B. Budde

Sixteenth Annual Conference on Mass Spectrometry and Allied Topics

May 12-17, 1968
Pittsburgh, Pennsylvania

Arranged by the Officers of
ASTM Committee E-14

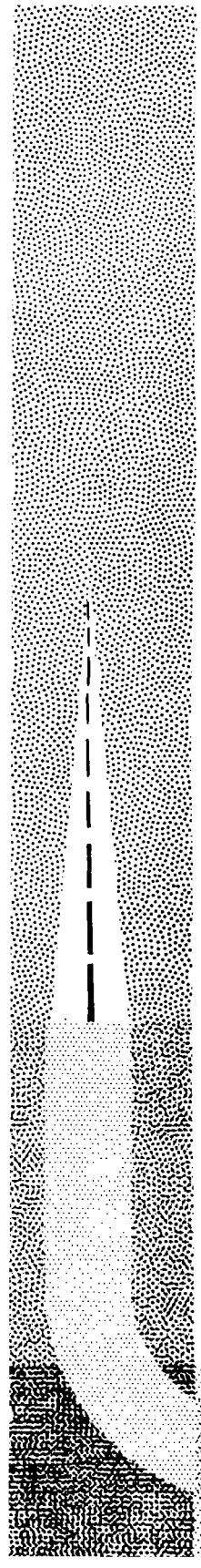

Sixteenth Annual Conference on Mass Spectrometry and Allied Topics

May 12-17, 1968
Pittsburgh, Pennsylvania

Arranged by the Officers of
ASTM Committee E-14

Preface

This volume is a collection of papers presented at the Sixteenth Annual Conference on Mass Spectrometry and Allied Topics, held in Pittsburgh, Pennsylvania, May 12-17, 1968. It is intended that this volume be distributed only to registrants of the conference and, therefore, should not be considered as a publication.

It is suggested that any future references to individual reports be cited in the form: author(s), presented at the Sixteenth Annual Conference on Mass Spectrometry and Allied Topics, Pittsburgh, Pennsylvania, May, 1968.

J. L. Franklin, Program Chairman

Arranged by the officers of the ASTM Committee E-14

H. M. Rosenstock, Chairman
J. L. Franklin, Vice-Chairman
D. B. Harrington, Vice-Chairman
A. B. King, Secretary
E. E. Muschlitz, Member-at-Large
R. M. Teeter, Member-at-Large

* * * * IN MEMORIUM * * * *

ROBERT WILEY HIGGINS

1913-1968

Born to James and Mary Jane Higgins April 27, 1913, in New Hope, Pennsylvania, Robert Wiley Higgins graduated from New Hope High School in 1931, received his B.S. degree, Cum Laude, in 1936 from Franklin and Marshall College and in 1939 he was named a Fellow at Northwestern University, from which he obtained a Ph.D. in organic chemistry in 1940. He was an instructor at Franklin and Marshall College until January, 1942, when he entered the United States Field Artillery. He attained the rank of captain and served until February, 1946. Dr. Higgins returned to Franklin and Marshall College as an assistant professor. In the summer of 1947 he was a research chemist at Armstrong Cork Company, Lancaster, Pennsylvania. From September, 1947, to June, 1950, he was assistant professor of chemistry at Pennsylvania State University. He was named associate professor of Human Nutrition Research at the Ellen H. Richards Institute, University Park, Pennsylvania, where he remained until September, 1952.

In 1952 Dr. Higgins came to Texas Woman's University, Denton, Texas, as professor of chemistry and chairman of the combined Chemistry-Physics Department, which then consisted of four staff members. His tireless efforts led to a separate Chemistry Department now expanded to 11 full-time and two part-time staff members. Under Dr. Higgins' able influence, an existing Masters degree program in chemistry saw continuous growth and a Ph.D. program was approved and initiated. In 15 years as departmental chairman, he was major professor for 19 students for M.S. degrees and for two Ph.D. candidates. Dr. Higgins was instrumental in achieving increased recognition for the science program at TWU and also in the acquisition of a new Graduate Science Research Center. Prior to his resignation as chairman on November 28, 1967, he had participated in the following professional activities: Organic Chemist, U.S. Bureau of Mines, Bartlesville, Oklahoma, summer, 1955; Research Chemist, Oak Ridge National Laboratory, Oak Ridge, Tennessee, summer, 1956; temporary employee, Union Carbide Nuclear Company, Oak Ridge, Tennessee, summer, 1958; NSF Conference on Reactive Intermediates in Organic Chemistry, University of Vermont, August 23-September 2, 1965; special lecturer of the Oak Ridge Mobile Laboratory Program for two years.

Dr. Higgins' research interests were in the area of synthetic organic chemistry with emphasis on organic sulfur and iodine compounds. He had recently synthesized isotopically labeled molecules for mass spectrometric studies. His research was supported by The Robert A. Welch Foundation, Houston, Texas, and University Institutional Grants. As an academic contributor to the work of the American Petroleum Institute's Research Project 48, his efforts led to donations of more than 150 previously unreported sulfur compounds, an appreciable number of which are in the API-44 list of mass spectral data. He was a member of numerous honorary and professional organizations. These included: Phi Beta Kappa; Sigma Xi, of which he served as president of the TWU club; American Association for the Advancement of Science; American Chemical Society, for which he was chairman of the Dallas-Ft. Worth section and a Councilor from 1963-66; Texas Academy of Science, for which he had recently completed a term as Vice-Chairman of the Physical Sciences section. He is listed in American Men of Science and Who's Who in the Southwest.

On July 1, 1939, he was married to the former Pauline Leaman of Lancaster, Pa. The ceremony was performed by her uncle at the Cedarville Methodist Church, Cedarville, Pa.

Dr. Higgins died on May 9, 1968, after a year's illness. Survivors include his widow, a son, Ronnie, who attends North Texas State University, a daughter, Mrs. Dwayne (Jean) Foster, all of Denton; a son, Jere, Senior Systems Analyst at the Texas Bank of Commerce, Houston, Tex.; three grandchildren of Denton; a brother, Leon Higgins, Philadelphia, Pa.; and four sisters, Miss Edith Higgins and Mrs. Ruth Denson of New Hope, Pa., Mrs. Sara Eastburn, Pittsburgh, Pa., and Mrs. Esther Laney, Highland Mills, N.Y.

* * * * IN MEMORIUM * * * *

DWIGHT A. HUTCHISON

1918-1967

Dwight A. Hutchison, Associate Chemist with Argonne National Laboratory, died suddenly October 18, 1967, at the age of 49. Dr. Hutchison was born in Madison, Indiana. In 1948 he was awarded his Ph.D. from the Ohio State University. This was preceded by five years as an Instructor at the Georgia Institute of Technology. He was associated with Argonne for the past 19 years where his primary research was centered in mass spectrometry.

Much of Dr. Hutchison's research was in the field of low-energy electron impact studies and involved the design and use of an electrostatic parallel-plate electron energy selector for determination of critical ionization potentials. He also devised a method for electronically differentiating ion appearance potential curves. Work was continued on the effects of electron energy distributions on appearance potential measurements and for determination of experimental threshold laws for ionization in the rare gases.

Some of Dr. Hutchison's earlier research concerned the study of ion-molecule reactions in the gas phase and the effects of surface reactions on mass spectra. The investigation of stable isotopic exchange reactions in various systems also occupied his attention.

His most recent research involved field ionization mass spectrometry. He wished to pursue the investigation of life-time distributions for field-induced fragment ion reactions. At the time of his death a new field ionization source was nearing completion.

Dr. Hutchison will be missed by all those who were acquainted with his work and the care with which he carried out his experiments.

TABLE OF CONTENTS

SIXTEENTH ANNUAL CONFERENCE ON MASS SPECTROMETRY

AND ALLIED TOPICS

PITTSBURGH, PENNSYLVANIA, May 12-17, 1968

* Invited Paper

*Invited Paper

*Invited Paper

*Invited Paper

*Invited Paper

*Invited Paper

1. An Automated Retarding Potential Difference Technique Using a Multichannel Analyzer*

P. J. Chantry
Westinghouse Research Laboratories
Pittsburgh, Pennsylvania 15235

Abstract

A commercially available multichannel analyzer** has been adapted so as to automatically accumulate data from a mass-spectrometer whose ion source is operated with the Retarding Potential Difference Technique for reducing the effective energy spread of the electron beam. Internally generated channel advance pulses sweep the analyzer alternately in the add and subtract modes. The difference electron current and the corresponding difference ion current are accumulated essentially simultaneously as functions of the electron energy by using digital to analogue conversion of the "live" channel address to generate a staircase electron accelerating voltage waveform. The lower and upper limits of the electron energy sweep are adjustable in a continuous fashion over a wide range. An important advantage of the system is that the electron energy may be swept twice (add, subtract) in a time short compared to possible drifts in electron current, pressure, multiplier sensitivity, etc., yet data may be accumulated over an arbitrarily long period, thereby increasing the signal to noise ratio.

*This work supported in part by the Advanced Research Projects Agency through the Office of Naval Research.

**Technical Measurements Corporation CAT 400 C.

2. A HIGH PRESSURE MAGNETIC ION SOURCE FOR DIRECT ATMOSPHERIC MEASUREMENTS IN THE D REGION

By

R. B. Lehotsky
Perkin-Elmer Aerospace Systems
Pomona, California 91767

Applying a Mass Spectrometer to space flight environments and conditions requires a reduction in the number of variables allowed for controlling and analyzing the mass spectra obtained. In particular, ion source operations are dictated by both simplicity in circuitry and power limitations. Consequently, the design philosophy must incorporate features which generally can be overlooked in the design of laboratory apparatus.

Two important features are the ion source linearity and time response. The linearity of the output current with ionizing region pressure is important since non-linear operation would only degrade the instrument sensitivity. Furthermore, linear operation removes the effects of sample interference.

Also, in a spacecraft moving through a changing atmospheric density at a relatively high velocity, the time response of the instrument becomes a critical factor in measuring constituent partial pressures as a function of the spacecraft altitude. For this reason, direct sampling of the external atmosphere becomes preferred over employment of a pressure-dividing inlet system. Therefore, for atmospheric measurements in the D region, from 70 to 120 kilometers, the objective of this study was to design an ion source such that a mass spectrometer system would be capable of analyzing pressures up to 10 microns, while maintaining linear operation and a low time response.

Figure 1 illustrates the model chosen as the basis for the design analysis. The ionizing region is bounded such that the gas flow into the analyzer is limited at two points, the electron entrance and the ion exit apertures. Ions formed in the electron beam are accelerated to the ion exit aperture using a defined extraction potential. The electron beam is magnetically aligned to maintain the electron beam dimensions. The dimensional variables are shown in this figure.

In the process of optimizing the ion source design, not only the pressure and the output current are variables but also all of the other parameters, such as dimensions, are considered to be variables. Consequently, in the work that follows, these parameters are scaled larger and smaller with other variables while the maximum pressure is allowed to change.

With such an ionizing region, the ion current reaching the ion exit aperture is defined by the following expression:

$$I^+ = PJ^- pt' R^2 \qquad (1)$$

where

P = probability of ionization

J^- = electron current density in the ionizing region

p = pressure in the ionizing region

t' = height of the electron beam in the ionizing region

R = radius of the ion exit aperture

This equation states that the output current will change proportionately with the pressure in the ionizing region as all the other parameters remain constant. Such an ion source will be then limited to a maximum pressure by the effects of ion space charge and decreasing mean-free-paths as the pressure is raised.

However, by defining a limit to these effects, expressions have been derived for ion source parameters in terms of the maximum ion source design pressure. The system in Figure 1 is designed to create a pressure differential between the ionizing region and the mass analyzer, by restricting the gas flow through the electron entrance and ion exit apertures. Thus, the effects of space charge and scattering within the analyzer remains constant. If the gas flow ratio between the two apertures is kept constant, then

for large differential pressures and for a constant length-to-diameter ratio of the ion exit aperture radius is expressed by:

$$R = C_1 \left(\frac{Q_a}{p_s} \right)^{1/2} \tag{2}$$

where Q_a = total gas flow through the analyzer

p_s = maximum ionizing region design pressure

C_1 = a constant

The electron beam thickness is defined by the acceptable ion energy spread of the mass analyzer, and is given by:

$$t' = \frac{\Delta V}{V_r} \; d \tag{3}$$

where ΔV = acceptable ion energy spread of the mass analyzer

V_r = ion extraction potential

d = repeller-accelerator spacing

To keep the ion transmission constant as the design pressure is increased, the distance, d, is related and scaled to the ion mean-free-path and is expressed by:

$$d = C_2/p_s$$

C_2 = a constant (4)

To keep the space charge effects constant as the design pressure is increased, the extraction potential is given by:

$$V_r = C_3 \, d^2 \, p_s^2 = C_4 \tag{5}$$

where C_3 = a constant

C_4 = a constant (the product of C_2^2 and C_3)

Substituting for the distance, d, shows that the ion extraction potential does not change with the design pressure. However, the gradient in the ionizing region will change as given by:

$$E_r = V_r/d = C_5 p_s \tag{6}$$

where C_5 = a constant (the ratio, C_4/C_2)

Consequently, the required electron beam thickness is seen to vary inversely with the maximum design pressure. The space charge parameters used to generate the expression for the extraction potential were derived from Brubaker's[1] work on ion source potential distribution. Another expression from Brubaker's[1] work enables the derivation of the electron current density as given by:

$$J^- = \frac{C_6 \, V_r}{wt'} \tag{7}$$

where w = width of the electron beam in the ionizing region

C_6 = a constant

A scaling factor is used to relate the beam width, w, to the ion exit aperture radius, such at the beam width will always remain greater than the aperture diameter. The expression for the electron current density is then given by:

$$J^- = C_7 \left(\frac{p_s^3}{Q_a} \right)^{1/2} \tag{8}$$

where C_7 = a constant

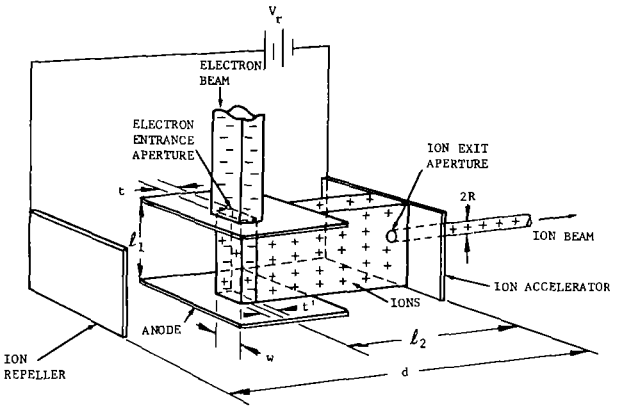

FIGURE 1
Model of the Ionizing Regions

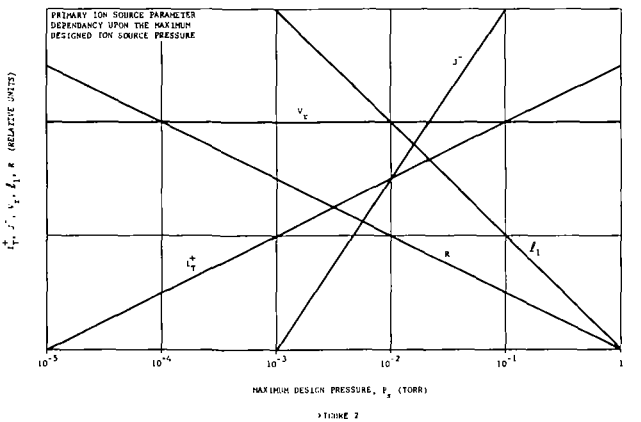

It is then seen that equation 1 becomes

$$I^+ = C_8 \left(Q_a \, P_s \right)^{1/2} \tag{9}$$

where C_8 = a constant

This equation states that with the use of scaling factors to define the geometrical relationships within the ionizing region, the maximum transmittable ion current arriving at the ion exit aperture increases with the square root of the maximum designed pressure limitation of the source. However, the linearity of the output current versus pressure would still be maintained.

As the maximum source pressure is increased, the result is (1) a shrinking of the ionizing region volume, (2) a decrease of the area of the electron entrance and ion exit apertures, and (3) an increase in the maximum transmittable ion current. The sensitivity of the source is then expressed by:

$$S = C_8 \left(\frac{Q_a}{P_s} \right)^{1/2} \tag{10}$$

This equation shows that the ion source sensitivity will decrease with the square root of the maximum design pressure, however, the number of ions available to work with has increased as seen by a previous equation.

The pumping system also governs the source conductance. Consequently, this independent control of the area for transmission allows for an increase in the transmittable ion current. This process of increasing the throughput cannot, however, continue indefinitely, since eventually the ion exit aperture will exceed the maximum object size for ion acceptability by the analyzer.

Figure 2 illustrates the dependence of the ion source design parameters upon the maximum design pressure. As seen, the relationships of the previous equations are shown with respect to the maximum design pressure. From the primary expressions derived above, relationships were then established to determine the dependence of the remaining ion source parameters under maximum design pressure. For a constant length-to-height ratio of the electron entrance aperture, it is found that the aperture height scales proportionally with the ion exit aperture radius. The magnetic field strength required can be expressed in terms of this aperture height, the electron beam thickness required, and the gradient in the ionizing region. Also, the walking angle of the electron beam in the orthogonal electric and magnetic fields can be determined from the magnitudes of these two fields.

The ion source was to be operated in conjunction with a small quadrupole mass spectrometer having an attached pumping system if 1 liter-per-second, and the ion energy spread acceptable for operation was 15 electron volts.

The design of the ion source was predicated upon direct analysis to 10 microns with a differential pumping ratio of 1,000. This defined the gas flow rate to be 1×10^{-5} torr-liters/second and an ion source conductance of 1 cc/sec. The gas flow was then divided equally through the two ion source apertures. With a length-to-diameter ratio of 2 defining the ion exit aperture, the required aperture diameter was found to be .005 inch. The repeller accelerator spacing calculated to be .028 inch. This spacing corresponded to 95% transmission of the ion beam when operated at 10^{-2} torr.

To obtain linear operation up to 10^{-2} torr, the design equations then predicted the following:

V_r = 40 volts

t = 0.003 inch

w = 0.020 inch

Ionizing electron current = 8 μamps at 52 ev.

Sensitivity = 1×10^{-8} amperes/torr

Aligning magnetic field = 800 gauss

Electron beam walking angle = 9.4°

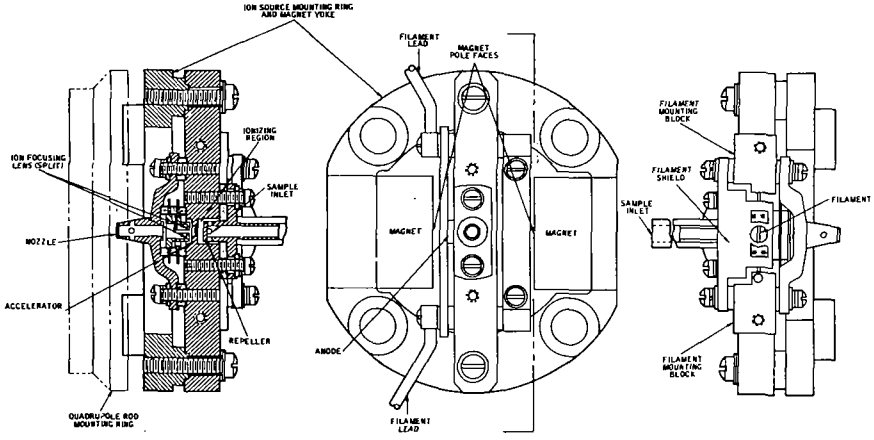

FIGURE 3
ION SOURCE ASSEMBLY

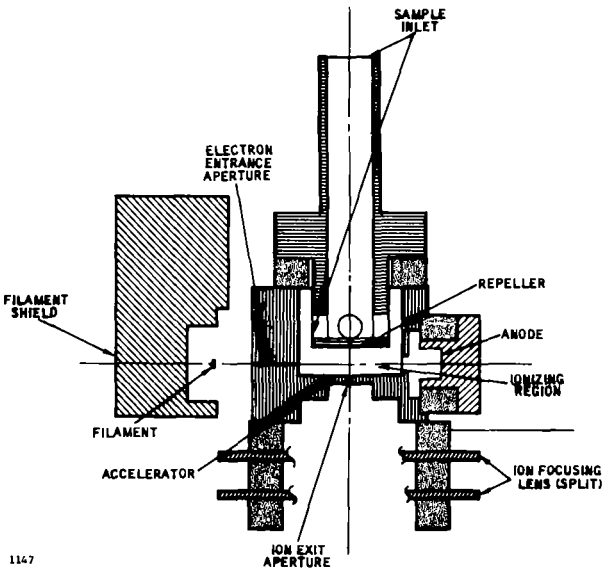

FIGURE 4
IONIZING REGION CROSS SECTION

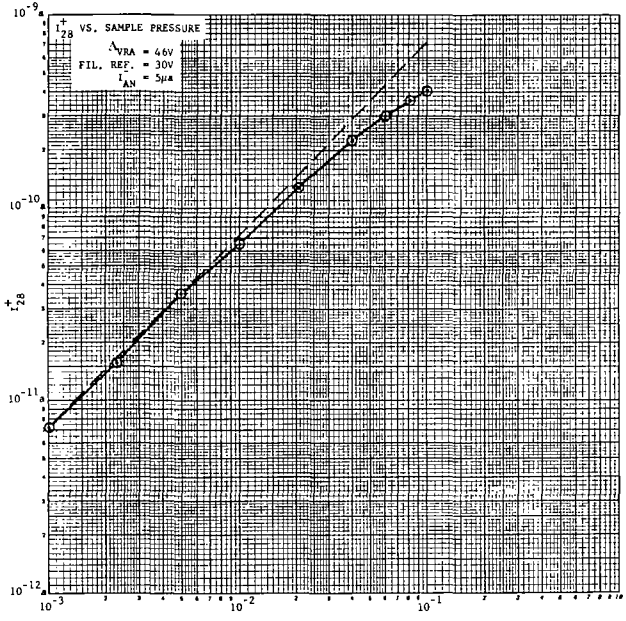

FIGURE 5

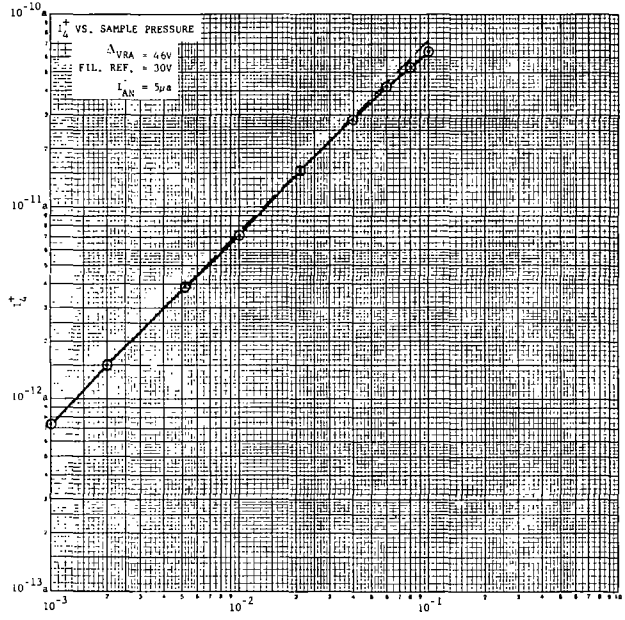

FIGURE 6

Figure 3 illustrates the ion source assembly as designed in the test model. The magnetic field was established utilizing Placovar magnets to establish the electron beam aligning field. This material was chosen due to its good vacuum properties. Figure 4, shows a cross-section of the ionizing region.

The ion source was tested in a small quadrupole operating in the 100% transmission mode, and after tuneup, the linearity versus pressure data was taken over the range from 1 to 100 microns. The sample pressure, however, was measured using a CEC Micromanometer which has an operating pressure range from 1 to 150 microns and a reproducibility of 0.5 microns. Consequently, the accuracy of the pressure measurement at 1 micron was limited by the measuring equipment.

Figure 5, shows the output linearity of the ion source using a nitrogen sample. From this curve it was seen that a non-linearity of less than 10% was obtained at the maximum design pressure of 10 microns. Extensive adjustments of the potentials was done, and it was found that the best results were obtained using average electron energies of 53 electron volts which was only 1 ev. higher than the theoretical prediction. The sensitivity obtained was 7.4×10^{-9} amperes-per-torr with 5 microamperes of ionizing current. While this was lower than predicted, the electron current at this time was not at the theoretical 8 microamperes, and this would reduce the sensitivity from the design level. It should also be noted that for laboratory use, it appears that operation could be extended to 1 torr by calibration of the output versus pressure. For this application, though, the reasonable output pressure limit appears to be 100 microns by accepting some degree of non-linearity, which was a decade higher than the design goal.

Figure 6, shows the output linearity versus a helium sample from monitoring the m/e 4 peak. These data appear quite promising, as the linearity extends well up the pressure scale. However, this effect was predicted, since the non-linearity due to space charge is known to be a function of both mass and ionization cross-section, and helium does not create space charge effects at pressures where both N_2 and O_2 do.

The time response for this particular ion source was calculated using a digital computer. It was found that the time constant of the source to sample changes was 833 microseconds.

In conclusion, we have found that the development of the design equations for extending ion source operations to higher pressures have agreed well with data taken on a test model, and are felt to be reliable for future design work.

REFERENCES

1. W. M. Brubaker, J. App. Phys., Vol. 26, No. 8, August, 1955.

4. A METHOD FOR MAKING PRECISE VELOCITY DISTRIBUTION MEASUREMENTS WITH A TIME-OF-FLIGHT MASS SPECTROMETER

Frank T. Greene
Midwest Research Institute
Kansas City, Missouri 64110

When using a time-of-flight mass spectrometer to follow very rapid processes, a problem may arise due to the intermittent operation of the mass spectrometer. At an operating frequency of 10 kc, one usually obtains information only during a 0.25 to 1.0 usec period which occurs at 100 usec intervals. When following processes which are short compared to 100 usec, one obtains no information during most of the mass spectrometer operating cycles, but one will accumulate noise during all cycles. If the process is repetitive and of the same order or shorter than the period between operating cycles, one can generally obtain a complete intensity distribution with time, but only by waiting for the phase of the master oscillator with respect to that of the process studied to drift through a complete cycle a statistically significant number of times. Hopefully, the two phases aren't accidentally locked.

A much more efficient procedure is to slave the mass spectrometer to the process being studied, and cycle the mass spectrometer only at the time of interest. This can be easily accomplished by substituting an external timing pulse from a pulse or delay generator for the pulse from the master oscillator. It is desirable but not necessary to operate the filament of the electron gun from a DC supply. By varying the delay between some fixed time on the repetitive process and the timing pulse, one obtains intensity as a function of time.

This has a number of advantages. It substantially reduces the time for a measurement and avoids the somewhat troublesome problem of obtaining an output circuit with very rapid response. One can obtain time resolution of 250 nanoseconds (or less) and still use unlimited integration times. And it is possible to make these measurements with no additional equipment other than a delay generator.

Although this technique is particularly applicable to measuring velocity distributions of species in molecular beams by the time-of-flight method, it can also be applied to any repetitive process in which time resolved spectra are required.

6. RATES OF SOME H_3^+ REACTIONS AT THERMAL ENERGIES,

J. A. Burt, M. J. McEwan, J. L. Dunn & H. I. Schiff
Centre for Research in Experimental Space Science,
York University, Toronto, Canada.

The reactions were studied in a fast flowing afterglow system, essentially similar to the one described by Fehsenfeld et al.[1] H_3^+ ions were produced by subjecting molecular H_2 either to a hollow cathode discharge or to an ionizing electron beam. Both these sources gave predominantly H_3^+ ions with H^+, H_2^+ and H_3^+ formation being at least two orders of magnitude lower.

Reactions of H_3^+ with CO, N_2, CO_2 and N_2O occurred by simple proton transfer

$$H_3^+ + X \rightarrow HX^+ + H_2$$

the HX^+ ion being the only product detected. The rate constants were all in the vicinity of 10^{-9} cm^3 sec^{-1}, within a factor of two of the classical collision frequency value.

The reaction of H_3^+ with NO showed two parallel channels, proton transfer and charge transfer, with proton transfer being the faster. In addition NO^+ was found to be formed by the secondary charge transfer reaction

$$NOH^+ + NO \rightarrow NO^+ + HNO$$

No proton transfer was observed when H_3^+ reacts with NO_2. A small amount of charge transfer occurred but the major product ion was NO^+ for which the reaction

$$H_3^+ + NO_2 \rightarrow NO^+ + OH + H_2$$

or

$$\rightarrow NO^+ + H_2O + H$$

is postulated. At higher NO_2 reactant flows complex ions such as $NO_2.NO^+$, $N_2O_4.NO^+$, $N_2O_4^+$, were detected.

With NH_3 proton transfer occurred rapidly and at higher reactant flows the first cluster ion $NH_4.NH_3^+$ was observed.

Only CH_5^+ was observed in the reaction with CH_4 but no CH_3^+ as reported from investigations of this reaction in mass spectrometer ion sources.

On the other hand the primary reaction between H_3^+ and C_2H_6 yields both $C_2H_7^+$ and $C_2H_5^+$ with the latter product being formed at twice the rate of the former. Secondary products from these ions reacting with C_2H_3 were also observed.

The reaction with C_2H_4 also yielded two primary products, $C_2H_3^+$ and $C_2H_5^+$. The latter product reacted further with C_2H_4 to form $C_4H_9^+$, while $C_2H_3^+$ formed $C_3H_5^+$.

H_3^+ reacted by means of a rapid 3 body process with H_2O to form H_3O^+. Addition of further H_2O resulted in formation of successively higher hydrates $(H_3O.nH_2O)^+$. With the experimental conditions used hydrates with $n \leq 4$ were observed. They appeared to be formed from their next lower hydrate with third order rate constants of about 10^{-29} cm^6 sec^{-1}.

The most surprising result was obtained with O_2 which was found to react very slowly with H_3^+. Only very small amounts of HO_2^+ were observed. At higher O_2 flows the major product was found to be HO_4^+ which was shown to be formed by the three body process.

$$H_3^+ + O_2 + O_2 \rightarrow HO_4^+ + H_2$$

The rate constant for this process was surprisingly large, of the order of 10^{-28} cm^6 sec^{-1}.

A number of proton transfer reactions involving N_2H^+ were also studied. The N_2H^+ source was provided by adding N_2 through an upstream inlet in sufficient quantities that all the H_3^+ ions are converted to N_2H^+. The second reactant is then added through an inlet located further downstream. Proton transfer from N_2H^+ to CO_2, N_2O, NH_3 and CH_4 was found to occur rapidly but no proton transfer to O_2 was observed.

The measurements permitted limits to be placed on the heat of formation of H_3^+. Failure to observe charge transfer with C_2H_4 or NH_3 places an upper limit at 12.5 ev. Observation of charge transfer with NO_2 puts a lower limit of 12.04 ev. if one accepts the ionization potential of NO_2 to be 9.80 ev. However this limit is inconsistent with recent findings of Chupka.[2] This inconsistency implies that either the ionization potential of NO_2 is too high or that the small amount of NO_2^+ found in our work arises from some process other than charge transfer with thermal energy H_3^+ ions.

A full report of this work will be published in the Journal of Chemical Physics.

References.

1. F.C. Fehsenfeld, A.L. Schmeltekopf, P.D. Goldan, H.I.Schiff and E. E. Ferguson. J.Chem. Phys., 44, 4087 (1966).

2. W. Chupka, private communication.

7. STUDIES ON THE MECHANISM OF $O^+ + O_2 \rightarrow O_2^+ + O$

John F. Paulson
Air Force Cambridge Research Laboratories (OAR)
Bedford, Massachusetts

The reaction $O^+ + O_2 \rightarrow O_2^+ + O$ may in principle proceed through charge exchange, oxygen atom pickup, or reaction complex mechanisms. For a given kinetic energy of the incident O^+ ion, KE(O^+), the kinetic energy of the O_2^+ product is thermal, 1/2 KE(O^+), or at least 2/9 KE(O^+), respectively, for these mechanisms. Using a double mass spectrometer system, retarding potential analyses of the reactant and product ions indicate that the charge exchange mechanism predominates in the range of incident ion kinetic energies from 0.7 to 20 eV when the O^+ ions are produced from dissociative ionization of O_2 at 30 eV.

Information on the reaction mechanism can also be obtained from isotopic analysis of the product ions when $^{18}O^+$ is incident upon ordinary O_2. Charge exchange can lead only to $^{16}O^{16}O^+$, atom pickup only to $^{16}O\,^{18}O^+$, and complex formation to both of these products in the ratio 1 to 2 (for the complete scrambling case). The use of $^{18}O^+$ as reactant shows that an ion-molecule reaction does occur, its cross section decreasing from about 1×10^{-16} cm^2 at 0.7 eV to 0.33×10^{-16} cm^2 at 14 eV. In this same energy range, the charge transfer cross section is constant at 4.6×10^{-16} cm^2. Retarding potential analyses of the $^{16}O^{18}O^+$ product of the ion-molecule reaction suggests that both complex formation and atom pickup mechanisms occur.

8. SOME OBSERVATIONS ON O_3^+, O_5^+, AND O_7^+

John F. Paulson and Fred Dale
Air Force Cambridge Research Laboratories (OAR)
Bedford, Massachusetts

Evidence has been obtained for the production of O_3^+, O_5^+, and O_7^+ in an electron bombardment ion source containing O_2 as sample gas. These species are generally observed to dissociate before their entry into the magnetic field of a 2.54 cm 90 degree magnetic sector mass spectrometer which is coupled to a 45.7 cm quadrupole mass filter. Thus the ionic dissociation product (O_2^+) may be observed directly with the mass filter when the sector mass spectrometer is tuned to the "metastable" mass number. In addition, the kinetic energy of the ionic dissociation product can be determined by retarding potential analysis. In the case of O_5^+, for example, an O_2^+ peak is observed with the mass filter when the sector mass spectrometer is tuned to m/e 12.8, i.e., $(32)^2/80$. The kinetic energy of this O_2^+ is 2/5 of the kinetic energy of the O_5^+ parent, as expected. Some O_3^+ ions have been observed to dissociate after their passage through the magnetic field of the sector mass spectrometer.

We have recently attempted to observe these metastable peaks from O_3^+, O_5^+, and O_7^+ in a 15 cm 60 degree sector mass spectrometer at various sample pressures, ionizing energies and ion accelerating voltages. Only the dissociation of O^+ to O_2^+ could be seen in this system. Indirect observation of the O_5^+ and O_7^+ species by their transitions in the double mass spectrometer system may have been favored by the deep potential well in the ion source of this system. However, these observations must be regarded as questionable until confirmed in another apparatus. The existence of polymeric neutral species in oxygen is known from other work, but the expected abundances are not sufficient to account for our observations.

9. Some Recent Developments in Field Ionization Mass Spectrometry.

H.D. Beckey

Institut für Physikalische Chemie der Universität Bonn

Previous reviews on Field Ionization (FI) Mass Spectrometry have been given elsewhere (1 - 3). This paper gives an account of the more recent work of the author's group. The names of the co-authors are given at the beginning of the different sections.

Two of the most specific features of FI are the following. Very little energy is transferred to the molecular ions by FI. This leads to the well known brief statement:

A. Field ionization is a very "soft" method of ionization.

A second feature not so generally known, but pointed out recently (4) is the greatly different time scale for ion decomposition in FI and EI (electron impact) source. EI fragments are formed within several times 10^{-14} - 10^{-6} sec after ionization. However, fragment ions at "normal" mass positions in FI mass spectra are formed within several times 10^{-14} - 10^{12} sec after FI. Summarizing:

B. Field ionization is a very "fast" method of fragment formation. (with respect to fragments at normal mass positions relative to parent ions)

Point B is discussed in greater detail in the paper.

I. Kinetics of fast unimolecular decomposition of organic ions.

a) Method of life time measurements by FI mass spectrometry.

Assume a molecule is field ionized at the surface of a FI tip which is at a positive potential U_o with respect to a cathode. If a fragment ion m is formed instantaneously, this will obtain the full kinetic energy $mv^2/2 = eU_o$. The potential drops rapidly with distance Δx from the tip. A fragment ion m formed at Δx starts from a lower potential. Its kinetic energy will be smaller than that of fragments starting at the tip by an amount which can be calculated by ΔU. It is observed at a mass position $m - \Delta m$ in the mass spectrum. The observed mass shift Δm is correlated with ΔU by the equation for a magnetic sector mass spectrometer $M U = c(H R)^2$, where H is the magnetic field strength and R the radius of deflection. Δx can be calculated as a function of ΔU from the potential distribution near the tip, which depends on the geometric shape of the tip and the cathode. Then the life time Δt of the parent ion is calculated by integration of the equations of motion. The complete calculation scheme is:
$\Delta M_{obs} \rightarrow \Delta U \rightarrow \Delta x \rightarrow \Delta t$. (see 5).

b) Mechanismus of field induced decomposition. $\tau = 3\times10^{-14}$-3×10^{-12} sec. (H.Knöppel).

Four different mechanisms for field induced decomposition have been described (5). 1.) Field induced spontaneous decomposition within one vibrational period ($\tau \approx 3\times10^{-14}$ sec) by a Franck-Condon transition to an ionic state, the dissociation energy of which is reduced almost to zero. 2.) Tunneling of free radicals through a potential barrier slightly below the potential maximum. ($\tau = 3\times10^{-14}$-3×10^{-12} sec). 3.) Delayed dissociation due to re-orientation of the molecular ion. ($\tau_{max} \approx 3\times10^{-12}$ sec.) 4.) Field induced statistical dissociation. ($\tau_{max} \approx 3\times10^{-12}$ sec.)

c) Normal metastable decomposition. $\tau = 1\times10^{-8}$ - 3×10^{-6} sec. (G.Tenschert)

Normal metastable ions are formed, as in the case of EI, in the field free drift tube of a M.S. in the case of FI. They have a range of life times of 1×10^{-8} - 3×10^{-6} sec. (Only about 1 - 3 x 10^{-6} sec with EI). A retarding potential technique was developed for measurement of the life time distribution of the metastable ions. (Special FI source with a retarding source of variable height and length (6)). Ions decomposing on the retarding potential plateau cause a new "metastable plateau peak", the position of which is variable between m and $m^* = m^2/M$, depending on the potential height. (M=mass of the molecular ion)

From the observed change of the metastable plateau peak intensity with variation of the ion residence time one can derive a "decay function" $g(t) = - dN(t)/N(t)dt$ which is an average velocity constant at the time t after field ionization.

d) Fast metastable decomposition. $\tau \approx 10^{-11} - 10^{-8}$ sec. (Tenschert)

A broad intermediate peak between the "normal fragment peak" (m) and the "normal metastable peak" (m^*) is termed "fast metastable peak". It arises from fragment ion formation in space some distance from the tip. (Knöppel) Tenschert analyzed the life time distribution of fast metastable ions from molecules such as tert. butyl benzene and n-heptane. (Using the calculation scheme indicated in section a)) See fig. 1.

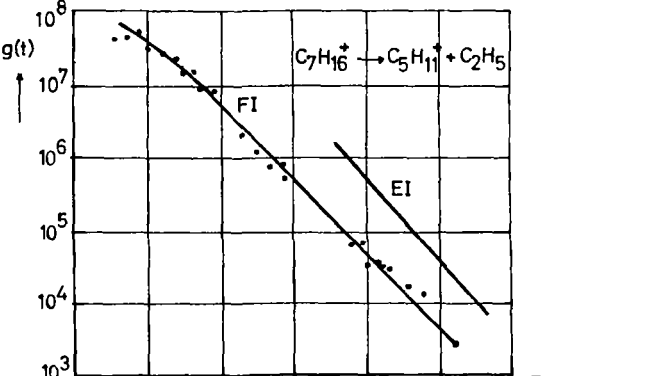

Decay function g(t) of n-heptane

The curve comprizes points originating from the fast metastable peak, from the metastable plateau peak (retarding technique), and the normal, unretarded metastable ions. In qualitative agreement with the statistical theory of mass spectra, there exists a continuous, extremely broad distribution of velocity constants, measured in the time interval between several times 10^{-11} and 10^{-6} sec. The corresponding electron impact curve of Hertel and Ottinger (7) is also shown. It is shifted to higher g(t) values because of larger energy transfer in the case of EI.

II. Rearrangement reactions. (H.Hey, H.Krone, K.Levsen.)

The time available for formation of a "normal" FI fragment ion (3×10^{-14} - 3×10^{-12} sec) is not sufficient for a rearrangement reaction requiring a large activation entropy, and for multi-step decomposition processes. Therefore, such FI peaks are not observed, even if the corresponding intensities are very large in EI spectra. A ratio R is defined

$$R = \frac{I^i_{FI}/I^b_{FI}}{I^i_{EI}/I^b_{EI}},$$

where I are the intensities, and the indices i and b refer to the i th fragment and the base peak, respectively. A new rule concerning comparative interpretation of FI and EI mass spectra states that a rearrangement or a multi-step process can be concluded to occur from the spectra if $R < 3\times10^{-4}$ is observed, whereas $R > 5\times10^{-2}$ is indicative of direct single step bond rupture. (Only peaks with $I^i/I^b > 0{,}20$ in the EI spectra should be evaluated).

The rule is applicable only to rearrangement reactions connected with pronounced displacement of the nuclei during transition from the normal state to the activated complex (high activation entropy). Electronic rearrangement without change of nuclear positions does not fall into this category. (Decomposition of di-cyclopentadiene into two pentadiene molecules, for example).

III. Surface reactions. (F.W. Roellgen)

The field impulse desorption method as described by Inghram and Gomer and by Block has been used for the study of catalytic reactions of organic substances on platinum and for investigation of reactions within adsorbed layers on FI emitters. A detailed account will be published in Intern. J. of Mass.Spectry. (Also on points I and II, and on new carbon filament FI emitters and whisker growth).

References.

(1) H.D.Beckey, Adv.in Mass Spectr.Vol II, Perg.Press (1962), (2) ibid. vol.III, Inst.Petr.(1966). (3) J.Block, ibid, Vol IV,(1968). (4) H.D.Beckey, Int.J.Mass Spectr. 1, 93 (1968). (5) H.D.Beckey and H.Knöppel, Z.Naturf. 21a, 1920 (1966). (6) H.D.Beckey, A.Heindrichs and G.Tenschert, Z. Instr.75, 195 (1967). (7) I.Hertel and CH.Ottinger, Z.Naturf. 22a, 1141 (1967). (9) H.D.Beckey and H.Hey,J.Org.Mass Spectr. 1, 47 (1968).

10. FIELD EVAPORATION OF Fe, Co AND Ni IN THE PRESENCE OF N_2, O_2 AND CO*

Douglas F. Barofsky and Erwin W. Müller

Department of Physics, The Pennsylvania State University
University Park, Pa. 16802, U.S.A.

Mass spectrometric analysis of the products of low temperature field evaporation is a new and important technique through which surface phenomena can be investigated. Field evaporation[1] can be treated as the field ionization of a metal surface atom followed by its thermal activation over or its tunneling through a field reduced energy hump. The general mathematical treatment of this process has been treated in great detail in a number of publications[1, 2, 3, 4, 5].

In designing our simple, prototype, field evaporation mass spectrometer the operating conditions of the low temperature field ion microscope were preserved in order to allow better correlation between the results of the mass spectrometric studies and those of the field ion microscope[6]. In anticipating that very simple spectra would be dealt with we employed only the simplest magnetic sector lens mass analyzer. The experimentally determined resolution of the resulting instrument is about 80. The analyzer samples a cross-section of ions originating from the center of an emitter tip surface to those coming from its edge. The transmission of the analyzer is about 1.5×10^{-2}. A high gain, low noise, resistance strip electron multiplier capable of single particle detection provides the necessary sensitivity of the instrument.

The instrument used in this work served in part as a prototype of the atom-probe field ion microscope[7]. This unique instrument utilizes the single atom resolution capabilities of the field ion microscope[8] in conjunction with the single particle sensitivity of existing electron multipliers to make a mass spectroscopic analysis of one single surface atom.

Our simple field evaporation mass spectrometer was used to analyze some of the low temperature (78^0K-300^0K) field evaporation products of Fe, Co and Ni at a background pressure of 10^{-7} Torr. The additional products formed when these three metals are field evaporated in the presence of N_2, O_2 and CO were also investigated.

At the background pressure of the system (10^{-7} Torr) and at 78^0K the field evaporation spectra consisted almost entirely of the doubly charged ion species of the emitter material. As the temperature of the tips was allowed to gradually increase to room temperature from 78^0K, the mass spectra became complicated with the formation of oxides and water associations. All three metals make a transition from doubly charged ions to singly charged ions with increasing temperature, and thus lend weight to the ionic tunneling theory[5, 6].

The introduction of one of the three gases, N_2, O_2 or CO, into the system at 78^0K had almost negligible effect on the field evaporation spectra despite a noticeable reduction in the evaporation fields of the emitters. Only in the case of iron were minute traces of FeN_2^{++}, FeO_2^{++} and $FeCO^{++}$ observed at 78^0K. At temperatures above 78^0K more reaction products attributable to the presence of one of the above gases were observed.

At the very low temperatures the mass spectra are in general simple and the ion species correspondingly easy to identify. However, at temperatures above 100^0K the uncertainties in the mass scale of our simple mass spectrometer are a basic limitation in identifying with certainty the numerous mass peaks which begin to occur. We now feel, however, that the need for improving the instrumentation and continuing the experiments on field evaporation has been established.

REFERENCES

1. E.W. Müller, Phys. Rev. 102, 618 (1956).
2. R. Gomer, J. Chem. Phys. 31, 341 (1959).
3. R. Gomer and L.W. Swanson, J. Chem. Phys. 38, 1613 (1963).
4. D.G. Brandon, Surface Sci. 3, 1 (1965).
5. T.T. Tsong, Surface Sci. 10, 102 (1968).
6. D.F. Barofsky and E.W. Müller, Surface Sci. 10, 177 (1968).
7. E.W. Müller, J.A. Panitz and S. Brooks McLane, Rev. Sci. Instr. 39, 83 (1968).
8. E.W. Müller, Advances in Electronics and Electron Physics, Vol. 13, Academic Press Inc., New York, 1960.

*Supported by the National Science Foundation and the American Iron and Steel Institute. To be published in the International Journal of Mass Spectroscopy and Ion Physics.

11. Elemental Composition Determination by Field-Ion Mass Spectrometry[1]

E. M. Chait, T. W. Shannon, W. D. Perry,
G. E. VanLear and F. W. McLafferty

Department of Chemistry, Purdue University
Lafayette, Indiana 47906

The unambiguous determination of the elemental composition of a compound is possible if the mass of the molecular ion can be measured with sufficient accuracy.[2] A major limitation of the use of electron-impact mass spectrometry for these valuable measurements is that such spectra often show no measurable molecular ion. Field ionization,[3-5] whose development is due especially to Beckey, is reported to produce relatively abundant molecular ions for all compounds examined.[4] No general study of the application of exact mass measurement techniques to field-ion mass spectra has been described;[6] indeed, relatively few low resolution[7] spectra have been reported for non-hydrocarbon compounds.[3-5] We report here that accurate mass measurements of field ions of a wide variety of compounds can be made relatively simply in conjunction with such measurements of the electron-impact spectrum.

The standard electron-impact ion source of a CEC 21-110B mass spectrometer was modified[8] so that a razor blade anode[3,9] 4.5mm wide can be inserted between the repellers, with insulation so that a potential of 8-10 kv can be applied between the blade and the ion exit slit (distance 0.25 mm). The blade can be adjusted externally for distance and angle and removed through a vacuum lock without venting the instrument. Details of the source are shown in Figure 1. All other operating parameters of the instrument are similar to those for electron impact; resolution (10% valley definition) of 32,000 by electron impact and 20,000 by field ionization is obtainable. Conversion from field-ion to electron-impact operation can be achieved in two minutes without interrupting the volatilization of a sample directly in the ion source. Sensitivities are highly dependent on blade condition, but the total ionization monitored can be as high as an order of magnitude below that observed using a 100 μamp electron current.

The field ion spectra of more than fifty different compounds of many types have been obtained to date; most show abundant molecular ions even when none are observed in the electron impact spectrum. In contrast to the spectra of all other compounds reported,[4] CCl_4 shows a negligible (<0.02% versus CCl_3^+) molecular ion. Molecular ions are also of low abundance in other perhaloalkyl-compounds [0.3% in $(n\text{-}C_4F_9)_3N$]. Representative mass measurements are shown in the Table. In all cases the molecular ion measurements are with the 3 millimass unit tolerance acceptable for electron impact measurements under similar conditions. A number of larger molecules such as glyceryl trilaurin (MW 683), $C_{30}H_{26}SnBr_2$ (MW 664), and the cyclic peptide evolidine (MW 770) yield measurable molecular ions, but exact mass measurements in this range are less satisfactory at present because of the lack of reference ion lines similar in mass. The dearth of fragment ions in the field ion spectra of most compounds plus the low sensitivity of the volatile fluorocarbons used as mass standards for electron impact spectra create this problem at higher masses.

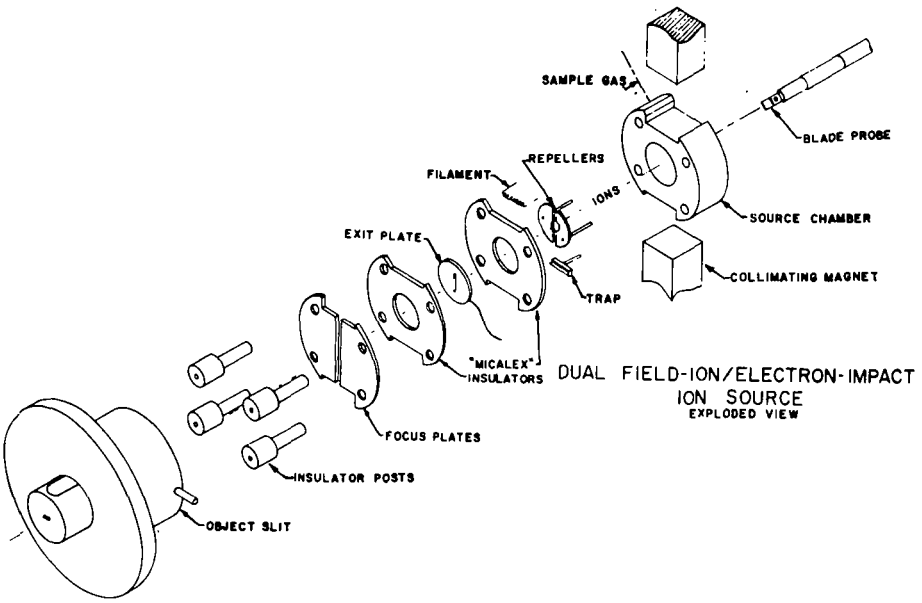

Figure 1. Dual Field-Ionization/Electron-Impact Ion Source

Table I. Mass Measurement of Field Molecular Ions from Compounds Which Do Not Give Electron-Impact Molecular Ions

Compound	Ion	Formula	Measured[a]	Calculated	Error[b]	Reference[c]
Serine ethyl ester	M[d]	$C_8H_{11}O_3N$	133.0765	133.0739	+2.6	$C_9H_{10}O$
Threonine ethyl ester						$C_9H_{12}O$
Ribose[e]	M	$C_5H_{10}O_5N$	147.0886	147.0895	−0.9	$C_9H_{11}O$
						$C_{10}H_{13}O$
	M − 1	$C_5H_9O_5$	149.0465	149.0499	+1.6	$C_9H_{11}C$
	M	$C_5H_{10}O_5$	150.0517	150.0527	−1.0	$C_{10}H_{14}O$
	M + 1	$C_5H_{11}O_5$[f]	151.0584	151.0606	−2.2	
Glucose	M	$C_6H_{12}O_6$	180.0653	180.0633	+2.0	$C_{11}H_{16}O$
	M + 1	$C_6H_{13}O_6$	181.0666	181.0711	−4.5	$C_{12}H_{13}O$
		$C_5C^{13}H_{13}O_6$		181.0666	0.0	
Diethyl sebacate	M	$C_{14}H_{26}O_4$	258.1848	258.1830	+1.8	$C_{17}H_{14}O$
	M + 1	$C_{14}H_{27}O_4$[f]	259.1939	259.1908	+3.1	$C_9H_7{}^{79}Br_3$
Abcisin II[g]	M	$C_{15}H_{16}O_4$	264.1337	264.1360	−2.3	$C_{18}H_{20}O$
						$C_{17}H_{12}O$

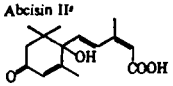

[a] Photoplate spectra were measured automatically with a Grant-Datex plate reader with computer calculation of the results (*14*).
[b] Millimass units.
[c] Molecular ion of the corresponding 2-alkanone or 1,1,2-tribromoethane.
[d] Molecular ion.
[e] Reference (*2*).
[f] Part of peak is due to M containing ^{13}C. This tends to make the measured mass lower than the calculated mass.
[g] Reference (*15*).

Thus, it appears that field ionization can extend the capability of high-resolution mass spectrometry for determining the elemental composition[10] of submicrogram samples to a much wider variety of compounds.

---

(1) The generous support of the National Institutes of Health, GM12755 and FR00354, is gratefully acknowledged.

(2) J. H. Beynon, "Mass Spectrometry and Its Applications to Organic Chemistry," Elsevier, Amsterdam, 1960; for a recent review see F. W. McLafferty, Science, 151, 641 (1966).

(3) H. D. Beckey, H. Knoppel, G. Metzinger, and P. Schulze, "Advances in Mass Spectrometry," Vol. 3, W. L. Mead, Ed., The Institute of Petroleum, London, 1966, p. 35, and references cited therein.

(4) H. D. Beckey, H. Heising, H. Hey, and H. G. Metzinger, Preprints, International Mass Spectrometry Conference, Berlin, Sept. 1967.

(5) G. G. Wanless and G. A. Glock, Anal. Chem., 39, 2 (1967).

(6) The only measurements reported reflect the experimental difficulties of this technique. W. L. Mead, A. R. West, J. S. Halliday, A. Riddoch, and H. Howarth, ASTM E-14 Conference on Mass Spectrometry, Denver, Colo., May, 1967, studied sulfur-containing hydrocarbon mixtures; both the resolution and mass measuring accuracies reported are an order of magnitude below the performance of their instrument (AEI MS-9) with electron impact ionization.

(7) High-resolution field-ion mass spectra have been reported by J. H. Beynon, A. E. Fontaine, and B. E. Job, Z. Naturforschg., 21a, 776 (1966); C. Brunnée, G. Kappus, and K. H. Maurer, ASTM E-14 Conference on Mass Spectrometry, Denver, Colo., May, 1967; and H. D. Beckey, Univ. of Bonn, private communication, Aug. 1967. Both of the latter authors report resolution in excess of 15,000, which indicates that their instruments should also be capable of accurate mass measurements.

(8) Detailed drawings will be supplied on request.

(9) A. J. B. Robertson and B. W. Viney, "Advances in Mass Spectrometry," Vol. 3, W. L. Mead, Ed., The Institute of Petroleum, London, 1966, p. 23.

(10) A disadvantage of field ionization compared to electron impact is that ion-molecule reactions often produce abundant ions,[3] such as $(M + 1)^+$ (see Table), which might be mistaken for the molecular ion, M^+. Determination of the elemental composition will distinguish between even-electron ions, such as $(M + 1)^+$, and the odd-electron M^+.

12. SOME OPERATIONAL PRINCIPLES OF FIELD IONIZATION MASS SPECTROMETRY [a]

by

Fred P. Abramson and Royce F. Howard
Analytical Instruments Division
Consolidated Electrodynamics Corporation
Monrovia, California

A field ionization source has been built and tested on a CEC Model 21-110B double focusing mass spectrometer. A razor blade has been used as the ionizing device. We have investigated the effects of a number of operational parameters on the quality of our field ionization mass spectra and have attempted to relate some of them to the physical phenomena which cause them. For example; the potential of the blade, the temperature of the source, and the presence of other species in a mixture have all been shown to produce significant effects on field ionization mass spectra.

The effects of voltage appear most significant when examining the spectrum of a material which readily fragments, even under the conditions of field ionization. Neohexane is such a compound. The molecular ion represents almost 12% of total ionization at 10 Kev emitter potential and drops to 6% when the emitter potential is raised to 12.5 Kev. We will also discuss some effects of voltage in the consideration of mixture phenomenon and ion-molecule reactions. There does not appear to be a significant amount of energy spread from this source. The maximum resolution with the field ionization source produced a 23% valley for the flourene-dimethylnitroanaline molecular ion doublet where the mass difference is less than 1 part in 40,000. This is essentially identical with the resolution obtained with a gas source.

When mixtures of hydrocarbons were analysed, it was noted that the quantitative accuracy was surprisingly poor. Further investigation revealed that this quantitative inaccuracy resulted from greatly different sensitivities when a substance was examined by itself and when it was examined in the presence of certain other molecular species. The phenomenon manifests itself in the following way. When some saturated hydrocarbon is introduced into the mass spectrometer, some particular sensitivity is noted. In fact, the relative sensitivity of pure hydrocarbons compared to aromatic or other functional species is rather low, say a factor of 1/5 for the case actually considered; neohexane and ethylbenzene.

[a] publication is anticipated in International Journal of Mass Spectrometry and Ion Physics.

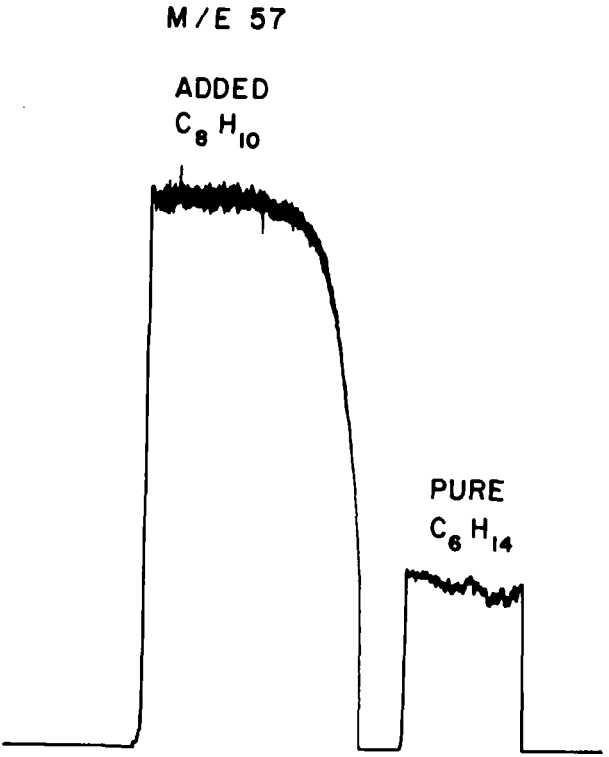

FIGURE 1

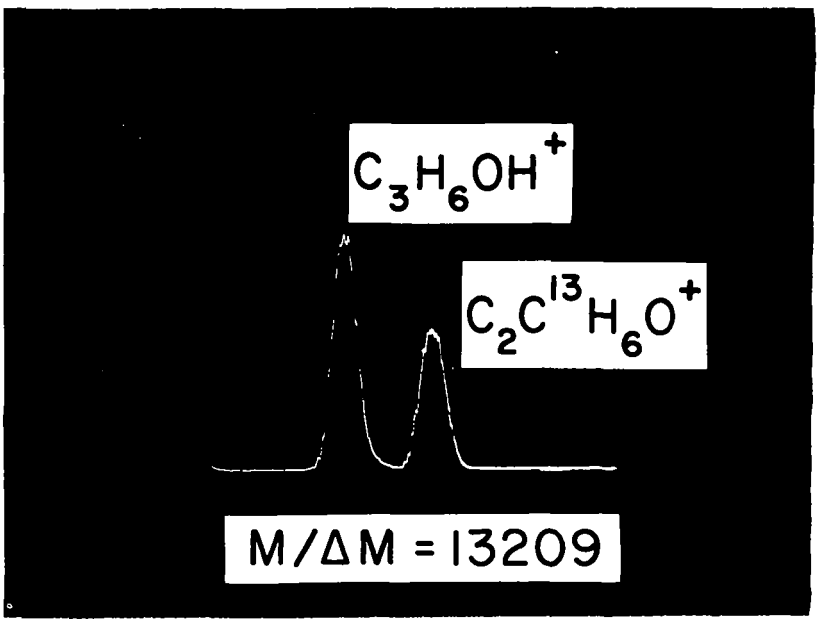

FIGURE 2

This sensitivity is greatly increased when some more strongly ionizing material is in the mass spectrometer at the same time. Figure 1 shows the m/e 57 peak from neohexane. The rightmost portion represents the signal from a pure sample of neohexane. The sample reservoir was isolated, the inlet line was evacuated and the signal decayed. An equal sized sample of ethylbenzene (which itself produces no m/e 57) was allowed to mix with the neohexane and then this mixture was readmitted to the mass spectrometer. As can be seen, the m/e 57 signal has increased by a factor of 3. The enhancement doesn't appear to be pressure sensitive but increasing the potential on the blade by 2 Kev reduces the enhancement by 25%.

According to what is currently known about ion-molecule reactions, processes such as proton transfer should have essentially no temperature coefficient and be quadratic with respect to pressure. When acetone is introduced into our field ion source, one generally sees a peak at m/e 59 which is considerably in excess of the expected isotopic contribution. The nature of the m/e 59 peak may be investigated using high resolution. Figure 2 shows the m/e 59 doublet with the source at 150°C and 11.5 Kev on the blade. The ratio of the proton transfer peak to the C-13 peak is 1.7. When the potential on the blade is lowered to 8 Kev, this ratio rises to 3.3. At 8 Kev, if the source is cooled to 40°C, the ratio becomes greater by a factor of at least 2.5.

Presumably, the temperature effect is a manifestation of the relative thickness of a "liquid" layer on or around the emitter surface. The effect of voltage here, as well as in the mixture phenomenon, seems to suggest that both the surface of the blade and the gas phase around it are sites for ionization. That these phenomenon occur at all suggests that the surface must play a significant role. However, we interpret the decrease in the relative amount of ion-molecule interaction and the decrease in the enhancement of our mixtures with increased emitter potential as follows: the substantial fraction of ionization takes place in the gas phase and, as the voltage is increased, the probability of reaching the surface of the emitter without becoming ionized decreases. Thus, the amount of ionization which occurs homogeneously will increase steadily as the emitter potential is increased.

13. Translational Energy Effects for Negative Ion-Molecule Reactions*

Thomas O. Tiernan and B. Mason Hughes

Aerospace Research Laboratories
Office of Aerospace Research
Wright-Patterson Air Force Base, Ohio 45433

Introduction

Studies of the energy dependence of ion-molecule reaction rates permit a critical assessment of existing theories concerning ion-molecule interactions. Moreover, when applied in conjunction with isotope techniques, such studies often provide considerable insight into the detailed mechanism of these reaction processes. While translational energy effects for positive ion-molecule reactions have been rather extensively explored in several laboratories[1], similar investigations for negative ion reactions are almost nonexistent. We have therefore undertaken an examination of the translational energy dependence of several types of negative ion-molecule reactions. The preliminary results of these studies are presented here.

Experimental

The experiments discussed in this paper utilized a dual stage mass spectrometer designed for the identification of ionic products from the impact of mass and energy analyzed ion beams on a target gas. The basic instrument has been previously described[2], but several modifications were required to permit observation of negative ion reactions. An important consequence of these modifications was the development of a mode of ion source operation which results in reactant negative ion beams comparable in intensity to those usually obtained for positive ions, that is, 10^{-8} - 10^{-9} amp. measured at the β- or energy defining slit. Briefly, the operating conditions required for this mode of source operation are, 1) a rather high impacting electron energy (~100 eV); 2) accessibility of the electron trap to the ionization chamber; 3) high trap or anode currents; 4) the anode must be operated at source potential. These conditions and other pertinent observations which cannot be discussed here have led us to conclude that this operating mode results in the ejection of relatively large quantities of secondary electrons from the anode into the source region which have energies appropriate for resonance electron capture. Moreover, operation with the higher energy electron beam permits the source pressure to be elevated considerably above that which would be possible with low energy beams in the resonance capture region, since with the latter, beam collimation and penetration into the ionization chamber are significant problems. This in turn means that three-body capture processes are probable in our mode of operation, again increasing the probability of formation of negative ions. The source design and further discussion of operating parameters will be presented in a forthcoming publication.

Results and Discussion

The first reaction type for which the energy dependence was determined was the exothermic charge transfer process,

$$O^- + NO_2 \rightarrow NO_2^- + O \qquad (1)$$

This reaction has been observed previously by several workers[3-5]. The dependence of the reaction rate on kinetic energy of the impacting ion in the laboratory scale of coordinates is shown in Figure 1. The indicated energy "zero" here actually corresponds to our lowest attainable energy, ~ 0.3eV. It can be seen that the reaction rate falls off somewhat with increasing reactant ion energy, finally reaching a plateau region. This behavior is quite similar to that observed for exothermic charge transfer in positive ion systems[6]. These observations are logically explained by the assumption that at low energies the traditional ion-induced dipole complex is formed and then decomposes to yield the charge transfer product. At higher kinetic energies, however, the orbiting complex cross-section falls off rapidly and above about 10eV a long-range electron transfer will be the dominant mechanism.

As an example of endothermic charge transfer, the reaction of Cl^- with Cl_2 was investigated as a function of impacting ion energy.

$$Cl^- + Cl_2 \rightarrow Cl_2^- + Cl \qquad (2)$$

The observed energy dependence is shown in Figure 2. The endothermic reaction channel shows a distinct threshold implying that reactant ion kinetic energy is being used to drive the reaction. The slight differences in the curves observed

*A more detailed account of this work will be submitted for publication in the Journal of Chemical Physics.

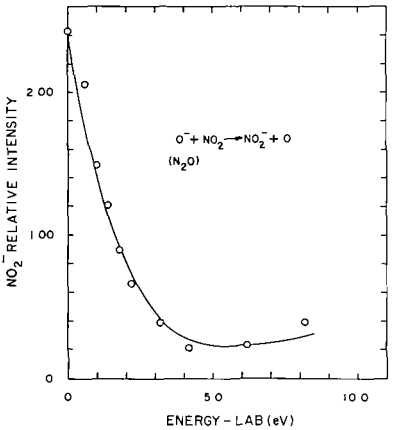

Figure 1. Energy dependence for exothermic charge transfer in a negative ion-molecule reaction.

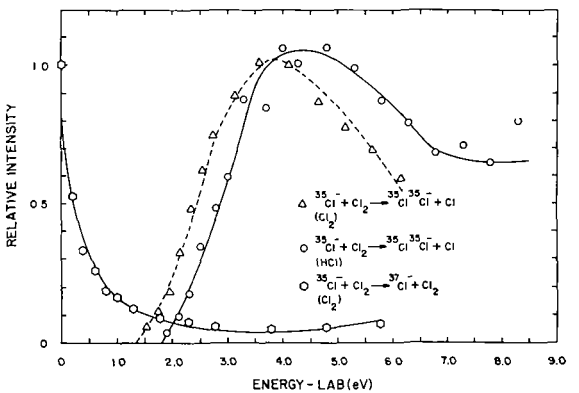

Figure 2. Energy dependence for endothermic charge transfer in a negative ion-molecule reaction.

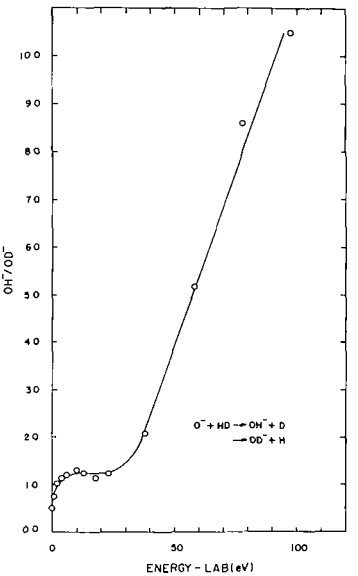

Figure 3. OH^-/OD^- from the reactions of O^- wit HD as a function of reactant ion energy in the laboratory system.

for Cl^- ions from Cl_2 as compared to those from HCl probably indicated differing amounts of internal excitation of the ions derived from these two sources. Again, the observed behavior is very similar to that which Maier[6] found for such endothermic processes. It is also noted that there is an exothermic channel yielding Cl^- product which exhibits the same behavior as that already described for exothermic reactions.

In the last reaction which was examined in this study, energy dependent isotope effects were determined for the reactions,

$$O^- + HD \rightarrow OH^- + D \quad \Delta H = -0.5eV \qquad (3a)$$

$$\rightarrow OD^- + H \qquad (3b)$$

While the orbiting complex model for ion-molecule reactions appears to be valid at low interaction energies, it is now reasonably well established for certain simple positive ion reactions that at higher energies a so-called "spectator stripping" model is dominant[7]. This process may be visualized as the stripping off of one fragment of the neutral by the impacting ion, leaving the remaining fragment undisturbed. The investigation of isotope effects for simple positive ion-molecule reactions as a function of energy has demonstrated a transition from the low energy mechanism to the stripping process[7]. These transitions do not appear to be very sharp for positive ion reactions, however. The energy dependence of the negative ion reactions discussed above was examined for similar mechanistic transitions. On the basis of conservation of momentum, it can be established that the internal energy of an ion formed in a stripping reaction such as (3) is given by the relation,

$$E_i = E_{O^-} \left[\frac{M_i}{M_{O^-}+M_i}\right] + \Delta H \qquad (4)$$

where M_i is the mass of the product ion, E_{O^-} and M_{O^-} are the energy and mass respectively of the impacting O^- ion and ΔH is the heat of the reaction. In this instance ΔH is approximately (-0.5)eV. In order for the product ion to be observed, the internal energy must be $E_i \leq D_i$, where D_i is the dissociation energy of the product ion. Taking $D_{OH^-(OD^-)} = 5.0eV$, and applying the relation given in equation (4), it can be deduced that OH^- should not be observed above an impacting O^- energy of 99eV while OD^- should be detected only at O^- energies below 52eV. From these considerations it is clear that the ratio of OH^-/OD^- from reaction (3) as a function of O^- energy should go to infinity at 52eV O^- energy in the laboratory scale. The plot given in Figure 3 for this reaction shows that the ratio rises sharply in this region of impacting ion energy. This apparently confirms the transition in mechanism for the reaction and it is notable that this transition is much more evident than has been detected for analogous positive ion processes.

It appears from the data discussed that the energy dependence for negative ion-molecule reactions is very similar to that previously observed for positive ion reactions. Thus, apparently, the reaction models applicable to positive ions are also useful in describing negative ion systems. Considerably more experimental data is necessary, however, before these conclusions can be applied generally to negative ion-molecule interactions.

References

1. Excellent reviews of such studies are given in Adv. Chem. Series 58, (1966), "Ion-Molecule Reactions in the Gas Phase", P. Ausloos, ed., American Chemical Society, Wash., D.C.
2. J. H. Futrell and C. D. Miller, Rev. Sci. Instr. 37, 1521 (1966).
3. R. K. Curran, Phys. Rev. 125, 910 (1962).
4. A. Henglein, G. A. Muccini, "Chemical Effects of Nuclear Transformations", p. 89, International Atomic Energy Agency, Vienna, 1961.
5. J. F. Paulson, Adv. Chem. Series 58, 28 (1966).
6. C. F. Giese and W. B. Maier, J. Chem. Phys. 39, 197 (1963); ibid, 39, 739 (1963).
7. A. Henglein, Adv. Chem. Series 58, 63 (1966).

14. Hydration of Negative Ions in the Gas Phase

By

P. Kebarle, M. Arshadi and
J. Scarborough

Chemistry Department
University of Alberta
Edmonton, Alberta, Canada.

Accepted in J. Chem. Physics to appear in 1968

ABSTRACT

The attachment of water molecules to the ions F^-, Cl^-, Br^-, I^-, O_2^- and NO_2^- was observed in the gas phase at water pressures from 0.1 to 1.5 torr and 292°K with an alpha particle ion source attached to a mass spectrometer. The negative ions were produced by adding a suitable compound RX to the 8 torr oxygen carrier gas. The reaction involved was: $RX + O_2^- = X^- + R + O_2$. Equilibrium constants for a number of clustering reactions (n-1,n): $X^-(H_2O)_{n-1} + H_2O = X^-(H_2O)_n$ were determined. The hydration of the ions falls off with increase of ionic size. Comparison of the free energies $\Delta G°_{2,3}$ and $\Delta G°_{3,4}$ of the halogen and alkali ions with the Pauling radii show that negative ions solvate more strongly than positive ions. Comparison with the Latimer Pitzer and Slanski [17] radii shows that these radii predict stronger (2,3) and (3,4) hydration for positive ions. The radii based on X-ray measurements [16] predict equal (2,3) and (3,4) hydration energies for positive and negative ions. The present data suggest that the single ion hydration energies derived by Latimer et al [17] and Verwey [18] are either incorrect or due to stronger solvation by negative ions not in the inner hydration shell but in the subsequent hydration interactions.

15. Negative Ion Impact Studies*

B. Mason Hughes and Thomas O. Tiernan

Aerospace Research Laboratories
Office of Aerospace Research
Wright-Patterson Air Force Base, Ohio 45433

Negative ion-molecule reactions have not been extensively investigated by the mass spectrometric techniques which have been so widely applied to positive ion processes and thus little is known about the reactions of even simple negative species. This has been due, in part, to the difficulty in obtaining negative ion beams of sufficient intensity to permit observation of reaction products. The development in our laboratory of a mode of operation for ion sources which yields negative ion beams of quite reasonable intensity, prompted an examination of selected negative ion-molecule reactions. In the present investigation, the reactions of O^-, OH^- and NH_2^- derived from N_2O, H_2O and NH_3 respectively, with a variety of neutral molecules were examined using the ARL tandem mass spectrometer[1], appropriately modified for negative ion studies. In addition to the identification of the various reaction channels for the negative ions indicated, relative rate constants for these interactions were determined. In some cases, isotopic studies were conducted in order to obtain information relative to the reaction mechanism.

Reactions of O^- with Inorganic Molecules

The reactions of O^- with N_2O, NO_2, NO, CO_2, CO and O_2 were investigated using an ion beam of 0.3 eV kinetic energy. The pressure of the neutral reactant gas in the collision chamber was maintained at 5 microns in all these experiments. When $^{16}O^-$ was employed as the impacting ion, reactions were observed only in the case of N_2O and NO_2. However, with the in-line geometry of our tandem spectrometer, the reactant ion beam is detected simultaneously with the products and therefore obscures any product having the same mass, that is a reaction yielding the original reactants. That such a reaction actually does occur for all the cases mentioned above was established by isotopic studies. In Table I are shown the product distributions from the reaction of $^{16}O^-$ with $N_2{}^{18}O$ and from the corresponding interaction of $^{18}O^-$ with $N_2{}^{16}O$. One of the products of this reaction is NO^-, as was observed previously by Paulson[2] on the basis of single-source experiments. More importantly, however, the data in Table I show that the major reaction channel is that yielding O^-. With $^{16}O^-$ impacting ions $^{18}O^-$ is produced, while $^{18}O^-$ reactant yields $^{16}O^-$ as the product ion. This fact clearly indicates that this reaction proceeds via an intermediate $[N_2O_2^-]^*$ complex anion rather than by a dissociative charge transfer mechanism. Such a complex intermediate is further substantiated by the fact that $N^{16}O^-$ and $N^{18}O^-$ are formed in approximately equal intensities from these reactions. Also, since both sets of reactants yield quite similar product distributions, an intermediate of common structure and internal energy is indicated. From similar studies with $^{14}N^{15}NO$, Paulson[2]

Table I. Product Distribution From the Reaction of O^- with N_2O Using Isotopically Labelled Reactant Ions and Neutral Molecules

$$^{16}O^- + N_2{}^{18}O \xrightarrow{1} [^{16}O\text{-}N_2\text{-}{}^{18}O]^* \xrightarrow{2} {}^{18}O^- + N_2{}^{16}O$$

Relative Distribution for Reaction 1			Relative Distribution for Reaction 2	
NO^- Product	Total Products		Total Products	NO^- Product
52.2	15.6	$N^{16}O^- + N^{18}O$	18.0	51.1
47.8	14.2	$N^{18}O^- + N^{16}O$	17.3	48.9
	--[a]	$^{16}O^- + N^{18}O$	64.7	
	70.2	$^{18}O^- + N^{16}O$	--[a]	

[a]Product ion cannot be observed since it has the same mass as the reactant ion.

*A more detailed account of this work will be submitted for publication in the Journal of Chemical Physics.

tentatively concluded that the $O^- - N_2O$ reaction involved a complex intermediate, although he could not entirely rule out contributions to the NO^- product from dissociative attachment in his single-source measurements. It is also notable that our data for the reaction of O^- with N_2O does not provide any evidence for the production of either O_2^- or NO_2^- as proposed by Burtt and Henis[3]. This suggests that previous observations of these products in single-source studies with N_2O were probably the result of impurities such as NO_2.

The reactions of O^- with NO_2 observed in the present study are shown below.

$$^{18}O^- + N^{16}O^{16}O \rightarrow {}^{16}O^- + N^{16}O^{18}O \qquad 0.169 \qquad (1a)$$

$$\rightarrow N^{16}O^{16}O^- + {}^{18}O \qquad 0.762 \qquad (1b)$$

$$\rightarrow N^{16}O^{18}O^- + {}^{16}O \qquad 0.069 \qquad (1c)$$

The isotopic experiments clearly establish that the major reaction mode is charge transfer. While this probably occurs principally by a long range transfer, since most of the charge transfer product shows no incorporation of the reactant ion, (reaction 1b), at least part of this product must be formed from a complex intermediate, (reaction 1c). If it is assumed that $^{18}O^-$, which cannot be detected in this experiment, is produced to the same extent as $^{16}O^-$, then the following reaction scheme is deduced,

$$O^- + NO_2 \xrightarrow{0.62} NO_2^- + O \qquad (2a)$$

$$\xrightarrow{0.38} [NO_3^-]^* \xrightarrow{0.76} O^- + NO_2 \qquad (2b)$$

$$\xrightarrow{0.24} NO_2^- + O \qquad (2c)$$

Paulson[2] also reported the formation of O_2^- from reaction (1) but we did not detect this product in our studies. Again this suggests that O_2^- may have been produced by dissociative attachment of electrons to NO_2 under Paulson's conditions.

As already mentioned, O^- ions appear to be unreactive with NO, CO_2, CO and O_2 unless isotopic techniques are employed. The use of $^{18}O^-$ ions as reactant species shows that O^- ions are produced from all these compounds, apparently through complex intermediates. These reactions and their rate constants determined in this study are shown in Table II. In most instances, the measured rates are

Table II. Rate Constants for Production of $^{16}O^-$ from Reaction of $^{18}O^-$ with Various Inorganic Molecules

Reaction	Rate Constant[a.] ($\times 10^{9}$ cm^3 molecule^{-1} sec^{-1})
$^{18}O^- + N^{16}O^{16}O \rightarrow {}^{16}O^- + N^{16}O^{18}O$	0.30
$^{18}O^- + C^{16}O \rightarrow {}^{16}O^- + C^{18}O$	0.46
$^{18}O^- + {}^{16}O^{16}O \rightarrow {}^{16}O^- + {}^{16}O^{18}O$	0.48
$^{18}O^- + N_2{}^{16}O \rightarrow {}^{16}O^- + N_2{}^{18}O$	0.60
$^{18}O^- + N^{16}O \rightarrow {}^{16}O^- + N^{18}O$	0.98
$^{18}O^- + C^{16}O^{16}O \rightarrow {}^{16}O^- + C^{16}O^{18}O$	2.87

a. Rate constants are based on the value of 1×10^{-9} cm^3 molecule^{-1} sec^{-1} for the charge exchange reaction of O^- with NO_2 as given in Ref. 2.

somewhat lower than typically observed for bimolecular ion-molecule processes. The large value observed for the rate of the $O^- - CO_2$ reaction is in sharp contrast to the other reactions. This indicates that a substantial portion of the O^- ions produced in pure CO_2 must undergo this reaction.

It is interesting to note that the formation of CO_3^- in a three-body reaction,

$$O^- + CO_2 + CO_2 \rightarrow CO_3^- + CO_2 \qquad (3)$$

has been proposed by Moruzzi and Phelps[5]. In view of the above results, it seems likely that at least a portion of this product must be produced as a third order product by a mechanism involving the charge transfer sequence for O^- ions. Similar comments are applicable to the formation of O_3^- which was also reported by the investigators cited above to be produced in a three-body process,

$$O^- + O_2 + O_2 \rightarrow O_3^- + O_2 \qquad (4)$$

It is not surprising that the charge transfer reaction between O^- and O_2 is not detected in our studies since previous work[5] has shown that energetic O^- ions are required for this reaction.

Reactions of O^- with Organic Molecules

In reactions 5-8 are reported relative cross-sections for the interaction of O^- with methyl chloride and with saturated and unsaturated hydrocarbons.

			Relative Reaction Rates	
$O^- + CH_3Cl$	$\rightarrow$	$OH^- + CH_2Cl$	0.47	(5a)
	$\rightarrow$	$Cl^- + CH_3O$	0.12	(5b)
	$\rightarrow$	$CHCl^- + H_2O$	0.41	(5c)
$O^- + C_2H_2$	$\rightarrow$	$OH^- + C_2H$	<0.01	(6a)
	$\rightarrow$	$C_2H^- + OH$	0.93	(6b)
	$\rightarrow$	$C_2OH^- + H$	0.07	(6c)
$O^- + C_3H_6$	$\rightarrow$	$OH^- + C_3H_5$	0.93	(7a)
	$\rightarrow$	$C_3H_4^- + H_2O$	0.06	(7b)
	$\rightarrow$	$C_3H_5^- + OH$	0.01	(7c)
$O^- + CH_4$	$\rightarrow$	$OH^- + CH_3$		(8)

Except for the case of acetylene, the dominant reaction of O^- in each of these instances is H-atom abstraction. H_2 and H_2^+ transfer are also seen to be significant reaction modes for O^- with CH_3Cl. For the reaction with acetylene, C_2H^- is the principal product. Since C_2OH^- is also observed as a product, it is probable that the reaction involves formation of the anion complex followed by dissociation to give the indicated products. Neuert and coworkers[4] detected the same reaction products in single-source experiments with mixtures of NO_2 and C_2H_2. They reported $k_{6b}/k_{6c} = 10$, in reasonably good agreement with our value of 13 for this ratio.

The reactions of O^- with methanol and ethanol were also examined. Again, isotopic studies were conducted in order to determine the source of hydrogen atoms or protons transferred from the neutral alcohol. These reactions are shown below

			Relative Reaction Rates	
$O^- + CH_3OH$	$\rightarrow$	$OH^- + CH_3O$	0.691	(9a)
	$\rightarrow$	$CH_3O^- + OH$	0.309	(9b)
$O^- + CD_3OH$	$\rightarrow$	$OH^- + CD_3O$	0.658	(10a)
	$\rightarrow$	$OD^- + CD_2OH$	0.063	(10b)
	$\rightarrow$	$CD_3O^- + OH$	0.279	(10c)
$O^- + C_2H_5OH$	$\rightarrow$	$OH^- + C_2H_5O$	0.401	(11a)
	$\rightarrow$	$C_2H_3O^- + OH + H_2$	0.321	(11b)
	$\rightarrow$	$C_2H_5O^- + OH$	0.277	(11c)
$O^- + C_2D_5OH$	$\rightarrow$	$OH^- + C_2D_5O$	0.338	(12a)

	→	$OD^- + C_2D_4OH$	0.115	(12b)
	→	$C_2D_3O^- + D_2 + OH$	0.232	(12c)
	→	$C_2D_5O^- + OH$	0.315	(12d)
$O^- + CH_3CD_2OH$	→	$OH^- + C_2D_2H_3O$	0.425	(13a)
	→	$OD^- + C_2DH_3OH$	0.022	(13b)
	→	$CH_2CDO^- + HD + OH$	0.248	(13c)
	→	$CH_3CD_2O^- + OH$	0.304	(13d)

It is clear from the observed reactions that both H and H^+ abstraction are significant reaction modes for the alcohols. In methanol, H atom abstraction is about twice as important as the H^+ transfer while in ethanol the two processes are of about comparable importance. The hydrogen entity transferred from methanol in the reaction with O^- comes almost exclusively from the hydroxyl group. With ethanol, transfer of hydroxyl hydrogens is also favored but to a lesser extent than for methanol. Also as reaction (13) indicates, almost none of the hydrogen transferred comes from the α-carbon atom of the ethanol molecule. The $C_2H_3O^-$ product observed from the reaction of O^- with ethanol probably is formed by H_2 elimination from the $C_2H_5O^-$ product ion. If this is in fact the case, then it can be seen from reaction (13) that this hydrogen loss occurs by elimination of H atoms on adjacent carbon atoms.

Reactions of OH^- and NH_2^-

The reactions of OH^- and NH_2^- with selected organic molecules were also determined and these are shown in reactions (14-23)

$OH^- + CD_3OH$	→	$CD_3O^- + H_2O$		(14)
$OH^- + C_2D_5OH$	→	$C_2D_5O^- + H_2O$		(15)
$OH^- + CH_3Cl$	→	$Cl^- + CH_3OH$		(16)
$OH^- + C_2H_2$	→	$C_2H^- + H_2O$		(17)
$NH_2^- + CD_3OH$	→	$CD_3O^- + NH_3$		(18)
$NH_2^- + C_2D_5OH$	→	$C_2D_5O^- + NH_3$		(19)
$NH_2^- + HCl$	→	$Cl^- + NH_3$		(20)
$NH_2^- + CH_3Cl$	→	$Cl^- + CH_3NH_2$	0.189	(21)
	→	$CH_2Cl^- + NH_3$	0.811	(22)
$NH_2^- + C_2H_2$	→	$C_2H^- + NH_3$		(23)

Not surprisingly OH^- reacts entirely by H^+ abstraction. As in the reactions discussed earlier, methyl chloride is again an exception in this respect. The reactions of NH_2^- are also much as expected, also involving H^+ abstraction. Here, too, methyl chloride reacts in a different manner. The striking differences observed for these negative ion reactions with alkyl chlorides suggests that the intermediates in such cases must be of quite different nature than for the alcohols and hydrocarbons. Additional studies of these reactions are indicated.

References

1. J. H. Futrell and C. D. Miller, Rev. Sci. Instr. 37, 1521 (1966).

2. J. F. Paulson, Advances in Chemistry Series 58, 39 (1966).

3. B. P. Burtt and J. Henis, J. Chem. Phys. 41, 1510 (1964).

4. H. Neuert, R. Rackwitz and D. Vogt, International Mass Spectrometry Conference, Berlin, 1967, Institute of Petroleum, London, p. 3.

5. J. L. Moruzzi and A. V. Phelps, J. Chem. Phys. 45, 4617 (1966).

16.

Reactions of C^+ Ions with CH_4

P. J. Sullivan, R. W. Rozett and W. S. Koski

Department of Chemistry

The Johns Hopkins University

Baltimore, Maryland 21218

(to be published in J. Chem. Phys.)

The cross sections for the reactions of C^+ with methane have been studied over an ion energy range of 5 - 100 eV. A tandem mass spectrometer which was previously described[1] was used in these studies. The instrument consists of a small 180°, 1 cm radius of curvature, primary mass spectrometer. The second analyzing spectrometer was a 60° magnetic sector instrument with an 8-inch radius of curvature. The product ions were extracted at 90° to the bombarding ion beam.

Cross sections for the charge transfer products, CH_4^+, CH_3^+, CH_2^+ and CH^+, and for the mass transfer products $C_2H_3^+$, $C_2H_2^+$ and C_2H^+, were determined as a function of energy.

The C^+ ions were produced by electron bombardment of CO. For 70 eV, the beam was found to consist of 27% ^4P state and 73% ^2P state. The composition of the beam could be changed by varying the electron energy. At 23 eV, the C^+ beam was predominantly in the ground ^2P state. By studying the reaction cross section as a function of electron energy and positive ion energy, it was possible to determine the contribution of both states to the total cross section.

The charge transfer reactions could be qualitatively interpreted in terms of Massey's adiabatic hypothesis, and the mass transfer reactions could be interpreted in terms of the spectator stripping mechanism.

1. E. R. Weiner, G. R. Hertel and W. S. Koski, J. Am. Chem. Soc., 86, 788 (1964).

18. Ionic Chemistry of Ketones*

Jack O. Terry and Thomas O. Tiernan

Aerospace Research Laboratories
Office of Aerospace Research
Wright-Patterson Air Force Base, Ohio 45433

Recent papers from our laboratory have been concerned with the significance of intermediate complexes in ion-molecule reactions.[1,2] In view of the extensive reactivity of the ketones and their tendency to form ion clusters we have undertaken a study of the ionic chemistry of these compounds using the techniques of high pressure mass spectrometry at source pressures up to 1 torr.[3] In addition, reactions of specific ions in the systems were identified in some cases with a dual stage mass spectrometer in which a mass and energy selected ion beam is impacted on target molecules of interest.[4] Particular emphasis was placed on the observation of higher mass ion clusters in these systems at elevated pressures. In an attempt to assess the effects of structural characteristics on ionic reactions in the ketones, several classes of these compounds have been examined, including simple alkanones, alkenones and cyclic alkanones.

Table I summarizes the spectra of the alkanones at various pressures. It can be seen that in all cases the primary ions have undergone essentially complete reaction at a source pressure of 60 microns. The observed ion-molecule products are formally similar for all the alkanones and consist of the protonated monomer, monomer carbonyl complex and the disolvated proton. The disolvated proton is clearly the most abundant product at higher pressures. No evidence was obtained for the formation of clusters of higher mass than the disolvated proton, even at source pressures up to 1 torr. This lends further support for the clustering model suggested by Munson[5] in which the extra hydrogen is bound to an oxygen atom in the protonated molecule ion and serves as a bonding bridge for the oxygen atom of an additional ketone molecule.

It is interesting to observe that 2-pentanone is exceptional among the alkanones studied in that no ion-molecule product corresponding to the parent ion carbonyl complex, RCO(RCO)R', is detected. As will be noted later, single ion experiments with acetone show that this product type is formed by reaction of the parent ion. Therefore, the absence of this product in the former case is probably due to the ability of the 2-pentanone parent ion to rearrange by a γ-hydrogen shift.[6] Apparently, this rearrangement occurs with a sufficient rate to compete with the alternative ion-molecule condensation. Other methyl ketones with available γ-hydrogen atoms have also been studied and again no parent ion carbonyl complexes were observed for these types of ketones.

In order to establish the mechanisms for formation of the observed ion-molecule products in the ketone systems, the individual ionic reactions in acetone were investigated in the tandem spectrometer using perdeuteroacetone and its ionic fragments. The results of these experiments are shown in Table II. The methyl ion reaction produces several products of lower mass than the parent ion and the isotopic studies reveal that the major portion of these are formed by dissociative charge transfer. Taking these into account, it is apparent that charge transfer is about equally important as the other ion-molecule reaction modes for methyl ion. Some of these lower fragments, however, are produced through an intermediate complex since some are observed to contain deuterium. In fact, the complex itself is observed in relatively large abundance in this case.

The reaction of CH_3CO^+ with acetone yields only one product which corresponds to that formed by H^+ transfer. The analogous reaction with CD_3CO^+ confirms that the mechanism does indeed involve only simple proton transfer. The parent ion reaction with acetone yields, as the isotopic studies show, an ion which is nominally that resulting from charge transfer. However, since small amounts of proton transfer product are also detected, it seems likely that the parent ion from this reaction is formed by dissociation of the proton transfer product which is probably produced by a highly exothermic reaction. This interpretation is consistent with the trends observed in the high pressure spectrum of acetone where the proton transfer product initially increases with pressure at the expense of the parent molecule ion, implying a collisional stabilization of the former at elevated pressures.

*A more detailed account of this work will be submitted for publication in the Journal of Physical Chemistry.

The reaction of the protonated parent ion in acetone could not be observed directly in the tandem spectrometer since the pressure in the first stage cannot be raised sufficiently to produce this species as an impacting ion. However, by impacting CH_3CO^+ ions on acetone at collision chamber pressures of 25μ, the further reactions of $CH_3COHCH_3^+$ ions produced in the chamber can be observed. In this manner, it was confirmed that the protonated parent ion reacts with acetone to produce the disolvated proton. The set of reactions shown for acetone can quite reasonably be generalized to the entire alkanone series with the few exceptions already mentioned.

For the alkenones investigated, the mass spectra as a function of pressure are shown in Table III. The ion-molecule products observed are quite similar in nature to those found for the alkanones. One interesting difference is that the parent ion-carbonyl product in the alkenones involves addition of an unsaturated carbonyl fragment, (C_2H_3CO or C_3H_5CO), rather than the CH_3CO addition which occurs with the alkanones.

In order to determine the mechanisms involved for product formation in the alkenones, 3-butene-2-one was selected for more detailed examination in the tandem mass spectrometer. Again the observed reactions are much the same as determined for acetone. The hydrocarbon ions undergo reactions which are apparently dissociative proton transfer. The methyl carbonyl and unsaturated carbonyl ions both proton transfer to the neutral ketone molecule, but the unsaturated carbonyl ion is considerably less reactive than the corresponding saturated ion. The parent ion yields mainly the protonated monomer and a small amount of the unsaturated carbonyl complex. The intensity of the latter product observed in the high pressure spectrum is greater than would be expected from the amount of parent ion which reacts. This may indicate that the unsaturated carbonyl complex is formed directly from $C_2H_3CO^+$ at higher pressures. Unfortunately, we are unable to verify this since the $C_2H_3CO^+$ does not react at pressures below about 40 microns, which is the pressure limit of our tandem instrument. As in the case of acetone, the formation of the disolvated proton from the protonated parent ion was confirmed for 3-butene-2-one by producing the latter ion in the collision chamber at pressures sufficiently high to induce further reaction.

The cycloalkanones investigated, for which the spectra at several pressures are summarized in Table IV, differ in some respects from the other two classes of ketones studied. One of the most striking differences is the formation of a dimer ion for both cyclobutanone and cyclopentanone. There are also rather obvious differences in the products from these two cyclic ketones themselves. In cyclobutane there is no ionic product corresponding to the disolvated proton which does appear in the cyclopentanone spectrum. On the other hand, the dimer carbonyl ion found in cyclobutanone is not observed in cyclopentanone. The disolvated proton has been shown to result from the protonated parent ion in these ketone systems and an alcohol type structure for the latter ion is consistent with the products formed. Since no disolvated proton is observed for cyclobutanone, it appears that the protonated parent ion in this case may have a different structure. A conceivable mechanism which might be invoked for this case would involve opening of the cyclobutanone ring prior to or during protonation. The protonated parent ion might then be formed with an aldehyde structure by protonation at the hydrocarbon end of the molecule. The ion with this structure could not readily yield the disolvated proton. In contrast, cyclopentanone, being a more stable ring structure, might well remain intact during protonation, and the protonated parent ion would therefore have the alcohol type structure appropriate for addition of another ketone molecule.

Studies with the tandem spectrometer were also accomplished for both cyclobutanone and cyclopentanone. In cyclobutanone, the hydrocarbon type ions undergo both charge transfer and proton transfer reactions, while the carbonyl ion reacts only by charge transfer. For the parent ion, products corresponding to addition of CH_2 and C_2H_2O were observed. The formation of the dimer ion could not be observed in the tandem from reaction of either parent ion or the carbonyl ions even at a collision chamber pressure of 40 microns. The reason for this is not clear since the high pressure data indicate that the dimer ion is third order in cyclobutanone pressure. Internal excitation energy of the reactants may be an important factor in formation of the dimer.

For cyclopentanone, the tandem studies show a somewhat different reaction mechanism. Here the carbonyl ion undergoes predominantly proton transfer rather than charge transfer. The parent cyclopentanone ion does not yield the carbonyl addition product but does react by proton transfer to the neutral reactant. As in the other ketones, the protonated parent ion was found to yield the disolvated proton. It is also interesting that the protonated parent ion was shown to be a precursor of the dimer ion in cyclopentanone.

Table I

Relative Intensities of the Principal Primary Ions and Ion Molecule Reaction Products for Straight Chain Alkanones

Compound:	CH_3-CO-CH_3			CH_3CH_2-CO-CH_3			CH_3-CH_2-CH_2-CO-CH_3			CH_3-CH_2-CO-CH_2-CH_3		
Reactant or Product Ion Type	10μ	30μ	60μ	10μ	30μ	60μ	10μ	30μ	60μ	10μ	30μ	60μ
	CH_3^+			$C_2H_3^+$			$C_2H_3^+$			$C_2H_3^+$		
$C_NH_N^+$	.042	trace	-	.042	-	-	.042	-	-	.061	-	-
				$C_2H_5^+$			$C_3H_5^+$			$C_2H_5^+$		
				.073	-	-	.053	.015	-	.235	-	-
	CH_3CO^+			CH_3CO^+			$(C_3H_7^+;CH_3CO)^+$			$C_2H_5CO^+$		
	.505	.276	.071	.431	.090	.012	.490	.222	-	.423	.293	.054
RCO^+				$C_2H_5CO^+$								
				.050	.052	.016						
	$CH_3COCH_3^+$			$CH_3COC_2H_5$			$CH_3COC_3H_7^+$			$C_2H_5COC_2H_5^+$		
$RCOR'^+$	.160	.061	-	.104	.046	.010	.058	.047	-	.086	.021	.005
	$(CH_3COCH_3)H^+$			$(CH_3COC_2H_5)H^+$			$(CH_3COC_3H_7)H^+$			$(C_2H_5COC_2H_5)H^+$		
$(RCOR')H^+$	.196	.439	.178	.277	.398	.066	.171	.416	.054	.178	.262	.051
	$CH_3CO(CH_3CO)CH_3^+$			$CH_3CO(CH_3CO)C_2H_5^+$						$(C_2H_5)_2CO(C_2H_5CO)^+$		
$RCO(RCO)R'^+$	.021	.075	.128	.023	.069	.057	-	-	-	.016	.151	.235
	$(CH_3COCH_3)_2H^+$			$(CH_3COC_2H_5)_2H^+$			$(CH_3COC_3H_7)_2H^+$			$(C_2H_5COC_2H_5)_2H^+$		
$(RCOR')_2H^+$	-	.094	.558	-	.311	.756	-	.253	.759	-	.252	.592

Table II

Relative Intensities of Products from the Reactions of Primary Ions with Acetone in the Tandem Mass Spectrometer at a Collision Chamber Pressure of Five Microns

Reactants	I/ I	Products	Reactants	I/ I	Products
CH_3^+ + Ace	.068	CHO^+	CD_3^+ + Ace	.049	CHO^+
	.079	$CHCO^+$		.097	$CHCO^+$
	.208	CH_3CO^+		.187	CH_3CO^+
	.060	$CH_3CH_2O^+$		.055	CH_2DCO^+
	.070	$C_4H_7^+$		.065	$CD_3CH_2O^+$
	.219	$CH_3COCH_3^+$		.065	$C_4H_5D_2^+$
	.044	$CH_3COHCH_3^+$		.153	$CH_3COCH_3^+$
	.156	$CH_3CO(CH_3)CH_3^+$		.034	$CH_3COHCH_3^+$
				.019	$CH_3CODCH_3^+$
				.138	$CH_3COCD_3CH_3^+$
CH_3CO^+ + Ace	.990	$CH_3COHCH_3^+$	CD_3CO^+ + Ace	1.00	$CH_3CODCH_3^+$
$CH_3COCH_3^+$ + Ace	.085	CH_3CO^+	$CD_3COCD_3^+$ Ace	.700	$CH_3COCH_3^+$
	.442	$CH_3COHCH_3^+$		.048	$CH_3CODCH_3^+$
	.473	$CH_3CO(CH_3CO)CH_3^+$		.069	$CD_3COHCD_3^+$
				.010	$CH_3COCH_3COCH_3^+$
				.087	$CH_3COCD_3COCH_3^+$
				.087	$CD_3COCH_3COCD_3^+$

Table III

Relative Intensities of the Principal Primary Ions and Ion Molecule Reaction Products for Straight Chain Alkenones

Compound	CH_3-CO-CH=CH_2			CH_3CO-CH=CH-CH_3			CH_3-CH_2-CO-CH=CH_2		
Reactant or Product Ion Type	10μ	30μ	60μ	10μ	30μ	60μ	10μ	30μ	60μ
	$C_2H_3^+$			$C_3H_3^+$			$C_3H_3^+$		
$C_NH_N^+$	.130	-	-	.110	.047	0.0	.149	.020	-
				$C_3H_5^+$			$C_2H_5^+$		
				.199	.010	-	.088	.010	-
	CH_3CO^+			CH_3CO^+			$C_2H_3CO^+$		
	.216	.049	-	.143	.013	-	.548	.429	.077
RCO^+	$C_2H_3CO^+$			$C_3H_5CO^+$			$C_2H_5CO^+$		
	.385	.360	.124	.305	.218	.043	.063	.044	-
	$C_2H_3COCH_3^+$			$C_3H_5COCH_3^+$			$C_2H_3COC_2H_5^+$		
$RCOR'^+$	.085	.021	-	.066	-	-	.064	.027	-
	$(C_2H_3COCH_3)H^+$			$(C_3H_5COCH_3)H^+$			$(C_2H_5COC_2H_3)H^+$		
$(RCOR')H^+$	.145	.353	.056	.177	.188	.026	.087	.197	.033
	$C_2H_3CO(C_2H_3CO)CH_3^+$			$C_3H_5CO(C_3H_5CO)CH_3^+$			$C_2H_3CO(C_2H_3CO)C_2H_5^+$		
$RCO(RCO)R'^+$	-	.045	.242	-	.094	.198	-	.123	.344
	$(C_2H_3COCH_3)_2H^+$			$(C_3H_5COCH_3)_2H^+$			$(C_2H_3COC_2H_5)_2H^+$		
$(RCOR')_2H^+$	-	.110	.521	-	.292	.502	-	.116	.418

Table IV

Relative Intensities of the Principal Primary Ions and Ion Molecule Reaction Products for Cyclic Alkanones

Product	Cyclobutanone (I/ I)			Cyclopentanone (I/ I)		
	10μ	30μ	60μ	10μ	30μ	60μ
$C_NH_N^+$	$C_2H_4^+$			$C_2H_3^+$		
	.048	-	-	.065	-	-
	$C_3H_5^+$			$C_3H_5^+$		
	.080	.029	-	.107	.039	-
RCO^+	$C_2H_2O^+$			$C_3H_3O^+$		
	.353	.071	-	.324	.229	.034
				$C_3H_4O^+$		
				.088	.041	-
$(Cycl\ Alk)^+$	$C_3H_6CO^+$			$C_4H_8CO^+$		
	.330	.470	.116	.171	.203	.023
$(Cycl\ Alk)H^+$	$(C_3H_6CO)H^+$			$(C_4H_8CO)H^+$		
	.052	.117	.047	.094	.184	.018
$(Cycl\ Alk)RCO^+$	$(C_3H_6CO)(C_2H_2O)^+$			$(C_4H_8CO)(C_3H_3O)^+$		
	-	.114	.357	-	.045	.149
$(Cycl\ Alk)_2^+$	$(C_3H_6CO)_2^+$			$(C_4H_8CO)_2^+$		
	-	-	.141	-	.057	.213
$(Cycl\ Alk)_2H^+$				$(C_4H_8CO)_2H^+$		
				-	.115	.480
$(Cycl\ Alk)C_NH_N^+$	$(C_3H_6CO)(CH_2)^+$			$(C_4H_8CO)(C_3H_5)^+$		
	.013	.101	.099	-	.046	.061
	$(C_3H_6CO)(C_3H_5)^+$					
	-	.018	.045			
Other	$(C_3H_6CO)_2(C_2H_2O)^+$					
	-	-	.049			

References

1. J. H. Futrell and T. O. Tiernan, J. Phys. Chem. 72, 158 (1968).
2. T. O. Tiernan and J. H. Futrell, J. Phys. Chem., in press (1968).
3. J. H. Futrell, T. O. Tiernan, F. P. Abramson and C. D. Miller, Rev. Sci. Instr. 39, 340 (1968).
4. J. H. Futrell and C. D. Miller, Rev. Sci. Instr. 37, 1521 (1966).
5. M. S. B. Munson, J. Am. Chem. Soc. 87, 5313 (1965).
6. F. W. McLafferty, Anal. Chem. 31, 82 (1959).

19. Ion-Molecules Reactions in Silane-Ethylene Mixtures

D. P. Beggs and F. W. Lampe

Department of Chemistry
The Pennsylvania State University
University Park, Pa. 16802

Previously in this laboratory we have studied the ion-molecule reactions in pure SiH_4 and we have also examined the radiolysis of pure SiH_4 and C_2H_4-SiH_4 mixtures. Certain aspects of the radiolytic behavior of the SiH_4 and the C_2H_4-SiH_4 mixtures point to chain reactions propagated by species that are not free radicals and which we have suggested to be ionic. For a more complete understanding of the radiation chemistry of these simple silane systems we have carried out a detailed study of the ion-molecule reactions in SiH_4-C_2H_4 mixtures. The results of this study has been of considerable help in clarifying the reaction mechanism.

The products and reactants of this system are identified by following the ion fractions ($I_i/\Sigma I_i$) of the various masses. Within experimental error $I_i/\Sigma I_i$ for m/e 24,27,29 and 32 is independent of source pressure and delay time.[1] This indicates that C_2^+, $C_2H_3^+$, SiH^+ and SiH_4^+ are neither products nor reactants in secondary reactions. On the other hand, $I_i/\Sigma I_i$ for m/e 25,26,28 and 30 decreases with an increase in pressure or delay time, thus indicating that these primary ions are reactants. The very small concentration of C_2H^+, m/e 25, precludes this as a major reactant. $C_2H_4^+$ and Si^+ both contribute to m/e 28, but, since Si^+ has been previously found to be non-reactive with respect to the formation of secondary ions in pure silane,[1] it is assumed that Si^+ is non-reactive in the silane-ethylene system and that $C_2H_4^+$ is the only reactive ion of m/e 28. We thus conclude that the major reactant ions are $C_2H_2^+$, $C_2H_4^+$, and SiH_2^+. For m/e 31, the $I_i/\Sigma\ I_i$ increases with increasing pressure or time delay. This indicates that SiH_3^+ is a secondary product as well as a primary ion. This result has been observed and discussed earlier.[1] The secondary ions of pure silane and pure ethylene have already been identified and studied.[1,2] Thus, this investigation is concerned with identifying and studying the cross-reactions of a silane-ethylene system (The reactions between an ion from ethylene with silane and between an ion from silane with ethylene).

A typical secondary spectra of the silane-ethylene system is shown in Table I. When compared to the secondary spectra of pure ethylene and pure silane, it can be seen that the cross reaction products must include ions at m/e 43,55,56,57 and 58. To aid in the elucidation of which primary ion is reacting to form a given product ion, one can measure the appearance potential of the product ion and compare it with the appearance potentials of the possible reactants. The primary ion which has an appearance potential closest to that of the product ion is taken to be the reactant ion provided the reaction is not energetically impossible. If more than one primary ion is responsible for production of a product ion, a change in the slope of the ionization efficiency curve will often denote the onset of another reaction involving a different reactant ion. The R.P.D. studies along with mass and energy considerations establish the cross reactions in a silane-ethylene system to be those shown in Table II.

A kinetic analysis using suitable assumptions results in an equation defining the ion fraction of the product ion:

$$X_p = \frac{X^\circ\ k_p\ [M]\ t}{1 + \Gamma} \qquad (1)$$

where X° is the initial concentration of the reactant ion, k_p is the specific rate constant for the formation of the product ion, [M] is the total pressure and

$$\Gamma = \gamma = \frac{[C_2H_4]}{[SiH_4]} \quad \text{if the reactant ion is } SiH_2^+$$

$$\Gamma = \gamma' = \frac{[SiH_4]}{[C_2H_4]} \quad \text{if the reactant ion is } C_2H_2^+ \text{ or } C_2H_4$$

From equation (1) it can be seen that the quantity $(k_p t)_{total}$ is obtained from the slope of a line through the points on a plot of $I_i/\Sigma\ I_i$ vs total pressure. As was discussed in an earlier paper[1], a plot of $(k_p)_{total}$ vs delay time should produce a straight line whose slope is

$(k_p^{th})_{total}$, the thermal rate constant.

The total ion fraction of any one product ion is the sum of the contribution from each different ion-molecule reaction:

$$(X_p)_{total} = (X_p)_a + (X_p)_b + (X_p)_c \qquad (2)$$

where

a	represents	$C_2H_4^+ + SiH_4$
b	"	$SiH_2^+ + C_2H_4$
c	"	$C_2H_2^+ + SiH_4$

where one or more of these contributions may be zero. Combining equation (1) and (2) and applying this to m/e 43

$$\frac{(k_p)_{total}}{[M]\,t} = \frac{[X^\circ_{C_2H_2^+}]\,k_7}{1+\gamma} + \frac{[X^\circ_{SiH_2^+}]\,k_4}{1+\gamma} \qquad (3)$$

Two experiments were performed, each using a different mixture ratio of ethylene and silane. The partial pressure ratios were $\frac{[C_2H_4]}{[SiH_4]} = 0.36$ and 1.67. Application of equation (3) to the data of these two mixtures produces two simultaneous equations which can be solved for k_4 and k_7. This procedure was repeated for every case where $C_2H_4^+$ did not contribute to the formation of the product ions.

In the case of m/e 56 and 58 where $C_2H_4^+$ does make a contribution, data from a separate experiment involving two different mixtures of acetylene and silane were used to determine $(k_p)_c$. This rate constant was inserted into equation (2) to give:

$$\frac{(k_p)_{total}}{[M]\,t} = \frac{[X^\circ_{C_2H_4^+}]\,(k_p)_a}{1+\gamma} + \frac{[X^\circ_{SiH_2^+}]\,(k_p)_b}{1+\gamma} + \text{constant}$$

Two simultaneous equations of this form were then available from the ethylene-silane data and the $(k_p)_a$ and $(k_p)_b$ could be calculated. $X^\circ_{C_2H_4^+}$ was calculated as a ratio of the $X^\circ_{C_2H_2^+}$.

As was noted earlier, the results indicate that SiH_2^+ does not react with C_2H_4 to produce a product at m/e 57 and 58. Likewise $C_2H_2^+$ does not form products at m/e 58, and $C_2H_4^+$ forms no products at m/e 43,55 and 57. The results are tabulated in Table II.

It is interesting to note that a SiH_2^+-C_2H_4 reaction favors production of $SiCH_3^+$ while a $C_2H_2^+$-SiH_4 reaction favors formation of higher mass products. This may be linked to the structure of the intermediate formed in these reactions. The SiH_2^+-C_2H_4 intermediate would tend to undergo a hydrogen shift and subsequent detachment of CH_3. While the $C_2H_2^+$-SiH_4 intermediate cannot form CH_3 as easily but would have a tendency to lose hydrogen atoms bonded to the silicon atom.

Comparison of the summation of the rate constants for the specific reactant ions (Table II) with the total rate constant for the loss of these ions shows satisfactory agreement.

A more complete text of this manuscript has been submitted to "The Journal of Physical Chemistry".

1. G. G. Hess and F. W. Lampe, J. Chem. Phys., 44, 2257 (1966).
2. F. H. Field, J. L. Franklin and F. W. Lampe, J. Am. Chem. Soc., 79, 2419 (1957).

Table 1

Silane - Ethylene Secondary Spectra

m/e	Relative Intensity	Cross Reaction Ion
39	28	
40	3	
41	100	
42	7	
43	61	$SiCH_3^+$
53	19	
55	26	$SiC_2H_3^+$
56	30	$SiC_2H_4^+$
57	24	$SiC_2H_5^+$
58	36	$SiC_2H_6^+$
59	15	
60	24	
61	3	

Table II

Ionic Reactions in a Silane - Ethylene System

		kx10^{11} (cm^3/mol.sec.)	A (Å^2)
$C_2H_4^+ + SiH_4$	k_1: $SiH_2^+ + C_2H_6$	1.4±0.3	2.3
	k_2: $SiC_2H_4^+ + 2H_2$	2.4±0.4	4.3
	k_3: $SiC_2H_6^+ + H_2$	7.1±0.9	11.9
$SiH_2^+ + C_2H_4$	k_4: $SiCH_3^+ + CH_3$	14.0±1.4	24.2
	k_5: $SiC_2H_3^+ + H_2 + H$	0.9±0.1	1.5
	k_6: $SiC_2H_4^+ + H_2$	0.6±0.1	1.0
$C_2H_2^+ + SiH_4$	k_7: $SiCH_3^+ + CH_3$	7.0±0.7	11.3
	k_8: $SiC_2H_3^+ + H_2 + H$	3.7±0.5	6.0
	k_9: $SiC_2H_4^+ + H_2$	2.2±0.3	3.5
	k_{10}: $SiC_2H_5^+ + H$	6.7±0.8	10.8

20. Kinetics of the Formation of Rare Gas Molecular Ions

J. J. DeCorpo and F. W. Lampe

Department of Chemistry
The Pennsylvania State University
University Park, Pa. 16802

The homonuclear diatomic ion of He has been studied by a pulsed mass spectrometric technique. These investigations of the bimolecular formation of He_2^+ show at least four families of excited states take part in the process. Three of these states have excitation functions with peaks at 36, 58, and 68 eV, while the fourth peaks between 30-34 eV. Kinetic studies performed at these electron energies yielded the effective lifetimes, as well as specific reaction rates for the corresponding families of the excited states. The kinetics of the formation process can be interpreted in light of the following reaction scheme.[1,2,3]

$$He + e \xrightarrow{\sigma_{ej}} He_j^* + e \qquad (R1)$$

$$He + e \xrightarrow{\sigma_o} He^+ + e \qquad (R2)$$

$$He_j^* + He \xrightarrow{k_j} He_2^+ + e \qquad (R3)$$

$$He_j^* \xrightarrow{\tau_j^{-1}} He' + h\nu \qquad (R4)$$

where σ_{ej} represents the cross-section for excitation to the jth state, σ_o represents the cross-section for ionization, τ_j is the effective lifetime of the jth state, k_j the specific rate constant for the Hornbeck-Molnar process, and He'represents helium in some state of insufficient energy to undergo Reaction (R3).

The basic instrument utilized in this investigation was a Bendix Model 14-101 time-of-flight mass spectrometer. A variable time delay (t_d) was installed as previously described.[4] The time delay (t_d) is the time between the end of the ionizing electron beam pulse and the beginning of the withdrawal pulse, i.e. reaction time for R3, for an infinitely short electron pulse.

Ionization-efficiency curves of He_2^+ with electron pulses of 0.25 and 1.44 μsec at various delay times, are shown in Figures 1 and 2. The ordinates of the He_2^+ curves have been shifted vertically to avoid overlapping, and to point out the structure of the curves. The ordinates are expressed in arbitrary units, while the abscissas represent the nominal or uncorrected electron energy. The structure in the He_2^+ curve is real, and not a result of instrumental conditions, as demonstrated by the included ionization-efficiency curve for He^+. Excited states of short affective lifetimes tend to reach their steady-state concentrations in the source at shorter electron bombarding times than the states of longer effective lifetimes. Thus, the use of the longer electron pulse should result in an increased contribution from the longer-lived states to the total He_2^+ formation. The ionization-efficiency curves, shown in Figure 1 were obtained with a 1.44 μsec electron pulse as opposed to the 0.25 μsec pulse in Figure 2. The change in the relative heights of the maxima with electron pulse duration indicates that τ_{36}, τ_{30} and $\tau_{58} > \tau_{68}$. Another test for this premise is the examination of the He_2^+ curves as a function of only time delay. As the reaction time is increased, the relative contributions of states with longer radiative lifetimes will predominate.

Examination of Figure 1 shows that the radiative lifetimes of the states corresponding to the maxima are in the order: $\tau_{36} \geq \tau_{30} > \tau_{58} > \tau_{68}$. It is not entirely clear whether another peak is present at 49 eV.

It can easily be demonstrated that as the delay time used becomes very small, i.e. as $t_d \to 0$, that

$$I_{He_2^+} \alpha \sum_j \sigma_{ej} \qquad (1)$$

Therefore, we conclude that the overall ionization-efficiency curve is a superposition of the electron-impact excitation functions for the states of helium that undergo the Hornbeck-Molnar process. This conclusion merits support if these curves are compared with the electron-impact

1. J. A. Hornbeck and J. P. Molnar, Phys. Rev. 84, 621 (1951).
2. F. J. Comes. Z. Naturforschq. 17a, 1031 (1962).
3. W. Kaul, Z. Naturforschung. 18a, 432 (1963).

excitation functions of helium determined by Lin et al.[5] Further support comes from Huffman and Katayama[6] who observed that all optically allowed states undergo Reaction R3.

The shoulder at 30 eV, and the peaks at 36 eV and 58 eV are characteristic of the electron-impact excitation function for the ^3P, ^3D, and ^1D family of states respectively.[5] These states are optically forbidden transitions (long radiative lifetimes), while the high energy maxima at 68 eV is characteristic of the excitation function for the optically permissable transition (short-lived lifetimes), the ^1P family, even though the energy of the maxima is somewhat less than observed by Lin et al.[5]

A study of the ionization-efficiency curves for short electron pulses and short delay times (Figure 2), reveals the anticipated large contribution from the short-lived ^1P family in support of this hypothesis.

An exhaustive kinetic study of the process involved in He_2^+ formation requires the calculation of each τ_j, k_j, and σ_{ej}/σ_o. Becker and Lampe[4] noted that the ionization-efficiency curves in Figures 1 and 2, are indicative of a method for determining these quantities. This method involves the investigation of the rate of He_2^+ formation at each of the maxima in the excitation function of the participating excited states; that is at 30, 36, 58, and 68 eV. Inspection of the individual excitation function curves,[5] however, reveals considerable overlap taking place in Figures 1 and 2. Thereby, only a partial separation is possible for the shoulder at 30 eV, and the peak at 36 eV. The values obtained at 58 and 68 eV, based on the excitation functions of Lin et al,[5] should be fairly good approximations for the formation of He_2^+ by the ^1D family, and the short-lived optically allowed ^1P family, respectively. $\frac{[He_2^+]}{[He^+]}$

It is much more convenient to work with ion-current ratio, $\frac{I_{He_2^+}}{I_{He^+}}$, than with absolute currents. Thus, assuming an infinitely short electron pulse, it is easily shown that:

$$\frac{I_{He_2^+}}{I_{He^+}} = [He] \sum_j \frac{\frac{\sigma_{ej}}{\sigma_o} k_j}{\tau_j^{-1} + k_j[He]} \left[1 - e^{-(\tau_j^{-1} + k_j[He])\, t_d}\right] \quad (2)$$

Kinetic measurements are made within the framework of (2). For a given electron energy, the ion-current ratio $I_{He_2^+}/I_{He^+}$, can be measured as a function of t_d. Considering, then, the initial slopes and the asymptotes of a plot of $I_{He_2^+}/I_{He^+}$ versus t_d, it is observed that:

$$\frac{\lambda_o}{A} = \frac{\lim_{t_d \to o} \frac{d\left(\frac{I_{He_2^+}}{I_{He^+}}\right)}{dt_d}}{\lim_{t_d \to \infty} \left(\frac{I_{He_2^+}}{I_{He^+}}\right)} = \frac{\sum_j \frac{\sigma_{ej}}{\sigma_o} k_j}{\sum_j \frac{\sigma_{ej}}{\sigma_o} k_j \, (\tau_j^{-1} + k_j[He])^{-1}} \quad (3)$$

The ratio $I_{He_2^+}/I_{He^+}$ (corrected for thermal drift and scattering), is plotted as a function of the delay time various pressures. The asymptotic value of the ratio was observed to be approached more rapidly in the order 68>58>36 eV, as should be the case if the effective lifetimes are in the increasing order $\tau 36 > \tau 58 > \tau 68$, as described previously. If only one state or family of states is involved for 58 and 68 eV, then (3) reduces to:

$$\frac{\lambda_o}{A} = \tau^{-1} + k\,[He] \quad (4)$$

Accordingly, the radiative lifetimes and specific reaction rates can be obtained from the intercepts and slopes of the plots of $\lambda o/A$, as a function of helium concentration. The separation of the reaction for the forbidden states at ~30, and 36 eV is not possible. Becker and Lampe[4] demonstrate, however, that the effective values, $\bar{k}$ and $\bar{\tau}^{-1}$, at 30 and 36 eV should be weighted more heavily with respect to those states whose excitation functions peak at these electron energies. No attempt was made to obtain a value for the shoulder at 30 eV, as the exact location

4. P. M. Becker and F. W. Lampe, J. Chem. Phys. 42, 3857, (1965).
5. R. M. St.John, F. L. Miller, and C. C. Lin, Phys. Rev. 134, A888 (1964).
6. R. E. Huffman and D. H. Katayama, J. Chem. Phys. 45, 138 (1966).

of the peak was uncertain.

Where k is known, σ_e/σ_i can be obtained from the initial slope λ_o. In agreement with the theory the plots were linear and the effective lifetimes and specific rate constants determined from these plots are shown in Table 1.

Table 1: Radiative Lifetimes and Specific Reactions Rates

Electron Energy (eV)	τ(μsec)	$k_i \times 10^{10}$ (cc molecule^{-1}sec^{-1}	$(\sigma_e/\sigma_i) \times 10^2$
36	1.33±0.10	4.67±0.2	0.75±0.4
58	0.59±0.03	5.92±0.2	0.21±0.2
68	0.47±0.03	3.07±0.2	0.31±0.4

The values reported by Kaul,[7] 0.28 and 2.6 μsec, for the effective lifetimes of the two states he observed, are not as discordant with the above values as might be supposed. Since the kinetic values were determined with 0.25 μsec electron pulse, our τ values for the long-lived state might be expected to be somewhat lower. Thus under our conditions of a short electron pulse, the long-lived excited states do not reach as high a concentration during the pulse as in Kaul's work,[7] where a 1.0 μsec pulse was used.

The values of the product kτ are higher than the value 0.58×10^{-16} (cc/molecule) previously reported by Dahler et al.[8] Observed values of σ_{ei}/σ_i are considerably lower than the values of k_a/k_i reported by Dahler et al.[8] This is probably a result of the different averaging that occurs when one uses steady state and pulse conditions.

The reaction cross-sections can be determined from the rate constants by using the following expression:

$$\sigma_{H-M} = \frac{k_i}{\bar{V}_{rel}} \qquad (5)$$

where $\bar{V}_{rel}$ is the average relative velocity of the atoms.

Observed values reflect contributions from a family of given state, i.e. $n(^3D), n \geq 3$. Nevertheless, it is interesting to compare these results with the work of Teter et al.[9] Using a completely different method, Teter reported Hornbeck-Molnar cross-sections for the n=3 states of helium. These results are shown in Table 2.

Table 2

State	H-M cross-section[19] m=3, 400°K	H-M cross-sections for rate constants cm^2 $n \geq 3$
3^3D	2.1×10^{-15} cm^2	2.5×10^{-15} at 36 eV
3^3P	1.4×10^{-16} cm^2	~ 30 eV
3^1D	4.6×10^{-16} cm^2	2.9×10^{-15} at 58 eV
3^1P	1.9×10^{-16} cm^2	1.5×10^{-15} at 68 eV

One might expect that our observed values, which include contributions from all states with $n \geq 3$, would be expected to be larger, but even the degree of agreement shown in table 2 between the two divergent methods indicates some validity to the postulate. In addition, the collision diameters obtained from the rate constants (assuming unit collision efficiency), may be compared with those derived from simple theoretical considerations.

7. W. Kaul, Conf. Inter. Phenomenes Ionisation Gas, 6, Paris I, 169-71 (1963).
8. J. S. Dahler, J. L. Franklin, M. S. B. Munson, and F. H. Field, J. Chem. Phys. 36, 3332 (1962).
9. M. P. Teter, F. E. Niles, and W. W. Robertson, J. Chem. Phys. 44, 3018 (1966).

$$\sigma_{obs} = \left(\frac{k_j}{\pi V_{rel}}\right)^{1/2} \qquad (6)$$

where σ_{obs} is the collision diameter. The results of Equation (6), are listed in Table 3.

Table 3: Observed Calculated Collision Diameters

Electron energy (eV)	σ_{obs} (Å)	$\sigma_{1s\,^3P}$ (Å)
36	3.3	7.8
58	4.0	7.8
68	2.6	7.8

The lowest reported appearance potential for He_2^+ is 23.1 ± 0.05.[10] According to published spectral term values for helium,[11] the "smallest" electron configuration at threshold is 1S3P. Employing the method outlined by Hirschfelder and Eliason,[12] the atomic radii of this configuration can be estimated, where:

$$\overline{r} = n^* (2n^* + 1)\ a_o/2\ (Z-S)$$

Slaters' rules were used to estimate the screening constant S and the effective principal quantum number n^*. The collision diameters can be obtained by application of Hirschfelder and Eliason's empirical rule, where:

$$\sigma = \overline{r}_{ground} + \overline{r}_{excited} + 1.8\ \text{Å}$$

The close proximity of the values adds support for the large determined rate constants.

A complete description of these investigations has been submitted for subsequent formal publication in the "Journal of Chemical Physics".

10. R. K. Curran, J. Chem. Phys. 38, 2974 (1963).
11. C. E. Moore, Natl. Bur. Std. Circ. No. 467 (1949).
12. J. O. Hirschfelder and M. A. Eliason, Ann. N. Y. Acad. Sci. 67, 451 (1957).

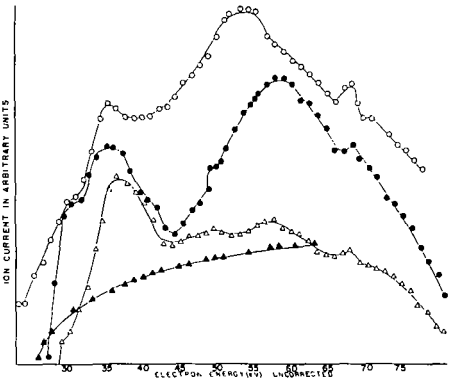

Figure 1. Ionization-efficiency curves in helium as a function of delay time. Source pressure - 20 μ; electron pulse = 1.44 μsec; ▲He^+ with delay time of 0.0 μsec; OHe_2^+ with delay time of 0.0 μsec; ●He_2^+ with delay time of 0.5 μsec; ΔHe_2^+ with delay time of 0.8 μsec.

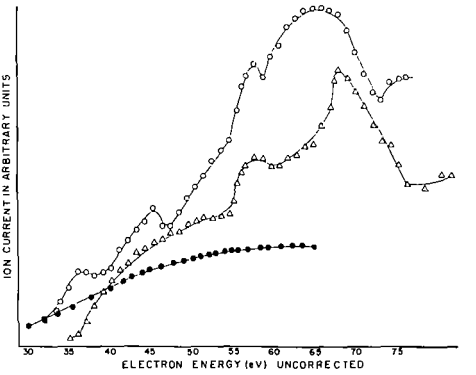

Figure 2. Ionization-efficiency curves in helium as a function of delay time. Source Pressure = 20μ; electron pulse = 0.25 μsec; ●He^+ with delay time of 0.0 μsec; ΔHe_2^+ with delay time of 0.0 μsec; OHe_2^+ with delay time of 0.7 μsec.

21. FRAGMENTATION IN FIELD IONIZATION MASS SPECTROMETRY

by
M. Barber, R.M. Elliott, T.R. Kemp and J.S. Halliday,
GEC-AEI Electronics Limited,
Scientific Apparatus Division,
Manchester, England.

The principal advantage which has usually been attributed to field ionization is the intensity of the molecular ion peak in field ionization spectra, not in an absolute sense but relative to the fragment peaks. This has led to a commonly-held belief that little fragmentation of the molecular ions takes place and hence that little useful information could be obtained from the fragment ions.

Exceptions to this general conclusion were in fact evident at an early stage, since it was shown by Beckey in 1961 (1) that rate-constants for very fast dissociation reactions could be deduced from the shape of low-mass tails on fragment peaks.

Wanless then showed (2) that high intensity metastable peaks occurred in the field ionization mass spectra of many aliphatic compounds, although in many cases the peaks due to the resulting fragment ions were negligibly small. These metastable peaks must be due to fragmentation processes where there is a high probability of that fragmentation occurring during the flight of the ion through the mass spectrometer. The only reason why the corresponding true fragment peaks are not equally intense is that the time spent by ions in the region of formation is so extremely short. However, the fragmentation can be observed equally conveniently in the metastable spectrum and Wanless showed how this could be used for deducing structures.

Our own observations of metastable peaks in field ion spectra have confirmed that in many cases the likelihood of fragmentation of the molecular ion in a given period of time is comparable with electron impact. Hence fragmentation processes in field ionization spectra can be readily studied, but by observation of the metastable peaks rather than the fragment peaks themselves. In recent papers (3,4) Beckey has shown how a comparison of intensities of fragment peaks and the corresponding metastable peaks in field ionization and electron impact spectra can be used to deduce whether a fragmentation is due to single-step direct bond rupture or the multi-step or rearrangement processes.

McLafferty et al (5) have observed metastable peak intensities in electron impact mass spectra, and have shown that for a given secondary fragmentation process $B^+ \rightarrow C^+ + D$ in a homologous series A_n, the logarithm of the ratio of intensities of the corresponding metastable peak m^* to that of the precursor B^+ is inversely proportional to the number of vibrational degrees of freedom in the parent molecule-ion. This they attribute to the increase in molecular size mainly affecting the internal energy by providing more degrees of freedom over which the internal energy can be randomized, the presence of a functional group giving rise to a substantial and characteristic part of the internal energy of the original molecule-ion.

It was therefore of interest to see whether a similar relationship holds in the case of field ionization. In field ionization the majority of fragmentation processes observable as metastable peaks are due to primary fragmentation of the parent ion A^+, and it is therefore not possible to study secondary processes. The series of primary processes $A_n^+ \rightarrow (A_n - X)^+ + X$, where the parent ion in a homologous series loses the same neutral fragment each time, can however be studied.

The field ionization spectra of a series of alkanones were run and the metastable intensities measured. Figure 1 shows the plot of log $\left[\frac{m^*}{m_1}\right]$ for alkanones (m_1 being the parent and m^* the metastable peak due to loss of H_2O from the parent) against the reciprocal of the vibrational degrees of freedom in the original molecule; this is compared with the equivalent data for the analogous loss of H_2S in thiols reported by Wanless (2). As can be seen a good straight line is obtained over the range C_3 to C_{18}, the slope being the reverse of that obtained by McLafferty in his investigations.

On the other hand similar plots for the loss of alkyl fragments in the same alkanones do not show this uniform behaviour, there being evidence (see Fig. 2) for abrupt changes in slope as the homologous series is ascended. Similar behaviour is observed if the results of Wanless on the loss of C_2H_5 and C_2H_6 from hydrocarbons (2) are plotted in the same way, as shown in Fig. 3.

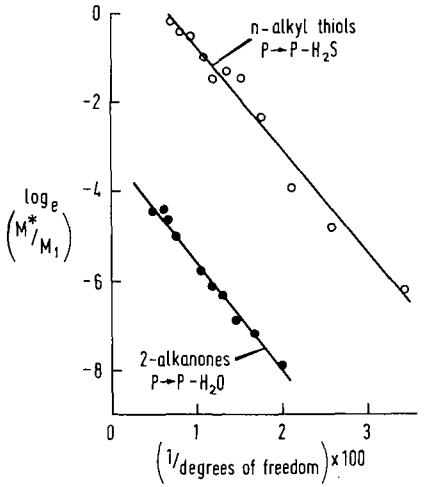

Fig. 1.

Variation in the ratio of metastable to parent peak intensities with the number of vibrational degrees of freedom for the loss of H_2O in 2-alkanones and H_2S in n-alkyl thiols.

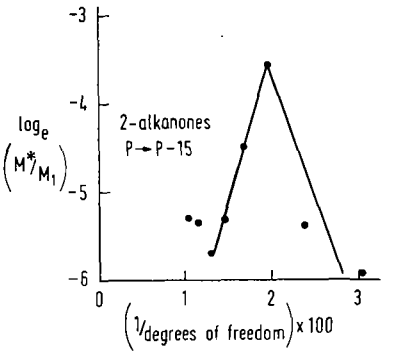

Fig. 2.

Variation in the ratio of metastable to parent peak intensities with the number of vibrational degrees of freedom for the loss of CH_3 in 2-alkanones.

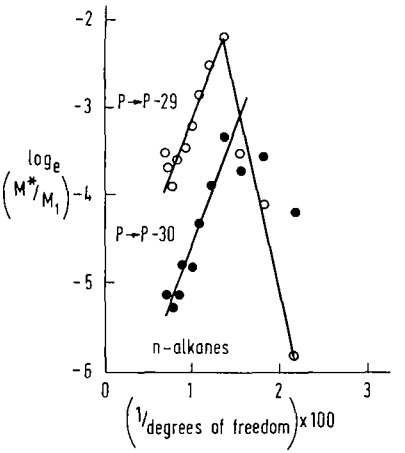

Fig. 3.

Variation in the ratio of metastable to parent peak intensities with the number of vibrational degrees of freedom for the loss of C_2H_5 and C_2H_6 in n-alkanes.

A possible explanation for this could be that the loss of H_2O and H_2S from ketones and thiols is relatively well localised and probably goes via a specific type of reaction. On the other hand the loss of a small radical from a hydrocarbon or from an alkyl chain in a ketone is not necessarily a localised loss, but can proceed via a series of different reactions and rearrangements from any part of the chain. Competition between these paths could change markedly with chain length, giving rise to the changes in slope.

These observations of systematic variations in metastable peak intensities are not at present fully explained but illustrate that considerable information on the nature of fragmentation processes is available in field ionization spectra.

References:

1. H.D. Beckey in Advances in Mass Spectrometry Vol. II, R.M. Elliott (ed) Pergamon Press (1963) p.1.

2. G.G. Wanless and G.A. Glook, Jr. Anal Chem. 39, 2 (1967)

3. H.D. Beckey, J. Mass Spectrometry and Ion Physics, 1, 93-97 (1968)

4. H.D. Beckey, A.S.T.M. E-14 Conference on Mass Spectrometry, Pittsburgh (1968)

5. F.W. McLafferty, T. Wachs and W.T. Pike in Advances in Mass Spectrometry Vol. IV, E. Kendrick (ed) Institute of Petroleum, London, 1968, p.153.

22. Field-Ion Mass Spectra of C_{18} Compounds Having Various Functional Groups

William K. Rohwedder

Northern Regional Research Laboratory, Peoria, Illinois 61604

Abstract

Mass spectra of C_{18} compounds having various functional groups were measured in a spectrometer equipped with a field-ion source. The sensitivity of the source was determined versus the nature of the functional group and the temperature of the ionizing blade.

- - - - - - - -

The usefulness of field-ion mass spectra in determining molecular weights of compounds, either singly or in mixtures, depends on the relative sensitivities of the molecular ion peak. Wanless and Glock (1) in their study of saturated hydrocarbons showed that the molecular ion peak sensitivity was approximately proportional to the molecular weight of the hydrocarbon when measured with a wire emitter. Sensitivities with a blade emitter source also appear to depend upon compound volatility.

The Nuclide source with which most of the work reported here was done, is an open source with the blade mounted perpendicular to the slit similar to that described by Robertson (2).

Figure 1 shows a field ion mass spectrum of a mixture of methyl esters from C_{14} to C_{20}, plus C_{22}. The peak at C_{21} is due to an impurity. The C_{15} and C_{17} esters are rare, and it was possible to use only half as much of these in the otherwise equal weight mixture. Figure 2 is a plot of the molecular intensity versus the chain length of the acid for the methyl ester mixture. Figures 1 and 2 show that for the higher molecular weight esters, sensitivity almost doubles for each additional two carbon atoms. Figure 3 is a plot of molecular intensity versus chain length for a mixture of hydrocarbons which should be comparable to Wanless' results. But again, sensitivities almost double for each two carbon atoms added to the chain.

It is difficult to explain such a great change in sensitivity by either chemical or ion optical effects. An increase of two carbon atoms on a chain 16 carbon atoms long doubles the sensitivity; such an increase is beyond any reasonable chemical effect. Similarly, an ion optical effect would be expected to show up as some form of mass discrimination where the change in sensitivity would be greater at the shorter chain lengths rather than at the longer chain lengths.

There are no vapor pressure data available for methyl esters in the 10^{-5} to 10^{-6} Torr region, but data for similar material in the millimeter region indicate that vapor pressure decreases by about a factor of two for each increase of two carbon atoms to the chain. The vapor pressure of methyl stearate is such that one obtains satisfactory spectra with the source temperature at 60° but the higher homologues require higher temperatures to prevent condensation. Wanless and Glock using wire emitters did not observe this extreme increase in sensitivity with chain length.

All these observations indicate that sensitivity changes may be caused by sample vapor condensing on the blade. Figure 4 is a diagram of the blade edge region. Both condensable and noncondensable sample molecules approaching the blade edge are ionized. Noncondensable sample molecules hitting the side of the blade bounce off without ionization, whereas condensable samples hit the blade, condense, and then migrate to the blade edge for ionization. In a wire emitter the effective area available for sample collision is the same for both condensable and noncondensable samples. The blade has a much larger area available. If condensation and migration occur, one would expect greatly increased sensitivities for compounds with lower vapor pressures over a limited range. The upper limit of sensitivity would occur when the vapor pressure of the sample is so low that

it condenses on other parts of the source or when the sample is too viscous to migrate to the edge rapidly. The lower limit of the effect exists when vapor pressure of the sample is so high that it does not condense significantly or revaporates before it migrates to the edge.

A razor blade field emission source was designed and built in which the temperature of the razor blade could be varied from 5° to 120° C. The source was enclosed and could be heated separately. The instrument was focused on the molecular ion of a compound, the blade temperature was varied, and the intensities were recorded. The results were not very satisfactory because it was necessary to refocus the instrument at each temperature and the total ion current and the analyzed current did not follow the same curve. The data were not reproducible. It would appear that to make a satisfactory source to prove this point, one would have to have mechanical blade adjustments, both translational and rotational.

Figure 5 shows the molecular intensity of several compounds. Two chloride isotopes have been added together as have the two bromide isotopes. The four compounds--methyl stearate, MeSt; methyl oleate, MeOl; methyl linoleate, MeLo and methyl linolenate, MeLn--are identical except for the number of double bonds, but yet there is considerable variation in their molecular intensity.

References

1. G. G. Wanless and G. A. Glock, Jr., Anal. Chem. 39, 2 (1967).

2. A. J. B. Robertson "Advances in Mass Spectrometry, III," p. 23, Institute of Petroleum, London, 1966.

Presented at the Sixteenth Annual Conference on Mass Spectrometry and Allied Topics, Field Ionization Symposium, Pittsburgh, Pa., May 12-17, 1968.

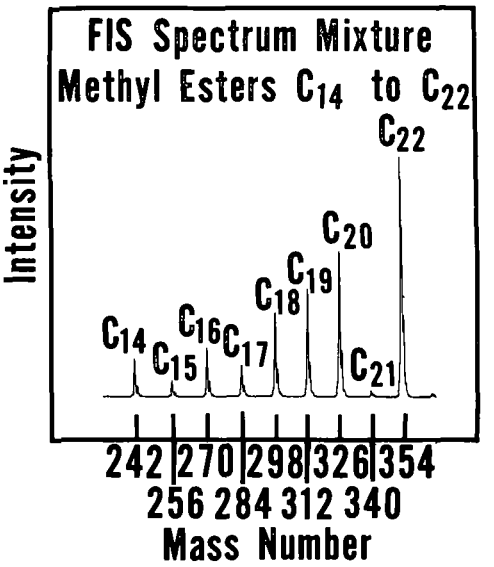

Figure 1. Photograph of field ionization spectrum of a mixture of methyl esters C_{14} to C_{22}.

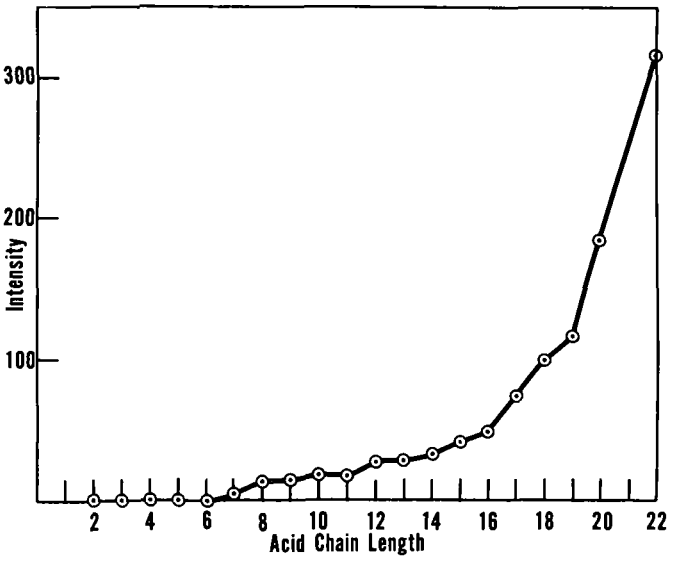

Figure 2. Plot of molecular intensity of methyl esters versus the chain length of the acid.

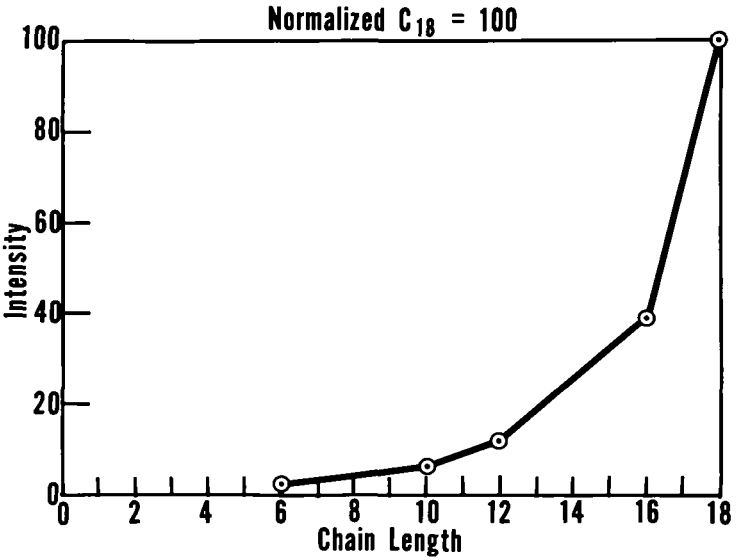

Figure 3. Plot of molecular intensity of hydrocarbons versus chain length.

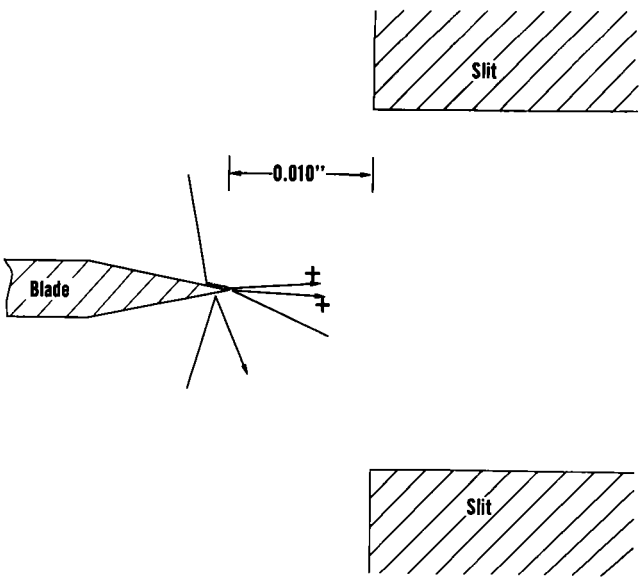

Figure 4. Schematic diagram of field ion blade emitter and slit.

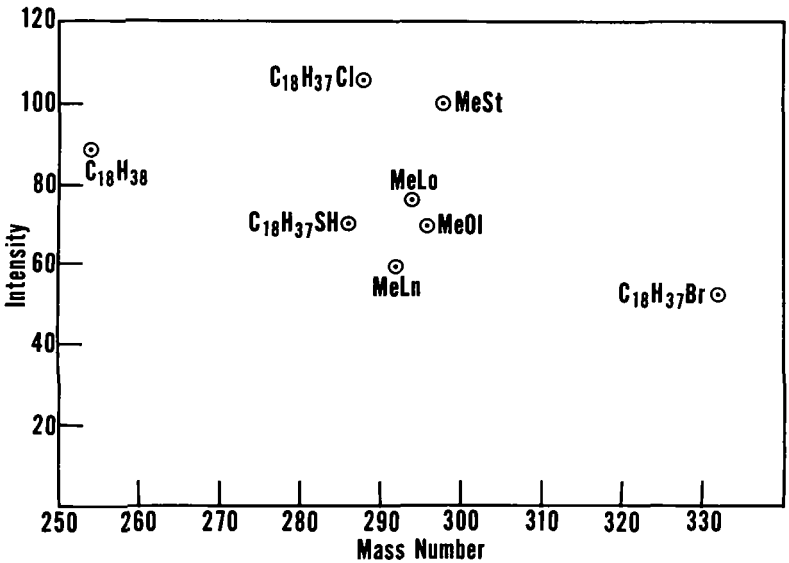

Figure 5. Plot of molecular intensity of a variety of compounds versus mass number. MeSt, methyl stearate; MeOl, methyl oleate; MeLo, methyl linoleate; and MeLn, methyl linolenate.

23. Field Ionization Spectra of Some Pesticidal and Other Biologically Significant Compounds, J. N. Damico, R. P. Barron, and J. A. Sphon, Division of Food Chemistry & Technology, Bureau of Science, Food and Drug Administration Department of Health, Education and Welfare, Washington, D. C. 20204

Field ionization spectra of some pesticidal and other biologically significant compounds of low vapor pressure were obtained with a combination electron impact field emission ion source. With this system it is also possible to obtain both types of spectra on the same sample charge. Switching from one mode of operation to another requires only a few minutes. The samples were introduced directly into the ion source with a molecular beam inlet system. This system permits the sample temperature to be maintained independent of the ion source temperature when the probe tip is placed a short distance (2mm) from the ionization chamber (1). The following conditions apply to both modes of operation: acceleration voltage, 3kv; magnetic scanning; ion source temperature 200°C.; sample temperatures approximately 20° C. unless specified (in Table 1 this is indicated under the heading T_c). Electron impact spectra were recorded at 70 ev. Field ionization data were obtained using a Pt wire emitter of 2 mm length and approximately 2.5 microns in diameter, a cathode potential of -6 kv, and an anode potential of +2 kv, with the distance between the anode and cathode at 2 mm. Emitter wires were activated overnight at a high source pressure of acetone (ca. 5×10^{-5} Torr) with the voltages applied. Overnight conditioning is usually sufficient to obtain a reasonable working sensitivity (10-30μg of sample required).

Since this work is to be submitted for publication in the International Journal of Mass Spectrometry and Ion Physics, only a limited amount of the data will be presented. The data in Table 1 summarize some of the rearrangement and multi-step processes produced by both electron impact and field ionization which are observed with some of the compounds in this study. Detailed studies of the time-of-flight spectra of the compounds shown in Table 1 have been reported (2,3,4); structures of all the compounds listed in the table are included in the publications just cited.

Molecular ion intensities were enhanced by field ionization for all the compounds examined. Molecular ions were not observed for Temik sulfoxide and Delnav and were only of very weak intensity for Temik and Temik sulfone in the electron impact mode. However, they were of appreciable abundance in the field ion mode.

TABLE 1.

CHARACTERISTICS OF SOME REARRANGEMENT AND MULTI-STEP PROCESSES PRODUCED BY ELECTRON IMPACT AND FIELD IONIZATION OF SOME PESTICIDAL COMPOUNDS.

Compound	T_c (°C)		m/e	Electron Imp. $\%\Sigma_{35}$	Electron Imp. R.I.%	Field Ion. $\%\Sigma_{35}$	Field Ion. R.I.%	Mechanism	
Carbaryl	EI	FI	57	8.6	31.1	39.8	100.0	Two-step dissociation	m* ?
	40	45	144	27.9	100.0	30.8	80.0	Rearrangement	m* = 1.2%
Bayer 37344			57	5.5	26.2	9.7	14.3	Two-step dissociation	m* ?
			168	21.2	100.0	8.6	12.7	Rearrangement	m* = 0.3%
UC-10854			18	0.0	0.0	5.8	12.0	Multi-step process	m* ?
			57	0.8	4.0	48.4	100.0	Two-step dissociation	m* ?
			136	17.4	71.9	13.8	28.7	Rearrangement	m* = 2.8%
Bayer 39007			57	5.9	17.0	47.6	100.0	Two-step dissociation	m* ?
			152	7.0	19.8	13.5	28.3	Rearrangement	m* = 5.0%
IPC			93	58.4	55.0	2.9	4.3	Rearrangement	m* ?
			119	16.0	100.0	22.3	33.3	Rearrangement	m* ?
CIPC			127	9.4	58.0	0.6	1.6	Rearrangement	m* ?
			153	7.4	45.8	5.6	14.3	Rearrangement	m* ?
Temik (Compound 13)	32	25	88	1.1	14.3	7.8	10.8	Multi-step dissoc.	m* ?
			115	1.5	19.5	72.9	100.0	Two-step dissociation	m* ?
Temik Sulfoxide (Compound 14)			63	1.7	11.6	15.5	10.4	Multi-step process	m* ?
	65	70	68	3.3	23.1	11.9	51.3	Multi-step process	m* ?
Temik Sulfone (Compound 15)			68	4.0	21.0	11.9	52.1	Multi-step process	m* ?
	60	90	79	0.4	2.2	11.2	49.3	Multi-step process	m* ?
Malathion			128	1.6	15.6	5.6	9.7	Two-step dissociation	m* ?
			149	0.1	1.0	17.7	30.8	McLafferty Rearrange.	m* ?
Delnav	45		270	4.0	31.3	43.6	100.0	Skeletal Rearrangement	m* ?

m* = % Indicates the relative intensity of the metastable peak when observed in the field ion spectrum.

m* ? Indicates a metastable peak‡ is not observed in the field ion spectrum.

‡ No special effort was made to record peak intensities of less than 1%.

ACKNOWLEDGEMENTS

The authors are grateful to the manufacturers for furnishing pesticidal samples and to the Pesticides Standards Branch, Division of Food Chemistry and Technology, for supplying the purified pesticides as noted in Table 1.

REFERENCES

(1) G. Brunee, Fourteenth Annual Conference on Mass Spectrometry and Allied Topics, ASTM Committee E-14, Dallas, Texas, (1966) 410

(2) J. Damico, W. R. Benson, J. Assoc. Offic. Anal. Chemists, 48, (1965) 344

(3) J. Damico, Ibid, 49, (1966) 1027

(4) W. R. Benson, J. Damico, Ibid, 51, (1968) 347

24. A Combined Electron Impact/Field Ionization Source and Its Application in Organic Geochemistry*

P. Schulze, B. R. Simoneit and A. L. Burlingame
Department of Chemistry and Space Sciences Laboratory
University of California, Berkeley, 94720

A standard electron impact source for the CEC 21-110 double focussing mass spectrometer has been modified for use as a field ionization source as well. The mechanical modifications are the following: A vacuum lock has been attached to the ion source housing. A steel rod, supporting the field ion emitter and the necessary insulators, can be pushed through this vacuum lock, thus introducing the emitter into a hole in the back of the ionization chamber. By means of a micrometer screw driving the support rod, it is possible to determine the optimum distance between the emitter and the repellers which serve as cathode. The emitter is made of three razor blades spotwelded together and is positioned parallel to the slit of the repellers. The triple blade was found to give a higher ion beam intensity than a single blade, due to the different field distribution rather than a larger emitting area. The proper voltages are supplied by a suitable voltage divider network. Changing from one mode of operation to the other is done by switching a multiconnector plug. The ion beam intensity is high enough to obtain a resolution of 22,000 (10% valley) in the field ionization mode. This is verified by resolving the doublet at m/e 99 in cyclohexanone, which consists of the C^{13} containing molecular ion and the molecular ion with one H-atom attached. Mixtures of fatty acid methyl esters and free fatty acids isolated from the Green River formation kerogen were analyzed in the field ionization mode.

The virtual absence of fragment ions in field ionization mass spectra makes it difficult to establish a mass scale and perfluorokerosene can therefore not be used as a mass standard. Since it was found that the scan reproducibility of the CEC 21-110 is excellent, the following procedure to set up a mass scale has been adopted. A perfluorokerosene spectrum is digitized online in the electron impact mode. Then the field ionization mass spectrum of the unknown sample mixture containing acetone, methylbutanone and cycloheptanone is taken in the real-time mode. All masses in the field ionization spectra are calculated by superimposing the elapsed times and masses of the three standard compounds on the slope of the

* A complete paper is in the press of the Journal of Mass Spectrometry and Ion Physics.

mass vs. time curve of the electron impact spectrum of perfluorokerosene. The masses calculated in this manner were found to be in error by approximately 0.15 mass units in the region of m/e 300 to 0.25 mass units in the region of m/e 450. All errors were below the theoretical value and thus using calibration compounds of higher masses improved these results considerably.

25. Kinetic Energies of N^+ Ions Formed by Dissociative Double Ionization of N_2

K. E. McCulloh and H. M. Rosenstock
National Bureau of Standards
Washington, D. C. 20234

Dissociative double ionization of N_2 by 1-kV electrons was studied by coincidence detection of the resulting pairs of N^+ ions in a system designed for kinetic energy measurements[1]. The kinetic energy distribution exhibits a peak at about 7.5 eV and cuts off sharply below 3.5 eV. This cutoff is interpreted as resulting from a maximum in a low-lying N_2^{++} potential energy curve. Such curves have been published by Hurley[2]. The peak at about 7.5 eV is most readily explained as resulting from vertical ionization to another completely repulsive, curve of N_2^{++}. Nothing definite is known about such a state or states in doubly-ionized nitrogen.

1/ K. E. McCulloh and H. M. Rosenstock, J. Chem. Phys. 48, 2084 (1968).

2/ A. C. Hurley, J. Mol. Spectroscopy 9, 18 (1962).

26. CORRELATION OF EXCESS ENERGIES OF ELECTRON IMPACT DISSOCIATIONS WITH THE TRANSLATIONAL ENERGIES OF THE PRODUCTS *

Max A. Haney and J. L. Franklin
Department of Chemistry
Rice University
Houston, Texas
77001

ABSTRACT

Translational energies of products of unimolecular dissociations resulting from electron impact have been measured at the appearance potentials of the fragment ions. Excess energies for each process were determined from the measured appearance potentials and the known heats of formation of ground-state products and reactants. Results are compared with the predictions of the Statistical Theory and found to be in agreement if the classical density of states is used. Application of the method to accurate determinations of heats of formation of radicals and radical-ions is demonstrated.

* This work was supported by The Robert A. Welch Foundation.

To be published Journal of Chemical Physics.

27. APPARATUS FOR MEASUREMENTS OF ION PAIR PRODUCTION

T. E. Sharp, J. T. Dowell, and B. Mass
Lockheed Palo Alto Research Laboratory, Palo Alto, California 94304

In ion pair production a positive fragment ion and a negative fragment ion are formed from the same molecule. The process may be induced by photon impact or by electron impact. Ion pair production is of interest because it is an important source of negative ions in the upper atmosphere and in radiolysis of gases. A comparison of ion pair production with dissociative attachment of electrons, another source of negative ions, shows that dissociative attachment is a resonant process peaking at low electron energies, while ion pair production is not a resonant process for electron impact, onsets at higher energies, and extends over a larger energy range. The cross sections for the two types of processes are often comparable and much smaller than ionization cross sections.

Because the products of an ion pair process are oppositely charged, the potential curve leading to these products is an attractive curve, often having a broad minimum. The shape of the cross section as a function of energy depends on the location of the intersection of the product energy with the repulsive part of this curve. If the intersection lies at a larger internuclear distance, outside the Franck-Condon region, then in photon impact the cross section for ion pair production will be proportional to the square of the reflection of the ground state wave function in the continuum wave functions of the repulsive part of the curve. In this case the cross section is bell-shaped and has no sharp onset. The ions are formed with some initial kinetic energy. An example of this behavior occurs in CH_3Cl (Ref. 1). On the other hand, if the product energy intersection lies within the Franck-Condon region, then a sharp onset will be observed in ion-pair production exactly at the product energy. The cross section resembles the square of the reflection of the ground state wave function in that portion of the repulsive part of the curve which lies above the product energy. The ions are formed without initial kinetic energy at threshold. An example occurs in O_2, where a sharp rise followed by tailing-off appears in photon impact (Ref. 2). If the threshold behavior in electron impact is linear and that in photon impact is a step function, then the electron impact cross section should look like the integral of the photon impact data.

The conventional method of studying ion pair production is to examine the positive ions separately from the negative ions. As a result, several ambiguities may arise: (1) Undetermined mechanism--what positive fragment ion is produced with a given negative fragment ion? (2) Hidden processes--an ion and an excited state may be formed instead of an ion pair, and this process may be buried in the apparent ion pair current. (3) Obscured onset--the energy at which ion pair production onsets may be obscured by other processes if the positive ions and the negative ions are measured separately. These ambiguities can be eliminated by simultaneous detection of positive and negative fragment ions in coincidence.

An apparatus to perform such measurements has been constructed in our laboratory. The heart of the instrument is a pair of 180° magnetic mass spectrometers, mounted "back-to-back" on the same ion source. The apparatus is mounted in a 6 inch ID stainless steel tube, around which is wound a solenoid. The magnetic field of 600 G, which provides the field for mass analysis, also serves to collimate the electron beam and to supply the field for operation of two resistance strip multipliers used for detection of positive and of negative ions. Provision is also made for total collection of ions, to permit determination of the gas pressure in the ion source. The radius of curvature for the positive ions is 4.5 cm, and for the negative ions, 3 cm. The difference is due to the requirement of pointing the strip multipliers, placed "back-to-back", in opposite directions. The arrival of an ion at the mass spectrometer collector is signalled by a pulse from the multiplier. The pulse is amplified, shaped, fed into a discriminator, and the resulting signal is fed into a delayed-coincidence circuit. The number of arrivals of single positive and negative ions is counted as well as the number of delayed coincidences. A background rate in each singles counting channel of one or two counts per second has been achieved using a low discriminator setting.

Several modes of operation are possible. The electron beam can be run continuously, and the difference in arrival times converted to pulse height which is displayed on a multichannel analyzer. Because positive ions also arise from dissociative ionization, the arrival of a negative ion is used as the start pulse. Ion energy analysis can be achieved by applying a retarding potential just before the multiplier. Alternatively, the electron beam may be chopped, and both the arrival time of one ion and the difference in arrival time of the second ion may be measured. The performance characteristics of the apparatus are still under test.

1. V. H. Dibeler and J. H. Walker, J. Chem. Phys. 43, 1842 (1965)
2. V. H. Dibeler and J. H. Walker, J. Opt. Soc. Am. 57, 1007 (1967)

29. ENERGETICS OF THE ELECTRON-IMPACT FRAGMENTATION OF ARYL-ALKYL ETHERS AND THIOETHERS.

J. L. Occolowitz
Eli Lilly & Co., Indianapolis, Indiana
and
R. G. Gillis, G. J. Long and A. G. Moritz
Defense Standards Laboratories, Maribyrnong, Victoria, Australia

Abstract

[M-olefin] fragments derived from phenyl alkyl ethers and thioethers are shown to have higher enthalpies than the isomeric ions derived from phenol and thiophenol. Although this indicates a non-phenolic structure for the fragment ions, there are insufficient experimental data to postulate an alternative structure.

Experimental data show that the anthrone molecular ion has an enthalpy higher than that of the tautomeric ion derived from 9-anthrol and close to the enthalpy of the $[M-C_2H_4]$ fragment ion from 9-anthrol ethyl ether. On this basis a ketonic structure is postulated for the fragment from 9-anthrol ethyl ether and by analogy for the fragments from the phenyl ethers.

To be published in Organic Mass Spectrometry.

30. Neutral Fragments from Electron Impact Studies

Masahiko Tsuchiya, Frank J. Preston, Harry J. Svec
Dept. of Chemistry, Institute for Atomic Research
Iowa State University, Ames, Iowa 50010

The chemical reactions that take place in electron bombardment ion sources involves positive and negative ions and neutral fragments. For many years we have been concerned with the problem of obtaining thermochemical information about reactive inorganic substances by means of ionization effiency studies. Many of these substances contain highly electronegative groups and thus readily form negative ions as well as positive ions. The reactive nature of these molecules prompted us to develope the simultaneous positive-negative ion mass spectrometer which was described at a previous conference. Despite the fact that results with this instrument have been extremely interesting, we declined to say anything about them this year in an attempt to follow the program chairman's suggestion of reducing contributions from a single laboratory. It seemed appropriate however that we say something about our work to determine the identity of the neutral fragments which are formed as a result of the chemical reactions taking place in ion sources.

We have talked about ways of doing this as long as seven years ago but the effort which went into the development of the positive-negative instrument side-tracked any serious development. The problem concerns carrying out the ionization of molecules in one electron beam; drawing aside the ions formed by appropriate electron fields; allowing the neutral fragments formed to diffuse into a second electron beam where they are ionized and perhaps further fragmented, and then mass analysing the positive and/or negative ions formed from the neutral fragments. Provisions must be made for controlling the electron energy and the electric fields in such a way as to be able to measure appearance potentials of radicals and other neutrals, excitation states of neutrals and ions and the kinetic energy of ions. In addition provisions must be made to minimize the effects of wall collisions and ion trapping in the electron beam.

A good idea isn't unique among scientists and this one way no exception. Beck and Osberghaus described a crossed, two electron beam ion source in 1960 with which they were able to identify neutral fragments and measure their appearance potentials. During the next few years further examples of work with this ion source was described by Beck and Niehaus (1962) and by Genzel and Osberghaus (1966). In the middle 60's, C. E. Melton also described a similar development and extended the ideas to studies in radiation chemistry and catalysis. Our own development differed somewhat from that of the foregoing authors in that our intent was to use ion source conditions more commonly used in conventional mass spectrometry. The electron beams are parallel and well collimated by means of magnetic shunts and the structure of the primary electron gun is open. Large mesh screens (>99% transparent) are used to maintain the integrity of the electric fields in the ionizing region. A liquid-nitrogen cooled surface opposite a molecular beam collimator reduces the probability that a condensable molecule passes through the ionizing region more than once. Figure 1 shows diagrammatically an end and side view of the electron gun structure. Note the ion draw out plate (1) above the primary electron gun which is electrically negative with respect to the shield, and the repeller electrode (high transparent mesh) of the second electron gun. Figure 2 is a photograph of the assembly with the ion draw-out plate (1) removed. Armco iron blocks serve to support both filament and trap structures and serve to control the position and uniformity of the collimating magnetic fields. The electron currents employed in most experiments are kept as low as possible to avoid problems due to ion-trapping. (EB-1 <100μa; EB-2 <25μa.)

Provisions are made for operating the electron guns in a d.c. mode and a pulsed mode. Pulsing the primary electron beam is achieved by controlling the grid potential while maintaining all other electric fields and the filament power constant. A tuneable lock-in amplifier simplified the mass spectrometer read-out problem. Appearance potential measurements are automatically recorded by means of an X-Y recorder. Fig. 3 is a schematic diagram of the general electronic circuitry.

The mass spectrometer detection system makes use of a 10-stage Allen-type electron multiplier to provide sufficient read-out sensitivity.

In the remainder of this paper we will give some examples of the kinds of results we have been obtaining. These are meant more to demonstrate the potentialities of the equipment than to indicate detailed results in systematic studies which are underway.

Despite attempts to obtain well collimated molecular beams and to limit them to a single pass through the ionization region, some primary molecules get into the secondary electron beam and are ionized. Figure 4 illustrates this fact and in addition the manner in which ions from neutral fragments are observed. One sees an ion current when the secondary beam is on; this increases when the primary beam is turned on and increases further when the latter current is increased and decreases when it is decreased. When the primary beam is turned off by means of the grid, the ion current is the same as previously observed. It is the difference in ion currents under varying source conditions which indicates the relative amounts of neutral fragments formed. In the case of CH_4^o and CH_3^o from propane the amounts are linear with sample pressures as indicated in Figs. 5 and 6. Thus, these are from primary reactions in the ion source. However, as is shown in Fig. 7, $C_2H_2^o$ is not linear with pressure and thus its origin is more complicated. At least part of it may arise by the interaction of two CH^o radicals. Table I summarizes the neutral fragment mass spectra from propane at two different sample pressures.

Appearance potential measurements can be made by varying the energy of either electron beam. Fig. 8 shows results for methyl radical when the energy of EB-1 is varied. Note that curve B covers only a 12 volt energy range. In Fig. 9 we illustrate what happens when the energy of EB-2 is varied. Curve A was obtained with no ionizing current from EB-1 but the filament on. This was done to keep possible thermal effects consistent. Curve B, is the result when both ionizing beams are present. The difference between these curves is due to ions from neutral CH_3^o. This is shown in Fig. 10 with the calibration correction of the electron energy for EB-2 also shown. The appearance potential derived from these data indicates that CH_3^o occurs in an excited state. Other excited states inferred from these data agree with those observed by Melton. Similar studies are possible with any other neutral fragment.

It is also possible to determine excitation energies of neutral species. This is accomplished by varying the electron energy of EB-1 below that of the ionization potential of a species and then ionizing the excited species formed by means of EB-2.

A typical example of an excitation function for a highly excited state of argon is shown in Fig. 11. Here the energy of EB-1 was varied while that of EB-2 was maintained at 5.0 eV. The resulting argon ion currents due to ionization of excited neutral argon atoms were observed in the mass analysing portion of the instrument. A series of such measurements were made at various EB-1 currents. At the same time a calibration of the energy scale of EB-1 was made by observing the appearance potential of Ar^+ at the ion draw out plate (1) as a function of electron energy current. The results are shown on the left in Fig. 12. Assuming a value of 15.76 eV for the ionization potential of Ar^+ indicates the highly excited states of A* under observation to be $\sim$0.15 eV lower than the ionization potential or 15.61 eV above the atomic ground state. This state has a life time $\geq 10^{-6}$ secs. It is probably the excited state assumed by Hornbeck and Molner and by Melton to account for the formation of Ar_2^+ which has an appearance potential just below that of the ionization potential of argon. There were no other states near this energy which had a life time long enough to observe in our experiment.

If one changes the experiment to use a fixed energy for EB-1 and a variable energy for EB-2 one can observe IE curves for Ar*. From these one can determine the energy at which the ionization probability of the above excited state of argon is a maximum. A typical ionization efficiency curve from EB-2 is shown in Fig. 13. Here the energy of EB-2 was varied at 18μa of ionization current. On the right side of Fig. 12 the maxima of a series of such curves obtained at different electron currents

are plotted as a function of the electron energy in EB-2. An energy calibration using the appearance potential of Ar^+ is also shown. The maximum cross section for ionizing this excited species is at 5.80 eV.

Another interesting measurement concerns the determination of kinetic energy mass spectra. By varying the voltage applied to the repeller associated with EB-2 and at the same time shutting off the electron current, only those ions whose kinetic energy in eV exceeds the repeller voltage are detected. Fig. 14 shows four kinetic energy scans of the benzene fragmentation by 75 eV electrons. Note that the mass scales for each scan is displaced sideways to avoid overlapping. The lowest spectrum represents ions whose kinetic energies are $\gtrsim$0.1 eV. Note from the upper scan that very few of the ions have kinetic energies exceeding 2.0 eV even for interactions with 75 eV electrons.

Similar experiments in which the primary electron energy was decreased stepwise indicates that for molecules as complex as propane and benzene none of the fragments have kinetic energies >0.1 eV when the energy of the bombarding electrons is less than 30 volts. This kinetic energy may actually be nearer 0.0 eV since the uncertainty in the kinetic energy measurement indicates 0.1 eV to be an upper limit. This is an important observation since it allows people who measure appearance potential values of fragment ions to forget about kinetic energy effects and to concentrate on attempting to determine electronic and vibrational excitations of these ions. It should be possible to determine these excitations with this ion source.

One remaining part of the development has not been done yet. We would like to be able to form negative ions from neutral fragments and to determine their electron capture energy.

References

D. Beck and O. Osberghaus, Z. für Physik, 160 406-19 (1960).
D. Beck and A. Niehaus, J. Chem. Phys., 37 2705 (1962).
D. Beck, Disc. Faraday Soc., 36 56 (1964).
C. E. Melton, J. Chem. Phys. 45 4414 (1966).
C. E. Melton, J. Sci. Inst. 43 927 (1966).
H. Genzel and O. Osberghaus, Z. Naturforsch. 22a 331 (1967).
C. E. Melton and P. S. Rudolph, J. Chem. Phys. 47 1771 (1967).

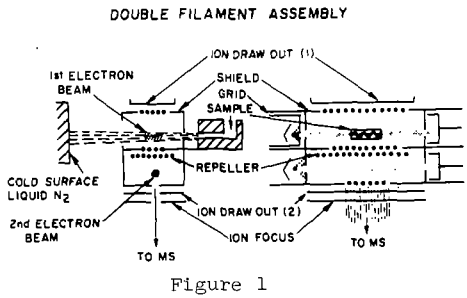

Figure 1

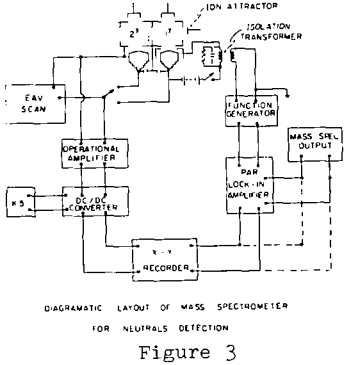

Figure 3

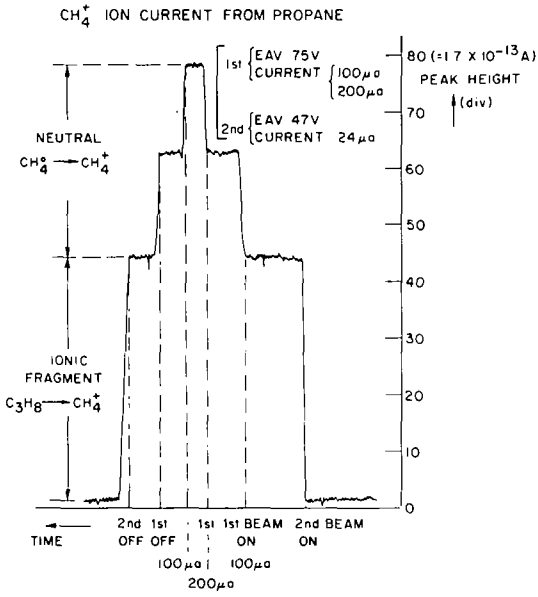

Figure 4

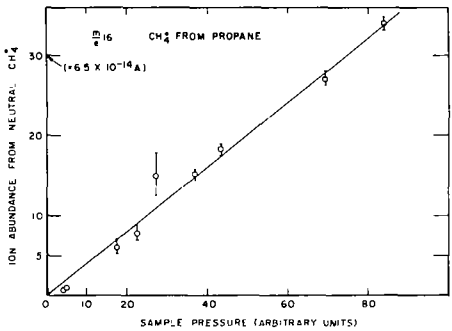

Figure 5

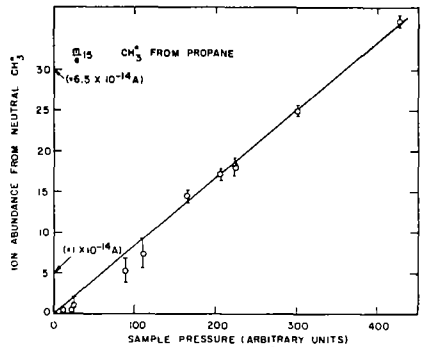

Figure 6

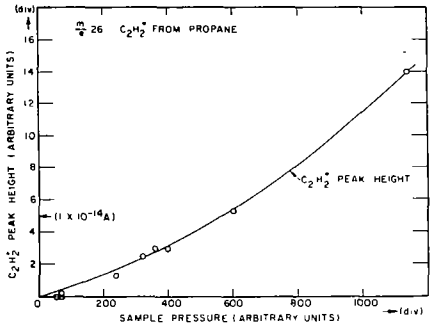

Figure 7

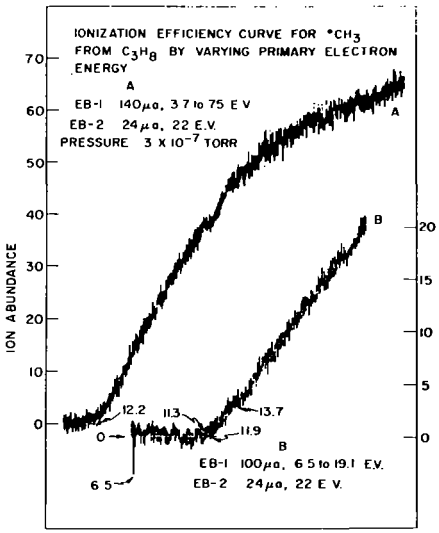

Figure 8

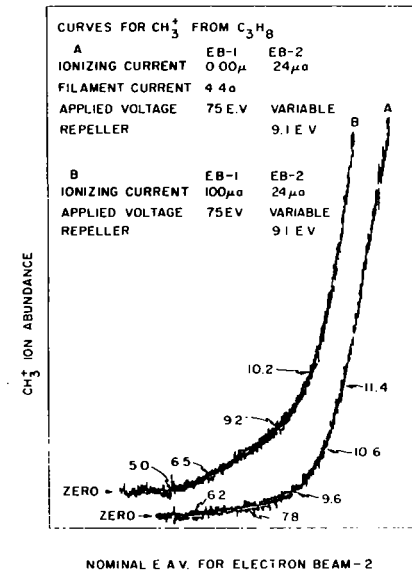

Figure 9

Table I.

Relative Abundances of Neutral Fragments from Propane

m/e			
2	H_2	12	9
12	CH	4	5
14	CH_2	16	17
15	CH_3	100	100
16	CH_4	97	97
25	C_2H	1	4
26	C_2H_2	2	25
42	C_3H_6	20	19
Pressure (Torr)		0.2×10^{-6}	1.2×10^{-6}

Ionizing Currents - Primary 100μa, 60 e.a.v.; Secondary 20 μa, 50 e.a.v.

Table I.

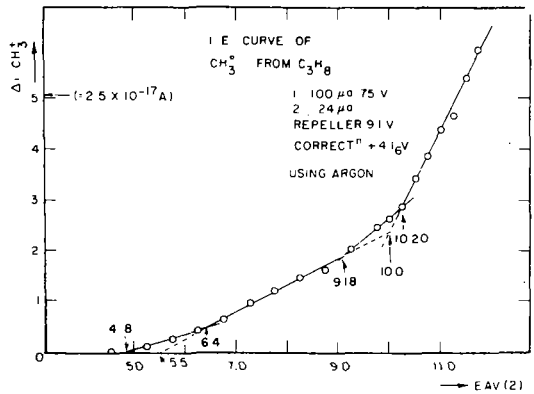

Figure 10

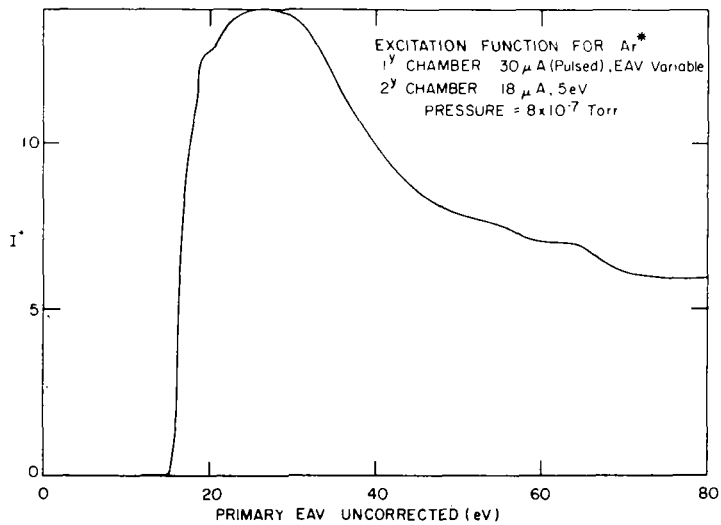

Figure 11

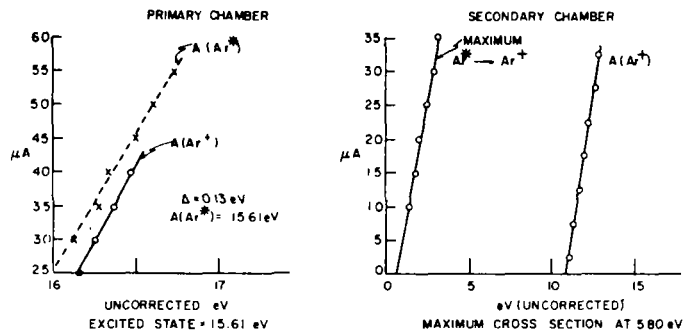

Figure 12

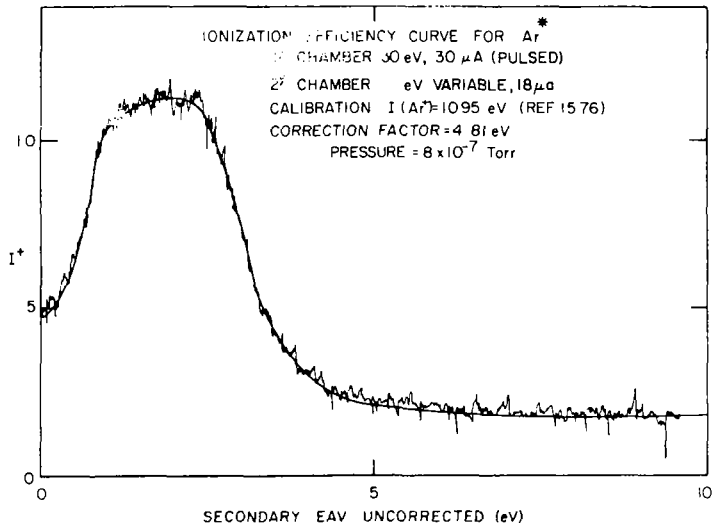

Figure 13

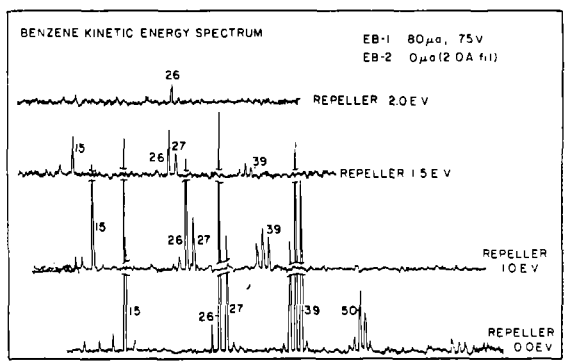

Figure 14

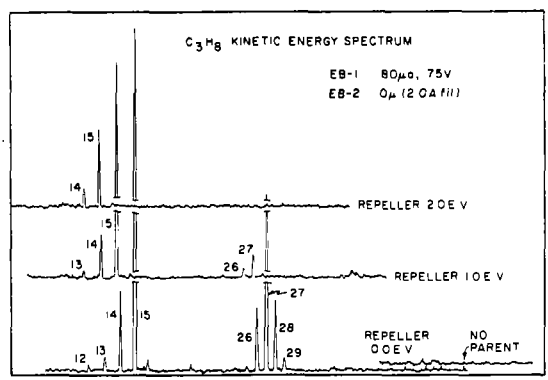

Figure 15

31. SECOND DIFFERENTIAL IONIZATION EFFICIENCIES OF C_4H_8 MOLECULES

by

G. G. Meisels, J. Y. Park, and B. G. Giessner
Department of Chemistry
University of Houston
Houston, Texas 77004

ABSTRACT

Appearance potentials of $C_4H_8^+$, $C_3H_5^+$, and $C_2H_4^+$ from cis- and trans-butene-2, butene-1, 2-methylpropene, methylcyclopropane, and cyclobutane have been evaluated using the second differential ionization method. Heats of formation of the fragment ions have been calculated. $\Delta H_f(C_3H_5^+)$ is 232±3 kcal/mole irrespective of the C_4H_8 structure, indicating that it is allyl ion. A second onset of $C_3H_5^+$ formation from methylcyclopropane and 2-methylpropene is interpreted as cyclopropyl ion formation with a substantial barrier. The absence of such processes for the other molecules suggests that at low energies carbon skeleton rearrangement, if any, should occur only by a head-to-tail cyclization mechanism.

INTRODUCTION

It is well known that the double bond in olefin cations migrates readily (1). This may proceed by hydrogen atom or hydride ion migration, and a typical sequence could be written as a 1-3 shift: $[CH_3\text{-}\overrightarrow{CH = CH}\text{-}CH_3]^+ \rightarrow [CH_2 = CH\text{-}CH_2\text{-}CH_3]^+$

While this rationalization could account for the similarity of the mass spectra of the linear butenes, it is inconsistent with the suggestion that fragmentation of 2-butene-$4d_3$ results in an essentially random distribution of labeled $C_3(H,D)_5$ ions (3,4).

While this problem can be studied by isotopic labelling, useful information can also be derived from appearance potentials and a consideration of the fragmentation energies of the six C_4H_8 isomers. Substantial differences in the structures of the precursors of fragmentation could make themselves apparent by variations in the heats of formation of product ions calculated from such data. It must be emphasized, however, that this and all other arguments based on fragment ions alone can only yield information on the excited precursors of the fragments.

The difficulty in the assessment of ionization and fragmentation thresholds is well known. Threshold behavior of complex molecules almost certainly deviates from linearity with excess electron energy. Contribution of vibrational excitation (5-7) and the possible applicability of a 1.127 power law (8-10) combine to make the expectation of a simple behavior unrealistic. Since the present argument depends on a reliable assessment of relative appearance potentials, all methods which do not give unique and unambiguous points at such energies must be suspect. Of the various means of assessing ionization onset by impact of electrons with thermal energy spread, the second differential ionization efficiency method of Morrison (11,12) is the only one which cannot be so criticized. While the argument of Morrison is based on a linear threshold law for single ionization, a maximum in the second derivative will also exist if the 1.127 power law holds.

EXPERIMENTAL

Materials: The butenes (Matheson & Co.) contained less than two percent impurities, mostly other structural isomers, normal and isobutane, and traces of butadiene. Methylcyclopropane (Chemical Procurement Laboratory) contained one percent n-butane, 1% one- or isobutylene, 0.4% ethylene, and 0.14% cyclopropane. Frinton Laboratories cyclobutane was purified to 99.9% by preparative Gas Chromatography.

Instrumentation: (Figure 1) A plastic junction box was inserted between the ion source and the power supply cable of an Atlas CH-4 mass spectrometer, and the filament power supply in the normal chassis of the instrument was isolated. Ionizing voltage was supplied from mercury batteries and a ten-turn 0.1% linear potentiometer. It was ganged with a second potentiometer using plastic gearing; the output of this potentiometer was employed to drive the x-axis of the Hewlett-Packard Model 2D3 x-y recorder. D.C. potentials in precisely reproducible multiples of .07V and the output from a Hewlett-Packard Model 3300A function generator could be superimposed on the ionizing voltage. The peak to peak modulation voltages at the filament were calibrated using a Tektronix Model 564 oscilloscope with 3A72 and 2B67 plug-in units while the high voltage was off. In early experiments the D.C. ionizing voltage was measured using a Leeds and Northrup K-3 potentiometer, and was calibrated against the x deflection of the x-y recorder again with the high voltage off. In later experiments, a Trimetrics digital voltmeter with .01% accuracy, powered from an isolation transformer, permitted ionizing voltage measurements during each run. The by-pass capacitor (5μF) between filament and high voltage ground reduced the 60 cycle noise to approximately 5-7 mV ptp. The modulation voltage between filament and box was independent of frequency between 40 Hz and 400Hz, dropping off by

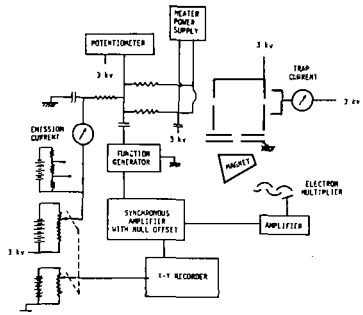

Figure 1: Schematic of circuits used for determination of second differential ionization currents

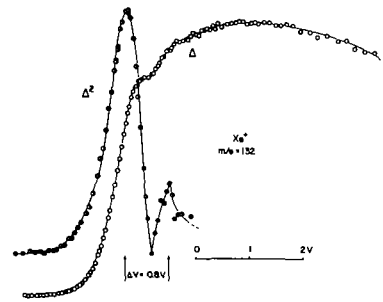

Figure 2: First and second differential ionization efficiency curves for xenon

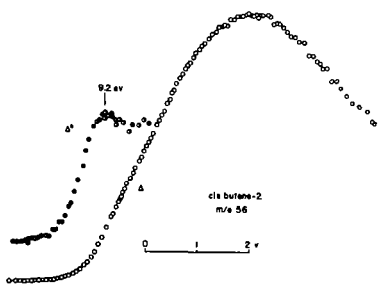

Figure 3: First and second differential ionization efficiencies for $C_4H_8^+$ from cis-butene-2

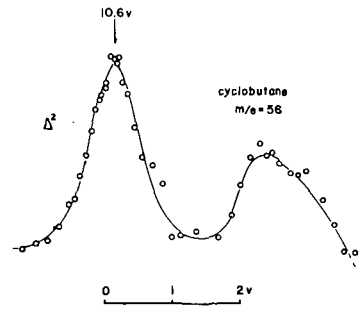

Figure 4: Second differential ionization efficiency of cyclobutane parent ion

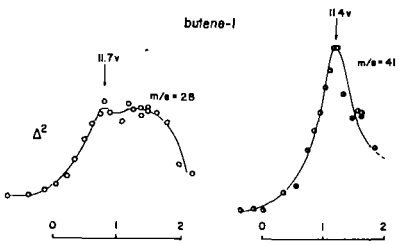

Figure 5: Second differential ionization efficiencies for $C_2H_4^+$ and $C_3H_5^+$ from butene-1

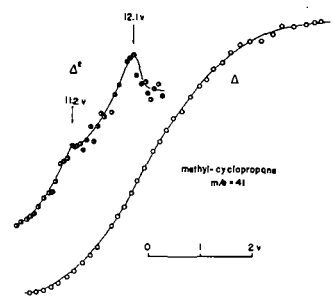

Figure 6: First and second differential ionization efficiencies for $C_3H_5^+$ from methylcyclopropane

10% at 10 Hz and 1.5 kHz respectively. Modulation voltage in all experiments was 0.08 volts peak to peak.

The filament shield was maintained at -.6V with respect to the filament, and the draw-out potentials were equally set at -0.6V each. The electron energy distribution was determined directly using a retarding potential on the electron collector and synchronous amplification of the modulated retarding potential (2kHz) as described for ion current detection below. The width at half-height of the Maxwellian - shaped distribution function was 0.6 eV.

The ion beam was defined by a 0.1 mm source slit and a 0.9 mm collector slit to obtain optimum peak flatness, a necessity since the A.C. resistance of the high voltage power supply is not negligible and a small amount of high voltage modulation is introduced.

The output of the electron multiplier went through one stage of amplification, and then to a Model 121 Princeton Applied Research Corporation lock-in amplifier. The reference A.C. signal for the synchronous amplifier was provided from the second output of the function generator.

First differential ionization efficiency curves were point-plotted directly. Second differential ionization efficiency curves were obtained by increasing the sensitivity of the lock-in amplifier by a factor of 10, and nulling the amplifier using zero offset. Ionizing voltage was then increased by 0.07 volts, and the increase in the differential current recorded. The step switch was then returned to the original position, the voltage increased and the procedure repeated.

RESULTS

The first and second differential ionization efficiency curves of xenon are shown in Figure 2. The maximum, corresponding to the first onset, is clearly defined and can be ascertained within $\pm$0.05 eV. The width at half-height is 0.68 eV; it is reproducible to within 5% in repetitive determinations and reflects primarily the electron energy distribution as expected. The energy span between the 25% height and the maximum height is 0.55 eV. A second peak is 0.8 $\pm$0.05eV above the lowest one. This separation is considerably less than the 1.31 eV difference between the ground state and the first excited state. It is probably best ascribed to autoionization and has been observed previously using second differential ionization (11), velocity selected beams (13), and the RPD technique (14). It was not observed by the energy distribution difference technique (15) as well as in a number of other investigations.

The ability to assess ionization potentials accurately was checked by obtaining the second differential ionization efficiency curve for krypton, which yielded a maximum at 14.05 $\pm$0.10 eV when xenon was used as the calibrating gas. This value is in good agreement with the spectroscopic ionization potential of 13.996 eV.

Representative second differential ionization efficiency curves for the parent ions of cyclobutane and cis-butene-2, and for fragment ions from butene-1 and methylcyclopropane are shown in Figures 3-6. The positions of the maxima or the onsets of plateaus are also summarized in Table I.

The following comments on the behavior of individual ions need to be added. Parent and fragment ions ($C_4H_8^+$, $C_3H_5^+$ and $C_2H_4^+$) of the 2-butenes did not show clear, well-defined "normal" maxima (Figure 3). Instead, relatively broad "plateaus" were observed. Such plateaus were also encountered for the $C_2H_4^+$ ions from all other isomers except that from cyclobutane, which showed fine structure with discernible peaks at 11.9 $\pm$ 0.15, 12.6 $\pm$ 0.1 and 13.0 $\pm$ 0.2 eV. "Normal" maxima were observed for all other parent ion peaks although cyclobutane showed a pronounced second maximum at 13.3 $\pm$ 0.2 eV (Figure 4). $C_3H_5^+$ ions were "normal" (Figure 5) except that from methyl cyclopropane (Figure 6), whose structure has a probable maximum at 11.2 $\pm$ 0.2 eV and an unmistakable one at 12.1 $\pm$ 0.1 eV. $C_3H_5^+$ from methylpropene has an uncertain second maximum at 12.5 $\pm$ 0.2 eV.

DISCUSSION

The maximum in the second differential ionization efficiency curves can often be ascertained easily, but many of the other ions such as the parent ions of the 2-butenes and essentially all $C_2H_4^+$ ions show broad plateaus. Dorman (16) suggested that in such cases one could not meaningfully assess the ionization threshold. While uncertainty is introduced by such irregular behavior, some confidence in the association of the onset of the plateau with the minimum energy required to form an ion can be derived from the shape of the low energy tail. When the xenon curve scaled to the assigned maximum is overlaid, the "tails" superimpose. On the basis of this argument we shall therefore take the maxima and plateau onsets as the minimum energies required to form a given ion, and the values summarized in Table I correspond to this interpretation. The agreement with values reported in the literature (16-21) is excellent where previous measurements are reliable.

The appearance potential data of Table I can be combined with the known heat of formation of ethylene (22) to obtain heats of formation of the $C_2H_4^+$ ion produced on fragmentation of the six isomers (Table II). $\Delta H_f(C_2H_4^+)$ calculated from the olefins is 258 kcal/mole, only slightly higher than the established value of 254 kcal/mole (23).

TABLE I

APPEARANCE POTENTIALS OF SOME MAJOR IONS FROM C_4H_8 ISOMERS (eV)

ION / ISOMER	$C_4H_8^+$		$C_3H_5^+$		$C_2H_4^+$	
	This investigation	Literature	This investigation	Literature	This investigation	Literature
Cyclobutane	10.6 ± 0.1	10.6[a]	11.2 ± 0.2	---	11.9 ± 0.15	---
Methylcyclopropane	10.2 ± 0.2	9.9[b]	11.2 ± 0.2	---	12.5 ± 0.2	---
Butene-1	9.6 ± 0.1	9.6[c]	11.4 ± 0.1	11.5[d,e]	11.7 ± 0.2	12.4[e]
Methylpropene	9.2 ± 0.08	9.2_3[c]	11.8 ± 0.2	11.4[f]	12.0 ± 0.2	12.2[f]
Cis-butene-2	9.0 ± 0.15	9.1_3[c]	11.6 ± 0.15	11.6[e]	11.7 ± 0.25	12.2[e]
Trans-butene-2	9.1 ± 0.15	9.1_3[c]	11.7 ± 0.15	11.8[f]	11.8 ± 0.25	---

a-ref. 18
b-ref. 19
c-ref. 17
d-ref. 16
e-ref. 20
f-ref. 21

TABLE II

HEATS OF FORMATION OF $C_3H_5^+$ AND $C_2H_4^+$ FRAGMENTS

C_4H_8	$\Delta H_f(C_3H_5^+)$ kcal/mole	$\Delta H_f(C_2H_4^+)$ kcal/mole
Cyclobutane	230 ± 5	267 ± 4
Methylcyclopropane	231 ± 5	280 ± 5
Butene-1	228 ± 2	257 ± 5
Methylpropene	234 ± 5	259 ± 5
Cis-butene-2	233 ± 3	257 ± 6
Trans-butene-2	235 ± 3	259 ± 6

Apparently there is little excess kinetic or electronic energy involved in the formation of this ion from the butenes. Considerably more energy is required, however, for the fragmentation of cyclobutane and methylcyclopropane ions to yield $C_2H_4^+$. This may indicate that a four-center dissociation is involved and that ring opening does not precede the fragmentation.

Similar calculations can be carried out for the formation of the $C_3H_5^+$ ion (Table II), yielding an average $\Delta H_f(C_3H_5^+)$ = 232 ± 3 kcal/mole. Near onset this ion is apparently produced with allylic structure from all isomers since $\Delta H_f(allyl^+)$ is probably 229 kcal/mole (23). The cyclopropyl structure, whose heat of formation is probably 239 kcal/mole (23), is clearly excluded since this value is well outside experimental error. These observations indicate that the ring opens in cycloalkanes. This was suggested previously after an examination of metastable peaks (24).

There is a pronounced second maximum in the curve for $C_3H_5^+$ from methylcyclopropane corresponding to a heat of formation of the ion of 252 kcal/mole. Similarly, there may be a barely discernible maximum when this ion is produced from 2-methylpropene, corresponding to $\Delta H_f(C_3H_5^+)$ = 250 kcal/mole. While this may simply be a result of excited allyl ion formation, it is more attractive to accept these two maxima as evidence for a common precursor with a cyclopropyl structure. Even then there must be a barrier to the dissociation, and these ions should be formed with equal excess energies. Alternately, this may also correspond to the formation of the cyclopropenyl ion in an excited state. In either case, a tertiary carbon structure would be required. Such a path and fragment ion structure are apparently not accessible to the linear alkenes and cyclobutane. This suggests that any skeletal rearrangement could proceed at low energies only through a head-to-tail (1 to 4) cyclization and ring opening.

ACKNOWLEDGEMENTS

This investigation was supported in part by the U.S. A.E.C. under Contract AT(40-1)-3606, and was made possible by the use of equipment obtained with a grant from the National Science Foundation. A more complete report will be published elsewhere.

LITERATURE CITED

1. K. Bieman, "Mass Spectrometry," McGraw Hill, New York (1962)
2. J. C. Lorquet, Bull. Soc. Roy. Sco. Liege, 5-6, 161 (1958); Catalog of Mass Spectral Data, API Project 44, Texas A & M University. College Station, Texas (1947-1961)
3. W. A. Bryce and P. Kebarle, Can. J. Chem. 34, 1249 (1956)
4. S. Meyerson, J. Chem. Phys. 34, 2046 (1961)
5. J. D. Morrison, J. Chem. Phys. 14, 1305 (1951)
6. W. A. Chupka, J. Chem. Phys. 30, 191 (1959)
7. E. Murad and M. G. Inghram, J. Chem. Phys. 40, 3263 (1964)
8. G. H. Wannier, Phys. Rev. 90, 807 (1953)
9. J. W. McGowan, M. A. Fineman, E. M. Clarke, H. P. Hanson, Phys. Rev. 167, 52 (1968)
10. C. E. Brion and G. E. Thomas, Internatl. J. Mass Spectry. Ion Phys., 1, 25 (1968)
11. J. D. Morrison, J. Chem. Phys. 21, 1767 (1953)
12. J. D. Morrison, J. Chem. Phys. 39, 300 (1963)
13. S. N. Foner and B. H. Nall, Phys. Rev. 122, 512 (1961)
14. C. E. Melton and W. H. Hamill, J. Chem. Phys. 41, 546 (1964)
15. R. E. Winter, J. H. Collins and W. L. Courchene, J. Chem. Phys. 45, 1931 (1966)
16. F. H. Dorman, J. Chem. Phys. 43, 3507 (1965)
17. K. Watanabe, T. Nakayama and J. Mottl, J. Quant. Spectry. Radiat. Transfer 2, 369 (1962)
18. R. F. Pottie, A. G. Harrison and F. P. Lossing, J. Am. Chem. Soc. 83, 3204 (1961)
19. F. H. Field, footnote in J. L. Franklin, J. Chem. Phys. 22, 1304 (1954)
20. I. Omura, Bull. Chem. Soc. Japan 35, 1845 (1962)
21. F. H. Field and J. L. Franklin, "Electron Impact Phenomena," Academic Press, New York (1957)
22. F. D. Rossini, D. D. Wagman, W. H. Evans, S. Levine and I. Jaffe, Natl. Bur. Stand. Circ. No. 500 (1952)
23. Critical Data Compilation on Mass Spectrometry; Data as of Jan. 1, 1967. Natl. Bureau of Standards, Washington, D.C.
24. P. Natalis, Bull. Soc. Roy. Sci. Liege 29, 94 (1960)

32. The Kinetic Energies of Some Penning Ions Produced on Impact with Metastable Helium and Neon*

K. D. Foster and E. E. Muschlitz, Jr.
Department of Chemistry, University of Florida, Gainesville, Florida 32601

Introduction

By obtaining information on the presence or absence of excess kinetic energy of ions and/or electrons[1] resulting from Penning and related ionization processes, e.g.

$$A^* + B \rightarrow A + B^+ + e \qquad (1)$$

it should be possible to gain insight into the states of the species involved and the nature of the energy transfer.

The present authors have attempted to investigate the kinetic energy of ions produced on impact of metastable He and Ne atoms with various target molecules, by a retarding potential technique.

Experimental

The apparatus consisted of three separately pumped chambers: the source region, the collision region and the mass analysis region. Beam definition by a capillary array and excitation by electron impact were achieved in the source region. In the collision region, the beam passed through an electric field of 8kV/cm, which served to remove charged species and quench possible highly excited states, before entering a collision box which contained some target gas. The bottom of the box (parallel to the beam) could be maintained at a positive or negative potential with respect to the top. The beam therefore entered along an equipotential plane, and the ions which were produced, could be accelerated toward, or retarded by, the top of the box (J_1). After passing through a slit in J_1 the ions were accelerated, focused and mass analyzed. The detection system was comprised of a secondary electron multiplier, a wide band amplifier, pulse shaper and counter. A printer, which provided automatic read out, was coupled to the counter.

Results and Discussion

Several systems have been studied. Among these are Ar^+ from He* + Ar, N_2^+ (He* + N_2), Ar^+ and $NeAr^+$ from Ne* + Ar. These ions have retarding curves which are almost superimposable and are therefore believed to be produced with thermal energies. The last ion will be recognized as an associative ion which accounts for about 20% of the total ionization in collisions of Ne* and Ar. The excess energy in the above reactions is presumably carried away by the electrons.

The ions H_2^+ and D_2^+, from the impact of He* on H_2 and D_2, appear to be formed with a slight excess of kinetic energy, although the curves almost coincide with the thermal ion curve at lower retarding potentials. H_2^+ has been reported previously by Penton and Muschlitz[2] to have excess kinetic energy on its formation. They explain the existance of excess K. E. in H_2^+ by a "curve-crossing" mechanism in which the H_2 is promoted to a preionizing state. The energy difference between the metastable He and this state is manifest as K. E. of separation of He and H_2*. The H_2* (which need only live for ca. 10^{-12} sec) may then undergo the following steps

$$H_2^* \rightarrow H^+ + e \qquad (2)$$

$$\rightarrow H + H \qquad (3)$$

Although it is not necessary to invoke a "curve-crossing" mechanism to explain the existance of excess K. E. in the product ion, it is a more logical explanation for the observed isotope effect in the Penning ionization cross sections of H_2, HD and D_2. Our retarding curves for H_2^+ and D_2^+ show H_2^+ to have the greater energy. This is to be expected if one considers the mass difference in the separation of the final products. However, there remain some unexplained features of the mechanism of this reaction.[3]

Retarding curves for the ions CH_4^+, CH_3^+ and CH_2^+ produced on impact of metastable He with CH_4 show these ions to be produced at essentially thermal energies, although the fragment ion may be slightly more energetic than the CH_4^+. The difference in the curves was slight such that it is difficult to tell if the fragment ions do in fact differ from the CH_4^+.

The impact of He* with O_2 yields retarding curves for O_2^+ and O^+ which show that these ions are unmistakably produced at higher than thermal energies. O_2^+ shows a dependence which is similar to that of H_2^+ while the curve for O^+ indicates that it has about twice as much kinetic energy as O_2^+. Our data on the oxygen system however do not enable one to distinguish between a "curve-crossing" type of mechanism and one in which

*To be submitted to J. Chem. Phys.

This research is supported by a grant from the National Science Foundation

a Franck-Condon transition occurs to a point on the He + O_2^+ interaction curve which is repulsive by approximately 1 eV. Measurements of the Penning Ionization electron energy spectrum would be helpful, if not definitive, in this regard.

The average retarding potential required to stop each ion (obtained by measuring the area under each retarding curve) is summarized in the following table.

Average Retarding Potentials $\bar{V}$ for Various Penning Ions

System	Product Ion	$\bar{V}$ (eV)
He* + Ar	Ar^+	
+ N_2	N_2^+	0.096
Ne* + Ar	Ar^+	
	$NeAr^+$	
He* + CH_4	CH_4^+	0.096
	CH_3^+	
	CH_2^+	
He* + H_2	H_2^+	0.13
+ D_2	D_2^+	0.12
He* + O_2	O_2^+	0.12
	O^+	0.23

References

1. V. Cermak, J. Chem. Phys., 44, 3781(1966).
2. E. E. Muschlitz, Jr., J. R. Penton and J. A. Herce, Abstract, 5th Int. Conf. on the Physics of Electronic and Atomic Collisions, p. 604, Nauka, Leningrad (1967).
3. Recently in this laboratory it has been found that HeH^+ is formed in the He* + H_2 system and accounts for ca. 6% of the total ionization.

33. COMPUTER CONTROL OF MASS ANALYZERS

W. E. Reynolds, J. C. Bridges, R. B. Tucker, and T. B. Coburn
Instrumentation Research Laboratory
Genetics Department, Stanford University School of Medicine
Palo Alto, California

ABSTRACT

Extending the use of digital computers from passive data collection to active control has increased the efficiency of computer-mass spectrometer systems. One such system devised, and described in this report, used a small digital computer and integer resolution (quadrupole and time-of-flight) mass spectrometers. The computer, by teletype, queries the user for operating parameters. The computer then translates these into detailed control functions that operate the instrument. Calibration is effected by the computer valving into the mass spectrometer a reference gas prior to introduction of the unknown sample. After calibration, the sample data acquired by the mass spectrometer is made available to the researcher in an on-line graphic system. Examples of processing GLC effluent are given. This work was sponsored in part by National Aeronautics and Space Administration Grant NsG 81 and Air Force Office of Scientific Research Grant AF 49(638)-1599.

INTRODUCTION

Some of the motivation for the work of this report has been the desire to utilize the decision making capabilities of a computer to direct the operations of certain instruments, primarily mass spectrometers. The system described uses a computer to perform a precalibration by the use of a reference gas and then to actively direct the mass spectrometer during data acquisition.

The computer used is a classic LINC, with 2K memory and a tape operating system. However we are shifting our computer interface to a time shared IBM 360/50 with a slave IBM 1800 to allow greater program flexibility. Also we are waiting until then to expand the present mass range of 1 to 256. Two sets of interfacing hardware have been built, and the system has been used on three integer-resolution mass spectrometers: a time-of-flight and two different quadrupole mass spectrometers.

Hence, this paper shall confine itself to describing the approach and system concept. The results from each of the mass spectrometers is actually shown.

It will be useful to establish a definition for a mass set voltage, Vc, the principal control voltage.

Most mass spectrometers that have an ion collector and electron multiplier to detect the ion signal, have some electronic control parameter, or have been adapted to have an electronic control parameter. This parameter is termed Vc in this report. As indicated in Figure 1, there is normally a provision to make Vc a linear or exponential function of time so that some interesting portions of the mass spectrum may be investigated. Often then the recorded output of the mass analyzer is interpreted by considering m/e to be a function of time. Such a recording is often referred to as a "scan". Actually m/e is a function of Vc and other parameters that have been kept constant.

If $m/e = F(Vc)$ then the inverse function $Vc = f(m/e)$ may be determined. To investigate the signal from m/e ions, a signal of Vc_1 may be applied to the mass analyzer and the relative abundance read at the output of the electron multiplier. A manual method of applying this is diagrammed in the center portion of Figure 1. This may seem a step backward in technology, but remember a computer is superb in doing routine repetitive operations.

So as shown in the lower portion of Figure 1, the computer may supply the control voltage, Vc_1, and read the signal resulting from the m/e_1 ions passed by the mass analyzer.

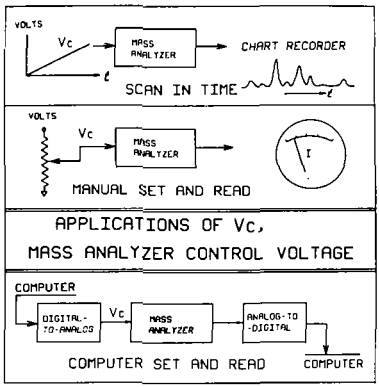

Figure 1

Applications of Vc, a mass analyzer control voltage.

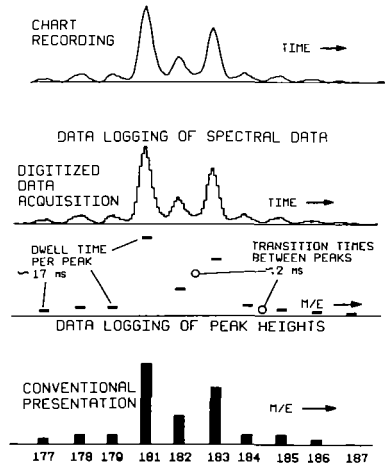

Figure 2

Evolutionary stages of data acquisition and presentation.

The rest of the report deals with the means and benefits of applying such signals Vc, to mass analyzer by computer logic. This is broad area and space will permit only the highlights of the systems concepts we have implemented or explored. Major points this report will cover are:

1. The applicability of this manner of control to various mass spectrometers.
2. The concept of reading a m/e signal amplitude rather than scanning.
3. A hardware implementation.
4. A software implementation.
5. Some results.

1. Different types of mass spectrometers.

Types of mass spectrometers suitable may be evaluated in terms of the character of Vc, the speed of response to Vc, the stability of the function in time, and the basic nature, linear, parabolic, exponential, etc.

Magnet controls by current has been judged to be rather slow for our purpose, time constants running in the order of 2 to 10 seconds. Other controls that do not have to change magnetic fields seem more amenable. Time constants of 0.1 to 2 milliseconds are readily obtainable.

The accelerating voltage of magnetic sector instruments would have good time response. The function of Vc to m/e, being a reciprocal function, does pose some problems. The distribution of peak positions with the accelerating voltage is very non-linear. To insure proper ion transmittance, digital-to-analog converters of very high precision are needed for accurate Vc generation.

Monopoles and Quadrupoles have a dc control voltage that control the amplitude of the ac/dc voltage ratio on the rod or rods. This is a linear function of m/e and most suitable. The time-of-flight mass spectrometer has a dc control voltage that controls the passage of the signal from ions of a specific m/e. In the time-of-flight the function is parabolic. We have implemented systems with both the quadrupole and time-of-flight type mass spectrometers.

The three dimensional mass spectrometer recently described by Dawson and Whetten should not be ignored. It has an interesting ion capture and holding property, and again a convenient dc control mode. And there are still other types that have some mode of Vc control.

Those that have dc voltage control are most easily amenable to computer control as high quality digital-to-analog converters are typically dc. And most such mass spectrometers have an easily identified connection point to apply the dc control voltage of proper polarity and range.

2. Some remarks about direct mass/charge (peak) measurements.

Typical conventional graphical recordings of mass spectrometer scans are similar to the portion shown at the top of Figure 2. If the continuium is sampled by a digital to analog converter for computer storage, the scan may be represented as in the next section. This is commonly done today; some thousands of data points are fed into a computer. A computer program then reduces this to a few hundreds of numbers, the amplitude of the integer m/e positions. Often this calls for rather sophisticated and fast computers. It is necessary to store or process in real time the thousands of sample points and have a rather extensive computer program to extract the values of the integer m/e positions, the basic data expected of a low resolution mass spectrometer. It might be argued that there is a lot of data taken that has a very low information content.

Area is sometimes taken as the amplitude. However for most purposes the simple peak heights are sufficiently representative of peak amplitude. Again in Figure 2, the digital measurement corresponding to the center of each peak is accentuated. This peak representation of amplitude is especially true if the peak shapes are uniform or known and/or the aperture (that affects mass spectrometer resolution) is broad enough.

Therefore, assuming that the integer m/e position can be forecast only the sample at that position need to be taken. This suggested by the next portion of Figure 2. With computer control, just that can be done. The intervening measurements need not be taken and no time is wasted on data of such low information content.

Actually such prediction is possible. Typical control times that we have achieved run about 2 milliseconds between any two samples and about 7 to 17 milliseconds upon a sample point. Each sampled point is at a specific m/e position and may be taken in any order the computer programmer desires.

We find best results if the aperture of the mass analyzer is broadened. This lowers the resolution. However, 10% valley criteria is meaningless as such. The only meaningful criteria is non-contribution to neighboring m/e positions.

Another benefit is the ability to use wide-band, electronically resetable, full integrators on the m/e signal instead of conventional RC bandpass amplifiers. These three factors: wide aperture, dwell time, and full integration, can be shown to effect a gain of about 13 in signal to noise ratio in comparable instances.

Such single data point logging is most modest in requirement of storage area in the computer and of speed necessary for analog-to-digital conversion. The data may be presented to the researcher as in the bottom portion of Figure 2, or in another manner, or just held in a computer file or tape for further logical analysis.

3. Hardware configuration.

The system hardware requirements may be divided into two portions, the source inlets and the electronics interface.

First the source system. The only thing unusual here is that we have fitted the gas inlet system with electro-pneumatic valves to enable their operation by computer control. The valves are ones of our own design and allow bake out to 225°C. On each of the three mass spectrometers we have instrumented, we have installed a reference gas system using FC-43, a reference widely used in mass spectroscopy. The valving of this into the mass analyzer is, as we shall see, a function of a control register driven by the computer. The reference gas is normally valved in, a calibration to the known peaks is made, and the gas pumped out before the unknown sample is introduced. Interpolation is used to locate all other integer m/e positions.

On two of the systems we have installed GLC inlets. It was found desirable in this case to provide for computer operated valves to keep these systems closed off from the mass spectrometer while the solvent peak was coming through the GLC.

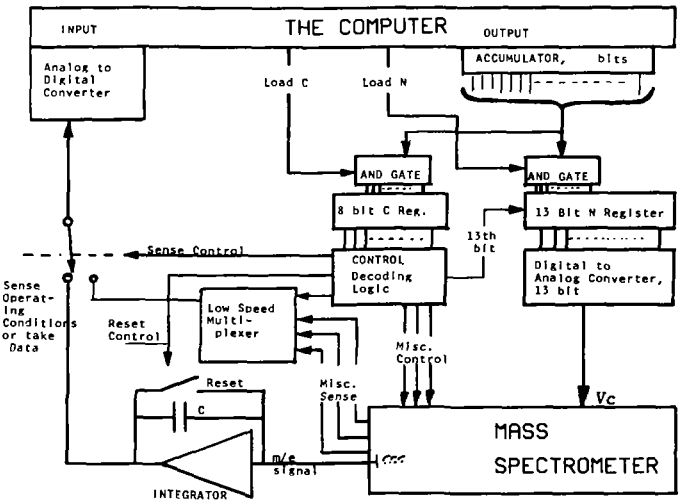

Figure 3

A block diagram of the interfacing electronics is shown in Figure 3. It includes two registers, an N register and a C register to hold command words from the computer. These are loaded by putting the predetermined word (number) into the accumulator and executing a load command, a pulse out on the N or C line. This causes the word to be passed and held in the appropriate register.

The N register directly drives the D to A converter that generates the control voltage Vc. Hence the "N" number sets the mass analyzer to pass a desired specie of ions.

The C register is a general purpose control register. We are using 8 bits that can be decoded into 128 functions. Actually, to simplify logic, we have provided for the use of only about 32. These control the gas inlet to the mass analyzer and some spectral display modes. There are relays which may be used for other desired function. We do anticipate the use of stepping motors to control key potentiometers.

There is relay multiplexing of analog signals to enable sensing of general operating parameters of the mass spectrometer. All these and the reset to the integrator are controlled from the C register.

The input to the computer must respond to program control, internally or externally causing an analog to digital conversion to be made.

We intend to experiment with dynamic control of various operating parameters such as ion energy, trap current, sample temperature, and sensitivity resolution settings.

4. The software.

It is the computer programming that makes a system out of what we have discussed. There are enumerable computer logic approaches to intelligently use the mass analyzer and control options outlined. A very fine exposure of this concept is made by R. J. Spinard in an October 1967 issue of Science magazine.

The following are the elements of such an interaction.

a. The computer is to accept Macro Commands from the user.

b. The computer is to generate the necessary Control Parameters.

c. These Control Parameters set the operating conditions of the Mass Spectrometer.

d. Spectral data is passed back to the computer.

e. And the computer should process this and present back an intelligent digest of the data.

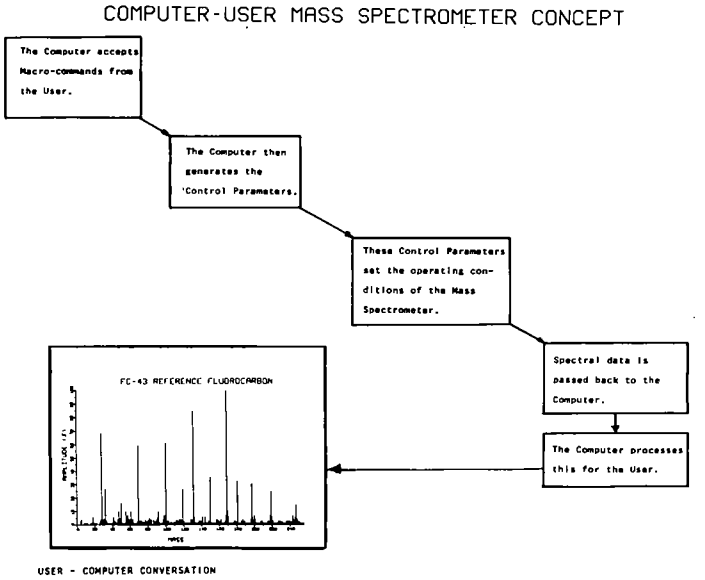

USER - COMPUTER CONVERSATION

```
SPECTRUM
GAS;*

REFERENCE GAS IS OFF
DO YOU WANT IT ON YES;
WAIT 15 SECS.

SPECTRUM
TAKE ONE;

TAKE ONE
T=2;
FILE NAME = MASS;
FILE # 2;
RETAKE? NO;

*Underlined items are User
  responses.
 Everything else is Computer
  prompting.
```

```
SPECTRUM
PLOT;

NAME; REFERENCE GAS CHECK;
FILE #S; 2;
J TO K BY T.
J= 10;
K= 650;
T= 1;
X DIMEN.= 10;
Y DIMEN.= 5;
BAR GRAPH? YES;

SPECTRUM
GAS;

REFERENCE GAS IS ON
DO YOU WANT IT OFF YES;
WAIT 15 SECS.
```

Figure 4

The logic concept of user-computer interaction and an example of user computer dialogue.

Figure 4 diagrams the concept and gives an example of user-computer conversation in our system. Presumably the suer wised to take a spectrum of the FC-43 reference gas to assure himself that everything was working. He has called and used three programs, one twice. There are about 15 such programs available, as will be shown later.

The user-computer conversation is shown at the bottom of Figure 4. The teletype and digital plotter are adjacent to the mass spectrometer. Hence this all transpired in the laboratory and took less than 10 minutes from valving in gas, giving parameters to the computer and receiving this plotted output.

The 15 odd programs in this realization are held in a monitor program called "SPECTRUM". Figure 5 helps diagram their functions. They may be divided into 4 classes. The top are the calibration group. Their general function is to allow the user to form and verify a correct "N" table. "GAS" controls the inlet valve for the reference gas. "LOCATE" is an initialization routine. "DISPLAY" and "MEASURE" will give detailed spectral information on a CRT or teletype, respectively. "TRACE" does a similar function on a digital plotter. "ALICE" is primarily to provide data dumps to a time shared 360/50. This has provided a data base for further program development.

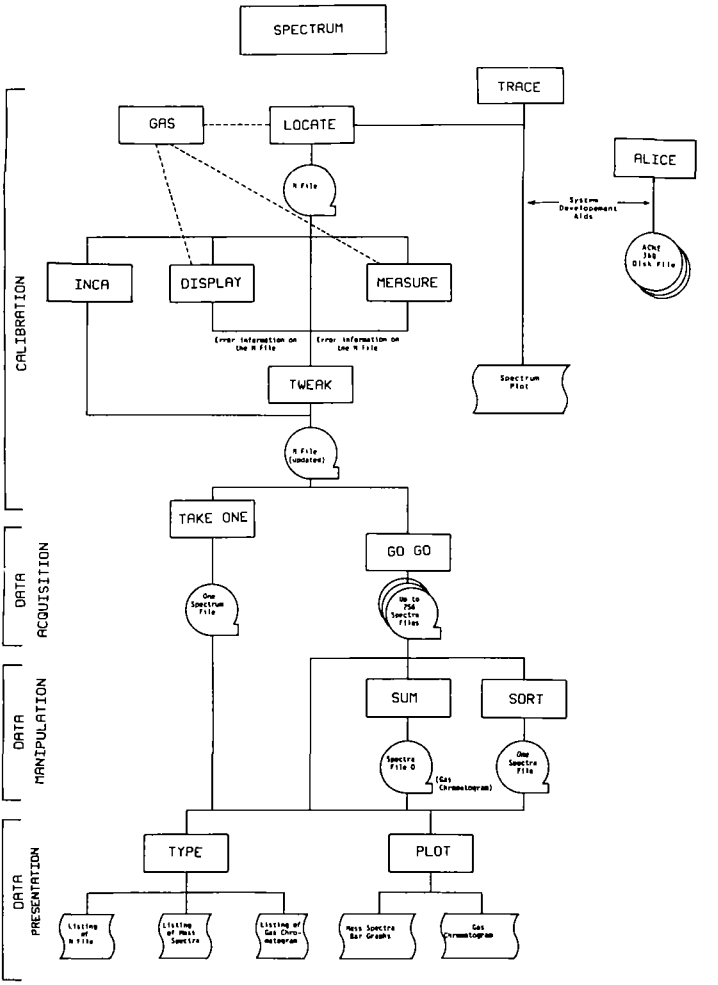

Figure 5. The software organization for system control.

"TWEAK" is a manual method of performing minor corrections to an "N" table from errors determiend by reference gas measurements. "INCA" is our latest addition and provides nearly automatic recalibration. "INCA" searches for and locates peaks in the reference gas, compares the found "N" position with that of a stored table, and makes such interpolation and corrections as necessary.

Figure 6 illustrates the type of work that can be done with four of these programs. These do not, repeat do not, result in stored spectral data as such.

Next, back in Figure 5, in the Data Acquisition section, are shown "TAKE ONE" and "GO GO". The first is for single spectra, such as may be obtained from solid samples. The later takes and stores a series (one about each 5 seconds) of spectra during a GLC run. These two programs, the ones that do useful work are perhapsthe simplest.

Last in Figure 5 are shown the Data Manipulation and Data Presentation groups. Some examples of their use is shown beginning with Figure 7. All results and usages are on-line, and at the site of the mass spectrometer. The computer is a few floors removed, but that is of little consequence. Figure 7 shows the result of a spectral run on a solid sample. The program for these plots asks and prompts the user to furnish the title and size. All other anotations and scalings are done by the program.

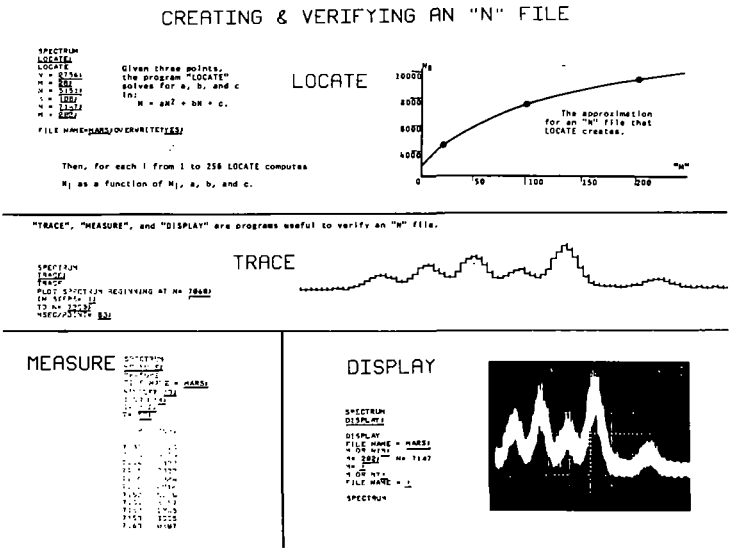

Figure 6. Examples of the calibration group.

We do get many questions from interested researchers that which to know what these programs can do. But the important thing is to realize what programs can be included. There is capability to store literally hundreds of programs to exploit the inherent capability of the hardware. All that has to be done is to write that program in machine language and give it an unique name so that it may be called when desired. This may be something of a task, but is no severe limitation. "INCA", as pointed out, is a late addition.

During a GLC run, "GO GO" took a series of spectra equally spaced in time. These individual spectra, about 217 in Figure 8, may be individually summed for a representation of total ions vs time. Actually the axis is numbered in spectrum indices. Any individual spectrum is available. In this case let us investigate the 6th major GLC peak at the 156th spectrum.

Figure 9 is a spectrum taken at the time of that GLC peak, hence of that faction.

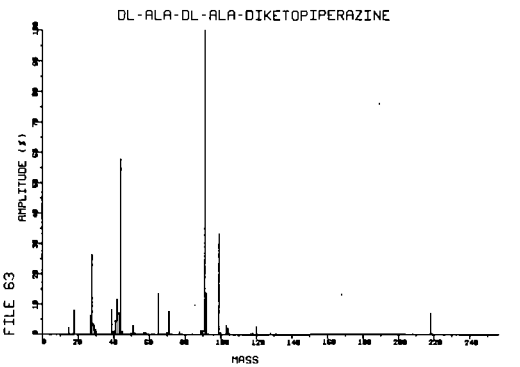

Figure 7. A spectrum from a solid sample.

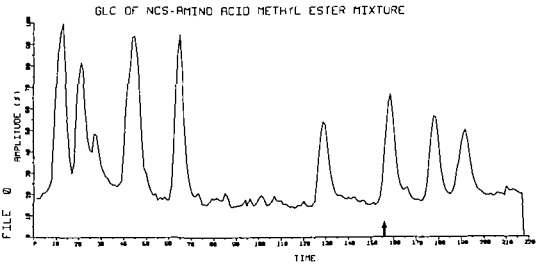

Figure 8. A summed ion plot from a GLC run.

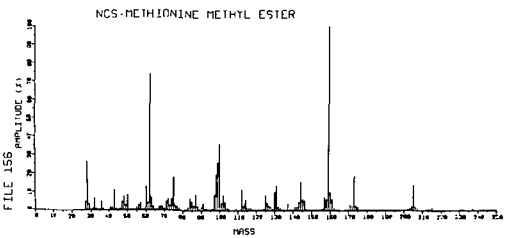

Figure 9. The 156th spectrum indexed in Figure 8.

CONCLUSION

The system described does give a laboratory researcher a highly efficient data acquisition and presentation system that is both economical of the researcher's time and computer requirements.

It is also felt that the concept of this system, precalibration and computer control of the mass analyzer and other parameters offers a fruitful development area for mass spectrometer instrumentation. This may be particularly so in development of remote instruments where the user, because of convenience, hazardous conditions, or space explorations, cannot personally operate the knobs.

REFERENCES

1. P. H. Dawson and N. R. Whetten, "Ion storage in 3-dimensional rotationally symmetric quadrupole fields", J. Vac. Sci. T. 5, 1, 1968.

2. R. J. Spinard, "Automation in the laboratory", Science 158 (3797), 55, 1967.

3. R. A. Hites and K. Biemann. "Computer recording and processing of low resolution mass spectra", International Mass Spectrometry Conference, Berlin, Sept. 1967.

4. W. E. Reynolds, J. Bridges and T. Coburn, "A computer operated mass spectrometer", Genetics Dept., Instrum. Research Lab. Technical Report IRL 1062.

5. C. A. McDowell, Ed., Mass Spectrometry, McGraw-Hill, New York, 1963.

6. B. Halpern, J. W. Westley, E. C. Levinthal, and J. Lederberg, "The Pasteur Probe: An Assay for Molecular Asymmetry", Life Sciences and Space Research IV, M. Florkin and A. Dollfus, Eds., p. 239-249, North-Holland, Amsterdam, 1967.

7. B. Halpern, J. W. Westley, I. von Wredenhagen, and J. Lederberg, "Optical Resolution of DL amino acids by gas chromatography and mass spectrometry", Biochem. Biophys. Res. Comm., 20, 710, 1965.

8. H. L. Friedman, H. W. Goldstein and G. A. Griffith, "Mass spectrometric thermal analysis of polymer decomposition products", Conference Proceedings of Fifteenth Annual Conference on Mass Spectrometry and Allied Topics, ASTM Committee E-14, Denver, Colorado, May 1967.

34. COMPUTER AIDED MASS DETERMINATION USING A SINGLE FOCUSING MASS SPECTROMETER

C.Brunnée, K.Habfast, U.Markwardt, S.U.Meier, and E.Wegner
VARIAN MAT GmbH, Bremen, Germany

Abstract

With a single focusing mass spectrometer of medium size (VARIAN MAT model CH5, deflection radius 20 cm, deflection angle 90°, ion accelerating potential 3 kV), mass determinations have been performed at a resolution between 2,500 and 10,000 (10% valley). The following techniques were used: 1) tuning the instrument to one or the other mass peak by manual alteration of the ion accelerating potential, 2) measuring the peak distances on the strip chart of an x-y-recorder, 3) digitizing the peaks at a sampling rate of 3 kHz and processing the data off-line with a computer. The accuracy obtained was better than 10 ppm in most cases. The possible influence of initial ion energies on the results is discussed.

The resolving power $m/\Delta m$ of a single focusing sector field mass spectrometer is determined by the dispersion K (i.e. mainly by the radius of magnetic deflection), further by the magnification G, the slit widths s_e and s_a, the initial energy spread $\Delta U/U$ of the ions, and the image errors ΔB, according to the following equation

$$\frac{m}{\Delta m} = \frac{K}{2(s_e G + s_a) + \frac{\Delta U}{U} K + 2\Delta B}$$

Since the slit widths s_e, s_a and the image errors ΔB can be made sufficiently small, $m/\Delta m$ is practically limited by the energy spread $\Delta U/U$ only. Thus ΔU has to be kept as small as possible to obtain maximum resolution.

ΔU consists 1) of the initial thermal energy spread, 2) of the energy distribution which fragment ions may obtain during the ionization process, 3) of the energy spread resulting from the fact that ion formation occurs not at a point but within a somewhat extended region of the electric field produced by the weak draw-out or pusher potential.

The thermal energy of molecular ions is smaller than 0.1 eV; the initial energy of fragment ions is in the same order of magnitude, provided that the fragments are not too small. The ion energy width caused by the extraction- and pusher-field can be reduced to a few tenths of an eV or less if a well defined electron beam is obtained, and a homogeneous and relatively weak electric field is produced in the ionization region. These three causes of energy spread combine to a ΔU between 0.1 and 0.3 eV, which yields a maximum theoretical resolving power of 10,000 or more for an ion accelerating potential of a few thousand volts.

We have studied these problems experimentally in some detail to determine whether a single focusing instrument of medium size can be used for precise mass determinations and for studies of initial ion energies. It turned out that after careful alignment of the slits and the magnetic field, and by using an ion source with a well-defined electron beam, a resolution approaching the theoretical limit as stated above can be obtained. The instrument used was a standard CH5 mass spectrometer (VARIAN MAT, Bremen) with a magnetic deflection radius of 20 cm and an ion accelerating potential of 3 kV.

Fig.1 shows the CO/N_2-dublet, recorded with this instrument. The measured resolution is about 10,000 (10% valley) which is equivalent to about 25,000 (50% peak width).

The instrumental sensitivity can be estimated from fig.2: at a resolution of about 4,000 (10% valley), the partial pressure sensitivity for atmospheric argon is approx. 2×10^{-6} A/torr (collector current/pressure in the ion source). The limit of detection at this resolution is still below 0.3 ppm.

In fig.3 the M^+ and the $(M-18)^+$ peak region of cholesterol is shown. By comparing the position of these peaks with those of reference peaks, their

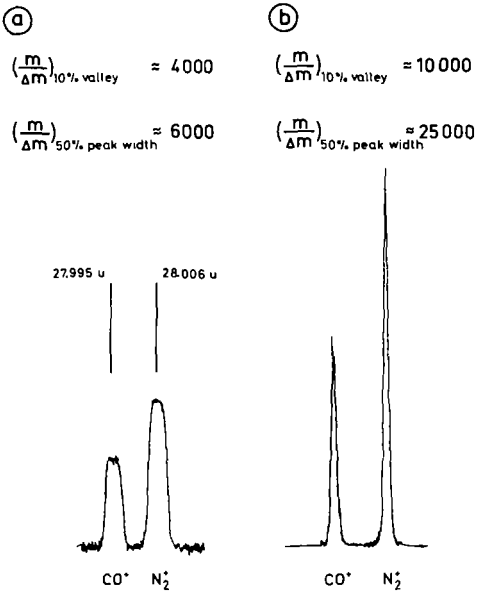

Fig. 1 Resolving power of the CH 5. Peaks recorded with a) Faraday collector, b) secondary electron multiplier

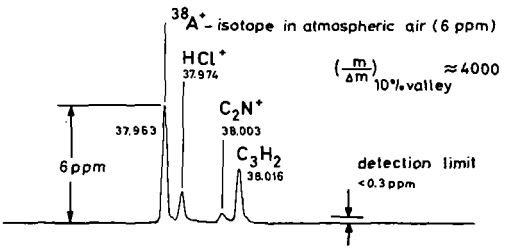

Fig. 2 ^{38}Ar isotope in atmospheric air, plus background. The detection limit at a resolution of 4000 is below 0.3 ppm.

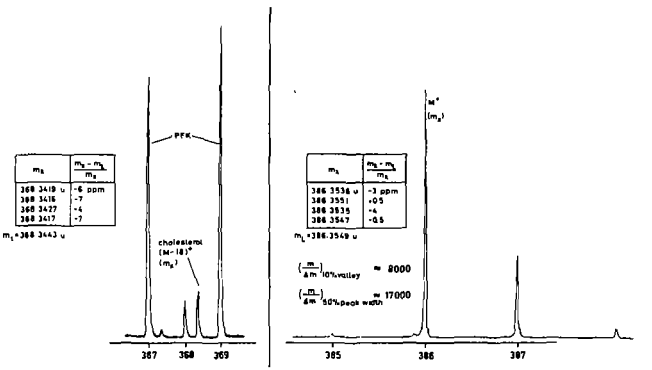

Fig. 3 Mass spectrum of cholesterol in the M^+ and $(M-18)^+$ peak region. Mass determination performed by manually changing the accelerating voltage.

$(\frac{m}{\Delta m})_{10\%\text{valley}} = 10\,000$	$m_x = m_1 + \frac{l_{1x}}{l_{13}}(m_3 - m_1)$
$(\frac{m}{\Delta m})_{50\%\text{peak width}} = 25\,000$	$m_x = 386.3533$ u $m_L = 386.3548$ u error -4 ppm

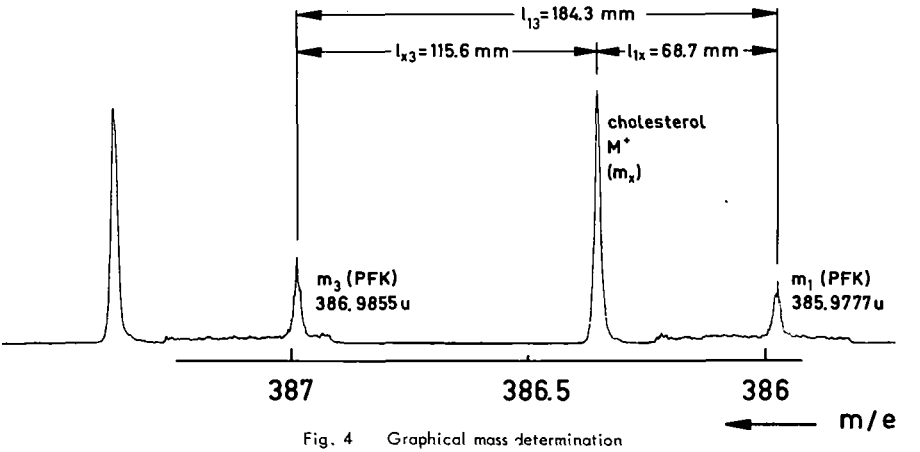

Fig. 4 Graphical mass determination

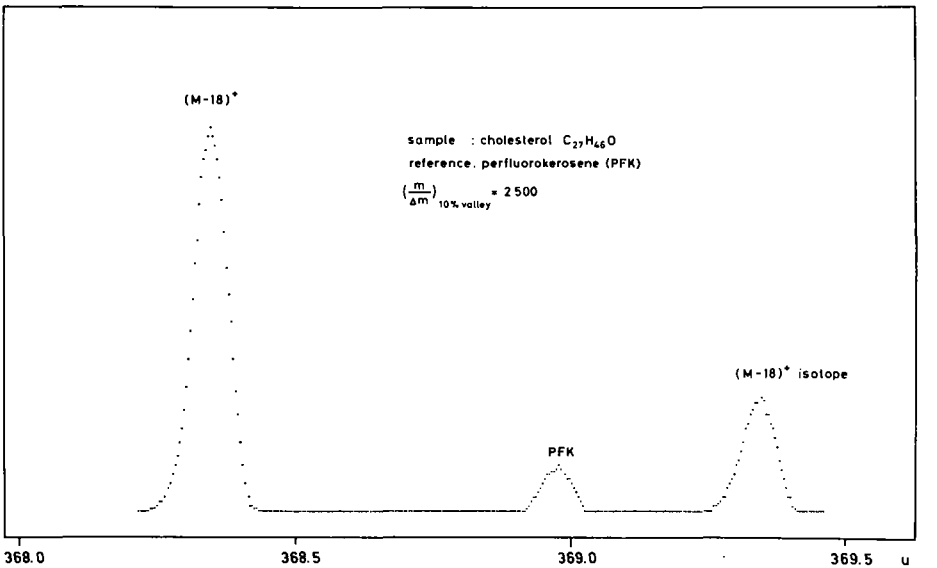

Fig. 5 Replot of digitized peaks

ⓐ

```
VARIAN MAT BREMEN / 10.04.68 / SPEKTRUM 29313

AUSGLEICHSPOLYNOM  GRAD  3 DURCH   7 MESSPUNKTE IM DIAGRAMM ZEITTAKT UEBER LOGARITHMEN DER MASSEN

KOEFFIZIENTEN   -5.15E 02    8.17E 02    9.99E 04    -4.73E 05

        MASSE       TAKT      INT              ABWEICHUNG
   210.234740    5484.86      52  0      .0022 U       .68 TAKTE     C15 H30
   211.242562    5791.26     108  0     -0.0031 U     -0.93 TAKTE     C15 H31
   212.245917    6097.31      17  0      .0009 U       .27 TAKTE     ISOTOPE
   218.985645    8099.59     227  1     -0.0006 U     -0.17 TAKTE     C4 F9
   219.989000    8391.49       9  0      .0003 U       .09 TAKTE     ISOTOPE
   224.250389    9611.65      46  0     -0.0011 U     -0.31 TAKTE     C16 H32
   225.258211    9895.80     105  0     -0.0022 U     -0.63 TAKTE     C16 H33
   226.261566   10178.92      17  0      .0030 U       .84 TAKTE     ISOTOPE
```

"unknown" (- 3 ppm)

ⓑ

```
AUSGLEICHSPOLYNOM  GRAD  3 DURCH   6 MESSPUNKTE IM DIAGRAMM ZEITTAKT UEBER LOGARITHMEN DER MASSEN

KOEFFIZIENTEN   -6.05E 02    9.08E 02    1.07E 05    -4.99E 05

        MASSE       TAKT      INT              ABWEICHUNG
   210.234740    5656.41      53       .0029 U       .88 TAKTE     C15 H30
   211.242562    5963.07     111      -0.0033 U     -0.99 TAKTE     C15 H31
   212.245917    6269.63      16       .0009 U       .26 TAKTE     ISOTOPE
   218.985645    8271.97     228  1    -0.0055 U     -1.61 TAKTE     C4 F9
   224.250389    9784.16      46      -0.0034 U     -0.97 TAKTE     C16 H32
   225.258211   10068.42     104      -0.0031 U     -0.89 TAKTE     C16 H33
   226.261566   10352.32      17       .0062 U      1.71 TAKTE     ISOTOPE
```

"unknown" (- 20 ppm)

Fig. 6 Computer printout from a single scan. Sample: pentacosane $C_{25}H_{52}$ plus perfluorotributylamine $(C_4F_9)_3N$. Determination of the mass of the $C_4F_9^+$ fragment. (MASSE ≙ literature mass values, INT ≙ peak heights, TAKT ≙ counts of the timing signal, ABWEICHUNG U ≙ deviation of the peak centroids from the mass values given by the polynomial).

```
VARIAN MAT BREMEN / 30.04.68 / SPEKTRUM 29306
EIN DIAG.ELEM. IN CHOLSYM WIRD = 2.47052942E-02
EIN DIAG.ELEM. IN CHOLSYM WIRD = 1.56250000E-02
EIN DIAG.ELEM. IN CHOLSYM WIRD = 6.10351563E-05

AUSGLEICHSPOLYNOM GRAD 4 DURCH  6 MESSPUNKTE, ZEITTAKT UEBER LOGARITHMEN DER MASSEN

KOEFFIZIENTEN   -5.5418708258E 01  4.1485801666E 02   7.1391183482E 01   8.0395170506E 04   -4.4763516573E 05

        MASSE       TAKT      INT              ABWEICHUNG
   266.297337   21919.44      52       .0009 U       .27 TAKTE     C19 H38
   267.305159   22225.69     155      -0.0030 U     -0.91 TAKTE     C19 H39
   268.308514   22532.11      30       .0023 U       .69 TAKTE     ISOTOPE
   270.255864   23120.31      37  1    .0026 U       .78 TAKTE     C17 H34 O2
   280.312986   26085.62      44       .0006 U       .17 TAKTE     C20 H40
   281.320808   26375.72     144      -0.0019 U     -0.56 TAKTE     C20 H41
   282.324163   26665.05      29       .0012 U       .35 TAKTE     ISOTOPE

STANDARDABWEICHUNG                     .0020 U       .59 TAKTE
```

"unknown" (+ 10 ppm)

Fig. 7 Computer printout from a single scan. Sample: pentacosane $C_{25}H_{52}$ plus methylpalmitate $C_{15}H_{31}COOCH_3$.

```
VARIAN MAT BREMEN / 30.04.68 / SPEKTRUM 29306
EIN DIAG.ELEM. IN CHOLSYM WIRD = 3.398213OOE-01
EIN DIAG.ELEM. IN CHOLSYM WIRD = 4.133986 42E-02
EIN DIAG.ELEM. IN CHOLSYM WIRD = 3.82732772E-02

AUSGLEICHSPOLYNOM GRAD  4 DURCH   8 MESSPUNKTE, ZEITTAKT UEBER LOGARITHMEN DER MASSEN

KOEFFIZIENTEN     3.1572257635E-02    1.9791909058E 02   -4.6770296434E 03   1.1474428279E 05   -5.0627433978E 05

        MASSE          TAKT     INT              ABWEICHUNG

   294.328635       30035.71      40          .0008 U        .21 TAKTE      C21 H42
   295.336457       30311.19     131         -0.0024 U      -0.66 TAKTE      C21 H43
   296.339812       30586.35      29          .0013 U        .34 TAKTE      ISOTOPE
   308.344285       33794.09      21          .0007 U        .19 TAKTE      C27 H44 * "unknown" (-7 ppm)
   309.352107       34056.78      88  1      -0.0021 U      -0.56 TAKTE      C22 H45
   310.355462       34318.71      19         -0.0001 U      -0.02 TAKTE      ISOTOPE
   322.359234       37380.58      12          .0019 U        .47 TAKTE      C23 H46
   323.367756       37631.34      57         -0.0025 U      -0.61 TAKTE      C23 H47
   324.371111       37881.78      13          .0003 U        .08 TAKTE      ISOTOPE

STANDARDABWEICHUNG                            .0016 U        .41 TAKTE
```

```
VARIAN MAT BREMEN / 03.04.68 / SPEKTRUM 29307
EIN DIAG.ELEM. IN CHOLSYM WIRD = 3.398312OOE-01
EIN DIAG.ELEM. IN CHOLSYM WIRD = 4.133986 42E-02
EIN DIAG.ELEM. IN CHOLSYM WIRD = 3.82732772E-02

AUSGLEICHSPOLYNOM GRAD  4 DURCH   8 MESSPUNKTE, ZEITTAKT UEBER LOGARITHMEN DER MASSEN

KOEFFIZIENTEN    -1.7184285028E-01    1.9792869745E 02   -4.5956818669E 03   1.1407174775E 05   -5.0636113519E 05

        MASSE          TAKT     INT              ABWEICHUNG

   294.328635       29770.37      38          .0002 U        .06 TAKTE      C21 H42
   295.336457       30046.18     136         -0.0022 U      -0.60 TAKTE      C21 H43
   296.339812       30321.48      30          .0015 U        .42 TAKTE      ISOTOPE
   308.344285       33530.72      21          .0014 U        .38 TAKTE      C22 H44
   309.352107       33793.11      93  1      -0.0030 U      -0.78 TAKTE      C22 H45 * "unknown" (-10 ppm)
   310.355462       34055.26      19         -0.0005 U      -0.13 TAKTE      ISOTOPE
   322.359234       37118.01      12         -0.0002 U      -0.06 TAKTE      C23 H46
   323.367756       37369.54      54         -0.0019 U      -0.48 TAKTE      C23 H47
   324.371111       37620.27      13          .0016 U        .40 TAKTE      ISOTOPE

STANDARDABWEICHUNG                            .0017 U        .43 TAKTE
```

```
VARIAN MAT BREMEN / 30.04.68 / SPEKTRUM 29308
EIN DIAG.ELEM. IN CHOLSYM WIRD = 3.398213OOE-01
EIN DIAG.ELEM. IN CHOLSYM WIRD = 4.133986 42E-02
EIN DIAG.ELEM. IN CHOLSYM WIRD = 3.82732772E-02

AUSGLEICHSPOLYNOM GRAD  4 DURCH   8 MESSPUNKTE, ZEITTAKT UEBER LOGARITHMEN DER MASSEN

KOEFFIZIENTEN     1.0037082108E-01    2.1885128190E 02   -5.1267305069E 03   1.1790233122E 05   -5.1482551016E 05

        MASSE          TAKT     INT              ABWEICHUNG

   294.328635       30048.63      40          .0016 U        .43 TAKTE      C21 H42
   295.336457       30324.19     136         -0.0020 U      -0.56 TAKTE      C21 H43
   296.339812       30599.04      29         -0.0002 U      -0.05 TAKTE      ISOTOPE
   308.344285       33809.17      21          .0006 U        .15 TAKTE      C22 H44
   309.352107       34071.93      90  1      -0.0024 U      -0.62 TAKTE      C22 H45 * "unknown" (-8 ppm)
   310.355462       34334.26      20          .0007 U        .18 TAKTE      ISOTOPE
   322.359234       37397.18      11          .0011 U        .26 TAKTE      C23 H46
   323.367756       37648.21      56         -0.0026 U      -0.65 TAKTE      C23 H47
   324.371111       37898.95      13          .0010 U        .24 TAKTE      ISOTOPE

STANDARDABWEICHUNG                            .0016 U        .41 TAKTE
```

Fig. 8 Computer printout from three subsequent scans. Sample: pentacosane $C_{25}H_{52}$.

CO^+ FROM CO

m_x	$\frac{m_x - m_L}{m_x}$
27 99494 u	+ 0.7 ppm
27.99508	+ 6
27 99479	- 5
27.99500	+ 3
27 99495 u	+ 1 ppm

CO^+ FROM CO_2

m_x	$\frac{m_x - m_L}{m_x}$
27.99476 u	- 6 ppm
27.99477	- 5
27.99493	+ 0.4
27.99506	+ 5
27.99488 u	- 1 ppm

(REFERENCE PEAKS: N_2^+, $C_2H_4^+$)

m_L = 27 99492 u

Fig. 9 Mass determination of CO^+ (manual change of ion accelerating potential).

accurate masses can be determined, for instance, by using the peak-matching method. Ryhage recently reported on such measurements performed with a single focusing instrument [1]. For our measurements, we have used some other techniques. The first was very simple: the spectrometer was alternately set to one or the other peak maximum by manually changing the ion accelerating potential. The mass values resulting from the indicated voltage differences - average values from 6 such individual determinations - are given in the figure. The max. deviation is 7 ppm.

Graphical interpolation of reference peaks on the strip chart record is another technique. Fig.4 shows this procedure: voltage scanning and plotting with an x-y-recorder have been employed to obtain a linear mass scale. The accuracy in this case is 4 ppm.

Comparable results were obtained by computer-aided mass determination. This technique is well established [2 - 6] but to our knowledge has not been used in connection with single focusing instruments. At a resolution between 2,500 and 4,000, a scanning time of 80 seconds per mass decade was chosen. The spectra were scanned exponentially, taking 25 to 50 samples per peak. The following instrumental setup has been used (DATAMASS N, VARIAN MAT): sample-and-hold amplifier (sampling rate 3 kHz) - A/D converter - magnetic core for formating - AMPEX TM7 magnetic tape recorder. The digitized data were processed off-line with a CDC 3200-computer. A replot of some digitized peaks is shown in fig.5. Peak positions were determined by calculating the centroids of the profiles. The mass scale was obtained in the usual way by fitting a polynomial to a few reference masses.

The results of mass determinations of the "unknown" fragment peak $C_4F_9^+$ from perfluorotributylamine at mass number 219 is shown in the computer printout fig.6. Reference sample was pentacosane. Errors: a) 3 ppm when using the isotope peak from $C_4F_9^+$ as an additional "known" reference peak and b) 20 ppm when using the $C_nH_m^+$-peaks from pentacosane as reference only, thus interpolating between peaks of 12 mass units difference.

Another example is given in fig.7. The molecular peak $C_{17}H_{34}O_2^+$ of methylpalmitate was considered "unknown". Error: 10 ppm when using the pentacosane peaks as reference only.

The reproducibility of mass determinations from three subsequent scans can be seen from the chart fig.8. The fragment $C_{22}H_{45}^+$ in the mass spectrum of pentacosane was considered "unknown". The errors are 7, 8 and 10 ppm. For three scans, the corresponding deviations of the 3 x 9 peak centroids from the values given by the polynomials are within about 1 mmu, or 3 ppm.

The question arises whether the initial energy of fragment ions will affect the accuracy of mass determination performed with a single focusing instrument. Theoretically, for a 3 kV ion accelerating potential, an increase of 0.03 eV of the ion energy will change the mass scale by 10 ppm. In practice we could not yet detect such changes, not even in the case of relatively small ions. In fig.9 the results of a number of mass determinations on CO^+ are summarized. CO^+ was present as molecular ion from CO, and as a fragment ion from CO_2. The maximum deviations from the literature values are about 5 ppm. The average values from the measurements agree to 1 ppm with the literature value. Hence, systematic error between the two measurements is not evidenced.

References

[1] R.Ryhage, Fifteenth Annual Conference on Mass Spectrometry and Allied Topics, Denver, p.162 (1967).

[2] C.Merrit, Jr., P.Issenberg, M.L.Bazinet, B.N.Green, T.O.Merron, and J.G.Murray, Anal.Chem. 37, 1037 (1965).

[3] W.J.McMurray, B.N.Green, and S.R.Lipsky, Anal.Chem. 38, 1194 (1966).

[4] C.Merrit, Jr., P.Issenberg, and M.L.Bazinet, International Mass Spectrometry Conference, Berlin (1967).

[5] H.C.Bowen, D.J.Shields, and H.M.Stanier, International Mass Spectrometry Conference, Berlin (1967).

[6] A.L.Burlingame, D.H.Smith, and R.W.Olsen, Anal.Chem. 40, 13 (1968).

35. THE IDENTIFICATION OF UNRESOLVED MULTIPLETS FROM ELECTRICALLY SCANNED SPECTRA

by M. Barber and B.N. Green
GEC-AEI Electronics Limited
Scientific Apparatus Division
Manchester, England

and

W.J. McMurray and S.R. Lipsky
Section of Physical Sciences
Yale University School of Medicine
New Haven, Connecticut U.S.A.

A mass spectral peak can be recognized as a multiplet if its width is significantly greater than the width of a singlet. On this statement is based of the method by which multiplets in electrically recorded scans can be isolated for later computer processing. Two criteria for specifying the peak width have been investigated. The first of these, the width of the peak at the threshold, has several disadvantages. The width varies with the intensity of the peak and in order to construct the relation between width and intensity for singlets, a large number of peaks have to be processed. This usually means the scan has to be completed or a calibration run has to be made. It is also difficult to eliminate peaks which are multiplets from the calibration data. A further complication is that small gradual changes in resolution cannot be easily allowed for.

The alternative criterion, that of specifying the width at a constant fraction of the peak height, overcomes these difficulties. Over a small mass range, the width will be essentially constant and by taking the average over a number of peaks an estimate of the reliability can also be made. A routine based on this second method of specifying widths is as follows. Starting at the high mass end of the spectrum, the width of every peak is measured. It is assumed that no multiplets occur in the first few peaks. This can usually be arranged by assuming that the first few peaks are reference peaks. The computer calculates the mean width and standard deviation of the first few peaks. It then compares the width of the next peak with the mean to see if it is significantly wider. If it is wider, the peak profile data is stored for subsequent deconvolution and the comparison is carried out on the next peak. If the next peak is not significantly wider than the mean, its width is used to recalculate the mean width and standard deviation, the first peak in the sequence being eliminated. In this way the width and standard deviation is continuously being updated, for a fixed number of peaks, as the scan progresses.

The width of peaks in electrically recorded scans varies for statistical reasons and Figure 1 indicates the accuracy to which the peak width can be measured. This data was obtained by making 5 spectra under similar conditions of 10,000 resolution and 35 seconds per decade scan speed. The standard deviation expressed as a percentage of the mean peak width is shown plotted against peak intensity for widths measured at 50% and 20% of the peak height. It can be shown by using a simple triangular model that the expected variations should be inversely proportional to the square root of the intensity and the curves have been drawn on this assumption. In spite of the scatter on the points, it can clearly be seen that the width measured at 20% is a more reliable estimate than the width measured at 50%. This holds for the reliability of the widths measured at 10%, the points being similarly placed to the 20% curve. The ratio in width between doublets and singlets also favours using a width measured as near to the base of the peak as practicable, at least for peaks in which the smaller component is a relatively small fraction of the larger component. This is indicated in Figure 2. The data in these curves were obtained by synthetically constructing doublets from the digital peak profile of a singlet. At this component peak separation (component peak separation equals 0.36 the 5% singlet width), there is a definite advantage in measuring the width at the lower levels except when the two components are nearly the same intensity, when there is least difficulty in detecting the doublet anyway. Curves showing essentially the same characteristics are obtained for component peak separations of ½ and ¼ the

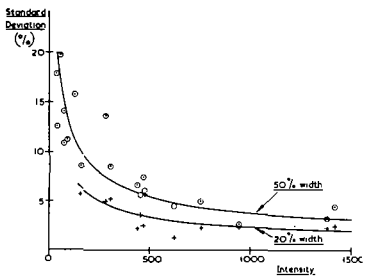

VARIATIONS IN SINGLET WIDTH, WITH INTENSITY

Fig. 1

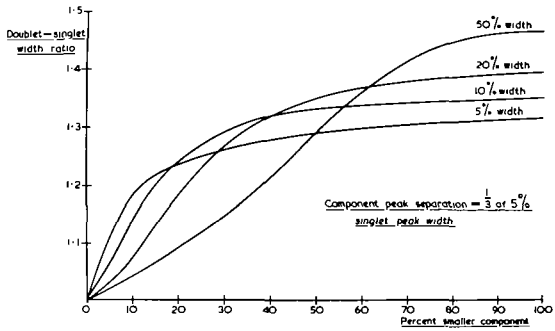

VARIATION OF DOUBLET PEAK WIDTH WITH INTENSITY OF SMALLER COMPONENT.

Fig. 2

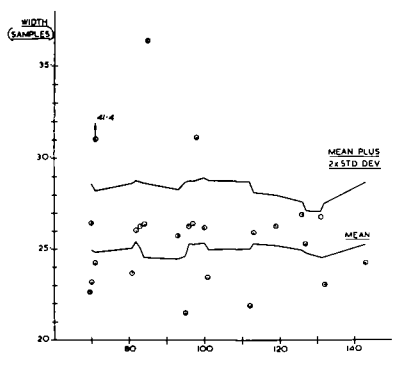

DISTRIBUTION OF PEAK WIDTHS MEASURED AT 20% OF THE PEAK HEIGHT (NONENE)

Fig. 3

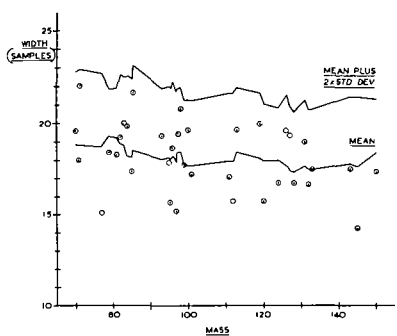

DISTRIBUTION OF PEAK WIDTHS MEASURED AT 50% OF THE PEAK HEIGHT (NONENE)

Fig. 4

TABLE 1

MASS	% INTENSITY OF SMALLER COMPONENT	EXCESS PEAK WIDTH IN STD. DEV. MEASURED AT			
		50%	20%	10%	5%
71.08	35	1.7	9.3	8.8	14.2
85.10	32	1.9	6.2	10.6	8.5
98.10	20	1.7	3.2	7.5	5.1
84.09	5.8	0.8	1.2	1.6	3.6
70.07	5.2	0.4	0.9	1.2	6.7

DETECTION OF MULTIPLETS BY EXCESS PEAK WIDTH (NONENE)

TABLE 2

Mass	% intensity of smaller component		Mass Difference (m.m.u.)
	Theoretical	Deconvoluted	
98.10	20	29	4.30
85.10	32	31	4.43
84.09	5.8	7.1	4.65
71.08	35	39	4.46
70.07	5.2	7.7	4.20

DECONVOLUTED MASS DIFFERENCES AND INTENSITIES OF CH-^{13}C DOUBLETS.

5% singlet width.

Figure 3 shows how the mean width at 50% of the height and the mean plus 2 standard deviations varies over the mass range 70 to 150 in a spectrum of nonene. Groups of 8 peaks were used to calculate the means at the mass indicated. The widths of the individual peaks are also shown. No peaks exceeded the mean width plus 2 standard deviations line, although there is a tendency for the 71, 85 and 98 peaks to be wider than the rest.

Figure 4 shows the much more favorable case where the width at 20% of the height was used as the criterion. The 71, 85 and 98 peaks are now obviously significantly wider than the rest. In these peaks the intensity of the smaller component was between 20 and 35% of the intensity of the larger one. No singlets appeared above the mean plus two standard deviations line.

Two other peaks in the sequence shown were only found to be doublets by comparing widths measured at the 5% level. In both cases, the smaller component was only about 5% of the height of the larger one. The results for all 5 identified doublets are summarised in Table 1. Tabulated are the number of standard deviations by which the doublet width exceeded the mean singlet width at the different levels of peak height. In particular it shows the significant increase in width in going from the 10% to the 5% level for the 2 peaks (84 and 70) which have the very low level component.

The data given in Figures 3 & 4 and in Table 1 refers to the identification of multiplets which only needed about a factor of 2 higher resolution to separate them (between 1.7 and 2.3) than the resolution at which the scans were run. However, it can be inferred from the data that had the separation been between 1/3 and 1/4 of the peak width, all the 5 peaks would have been still detected.

Table II shows the results of deconvoluting with known singlets the 5 peaks previously identified as doublets by a least squares fit method. (1) The mass differences are all within 4 ppm of the expected mass difference of 4.47 m.u.

In conclusion, it has been shown how the effective resolution of the data from electrically recorded scans can be improved by deconvolution. By a preliminary procedure, only those peaks worthy of deconvolution can be selected, thus considerably reducing the computer processing time. The indications are that the technique could be extended to data requiring a factor of at least 3 improvement in resolution and work is proceeding along these lines.

The authors would like to thank Mr. A. Grummitt of GEC-AEI Electronics Limited, for his assistance with the deconvolution program.

References

(1) T.R. Lusibrink, Ph.D. Thesis, University of California, August 1965.

36. ON-LINE DIGITAL RECORDING OF HIGH RESOLUTION MASS SPECTRAL DATA WITH SUBSEQUENT COMPUTER-PROCESSING

M. B. Neher, R. L. Foltz, M. E. Hassfurther, and R. B. Randall

Battelle Memorial Institute
Columbus Laboratories
505 King Avenue
Columbus, Ohio 43201

INTRODUCTION. The rapidly changing state of the art in digital computer technology and its application to mass spectrometry has resulted in a number of rather different approaches to obtaining data in a form suitable for computer processing. The papers presented in this program attest to the interest in this subject and to the variety of approaches.

Since we have an MS-9 at Battelle, our remarks are directed primarily to the direct electrical readout of the MS-9, although some of the same considerations apply to photo-plate instruments as well.

The decision about the type of data system to obtain was greatly influenced by the specific circumstances at Battelle. In view of the nature of our work, it was imperative that the system be as versatile as possible so that it could be used for a wide variety of projects. Also, it was imperative that the system chosen should have a minimum delay factor. Utilization of Battelle's large and very fast CDC 6400 computer appeared to offer significant advantages. Real-time, on-line operation was considered, but the location of the computer center with relation to the mass spectrometer lab and the inherent problems of on-line systems dictated an off-line operation.

BATTELLE DATA SYSTEM. A block diagram of the data system we decided upon is shown in Figure 1. It consists of two A-D converters, a multiplexer, core storage, digital tape recorder and the associated electronic controls. The system was designed and built by Mr. M. E. Hassfurther of Battelle's Systems Electronics Division.

For the peak intensity signal, we use a 14-bit A-D converter, capable of operating at 125 KH_z (Preston, Model VHS 8300). For monitor current we built a 6-bit A-D converter. This, as well as all the other electronic controls, was built from Honeywell Micropac electronic modules. The digitized data, fed through a digital filter, timing clock, and tape recorder control commands are multiplexed together and fed into the core storage unit (Ampex, Model RF2), which allows us to store data while the tape recorder is making the inter-record gaps required for computer-compatible tapes.

We have a number of operator selectable inputs for flexibility of the system. These are selectable from the control panel, and include digital switches for recording the data, the run number, A-D converter rate, the threshold level and number of samples required to consider input as a peak and the specification that a given run is background, or data, or include computer instructions to substract background from the data. The controls also include a Read-Write Coincidence alarm indicating overflow of the core storage, and selectors for the recording modes and tape density.

The tape recorder (an Ampex TM 4111), operates at 75 in/sec and 556 or 800 BPI. Recording in the Real Time mode, i.e., recording every digital data point, the system is limited to 12-1/2 KH_z, which permits scans of 40 sec/decade or slower.

The system as described so far is a more or less conventional analog-to-digital data system. The important feature of this system is a recording technique which permits recording only the portion of the spectrum that contains pertinent information.

For 10 sec/decade scans with resolution of 10,000, it has been shown that a digitizing rate of about 50 KH_z is required. To record such scans in the Real Time mode requires a high performance tape recorder. Such a recorder would make a data system unreasonably expensive.

For most of the time in any high resolution scan, there is no output signal. Conservatively, it is estimated that the output is at zero about 80 to 90 percent of the time. Hence, it was reasoned that by using the core storage, data could be digitized at the maximum rate of the A-D converter, store the results in the core storage memory until enough data accumulated to write one block of tape, provided that the periods in which data bursts occur were not so long that the data input would catch up with the relatively slow tape recorder.

Hence, a second recording mode was designed into the data system, a Compressed-Time Mode. In this mode, the core storage unit accumulates data only after successive digital points exceeds the threshold level. Both the number of digital samples and the threshold level are operator-selectable variables. This provides digital filtering to eliminate the majority of single ion events and random noise. Thus, recording begins in the core storage unit only when an actual peak occurs, and is terminated when the signal drops below the threshold level. The time at which the end of the peak occurs is recorded on tape immediately following the peak intensity data. With this recording format, 10 sec/decade scans can be recorded. The data system will actually operate at a digitizing rate suitable for 5 sec/decade scans, but the modified MS-9 electronics do not give a sufficiently high bandwidth for such a fast scan.

This compressed time format has worked so well that the Real-Time mode is not used. A complete mass spectrum (mass 700 down to 12) required from 1 to 8 feet of tape, depending on the complexity of the spectrum, whereas, the same scan in the Real-Time mode requires approximately 200 to 250 feet of tape.

OPERATION. The MS-9 data system has been in use for more than 6 months and its operation has proven to be remarkably simple. To enable the operator to have more control of certain of the operating parameters, Battelle-designed remote slit, magnet and probe positioning controls have been added. The magnet positioning control utilizes a digital stepping motor, with Selsyn feed-back to indicate the magnet position at the console within .001 in. The slit and probe controls utilize null-balancing servo circuits providing both push-button-switch-settable and infinitely variable positions. To set-up for operation, the slits are adjusted for the desired resolution, the magnet is adjusted for optimum position, and the proper effective bandwidth is selected. Both magnet position and effective bandwidth must be changed when the scan rate is varied.

A scan is started by push-button switch operating a relay system which simultaneously starts the mass spectrometer, the data system, and if desired, the UV recorder. The scan normally is terminated at a selectable point in the scan by an optical relay attached to the magnet scan meter (usually around mass 12), but can also be terminated manually.

Progress of the scan is monitored on a Tektronix storage oscilloscope, checking for width, height and shape of selected peaks. This method of checking has been entirely satisfactory. Analog recording has not been found necessary to determine whether a run is satisfactory.

COMPUTER PROGRAMS. Mass spectral computer programs have been described by others so the details of our computer programs will not be presented here. Briefly, the program computes the peak times and areas of all peaks, identifies the reference compound peaks, selects the most suitable of these and interpolates between them to determine the masses of unknown peaks, substracts out the background if desired, computes and records all formulas which fit the measured masses within specific error limits and considering hetero-elements which are specified, and finally, prepares a low resolution mass spectrum using the Calcomp plotter on the CDC 6400.

The standard output of the system includes:

1. A listing of unknown peaks, intensities, and molecular formulas. This listing shows the error in mass allowed in acceptable formulas, the number of heteroelements to be considered. For each peak it lists the observed mass and intensity, the calculated intensity of the corresponding C-13 peak, then the calculated mass and actual error in PPM for the formulas listed. Doubly ionized peaks are identified. If no satisfactory fit is found within the specified limits that fact is noted (Figure 2).

2. A computer plotted low resolution spectrum having a linear mass scale and an intensity scale from 0 to 100 percent.

3. A listing of background peaks substracted, if applicable.

4. Figure 3 shows a listing of reference peaks for mass measuring.

   The program uses a pattern recognition routine to identify reference peaks from data which are supplied with the program deck. The routine selects the most intense peak in the lower third of the spectrum, tentatively assigns this as the 69 peak, checks for the isotope peak at 70, then matches up and down from that point. If a satisfactory fit is not found, the next most intense peak is tried. If a fit is not found in five attempts, the run is terminated. Once a satisfactory fit is found, the routine then interpolates between reference peaks to obtain accurate masses of all other peaks using a polynomial interpolation routine.

5. Figure 4 shows part of the reference peaks not used for mass measuring with intensities and error in the observed masses. The average error of these peaks above mass 100 is computed and this value is used to set the error limits in computing the molecular formulas.

The entire calculation requires a single run on the CDC 6400 computer--about 10 seconds of central processor time and 1 minute of peripheral processor time. Turn-around-time depends upon the computer center backlog, but is often less than 30 minutes.

SPECIFIC PERFORMANCE RESULTS. Mass measuring accuracy of the system is, of course, dependent upon optimization of the mass spectrometer. However, using both perfluorokerosene and perfluorotributylamine as reference compounds we have been operating consistently with average errors of 3.5 to 6 ppm based on the relatively low intensity reference peaks which are not used for mass measuring. Figure 5 shows measuring error data for a number of runs using PFTBA and PFK. As might be expected, mass measuring accuracy decreases with increasing scan rate. In general, we have obtained satisfactory results with both PFK and PFTBA. However, we tend to prefer PFTBA because its spectrum is simpler than the PFK spectrum and has no peaks with positive mass defect. Figure 6 shows the average mass measurement error on selected peaks of perfluorotributyl amine on 40 sec/decade scans. These data were taken from a number of runs made under a variety of conditions--no attempt being made to make them identical. The average error calculated by averaging the error of all peaks is 4.9 ppm. However, if the average experimental mass is used to calculate the error of each peak, a considerably lower average error is obtained, 1.9 ppm, which means that averaging the values from several scans would give better mass measuring accuracy.

SUMMARY AND CONCLUSIONS.

1. Direct digital recording is satisfactory. Analog playback is not necessary.

2. The compressed time recording mode greatly reduces the amount of tape required, and therefore, reduces the computer processing time compared to the real-time recording mode.

3. PFK and PFTBA are about equally satisfactory as reference compounds.

4. The ability to make repetitive scans rapidly is very useful--actually essential for GC and probe samples.

5. The flexibility of a large, very fast computer to process data is extremely useful. The features not available with a smaller, slower computer are:

   a. Rapid processing of data

   b. Separate listing of reference peaks and unknown peaks

   c. Background subtraction

   d. Low resolution bar-graph computer plot.

The programs are currently being modified to handle automatic preparation of element maps, recognition of isotope multiplets, and program-averaging of multiple scans for improved mass measuring accuracy.

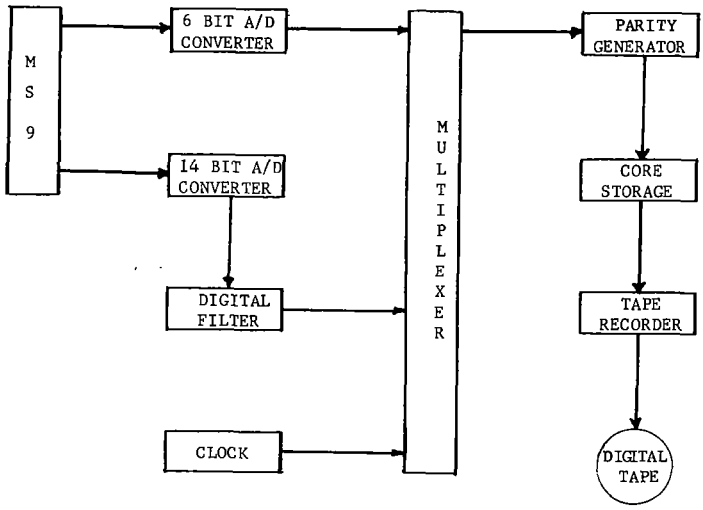

FIGURE 1. BLOCK DIAGRAM OF DATA SYSTEM

Battelle Mass Spectral Data
5/01/68 Run No. 2

Calculation Limits

Error	O	N	F	Cl	BR	I	S	P	Si	D	C13
.000011	2	2	0	0	0	0	0	0	0	0	0

Measured Mass	Relative Intensity Actual	Relative Intensity Theor. C(13)	Calculated Mass	Error PPM	Molecular Formula
15.0231	17.66	.19	15.0235	23.8	C H3
15.5090	.13		31.0179	Peak, Doubly Ionized	
15.9949	.22		15.9949	1.2	O
16.0270	.14			No Satisfactory Fit	
16.0311	.22		16.0313	15.1	C H4
17.0026	2.85		17.0027	6.6	H O
. . . . .					
143.0822	4.17	.28	143.0820	1.2	C6 H11 O2 N2
144.0900	19.56	1.29	144.0899	.7	C6 H12 O2 N2
145.0933	1.19	.13	145.0932	.8	C5 C(13) H12 O2 N2

Intensity of Weakest Peak = .050 Percent
Sum of Intensities of All Peaks = 574.7 Percent

FIGURE 2. TYPICAL COMPUTER PROGRAM OUTPUT

Mass AMU	Intensity Percent	Error Sec.
613.9647	2.39	-.0003
575.9679	1.75	.0005
537.9711	.45	.0000
501.9711	6.91	-.0003
463.9743	3.40	-.0005
425.9775	2.72	.0002
413.9775	4.08	-.0006
375.9807	.59	.0006
325.9839	.19	-.0001
313.9839	.40	-.0000
263.9871	9.71	-.0014
230.9856	.80	.0002
225.9903	.32	-.0002
218.9856	61.20	.0000
213.9903	.43	.0005
180.9888	1.60	-.0003
168.9888	3.54	-.0002
149.9904	1.55	.0004
130.9920	34.63	-.0001
118.9920	6.70	-.0000
113.9966	2.73	.0001
99.9936	9.97	.0001
92.9952	.61	-.0004
80.9952	.31	-.0008
68.9952	100.00	0.0000
49.9968	.46	.0010
30.9984	1.25	.0006
20.0062	.37	.0015
18.0105	4.22	.0007

FIGURE 3. REFERENCE PEAKS FOR MASS MEASUREMENT

Mass	Intensity	Error, PPM
614.9700	.12	3.0
525.9665	.19	8.8
502.9729	.54	3.1
464.9784	.19	1.5
414.9835	.28	6.3
280.9822	.24	.6
264.9898	.42	2.5
219.9895	3.17	2.5
175.9937	.46	1.4
163.9927	.53	4.7
161.9896	.16	4.9
144.9955	.42	3.0
142.9937	.25	11.8
131.9952	.81	1.2
111.9935	.33	.6
94.9965	.11	17.9
69.9984	.84	2.1
51.0037	.08	16.3

Average Error 3.8 PPM

Slope Calculated From 69-81 peaks = -.0599080
Slope Calculated From 69-70 Peaks = .0599323

FIGURE 4. REFERENCE PEAKS NOT USED FOR MASS MEASUREMENT

Reference Compound	Scan Rate, Seconds/Decade		
	80	40	10
PFTBA	3.8(7)	5.6(36)	7.2(2)
PFK	4.3(5)	4.9(29)	6.2(2)

FIGURE 5. AVERAGE MASS MEASURING ACCURACY IN PPM BASED ON NUMBER OF SCANS IN PARENTHESES

Calculated Mass	No. Of Scans	Average Mass	Averaged Error PPM	Error Of Average Mass PPM
614.9681	4	614.9684	6.2	0.4
502.9745	4	502.9736	4.6	1.9
464.9777	5	464.9777	4.2	0.0
414.9809	6	414.9817	5.7	1.9
264.9905	6	264.9907	3.9	0.7
219.9890	6	219.9897	3.8	3.1
163.9935	6	163.9934	3.1	0.4
131.9954	6	131.9961	7.7	5.1
		Average	4.9	1.9

FIGURE 6. MASS MEASURING ACCURACY WITH PFTBA 40 SECONDS/DECADE SCANS

37. DIGITAL DATA ACQUISITION AND REDUCTION SYSTEMS

IN REAL-TIME COMPUTER HIGH RESOLUTION MASS SPECTROMETRY[1,2]

D. H. Smith, R. W. Olsen and A. L. Burlingame
Department of Chemistry and Space Sciences Laboratory
University of California, Berkeley, California 94720

The digital computer is rapidly becoming a routine tool for the mass spectroscopist in many phases of the task of data handling. In high resolution mass spectrometry, past efforts utilizing the computer have been concentrated on data reduction and presentation, and initial efforts have been made toward interpretation of high resolution spectra. One of the most active areas of interest in the past two years, however, has been the use of the computer for data acquisition of electrically detected spectra. The digital computer, with its inherent fast response time, accuracy and programmable versatility, makes it ideally suited to the task of data acquisition. In this paper I would like to discuss some aspects of data acquisition and some improvements in our methods of data reduction programming since our last reports.[3,4,5]

It has been our experience that the variety of approaches to data acquisition is limited only by the imagination of the programmer working within the limitations of available computer hardware. I would like to discuss only two of the many possible different approaches. These approaches are quite general and both could be applied to many mass spectrometer-computer systems.

A block diagram of the system is shown in Figure 1. Several improvements have been made in this system since it was last discussed.[4] Control of the system is carried out by one character teletype commands given by the operator, allowing selection of whatever function the system is to perform. The 14 bit A/D is capable of operation at 100 KHz. The display has been converted from a point-by-point mode of operation to a vector mode so that a conventional bar graph may be constructed from the spectral data, or alternatively, the actual peak profiles may be traced out.

The first approach to data acquisition is summarized in Figure 2. This approach results in recording all data points above a pre-set threshold, thus saving all the peak profiles. With the profiles in hand, it is possible to accomplish peak position and intensity determinations by any of a variety of approaches from peak tops to curve fitting. The data are permanently available for a comparison of different data reduction techniques, for example.

Fig. 1 DATA ACQUISITION HARDWARE

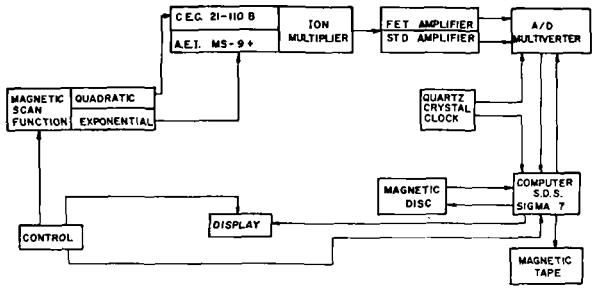

Figure 2

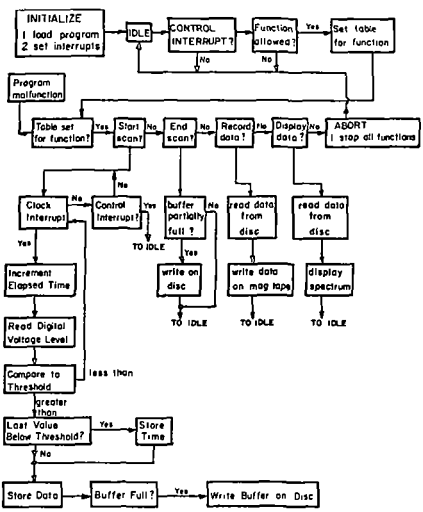

Figure 3

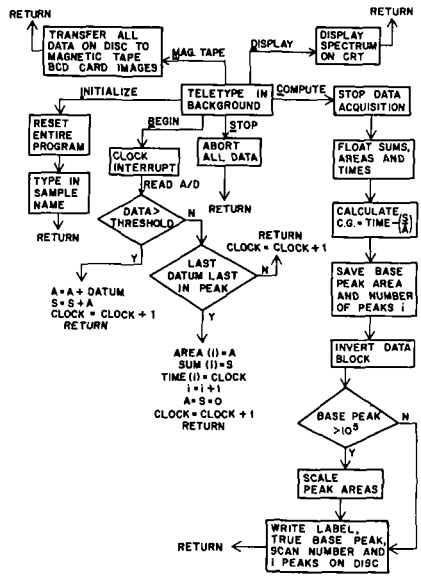

The operational flow of the program is as follows. A control interrupt provided by the teletype is used to begin data acquisition. With each interrupt from the external clock the clock register is incremented and the datum compared with threshold. Values greater than threshold are stored along with the time, which is stored once at the beginning of the peak. This program uses two buffers for the incoming data. As one buffer is being filled, the other buffer is emptied onto the disk. When the scan is terminated the data may be displayed and/or recorded. Spectra consisting of only the calibration mixture, PFK, as frequently occurs during work with the direct introduction probe may be rejected by the operator.

With this program, the most that has to be done within the computer occurs when a time word and a voltage level must be stored as a buffer is filled and must be written out on the disk. These procedures require 38 μsec., so the clock rate is limited to a maximum of about 25 KHz to avoid missing a clock interrupt. This limitation, however, has proven to be of little consequence to mass measurement accuracy for spectra taken at scan rates of 8 seconds/decade in mass, using the center of gravity as a peak position critereon, even though at this scan rate there are only 8 to 9 points/peak at 25 KHz clocking rate.

One of the primary arguements for acquiring peak profiles is that the profiles may be treated by deconvolution techniques to resolve unresolved multiplets. In routine work, however, many spectra are recorded of known compounds or mixtures of a known class of compounds such as hydrocarbons, esters and so forth. In these cases it is possible to scan at a resolution in excess of that required to separate commonly encountered multiplets, such as CH_2 vs. N, as required by the elemental composition(s) of the sample.

The doublets that remain consist of C^{13} vs. CH, and these may be treated during data reduction by a rather simple technique to be described in the following paper.[6] With these considerations, one needs only the center of gravity of the peak profile, a position criterion that has been shown to yield good results. The second approach to data acquisition is designed to save only those data necessary to determine the center of gravity. Figure 3 summarizes the operational flow of this procedure. This program is also under teletype control. Input of the letter I initializes the system and allows the operator to input the sample name. Data acquisition is initiated by the letter B for begin. Data below threshold are rejected while the clock register is incremented for each

Figure 4

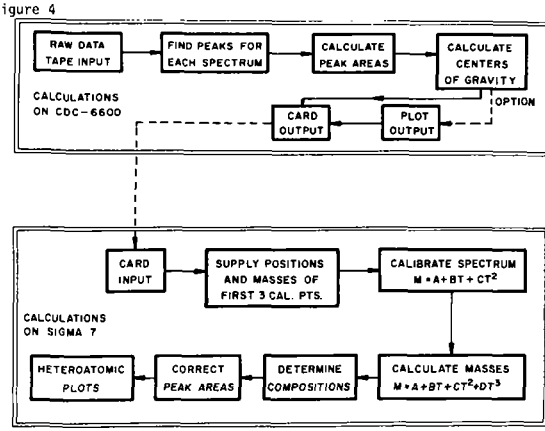

Figure 5

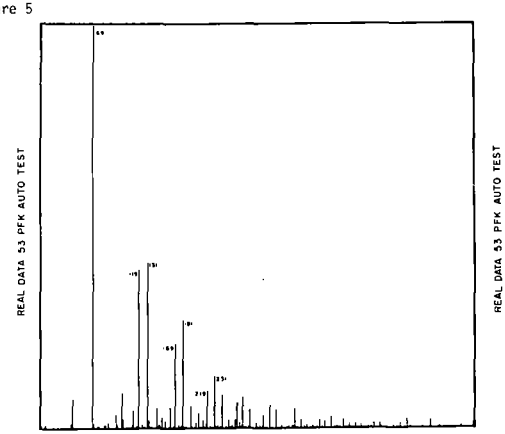

clock interrupt. Data above threshold are handled by adding the datum to the variable A. The contents of A are added to the variable S, and the clock register is incremented by one. When the peak drops below threshold, the values of S, A and time are stored, A and S are re-set to zero, and the clock register and i are incremented. The data acquisition process is stopped by typing C, for compute. The program then carries out the calculations summarized in Figure 3. Sums, areas, and times are converted to floating point numbers. The centers of gravity are calculated as C.G. = TIME $-\frac{(S)}{(A)}$. The base peak intensity is saved along with the number of peaks, i.

Because it has proven to be more convenient for calculating the lower end of the mass range (m/e 40 to 80) by beginning the calculations at low mass, the data block is inverted at this point and all times subtracted from a constant specified at *INITIALIZE*. This results in a block of data beginning at low mass, low time, and proceeding to high mass, high time.

The intensity scale is then converted to a scale in which the base peak equals 10^5, if the base peak was greater than 10^5. The data block is then transferred to the magnetic disc. These calculations require less than 1 second for the pre-set maximum of 2000 peaks/scan, and are thus easily completed before the magnet returns to high field for the beginning of the next scan.

The longest time required during the data acquisition cycle for this program is 29 μsec., restricting the maximum digitization rate to 34 KHz. It should be noted at this point that both data acquisition programs carry out the processes of clock count and thresholding within the computer. Both tasks could be more efficiently carried out using external hardware, thereby increasing the maximum digitization rate.

When the desired number of scans of the sample or samples have been recorded, the operator types M for magnetic tape, and the data are output to mag. tape from the disc. A normal data acquisition cycle would consist of Initialize, Begin, Compute, Display, Begin, Compute, and so forth, followed by Mag. tape, Intialize, Begin, Compute, Display and so forth. The input of S for stop aborts the data if they are not desired.

Proceeding now to data reduction, Figure 4 summarizes the computations for peak profile data taken with the 21-110. Under normal conditions, centers of gravity are calculated, and the resulting data output on cards, and optionally, on a plot that may be used for selection of the first three calibration points.

Figure 6

SCAN REPRODUCIBILITY

Scan Rate 1* - 170 seconds, m/e 605 to 51

Mass	T_1**	T_2	T_3	Difference***
604.96325	429314	429357	429381	67
504.96964	690525	690543	690579	52
404.97603	936084	936108	936153	69
304.98242	1194438	1194432	1194480	48
204.98882	1486483	1486489	1486527	44
99.99361	1873034	1873032	1873070	38
51.00463	2126227	2126264	2126308	81

Scan Rate 2* - 52.5 seconds, m/e 605 to 51

604.96325	270754	270732	270767	35
504.96964	436665	436627	436675	48
404.97603	589106	589097	589151	54
304.98242	748005	748001	748057	52
204.98882	925856	925855	925905	49
99.99361	1163442	1163454	1163517	75
51.00463	1320293	1320314	1320384	91

* Scan Rate 1 and Scan Rate 2, scans taken with clock rates of 10KHz and 20KHz respectively.

** T_n's are times, in elapsed clock pulses, for the given mass, for 3 successive scans at each scan rate.

*** Differences are the maximum differences noted among 3 scans, in clock pulses (50 clock pulses correspond to 5msec. and 2.5msec. for 10KHz and 20KHz respectively).

Figure 7

MASS MEASUREMENT ERRORS (in p.p.m.) USING LEAST SQUARES FIT TO TIME CONSTANT VS. TIME CURVE

PERCHLOROBUTADIENE NOMINAL MASS	NORMAL	# OF CAL. PTS./# OF COEFFICIENTS 7/3	7/5	5/2	5/4
223	-0.1	+0.1	-0.3	-1.3	+0.1
224	+0.6	+0.9	+0.3	-1.0	+0.8
225	-0.5	-0.1	-1.0	-2.6	-0.2
226	-0.3	+0.1	-0.8	-3.0	+0.1
227	-0.5	0.0	-0.9	-3.7	+0.1
228	-0.4	+0.1	-0.9	-4.2	+0.4
229	-0.7	-0.2	-1.3	-5.2	+0.1
230	-0.5	0.0	-1.1	-5.6	+0.6
231	-0.6	-0.2	-1.3	-6.4	+0.6

Mass calculation, composition determination, and plotting proceed as has been discussed previously. The area correction is based on the linear magnet current scan used with the 21-110, and is accomplished by simply dividing the peak area by the square root of the mass.

Calculations for the exponential data obtained from the modified MS-902 proceed in an analagous manner, with the appropriate Mass-Time realtionship and no correction for peak areas. Data taken with the center of gravity program may be handled entirely on the Sigma 7 by simply reading back the data tape generated during data acquisition.

Figure 5 represents the type of plot of the raw data that is generated. This plot may be used to choose 3 calibration points at the beginning of the scan. Some of the more intense peaks of PFK are indicated (the spectrum is of PFK only).

Recent experiments with the 21-110 have been aimed at making data reduction more automatic, with as little human intervention as possible. Working toward this goal, a reproducible scan has been accomplished. The scan is carried out with a high precision linear ramp generator, whose direction is changed with a digital pulse. This pulse is gated with the clock interrupt to the computer so that the computer begins time measurement at the instant the scan is begun. Figure 6 indicates the reproducibility that is achieved. The times given are the times in clock pulses for the indicated mass for three successive scans. The differences noted are of the order of a peak width.

The computer is supplied with three approximate times for the first three calibration points, and mass calculation is carried out automatically. A slight trend is noted in the times presented on the slide. The program compensates for this by continually updating the times for the first three points.

Another area of interest in data reduction is concerned with calculating data obtained from the modified MS-902. In the normal method of handling data from an exponential scan, a particular time is assigned to a particular calibration mass, and resulting calculated time constants used for mass calculation. This method does not consider possible variations in the mass-time curve resulting from instrumental imperfections, nor does it consider the fact that peak positions are affected by ion statistical considerations. With these considerations in mind, an investigation has been carried out on the effects of using least squares curve fitting techniques for the time constant vs. time curve. A wide range of numbers of calibration points

and numbers of coefficients were studied using least squares in an effort to determine the optimum combinations. With the coefficients determined for a particular set of calibration points, masses in the central part of the region covered by the calibration points were calculated. The data in Figure 7 are representative of the results obtained.

The mass measurement errors are the average of 9 successive scans of the spectrum of perchlorobutadiene, and are presented in parts per million (p.p.m.). The errors in the column titled NORMAL are those obtained from the conventional method of calculation. The other columns have headings representing the number of calibration points considered along with the number of coefficients used.

7 cal. pts./5 coefficients and 5 cal. pts./2 coefficients clearly yield results that are poorer than the normal results. 5 cal. pts./4 coefficients yield a marginal improvement. The results obtained with 7 cal. pts./3 coefficients are representative of the fact that this combination generally yields, for this particular instrument, a marked improvement in mass measuring accuracy.

In conclusion, I have attempted to present a brief survey of the current areas of interest in our laboratory toward improvement of the real-time computer-mass spectrometer system. The following paper will be concerned with the results obtainable using such a system.

We wish to express our thanks to Mr. John McConnell and Miss Deborah Allen for the computer programming.

REFERENCES

1. Financial support was provided by NASA Grants NGR 05-003-134 and NSG 243, Suppl. 5.
2. For a detailed report of these studies, see "High Resolution Mass Spectrometry in Molecular Structure Studies, Part XX," D. H. Smith, R. W. Olsen and A. L. Burlingame, Chemical Instrumentation, in preparation.
3. A. L. Burlingame, D. H. Smith and R. W. Olsen, Anal. Chem. 40, 13 (1968).
4. A. L. Burlingame, in Advances in Mass Spectrometry Vol. 4, E. Kendrick Ed., Institute of Petroleum, London 1968, p. 15.
5. A. L. Burlingame, D. H. Smith and R. W. Olsen, 155th National American Chemical Society Meeting, Division of Physical Chemistry, San Francisco, March 31 - April 5, 1968, p. S 269.
6. A. L. Burlingame, D. H. Smith, R. W. Olsen and T. O. Merren, 16th Annual Conference on Mass Spectrometry and Allied Topics, May 12 - 17, 1968, Pittsburgh, Pa.

38. REAL-TIME HIGH RESOLUTION MASS SPECTROMETRY[1,2]

A. L. Burlingame, D. H. Smith, T. O. Merren[3] and R. W. Olsen
Department of Chemistry and Space Sciences Laboratory
University of California, Berkeley, California · 94720

ABSTRACT: Results obtained in this laboratory employing the Nier-Johnson geometry (modified G.E.C.-A.E.I. MS902) coupled to an S.D.S. Sigma 7 computer demonstrate an accuracy of mass measurement better than 0.5 p.p.m. for the "4- to 9-average" technique for entire real-time high resolution mass spectra. The detection and identification of unresolved doublets from error in accurate measurement of the center of gravity is described utilizing the very high accuracy in routine mass measurement with the system described.

INTRODUCTION: The mass spectrometer-computer system hardware configurations and software logic, in addition to an evaluation of the real-time data acquisition and processing technique developed in this laboratory, were discussed in detail in the previous paper (4). Previous work in this laboratory employing a C.E.C. 21-110B mass spectrometer coupled to the Sigma 7 has been reported demonstrating a standard deviation of accurate mass measurement of approximately 4 p.p.m. (5,6), employing a magnet scan function varying quadratically in mass.

RESULTS:

Mass Measurement Accuracy(8): One of the primary investigations of interest was the degree of mass measurement precision and accuracy that could be attained employing a mass spectrometer capable of providing a static resolution (M/ΔM) of 1 part in 70,000 (modified G.E.C.-A.E.I. MS902). This has been evaluated at different resolutions, scan and A/D clock rates. Spectra were scanned exponentially by sweeping the magnetic field to cover a selected decade in mass from high to low masses.

In order to assess the accuracy of mass measurements attainable, nine successive spectra were determined at resolution (M/ΔM) 25,000, employing a scan rate of 35 seconds per decade in mass. The multiplier-amplifier voltage output was digitized at 24 KHz. Perchlorobutadiene was chosen for these scans as a compound in which the accurate masses of fragment ions are known unambiguously. The sample flow rate into the ion source from a heated glass inlet system was less than 10 nanograms per second.

For each of these scans, the actual differences between the observed (calculated from PFK internal standard) and the true masses were determined for all peaks in the mass spectrum. The distribution of these actual errors in the resulting 266 calculated accurate mass values covering the mass range 100 to 266 for peaks greater than 2% of the base peak are presented in Figure 1 in the form of histograms. Histogram A in Figure 1 illustrates the percentage of errors (absolute values are plotted) falling within the ranges 0-2, 2-4 p.p.m., and so forth. It can be seen that in 70% of the measurements, the observed (calculated) mass differs from the true mass by less than 2 p.p.m.

A significant improvement in precision is obtained by calculating the mean mass for each peak in several scans. If the errors in individual observed masses are random, then both precision and mass measurement accuracy should be improved by a factor of 2, by taking the mean mass in four scans, and a factor of 3 taking the mean mass for nine scans, etc. If, however, the observed deviations in calculated masses are due to systematic errors in the data acquisition and/or reduction systems, mass measurement accuracy should not be significantly better than for single scans.

In order to statistically evaluate the raw data taken on nine successive scans, the "4-average" mean masses were calculated for scans 1-4 and 5-8. The 58 differences obtained are plotted in Figure 1 as Histogram B. In this case, the error ranges are 0-1, 1-2 p.p.m., and so forth. Comparison with Histogram A shows that the errors are reduced by about a factor of 2, with 77% of the errors now less than 1 p.p.m.

The differences obtained from utilizing the mean of all nine scans are presented as Histogram C in Figure 1, and are plotted over the error ranges 0-0.5, 0.5-1 p.p.m., and so forth. Again, the accuracy has been improved. In this case, 60% of the error values are less than 0.5 p.p.m. These results are consistent with the hypothesis that the observed mass measurement accuracy is due to random rather than systematic errors.

Routine results of real-time data on organic compounds may be illustrated by an evaluation of eight scans of methyl arachidate taken at a resolution of 25,000 over a dynamic range of 500 to 1. For these data, 65% of the mass differences from the mean accurate masses for the eight scans fall within 1 p.p.m. of the true values for those above m/e 100. Considering all masses above m/e 40 in the "8-average" scan, 61% of the mass differences are within 1 p.p.m. of the true values. The largest error noted is that of the isotope peak m/e 44 ($C_2{}^{13}CH_7$), 0.22 m.m.u., or 5.0 p.p.m. The slight decrease in mass measurement accuracy below m/e 100 is relatively unimportant, since there are many

fewer possible ambiguities in the assignment of elemental composition.

An evaluation of precision and accuracy of relative abundance measurements for this instrument on-line to the Sigma 7 was accomplished using the calculated abundance ratios for peaks in the mass spectra of perchlorobutadiene $[(Cl^{35} + Cl^{37})^m$ where $Cl^{35} = 0.758$; $Cl^{37} = 0.242$ and m is the number of chlorine atoms in the species].

Peak abundances may be conveniently expressed as percentages of the total isotopic peaks in a group, i.e.:

$$\frac{n_i}{N} \times 100 \qquad \text{where } n_i \text{ is the number of ions in peak i}$$

(obtained as discussed in reference 9) and $N = \Sigma n_i$ is the total number of peaks (ions) in the group.

These percentage abundances can be assigned theoretical standard deviations according to the equation:

$$\delta_{\text{theoret.}} = \frac{\sqrt{n_i}}{N} \times 100$$

This form of the equation for $\delta_{\text{theoret.}}$ results in the standard deviation expressed in the same units (percentage of total ions in the group) as the abundance value itself.

Nine successive scans of perchlorobutadiene at each of the two resolutions (M/ΔM) 11,300 and 30,000 were obtained and these data were used to evaluate the accuracy of relative abundance measurements. Representative data are presented in Table 1 which compare the mean observed abundances with the true abundances and the observed standard deviations with the theoretical values.

Precision may be evaluated by comparing the observed and theoretical standard deviations in Table 1. It can be seen that they agree very closely, indicating that variations in relative abundance measurements are fully accounted for by ion statistical considerations. This confirms the conclusions reached by McMurray et al. (9) from a limited number of peaks at 10,000 resolution and extends them to a larger population, wider relative abundance range and resolutions as high as 30,000.

Applications to Organic Analysis: Having at hand a detailed evaluation of a computer coupled high resolution mass spectrometer system (MS902-Sigma 7), it is of interest to examine the significance of the "4-average" accuracy of 1-2 p.p.m. in the determination of high resolution mass spectra.

As an example, eight successive scans of the spectrum of methyl arachidate were recorded at 10,000 resolving power (MS902, 32 seconds per decade with a digitization rate of 24 KHz). Mass measurement accuracy was evaluated in calculating average mass differences (in p.p.m.) between observed and assigned mass for spectral groups: 1→4, 5→8 and 1→8. Some data representative of those observed for the complete spectrum are presented in Table 2.

An examination of Table 2 reveals two sets of measurement accuracy data. One set, comprising the majority of the table, includes those data in the 1-2 p.p.m. range expected on the basis of foregoing discussions; the other set, comprising nominal masses 70, 88, 130, 186, 214, include those data which exhibit very large differences (cf. errors). These entries may then represent unresolved doublets, with the contribution from a second compositional component shifting the peak center of gravity sufficiently to yield errors larger than expected from the instrument-computer system.

To illustrate this in more detail, the digital peak profiles (plotted from one scan) of the suspected unresolved ^{13}C vs. CH doublets (ΔM = 0.00446 a.m.u.) at m/e 88 and 130 are presented in Figure 2. Peak widths at 10,000 resolution, 35 seconds per decade, should be approximately 1500 μsec. The calculated positions of the centers of gravity (labelled C.G., Figure 2) are indicated. The presence of an unresolved ^{13}C isotope peak under the peak profile should result in a shift of the center of gravity to slightly lower mass depending upon the relative abundances of the two components in the unresolved doublet. The profile of m/e 130 in Figure 2 is a particularly striking example of how little the peak profile need be distorted to yield a relatively large mass measurement error.

Mass measurement thus provides a criterion for the detection and definition of unresolved doublets. Detection of doublets on this basis depends upon the mass defect of the homogeneous (isobaric) components and the ratio of their abundances. These parameters determine the shift in the observed center of gravity for the unresolved doublet. An equation has been derived to relate this shift, E, of the larger peak to the abundances I_1 and I_2, and the theoretical component separation, S (reciprocal of the theoretical resolution ΔM/M):

$$E = \frac{I_2 S}{I_1 + I_2}$$

Figure 1

DISTRIBUTION OF MASS MEASUREMENT ERRORS
AT RESOLUTION OF 25,000

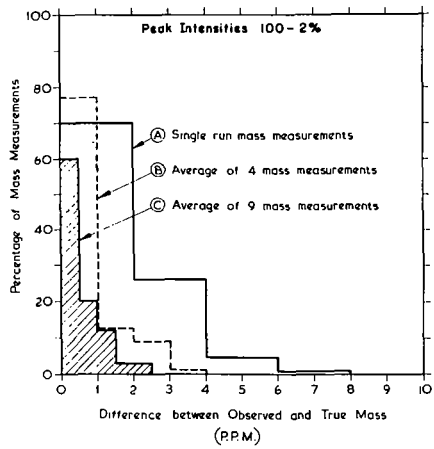

Figure 2

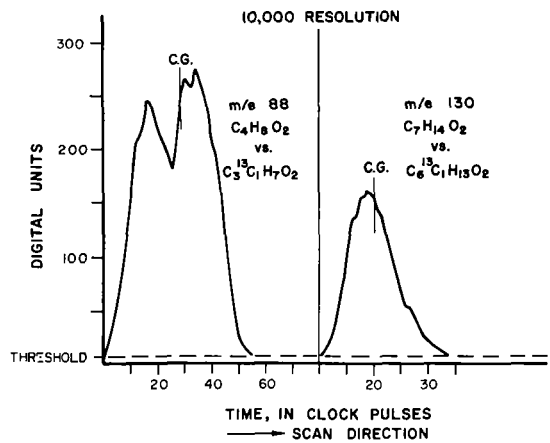

Figure 3

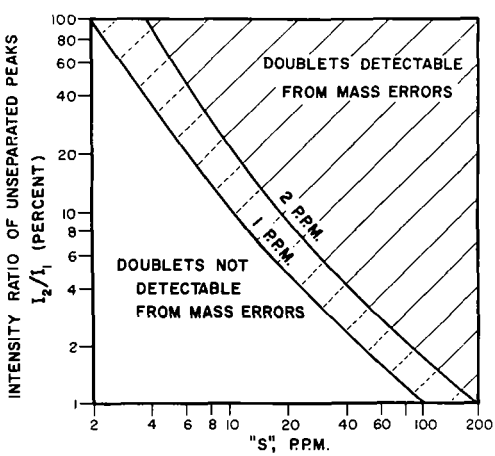

TABLE 1

Species	m/e	True Abundance	Resolution 11,300				Resolution 30,000			
			Mean Observed Abundance	Standard Deviation	Theoretical Standard Deviation	Error in Mean Abundance	Mean Observed Abundance	Standard Deviation	Theoretical Standard Deviation	Error in Mean Abundance
C_4Cl_6	258	19.0	18.8	± 0.5	0.5	-0.2	18.8	± 1.3	1.5	-0.2
	260	36.3	36.5	± 0.4	0.7	+0.2	36.6	± 2.2	2.1	+0.3
	262	29.0	28.9	± 0.8	0.7	-0.1	28.7	± 1.6	1.9	-0.3
	264	12.4	12.4	± 0.3	0.4	0.0	12.6	± 0.9	1.2	+0.2
	266	2.96	3.00	± 0.17	0.22	+0.04	3.12	± 0.41	0.61	+0.16
	268	0.38	.35	± 0.12	0.07	-0.03	0.38	± 0.20	0.22	0.00
	270	.02	-	-	-	-	-	-	-	-
C_4Cl_5	223	25.0	25.0	± 0.5	0.4	0.0	24.5	± 1.5	1.2	-0.5
	225	39.9	39.6	± 0.5	0.5	-0.3	40.2	± 1.6	1.5	+0.3
	227	25.6	25.7	± 0.4	0.4	+0.1	25.8	± 0.9	1.2	+0.2
	229	8.16	8.31	± 0.20	0.24	+0.15	8.24	± 0.54	0.68	+0.08
	231	1.32	1.34	± 0.14	0.09	+0.02	1.25	± 0.15	0.26	-0.07
	233	.08	-	-	-	-	-	-	-	-
C_4Cl_4	188	33.0	33.1	± 0.7	0.8	+0.1	32.7	± 1.6	2.3	-0.3
	190	42.2	42.3	± 0.5	0.8	+0.1	42.2	± 2.5	2.6	0.0
	192	20.2	20.3	± 0.8	0.6	+0.1	20.5	± 2.3	1.8	+0.3
	194	4.31	4.35	± 0.27	0.28	+0.04	4.56	± 0.72	0.85	+0.25
	196	0.30	-	-	-	-	-	-	-	-
C_4Cl_3	141	43.6	43.7	± 1.1	1.1	+0.1	43.8	± 5.1	3.3	+0.2
	143	41.7	41.6	± 1.1	1.1	-0.1	42.3	± 2.3	3.3	+0.6
	145	13.3	13.3	± 0.5	0.6	0.0	12.8	± 1.9	1.8	-0.5
	147	1.42	1.38	± 0.28	0.20	-0.04	1.10	± 0.53	0.57	-0.32
C_4Cl_2	118	57.5	56.8	± 1.3	1.3	-0.7	57.7	± 3.6	4.3	+0.2
	120	36.7	37.4	± 1.1	1.1	+0.7	36.0	±3.9	3.4	-0.7
	122	5.80	5.81	± 0.48	0.42	+0.01	6.30	± 1.37	1.41	+0.50

TABLE 2

Mass Measurement Accuracy, Methyl Arachidate

Assigned Composition	Assigned Mass	Average Difference (in p.p.m.) 1-4	5-8	1-8	Average Intensity
C_3H_5	41.03912	- 0.51	- 1.62	- 1.06	7.81
$C_2{}^{13}C_1H_4$	42.04247	- 0.48	- 1.97	- 1.32	0.26
C_3H_6	42.04694	- 1.03	0.26	- 0.39	2.49
$C_2H_3O_2$	59.01330	1.32	0.85	1.08	1.43
C_5H_9	69.07042	- 0.53	- 0.37	- 0.45	12.45
C_5H_{10}	70.07824	-11.86	-12.53	-12.20	3.50
$C_3H_6O_2$	74.03677	0.27	- 0.95	- 0.34	100.00
$C_4H_7O_2$	87.04459	0.43	0.68	0.50	65.14
$C_4H_8O_2$	88.05242	-27.48	-25.30	-26.39	5.51
$C_5H_9O_2$	101.06024	- 0.35	0.67	0.16	6.81
C_9H_{13}	121.10172	- 0.76	- 1.55	- 1.15	0.98
$C_7H_{13}O_2$	129.09155	- 1.52	- 0.38	- 0.95	7.19
$C_7H_{14}O_2$	130.09936	- 9.03	- 7.87	- 8.45	2.30
$C_8H_{15}O_2$	143.10719	0.25	- 0.37	- 0.06	19.84
$C_{12}H_{19}$	163.14866	- 0.18	0.82	0.32	0.39
$C_{11}H_{22}O_2$	185.15414	0.28	- 0.09	0.10	4.93
$C_{11}H_{23}O_2$	186.16196	-12.79	-12.21	-12.45	1.13
$C_{13}H_{25}O_2$	213.18544	0.62	- 0.13	0.25	2.05
$C_{13}H_{26}O_2$	214.19326	-10.05	- 8.68	- 9.38	0.70
$C_{18}H_{34}$	250.26603	- 0.48	1.17	0.25	0.18
$C_{18}H_{35}O_2$	283.26368	0.25	- 0.46	- 0.10	8.82
$C_{19}H_{37}O_2$	297.27933	- 0.51	0.47	- 0.02	1.82
$C_{21}H_{42}O_2$	326.31846	- 0.28	- 0.63	- 0.45	15.34

This equation is, of course, independent of actual instrument operating resolution.

This equation is used to obtain the error confidence limits in Figure 3 at the 1 and 2 p.p.m. level. For example, if one is confident that a series of mass measurements should yield an accuracy of better than 1 p.p.m. for single resolved peaks, then doublets with a separation S = $\Delta M/M$ of 4 p.p.m. are detectable if $I_2/I_1 \geq 35\%$, and doublets with $\Delta M/M$ = 20 p.p.m. are detectable if $I_2/I_1 \geq 5\%$.

This equation may then be applied and tested for the CH vs. ^{13}C doublets noted above. The abundance I_2, the ^{13}C contribution, may be calculated on the basis of the corresponding peak one mass unit lower. S and $(I_1 + I_2)$ are known quantities. Data in Table 3 reflect the results of using this procedure to correct the observed error of the doublet for the ^{13}C component in the spectrum of methyl arachidate at an instrument operating resolution of 10,000.

Table 3

Nominal Mass	Observed Error (p.p.m.)	Mass Measurement Error, CH Species (p.p.m.)
70	-12.20	0.2
88	-26.39	-0.1
130	- 8.45	-0.3
186	-12.45	-0.3
214	- 9.38	-0.8

REFERENCES:

1. Financial support was provided by the National Aeronautics and Space Administration, Grants NGR 05-003-134 and NsG 243, Suppl. 5.

2. For a more extensive report of these studies, see "High Resolution Mass Spectrometry in Molecular Structure Studies, Part XXI," A. L. Burlingame, D. H. Smith, T. O. Merren and R. W. Olsen, Anal. Chem., in press.

3. G.E.C.-A.E.I. Ltd., Scientific Apparatus Division, Manchester, England.

4. D. H. Smith, R. W. Olsen and A. L. Burlingame, 16th Annual Conference on Mass Spectrometry and Allied Topics, May 12-17, 1968, Pittsburgh, Pa.

5. A. L. Burlingame, D. H. Smith and R. W. Olsen, Anal. Chem. 40, 13 (1968).

6. A. L. Burlingame in Advances in Mass Spectrometry Vol. 4, E. Kendrick, Ed., Institute of Petroleum, London, 1968, p. 15.

7. A. L. Burlingame, R. W. Olsen, D. H. Smith, 15th Annual Conference on Mass Spectrometry and Allied Topics, May 14-15, 1967.

8. A. L. Burlingame, D. H. Smith and R. W. Olsen, 155th National American Chemical Society Meeting, Division of Physical Chemistry, San Francisco, March 31-April 5, 1968, p. S 269.

9. W. J. McMurray, S. R. Lipsky and B. N. Green in Advances in Mass Spectrometry Vol. 4, E. Kendrick, Ed., Institute of Petroleum, London, 1968, p. 77.

39. Comparison of Data Acquisition and

Computation Systems for High-Resolution Mass Spectra

R. Venkataraghavan, J. W. Amy, R. D. Board,

R. D. Brown, R. J. Klimowski and F. W. McLafferty

Department of Chemistry, Purdue University, Lafayette, Indiana 47907

Introduction

High-resolution mass spectral data are acquired in our laboratory both from photoplate recorded spectra and from direct electrical recording.[1] Photoplate high-resolution spectra are digitized and recorded onto magnetic tape using a modified Grant-Datex comparator microdensitometer system. This particular instrument scans the plate, takes a transmission sample every 0.25 micron across the line above a preset threshold and records the information onto tape at 200 bpi. density. The results obtained from this instrument, as well as some of its basic limitations, have been previously reported.[2] Recently we have examined the data more critically to evaluate the precision and accuracy obtainable with this system and would like to report several of the interesting observations made during the course of this study.

Several experiments were performed to evaluate the precision with which the mass of fragment ions can be measured. Spectra of 2-nonadecanone and perfluoro-kerosine were recorded onto photoplates under identical conditions and were digitized on the same day and on different days. The data were processed on a C.D.C. 6500 computer using the techniques we described previously.[3] The results of this precision study are shown in Table I, showing the data sets compared, the total number of lines compared and the mean difference between measured masses. On the same day, same plate and spectrum, for 76 lines studied the mean difference was 0.13 mmu. Spectra measured on different days using the same plate and spectrum showed a mean difference in mass of 0.26 mmu for 77 lines compared. Results from different spectra taken from the same plate showed a mean mass difference of 0.47 mmu. In a random experiment in which data were obtained from different photoplates and compared, the mean difference in measured mass of 49 lines compared was 0.33 mmu. In that for all these cases the mean difference in measured mass was within 1 mmu., these experiments show that highly reproducible data can be obtained from the Grant-Datex plate reader system if proper care is exercised in measuring the spectra. In the absence of determinate errors, the accuracy of mass measurement should be equally good.

In routine applications some of the lines in high-resolution data are not well resolved due to lack of sufficient mass spectrometer resolution, photoplate grain structure and other factors. In these instances, if the lines are assumed to result from single species, an error is introduced which depends on the degree of overlap of the interfering specie. In most cases appreciable overlapping occurs due to the contributions from ^{13}C species. Several experiments were carried out to determine the effect of this overlap on mass measuring accuracy. Table II illustrates typical results obtained on lines where there was no contribution from ^{13}C species. For 29 lines involving different ion types the average standard deviation was 0.30 mmu and the average mass error was around 0.4 mmu.

When an overlapping profile is encountered it is desirable to separate the individual components to improve the mass measuring accuracy. Shown in Table III is the effect of deconvolution on mass measuring accuracy for several ion types. All the ions shown had a significant contribution from C species. The error in measured mass is shown in the second column, noting that each line was assumed to result from a single ionic specie. Since we know that all of the lines contained significant ^{13}C contribution, the profiles were subjected to deconvolution and the resulting data are shown in the last column. A definite improvement in mass accuracy results from deconvolution.

RECORD NO.	NO. OF ITERATIONS	STANDARD ERROR	TIME (SEC.)	POSITION (MM.)	INTENSITY	WIDTH (MICRONS)	WEIGHTING FACTOR	TOTAL POINTS	STEPS
11	3	1.27		22.97672	31.77	14.29	1.321	102	1

••••••••••PROFILE FOR ABOVE RECORD SUSPECTED TO BE DOUBLET BASED ON WIDTH,NUMBER OF BANDS,AND TOTAL POINTS.

DECONVOLUTION INITIATED.

11	3	1.01	22.97410	16.65	13.35	.231	102	1
			22.97920	15.39	12.28	.231		

CALC	ERROR	C12/13	M	U
103.05363	.18	8/0	5	1
103.05478	1.58	8/0	7	0

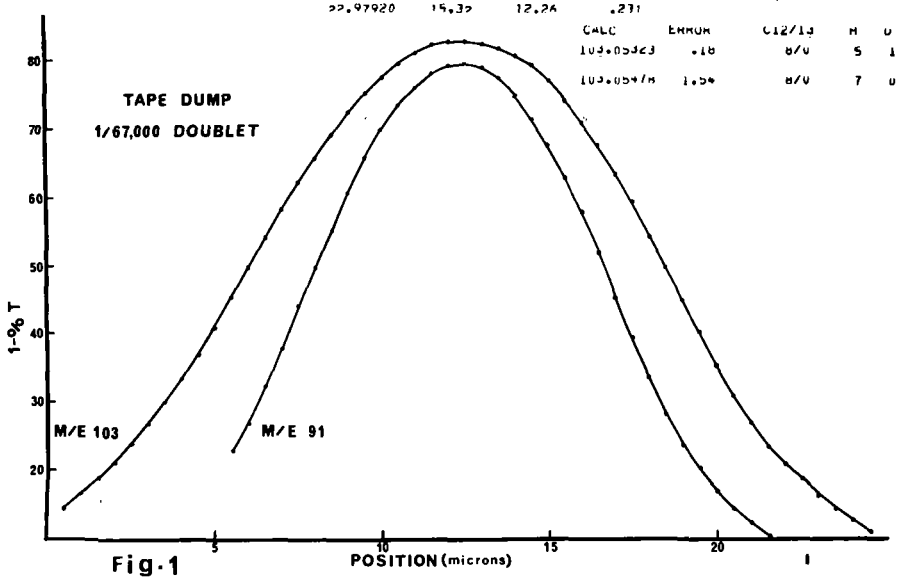

Fig.1

Plot of Tape Dump

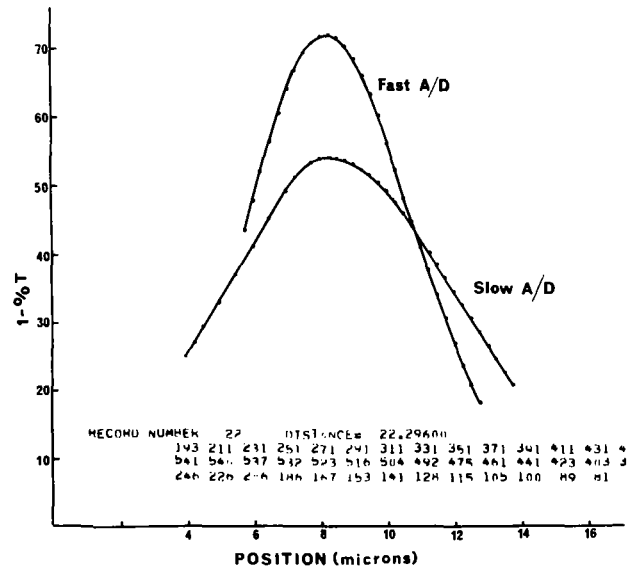

RECORD NUMBER 22 DISTANCE= 22.29600

193 211 231 251 271 291 311 331 351 371 391 411 431 451 471 491 511 531 534 537
541 544 537 532 523 516 504 492 475 461 441 423 403 386 366 346 326 306 286 266
246 226 206 186 167 153 141 128 115 105 100 89 81 75 70 66 61 56 53 49

Fig: 2

MASS SPECTROMETER + COMPUTER SYSTEM

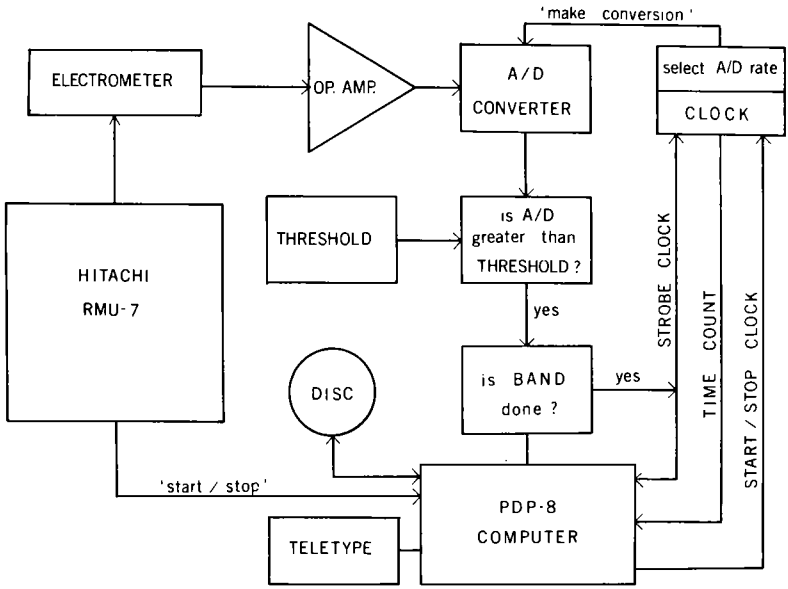

Fig. 3

BENZENE - PYRIDINE DOUBLET

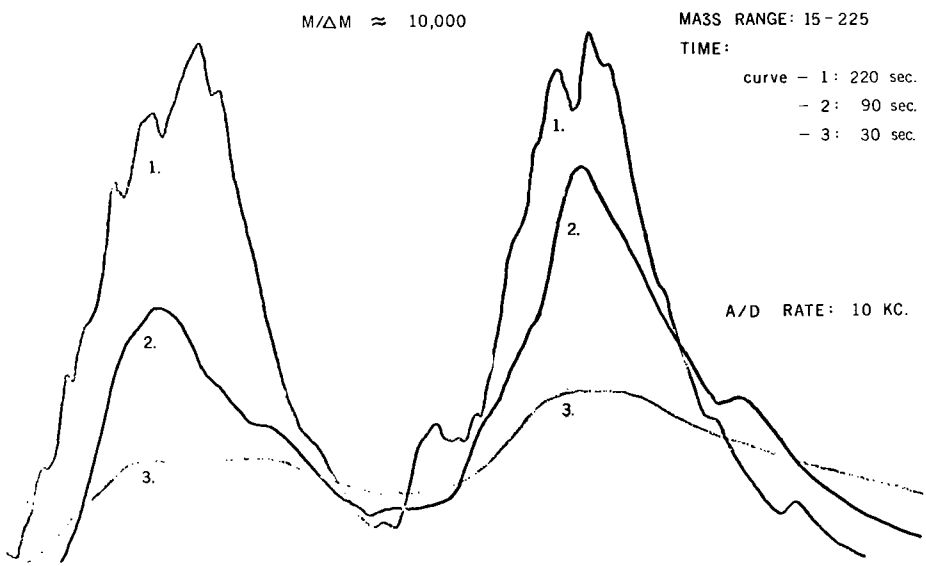

Fig. 4

The computer program developed to deconvolute the overlapping peaks uses a curve fitting technique employing least squares criterion. Further, checks are made on each profile regarding the width, total number of points, and other factors to detect the presence of a multiplet. If these parameters differ from those for a singlet, deconvolution is initiated to resolve the component peaks. Fig. 1 illustrates the application of these techniques to a 67,000 doublet containing the ion types $C_3H_5D^+$ and $C_3H_7^+$. For comparison the profile of a singlet is also shown. Deconvolution was initiated since the parameters were different from those for a singlet. Further analysis of the data leads to the mass and elemental composition for each of the ion types constituting the overlapping profile.

A careful examination of the raw data obtained from the plate reader revealed some of the inadequacies of the analog-to-digital converter present in the existing equipment. It was felt that if the signal from the photomultiplier were followed more closely, it should be possible to define the profile more accurately. This would enable one to look at the fine structure of the profile and consequently to increase the capabilities of the system significantly. We have incorporated a new A/D converter in the plate reader, results from which are plotted in Fig. 2. Results from the old A/D converter are plotted for comparison. The effect of convolution is apparent if the signal from the photomultiplier is not followed closely by the A/D converter. We are also in the process of making extensive modifications to completely eliminate the loss of data necessitated by turning on and off the magnetic tape recorder in the Datex system.

Recently, we have been investigating the potentialities of a system compromised of a PDP-8 computer and a high-resolution Perkin-Elmer-Hitachi RMU-7 mass spectrometer. Fig. 3 shows the block diagram of the system. The system contains an A/D converter, digital hardware threshold logic and an external crystal clock. The clock has a divider and the triggering rate can be selected before hand to suit the experiment. The data from the clock is stored in a 24 bit register and is available to the computer at any time during a scan. The computer itself has 4K of core memory with a teletype input output capabilities. The key to the whole system is a low cost disk with 64K words of auxillary storage. We found that this is extremely valuable as a high speed I/O device as well as a mass storage medium. Further this has enhanced the capability of the system, in the sense that all the software is held on the disk and brought into core only when it is necessary.

The software developed for this system is modular and makes use of the disk extensively.

First phase of the software concerns itself with acquiring the data. This section of the program uses the interrupt feature of the computer. The data is collected over the peak profiles at preselected rate over a preset threshold and stored on the disk. When the scan is completed an interrupt is generated and this brings in the next phase of the program to determine the line positions. To execute the program, data is retrieved from the disk and operated on the core. This of course has the advantage of using techniques that cannot possibly be used in real time using a small computer. We are investigating the advantages and disadvantages of using various methods of determining the peak centers. After completing this, the third phase of the program is brought in from the disk to establish the relationship between time and mass using the data from the calibration compound. After establishing this relationship all the time values are converted to the corresponding mass values in the fourth phase. Finally the elemental compositions are determined for all the mass values stored, in the fifth phase of the software. All these operations are continuous and no operator intervention is necessary. Flexibility of the system was kept in mind throughout the development of software. Several options are built into the programs at various stages. For example if one would like to examine the raw data, then by setting the proper register switches one can get a complete data dump. Several data dumps have been taken and Fig. 4 shows a plot of the data obtained on scanning over a 10,000 doublet at different scan rates.

Table 4 lists some of the criteria that should be taken into consideration for comparing the two data acquisition systems. The quality of data obtained from the photoplate spectra are much superior to the data obtained from direct electrical recording because there is an integrating effect on the photoplate spectra. The effective resolution that one can obtain remains fairly constant with electrical recording whereas it increases with increasing mass on photoplate recorded spectra. It is fairly easy to obtain more reliable abundance data from electrically recorded spectra than from photoplate recorded spectra. In the photoplate technique calibration of the emulsion is necessary to obtain reliable abundance values. For a small amount of sample, at a given resolution over the same mass range the sensitivity of the photoplate is better than in electrical recording.[4] Photoplate recorded spectra can

be stored permanently without any added effort. Flexibility of computer systems should be taken into consideration for comparing the two modes of data acquisition. The capabilities of a small computer when it is used for on line data processing impose a limitation on how far the analysis of data can be carried out. Of course this limitation is not applicable to off line data processing systems, particularly with the availability of a centralized large computing system. The great advantage of electrical recording and on line processing is that one can get the final results within a short period of time and this would of course enable the scientist to decide on the future experiments.

Acknowledgements: We would like to thank Mr. Hank Yosel for his help on building most of the hardware described in this work. The generous financial support of the National Institutes of Health (GM 12755 and FR 00354) is gratefully acknowledged.

References

1. R. Venkataraghavan, F. W. McLafferty and J. W. Amy, Fourteenth Annual Conference on Mass Spectrometry (ASTM E-14), Dallas (1966).
2. R. Venkataraghavan, R. D. Board, R. Klimowski, J. W. Amy and F. W. McLafferty, International Mass Spectrometry Conference, Berlin, 1967.
3. R. Venkataraghavan, F. W. McLafferty and J. W. Amy, Anal. Chem., 39, 178 (1967).
4. K. Habfast and K. H. Maurer, Fourteenth Annual Conference on Mass Spectrometry (ASTM E-14), Dallas (1966).

Table I.

MASS PRECISION

	Total lines compared.	Avg. Dif. in means.
1. Same Day, Same Plate, Same Spectrum	76	0.13mmu.
2. Different Day, Same Plate, Same Spectrum	77	0.26mmu.
3. Same Plate, Different Spectrum	66	0.47mmu.
4. Different Plate, Different Spectrum	49	0.33mmu.

Table II.

ERROR AND PRECISION OF ISOLATED LINES

Ion Type	Mass Error (mmu.)	Std. Dev. (mmu.)
C_4H_6O	0.15	0.24
C_6H_9O	-0.35	0.27
$C_{14}H_{26}$	-0.15	0.26
$C_{19}H_{38}O$	-0.15	0.33

For 29 lines: Average standard deviation = 0.30mmu.
Average mass error = 0.39mmu.

Table III.

Errors Before and After Deconvolution

Ion Type	Mass Before Error(mmu)	Mass After Error(mmu)
C_6H_6	-0.96	0.18
C_7H_{14}	-2.33	-0.70
C_8H_{17}	-1.93	-0.19
C_9H_{16}	-1.25	0.45

Average errors for 21 lines studied:

Before Deconvolution 1.51mmu.

After Deconvolution 0.40mmu.

Table IV.

Criteria for Comparison of Data Acquisition Techniques

1. Quality of Data
2. Effective Resolution
3. Accuracy of Abundance Data
4. Sensitivity vs. Mass Range
5. Permanent Data Storage
6. Flexibility of Computer Systems
7. Elapsed Time for Final Results

40. Recent Studies on the Franck-Condon Principle for Polyatomic Molecules.

H. M. Rosenstock* and R. Botter

Centre d'Etudes Nucleaires, Saclay, France

Recent experimental results from photoelectron spectroscopy and photoionization mass spectrometry have provided much material suitable for interpretation by the Franck-Condon principle. Three examples will be discussed: carbon dioxide, water and ammonia. These examples illustrate a number of the possibilities and problems of interpretation of experimental results. These problems include assumptions concerning the energy dependence of photoionization cross sections, the type of force fields leading to molecular vibrations, adequacy of the harmonic oscillator model, and problems arising from autoionization structure near the ionization threshold.

---

* Guest worker at the Centre d'Etudes Nucleaires, Saclay, France. Permanent address: National Bureau of Standards, Washington, D. C.

41. Applications of Photoionization Mass Spectrometry With High Photon Resolution*

William A. Chupka and Joseph Berkowitz

Argonne National Laboratory, Argonne, Illinois

The capability of performing photoionization mass spectrometry on gaseous molecules with photon band widths as narrow as 0.04Å (corresponding to ca. 0.0007 eV at 800Å) and at temperatures from 300°K down to 78°K (to reduce thermal vibrational and rotational energy) has proved to be a very useful tool in the study of a variety of phenomena. The characteristics of the autoionization observed near threshold for some monatomic and diatomic gases, especially H_2, have been studied in considerable detail and the results compared with theoretical predictions. Studies of other diatomic and polyatomic molecules have yielded very precise values for ionization potentials bond energies and electron affinities as well as structural information for polyatomic ions in some cases. Ions have been prepared in known vibrational and electronic (and in some cases rotational) states and their reactions studied as a function of their state of excitation. Chemi-ionization reactions of H atoms and H_2 molecules in known excited states have also been studied.

---

* Work performed under the auspices of the U.S. Atomic Energy Commission.

42. Mass Spectrometric Study of the Photoionization of H_2S and SO_2*

Vernon H. Dibeler and Susan K. Liston

Institute for Materials Research
National Bureau of Standards
Washington, D. C. 20234

A number of photon absorption and electron impact studies of hydrogen sulfide and sulfur dioxide have been reported. In the case of H_2S, Rydberg series (1), photoionization without mass analysis (2), photoelectron spectroscopy (3), and electron impact (4,6), are generally in agreement in reporting the first ionization threshold at 10.45 ± 0.05 eV. Thresholds for electronically excited states of the molecule ion have also been reported (3,5), although not in good agreement. The ionization energy of the SH radical has also been obtained from absorption spectra (7) and from electron impact studies (8). Both results agree within combined uncertainties.

For SO_2, a rough extrapolation of Rydberg series (9) resulted in $I(SO_2)$ = 12.05 ± 0.05 eV. This is very probably too low by an amount greater than the estimated uncertainty as Inn (10) and Watanabe (11) report photoionization results of 12.42 ± 0.02 eV and 12.34 ± 0.02 eV, respectively. Good agreement with the latter has also been obtained by means of photoelectron spectroscopy (3). In addition, recent electron impact measurements (12,14) also agree, within the stated uncertainties, although they are generally higher than the photoionization values. Blanchard and LeGoff (15) observed a diminution in threshold for the SO^+ ion from SO_2 when the latter was exposed to a heated tungsten ribbon. They ascribed the lower value, 12.5 ± 0.3 eV to the ionization energy of the SO radical. An indirect measure (12) of the same quantity resulted in the upper limit, I(SO) < 11.0 eV.

Thus, although molecular ionization thresholds in H_2S and SO_2 are established within rather narrow limits (± 0.05 - 0.1 eV) there remains considerable uncertainty regarding dissociative ionization of these molecules. The difficulties in obtaining accurate threshold values (± 0.01 eV, or less) for dissociative ionization of complex molecules and, thereby, bond dissociation energies by means of electron or photon impact have been discussed (16,18). Also, from recent reviews of bond dissociation energies (19,20) and of mass spectrometric studies of elemental sulfur (21), it is apparent that the "high" value of $D_0(S_2)$ is well established, although the uncertainty is at least 0.1 eV. Other values of sulfur bonds such as D_0(HS-H), D_0(HS), ΔHf°_0(SO), and dependent quantities are ill-defined. The present work was undertaken in an attempt to reduce the limits of uncertainty and to improve the related thermodynamic values.

Measurements were made by means of the combined vacuum ultraviolet monochromator - mass spectrometer described in detail in the first paper of this series (22), but incorporating certain significant changes described in subsequent reports (23).

H_2S: The relative abundances of positive ions, H_2S^+, HS^+, S^+ and S^+(m) at 21.23 eV are 1.00, 0.76, 0.46, and 0.01 respectively. The observation of a metastable transition $H_2S^+ \rightarrow S^+$ ($^m/_e$ = 30.1) + H_2 with an unusually large relative abundance has been noted previously (6). One other possible metastable due to the transition, $HS^+ \rightarrow S^+ + H$, was also observed but with a relative intensity too low (0.003) for threshold measurements.

* This work was supported in part by the U. S. Atomic Energy Commission. A more nearly complete version has been accepted for publication in the Journal of Chemical Physics.

The ion yield curve for the H_2S^+ ion has a sharp onset at 1189Å (10.43 ± 0.01 eV). This minimum ionization energy is in excellent agreement with 10.42 eV reported by photoelectron spectroscopy (3). It may be significantly lower than the results obtained from Rydberg extrapolation (1) and previous photoionization (2) if the uncertainties are as quoted by the authors. It is generally in good agreement with recent electron impact results although not always within the uncertainties claimed. Taking the present threshold value as the heat of reaction, ΔH_o = 240.5 kcal mol^{-1}, for $H_2S + h\nu \rightarrow H_2S^+ + e$, and adding the heat of formation (24), $\Delta Hf^\circ_o(H_2S)$ = -4.232 kcal mol^{-1}, we obtain $\Delta Hf^\circ_o(H_2S^+)$ = 236.3 kcal mol^{-1}. This and following thermodynamic values are summarized and discussed in the paper to be published.

The threshold of the HS^+ ion definitely appears at 869Å (14.27 ± 0.02 eV). The remainder of the curve is a remarkable smooth and apparently featureless continuum to 600Å, although the portion below 800Å was taken in 5-Å steps. Taking the threshold to be the heat of reaction, ΔH_o = 329.1 kcal mol^{-1} for $H_2S + h\nu \rightarrow HS^+ + H + e$ the usual summation of heats of formation (24) results in $\Delta Hf^\circ_o(HS^+)$ = 273.2 kcal mol^{-1}. Subtracting Morrow's (7) value of I(SH) = 239.8 ± 0.7 kcal mol^{-1} gives $\Delta Hf^\circ_o(SH)$ = 33.4 ± 0.7 kcal mol^{-1} and permits us to derive $D_o(HS-H)$ = 89.3 ± 0.7 kcal mol^{-1}.

The S^+ ion appearing in the mass spectrum at $^m/_e$ = 32.0 exhibits a rapidly rising onset at 925Å (13.40 ± 0.02 eV). However, the production of ground-state products according to the reaction,

$$H_2S(^1A_1) + h\nu \rightarrow S^+(^4S) + H_2(^1\Sigma_g^+) + e$$

is forbidden by the spin conservation rule. Although the uncertainty in evaluationg either normal or metastable threshold is about ± 1Å, the S^+ ion formed by metastable transition and observed at $^m/_e$ = 30.1 clearly has a lower energy onset than the S^+ ion observed at $^m/_e$ = 32.0. Therefore, subtracting I(S) from the metastable threshold results in $\Delta Hf^\circ_o(S)$ = 65.0 ± 0.5 kcal mol^{-1}. From the heat of formation (24) $\Delta Hf^\circ_o(S_2)$ = 30.647, we derive the bond dissociation energy, $D_o(S_2)$ = 99.4 kcal mol^{-1}. Also, from the above ΔHf°_o (HS) = 33.4 kcal mol^{-1} we obtain $D_o(HS)$ = 83.2 kcal mol^{-1}.

SO_2: The two principal ions observed at 21.23 eV are the SO^+_2 and SO^+ ions with relative abundances of 1.00 and 0.75 respectively. Except for the equally abrupt onset, the ion-yield curve for SO_2 is quite unlike that of H_2S. The first ionization threshold has a mid-point at 1006Å (12.32 ± 0.01 eV). This threshold energy together with the heat of formation (24), $\Delta Hf^\circ_o(SO_2)$ = -70.336 kcal mol^{-1} gives the ionic heat of formation, $\Delta Hf^\circ_o(SO_2^+)$ = 213.8 ± 0.2 kcal mol^{-1}.

The SO^+ ion shows a weak but step-like onset at 784Å (15.81 ± 0.02 eV). Unfortunately, an accurate direct measurement of I(SO) has not been reported. However, Brewer (26) and Marsden (27) have discussed briefly the spectroscopic evidence for $D_o(SO)$ = 5.357 eV (124.14 kcal mol^{-1}), and Warneck, Marmo, and Sullivan (28) have reported an upper limit only slightly greater. Accepting this value and $\Delta Hf^\circ_o(S)$ = 65.0 kcal mol^{-1} determined above we calculate $\Delta Hf^\circ_o(SO)$ = - 0.16 kcal mol^{-1}. This results in a value of $D_o(OS-O)$ = 129.2 kcal mol^{-1} and I(SO) = 10.21 eV.

References

(1). W. C. Price, J. Chem. Phys. 4, 147 (1936).

(2). K. Watanaba and A. S. Jursa, J. Chem. Phys. 41, 1650 (1964).

(3). M. I. Al-Joboury and D. W. Turner, J. Chem. Soc. 1964, 4434.

(4). J. D. Morrison, J. Chem. Phys. 19, 1305 (1951).

(5). D. C. Frost and C. A. McDowell, Can. J. Chem. 36, 39 (1958).

(6). V. H. Dibeler and H. M. Rosenstock, J. Chem. Phys. 39, 3106 (1963).

(7). B. A. Morrow, Can. J. Phys. 44, 2447 (1966).

(8). T. F. Palmer and F. P. Lossing, J. Amer. Chem. Soc. 84, 4661 (1962).

(9). W. C. Price and D. M. Simpson, Proc. Roy. Soc. (London) A165, 272 (1938).

(10). E. C. Y. Inn, Phys. Rev. 91, 1194 (1953).

(11). K. Watanabe, J. Chem. Phys. 26, 542 (1957).

(12). R. M. Reese, V. H. Dibeler, and J. L. Franklin, J. Chem. Phys. 29, 880 (1958).

(13). R. Hagemann, Compt. Rendu 255, 1102 (1962).

(14). R. Botter, R. Hagemann, G. Nief, and E. Roth, Advances in Mass Spectrometry, Vol. 3. The Institute of Petroleum, 1966, p. 951.

(15). L. P. Blanchard and P. LeGoff, Can. J. Chem. 35, 89 (1957).

(16). B. Steiner, C. F. Giese, and M. G. Inghram, J. Chem. Phys. 34, 189 (1961).

(17). F. A. Elder, C. F. Giese, B. Steiner, and M. G. Inghram, J. Chem. Phys. 36, 3292 (1962).

(18). W. A. Chupka, private communication.

(19). S. W. Benson, J. Chem. Educ. 42, 502 (1965).

(20). J. A. Kerr, Chem. Revs. 66, 465 (1966).

(21). J. Berkowitz, Chapt. in Elemental Sulfur, edited by B. Meyer, Interscience Publishers, New York, 1965.

(22). V. H. Dibeler and R. M. Reese, J. Res. NBS, 68A, 409 (1964).

(23). For the preceeding paper of this series, see: M. Krauss, J. A. Walker and V. H. Dibeler, J. Res. NBS.

(24). D. D. Wagman, W. H. Evans, V. B. Parker, I. Halow, S. M. Bailey, and R. H. Schumm, Natl. Bur. Std. (U.S.) Tech. Note 270-3 (1968).

(25). C. E. Moore, Natl. Bur. Std. (U.S.) Circ. No. 467 (1952).

(26). L. Brewer, J. Chem. Phys. 31, 1143 (1957).

(27). D. G. H. Marsden, J. Chem. Phys. 31, 1144 (1957).

(28). P. Warneck, F. F. Marmo, and J. O. Sullivan, J. Chem. Phys. 40, 1132 (1964).

44. HIGH RESOLUTION MASS SPECTRAL PHOTOPLATE DATA ACQUIRED AND REDUCED WITH A REAL TIME REMOTE DIGITAL COMPUTER

D. M. Desiderio, Jr.* and T. E. Mead
American Cyanamid Company
Stamford Research Laboratory
Stamford, Connecticut 06904

A data reduction system was desired in American Cyanamid's Stamford Research Laboratory to obtain high resolution mass spectral data from photoplates with the maximum accuracy obtainable from a photoplate, at a minimum in cost and human intervention, a maximum of convenience to the comparator operator, and the fastest return of results from the computer. A microdensitometer-comparator connected remotely to an existing computer appeared to be the best design to achieve the above desiderata.

Photoplates are read by a Gaertner comparator Model C9418 and the resulting data encoded with a Datex optical encoder Model 03-507-9. The photomultiplier analog output is amplified by an SDS Model 925 digital computer.

The system described combines the automatic comparator-microdensitometer to read transmission values every 0.5 microns and the medium size, high speed digital computer connected via a direct cabling system of 500 feet length to transmit high resolution mass spectral photoplate data. The digital data are processed by a machine language data acquisition program resident in the computer, and those data above a threshold are stored on a disc file. During acquisition the computer program automatically follows an increasing or decreasing photoplate background and corrects each datum accordingly. The rate of comparator travel is continuously variable from 0 to 125 mm/min., enabling an exposure to be scanned in 3-4 minutes.

Before initiating plate travel, input parameters are sent to the computer with a teletypewriter located next to the comparator. This input procedure is one of a "dialogue" nature with the computer. Previously written questions are asked by the machine language acquisition program and the comparator operator answers each question with a number until the input parameters are fulfilled, at which point the computer instructs the comparator operator to commence measurement.

*Present Address: Institute for Lipid Research, Baylor University College of Medicine, Texas Medical Center, Houston, Texas 77025

While the comparator slews back to begin reading another exposure, the computer transfers the acquired data from the disc to a magnetic tape. This procedure repeats until all spectra of interest are transmitted and stored sequentially on magnetic tape.

The data are then reduced at the computer operator's convenience. A FORTRAN program reads the peaks into memory, calculates peak centers and areas, resolves overlapping peaks by a non-linear, least squares, iterative procedure, calculates masses, elemental compositions, and prints an element map and a "low resolution spectrum" with a list of all elemental compositions found.

The system explained here is offered in the hope that it represents the terminal developmental step in the acquisition of data, namely, by direct communication with the computer.

45. Improved Acquisition and Processing of High Resolution Data from Photoplates.

F. Aulinger, J. Franzen, W. Riepe, D. Stüwer
(Institut für Spektrochemie und angew. Spektroskopie, Dortmund)

E. Wegner, U. Markwardt, K. Habfast
(Varian MAT GmbH, Bremen)

This paper deals with preliminary results obtained with the Varian MAT SM1A mass spectrometer, the automatic photoplate reader Leitz-Varian SAM 1 and a line identification computer program. The work is aimed at the unambiguous identification of mass spectral lines of unknown substances with molecular masses as high as 400 to 500 u.

The entire experimental procedure is diagrammatically shown in fig. 1. Our SM1 instrument yields, at a photographic resolution of some 40000, lines between 2 - 6 µm wide on Ilford Q2 plates, provided the lines are not overexposed. The SAM1 automatic plate reader samples the line profile, above a variable threshold, in precise steps of 0.2 µm. A computer program deconvolutes broad mass lines; the position values of narrow lines are determined by computing the center of gravity. The reproducibility of distance measurements was found to be better than 0.01 µm, based on repeated measurements on a photographically produced reference scale. - The integrated areal line blackening $B = 1 - T$ (T = line transparency) turned out to be proportional to the logarithm of the total number of ions which produced this line.

The line identification computer program allows the consideration of up to 5 different kinds of hetero elements two of which may be made up of up to 7 isotopes. The computer program provides three restrictions which limit the number of possible hetero atom combinations for a given mass line:

1. If minor isotope lines are to be expected with sufficient intensity for a given combination, then they must be detected, or else this combination will be discarded;
2. The user may voluntarily disregard certain hetero element combinations, based on his previous chemical knowledge, or based on preliminary results.
3. If a line should, at this point of the program, not be uniquely identified, then the computer program will initiate an investigation as to which of the remaining combinations can be eliminated because of their being far less probable than others. The probability of a certain combination to be true is determined by considering
   a) the difference between the computed and the experimental mass values,

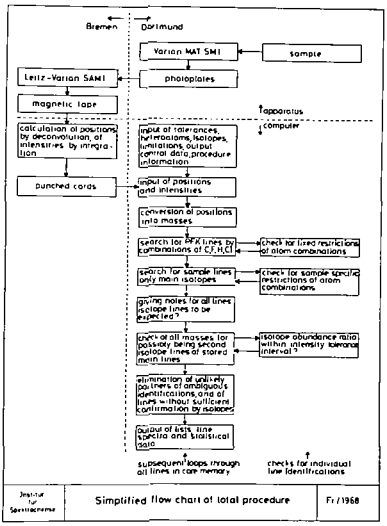

Fig. 1 Simplified flow chart of total procedure

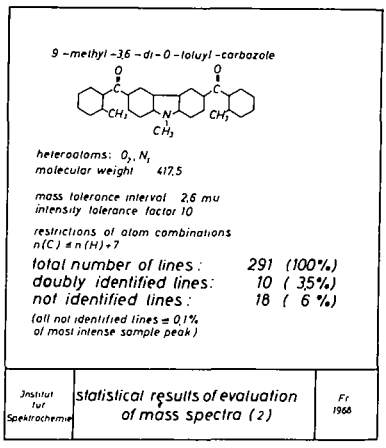

Fig. 2 Statistical results of evaluation of 9-methyl-3,6-di-O-toluyl-carbazole

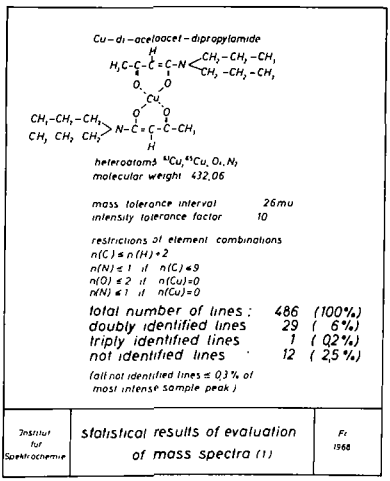

Fig. 3 Statistical results of evaluation of Cu-di-acetoacet-dipropylamide

mass range (u)	nr. of lines	standard errors $\tilde{s}_{abs}$ (mu)	$\tilde{s}_{rel}$ (ppm)
0 - 100	84	0,6	7,4
100 - 200	202	0,9	6,1
200 - 300	96	1,1	4,7
300 - 400	46	0,9	2,5
400 - 500	13	0,9	2,1
(Cu - di - acetoacet - dipropylamide)			
0 - 100	24	0,6	6,9
100 - 200	97	0,7	5,0
200 - 300	86	0,8	3,3
300 - 400	39	0,8	2,6
400 - 500	15	1,0	2,4
(9 - methyl - 3,6 - di - O - toluyl - carbazole)			

Institut für Spektrochemie — Accuracy of mass determination (statistical data) — Fr / 1968

Fig. 4 Accuracy of mass determination

and

b) the isotope abundance pattern of all elements contained in that combination.

The computer printout may consist of bar graphs with line identifications, or of lists of identified lines, above a variable threshold, and with or without unidentified lines, minor isotope lines, doubly-charged lines etc.

The results we obtained so far, for two samples with molecular weight 417 and 432, respectively, are shown in figs. 2 and 3. On each photoplate, only one exposure trace, covering a dynamic range of $1 : 10^5$, was evaluated.

The accuracy of mass determination is shown in fig. 4. The "standard errors" were obtained in an analogous manner to the calculation of "standard deviations", except that the deviation of the experimental values from the "true" (tabulated) values, and not from the "mean" values, were computed. The standard error of 2.5 ppm at nominal mass 400 corresponds to an apparent error of 0.3 µm in line distances. This is, in our opinion, not the limit: a non-linear interpolation between the square roots of reference masses will increase the accuracy of scale conversion (photographic line position to mass); the elimination of gelatine shrinkage by modified photoplate fixing techniques will improve the fidelity of line positions after plate processing; elimination of change build-up on the photoplate surface by ions and secondary particles will avoid incontrollable line shifting.

Further results of this work will be published elsewhere.

46. A NEW CONCEPT IN SPECTRA READOUT

Raymond A. Meyer and George Lauer
Science Center
North American Rockwell Corporation
Thousand Oaks, California 91360

I will describe the feasibility study on our visual-digital converter. Bear in mind that this is only the start and many questions remain unanswered at the moment. Assuming that the ions of a mass spectrometer can be made to activate a scintilator plate without loss of resolution, the spectra may be presented as a series of bars of light with both X significance giving the m/e and Z or intensity significance giving ion beam density. My concept is that of a ½" x 12" scintilator replacing the photo plate and forming the vacuum barrier. Thus, ions striking the scintilator will result in bars of light visible from the rear of the spectrometer. Since the scintilator plate is not yet in existence, a series of black and white bars were drawn and photographed to construct the grid showin in Figure 1. It measured 3/8" x 1/2" and was transilluminated. Thus, presenting a bright bar 100 mills wide followed by a dark segment 50 mills wide, etc. The minimum was a 5 mill bar of light and a 5 mill dark area. This grid was used in all testing.

The spectra readout system or visual-digital converter is based on a television camera focused on the spectra with the video signal fed in digital form into a computer. Figure 2 shows the output from a single horizontal scan line. The active scan takes place during a 53 microsecond period and a new line is scanned every 63 microseconds. A complete frame is scanned every 33,000 μseconds if a 525 line scan is used. The sync level is used to command the computer and the video portion, of course, contains the line intensity information. Figure 3 shows the output from the camera as it looks at a single scan line. In the top line, the camera is looking at a dark subject. The center line shows what we would see if the scan lines were oriented the way we would expect to see them when looking at our simulated spectra. This information is of little value because we can't look at a single spectra line but rather look across all of them. However, if the camera is turned on its side, the scan lines become aligned with the spectra as shown in the lower line and thus present a signal that is usable. The area under the video signal is a measure of the total light which has been emitted by the scintilator in the area scanned. If the spectra bar is very narrow, the next scan line will be like the top one and show no light. If it is a wide bar, the next several may show light such as shown in the small screen reproduction.

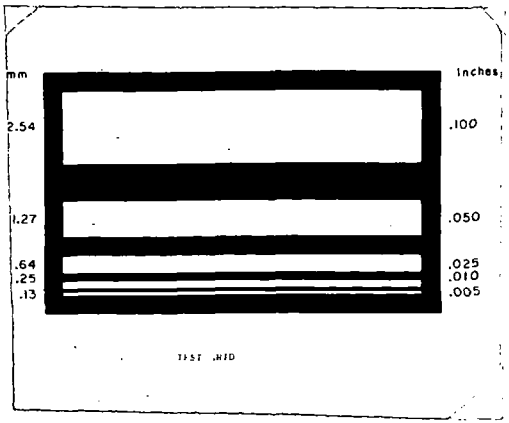

Figure 1. Test Grid

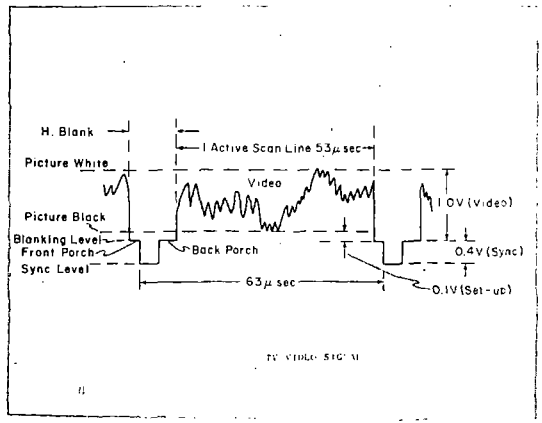

Figure 2. Video Signal

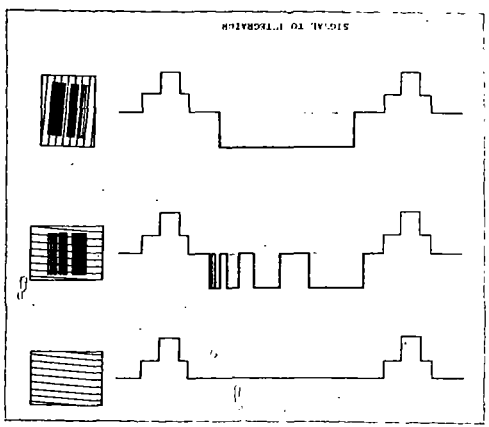

Figure 3. Signal to Integrator

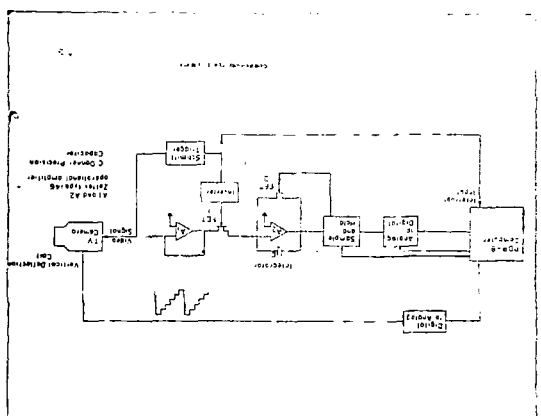

Figure 4. Camera-Computer Schematic

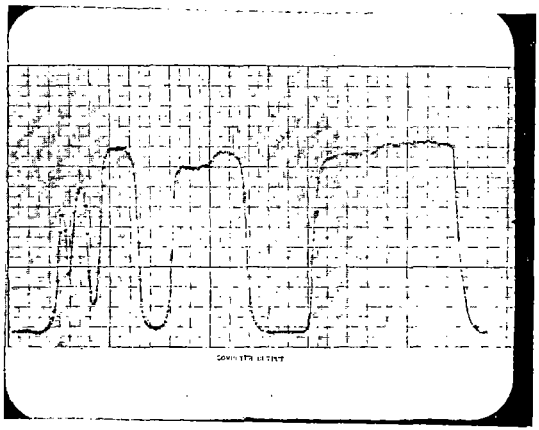

Figure 5. Computer Output

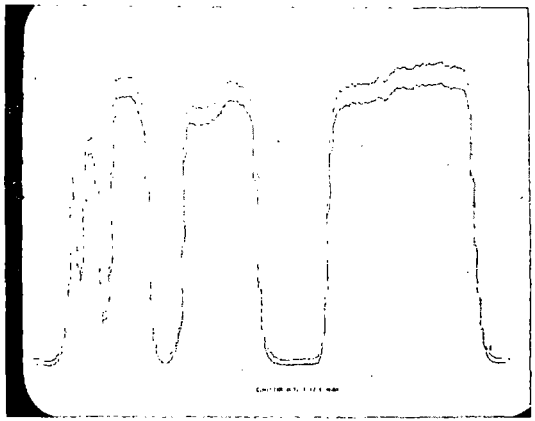

Figure 6. Computer Line Output

TABLE II

Output vs. Lens Stop

f Stop	Run 1	Run 2	Theory
1.4	100%	100%	100%
2	63	61	49
2.8	38	33	25
4	19	19	12
5.6		10	6
8		4	3

OUTPUT VS. LENS STOP

Figure 7. Output vs. Lens Stop

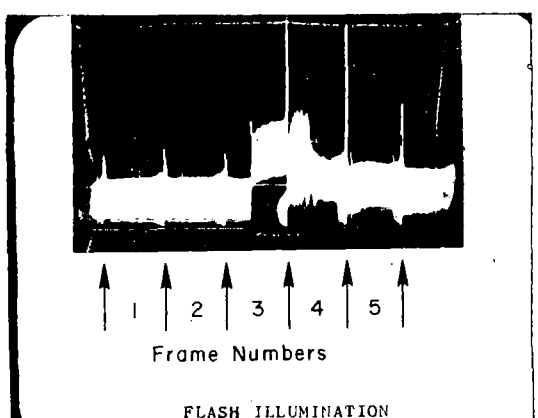

Figure 8. Flash Illumination

To reemphasize, the camera is turned on its side so the horizontal scan lines become vertical and thus aligned with the bar of light on the scintilator. Thus, the spectra may be converted into an electrical signal. Without my co-author, Dr. Lauer, that is where it could well have stopped. Figure 4 presents the circuitry used to control, digitize, and store the video information. Let us consider the operation during a single (ex-horizontal now vertical) scan line. The signal is fed into an operational amplifier to establish the proper level and then to another amplifier used as an integrator at the end of the line scan. The voltage on condenser C accurately represents all the light present in that portion of the spectra. The end of the scan is signaled by the start of the blanking pulse. The video signal is removed from the integrator and the condenser voltage is stored in the sample and hold portion of the computer. When the integrated signal is safely stored, F.E.T. 1 closes and discharges the condenser preparing it to receive the next line.

The vertical positioning of the scan lines has been placed under computer control to insure that, for example, line 260 from Frame 1 accurately coincides with line 260 from Frame 2, etc. The staircase voltage establishing vertical position is incremented by one step at this time and the camera is ready for another scan line. During the 53 μsec of the next scan, the computer has time to digitize the data stored in the sample and hold section and add it to all data previously stored for that scan line from previous frames. Thus, line by line the spectra is scanned and the integral of the light determined, digitized and stored. The entire frame is repeated every 1/30 of a second if the normal 525 lines are scanned and the data from each succeeding frame summed.

The stored data may be handled in any manner. With proper programming and prestorage of calibration data the end of the sparking time could be signaled by a typewriter output of the complete analysis. We chose a graphical output and Figure 5 shows a scan line by line output of our test grid. It is perhaps easier to see in Figure 6 where the X-Y recorder was allowed to draw continuous lines. The line distortion is a function of the recorder.

Figure 7 shows a cursory look at linearity. These data show response as a function of camera level aperature. The lens diaphragm is uncalibrated but is a F 1.4 Nikon from my Leica.

Does the vidicon integrate and store all the light falling on it between scans of the electron beam? We studied this by illuminating a white card with a 3 microsecond flash of light. The light pulse is obviously much shorter than the

3×10^4 microseconds required to scan a complete frame. Figure 8 shows an oscilloscope display of five complete frames. The light pulse occurred during the third frame and was reasonably constant during a single scan. The wipe-off is also shown to be good and is almost complete after two frames. The wipe-off is the parameter that determines memory from a single scintilation, for example.

Thus, this preliminary study of a new technique has found no performance limiting factors. The system shows 5 mill resolution, linearity of response, and integration. This study was done with a Shibadena HV 14 camera costing only 400 dollars and having a resolving power of 400 lines.

Where do we go from here? Obviously a more expensive camera would provide better resolution. Westinghouse has perfected a more adaptable camera tube, The Secondary Electron Conduction Tube. It has demonstrated integration times of 5 minutes with wipe-off in one pass of the electron beam. Resolving powers of over 1000 lines have been demonstrated. The scintilator remains to be studied and perfected. None of these seem at present, to present unsurmountable difficulties. Certainly, much remains to be done, but the new detector does appear feasible in the preliminary study.

47. A COMPUTER-CONTROLLED SYSTEM FOR AUTOMATICALLY SCANNING AND INTERPRETING PHOTOGRAPHIC SPECTRA

C.A. Bailey, R.D. Carver, R.A. Thomas, and R.J. Dupzyk

Lawrence Radiation Laboratory, University of California
Livermore, California

The Lawrence Radiation Laboratory has had a CEC 21-110 Spark Source Mass Spectrometer in operation for five years. Two years ago the chemists and electrical engineers started looking for a way to simplify and improve the reduction of the data which is taken on photographic plates.

Several available systems of both plate reader and densitometer were looked into and found to have hard wired programs not applicable to what we wanted to do. We concluded that we had to design the system ourselves.

The Grant Microdensitometer was found to be an excellent plate reader capable of being operated by computer controlled stepping motors. The densitometer was coupled to a Digital Equipment Corporation PDP-8 computer to construct our present system.

The first component in the system is a Spark Source Mass Spectrograph, CEC 21-110. The ions from a sample are collected on a 2" x 15" glass photoplate. The mass lines occurring on the plate come from elemental and compound ions, singly and multiply charged. Twenty graded exposures can be collected on a plate. Each exposure is 2mm in length. For our purposes "exposure" means the number of ions striking the photographic plate; this value is expressed in Coulombs. The second component in the system is a Grant Microdensitometer. It has an accuracy of $\pm$ 1 micron in the X and Y directions. The densitometer is stepped in one micron increments in the X direction and five micron increments in the Y direction. There are two viewing screens available. One is a projection through a 22 power zoom lens which allows a closeup of the area being scanned. The second screen is an analog signal from the detector displayed on a cathode ray tube. It is used for adjusting the scanning slits.

The readout is an analog-to-digital converter (ADC) connected to the photomultiplier output. The ADC is capable of twelve-bit resolution with a digitizing time of 35 microseconds.

The actual plate stage drive is accomplished by using two hundred steps per revolution digital stepping motors. The X-drive incorporates a 5:1 gear reduction which results in a scale of one micron per step. No gear reduction is used on the Y-drive, therefore the scale is 5 microns per step. Motor speed was selected to allow instant start-stop-reverse response without resorting to controlled speed-up to compensate for inertial effects.

The interface from the PDP-8 to the microdensitometer uses only one device selector. The device selector, by program control, puts out any one, or a combination of three IOT pulses.

IOT-TWO is used to transfer nine status conditions, such as X ready, Y ready, + X limit, etc., into the accumulator. All but two of the status conditions set the flag. IOT-FOUR actuates any one of nine different control functions depending on what bit or bits are set in the accumulator. Typical control functions are, step + X, step - Y, clear flag, interrupt on, etc.

The interface provides interrupt capability, but it is not being used with the present program.

The third component is the Digital Equipment Corporation PDP-8. It is the 4k version equipped with two Dectape transports and the extended arithmetic element (EAE). The code occupies all of core. The floating point package-D is used for all the input, output, and most of the calculations. Control and operation of the system is done entirely with software.

The following describes the interaction between the operator and the Grant/PDP-8 system. The emulsion calibration for the plate is made by exposing the plate to the rhenium isotope spectrum at varying intensities, changing the magnet setting between exposures in order to offset the lines. These line-density-ratios are fitted into the Hull equation relating plate density to exposure (Fig. 1). The exponent R is calculated to be used later to calculate relative abundances of the ions striking the plate.

The input for this process is through the teletype (TTY). The operator types the number of rhenium lines to be read and a value for the transmission at infinite exposure (T_{inf}).

When the specified number of lines has been read the computer waits for the operator to realign the stage to read from low mass to high mass over the range he desires. When alignment is complete the operator types in a starting and a final location in microns, four mass numbers, and their locations on the plate. These masses are carefully chosen prominent lines distributed across the range of interest and are fitted into a mass number calibration equation (Fig. 2). "A" and "B" are determined and used later to calculate the mass number of each unknown line from its location on the plate. Twenty exposure values are typed in corresponding to the number of Coulombs each line was exposed. At this point the computer is put in complete control, and the operator is no longer needed.

The following is a description of the peaks encountered on a typical photographic plate and the way the computer code handles them.

The first peak is a singlet in a clean portion of the plate. The peak reading process always starts with the most intense exposure. The code calculates a peak detection threshold value. This value is an arbitrary decrease in the transmission calculated from the background values (Fig. 3). This value is updated every one ninth of a mass unit if a peak has not been detected. A peak is determined by testing to see if the incoming transmission value is below the peak detection threshold. If a peak is detected it is checked to see if it is an honest peak. This check is necessary because of noninformity in the emulsion. If it is an honest peak its peak top is determined and two background values one ninth of a mass unit on either side of the peak top are taken. One ninth of a mass unit is an arbitrary distance selected to reach over the very dense lines and yet not encounter other mass lines from multiply charged ions. There are not a constant number of exposures for each mass line, so the following method is used to determine when all the lines for a individual mass have been read. Two questions are asked of the PDP-8. 1) Have twenty exposures been racked? If yes, then it does not look for more information; if no, the second question is asked. 2) Is the transmission of this peak top below a threshold value calculated from the background values of the previous exposure? If yes, then the stage is racked one exposure in the positive Y direction, the direction of lesser exposure, and the data are stored in a buffer in core. If no, then all the data from that line have been measured and the code racks back to the most intense exposure and continues to look for a new mass.

The second peak is a doublet. The first mass line encountered in a doublet is read in the same manner as a singlet except that the background values are now taken at one ninth mass unit on one side and at the minimum in the valley between the peaks. The computer is aware that there is a mass on its high mass side. When it has finished the first mass line it then scans the high mass line. Because the various exposures are not perfectly perpendicular to each other it was necessary to make sure that the stage returned to the peak top of the most intense exposure of each mass line encountered before starting to look for a new mass line. This was especially necessary in the case of doublets.

The third peak is one that lies in fog. Fog is caused by the ions from a very abundant element scattering due to residual charge build-up. Fog on plates may have a transmission value as small as 5%. The process of updating the peak threshold detection value every one ninth of a mass unit described earlier allows very light lines to be found in the very dark fog. The process of checking to see if the peak top value is darker than the threshold calculated from the previous exposure allows all the exposures for a mass line to be read.

The entire plate is read and the data are stored on the Dectapes in two block segments. The following information is stored: The mass number, from eq. 1 the transmission at the peak top, the transmission at the two background positions, and the exposure value.

The teletype output is shown in Figure 4

1) The percent transmission of the Re 185 and Re 187,
2) the R values for each Re ratio, calculated from the Hull equation,
3) and the average R value.

Following this are the data for all detected masses on the plate typed in the following fashion (Fig. 5)

1) The mass number,
2) the percent transmission of the peak top and the two background values,
3) the abundance of the peak top and the two backgrounds and a net abundance,
4) the average abundance and the percent error.

The average abundance is a weighted average so that all exposure values could be used in the calculation. The weighting function is parabolic.

It was found that the numbers from the Grant/PDP-8 system agreed with hand calculation to within 5%. This is very good agreement as spark source work is usually quoted to a factor of two. There is no reason to believe that the Grant/PDP-8 numbers are not better. Standard samples are difficult to prepare.

To conclude let us compare the time spent in reading and reducing the data from one plate. Starting from the time that the plate is developed, dried, and ready for reading until relative abundances are in hand:

1) The Grant/PDP-8 system takes one half hour of operator time, and for a typical geological sample about eleven hours of system time, approximately 5 hours for reading the plate and 6 hours for typing the data. It can be set up before closing time and answers are ready at opening time the next morning.
2) With the standard system an operator is almost always required to put the data out on chart paper, convert it to IBM cards and run a short code on a CDC 3600 taking a total time of three or four days.

The Grant PDP-8 system is a great improvement over the old system. It should be adapted readily to other plate or film reading systems.

We would like to thank Dr. G. W. Barton, Jr. for his help in deriving the equations to weight the average abundance and to calculate a percent error for the average abundance.

This work was performed under the auspices of the United States Atomic Energy Commission.

FIGURE I

HULL EQUATION FOR EMULSION CALIBRATION

$$Emi = \left[\frac{T_o - T}{T - T_{inf}} \right]^{\frac{1}{R}}$$

FIGURE 2

MASS CALIBRATION EQUATION

$$MASS = \left[\frac{Loc - A}{B} \right]^2$$

FIGURE 3

THRESHOLD EQUATION

Threshold = Average Bkg. - (% * Average Bkg.)

FIGURE 4

RHENIUM DATA AND R VALUE

%T RE 185 and RE 187

+ϕ.4749693E+ϕ2	+ϕ.3592184E+ϕ2
+ϕ.49ϕ1ϕ98E+ϕ2	+ϕ.3636140E+ϕ2
+ϕ.5264959E+ϕ2	+ϕ.3936508E+ϕ2
+ϕ.5235654E+ϕ2	+ϕ.4119656E+ϕ2
+ϕ.56ϕ1952E+ϕ2	+ϕ.4483516E+ϕ2
+ϕ.648596ϕE+ϕ2	+ϕ.5196582E+ϕ2
+ϕ.6923ϕ75E+ϕ2	+ϕ.56ϕ4394E+ϕ2
+ϕ.691ϕ865E+ϕ2	+ϕ.5633699E+ϕ2
+ϕ.8329668E+ϕ2	+ϕ.7479852E+ϕ2
+ϕ.78ϕ2197E+ϕ2	+ϕ.6656897E+ϕ2

R VALUES

+ϕ.94673ϕ2E+ϕϕ
+ϕ.1ϕ2846ϕE+ϕ1
+ϕ.1ϕ62ϕ21E+ϕ1
+ϕ.8881528E+ϕϕ
+ϕ.8849648E+ϕϕ
+ϕ.1ϕ49275E+ϕ1
+ϕ.1114296E+ϕ1
+ϕ.1ϕ79682E+ϕ1
+ϕ.1ϕ14555E+ϕ1
+ϕ.1131831E+ϕ1

$$R = \text{Log}\left[\frac{\dfrac{T_o - T_{187}}{T_{187} - T_{inf}}}{\dfrac{T_o - T_{185}}{T_{185} - T_{inf}}}\right] \div \text{Log}\,(1.67)$$

AVE R VALUE +ϕ.9789795E+ϕϕ
1/R VALUE +ϕ.1ϕ21472E+ϕ1

FIGURE 5

DATA OUTPUT MASS, PERCENT TRANSMISSION FOR MASS,
AND RELATIVE ABUNDANCE FOR MASS

MASS +ϕ.3127783E+ϕ2

%T	%B1	%B2
+ϕ.1582418E+ϕ2	+ϕ.2749695E+ϕ2	+ϕ.242ϕϕ24E+ϕ2
+ϕ.2ϕ61ϕ5ϕE+ϕ2	+ϕ.3262516E+ϕ2	+ϕ.3ϕϕ61ϕ4E+ϕ2
+ϕ.27ϕ3295E+ϕ2	+ϕ.4163136E+ϕ2	+ϕ.3748472E+ϕ2

A (T)	A (B)	A (B)	A (NET)
+ϕ.3143612E-ϕ4	+ϕ.14913ϕϕE-ϕ4	+ϕ.1787448E-ϕ4	+ϕ.1504238E-ϕ4
+ϕ.445ϕϕ17E-ϕ4	+ϕ.23ϕ9754E-ϕ4	+ϕ.2616ϕ48E-ϕ4	+ϕ.1987115E-ϕ4
+ϕ.6113529E-ϕ4	+ϕ.3ϕ88ϕ63E-ϕ4	+ϕ.3698ϕ68E-ϕ4	+ϕ.272ϕ463E-ϕ4

AVE ABND +ϕ.2337621E-ϕ4 PCT ERROR +ϕ.1ϕϕ89ϕ4E+ϕ2

$$\text{Emi} = \left[\frac{T_o - T}{T - T_{inf}}\right]^{1/R}$$

$$\text{Abund} = \text{Emi} * \sqrt{\text{Mass}} \div \text{Exposure}$$

48. Computer-Aided Interpretation of Mass Spectra

R. Venkataraghavan, F. W. McLafferty, and G. Van Lear

Department of Chemistry, Purdue University, Lafayette, Indiana 47907

Abstract

Computer programs have been written to carry out major steps in the procedure for interpretation of high-resolution mass spectral data. These steps include identification and evaluation of the molecular ion, neutral fragments lost from the molecular ion and characteristic ion series, followed by elucidation of specific structural details using a subroutine for the particular compound class selected. The technique has been tested on several monofunctional and a few bifunctional compound types. The method shows promise of not only increasing the interpreter's efficiency but of providing more specific and detailed structural information from the spectral data. A publication describing the details of the technique is under preparation.

49. Orbital Symmetry Selection Rules for Mass Spectrometric Reactions

by
Ralph C. Dougherty and James G. Watt
Department of Chemistry
Ohio State University
Columbus, Ohio 43210

In order to apply electronic theories of organic reactivity to mass spectrometric reactions it is necessary that one specify the reactive electronic state of decomposing ions. If the density of electronic states is high enough to insure the non-existence of isolated electronic states, we can apply considerations of normal state lifetimes to gas phase ions. The preceding criterion is certainly satisfied for the majority of the ions produced by impact with 70 eV electrons on large organic molecules. Mass spectrometric reactions can thus be empirically divided into three classes based on the reaction time scale as shown by metastable ions and normal excited state lifetimes. Class I reactions are presumed to occur primarily from low-lying electronic states of the parent ion. This class includes all reactions of molecule ions which give rise to significant metastable peaks, and decomposition reactions of even-electron ions that were initially formed in low-lying singlet states. The PMO theory[1a] and orbital symmetry selection rules[1b] for ground state reactions may be immediately applied to these reactions. Class II reactions are presumed to occur primarily from excited electronic states. This class includes most of the decompositions of doubly ionized particles and reactions of molecule ions for which metastable peaks cannot be detected. The simplified theories of excited state reactivity may be applied to these reactions. Class III reactions are those reactions for which the reactive electronic states are indeterminant. This class must include many of the reactions of even-electron fragment ions and reactions of molecule ions for which only low intensity metastable ions are detected.

This approach has provided a very satisfactory account of the features of the hexahelicene rearrangement (loss of C_2H_4 from the hexahelicene[2] molecule ion), the retro-Diels-Alder reaction of 4-vinyl-cyclohexene[3] and the McLafferty rearrangement.[4] All three of these reactions are Class I electrocyclic processes and the PMO theory for radical cations gives results that

are in complete agreement with experiment.

Full papers dealing with the reactive states of ions and the PMO theory of radical cations[5] and the analysis of electrocyclic mass spectrometric reactions[6] will appear shortly. A full account of valence electron SCF and extended Hückel calculations as applied to electrocyclic mass spectral reactions is in preparation.[7]

Financial support from the National Institutes of Health is gratefully acknowledged.

(1) (a) M.J.S. Dewar, Tetrahedron, Suppl., 8, 75 (1966);
(b) R. Hoffmann and R. B. Woodward, Accounts of Chemical Research, 1, 17 (1968).
(2) M. S. Newman and D. Lednicer, J. Am. Chem. Soc., 78, 4756 (1956).
(3) E. P. Smith and E. R. Thornton, ibid., 89, 5079 (1967).
(4) F. W. McLafferty, " Interpretation of Mass Spectra," Benjamin, New York (1966).
(5) R. C. Dougherty, J. Am. Chem. Soc., in press (1968).
(6) R. C. Dougherty, ibid., in press (1968).
(7) J. G. Watt and R. C. Dougherty, to be published.

50. THE ELECTRONIC STRUCTURE OF THE SIX-MEMBERED TRANSITION STATE IN SOME γ-HYDROGEN REARRANGEMENTS[1]

F. P. Boer and T. W. Shannon, The Dow Chemical Company, Eastern Research Laboratory, Wayland, Massachusetts 01778 and F. W. McLafferty, Department of Chemistry, Purdue University, Lafayette, Indiana 47907

Despite the very substantial number of experimental studies[2] of the γ-hydrogen rearrangement, the question of whether the reaction proceeds via stepwise or concerted mechanisms, and whether the transferred entity should be labeled as a proton or a hydrogen radical, are still debated[3,4].

This represents an attempt to clarify this situation by theoretical studies of the electronic structure of the six-membered cyclic transition states generally accepted for these reactions.

Conditions For Rearrangement - The first task is to postulate the necessary conditions for γ-hydrogen transfer and to identify the reasons underlying the parallel reaction paths under electron impact and photolytic conditions. Useful insight into the problem may be provided by the simple three-orbital Huckel LCAO model.

Consider three atomic orbitals of the reacting system: X_C an sp^3 orbital on C_γ ; X_H, a hydrogen 1s orbital; and X_O, which can be a 2p orbital on the carbonyl oxygen. We also assume the diagonal elements of the Hamiltonian matrix, H_{CC}, H_{HH}, and H_{OO} are equal (to α) and use appropriate values of β for the off-diagonal elements H_{ij}. Ignoring non-orthogonality effects, the secular equations readily yield eigen values and eigen vectors (Fig. 1), for the molecular orbitals of the system.

Initially, we have $H_{CH} = \beta_1$ and $H_{HO} = 0$. The system contains two electrons in the C-H orbital ψ, at $\epsilon_1 = \alpha + \beta_1$; a single electron in the oxygen non-bonding orbital ψ_2 at $\epsilon_2 = \alpha$; and an unoccupied σ^* orbital ψ_3. The orbitals of the final state, defined by complete hydrogen transfer to oxygen, resemble those of the starting system. One electron is now in the carbon non-bonding orbital at $\epsilon_2 = \alpha$ while two electrons form the O-H bond at $\epsilon_1 = \alpha + \beta_4$.

In the transition state the hydrogen atom is placed between C and O such that $H_{CH} = H_{OH} = \beta_2$. The lowest MO is now a three-center bonding orbital analogous to bridge bonds in boron hydrides.[5] The eigen values depend on the magnitude of the C-O interaction ($H_{CO} = \beta_3$). In the limit of $\beta_3 = 0$, ψ_2 remains non-bonding while the bonding orbital ψ_1 has energy $\epsilon_1 = \alpha + \sqrt{2}\,\beta_2$. For $\beta_3<0$, repulsion between C and O lobes of opposite sign gives increasing antibonding character to ψ_2 while ψ_1 is further stabilized. For the case $\beta_3 = \beta_2$, $\epsilon_2 = \alpha - \beta_2$ while ϵ_1 goes to $\alpha + 2\beta_2$. The real transition state is between these two limits: more detailed calculations suggest that $\beta_3 \backsim 0.4\beta_2$ for a C-O distance of 2 Å.

These observations suggest the following hypothesis: The removal of an electron from the four-electron C-H···X system is a necessary condition for γ-hydrogen transfer with a low activation energy. Delocalization of an electron pair over three centers lowers the energy of the bonding orbital ψ_1, thus favoring formation of the transition state. However, the energy of ψ_2 is simultaneously raised. If ψ_2 is singly occupied these effects may approximately cancel and the transition state will be energetically accessible. If ψ_2 is doubly occupied, the antibonding terms will be much larger, giving a much greater activation energy for rearrangement.[6]

The Norrish II photoelimination of olefins from ketones is also a facile reaction.[7] In this system an electron has been removed by excitation to the carbonyl π^* orbital, which is orthogonal to the C-H-O plane and functions only as a sink for the fourth electron.

Rearrangement in 2-Pentanone - Detailed molecular orbital calculations were performed on 2-pentanone as a model system. The method used[8] includes all the electrons and all the atomic centers of the reacting system. The overlap and kinetic energy integrals between all atomic orbitals in the system are evaluated exactly. Parameters for constructing the Hamiltonian matrix are derived from S.C.F. calculations on appropriate model compounds.

The transition state is reached in two steps. First, rotation of C_γ about the C_α - C_β bond brings C_γ about 2.0 Å from the oxygen atom and the carbon and oxygen atoms all lie in a plane. In the second step, a 60° rotation about C_β - C_γ brings one of the γ-hydrogens in the reaction plane about 1.1 Å from the oxygen. The maximum bonding occurs when the ring angles are opened up about 15°. In this

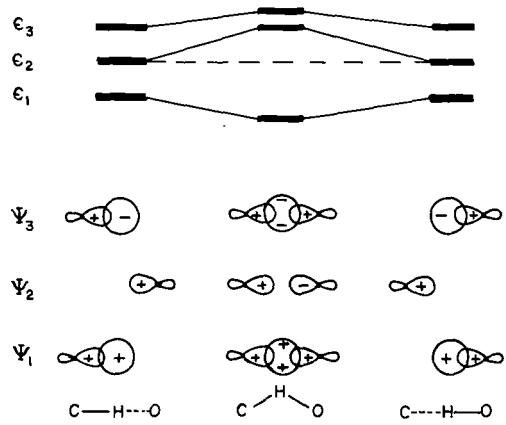

Figure 1
Wavefunctions and Energies From the Hückel Three-Orbital Model

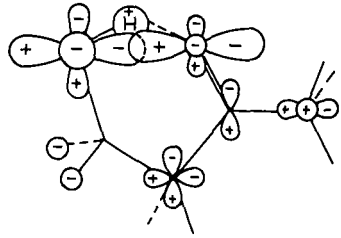

Figure 2 Wavefunction of the highest occupied molecular orbital of 2-pentanone in the transition state.

configuration the H atom is about 1.3 Å from C and 1.2 Å from O. In the final step C_γ swings away leaving H bonded to oxygen.

The highest occupied molecular orbital, ψ_n can be closely identified with the non-bonding MO ψ_2 from the Hückel analysis. The electron density of this orbital is given in Table I, and the wavefunction in the transition state is shown in Figure 2.

In the neutral ketone much of the electron density is localized on oxygen, in accord with the usual notation that the oxygen lone-pair electrons are ionized. As the reaction proceeds by rotation of C_γ about the C_α -C_β bond, significant density builds up on C_γ and the two γ-hydrogens nearest to the carbonyl group. The phase of the wavefunction on oxygen is opposite in sign to that on carbon and the two hydrogen atoms. A 60° rotation of the terminal methyl group places one of the γ-hydrogens slightly closer to oxygen than carbon; just past the node of the non-bonding orbital. The electron density is almost evenly divided between C_γ and O, slightly favoring C_γ. As C_γ swings away, the radical character which was originally concentrated on the carbonyl oxygen flows smoothly over to C_γ.

The question of proton or hydrogen atom transfer may now be considered. The proton transfer model assumes heterolytic cleavage of the C_γ -H bond and is expected to leave high residual negative charge on C_γ and a high positive charge on H. The unpaired electron is presumably localized on oxygen. In the case of hydrogen atom transfer, no formal charge is expected on either the hydrogen or the γ-carbon, and the latter atom becomes the radical site.

If one electron is removed from the highest filled molecular orbital by ionization this MO then defines the radical character associated with the molecule-ion. The unpaired density need not be localized on a single site. We have seen that the radical density (Table I) shifted over to the γ-carbon as the reaction proceeded. In the transition state the probability that the radical was located at C_γ was 0.37. From the point of view of unpaired density the H atom transfer mechanism seems to fit the MO results. Further, the proton transfer model places the unpaired electron on oxygen. However, when three electrons are available we would expect the O-H bonding orbital, which lies at a lower energy, to be doubly occupied and the lone-pair orbital on the oxygen singly occupied. Thus the requirement of the proton transfer model that the lone electron reside on the oxygen seems untenable.

A shift of our point of view to overall net charges (Table II) is quite instructive. The γ-carbon atom shows a high net negative charge (-0.44) in the transition state, while the hydrogen atom bears strong positive charge (+0.30). As the reaction proceeds, C_γ acquires even more negative charge (-0.79). These figures partially support a proton transfer model where heterolytic cleavage results in large residual net charges. Note that this model does not require migration of a proton to a positively charged oxygen since this atom remains nearly electrically neutral by virtue of its ability to withdraw charge from the carbonyl carbon.

In this instance, the MO wavefunction reconciles apparently contradictory features of the two mechanistic models cited. We conclude that a forced choice between proton and hydrogen atom transfer may be simplistic.

The problem of concerted versus stepwise[9] elimination of the olefin from the molecule-ion requires discussion. The concerted mechanism may be defined by the formation of a transition state with an electronic structure as shown in Fig. 3. This formulation requires the simultaneous formation of the O-H bond and the breaking of the bond between C_α and C_β.

Figure 3

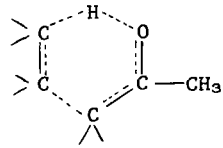

The detailed calculations show that a transition state with this electronic structure does not occur. The overlap populations indicate no appreciable weakening of the C_α -C_β bond. In addition, no increase is observed for the C_α -$C_{carbonyl}$ or C_β -C_γ overlap populations,

nor is there any diminution of the C-O double bond.

Further evidence for a stepwise mechanism appeared in calculations on "concerted" transition state geometries where the ethylene fragment was removed simultaneously as the O-H bond was formed. These states appeared to be substantially less stabilized by incipient bond formation than the "stepwise" intermediates.

The transfer of hydrogen appears to precede elimination of ethylene and therefore the overall reaction should be considered to occur via a stepwise mechanism. The driving force for olefin elimination appears to be the creation of a more favorable radical site rather than the appearance of any markedly antibonding regions in the ion formed after hydrogen transfer.

References

1. Submitted for publication to the Journal of the American Chemical Society.

2. H. Budzikiewicz, C. Djerassi and D. H. Williams, "Mass Spectrometry of Organic Compounds", Holden-Day Inc., San Francisco, California 1967

3. F. W. McLafferty and T. Wachs, J. Am. Chem. Soc., 89, 5043 (1967).

4. G. Spiteller and M. Spiteller-Friedmann, Monatsh., 95, 257 (1964).

5. W. H. Eberhardt, B. C. Crawford and W. N. Lipscomb, J. Chem. Phys. 22, 989 (1954)

6. A. Maccoll, J. Chem. Soc., 1958, 3398.

7. C. H. Niod, J. C. Calvert, J. Am. Chem. Soc., 89, 1790 (1967) and references cited therein.

8. M. D. Newton, F. P. Boer and W. N. Lipscomb, J. Am. Chem. Soc., 88, 2353, 2361, 2367 (1966)

9. F. W. McLafferty, Chem. Comm. 78, 1966.

Table I[a]

Charge Density in the Highest Occupied Molecular Orbital of 2-Pentanone

	Ground State	Step 1	Step 2 Transition State	Step 3
C(1)	0.16	0.09	0.09	0.06
C(2)	0.06	0.01	0.02	0.07
C(5)=C$_\gamma$	0.01	0.09	0.37	0.45
O	0.52	0.48	0.35	0.12
H(5)=H$_\gamma$	0.01 (3)	0.09(1) 0.08(2)	0.00(2) 0.00(1)	0.00(2)
H(O)	-	-	-	0.01(1)

(a) Multiplicities of the atoms given in parentheses.

Table II

Net Charge on the 2-Pentanone Molecule-Ion

	Ground State	Step 1	Step 2 Transition State	Step 3
C(1)	-0.23	-0.32	-0.29	-0.28
C(2)	+0.71	+0.64	+0.67	+0.74
C(5)=C$_\gamma$	-0.21	-0.11	-0.44	-0.79
O	+0.07	+0.18	+0.24	+0.40
H(5)=H$_\gamma$	+0.05(3)	+0.02(1) +0.16(2)	+0.07(2) +0.30(1)	+0.10(2)
H(O)	-	-	-	+0.18(1)

51. THE SIGNIFICANCE OF HYDROGEN-LOSS PATTERNS OF IONS PRODUCED BY ELECTRON IMPACT

Stuart W. Staley, John P. Erdman, and Timothy J. Henry
Department of Chemistry
University of Maryland
College Park, Maryland 20740

The determination of the structures of ions produced by electron impact is an important problem which has received a great deal of attention in recent years. A number of criteria, such as isotopic labeling results, ionization and appearance potentials, substituent effects, metastable ion characteristics, and the general appearance of fragmentation patterns, have been used to assign structures to ions. However all of these techniques are limited and are primarily of value in eliminating certain structures from consideration. As a consequence it is generally recognized that the myriad of structural formulae presented in papers dealing with mass spectrometric fragmentations are often useful only for "bookkeeping" purposes and that little solid evidence is available concerning the actual ion structures.

We suggest that a new criterion, based on the analysis of the patterns arising from the loss of hydrogen from molecular and fragment ions (which we refer to as hydrogen-loss patterns) can be of use in assigning ion structures in certain specific cases. The abundant loss of more than two or three hydrogen atoms from molecular ions is rare; nevertheless very small peaks, representing the extensive loss of hydrogen from molecular and fragment ions, are commonly observed in 70 eV spectra, particularly in those of hydrocarbons. For example, the spectra of propane, butane, pentane and hexane [1] show patterns of small peaks from the molecular ion peak down to m/e 36, 48, 60 and 72, respectively; we refer to these as the molecular ion regions. In general these regions show the normal alternation of intensity with the even-electrons peaks at odd m/e values being more intense than neighboring odd-electron or radical-cation peaks. However notable exceptions occur at m/e 38 in propane, m/e 50 in butane, m/e 62 in pentane and m/e 74 in hexane.[2] These peaks are much more prominent than surrounding odd-electron peaks and are comparable to or larger than many of the even-electron peaks. It can be seen that these peaks represent a series of ions with the general formula $C_nH_2^{+\cdot}$. We suggest that they have linear structures with the two terminal carbons being substituted by hydrogen. A significant feature of such a structure is that the two C-H bonds are "totally-orthogonal" to the electron-deficient π system on the carbon chain. By this we mean that there are no rotations which can occur in the ion which will allow overlap of the C-H bond with the π system, a condition which is necessary for additional loss of hydrogen via a relatively low energy pathway.

More saturated ions, such as $C_nH_3^+$ or $C_nH_4^{+\cdot}$, may also have ground state conformations in which all of the C-H bonds are orthogonal to the electron-deficient π system but at 70 eV enough excess energy is available for rotation to occur about the π bonds, thereby effecting overlap of C-H bonds with the π system. Thus it can be seen that the $C_nH_2^{+\cdot}$ ions are relatively abundant not because of any exceptional thermodynamic stability (although this factor will greatly influence their rate of formation) but because of relatively low rates of decomposition.

We therefore suggest that peaks which are relatively abundant in the context of the complete hydrogen-loss pattern may correspond to ions with totally orthogonal structures. An ion need not be linear to satisfy this criterion; planar cyclic structures are also included since no rotation can occur about the C-C bonds due to the constraint of the ring. For example, in the molecular ion region of 1-heptyne and other C_7H_{10} isomers the largest peak below m/e 95 (M-1) is at m/e 91; there is very little additional loss of hydrogen in the molecular ion region. Thus the m/e 91 peak appears to exhibit the characteristics of a totally orthogonal ion. The previously proposed tropylium ion [3] is a reasonable structure on the basis of this criterion whereas the benzyl ion is not. The largest peak below m/e 91 is at m/e 86 which is another ion in the $C_nH_2^{+\cdot}$ series.

In order to test these ideas further we have synthesized a series of 7-alkylcycloheptatrienes (methyl, ethyl, propyl, and butyl). The molecular ion regions have some interesting features which will be published at a later time. Significant odd-electron peaks which are reasonably formulated as totally orthogonal ions are found at m/e 102 (phenylacetylene $^{+\cdot}$), m/e 126 (phenylbutadiyne $^{+\cdot}$), and m/e 128 (naphthalene $^{+\cdot}$ or azulene $^{+\cdot}$). [4] Significant even-electron peaks are found at m/e 115 (indenyl or ethynyltropylium) and m/e 139, for which several structures, including a tricyclic one previously proposed by Beynon [5], can be written.

It should be noted that often several isomeric ions possess totally orthogonal structures and a choice between them cannot be made on the basis of this criterion.

This discussion can be extended to compounds other than hydrocarbons. For example, the molecular ion region of thiacyclohexane [1] shows loss of five hydrogens to give a relatively abundant m/e 97 peak; there is a virtual cessation of the hydrogen-loss pattern at this point. This behavior is consistent with that expected for the previously proposed thiopyrylium ion [6], which is isoelectronic with the tropylium ion.

The analysis of hydrogen-loss patterns can also be useful in the study of fragmentation mechanisms. We have obtained the mass spectra of thirteen cyclic $C_{10}H_{12}$ isomers, all of which have virtually the same hydrogen-loss pattern in the region immediately below the molecular ion. However the relative intensities of the molecular ions vary greatly, with those of benzenoid compounds generally being more intense. This suggests that the molecular ions of these latter compounds have at least two different structures, one which is unrearranged and a rearranged structure which is capable of decomposing to give the observed hydrogen-loss pattern. (The fact that most of the σ bonds in benzenoid compounds are orthogonal to the π system explains in part the well-recognized stability of the molecular ions of these compounds).

In a sense the hydrogen-loss pattern serves as a "fingerprint" for the molecular-ion precursor. The gross mass spectra of these $C_{10}H_{12}$ isomers are also quite different in many cases. This suggests that even though these isomers partially rearrange to a common molecular ion, in many cases low energy fragmentation pathways are available which compete effectively with rearrangement. Additional discussion regarding the significance of hydrogen-loss patterns will be presented at a later time.

Acknowledgement: We are pleased to acknowledge the support of this work by the Petroleum Research Fund of the American Chemical Society and the Advanced Projects Research Agency. The mass spectrometer was purchased with a grant from the National Science Foundation.

References

1. Index of Mass Spectral Data, American Society for Testing and Materials, Philadelphia, Pa., 1963, and references therein.
2. Nearly all hydrocarbons of sufficient molecular weight exhibit these peaks, not only in the molecular ion region but in fragment ion regions as well.
3. S. Meyerson, H. Hart and L. C. Leitch, J. Am. Chem. Soc., 90, 3419 (1968).
4. These structures have not been proved but represent the most reasonable possibilities on the basis of this criterion.
5. J. H. Beynon, Mass Spectrometry and its Applications to Organic Chemistry, Elsevier Publishing Co., New York, N. Y., 1960, p. 274.
6. V. Hanuš and V. Čermák, Coll. Czech. Chem. Commun., 24, 1602 (1959).

52. Distinguishing Diastereotopic Hydrogens by Mass Spectrometry. A Direct Probe into the Transition State of an Electron Impact Induced Elimination Reaction.

by Mark M. Green

Department of Chemistry, University of Michigan

It has been recognized for some time that acyclic diastereomers show mass spectral differences which are usually small and difficult to interpret. Thus, although interesting studies have been carried out on more restrictive cyclic stereoisomers, their acyclic counterparts remain essentially unexplored.

We have found that two acyclic diastereomers, which are isomers only by virtue of hydrogen deuterium substitution, can be easily distinguished by a stereoselective mass spectral elimination reaction.

Reaction of racemic-2,4-pentanediol with one equivalent of p-toluenesulfonylchloride and subsequent reduction of the derived tosylate with lithium aluminium deuteride leads by stereospecific reaction to (S,R)-2-deutero-4-hydroxypentane (I) (all compounds are racemic). The identical reaction sequence carried out on meso-2,4-pentanediol leads to (S,S)-2-deutero-4-hydroxypentane (II). Conversion of I to its chlorosulfite ester followed by heating in dioxane, a reaction known to involve retention of configuration, leads to III, while reaction of I with thionyl chloride in pyridine leads to IV. In a similar manner identical samples of III and IV are produced by the inverse reaction sequence from II (i.e. III in pyridine and IV in dioxane).

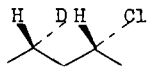

III

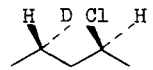

IV

Mass spectral analysis, at ambient temperature and low voltage, of the isomeric chlorides (III and IV) show that loss of hydrogen chloride involves the hydrogens on C-4 to approximately 55% and that loss of the diastereotopic hydrogens takes place to unequal extents as shown:

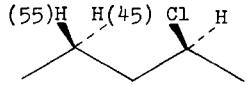

The stereoselectivity decreases to 6% at 70 ev and 135°C.

The significance of these results rests in the fact that (i) this reaction likely involves only transition state differences and therefore is a direct probe into these effects independent of the ground state, and, (ii) in the demonstration that this ubiquitous mass spectral reaction (i.e. elimination) is unusually sensitive to subtle structural effects.

These findings will be discussed in a communication to appear in the J. Amer. Chem. Soc., July issue (1968).

53. Metastable Ions in Mass Spectra

M. L. Gross, R. B. Fairweather, W. F. Haddon, F. W. McLafferty

Department of Chemistry, Purdue University, Lafayette, Indiana 47907

H. W. Major

Perkin-Elmer Corp., Downers Grove, Illinois

Introduction

In this paper we will discuss three techniques that are useful in observing metastable ions:

(a) *defocused metastable ions on double focusing mass spectrometers*
(b) defocused metastable ions on a time-of-flight mass spectrometer
(c) metastable ions on a cycloidal mass spectrometer.

and secondly to report some observations that we have made regarding relative metastable intensities and how these might be useful in determining the structure and internal energy of fragment ions.

Defocused Metastable Ions on Double Focusing Mass Spectrometers

Ions that decompose outside the source and before the electric sector of a double-focusing mass spectrometer will have insufficient kinetic energy to be transmitted by the electric sector and, therefore, will not be observed in normal operation. These metastable ions can be observed, however, by increasing the accelerating voltage such that the kinetic energy after dissociation will again be sufficient that the daughter ions will pass the electric sector. This technique was introduced by Barber and Elliott (1) in 1964 and further developed by Jennings (2) and by Futrell, Ryan and Sieck (3) in 1965.

These metastable ions can also be observed by lowering the electric sector potential by the factor m_2/m_1 or m^*/m_2 (which is identical to m_2/m_1) for the process:

$$m_1^+ \rightarrow m_2^+ + (m_1 - m_2)$$

and scanning the magnetic field in the region of the metastable mass. The method is very sensitive in that the metastable intensity is greater than for those metastables which decompose after the electric sector and for those observed in a single sector instrument under identical conditions of repeller voltage and electron energy. In n-decane, not only the 142 → 113 transition (loss of ethyl from the molecular ion) is observed, but also the 143 → 114 and the 144 → 115 (loss of ethyl from the single and double isotope peaks).

Defocused Metastable Ions on a Time-Of-Flight Mass Spectrometer

Ions which decompose in the drift tube (metastable ions) of a time-of-flight mass spectrometer are not normally observed separately. The daughter ions, the neutrals, as well as the undecomposed precursor ions will arrive simultaneously at the collector. The separation of the daughter ions (metastables) from the neutrals and the precursors can be accomplished by applying a variable retarding potential on a grid situated before the collector. Appearing first--or completely unretarded--will be the neutrals. Next the precursor ions will be observed, since these ions have lost no kinetic energy due to decomposition. Therefore, they will be retarded least of all the ionic species. Finally the daughter ions (metastables) will be observed: those of highest mass will appear first as they will be subjected to the least amount of retardation.

Interfering ions of masses higher than the precursor can be eliminated by pulsing a plate situated in front of the retarding grid. Details of the method as well as typical metastable spectra will be given in a later publication.

Metastables on a Cycloidal Mass Spectrometer

Metastable ions in a cycloidal mass spectrometer are observed to occur between the masses of the daughter ion and the precursor ion. The greatest intensity of metastable ions occurs on the high mass side of the daughter ion, and the intensity decreases in an exponential manner as we procede toward the precursor ion. The intensity at a given mass is related to the position in the cycloidal trajectory

at which decomposition occurs. Therefore, the intensity at a given mass is related to the number of decompositions occurring at some time, t, relative to formation of the precursor. Since mass spectrometric decompositions are unimolecular processes, we might expect a plot of logarithm of the intensity at a given time vs. time to be linear and the slope to represent the rate constant. What is generally observed is a curve of steadily decreasing slope indicating, we feel, a continuous distribution of rate constants for decomposition. Details of the calculations and typical plots can be found in a forthcoming publication.

Degree of Freedom Effects

It has been recently observed that the metastable ion intensity (relative to the precursor ion intensity) for decomposition of a primary or secondary fragment decreased with the size of the neutral fragment lost in the formation of the fragment ion.(4) For example, in a series of secondary alsohols, $RCH(OH)CH_3$, the metastable ion intensities for the following decompositions of the m/e = 45 ion

$$C_2H_5O^+ \rightarrow CHO^+ + CH_4 \quad m^* = 18.7$$
$$C_2H_5O^+ \rightarrow H_3O^+ + C_2H_2 \quad m^* = 8.02$$

were found to decrease as the size of R increased. In fact, a linear correlation was obtained when the logarithm of the relative metastable intensity was plotted vs. the reciprocal of the number of internal degrees of freedom in the molecular ion.(4) Closer scrutiny and a study of a number of other systems has revealed that the linear correlation is not always obtained. Also the slopes of the curves are found to increase as the electron energy is decreased. Details and possible explanations for these observations will be given in a later publication. Nevertheless, structural information concerning fragment ions can be obtained using degree-of-freedom correlations. Two examples will be briefly discussed.

(a) Structure of the $C_2H_5O^+$ Ion from $CH_3OCH_2CH_2OH$

First of all, we know that the metastable ion characteristics for $C_2H_5O^+$ ions from methyl ethers are different from those $C_2H_5O^+$ ions from appropriate alcohols and ethyl ethers:(5)

(1) the metastable at 8.02 corresponding to the loss of C_2H_2 is not observed, and

(2) the metastable at 18.7 corresponding to the loss of CH_4 is no longer flat-topped (no kinetic energy release), but rather gaussian in shape.

The metastable ion characteristics of the $C_2H_5O^+$ ion generated from 2-methoxyethanol are as follows:

(1) The metastable at 8.02 is observed but is of low intensity: approximately 10% of that which we might predict from a curve correlating the 8.02 metastable intensities for $C_2H_5O^+$ ions generated from ethyl ethers and larger 2-alkoxyethanols.

(2) The metastable intensity at 18.7 (of gaussian shape) is fairly well correlated with a degree-of-freedom plot for methyl ethers.

From these observations, we feel that approximately 90% of the $C_2H_5O^+$ ions from 2-methoxyethanol are of the structural type generated from methyl ethers ($CH_3O = CH_2$).

(b) Structure of the $C_2H_5O^+$ Ion from 1,3-Butanediol

It is apparent that two types of $C_2H_5O^+$ ions might be generated from 1,3-Butanediol:

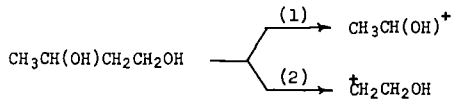

either an ion corresponding to that formed from primary alcohols by β-cleavage or that formed from secondary alcohols by α-cleavage. If the former were the case, we would expect the relative metastable intensity to be correlated by the series of primary alcohols. If the latter were the case, the intensity would be correlated by the series of secondary alcohols ($RCHOHCH_3$). An intermediate result was observed which corresponds to 71% of the $C_2H_5O^+$ ions being formed by pathway (1) above. This percent remained constant at lower electron energies. Details and further systems will be examined in a forthcoming publication.

Correlation of Relative Metastable Ion Intensities with Hammett's σ-Constants

We have seen that the size of the neutral lost in formation of a particular fragment ion will effect the metastable ion intensity observed in the decomposition of the fragment ion. We have also observed another cause for varying metastable

ion intensities. Substituted benzophenones are observed to decompose to form the benzoyl ion (m/e = 105) which in turn loses CO (m* = 56.5).

$$YC_6H_4COC_6H_5^{+\cdot} \rightarrow C_6H_5CO^+ \xrightarrow{*} C_6H_5^+ + CO \quad (m^* = 56.5)$$

The relative metastable ion intensity was found to decrease as the electron withdrawing ability of the substituent (Y) increased. In fact a fairly good linear correlation was obtained when the logarithm of the relative metastable intensity was plotted vs. the σ-constant for the substituent. These results were interpreted as indicating that the benzoyl ions were formed with a lower internal energy distribution as the substituent became more electron withdrawing. Details can be found in a recent publication.(6)

Finally, a similar result was obtained in the bibenzyl system. Bibenzyls are known to decompose to the $C_7H_7^+$ ion which can lose acetylene to form $C_5H_5^+$ (m* = 46.4).

$$YC_6H_4CH_2CH_2C_6H_5^{+\cdot} \rightarrow C_7H_7^+ \xrightarrow{*} C_5H_5^+ + C_2H_2 \quad (m^* = 46.4)$$

The relative metastable ion intensity at 46.4 was observed also to decrease as the electron withdrawing ability of the substituent (Y) increased. Again, a fairly good linear correlation was obtained when the logarithm of the metastable intensity was plotted vs. the σ-constant for the substituent. The slope of the correlation (ρ-value) was observed to increase as the electron energy decreased.

Acknowledgement

We are grateful to the National Institutes of Health (Grants GM12755 and FR00354) for their financial support.

References

(1) M. Barber and R. M. Elliott, paper presented at the 12th ASTM E-14 Meeting on Mass Spectrometry, Montreal (1964).

(2) W. Higgins and K. R. Jennings, Chem. Commun., 99 (1965).

(3) J. H. Futrell, K. Ryan, and L. W. Sieck, J. Chem. Phys., 43, 1832 (1965).

(4) F. W. McLafferty and W. T. Pike, J. Am. Chem. Soc., 89, 5951 (1967). F. W. McLafferty and W. T. Pike, ibid, 89, 5951 (1967).

(5) T. W. Shannon and F. W. McLafferty, J. Am. Chem. Soc., 88, 5021 (1966).

(6) M. L. Gross and F. W. McLafferty, Chem. Commun., 254 (1968).

54. A DETECTOR FOR THE METASTABLE IONS OBSERVED IN THE MASS SPECTRA OF ORGANIC COMPOUNDS

N. R. Daly, A. McCormick and R. E. Powell

Atomic Weapons Research Establishment, Aldermaston, Berkshire, England

A sensitive ion detector is described that can record all fragments in the mass spectrum of an organic compound. Alternatively it can suppress to a very high degree the normal spectrum and amplify the spectrum of the products of metastable decompositions which take place on either side of the magnet in a sector type mass spectrometer. It has been found that the "meta-stable spectra" or organic compounds having almost identical "normal" spectra may be sufficiently different to allow unambiguous identification.

Accepted for publication in the Review of Scientific Instruments

55. COMPETITIVE PRIMARY LOSS OF C_2H_4 AND CO FROM 1-TETRALONE UNDER ELECTRON IMPACT

Seymour Meyerson and R. W. Vander Haar

Research and Development Department, American Oil Company, Whiting, Indiana 46394

ABSTRACT

Competing primary reactions by which 1-tetralone loses C_2H_4 and CO give rise to a doublet at mass 118 in the high-resolution mass spectrum corresponding to 96.4% $C_8H_6O^+$ and 3.6% $C_9H_{10}^+$, respectively. However, study of the remainder of the spectrum suggests that these intensities constitute a poor measure of the relative importance of the two reaction paths. The $C_9H_{10}^+$ ion evidently degrades more readily than $C_8H_6O^+$, since an estimated 26% of the ions arising in these paths involve primary loss of CO. This estimate is supported by voltage dependence of the intensity distribution between the members of the doublet. As ionizing voltage is decreased, the intensity distribution is constant to about 20 volts, but between 20 and 10 volts the value for $C_9H_{10}^+$ rises smoothly from about 3.5% to about 25%.

To be published in Organic Mass Spectrometry.

56. Mass Spectrometric Study of Methoxy Compounds

by

Kermit R. Way (Michigan State University, East Lansing, Michigan) and Paul Skoug and Morley E. Russell (Northern Illinois University, DeKalb, Illinois)

In the mass spectra of compounds with the formula CH_3OCH_2R (R = e.g. H, CH_3, Cl, CH_2OH) the m/e 17 ion occurs as a doublet. The ion of lower mass is OH^+ and we have identified the higher mass ion as CH_5^+. It also has been shown that the CH_5^+ ion is linear with pressure which means it is not the product of an ion-molecule reaction but is a rearrangement ion.[1]

To ascertain the origin of this rearrangement ion, the following labeled compounds were synthesized:

$CD_3OCH_2CH_3$	$CH_3OCH_2CD_2OH$
$CH_3OCD_2CH_3$	$CH_3OCD_2CH_2OH$
$CH_3OCH_2CD_3$	$^{13}CH_3OCH_2CH_2OH$

(The n.m.r. of each of the deuterated compounds was examined and the labeling found to be correct.) The major ion in each case was the fragment ion resulting from a cleavage of the molecule ion. This ion then further decomposes to give CO and CH_5^+ (or the deuterated analogue).

A search was made for a metastable peak corresponding to the aforementioned reaction and in each case one was found. The data are summarized in Table I.

Table I CH_5^+ Metastable Peaks in the Spectra of Labeled Methylethylether and 2-Methoxyethanol

Parent molecule	Process	m* Calculated	m* Found
$CD_3OCH_2CH_3$	$CD_3OCH_2^+ \rightarrow CD_3H_2^+ + CO$	8.33	8.3
$CH_3OCD_2CH_3$	$CH_3OCD_2^+ \rightarrow CD_2H_3^+ + CO$	7.68	7.7
$CH_3OCH_2CD_3$	$CH_3OCH_2^+ \rightarrow CH_5^+ + CO$	6.42	6.4
$CH_3OCH_2CD_2OH$	$CH_3OCH_2^+ \rightarrow CH_5^+ + CO$	6.42	6.4
$CH_3OCD_2CH_2OH$	$CH_3OCD_2^+ \rightarrow CD_2H_3^+ + CO$	7.68	7.6
$^{13}CH_3OCH_2CH_2OH$	$^{13}CH_3OCH_2 \rightarrow {}^{13}CH_5^+ + CO$	7.04	7.1
	$\searrow CH_5^+ + {}^{13}CO$	6.28	6.3

High resolution spectra were obtained for the labeled methylethylethers in the region m/e 16 to m/e 20. These spectra confirmed the results on methylethylether given in Table I, i.e. the isotopic daughter ions given above were formed in each case.

Appearance potential measurements using dimethylether were made in order to calculate the enthalpy for formation of CH_5^+. The results are given in Table II.

Table II Appearance Potential Measurements and Enthalpy of Formation of CH_5^+ From Dimethylether

Process	CH_5^+ A.P., eV	CH_5^+ ΔH_f, kcal	A.P. Measurement
$h\nu + CH_3OCH_3 \rightarrow CH_5^+ + H + CO + e$	13.30 ± 0.06	$\leq$ 238	P.I.
$e + CH_3OCH_3 \rightarrow CH_5^+ + H + CO + 2e$	13.40 ± 0.20	$\leq$ 240	R.P.D.
$CH_4^+ + CH_4 \rightarrow CH_5^+ + CH_3$	12.60 ± 0.01[2]	$\leq$ 224	P.I.
$CH_3OCH_3 \rightarrow CHO^+ + H + CH_4 + e$	13.0 (calculated)[3]		

The above results show that the process which forms CH_5^+ has an activation energy of 14 kcal/mole or more. Another point to note is that CH_5^+ competes with CHO^+. The lower appearance potential would favor CHO^+ but the difference is not so great as to preclude CH_5^+ formation.

Acknowledgement

We are very grateful to Drs. W. A. Chupka and J. Berkowitz for the A.P. measurement (P.I.) on CH_5^+, and to H. W. Major for the high resolution spectra. We also wish to acknowledge the National Science Foundation for part of the funds used to purchase the mass spectrometer used in most of this study.

References

1. Kermit R. Way and Morley E. Russell, J. Phys. Chem., 69, 4420 (1965).
2. W. A. Chupka, Private Communication.
3. R. B. Bernecker and F. A. Long, J. Phys. Chem., 65, 1565 (1961).

57. MASS SPECTROMETRY OF AZOMETHANE

Z. Prášil and W. Forst
Department of Chemistry, Université Laval, Québec 10, Canada.

(Abstract)

The conventional mass spectrum of azomethane with 75 volt electrons, as well as the appearance potentials of ions at masses 15, 28, 43 and 58, has been redetermined. A high-resolution mass spectrum has shown peaks at masses 14, 27, 28 and 29 to be composite. This information is used to trace the decomposition mechanism of the azomethane ion. It proceeds principally by simple bond ruptures

$$CH_3N_2CH_3^+ \rightarrow CH_3^+ , \quad CH_3N_2CH_3^+ \rightarrow CH_3N_2^+ ;$$

and by the more complicated rearrangement process

$$CH_3N_2CH_3^+ \rightarrow CH_2N^+ .$$

The three fragment ions plus the parent ion account for 85% of the mass spectrum. Three appearance potentials were found at mass 28, corresponding to the three species contributing to this peak (CH_2N^+ , $C_2H_4^+$, N_2^+). Two appearance potentials were found for CH_3^+ at mass 15, the lower corresponding to formation of CH_3^+ directly from the azomethane ion, and the higher to formation of CH_3^+ from $CH_3N_2^+$. Within experimental error, the new appearance potential data are in good agreement with thermochemical data from other sources, notably the activation energy for the pyrolysis of azomethane. Previous appearance potential data for ions at masses 15 and 43 are shown to be in error due to instrumental effects.

(The full paper will appear in J. Am. Chem. Soc., issue of 19 June 1968)

58. SOME INVESTIGATIONS OF HYDROGEN ION TRAPPING AND REFLECTION IN METAL SURFACES. USING A 30 keV ULTRA HIGH VACUUM ACCELERATOR

G. M. McCracken
U.K.A.E.A., Culham Laboratory,
Abingdon, Berkshire, England

A 30 kV ion accelerator[1] has been used to investigate the interaction of hydrogen and deuterium ions with metal surfaces, particularly at large total doses, up to 10^{19} ions/cm^2. The incident ions were mass analysed in a magnetic sector field and their re-emission was investigated in an ultra high vacuum target chamber using a quadrupole mass filter. This detected mainly those ions which were re-emitted from the surface with low energies. In addition a 3cm radius, 127° electrostatic analyser, coupled to a channel multiplier as detector, has been used to measure the energy and angular distribution of ions re-emitted from the surface with an appreciable fraction of their incident energy.

Two principal mechanisms have been observed which contribute to re-emission. Firstly, the incident ions, after having slowed down to thermal energies, diffuse within the lattice either under thermal or bombardment induced diffusion. This leads to an equilibrium being set up between the number of ions arriving in the metal and those diffusing back to the surface[2]. Whether ions diffusing to the surface escape or not depends on the potential distribution at the surface. In the case of metals which do not react chemically with hydrogen the results are consistent with the assumption that every ion which diffuses back to the surface escapes. In the case of metals which react exothermically with hydrogen to form partial molar solutions, such as titanium or zirconium, the potential barrier at the surface allows the incident ions to be trapped for long periods of time over a wide range of temperatures[3]. At high temperatures and also at low temperatures, however, this trapping is much less efficient. A theory based on a solution to the diffusion equation with appropriate boundary conditions has been developed which explains the principal features observed experimentally.

The second method of re-emission involves scattering of the incident ions in the metal lattice before it reaches thermal energies. A small percentage (depending on the atomic number of the target metal) of the incident ions undergo sufficiently large angle scattering collisions, to be back scattered out of the solid. The 127° analyser has been used to detect those which come out in a charged state. The principal metal used for this investigation was molybdenum. A continuous energy

distribution from close to the incident energy down to less than 500 eV has been observed, with both H^+ and H^- ions, the number of negative ions being slightly less than half the number of positive. With incident ions normal, the shape of the energy spectrum does not alter radically between 27° and 75° with respect to the normal.

REFERENCES

1. G. M. McCRACKEN, J.H.C. MAPLE and H.H.H. WATSON, 1966, Review Sci. Inst. 37, pp 860-866.

2. G. M. McCRACKEN and J.H.C. MAPLE, 1967, Brit. J. of Appl. Phys. 18, pp 919-930

3. G. M. McCRACKEN, D. K. JEFFERIES and P. GOLDSMITH, 1968, Proceedings of the Fourth International Vacuum Congress, Manchester. April 1968 to be published.

59. The Application of an RF Quadrupole Mass Spectrometer to the Detection of Atomic and Molecular Beams*

Gilbert O. Brink

Cornell Aeronautical Laboratory, Buffalo, New York

ABSTRACT

One of the major problems associated with research work in atomic and molecular beams is that of the detection of the beam. While a number of detectors have been developed for use with particular beam materials, it would be desirable to have a detector available which can detect any beam. The last few years have seen a number of "universal beam detectors" developed based on the principal of ionization of the beam by electron bombardment followed by mass analysis of the resulting ions. These detectors, while being truly "universal" in the sense that they will detect any beam, have all suffered from poor detection efficiency.

An electron bombardment detector has recently been developed which has an overall efficiency of the order of one percent, and this detector and its associated equipment will be described. This detector is currently being used for work in atomic and molecular beam magnetic resonance, and it has proven itself to be satisfactory for the detection of not only ground state atoms and molecules, but also for the detection of atoms and molecules in metastable electronic states. The design of the detector will be described and representative data on its operation will be presented.

* This work has been published in Rev. Sci. Inst., 37, 857 (1966).

60. LOW ENERGY INTERACTION STUDIES WITH MERGING BEAMS

P. K. Rol

Space Science Laboratory, General Dynamics/Convair
San Diego, California, 92112

A new technique has been developed to measure two-body interaction cross sections in the energy range from near thermal to several hundred electron volts.[1] Two beams of relatively high laboratory energy (several keV) are merged and move in the same direction along a common axis. The relative energy of the particles in the two beams is

$$W = \mu\left[\left(\frac{E_1}{m_1}\right)^{\frac{1}{2}} - \left(\frac{E_2}{m_2}\right)^{\frac{1}{2}}\right]^2$$

where m_1 and m_2 are the masses, E_1 and E_2 are the energies of the particles in the two beams and μ is the reduced mass. For simplicity consider the case $m_1 = m_2$. Then the expression for the relative energy reduces to

$$W = \tfrac{1}{2}\left(E_1^{\frac{1}{2}} - E_2^{\frac{1}{2}}\right)^2$$

which may be expanded to give

$$W \approx \frac{\Delta E^2}{8E}$$

with $E = \frac{1}{2}(E_1 + E_2)$ and $\Delta E = |E_1 - E_2| \ll E$. Thus $W \ll \Delta E$. The energy spread δW in the relative energy, resulting from the sum of the energy spreads in the primary beams δE, is given by

$$\delta W \approx \left(\frac{W}{2E}\right)^{\frac{1}{2}} \delta E$$

which is quite small, since $W \ll E$. For example, if the primary beam energies are 5000 and 5100 eV, the relative energy $W = 0.25$ eV. An energy spread in each beam of 1.5 eV results in a spread in the relative energy $\delta W = 0.015$ eV.

The number of product particles per second produced in the interaction region is given by

$$N = \left[\frac{W}{2E_1E_2}(m_1 + m_2)\right]^{\frac{1}{2}} \sigma(W) \iiint J_1 J_2 \, dxdydz$$

where $\sigma(W)$ is the reaction cross section. In the overlap integral J_1 and J_2 are the flux densities of the primary beams and dxdydz is a volume element in the interaction region. J_1 and J_2 are determined from the beam profiles in the interaction region. Due to the high velocities of the particles, the number densities in the beams are low and therefore the ratio of the product signal to the primary beam intensity is extremely small.

The beams are generated in ion sources, magnetically analyzed and merged. One or both beams can be neutralized by passage through a charge exchange cell. In order to reduce transverse velocities both beams are well collimated. The required relative energy can be obtained in different ways. The most desirable method, when one or both species are charged, seems to be the adjustment of the applied voltages at the ion sources to give a relative energy for which the reaction cross section is small. The charged particles are then accelerated or decelerated to the desired relative energy by a pair of parallel grids at the entrance to the interaction region. The charged particles are decelerated or accelerated respectively, by the same voltage when they

leave the interaction region. If the reaction products are ionized, only those formed inside the interaction region show a net loss or gain in energy since they pass only through one pair of grids. In the case of neutral-neutral interactions the desired relative energy is determined by the voltages applied at the ion sources, but the net loss or gain of energy while leaving the interaction region through the second pair of grids still discriminates the products formed inside the interaction region from those formed outside. After the interaction region the ions are demerged. The primary beams are monitored separately and the product particles are collected. Because of their high energy the neutral particles can easily be detected. One or both beams are modulated so phase sensitive detection at the modulation frequency or the beat frequency can be utilized. If the product particles are ions, energy analysis can be performed. Additional deflection may be used to prevent energetic neutrals formed by the primary beams through collisions with the walls or the rest gas from reaching the detector.

The total reaction cross section can be measured directly, since all product particles are confined to a small forward cone in the laboratory coordinate system and are thus all detected. Energy analysis of the products can reveal details of the interaction mechanism. In charge rearrangement reactions the change in mass causes a considerable change in lab energy and facilitates detection of the products. Neutral product particles can only be observed if both reactant beams consist of ions, otherwise, the product can not be separated from the very intense primary beams.

The following types of reactions have been studied with this new technique at relative energies as low as 0.05 eV:

(1) charge exchange,[2,3]

(2) charge rearrangement (ion-molecule reactions),[4,5]

(3) mutual neutralization of positive and negative ions.[6]

In the short time since it has been developed, it has been shown that the merging beams technique is a powerful tool for the study of two particle interactions over a wide range of energies.

References

1. S. M. Trujillo, R. H. Neynaber, and E. W. Rothe, Rev. Sci. Instr. 37, 1655 (1966).

2. V. A. Belyaev, B. G. Breshnev, and E. M. Erastov, JETP Pis'ma v Redaktslyu 3, 321 (1966) [English Transl.: JETP Letters 3, 207 (1966)].

3. R. H. Neynaber, S. M. Trujillo, and E. W. Rothe, Phys. Rev. 157, 101 (1967).

4. R. H. Neynaber and S. M. Trujillo, Phys. Rev. 167, 63 (1968).

5. P. K. Rol and E. A. Entemann, to be published in J. Chem. Phys. (1968).

6. W. Aberth, J. R. Peterson, D. C. Lorents, and C. J. Cook, Phys. Rev. Letters 20, 979 (1968).

61. The Three Dimensional Quadrupole Ion Trap

P.H. Dawson and N.R. Whetten
General Electric Research and Development Center
Schenectady, New York 12301

Survey

In recent years, quadrupole mass filters and monopole mass spectrometers have come into widespread use. They depend on the action of radio-frequency quadrupole fields on the ions as they pass through the analyzers. Conditions may be chosen so that only ions with a narrow range of e/m values have trajectories that are stable and limited in amplitude, so that the ions are transmitted.

A three-dimensional quadrupole can be constructed (Fig. 1) in which ions that are formed in the field may have trajectories that are stable in all three coordinate directions. Ions of chosen e/m values can be stored in the device. Pioneering work on these devices was carried out at the University of Bonn by Fischer[1] and later by Rettinghaus.[2] They operated the ion trap so as to simultaneously contain ions of a wide range of e/m values. The presence of particular ions was detected by the power absorption in an auxiliary rf circuit tuned to the characteristic frequency of motion of those ions. This method is complex and suffers from the disadvantage that the presence of one ion in the trap influences the build-up in concentration of other ions. The authors[3,4] have operated three-dimensional quadrupoles so that only a particular ion species is trapped for a given set of voltage conditions. The ions are detected by periodically pulsing them from the trap into an electron multiplier.

Operation

Figure 1 shows the ion trap. It is a three-electrode structure, the electrodes being complementary hyperboloids of revolution. There are two identical "cap" electrodes and a "ring" or donut shaped electrode. A combination of rf and dc potentials in a fixed ratio is applied to the ring. The ratio of the dc to rf determines the mass resolution of the trap. Ions are formed within the trap by electron bombardment. The circuitry used is outlined in Fig. 2. The spectrum is scanned by keeping the dc/rf ratio fixed but varying the voltage amplitudes. Each ion in turn undergoes a time of stable oscillation, so that its concentration builds up in the trap. During that time, the ions are periodically pulsed from the trap and measured. At 10^{-9} Torr, a pulse repetition rate of 25 msec is typical. Reference 3 discusses the theory of operation.

Storage

Storage capability is demonstrated in Fig. 3 for the low resolution case with the dc voltage equal to zero. The electron beam was operated for a few seconds to saturate the trap with ions, and then was switched off. After the indicated time, ions were pulsed out to measure the number remaining. At low background pressures, ions can be stored for several days. The ion-loss curve corresponds to a second-order process so that the loss process is ion-ion scattering. At high background pressures, ion-neutral scattering may become dominant.

Mass Spectrum

A mass spectrum is shown in Fig. 4. The pressure was 5×10^{-8} Torr and the storage time was 25 msec. Resolution was 130 at half-height. This type of device frequently exhibits peak shape problems. These have been shown theoretically and experimentally to be the result of distortions

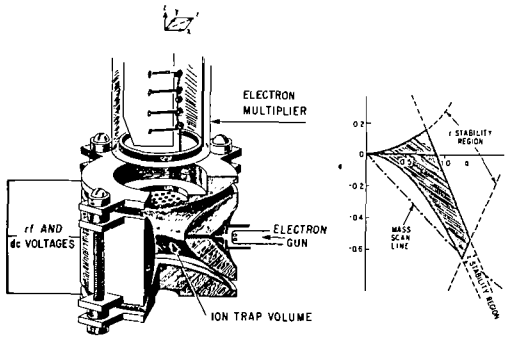

Fig. 1 - Quadrupole Ion Trap

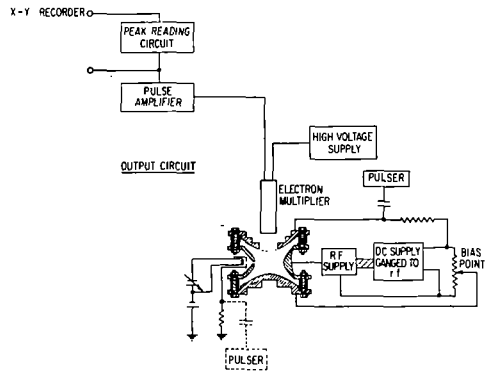

Fig. 2 - Circuit for 300 Mass Spectrometer

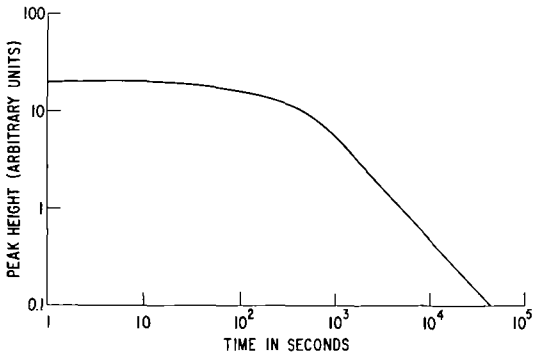

Fig. 3 - Ion Storage
Low Resolution, Pressure = 3 x 10^{-10} Torr

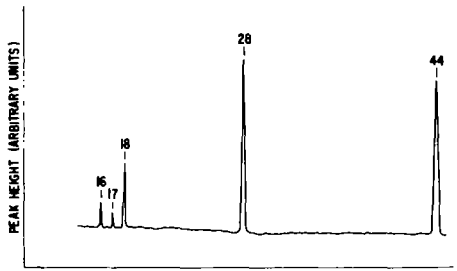

Fig. 4 - Background Mass Spectrum

in the electrode geometry.[5] They are corrected by applying a small bias voltage between the two end-caps.

Uses of Ion Storage

In partial pressure analysis, the storage principle has the following advantages: (1) Sensitivity--it stores or integrates the signal. (2) Path Length--there is a very long path length in a small device. This allows device miniaturization. The authors have constructed an analyzer section smaller than a 1" cube with a usable resolution of 150. The ion storage principle appears attractive for use in studies of ionization phenomena and ion-molecule reactions. It has already been used to trap ions for use in magnetic resonance experiments.[6,7,8]

References

1. E. Fischer, Z. Physik 156, 26 (1959).
2. G. Rettinghaus, Z. Angew. Phys. 22, 321 (1967).
3. P.H. Dawson and N.R. Whetten, J. Vac. Sci. & Technol. 5, 1 (1968).
4. P.H. Dawson and N.R. Whetten, J. Vac. Sci. & Technol. 5, 11 (1968).
5. P.H. Dawson and N.R. Whetten, to be published.
6. D.C. Burnham and D. Kleppner, Bull. Am. Phys. Soc., Series II, 11, 70 (1966).
7. C.B. Richardson, K.B. Jefferts, and H.G. Dehmett, Phys. Rev. 165, 80 (1968).
8. K.B. Jefferts, Phys. Rev. Letters 20, 39 (1968).

64. MASS SPECTRA OBTAINED USING A NEW

FAST-SCAN MAGNET SYSTEM AND DIRECT INLET PROBE

A. J. Smith, T. J. Eskew
Nuclide Corporation, State College, Pennsylvania

and

T. R. Kantner
Hershey Medical Center, Hershey, Pennsylvania

The Nuclide 12-90-G mass spectrometer has been designed for a wide range of applications in the field of chemistry. The very wide and rapid acceptance of mass spectroscopy as a tool by the various chemistry disciplines has created a continual demand for innovations and improvements in this type of instrumentation. The 12-90-G has kept pace with most of these demands as has been reported several times previously at this meeting in past years.

The present discussion will cover two recent changes to the instrument, namely, the magnet system and the direct sample introduction system.

Direct Sample Introduction System:

The direct sample introduction system is shown in line drawing form in Figure 1. It consists of a vacuum lock assembly and sample probe for direct insertion of the sample into the ion source of the mass spectrometer without breaking vacuum.

The probe tip contains a thermocouple, and heating element along with a glass sample container which is capable of being heated to over 400°C. The sample is contained in a glass capillary tube of one millimeter inside diameter and ten millimeters length which is glass-blown into an outer glass shield which surrounds the heater. This outer glass tube shields the probe tip from the high voltage on the ion source and is a convenient size for easy handling during loading. The sample holder is easily replaced and is held in place by a slight spring tension of the heater element. A 20° angular tilt of the probe with respect to the horizontal and the relatively deep sample container provide insurance against losing the sample upon introduction into the instrument.

The vacuum lock consists of a teflon pole valve for isolating the ion source high vacuum, a valved roughing line and a series of teflon packings which allow for differential pumping of the system when the probe is inserted.

Magnet System:

Completely new and all solid-state magnet electronics are now standard on the 12-90-G. They provide more versatility and scanning capability than was heretofore available.

Under fast scan conditions, whether voltage or magnetic, an apparent loss in resolving power and peak height results due to the limited bandwidth of the detection system. Exponential scanning of the mass spectra provides a scan time per peak which is independent of mass. As a result peak distortion is proportionally the same for all masses and the identifiable characteristics of the spectrum remain unchanged. Magnetic scanning is preferred to voltage scanning because the latter results in a net loss in sensitivity at higher mass numbers.

There are some drawbacks to rapid magnetic scanning, however, which if not overcome can seriously limit the useful mass range of an instrument. First, a true control of the magnetic field is required if an exponential scan is to be achieved. If the field does not change in an

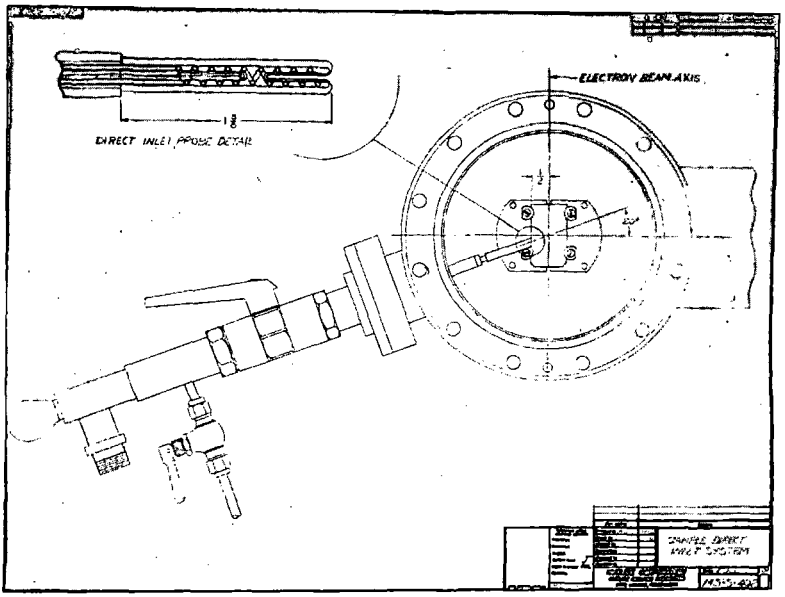

Figure 1

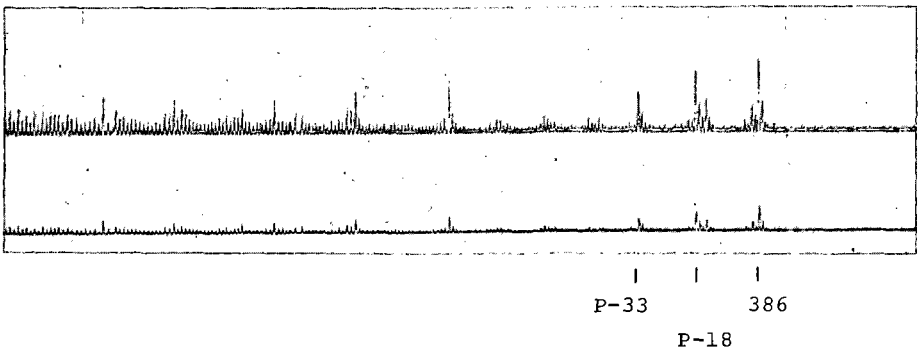

Cholesterol
Ion source at 350°C

Figure 2

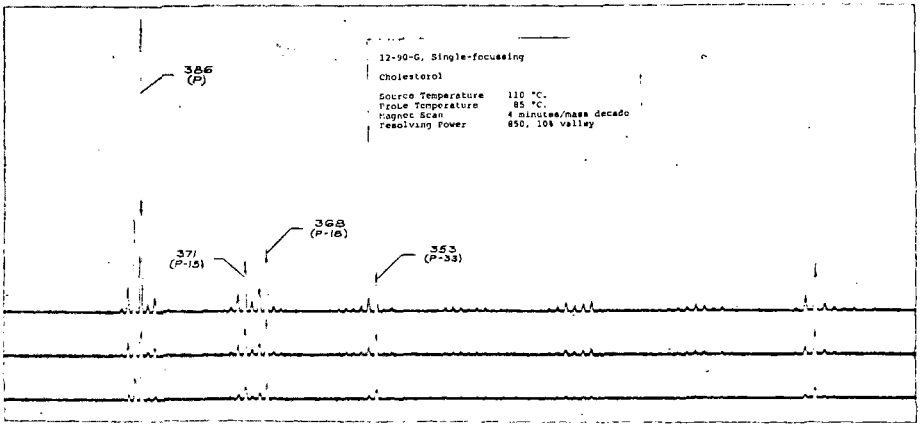

Cholesterol
Ion source at 110°C

Figure 3

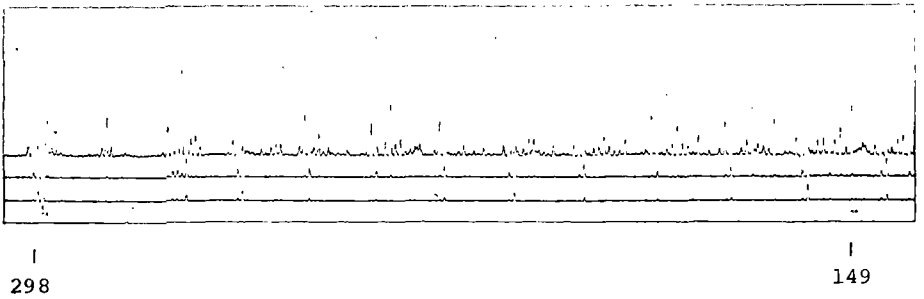

Methyl stearate

0.4 sec/octave; resolving power of 500

Figure 4

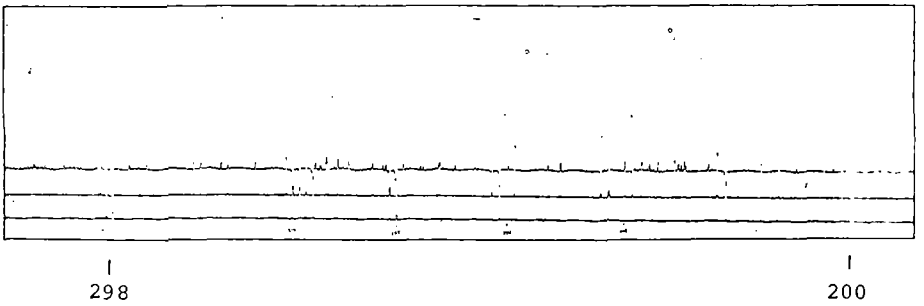

Methyl stearate

0.67 sec/octave; resolving power of 950

Figure 5

exponential fashion, then the apparent resolving power and sensitivity will change throughout the mass spectrum. In systems without a field controlled scan it is not unusual to expect the apparent resolving power and sensitivity to be different by a factor of three in different parts of a single spectrum. In a current-controlled magnet the effect of both hysteresis and circulating eddy currents generated during a scan is to slow down the scan both at high magnetic fields when scanning up-mass and at low magnetic fields when scanning down mass. Unless this is corrected the net effect is a serious deviation from an exponential change in field with a resultant distortion in resolving power and sensitivity at the high and low ends of the mass spectrum. Generally speaking, in instruments in which the scan has not been corrected for these effects as much as one-half the static magnetic field range of the magnet is not useable in fast scanning.

These problems have been overcome in the 12-90-G magnet system however and as a result fast scanning is possible over the entire range of the magnet. This is about 12,000 gauss, which corresponds to a mass range over 6000 amu at 1000 volts accelerating potential. Fast scanning of the field-regulated system has been made possible by providing an over voltage and current to overcome the inductance and eddy currents of the magnet and by allowing the magnet current to swing negative for a time on rapid down-mass scans.

Performance Results:

The maximum temperature at which the probe has been operated is in excess of 400°C. Heating time to go from ambient to 200°C is one minute and about another minute is required to reach 300°C. Cooling in a vacuum from 350°C to 150°C can be achieved in two minutes; cooling in atmosphere for the same temperatures can be achieved in less than one minute.

Total cycling time for introducing a sample with the probe - including the time required for removing the probe from the lock, loading a previously prepared sample holder, and inserting the probe and pump-down - is on the order of 30-45 seconds.

Water cooling at the probe tip to shield it from the heat of the ion source block is not essential in the 12-90-G as in some other instruments since the source can normally be maintained at a temperature of 100°C or even as low as 70°C if the electron emission from the source filament is reduced. However, if required the source can be operated at temperatures much higher than the probe temperature without serious loss of performance. The small cross-sectional area and depth of the capillary sample container in the probe tip effectively shield the sample from the heat of the ion source. Figure 2 shows a scan over a portion of the mass spectrum of cholesterol, a low boiling thermally unstable compound. The scan rate was 1 min/mass decade, the sample size was 10 nanograms and the probe temperature less than 100°C. Although the source block was at a temperature over 350°C, control of sample evaporation was maintained with the probe heater when the spectrum was obtained. The peaks at the P-18 and P-33 positions which are relatively large compared to the parent ion peak at mass 386 indicate the degree of thermal decomposition of the sample due to the high source temperature.

Figure 3 shows a portion of the cholesterol mass spectrum obtained for different temperature conditions. The probe temperature was 85°C but in this case the source temperature was only 110°C rather than 350°C as in the previous figure. It is apparent from the very small fragment peaks at the P-18 and P-33 mass position that the degree of thermal decomposition is considerably less. The peak height ratio of 386/368 is approximately 5/1, and is about the same as can be achieved when using a water-cooled probe tip. One can conclude from this data that good results on small size and thermally unstable compounds can be achieved without elaborate cooling of the probe tip providing that the probe design allows for some degree of shielding of the sample from the ion source and that a low source operating temperature can be maintained.

The remaining two figures show portions of the mass spectrum of methyl stearate obtained with the fast-scanning magnet system, scanning in the exponential mode. No slides are available to show the scan capability at either high fields on up mass scans or at low fields on down mass scans, but the results obtained to date indicate that peak widths are constant to within about a factor of 1.5 over the range from mass 12 to well in excess of mass 600. Scanning linearly one would expect the peak width to vary by a factor of seven over this range.

Figure 4 shows the spectrum from about mass 150 to mass 300; scanning time was in about 0.4 seconds. The electrometer bandwidth was set at 1000 Hz. The resolving power measured at the parent ion (mass 298) is 400 based on the 10% valley definition. The source and collector slits were set to give a static resolving power on the order of 500 (10% valley). It is evident from the trace that already at this scan rate and resolving power some of the peaks are not fully recorded because the galvanometer light beams are moving too fast to make a good impression on the record paper. Note that the relative peak widths remain constant throughout the scan in both this case and in the next slide.

Figure 5 shows a smaller portion of the mass spectrum of the same compound methyl stearate in order that the mass resolution can be shown in greater detail. The scan rate was 0.67 sec/mass octave and resolving power measured at the parent peak mass 298, is 950, 10% valley. The static resolving power was 2000 and the electrometer bandwidth about 3000 Hz.

65. SOME MASS SPECTRAL AND ANALYTICAL ASPECTS OF DEUTERIUM LABELING OF STRAIGHT-CHAIN OLEFINS

by

D. G. Earnshaw, F. G. Doolittle, and A. W. Decora
U.S. Department of the Interior, Bureau of Mines
Laramie Petroleum Research Center
Laramie, Wyoming 82070

Work done at the Laramie Petroleum Research Center has led to the search for a method to analyze for linear mono-olefins in products from Green River oil shale. A method utilizing deuterium labeling and mass spectrometry for identifying and analyzing linear mono-olefins is described. The method shows promise for the analysis of mixtures of linear mono-olefins after they have been homogeneously deuterated to the corresponding dideuterioalkanes using a tris(triphenylphosphine)rhodium catalyst. Five n-decanes (1,2-d_2, 2,3-d_2, 3,4-d_2, 4,5-d_2, and 5,6-d_2) and six n-alkanes-1,2-d_2 (undecane, dodecane, tridecane, tetradecane, pentadecane, and hexadecane) have been prepared and their 70-volt spectra have been obtained. The ultimate aim of this research is to extend the methods described to higher-molecular-weight compounds. Predictions of their spectra would eliminate the need to prepare these compounds to use as standards.

Correlations of mass spectra with the structures of the five vicinal dideuterio-n-decanes are presented. Those regions of the mass spectra are used where fragment ions form by simple carbon-carbon bond cleavage followed by reactions involving hydrogen loss. For the five vicinal dideuterio-n-decanes the C_6, C_7, and C_8 fragment ions are used.

The effect of deuterium labeling can be enhanced by removing contribution of ions that result from hydrogen loss from fragments formed by single carbon-carbon bond cleavage. It is assumed that this hydrogen loss occurs in the dideuterioalkanes exactly as it does in the protioalkanes. Deuterium loss has also been considered, but correction for deuterium loss did not improve results and consequently was not used in this work.

Study of the "enhanced" spectra shows that fragment ions in the C_6, C_7, and C_8 region can be readily explained by simple carbon-carbon bond cleavage followed by hydrogen loss. The fragment ions in the regions below C_6 cannot be so explained. However, the differences in peaks of the C_6-C_8 region are sufficient to identify each of the five vicinal dideuteriodecanes and to analyze a mixture of any of the five. The peaks in this region are shown in table 1. A least squares matrix using nine equations in five unknowns has been calculated using the data given in table 1. This matrix was used to analyze a test mixture of four dideuteriodecanes. The result of the analysis is shown in table 2. The

TABLE 1. - Selected peak heights used for calculation of least squares matrix

Fragment peak		Enhanced peak heights of five dideuteriodecanes[1]				
Carbon No.	m/e	1,2-d_2	2,3-d_2	3,4-d_2	4,5-d_2	5,6-d_2
6	85	726	762	734	75	82
	86	54	22	23	634	38
	87	631	677	706	699	1265
7	99	166	161	29	41	44
	100	7	11	136	-34	-38
	101	150	135	142	302	292
8	113	85	3	17	20	22
	114	17	83	-2	-14	-20
	115	101	107	174	182	185

[1] These peak heights have been "enhanced" by removal of contribution of ions resulting from hydrogen loss after simple carbon-carbon bond cleavage and normalized to a total ionization of 10,000.

TABLE 2. - Result of mass spectral analysis of a mixture of dideuteriodecanes

Dideuteriodecane, position of substitution	Test mixture composition, mole %		Error, mole %
	Known	Calculated	
1,2-d_2	31.5	37.8	+6.3
2,3-d_2	0.0	-3.2	-3.2
3,4-d_2	17.5	14.2	-3.3
4,5-d_2	23.5	23.7	+0.2
5,6-d_2	27.5	30.7	+3.2
Total	100.0	103.2	----

results on the test mixture indicate the promise of the method. However, additional data are needed to more fully establish precision and accuracy of the method.

Initial attempts have been made to predict the spectra of the C_{11}-C_{16} n-alkanes-1,2-d_2. These spectra were chosen because the compounds were available for comparison. To predict these spectra it was assumed that all the vicinal dideuterioalkanes having the same molecular weight produce constant sums of peak heights for each carbon-number region. It has been found that these sums are constant within ± 5 percent.

Studies indicate that the ratios of peaks in some carbon-number regions observed in the spectra of low-molecular-weight compounds are close to the ratios of peaks of higher carbon-number regions in higher-molecular-weight compounds. Although the results obtained thus far are not good enough for quantitative work, they are good enough to identify individual compounds and to encourage further work on the prediction process.

66. THIOLACETATE ESTERS AS OLEFIN DERIVATIVES FOR MASS SPECTROMETRY

By Richard M. Teeter
Chevron Research Company, Richmond, California 94802

The analysis of olefins and olefin mixtures is of great practical importance and has received attention in both industrial and academic laboratories. For complex mixtures, the combination of mass spectrometry with and without hydrogenation after separation in the gas chromatograph[1] has proven itself; but the technique is limited in the structural information it can provide. For a pure olefin, the structure of which is to be determined, the mass spectrum is frequently of little help because rearrangement processes mask the location of the double bond. Reaction of the double bond to form a derivative more amenable to mass spectrometric analysis has been applied quite successfully. Oxidation of the double bond to an epoxide followed by reaction with iodide ion and rearrangement to a mixture of ketones[2] or by reaction with dimethylamine to form a mixture of dimethylamino alcohols[3] leads ultimately to the identification of the double bond position. Oxidation with osmium tetroxide and formation of the dioxolane with acetone[4] gives a product whose mass spectrum can be very useful in this context.

In the hope of finding still another method to aid the analysis of olefins, the addition of thiolacetic acid to these compounds was investigated and the mass spectra of the products studied. The mass spectra of a large number of aliphatic thioesters, including 13 thiolacetates, were studied by McFadden, Seifert, and Wasserman in 1965.[5] This was very good work and I have drawn upon it heavily, but the thioesters were prepared from thiols and either acid chlorides or anhydrides and so there was no information in that source about the thiolacetic acid addition reaction. This, of course, is an essential part of the knowledge required if the reaction and its products are to be used analytically.

It is known[6] that the addition of thiolacetic acid proceeds via a free radical addition reaction since it is catalyzed by peroxides[7] and yields primarily the anti-Markownikoff product.[8] But there has been very little reported on the variations in products and yield with olefin structure, so this question was examined as well as the question of the suitability of the mass spectra for analysis.

The reaction is conveniently carried out on a small scale in a 1-ml reaction flask with a short sealed-on water condenser. Two-tenths milliliters of olefin is placed in the flask followed by 0.4 ml of redistilled thiolacetic acid and 1-2 mg of benzoyl peroxide, and the reaction mixture is heated under gentle reflux for 2 hours. Samples are removed for gas chromatographic analysis at roughly 30-minute intervals. Considerable variation was found in reaction rate, 2-methylheptene-1 reacting essentially to completion in 30 minutes, and 1-ethylcyclohexene requiring over an hour. All of the hydrocarbons studied gave relatively simple mixtures of products in over 95% yield except the two tetra-substituted olefins, 2,3-dimethylhexene-2 and 1,2-dimethylcyclohexene. These latter materials were slow, requiring over 2 hours for 90% reaction and yielded complex mixtures which have not been fully identified. The dimethylcyclohexene product gave at least six poorly resolved peaks in the chromatograph.

With 1-olefins, the reaction produces mainly the terminal thiolacetate, presumably by the familiar chain reaction involving a relatively stable II° radical as the intermediate. However, the 2-product is also produced in small amounts, small because the less stable I° radical is formed in small amounts. Four α-olefins were examined and the yields of I° and II° ester are presented in Table I.

Table I

Addition of Thiolacetic Acid to 1-Olefins
Product Composition

Olefin	I° Ester	II° Ester
Decene-1	97.8	2.2
Octene-1	97.7	2.3
3-Cyclopentylpropene-1	98.0	2.0
Vinylcyclohexane	98.4	1.6

The mass spectra were not required for identification of these products since the chromatographic retention times are different and reproducible enough to use the series of products given in Table II. Each of the four possible thiolacelates was trapped and the mass spectra were recorded.

Table II

Addition of Thiolacetic Acid to Octenes
Product Composition

Olefin	1-Ester	2-Ester	3-Ester	4-Ester
Octene-1	97.7	2.3		
Octene-2		54.7	45.3	
Octene-3			55.2	44.8
Octene-4				100.0

The same retention time technique was used to determine the product composition from the addition to the cyclic olefins shown in Table III. Note that the major product in each case results from the more highly substituted radical. The competition between I° and III° radical was examined in the cases of addition to 2-methylheptene-1 and 2,5-dimethylhexene-1, and in both cases the reaction went exclusively via the III° radical, yielding 100% of the terminal addition product.

Table III

Addition of Thiolacetic Acid to
Cyclohexane Octenes
Product Composition

Olefin	2-Cyclohexyl-ethane-1-thiol Acetate	1-Cyclohexyl-ethane-1-thiol Acetate	1-Ethylcyclo-hexane-1-thiol Acetate	2-Ethylcyclo-hexane-1-thiol Acetate
Vinylcyclo-hexane	98.3 II° Radical	1.7 I° Radical		
Ethylidene-cyclohexane		99.7 III° Radical	0.3 II° Radical	
2-Ethylcyclo-hexene			1.7 II°Radical	98.3 III° Radical

With a double bond in a ring, cis-trans isomerism becomes possible. Gas chromatography of the products from the olefins of Table IV gave, in addition to the small percentage of II° product, two peaks whose areas are given under "By GC." Both of these were trapped from the methylcycloheptene product, and their mass spectra were virtually indistinguishable. It was shown in 1957[9] that the addition of thiolacetic acid to 1-methylcyclohexene yields 85% cis and 15% trans products, so the major product here was expected to be cis. The NMR spectra of the crude reaction products confirmed this judgment, and integration of the appropriate peaks yielded the compositions given under "By NMR."[10]

Table IV

cis-trans Isomers
Product Composition

Olefin	II°-cis		II°-trans	
	By GC	By NMR	By GC	By NMR
1-Methylcycloheptene	72.0	70	28.0	30
1,4-Dimethylcyclohexene	76.5	76	23.5	24
1-Ethylcyclohexene	84.4	78	15.6	22

In the mass spectra of the thiolacetates which were studied, the largest peak was usually either the acetyl ion at m/e 43 or the ion corresponding to the original olefin. The parent peaks varied in relative size from 0.6% of the largest, or base, peak up to 6%. As observed by McFadden and his coworkers, it is difficult to predict the size of the parent peak on the basis of the amount of branching in the chain. 2-Methylheptane-1-thiol acetate shows a parent peak that is about one-fourth the size of that shown by the straight chain esters while that of the even more highly branched 3,4,4-trimethylpentane-2-thiol acetate is three times as large.

The most interesting fragmentation reported by McFadden is the loss of an alkyl sulfur species of mass 60, 74, or 88 from the parent ion. The nature of the lost neutral particle has now been confirmed by exact mass measurement on the residue. The reaction can be written as shown below.

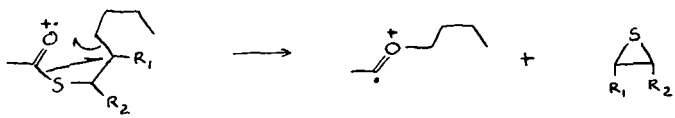

The data in Table V show, by underlining, the peaks which, on the basis of the above scheme, should be the largest in the series from M-60 to M-102. The expectations are borne out except in the last case.

Table V

Loss of $(CH_2)_nS$ from Parent Ion

Compound	R_1	R_2	Peak Height M-60	M-74	M-88	M-102
Octane-1-Thiol Acetate	H	H	8.6	0.6	1.0	1.5
Octane-2-Thiol Acetate	H	CH_3	0.3	8.9	1.1	1.4
Octane-3-Thiol Acetate	H	CH_2CH_3	0.2	1.4	9.4	3.4
Octane-4-Thiol Acetate	H	$CH_2CH_2CH_3$	0.0	1.0	2.2	5.2
2-Methylheptane-1-Thiol Acetate	CH_3	H	0.1	5.4	0.4	1.0
3,4,4-Trimethylpentane-2-Thiol Acetate	CH_3	CH_3	0.0	0.0	0.0	1.7

Another surprise in the spectrum of 3,4,4-trimethylpentane-2-thiol acetate was a pair of peaks at m/e 131 and 132, loss of 57 and 56, respectively, from the molecular ion. As expected, m/e 132 was found, by mass measurement, to be $C_8H_{12}OS^+$, implying the loss of C_4H_8. However, rather than $C_8H_{11}OS^+$, m/e 131 was found to be $C_7H_{15}S^+$ (loss of $C_3H_5O\cdot$) which requires a carbon-skeleton rearrangement. The two schemes shown below can be used to rationalize these two reactions although there is no evidence beyond consistency with the data and with each other.

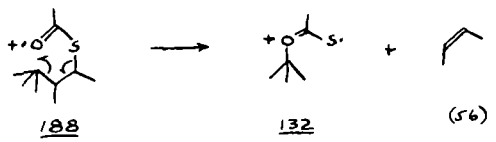

188 132 (56)

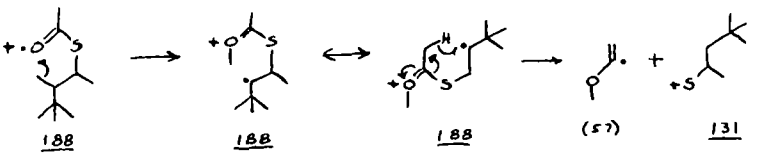

188 188 188 (57) 131

Two unsaturated thiol acetates were prepared, oct-7-enethiol-1 acetate, minor product from addition to 1,7-octadiene, and oct-1-enethiol-1 acetate, minor product from addition to octyne-1. Loss of 43 was prominent in the spectrum of the former while loss of 42 occurred with the latter. The presence of the adjacent double bond probably permits the following rearrangement.

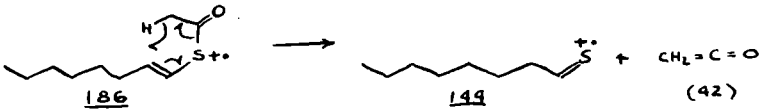

The major addition products (>95%) resulted, in each case, from the addition of two molecules of thiolacetic acid; but these were not purified adequately by gas chromatography, and so their spectra were not suitable for reporting.

References

1. R. M. Teeter, C. F. Spencer, J. W. Green, and L. H. Smithson, J. Am. Oil Chem. Soc. 43, 82 (1966).
2. G. W. Kenner and E. Stenhagen, Acta Chem. Scand. 18, 1551 (1964).
3. H. Audier, S. Bory, M. Fétizon, P. Longevialle, and R. Toubiana, Bull. Soc. Chim. France 1964, 3034.
4. R. E. Wolff, G. Wolff, and J. A. McCloskey, Tetrahedron 22, 3093 (1966).
5. W. H. McFadden, R. M. Seifert, and J. Wasserman, Anal. Chem. 37, 560 (1965).
6. C. Walling, "Free Radicals in Solution," John Wiley and Sons, 1957, pp 316-317.
7. R. Brown, W. E. Jones, and A. R. Pinder, J. Chem. Soc. 1951, 2123.
8. B. Hollberg, Arkiv Kemi Min. Geol. 12B, 3 (1938).
9. F. G. Bordwell and W. A. Hewett, J. Am. Chem. Soc. 79, 3493 (1957).
10. I am indebted to Dr. L. P. Lindeman for obtaining and interpreting the NMR spectra.

:am

67. ELECTRON IMPACT INDUCED REARRANGEMENT OF TRIMETHYLSILYL GROUPS IN LONG CHAIN COMPOUNDS

G. H. Draffan, R. N. Stillwell and J. A. McCloskey

Baylor University College of Medicine, Houston, Texas

In the mass spectra of certain long chain compounds there is considerable evidence that coiling or winding of the chains can occur allowing the interaction of otherwise remote sites in the molecules. It has been shown, for example (1), that elimination of CH_3OD occurs from the α-cleavage ion of methyl O-d, 12-hydroxystearate, thus implicating a 15-membered transition state. We have studied the mass spectra of the trimethylsilyl (TMS) derivatives 1 - 9 and with

$RO_2C(CH_2)_nCO_2R'$	1 - 4	n = 8, 10, 16, 20
	a	R = R' = TMS
	b	R = TMS, R' = CH_3
$TMSO_2C(CH_2)_nCN$	5	n = 8 ; 6 n = 10
$TMSX(CH_2)_{10}XTMS$	7	X = O ; 8 X = S ; 9 X = NH

the exception of compounds 7 and 9, have observed prominent ions arising from intact TMS group rearrangements. The transfer of these groups from donor to acceptor sites in the chains again requires the involvement of large ring transition states. In the identification of such ions, use has been made of exact mass measurement and also of the labeled silylating reagent d_{18}-(bistrimethylsilyl)acetamide (2).

There is already evidence in the literature that TMS groups undergo rearrangement on electron impact (2, 3). The ion of m/e 147, a, has been identified in the spectra of several polysilylated compounds (2, 3) and is especially prominent from polymethylene glycol di-TMS ethers of the type 7 (2, 3c).

$$(CH_3)_3\overset{+}{S}iO{=}Si(CH_3)_2$$

a, m/e 147

In the spectra of the diesters 1a - 4a the ions m/e 204 ($C_8H_{20}O_2Si_2$) and 217 ($C_9H_{21}O_2Si_2$) are prominent (3a : m/e 204, R.I. 63%, m/e 217, R.I. 34%). These ions, which retain both intact TMS functions evidently require interaction of the chain

termini. They may be assigned structures b and c (R = TMS) (4) and are then the structural analogs of the well-known methyl ester ions m/e 74 and 87. In the spectra of polysilylated carbohydrate derivatives (3b) m/e 204 and 217 have been formulated as b' and c'. Labeling the carbonyl carbon atoms of 3a with ^{13}C, results in retention of one atom of ^{13}C in 204 and 217, strongly supporting structures b and c rather than b' and c', which could not a priori be discounted. For the mixed esters 1b - 4b, b and c (R = CH_3) shift 58 mass units lower, in accordance with the transfer of the TMS function to the carbomethoxy group.

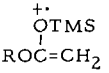

b

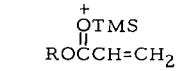

c

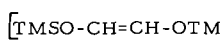

b'

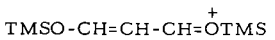

c'

Examination of the high resolution spectrum of 3a reveals a series of low intensity ions corresponding to the composition $(TMS)_2CO_2(CH_2)_nCH=CH_2$ for which n = o for m/e 217, ion b.

In the spectra of the cyano esters 5 and 6 two series of TMS rearranged ions have been identified. Thus from 6 the even electron ions $[TMS\text{-}NCC_nH_{2n-1}]^+$ are recorded for n = 2 - 10. The most abundant member (R.I. 23.5% when n = 9 in 6) corresponds to M - $C_2H_3O_2$. Odd electron ions $[TMS\text{-}NCC_nH_{2n}]^{+\cdot}$ are significant only when the radical is stabilised by conjugation (n = 1) or by cyclization (n = 4 - 5). The most prominent ion, when n = 5 (R.I. 17% in 6) may adopt the cyclic structure d.

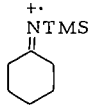

d

TMS rearrangement ions in the spectrum of decane diol di-TMS ether 7 have been discussed elsewhere (2, 5). These all involve loss of at least one silyl methyl group. In contrast, the spectrum of the dithiol derivative 8 contains the ions M - SH (R.I. 4%), M - $(CH_2)_nSH$ (n = 1 - 8, R.I. all ca. 0.5%) and TMS-$\overset{+\cdot}{S}$-TMS (R.I. 11%) which require transfer of a TMS group from one sulphur atom to the other, most probably at the molecular ion stage. A metastable ion is recorded for the formation of M - SH from M.

The sulphur analog e of m/e 147, a, prominent in the spectrum of the diol derivative 7, is derived at least in part, by loss of methyl from $TMS\text{-}\overset{+\cdot}{S}\text{-}TMS$.

$$TMS\text{-}\overset{+\cdot}{S}\text{-}TMS \xrightarrow{m^*} TMS\text{-}\overset{+}{S}{=}Si(CH_3)_2$$

e

Fragmentation of the diamine TMS derivative 9 is dominated by cleavage α- to the nitrogen, giving $[TMS\text{-}NHCH_2]^+$, 49% $\sum_{40}$. The nitrogen analog of ion a, m/e 146 $[(CH_3)_2\overset{+}{Si}{=}NH\text{-}Si(CH_3)_3]$, is observed at low abundance.

A number of interesting doubly-charged ions which have no singly-charged counterpart have been observed in the spectra of 1a - 4a and 7 - 9. It has been previously shown (2) for the C-22 homolog of 7 that silyl methyl groups are lost from opposite ends of the chain:

1a - 4a	$(CH_3)_2\overset{+}{Si}O_2C(CH_2)_nCO_2\overset{+}{Si}(CH_3)_2$	(n = 16, R.I. 2.4%)
7 - 9	$(CH_3)_2\overset{+}{Si}\text{-}X(CH_2)_{10}X\text{-}\overset{+}{Si}(CH_3)_2$	(X = O, R.I. 5.4%)

Weak doubly-charged ions resulting from α-cleavage and loss of a silyl methyl group have also been recorded from the 12-hydroxystearic acid derivatives 10 and 11.

$$TMSO_2C(CH_2)_{10}\underset{\underset{OR}{|}}{CH}(CH_2)_5CH_3 \longrightarrow (CH_3)_2\overset{+}{Si}O_2C(CH_2)_{10}\overset{+}{\underset{\underset{OR}{|}}{CH}}$$

10 R = CH_3, 11 R = TMS

In conclusion, since TMS derivatives are being increasingly used in mass spectrometry, an awareness of the tendency of the silyl function to undergo intramolecular rearrangement is important for the correct interpretation of their mass spectra. In addition this work provides further evidence for the existence of large transition states, permitting the interaction of remote groups in long chain compounds.

REFERENCES

(1) R. E. Wolff, M. Greff and J. A. McCloskey, in Advances in Mass Spectrometry", Vol. 4, E. Kendrick, Ed., Institute of Petroleum Press, London, 1968, p. 193.

(2) J. A. McCloskey, R. N. Stillwell and A. M. Lawson, Anal. Chem., 40, 233, (1968).

(3) W. J. Richter, M. Vecchi, W. Vetter and W. Walther, Helv. Chim. Acta, 50, 364 (1967); (b) O. S. Chizhov, N. V. Molodtsov and N. K. Kochetkov, Carbohydrate Res., 4, 273 (1967); (c) H. Budzikiewicz, C. Djerassi and D. H. Williams, "Mass Spectrometry of Organic Compounds," Holden-Day, Inc., San Francisco, 1967, p. 471-7; (d) P. Capella and C. Zorzut, Anal. Chem., in press.

(4) We thank Dr. W. J. Richter for first pointing out this possibility.

(5) See also ref. (3c).

68. ELECTRON IMPACT STUDIES XII. MASS SPECTRA OF SILAZANES

by

K. Ganesh Das and P.S. Kulkarni
National Chemical Laboratory, Poona-8, India

and

M.V. George and V. Kalyanaraman
Indian Institute of Technology, Kanpur, India

Abstract

Although the interest in organosilicon chemistry has increased in recent years, the information available in literature on the behaviour of Si-N bond on electron impact is scanty. We have initiated systematic work on the fragmentation of silicon-nitrogen compounds under electron impact. In the present studies we have examined the mass spectra of the following tetraaza-3,6-disilacyclohexanes.

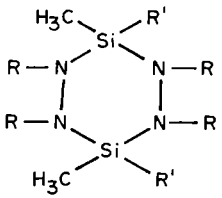

I R = C_6H_5, R' = CH_2=CH

II R = m-$CH_3C_6H_4$, R' = CH_2=CH

III R = m-$CH_3OC_6H_4$, R' = CH_3

I. 1,2,4,5-tetraphenyl-3,6-dimethyl-3,6-divinyl-1,2,4,5-tetraaza-3,6-disilacyclohexane.

II. 1,2,4,5-tetra(m-tolyl)-3,6-dimethyl-3,6-divinyl-1,2,4,5-tetraaza-3,6-disilacyclohexane.

III. 1,2,4,5-tetra-(m-anisyl)-3,3,6,6-tetramethyl-1,2,4,5-tetraaza-3,6-disilacyclohexane.

The silylhydrazines that we have studied include the following compounds.

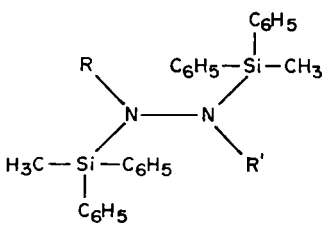

IV R = C_6H_5, R' = C_6H_5

V R = C_6H_5, R' = p-$CH_3C_6H_4$

VI R = C_6H_5, R' = p-$CH_3OC_6H_4$

VII R,R' = 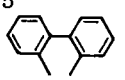

IV. N,N'-diphenyl-N, N'-bis(diphenylmethylsilyl) hydrazine.

V. N-phenyl-N'-(p-tolyl)-N, N'-bis (diphenylmethylsilyl) hydrazine.

VI. N-phenyl-N'-(p-anisyl)-N,N'-bis(diphenylmethylsilyl) hydrazine.

VII. N,N'-bis(diphenylmethylsilyl) dibenzodihydro pyridazine.

All the compounds that we have studied show intense molecular ions. Expulsion of (R-N·) and (R-N=N-R) from the molecular ion is a characteristic fragmentation mode of tetraaza-3,6-disilacyclohexanes. Hydrogen transfers and skeletal rearrangements are observed. Evidence for the decomposition of the doubly charged molecular ion into two singly charged ions and into a doubly charged ion and a neutral molecule was obtained. Two different types of metastable ions are detected which support many fragmentation modes. In general fragmentation modes leading to even electron ions are favoured.

The full paper will be published elsewhere.

69. INTRAMOLECULAR REACTION OF REMOTE FUNCTIONALITIES

IN LONG-CHAIN ALIPHATIC DIKETONES UPON ELECTRON IMPACT[1,2]

W. J. Richter, D. H. Smith, and A. L. Burlingame
Department of Chemistry and Space Sciences Laboratory
University of California, Berkeley, California 94720

The mass spectral fragmentation of several long-chain aliphatic 1,n-diketones (n>5) has been studied with respect to the possibility of interactions between remote functionalities. As might be anticipated for the introduction of an additional carbonyl group into the simple monoketonic model, the major part of the total ion production still reflects the independent behavior of both ketonic centers. Functional group interaction, however, is established by the occurrence of certain fragmentation reactions absent or negligible in the case of monoketones.

This is the case, for instance, for a particular type of β-cleavage. While the cleavage of α-β-bonds, associated with γ-hydrogen transfer (commonly referred to as McLafferty-rearrangement) is encountered in aliphatic mono- as well as diketones, such cleavage without hydrogen transfer has virtually no precedent in monoketonic models. A direct participation of the second distant functionality in this mode of fragmentation is therefore to be considered. In contrast to the McLafferty-rearrangement, which generally gives rise to odd-electron radical ions at even mass, the fragments formed in the course of this cleavage process possess even-electron configuration, occur at odd mass numbers, and more importantly, retain the charge on the alkyl-, or more precisely, the ketoalkyl portion of the molecule. This type of β-cleavage results in an overall loss of $RCOCH_2$- from the molecular ions and can be visualized as a two-step process:

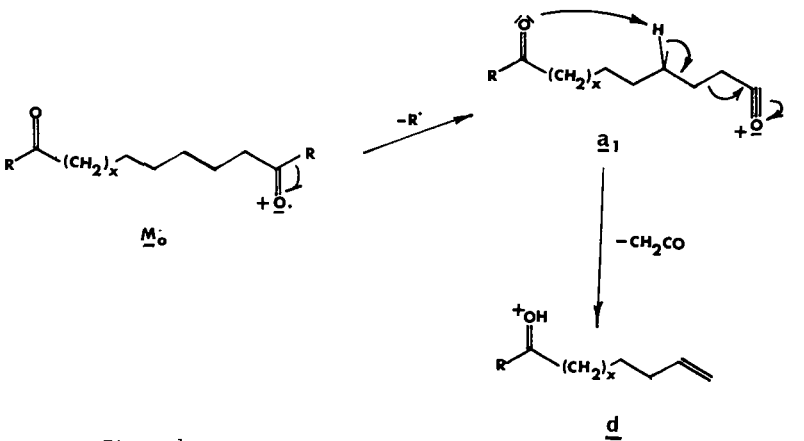

Figure 1

This sequence involves a normal α-cleavage, as observed in both mono- and diketones, followed by the attack of the remote carbonyl function at a specific position (γ'), resulting in abstraction of a proton from a favorable site. This second step which resembles a chemical Hofmann elimination would cause the loss of a neutral ketene molecule and would appear to be triggered exclusively by the "basicity" of the additionally present functionality.

As an alternative, a direct loss of an $RCOCH_2$ radical as an intact unit in a one-step process cannot be ruled out from the data available, particularly since confirming evidence from metastable peaks is lacking for either case. For instance, a radical-type abstraction of the same γ'-hydrogen atom could result in the observed cleavage as a direct consequence. Such a process might receive at least some favorable product development control by providing conjugation with the carbonyl-π-system for the radical species to be lost in that case. It could be favored over similar processes involving abstraction from other sites, which would produce only homologous, non-conjugated radicals.

An analogous behavior is exhibited by esters of comparable keto- and dicarboxylic acids.

Routine determinations of complete high-resolution mass-spectra, in addition to deuterium labelling, were employed to substantiate some of the mechanistical details proposed for the formation of these and other fragment ions regarded as products of an intervention of remote functional groups in normal monoketonic fragmentation.

FOOTNOTES

1. To be published in Journal of the American Chemical Society.

2. Financial support was provided in part by the National Aeronautics and Space Administration Grant NsG 101.

70. MASS SPECTRUM OF ACETOPHENONE AZINE. EVIDENCE FOR THE REARRANGEMENT OF METHYL, PHENYL, AND HYDROGEN DURING DECOMPOSITION

by

S. E. Scheppele, R. D. Grigsby, E. D. Mitchell, and D. W. Miller

Departments of Chemistry and Biochemistry, Oklahoma State University, Stillwater, Oklahoma 74074; and Department of Biochemistry and Biophysics, Texas A&M University, College Station, Texas 77843.

Migrations of alkyl, aryl, and other functional groups during the fragmentation of organic molecules are currently receiving considerable interest in mass spectrometry.[1] We have conducted a detailed study of the fragmentation pattern of acetophenone azine and have found evidence for the rearrangement of phenyl, methyl and hydrogen during decomposition induced by electron inpact. A full account of the investigation has been accepted for publication in the *J. Amer. Chem. Soc.*; consequently, the present manuscript will be limited to a presentation of the data followed by a brief summary of the more interesting rearrangement mechanisms.

In the table are given ions having intensities greater than $0.7\%\Sigma_{38}$ in the mass spectrum of the compound.

Peaks above $0.7\%\Sigma_{38}$ in the Mass Spectrum of Acetophenone Azine

m/e	$\%\Sigma_{38}$[a]	RA[b]	m/e	$\%\Sigma_{38}$[a]	RA[b]
51	4.4	25	132	2.1	12
76	1.1	6	133	1.6	9
77	15.1	85	159	4.1	23
91	1.6	9	180	2.1	12
103	0.8[c]	5[c]	194	1.2	7
103	2.6[d]	14[d]	195	0.7	4
104	2.0[e]	11[e]	221	17.8	100
104	0.7[f]	3[f]	235	2.5	14
117	1.1	6	236	10.1	37
118	6.8	38			

(a) Percent Total Ionization, (b) Relative Abundance, (c) Composition C_7H_5N, (d) Composition C_8H_7, (e) Composition C_7H_6N, (f) Composition C_8H_8

Elemental compositions for the principal ions were determined by high-resolution mass measurements. Metastable peaks were observed for the transitions m/e $236^+ \longrightarrow$ m/e $221^+ + 15$, m/e $221^+ \longrightarrow$ m/e $194^+ + 27$, m/e $194^+ \longrightarrow$ m/e $117^+ + 77$, and m/e $118^+ \longrightarrow$ m/e $77^+ + 41$.

Several of the observed rearrangement ions are given below along with the probable fragmentation pathways.

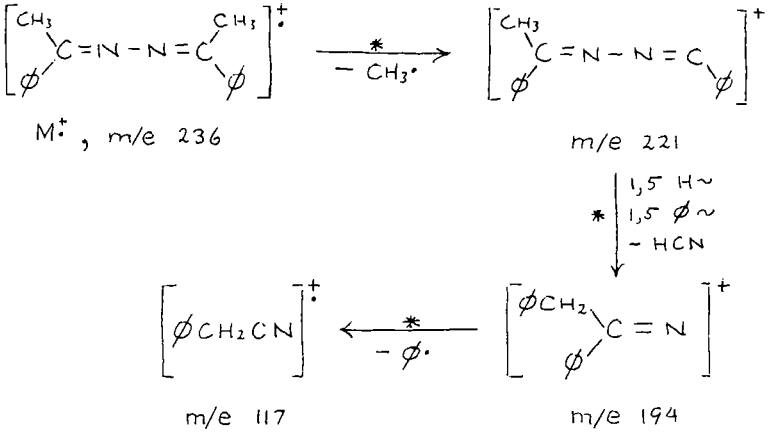

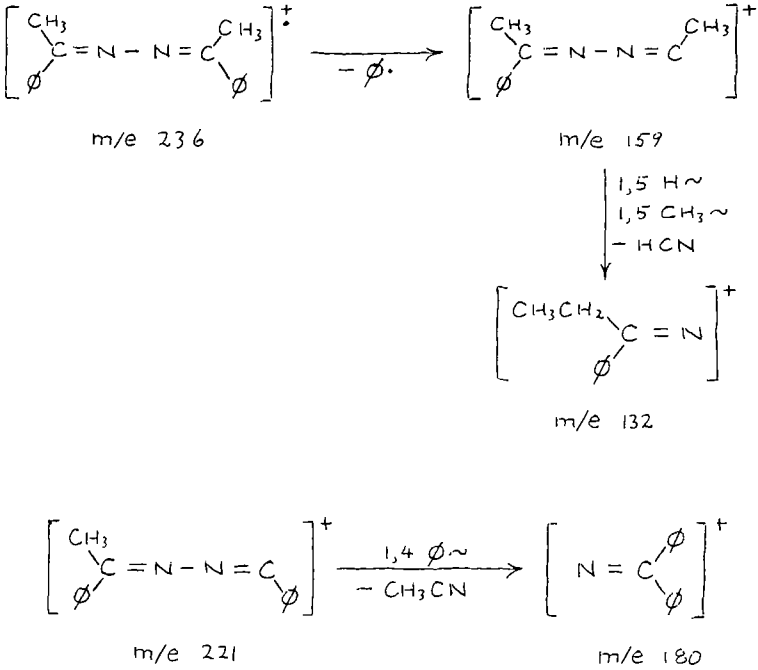

The most intense peak in the spectrum, m/e 221, is formed by loss of a methyl radical from the molecular ion, m/e 236. The rearrangement ion m/e 194 appears to originate from m/e 221 by 1,5 shifts of hydrogen and phenyl followed by loss of HCN. Although the structure shown has the rearranged phenyl group attached to the methylene carbon, it could also be located on the nitrogen. Loss of a phenyl radical from m/e 194 gives m/e 117, which corresponds to the molecular ion of benzyl cyanide.

By removal of a phenyl instead of a methyl radical from m/e 236, the ion at m/e 159 arises. The peak at m/e 132 may be formed from m/e 159 through a route analogous to the formation of m/e 194, except that a methyl group is shifted in place of a phenyl. As for m/e 194, the rearranged group (methyl) could be attached to nitrogen instead.

Another rearrangement peak appears at m/e 180. This ion could be formed from m/e 221 through a 1, 4 phenyl shift followed by loss of acetonitrile.

The driving force in the formation of these and other rearrangement ions observed in the spectrum appears to be extensive electron delocalization in both reactant and product ions as well as the formation of stable neutral molecules in the decomposition products.[2] The neutral species occurring most often are hydrogen cyanide, benzonitrile, and acetonitrile.

Evidently, azines are very useful compounds for the study of electron-induced rearrangements. A systematic investigation of the mass spectra of other azine derivatives of aldehydes and ketones is currently in progress and will be reported later.

---

[1]P. Brown and C. Djerassi, Angew. Chemie, Int. Ed. Engl., *6*, 477 (1967).

[2]F. W. McLafferty in "Mass Spectrometry of Organic Ions" (Ed. F. W. McLafferty) Academic Press, New York, 1963, Chapter 7.

71. THE MASS SPECTRA AND CORRELATIONS WITH STRUCTURE FOR SOME 1-(2-THIENYL)-1-THIAALKANES

by

Norman G. Foster, Diana Wong-Kiu Shiu and Robert W. Higgins[1]

Texas Woman's University, Department of Chemistry

Denton, Texas 76204

The mass spectra of eleven members of the thiaalkanes class have been obtained and correlations of the spectra with structures are reported. The fragmentation paths and rearrangement mechanisms are discussed. The significance of observed metastable peaks and their associated processes is considered. The presence of an abnormally large number of doubly charged ion species was noted.

In summary the correlations show moderately strong parent peaks for all members of the series. The base peak forms by alpha-cleavage to the chain sulfur atom, and always in a position beta to the thiophene ring. Rearrangement of a hydrogen atom occurs with this cleavage to produce an ion moiety at m/e 116. Relatively large amounts of hydrocarbon fragment ions are formed in contrast to only small amounts of ions typical of the alkylthiophenes and alkylsulfides. Alkyl substitution on the thiophene ring does not interfere with analytical detection since the alkyl group is carried along with the rearranged ion moiety at the corresponding larger m/e.

The formation of an expanded ring moiety for the rearrangement ion at m/e 116 may occur. This is considered in some detail. A fragment ion at m/e 82, characteristically stronger than the ions at m/e 84 and 85 is observed, and is a useful analytical clue. This may be a thiophyne ion, produced from either an unexpanded ring, or it may be an open chain ion.

Metastable processes proving that four fragment ions of substantial intensity arise from the m/e 129 ion species are observed. Thus, although the m/e 129 ion is of small intensity, it must be important in the fragmentation process. A small amount of m/e 64 (S_2^+) ion is observed. A metastable peak establishes that at least a portion of it comes from the m/e 129 ion. This suggests a 7 membered ring system as the possible structure of the m/e 129 ion, with a randomization of the carbon and sulfur atoms.

Isotopically labeled molecules with deuterium and carbon-13 in specific positions are suggested for establishing some of the mechanisms proposed above.

[1]Deceased

72. A MASS SPECTRAL CORRELATION STUDY OF ALIPHATIC ALCOHOLS

by

Mynard C. Hamming
Continental Oil Company
Ponca City, Oklahoma 74601

Correlation studies relating mass spectral data with molecular structures have proven to be a rapid means of identifying unknown substances from their mass spectra. In an effort to expedite the development and the application of such correlation studies a scheme has been devised of first systematically selecting peaks from a given spectrum and then deducing the significance of the selected peak by using interpretation maps. An interpretive peak is a peak which has an intensity greater than that of another peak 14 mass units higher or 14 mass units lower, and also greater than that of another peak one mass unit higher or one mass unit lower. Such neighboring peaks are easily visualized when a spectrum is arranged in the form of a rectangular array.

The study presented originated fron an examination of 75 mass spectra of aliphatic alcohols in the carbon range of C_6 to C_{12}. A representative series of twenty-five C_8 alcohols has been accepted for publication in the Thermodynamics Research Center Data Project, Thermodynamics Research Center, Texas A & M University, College Station, Texas.

****

Special thanks is due Dr. E. J. Eisenbraun and his students at Oklahoma State University who generously supplied the samples used in this study.

73. ELECTRON IMPACT INDUCED FRAGMENTATION PATTERNS OF SOME PHOSPHONIUM YLIDS AND IMINOPHOSPHORANES

L. Tőkés, S. Wong and G. Jones
Syntex Research Center, Stanford Industrial Park
Palo Alto, California

SUMMARY

The mass spectra of nine iminophosphoranes (I) and of ten phosphonium ylids of types II and III have been examined.

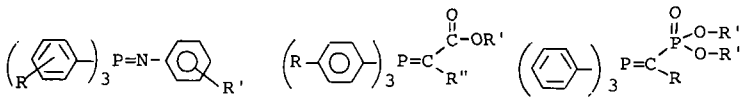

I II III

All spectra showed intense peaks corresponding to the molecular ion and to the loss of a hydrogen atom, the latter sometimes prevailing. The iminophosphoranes showed very little fragmentation which is consistent with the presumed[1] high degree of $d\pi$-$p\pi$ orbital overlap between the phosphorous and nitrogen atoms. The majority of the charge retaining fragments from the iminophosphoranes originate from the triphenylphosphine moiety, providing useful information about the location of the substituents in these molecules.

The triphenylphosphine fragmentation products[2] are apparent in the mass spectra of both phosphonium ylids II and III. In addition to those, there are cleavage products which are characteristic of the ester groups. In compounds II (R"=H) and III (R=H) the relative intensity of the fragment ions corresponding to the formal rupture of the CO-OR' or PO-OR' vs. the CH-CO or CH-PO bonds changes remarkably when the R' group is varied from methyl to longer chains. This is due to the formation of a methylene ylid V, via the transfer of a hydrogen atom as indicated on the ethyl ester IV, which is known[2] to undergo very facile loss of a hydrogen atom, yielding ion VI.

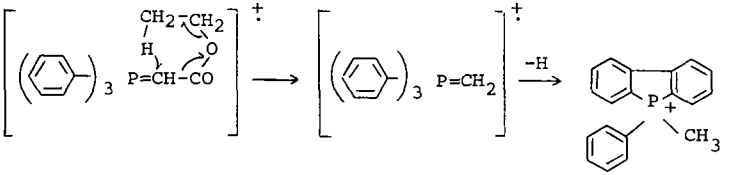

IV V, m/e 276 VI, m/e 275

The base peak (m/e 352) in the mass spectrum of the diphenoxyphosphinyl ylid III (R=H, R'=C_6H_5) is due to a rearrangement ion involving migration of a phenyl group to the charge retaining fragment (see VII). This rearrangement step is apparently an energetically very favorable one since the corresponding peak remains as the only dominant feature besides the molecular ion in the mass spectrum at low ionizing potentials.

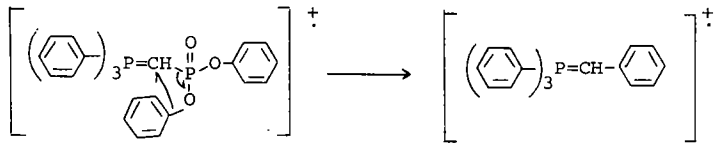

VII VIII, m/e 352

With the aid of high resolution analysis and deuterium labeling techniques other cleavage products in these spectra were also studied and possible mechanistic assignments will be discussed.

---

1. A. W. Johnson and S. C. K. Wong, Canadian J. Chem., 44, 2793 (1966).

2. D. H. Williams, R. S. Ward and G. Cooks, J. Am. Chem. Soc., 90, 966 (1968).

74. COMPARATIVE STUDIES OF ELECTRON-IMPACT AND THERMOLYTIC FRAGMENTATION: o-PHENYLENE CARBONATE

Don C. DeJongh * and David Brent
Department of Chemistry
Wayne State University
Detroit, Michigan 48202

* Alfred P. Sloan Research Fellow

In the mass spectrum of o-phenylene carbonate (1), CO_2, CO, and acetylene are sequentially eliminated from the molecular ion. This pathway is reviewed in Figure 1, along with speculative structures for ions.

Figure 1. The 70 ev mass spectrum of o-phenylene carbonate.

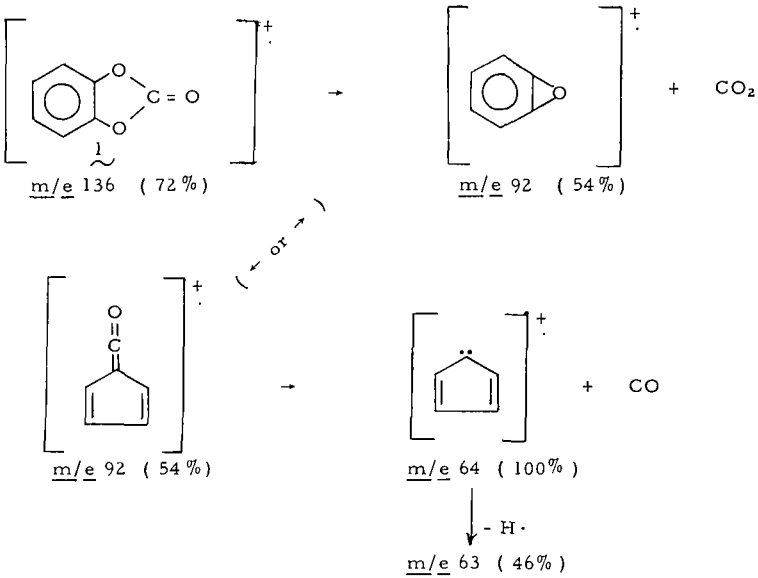

Compound 1 was pyrolyzed at 700° while passing through a 12" quartz tube with dry nitrogen carrier gas at 15 mm Hg. Two major products were obtained -- naphthalene (2 , 11.5%) and indene (3 , 7.8%). Naphthalene ($C_{10}H_8$) corresponds in elemental composition to the dimer of the peak at

m/e 64 ($C_5H_4^{+\cdot}$). Azulene (4), a $C_{10}H_8$ isomer, was obtained as a minor

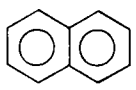

2

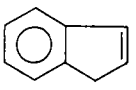

3

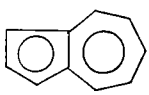

4

product. Compounds 2 and 4 could arise by the thermal rearrangement of fulvalene (5), also a $C_{10}H_8$ isomer:

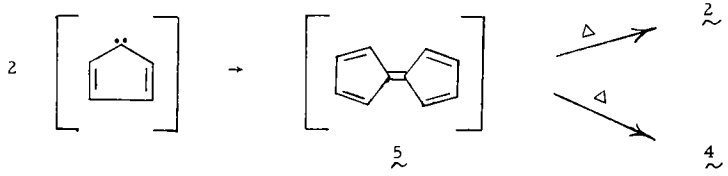

Naphthalene is the most stable of the three isomers (2 , 4 and 5).

One possible route for the formation of indene (3) is given in Figure 2.

Figure 2. A possible route for formation of indene (3) from the pyrolysis of 1 .

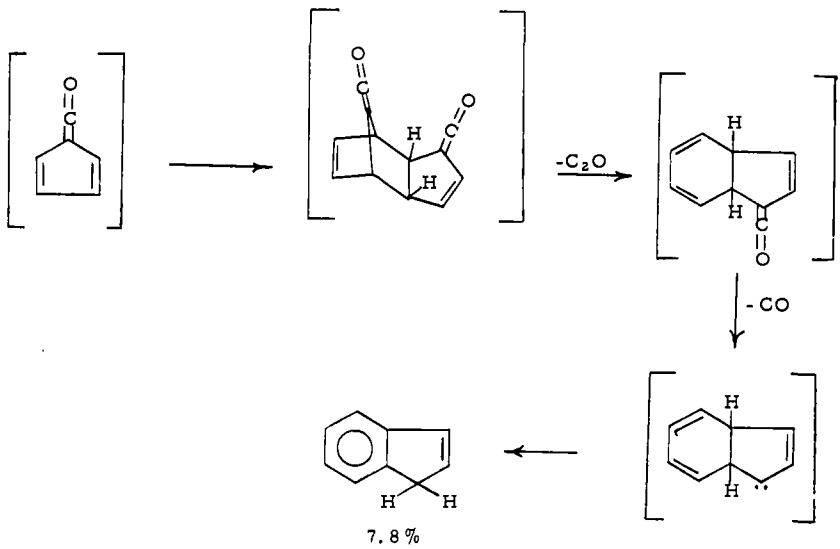

$$C_2O \rightarrow C_{(g)} + CO$$

The formation of both major products can be explained by structures which are suggested by the mass spectral fragmentation (Figure 1).

Acknowledgments. The project of which the work reported in this summary is a part is supported by research grants-in-aid from the Alfred P. Sloan Foundation and the Upjohn Company.

76. A New Miniature Mass Spectrometer for Partial Pressure Analysis

by

D. Allenden, R.D. Craig and R.G. Johnson.

Introduction

Mass spectrometric developments in the field of residual gas analysis have tended towards improved resolution and higher sensitivity. Instruments have, therefore, required more sophisticated design and have grown larger and more expensive, while their operation has become correspondingly more complex. There is, however, need for a small, low cost, simply operated partial pressure gauge which can separate the spectra of the common gases, read directly partial pressures down to 10^{-11} torr and has a reproducible performance.

Such a partial pressure gauge, capable of separating and identifying all the individual components commonly present in a vacuum system, overcomes a basic limitation of total pressure gauges of the ionization type, for example the Bayard-Alpert ion gauge, the magnetron gauge and the cold cathode trigger discharge gauge, in that these gauges all have widely different sensitivities for different gas compositions. Relative sensitivities for such gauges range from 3.0 for light hydrocarbons, about 1.0 for argon, nitrogen and carbon monoxide, to 0.4 for hydrogen and 0.2 for helium. Thus, apart from non-linear limitations such as the X-ray effect, these gauges can only give a meaningful absolute pressure if the gas composition is known.

The object in designing a miniature mass spectrometer is to provide direct partial pressure readings of each gas or vapour and thus give a better understanding of the vacuum, so enabling the total pressure of the system to be computed.

Design Considerations

In considering the development of a simple partial pressure gauge to replace conventional total pressure gauges, the following design criteria were regarded as the most important.

1. Comparable in size, convenience of operation and cost with an ion gauge, magnetron gauge or other total pressure measurement device.

2. Sufficent resolution for the identification and separation of the common gases and vapours encountered in vacuum work, such as H_2, H_2O, CH_4, the components of air, heavier hydrocarbons, diffusion pump vapours and mercury.

3. Capable of useful measurements in the 10^{-3} torr to 10^{-11} torr range.

4. Direct calibration of the control unit to read equivalent nitrogen pressure with a reproducibility of $\pm$ 10%.

5. Minimum disturbance to the vacuum system during operation of the gauge.

Description of the instrument

To meet these requirements, a miniature mass spectrometer known as the AEI Minimass partial pressure gauge has been designed. The instrument is based on the conventional 180° deflection of the ion beam in a magnetic field using a 1 cm radius path. Metal and glass envelope versions are shown in Figure 1.

Special consideration has been given to the filament and electron gun design to minimise outgassing and cracking of the gases in the system. A pure rhenium filament of 3 mm^2 area is employed and for the maximum ionizing electron current used of 60 μA the power dissipation is only 2 watts.

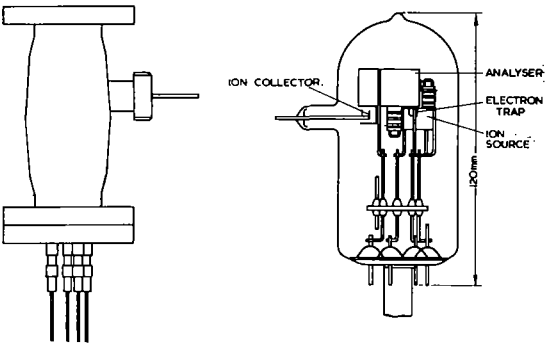

Fig. 1 Metal and glass envelope versions of the partial pressure gauge. The glass gauge can also be mounted, as is the metal gauge, on a $2\frac{3}{4}$ in (70 mm) o.d. flat copper gasket UHV flange. All gauges can be baked to 400° C.

The control unit provides both manual and repetitive automatic scanning and the scan circuit is such that the mass scale is truly linear, thus facilitating the identification of unknown masses. The mass range is from 2 to 240 and scan times are normally between 1 and 10 minutes.
The magnet, providing a field of 4000 gauss, is sufficiently light to be mounted as an integral part of the gauge head.

Resolution Requirement

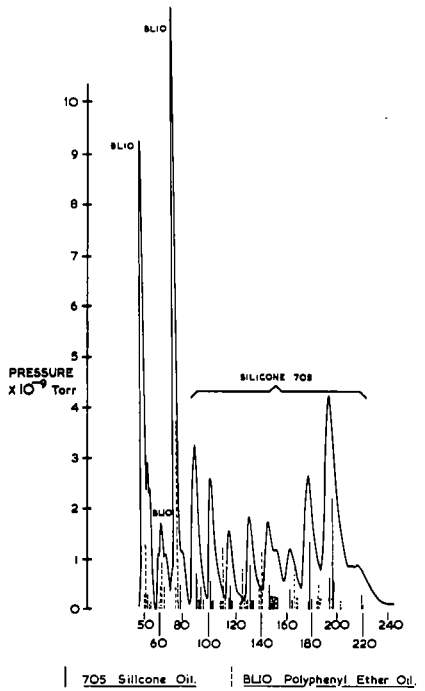

Fig. 2 Silicone 705 oil examined in the presence of BL10 polyphenyl ether oil (Minimass trace) with the cracking patterns obtained on a high resolution mass spectrometer superimposed.

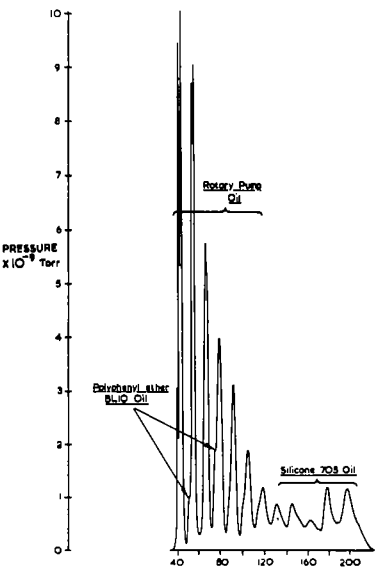

Fig. 3 'Fingerprint' spectrum of a mixture of rotary pump, BL10 polyphenyl ether and 705 silicone oil vapours.

The use of only partially resolved 'fingerprint' spectra for the identification and analysis of mixtures of high molecular weight vapours commonly occuring in vacuum systems has been discussed elsewhere (1). It has been shown that useful data can be obtained with an instrument, such as that used in the present work, whose resolving power is only 20 on the 10% valley definition. It may be claimed that these 'fingerprint' spectra simplify the identification of these high molecular weight vapours occuring in vacuum problems as compared with the complex multi-peak spectra obtained from high resolution instruments.

Figure 2 shows one example of such 'fingerprint' spectra for a mixture of polyphenyl ether and silicone diffusion pump oil vapours. Along the bottom of the figure are shown the normal cracking pattern spectra obtained with a high resolution spectrometer operated at 170°C.

Another example of fingerprint spectra showing the ability to separate the two previous diffusion pump vapours from the hydrocarbon vapours arising from rotary pump oil is shown in figure 3.

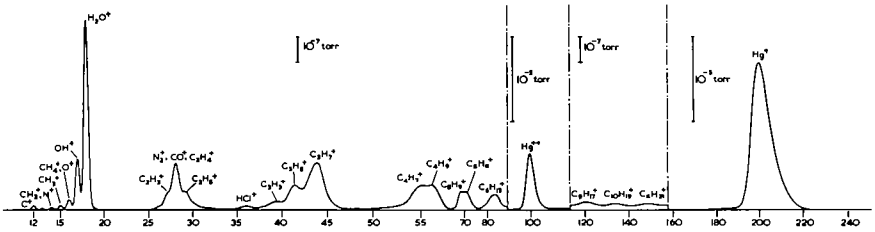

Fig. 4 Spectrum of unbaked vacuum system showing residual hydrocarbon and mercury vapour peaks.

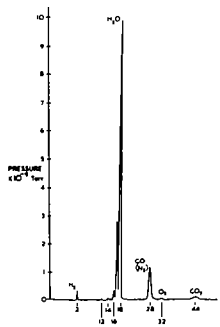

Fig. 5 Spectrum of simple gases present in a UHV system.

The ability to make useful measurements on mercury in the presence of a hydrocarbon background is shown in figure 4 while figure 5 shows a typical spectrum for a high vacuum system contaminated with water vapour.

Sensitivity for different gases

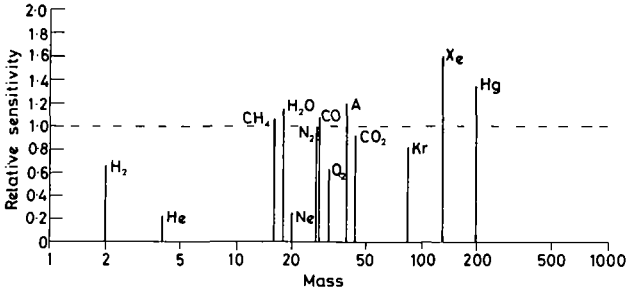

Fig. 6 Histogram showing the relative sensitivity of various gases to nitrogen.

Measurements of the sensitivities of various gases and vapours relative to nitrogen were made using a McLeod gauge, calibrated ion gauge, or a capsule gauge plus leak system. The results are given in the table and are summarised in figure 6.

Gas or Vapour	H_2	He	CH_4	H_2O*	Ne	N_2	
Relative Sensitivity	0.67	0.22	1.06	1.15	0.24	1.00	
Gas or Vapour	CO	O_2	A	CO_2	Kr	Xe	Hg*
Relative Sensitivity	1.09	0.63	1.19	0.91	0.81	1.60	1.34

* Results based on comparison with ion gauge pressure readings, corrected according to Dushman (2).

These relative sensitivity values relate to the normal operating conditions of 60 μA electron current at 75 eV energy.

Low pressure performance

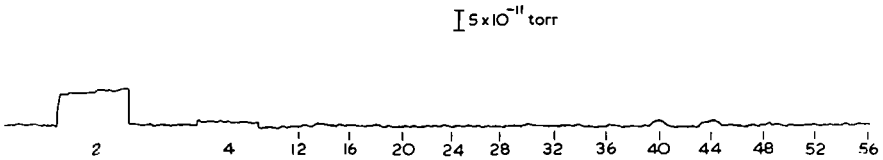

Fig. 7 Spectrum of residual gases in an ion pumped system giving a 1.3×10^{-10} torr (N_2 equivalent) reading on a trigger discharge gauge.

To confirm the low pressure sensitivity, the partial pressure gauge was connected to an ion pumped UHV system and a spectrum taken when the total pressure, indicated by a trigger discharge gauge, was 1.3×10^{-10} torr.

This spectrum is shown in figure 7 and it can be seen that the detection limit in terms of equivalent nitrogen pressure is better than 10^{-11} torr. The peak to peak noise on the recording is about 5×10^{-16}A.

Using the relative sensitivities quoted above, the sum of the partial pressures shown by the mass spectrometer is 2.3 x 10^{-10} torr (true pressure). The true total pressure calculated from the trigger discharge gauge indication, after correcting for the various gas sensitivites, amounted to 2.6 x 10^{-10} torr. These two values are considered to be in resonably good agreement.

High pressure performance

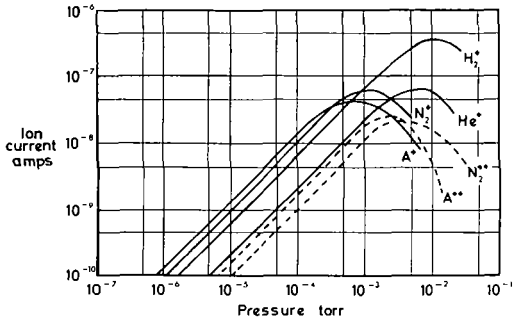

Fig. 8 High pressure linearity of the ppg for A,N_2, He and H_2.

To assess the performance of the spectrometer at high pressures, the ion current was plotted against pressure over the range 10^{-6} to 10^{-1} torr using a McLeod gauge. The results for A, N_2, He and H_2 are given in figure 8 and it can be seen that improved high pressure linearity is obtained for the higher mass gases by working with their low mass fragments (or doubly ionized) peaks. When this is done, there is reasonably good linearity up to 10^{-3} torr for all the gases. This high pressure linearity is about an order better than obtained on larger mass spectrometers, because of the short ion path associated with the use of a 180° 1cm radius geometry.

Conclusions

The performance data shows that the partial pressure gauge described, which is little more complex than many total pressure gauges, is capable of useful application in the vacuum field for studies ranging from foreline pressure up to 10^{-2} torr to ultra high vacuum of 10^{-11} torr.

The gauge is suited both for studies of the common gases, including leak detection, and for the identification and analysis of the high molecular weight vapours found in vacuum systems.

In addition to enabling calculations of true total pressures, the partial pressure gauge indentifies the main components limiting the vacuum, thereby indicating what action should be taken to make further improvements to the ultimate obtainable.

References (1) Coulson, J.A., Craig, R.D., and Johnson, R.G., 14th Nat. Vac. Symp. of AVS 1967, 73.

(2) Dushman, S., Sc. Found. Vac. Technique, John Wiley NY. 1949,350.

78. Time-of-Flight Mass Spectrometer with Axial Symmetry: Theory and Performance

by

M.F. Zabielski, H.T. Diem* and B.R.F. Kendall

Extended Abstract

A range of compact time-of-flight mass analyzers has been developed for use in measuring the ion composition of the upper atmosphere. High sensitivity is obtained by accelerating ions in a direction perpendicular to the axis of symmetry. This makes it possible to pulse ions from a source region having a volume as high as 100 cc while maintaining a comparatively small collector area.

The theory of cylindrically symmetrical mass analyzers with two accelerating regions has been developed. A computer program has been written which provides the space focusing conditions and flight times for an arbitrary set of spectrometer dimensions. A comparison of the space focusing conditions of equivalent linear and cylindrical spectrometers indicates that these conditions are more critical for the cylindrical spectrometer.

A spectrometer constructed in the shape of a wedge cut from a cylinder has been experimentally investigated. There is reasonable agreement between the predictions of the full cylinder theory and the experimental results of the wedge spectrometer. A wedge spectrometer with a total flight path of 4.4 cm has a resolving power of 5 as defined as width at half height. In spite of this low resolving power, this instrument is useful for most ionospheric studies since available computer techniques [1] can enhance the effective resolving power up to about 40.

A useful feature of this type of instrument is its ability to function at pressures as high as 10^{-1} torr without serious degradation in peak shape. An experimental calibration of the change in instrument sensitivity with pressure for the wedge spectrometer has been performed.

---

* Now at: CBS Laboratories, High Ridge Road, Stamford, Conn.

1 Kendall, B.R.F. and M.F. Zabielski, Proc. 15th Annual ASTM E-14 Conference on Mass Spectrometry, Denver, May 1967, p 377.

79. Recent Advances in Low Cost Time-of-Flight Mass Spectrometry

by
D. C. Damoth, C. J. Moorman, R. H. Lehman
The Bendix Corporation, Scientific Inst. Division

The low cost, solid state MA-1 Time-of-Flight Mass Spectrometer was described last year at this conference by the authors [1] and by Moorman and Bonham [2]. In the past year some novel and useful features have been developed. This paper will describe some of these in the areas of pumping, inlets and readout systems. Finally, some comments on computerizing the readout will be offered.

Through recent developments and by working with mass spectrometer users, a versatile array of pumping systems has been made available, so that now it is not necessary to use one system for all applications. A system can be chosen which best fits the application. The most commonly used system (Figure 1) still consists of a water cooled mercury diffusion pump, with a freon cooled trap and a liquid nitrogen cooled baffle. This system has been used for years on TOF and other mass spectrometers. (Figure 2) It gives good pumping speeds and an ultimate pressure in the 10^{-9} Torr range with liquid N_2 and sufficient bakeout. Normal operating pressure is in the low 10^{-7} range with liquid N_2 and low 10^{-5} range without liquid nitrogen. This system gives a very clean background and allows the ultimate sensitivity of the spectrometer to be more nearly utilized. Even without liquid N_2, the background remains clean over most of the spectrum with only the mercury peaks appearing. It is relatively unsusceptible to contamination and is not adversely affected by accidental exposure to air.

The next system (Figure 3) is similar to the first except that freon is used as a coolant for the diffusion pump instead of water. While retaining the advantages of the first system, it can be moved easily and used where no cooling water is available. While the cost is slightly higher, the increased mobility will offset this in many applications. One disadvantage of this system in some locations is that all of the heat from the diffusion pump is transferred to the surrounding air by the refrigeration system.

The next system, which is the lowest cost, provides adequate pumping speed and good ultimate pressure. (Figure 4) It consists of an oil vapor diffusion pump which is water cooled, a water cooled baffle and a liquid nitrogen trap. Various pumping fluids can be used in this system, but polyphenyl ether gives the best ultimate pressure which is adequate for most mass spectrometer applications. However, the pump fluid background is spread over a large mass range and makes it more difficult to use the great sensitivity of the MA-1. Where ultimate sensitivity is not paramount, this system is satisfactory. *

This system can also be used with freon cooling. (Figure 5) In this form it is also portable and, therefore, more versatile.

In addition to these pumping systems, a new series of inlet systems is being developed for use with the low cost TOF.

There is a new solid sample direct inlet probe system (Figure 6) which, while maintaining the advantages of the direct inlet probe systems used with other TOF's, is lower cost and more rugged. It incorporates a completely encapsulated and protected heater which requires no maintenance and is capable of temperatures over 600C. As in the other probes, a double ended crucible is used so the thermocouple is situated directly in the bottom chamber, thus maintaining fast temperature response. This is important during rapid heating or cooling cycles and in searching for thermally sensitive unknown compounds. The crucible is held at an angle from horizontal to minimize the possibility of losing the sample during insertion or removal from the source. That angle also makes the probe useful in analyzing low vapor pressure liquids.

* (Note added in final manuscript) In evaluating the relative effectiveness of polyphenyl ether fluids vs. mercury, as much as two decades difference in ultimate was obtained with different brands of polyphenyl ether. Bendix Vacuum Division-CVC Convalex 10 was the best tested.

The vacuum lock used with the direct inlet probe is designed so samples can be changed rapidly with only a slight perturbation of the vacuum inside the source.

The same vacuum lock is also used with other inlet systems, such as the continuous atmospheric pressure inlet and source arrangement. (Figure 7) It has a tightly enclosed source, an interchangeable molecular leak, a differentially pumped region, a small diameter connecting tube and a heated sampling valve.

In operation, gases at atmospheric pressure, or above if desired, enter through the heated sampling valve into a differentially pumped connecting tube which can be a few feet long. Gases in this tube then enter the mass spectrometer source through the molecular leak. The tube is terminated near the molecular leak and the source volume and pumping speed are designed so response times of about 50 milliseconds are achieved. The heated sample control valve reduces water vapor condensation and flow problems when this system is used for respiratory gas research. This arrangement is also useful for process control and monitoring reactions at higher pressures. The vacuum lock assembly used for the above inlets is incorporated into a sample handling manifold system (Figure 8) which provides a lot of flexibility. It is arranged so that with the probe withdrawn, sample gases can be admitted to the mass spectrometer from the standard gas inlet system as well as directly from a gas chromatograph or from a sample splitting or enriching system used with the gas chromatograph. The gas handling portion of the manifold can be heated. It is possible to switch from one inlet to another in the shortest time. This is important to users having many compounds in different forms to analyze.

A variation of this low cost TOF which is gaining popularity is the residual gas analyzer version. One exciting application is the proposed used of a TOF RGA inside a large shock tunnel. (Figure 9) The RGA will be mounted on a "stalk" enclosing the pump line to the analyzer housing and the electronic leads.

Due to the wide range of application of the TOF, there are many readout system variations which are mainly divided between oscilloscope and analog readouts. (Figure 10) The oscilloscope can be used alone as a complete spectrum monitor or in combination with the analog output. All mass peaks not previously gated out by the analog system appear on the oscilloscope. Visual perception of changes in the spectrum on the 'scope is most useful in the time range from 10 seconds to a few tenths of a second. Faster observation requires the use of photographic recording techniques. For continuous recording of the abundance of one or more masses with time constants of about one millisecond and longer, and for recorded scans of one second or longer, the analog system is used. The analog output is usually presented via a strip chart recorder chosen to match the scan rates and accuracies needed.

In addition to the scanner analog which presents a single peak or narrow mass range with fixed position manual set, single scan trigger, or automatically repetitive scanning, the total intensity of all the peaks in the spectrum above a chosen mass number may be integrated continuously with the Total Output Integrator. This device was described at this conference in 1966 by Bonham and Damoth [3]. The TOI has found widespread use in reaction monitoring, mass thermal analysis and gas chromatography.

The fast response of the oscilloscope output is required where analyses must be made in the millisecond range or faster. Photographic recording is necessary to translate the fast display into a slower display, usually translating time to displacement along the film. The drum camera is effective for this, but is expensive to purchase and operate, and is also cumbersome to operate. Consequently, techniques for electronically displacing the oscilloscope spectra with relationship to fixed film cameras have been developed and are widely used. The Z-axis gating unit (Figure 11) has been developed to simplify bar-graph presentation of two masses on a dual beam oscilloscope with cycle-by-cyble time resolution. However, information on peaks other than those chosen is missed.

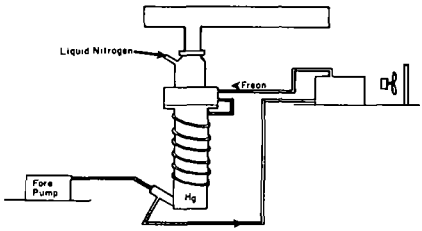

Fig. 3

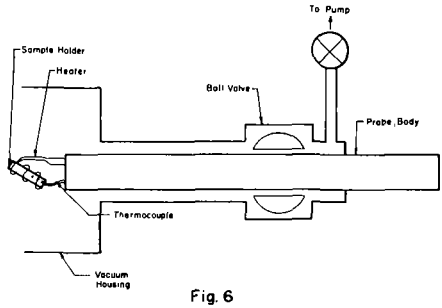

Fig. 6

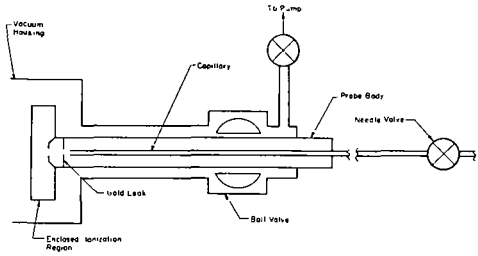

Fig. 7

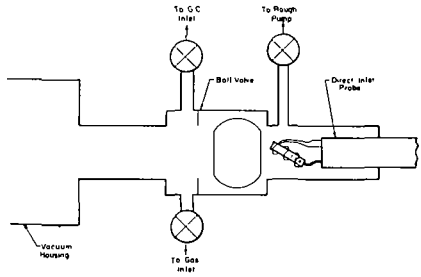

Fig. 8

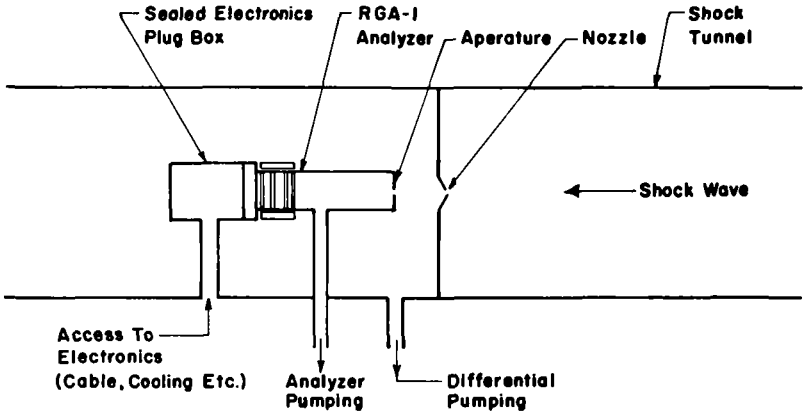

IN STREAM ANALYSIS OF SHOCK TUBE GASES

Fig. 9

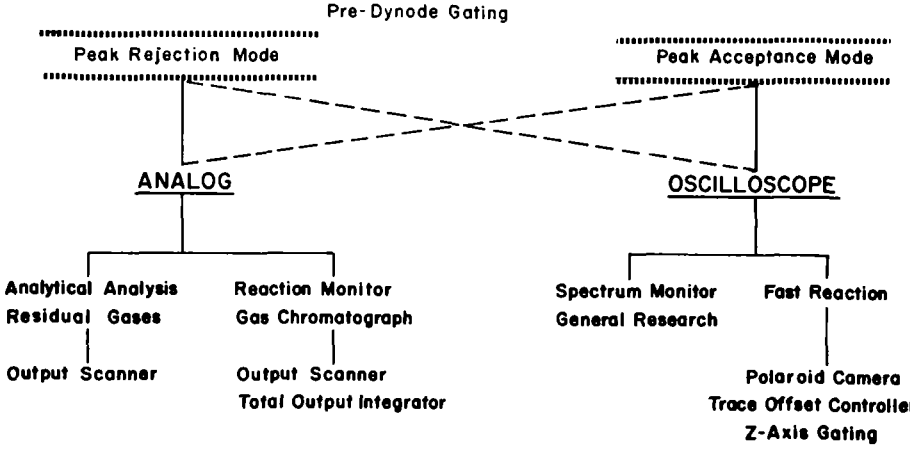

READOUT SYSTEM VERSATILITY

Fig. 10

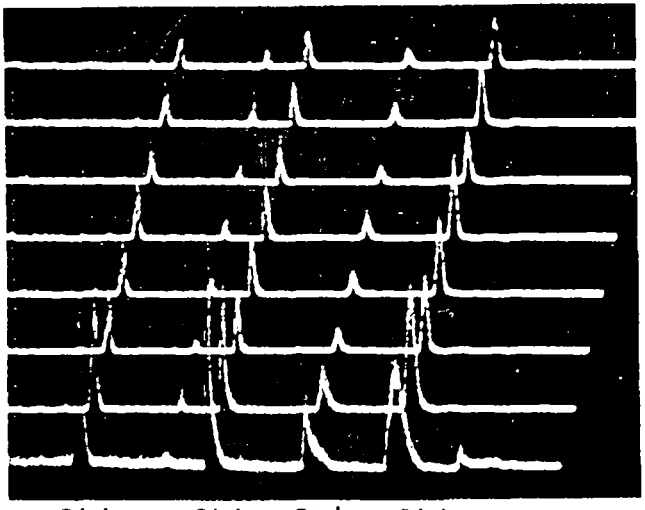

ANTIMONY SPECTRUM USING
TRACE OFFSET CONTROLLER
WITH OSCILLOSCOPE CAMERA

Fig. 12

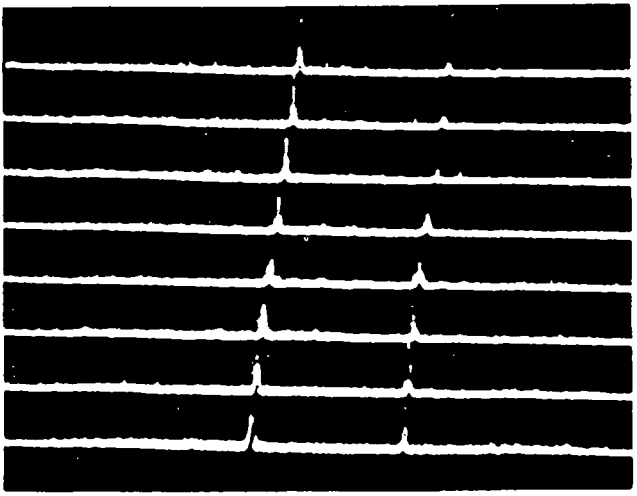

ALUMINUM SPECTRUM USING
TRACE OFFSET CONTROLLER
WITH OSCILLOSCOPE CAMERA

Fig. 13

Thus, the stepped raster display method described by Moulton and Michael[4] has led to the commercial Oscilloscope Trace Offset Controller unit. Figure 12 shows a wide mass range recording of the polymers of antimony produced by laser vaporization and Figure 13 shows a shorter mass range recording of aluminum also vaporized by laser. The trace offset controller permits spreading out as many as 64 separate spectra, even at 100,000 spectra per second on one or two oscilloscopes. If desired, 1, 2, 4, or 8 spectra can be superimposed on a single line to give an averaging effect as is obtained when the spectrum is viewed visually on the oscilloscope.

Another requirement frequently placed on the mass spectrometer is for maximum dynamic range. This has led to the two types of pre-dynode gating systems. (Figure 14) The first type, which rejects a selectable mass peak signal as it enters the magnetic electron multiplier was first developed to suppress the helium carrier gas signal in GC/MS applications. It has also found widespread usage in shock tube research and other applications where one to three large peaks can be profitably suppressed.

Conversely, it is sometimes desirable to select one or a few low intensity peaks and allow only these to be amplified in the multiplier. This can arise when there are a multiplicity of large peaks and it is desirable to record very small peaks. The technique is called peak acceptance pre-dynode gating. This device in combination with Z-axis gating or the trace offset controller makes a flexible, powerful means for fast reaction recording. Peak acceptance pre-dynode gating has also been employed by Dr. Martin Studier at Argonne National Lab and Dr. Don McAdams at Humble Oil Research in Baton Rouge to extend the sensitivity of GC/TOFMS combinations greatly.

The topic of computerized mass spectrometer output is very popular. Many publications have described the effectiveness of computer data reduction on high resolution spectra of organic compounds. These systems are usually costly and thus of academic interest to the typical analytical laboratory or low budget researcher. Large numbers of economically important but not highly dramatic sample mixtures are analyzed daily via gas chromatograph/mass spectrometer combinations. This undoubtedly gives a real glow of pride to Roland Gohlke and Vic Caldecourt who at Dow Chemical Company in 1957 pioneered this field with a TOF mass spectrometer.

The GC/MS combination is so powerful and generates data so rapidly that the bottleneck in the system is the data reduction and correlation process. A single scan of an organic compound with one hundred peaks and intensity variations over a range of 1000:1 performed in one second generates over 10^5 bits of information, to say nothing of instructions and correlation of unknown with known spectra.

The loss of efficiency of coupling mass spectrometer outputs into computers via conventional program language is high. It is logical to predicate close functional coupling of the computer programming with the mass spectrometer scan and output functioning. This is especially attractive in the TOF mass spectrometer with the analog output.

One drawback of this approach in the past has been the lack of the required degree of relative time stability of the mass peaks in the TOF output spectrum. This is similar to the non-linearity and hysterisis effects in magnetic scanning and R.F./D.C. instabilities in quadrupole instruments.

The time stability of the MA-1 is sufficient to allow the close coupling of the TOF to on-line or off-line computers and direct data reduction. In the near future this capability will facilitate mass spectra to be developed, reduced and correlated at an unprecedented rate.

(1) *A New Low Cost/RGA Time-of-Flight Mass Spectrometer*
D. C. Damoth, R. H. Lehman, C. J. Moorman, 15th. Annual ASTM E-14 Conference, Denver, 1967

(2) Factors Influencing the Resolution of a TOFMS
C. J. Moorman and R. W. Bonham

(3) Performance Characteristics of a New Time-of-Flight Mass Spectrometer
R. W. Bonham and D. C. Damoth, 14th. Annual ASTM E-14 Conference
Dallas, 1966

(4) Stationary Film Recording of Time-Resolved Mass Spectra
D. Mc L. Moulton and J. V. Michael, R.S.I. 36, Feb., 1965, pp 226-8

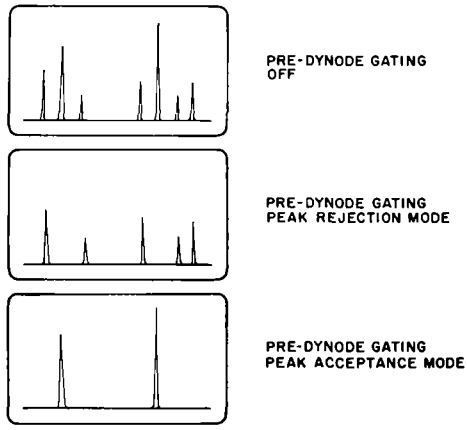

PRE-DYNODE GATING OSCILLOSCOPE DISPLAY

Fig. 14

80. "A VERSATILE 'MONOENERGETIC' ELECTRON IMPACT SPECTROMETER FOR THE STUDY OF INELASTIC COLLISION PROCESSES"

by C.E. Brion, C.R. Eaton, L.A.R. Olsen, and G.E. Thomas

ABSTRACT

A system consisting of a double 127^{o} electron monochromator and monopole mass filter (see A.S.T.M. meeting Denver 1967) has been improved to give a highly versatile instrument capable of studying positive ions, negative ions, electron scattering by energy loss, and excited neutrals by scavenging. The improved instrumentation and results for simple atoms and molecules are discussed. This includes direct positive ionization, autoionization, resonance capture, dissociative capture, ion pair processes, and excitation of neutrals to allowed and optically forbidden states.

This work has now been published in the International Journal of Mass Spectrometry and Ion Physics Volume 1, page 25 and Volume 1, page 102 (1968).

81.

DESIGN OF A TANDEM MAGNET SYSTEM FOR ANALYZING IONS FROM 10 TO 100 KEV

F. A. White and T. Wilson Whitehead, Jr.

Division of Nuclear Engineering and Science
Rensselaer Polytechnic Institute
Troy, New York 12181

Abstract

Two large magnets have been designed and constructed for an ion analyzer system which can function either as an isotope separator or a research mass spectrometer. The magnets are homogeneous magnetic field sectors of 86° with a beam radius of curvature of 48 inches and a 2-inch pole gap. Exciting coils are air-cooled and consist of about 11,600 turns of 0.081-in-dia. formex-coated copper wire. A commercial 60 volt 20 amp power supply develops a maximum field, for a single magnet, of 7000 gauss over a pole face area of about 900 sq-in. Construction features and results of a computer analysis to determine the focal properties are described.

Introduction

The RPI Tandem Isotope Separator has been conceived from the point of view that it will contribute primarily to nuclear and solid-state physics. However, this apparatus should be potentially useful in special problems relating to physical chemistry, environmental science, the investigation of plasmas, geophysics, and other disciplines where either isotopic ratio measurements or determinations of ion specie, ion energy, and charge state are required. General considerations leading to the design of this multiple magnet system were derived, in part, by experience with several previously constructed multiple magnet spectrometers.[1,2,3]

One spectrometer was constructed with an "S"-shaped trajectory in which positive ions were deflected by the first magnet in a clockwise direction, and bent in a counter-clockwise direction by the second magnetic sector. Two other spectrometers possessed "C"-shaped trajectories in which the ion beam was deflected in the same sense by both magnets. The principal advantage of the "S"-shaped configuration is that the mass dispersion is doubled when two analyzers are arranged in tandem, but the resolution is usually reduced because of geometric aberrations. In the case of the "C"-shaped geometry, it is essential that the defining slit between the two magnets must be substantially smaller than the dispersion for adjacent isotopes. With this restriction, the dispersion is essentially the same as for the case of single magnetic analyzer. However, the "abundance sensitivity" is greatly increased for either tandem system.

Requirements

The general concept of the complete analyzing system was that it should serve the dual function of (1) operating as an isotope separator o. very high purity, but modest ion current, and (2) being used as a highly specialized and programmable tandem system for investigating the interaction of ions with matter. Both of the above considerations led to the decision to complement the magnetic analyzers with two electrostatic lenses, in order that the facility might be utilized as two double-focusing systems in tandem.

Specifically desired characteristics for the tandem magnet system were (1) capability for analyzing singly charged ions to mass number 250, at energies up to 100 kev; (2) exciting coils impedance matched to commercially available power supplies; (3) programmability either as a coupled tandem system, or as independent units, and (4) provision for experimental

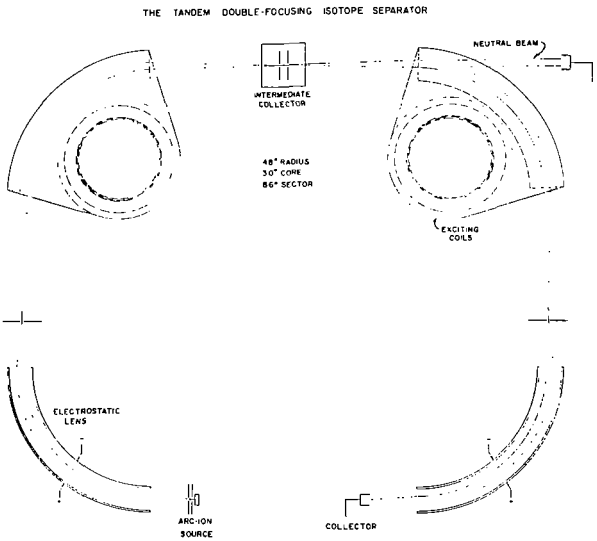

Figure 1

Location of Magnets and Electrostatic Lenses in Tandem Isotope Separator.

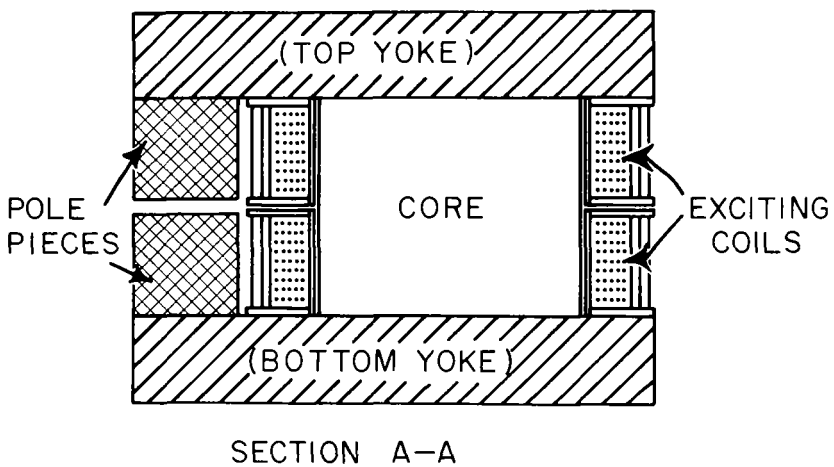

Figure 2

Section through a magnet.

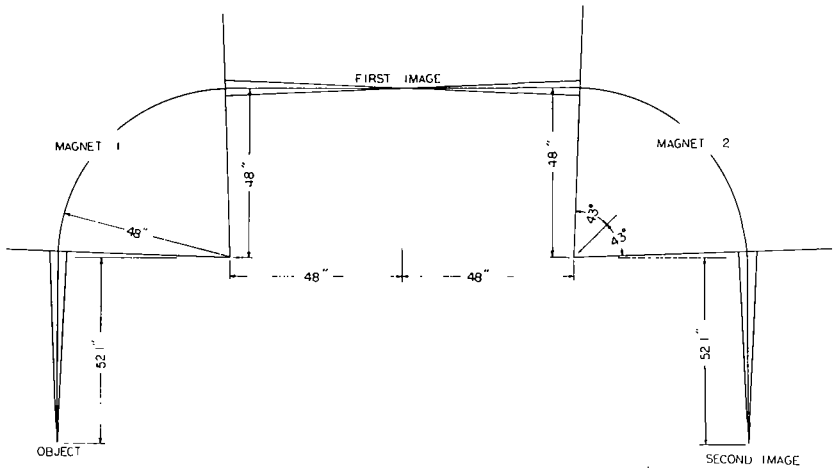

Figure 3
Ion Optical Layout for the Pair of Magnets.

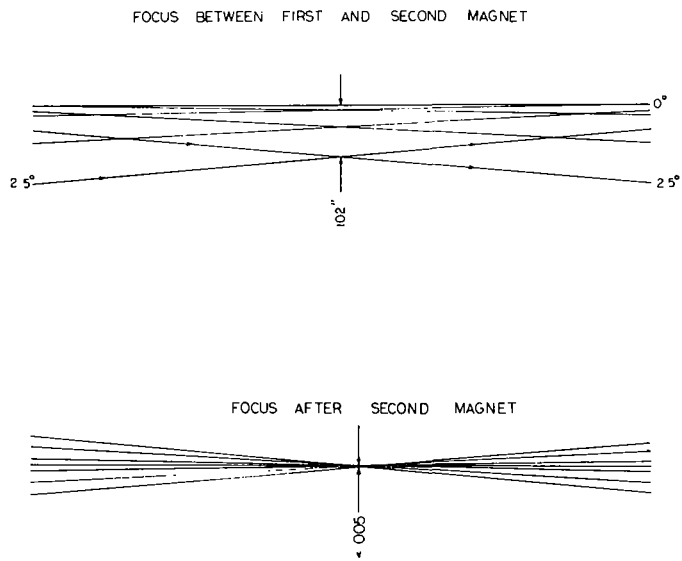

Figure 4
First and Final Magnetic Focusing of a Group of Ion Trajectories.

optimization of the ion beam optics by means of convenient mechanical positioning of the magnets. In addition, provisions were made for a high degree of beam collimation, accessability through ports at every focal point and a neutral beam monitor.

Equipment

Figure 1 shows a top view of the four lens components of the tandem isotope separator. Both the electrostatic and the magnetic sectors operate on a 48" radius. All of the magnet parts were fabricated from low-carbon, annealed steel. The inner and outer radii of the pole pieces are 42" and 54" and the pole gap is 2". The gap parallelism is determined by duraluminum space blocks inserted between the pole pieces.

Figure 2 shows a cross section of one of the magnets. The air-cooled exciting coils were designed to impedance match commercially available 60 volt - 20 amp power supplies. This supply delivers current to a total winding of 11,600 turns of #12 formex coated copper wire through a parallel arrangement of eight subcoils. The maximum magnetomotive force for one magnet is 29,000 ampere-turns which energizes the assembly to a field strength of 7,100 gauss across the 2" gap.

Focal Properties

For a large magnet spectrometer of this type, the effect of the fringing magnetic field on the ion trajectories is considerable and should be taken into account in the magnet design. Shielding of the beam tube near the entrance and exit positions offers some remedy, but a transition region in the field that is not well-defined without measurements still exists. Also, for the RPI beam analyzer, the realization of this beam shielding would have been a task of considerable magnitude. Since a nearly linear relationship between fringing field magnitude and excitation current obtains here, we decided to forgo the shielding and compensate for the fringing field effect in the choice of sector angle and magnet position.

Two general methods are available for initial design studies of this type: a theoretically predicted description of the field, or the construction of a working model. Either or both of these methods would lead to useful results. Our choice was to make an estimate of the fringing fields and design the magnets. Since the position of the magnets is adjustable, we felt that minor orbit adjustments could be made without difficulty.

As a first approximation to this problem, the two-dimensional field of a parallel plate capacitor was used as a model. Clearly this model has some deficiencies, such as neglecting the coil effect, the thickness of the pole pieces and yoke, and at large distances, the finite extent of the magnet. Nevertheless, it is a decided improvement over ignoring the problem.

The fringing field of the capacitor can be evaluated by means of a Schwarz-Christoffel transformation, and a computer program was written to calculate orbits in a field of this shape. Using this program, it was found that the sector angle for a magnet with a 2" gap should be reduced from 90° to 86°, and the object should be moved back 4.1". It was arbitrarily decided to preserve the distance between the magnet centers at 96" and take up the fringing field correction in the manner shown in Figure 3.

One of the most interesting properties of this magnet system is due to the zero dispersion effect. With the magnets arranged in the present configuration, the geometric aberrations essentially vanish at the second focal point. Momentum dispersion occurs at the first focal point and separation can be carried out here. The transmitted beam then refocuses to a nearly perfect image shown in Figure 4.

After the magnets were constructed, the actual field generated by them was measured, and these data served as a guide to the final design and positioning of the beam slits and vacuum envelope. The results of this

field measurement, taken with Hall effect transducers, are indicated in Figure 5. These data were actually taken on a two-dimensional grid in the magnet midplane, and, strictly speaking, there is some variation in the function at different distances from the center of the magnet. The field intensity coordinates for the computation were generated by passing a mathematical sheet through a group of thirteen of the measured data points surrounding the point of computation and interpolating field values at off-net points. Also, since the midplane field intensity is a boundary condition that determines the three-dimensional field shape, this localized data grid may be used to specify the field components outside the magnetic midplane so that three-dimensional studies of particle orbits can be made with good accuracy.

The more exact calculation based on the field of the completed magnets showed that the center of the beam radius of curvature in the magnet should be displaced toward the center along the symmetry axis by 0.8" and the object and second image points are to be moved back from the magnets by 1.1". These calculated foci should be accurate to about $\pm \frac{1}{4}$" along the beam direction since the current densities of this system will generally be quite low and space charge effects should be negligible.

Acknowledgements

It is a pleasure to acknowledge assistance by the staff of Transformer Shop of the General Electric Research and Development Center, J. C. Sheffield, M. Trzepacz, J. F. Lewis, and G. L. Struthoff. A number of graduate students also provided valuable aid during various phases of the assembly and testing of this magnet system.

References

(1) F. A. White and T. L. Collins, Appl. Spectroscopy, 12, No. 1, 12 (1958).

(2) F. A. White, J. C. Sheffield, and F. M. Rourke, Appl. Spectroscopy, 12, No. 46 (1958).

(3) F. A. White and L. Forman Rev. Sci. Inst., 38, 355 (1967).

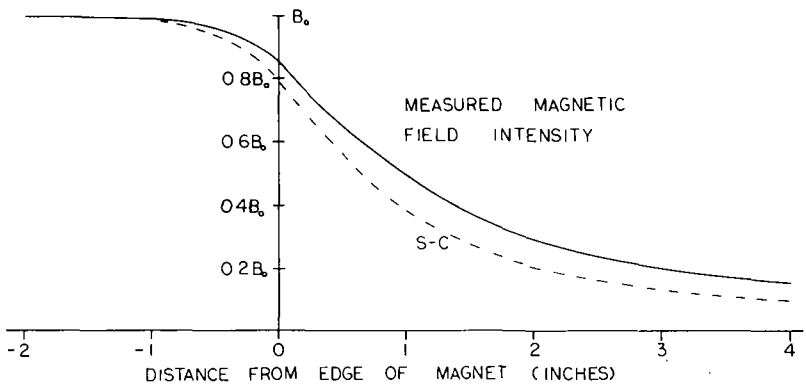

Figure 5
Measured Field Intensity Compared with the Schwarz-Christoffel Functions.

82.

SECONDARY ION EMISSION MICROANALYSER

J-M. ROUBEROL, J. GUERNET, P. DESCHAMPS, J-P. DAGNOT
and J-M. GUYON de la BERGE

CAMECA - COURBEVOIE (92) FRANCE

I. Introduction

The secondary ion emission Microanalyser was first described by Castaing and Slodzian in 1962 (1), and was exhibited at the French Society of Physics exhibition in that year.

This first experimental model, with simple magnetic filtering of mass, was followed by a second apparatus, described at the Orsay Microanalysis Conference in 1965 (2). This second version of the Microanalyser included a double filtering system, with magnetic filtering of mass and electrostatic filtering of energy, permitting extension of the useful range of the instrument to higher masses.

The Microanalyser described below was developed by Cameca. It uses the double filtering principle of the second version of the Castaing and Slodzian Microanalyser and includes significant improvements over the original experimental apparatus.

General Principle

The Ion Microanalyser is an instrument which combines a mass spectrometer with an ion emission microscope to form a surface distribution map of the components of a specimen. The limit of resolution attained in practice is of the order of one micron.

The instrument operates as follows : the specimen is bombarded by an ion beam with an energy of 10 kV. Under the action of these primary ions, particles are sputtered from the specimen surface. Some of these particles are ionized atoms or groups of atoms. These secondary ions, characterizing the elements or isotopes of the specimen, are accelerated and focussed by an electrostatic lens into a beam which carries a real image formed by all of the types of ions extracted from the specimen.

This image, which would be an enlarged material reproduction of the specimen surface, is not allowed to form, but the beam which carries it is separated by a mass spectrometer, isolating the various elementary images, each corresponding to an ion of specified mass.

The mass spectrometer is of a special type known as stigmatic, having both radial and transverse focussing properties, which forms an image of the specimen after deflection of the beam in the spectrometer.

The elementary ion image, isolated by the exit window of the spectrometer, is projected on the cathode of an image converter to form an electron image which is displayed on a fluorescent screen. By changing the adjustment of the mass spectrometer, it is possible to observe in succession the distribution maps of the emission of the various ions from the specimen surface.

II. Ion Optics

All of the secondary ions do not leave the specimen with the same initial velocity. In order to obtain a sufficiently high mas resolution, a design permitting both momentum filtering and energy filtering is used.

Deflection of the beam in a magnetic prism provides the momentum filtering. Energy filtering is accomplished with an electrostatic mirror. The beam, after isolation of ions of selected momentum, is directed into an electrostatic mirror which is adjusted to reflect only ions with a velocity lower than a certain value, thus eliminating ions of higher velocity.

The magnetic prism and electrostatic mirror are shown in figure 1. A detailed study of the optical properties of this design has already been published. The following is a brief statement of the operation and principal characteristics of the ion optical system :

The secondary ions are accelerated by an applied potential difference of the order of 5 kV in an immersion lens, and the lens forms a real image A_1B_1 of the object AB. An aperture, placed at the crossover C_1 of the immersion lens permits elimination of secondary ions with too much lateral energy, and also provides an entrance window to the first magnetic deflection.

The exit window which provides selection of momentum, consists of an aperture C_2 placed in front of the electrostatic mirror.

Although the field in the prism is uniform, the beam, in the course of this first deflection, is subject to a transverse focus in addition to the classical radial focus. The beam enters the prism at an angle of incidence ε so that the fringing field of the magnet has a transverse action on rays inclined with respect to the radial plane of symmetry.

By proper selection of the angle ε, it is possible to adjust this transverse focussing effect so that the transverse focal point coincides with the radial focal point.

As shown in Figure 1, the angle of incidence is about 45°, and the leakage field causes convergence of the beam to form two pairs of stigmatic points, one pair representing real images and the other representing virtual images. The apertures C_1 and C_2 are placed at the real stigmatic points, C_1 at the object and C_2 at the image. The immersion lens is adjusted to form the image A_1B_1 at the virtual stigmatic object point.

Following the aperture C_2, the beam then seems to come from a stigmatic image A_2B_2 at the virtual stigmatic point.

The electrostatic mirror is adjusted to be equivalent to a convex mirror with its apex in the plane of A_2B_2 , the virtual image of the magnetic lens, and its center at C_2. Under these conditions, the intermediate image A_3B_3 formed by the mirror, and acting as a virtual object for the second passage through the magnetic lens, coincides with A_2B_2.

The prism being symmetric with respect to the axis of the mirror, the beam after the second magnetic deflection, seems then to come from a virtual stigmatic image A_4B_4, symmetrical with A_1B_1 , and there is formed at C_3, symmetrical with C_1, a crossover which is a real stigmatic image of C_2.

Figure 2 shows the analogy between the electrostatic mirror used and a conventional immersion lens. The center and the apex of the mirror correspond respectively to the crossover and the image at the center of the cathode of the analogous immersion lens.

The mirror being convex, the dispersion of the beam by the second magnetic deflection acts in the opposite sense to the first deflection, so that the angular dispersion at the exit of the second prism is very small.(It would be zero if the apex of the mirror were at the point O.)

Because of this compensation and also the filtering of the beam in energy, the final image A_4B4 has a very small chromatic aberration.

Figure 3 shows a schematic of the electronic power supply for the different parts of the analyser. Provision is made for two cases, analysis of positive secondary ions and negative secondary ions.

The upper limit of the energy of the ions which contribue to the formation of the image is fixed by the potential difference between the specimen and the "cathode" of the mirror, which can be adjusted by a potentiometer. The ions whose energy corresponds to a potential difference greater than this, reach the cathode and are neutralized and eliminated from the reflected beam.

After the second deflection, the secondary ions enter the image converter which consists of the following main optical elements :

1) a post-acceleration lens with two electrodes;
2) a projection lens with 3 electrodes; and
3) the image converter itself, which consists of an immersion lens whose cathode is bombarded by the ion beam and emits secondary electrons.

The adjustment of the projection lens is such that the telescope objective which it forms along with the post acceleration lens projects the virtual image A_4B_4 as a real image on the cathode of the converter. Secondary electrons are then emitted, accelerated in the opposite direction, and focussed by the immersion lens of the converter as an electron image which can be observed on a fluorescent screen.

The purpose of the post acceleration of the ions is to reduce the contraction of the ionic image which is caused by acceleration or deceleration of the ions in the anode-cathode space of the converter. This is accomplished for both positive ions which are accelerated in the converter and for negative ions which are decelerated in the converter.

Finally, we note that the potential difference for acceleration of the electrons is constant at 30 kV for both positive and negative ions.

III. Apparatus

Figure 4 is a horizontal cross-section showing the entire microanalyser. Figure 5 is a vertical cross-section of the image converter. Figure 6 is a schematic drawing of the vacuum system.

A. Specimen Compartment

The specimen is supported on a rod penetrating into the chamber through a metallic bellows. A mechanism for displacement in X, Y and Z is located outside the chamber.

A fixed angular movement of the arm of the specimen holder permits the specimen to be placed either in the analysis position or in the viewing position. In the viewing position the specimen is viewed with a 50 power metallographic microscope.

When the sample holder is in the viewing position the sample can be changed using a vacuum lock. The inlet opening is made of a demountable window to permit viewing of the sample.

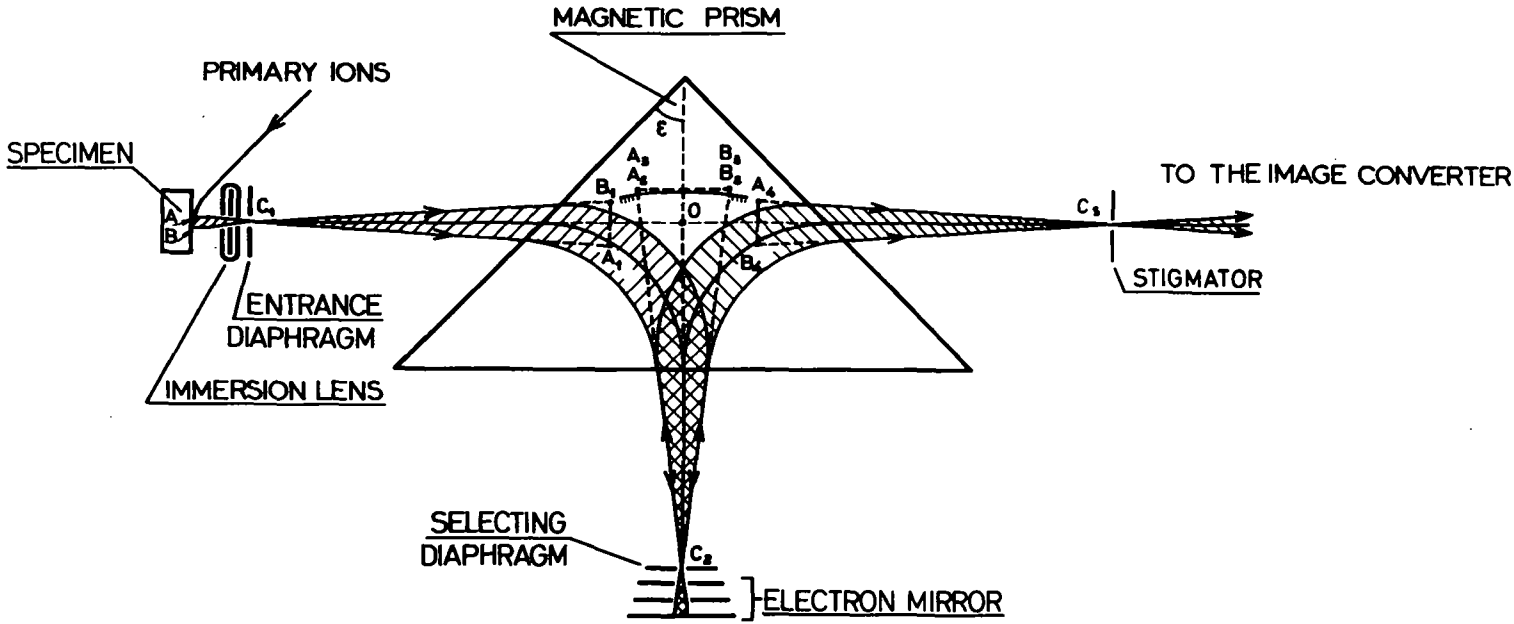

MOMENTUM AND ENERGY FILTERING SYSTEM

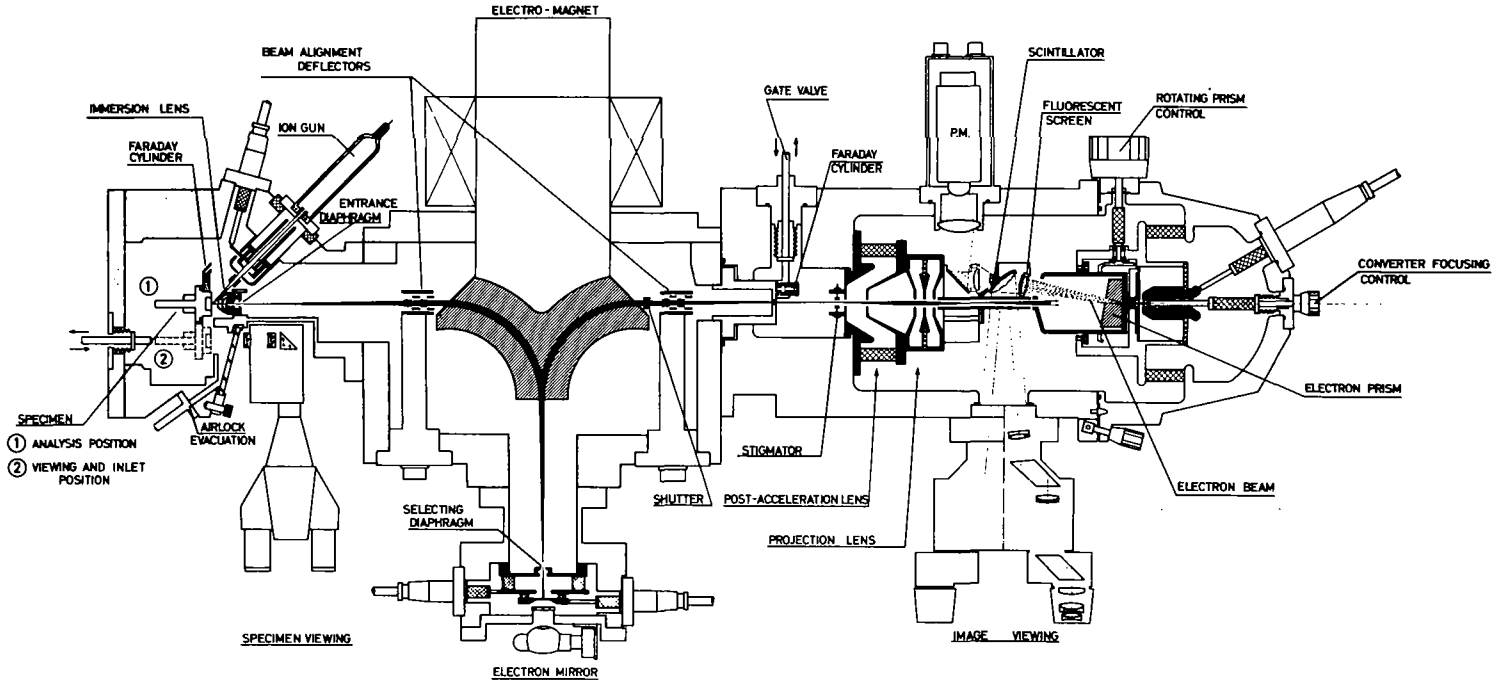

İON MİCROANALYZER CAMECA

The ion gun, a radio-frequency ion source, is followed by a 3 electrode electrostatic condenser and an electrostatic system for centering the beam on the specimen. The primary ions used are generally argon or oxygen.

B. Prism-Mirror Assembly

The double magnetic prism is an electromagnet whose pole pieces are under vacuum inside the central body of the apparatus. The magnet gap is 5 mm and the radius of deflection 110 mm.

The cathode of the electrostatic mirror, whose surface is carefully polished is heated to avoid contamination, using a tungsten filament lamp located outside the vacuum system.

At the entrance and exit to the double magnetic prism there are electrostatic deflectors used for general alignment of the ion beam.

Near the exit deflector there are a pair of plates which permit the beam to pass for a fixed time. These serve as a shutter to control exposure of the film.

A removable Faraday cylinder at the exit crossover of the magnetic analyser system, permits measurement of the intensity of the total ionic beam.

C. Image Converter

The image converter can be used in the following four different ways.

1) Visual Observation : The electron image is displayed on a fluorescent screen, observed in transmission by a 5 power binocular telescope.
2) Image Recording : The electron image is recorded directly on film in a camera placed within the converter chamber.
3) Measurement of Total Ion Current : The fluorescent screen is replaced by an aperture corresponding to an area of about 125 microns diameter on the specimen surface. The beam then strikes a plastic scintillator which is coupled by high aperture optics to a photomultiplier located outside the converter. With conversion of the ions to 25 kV electrons and then to photons, the photomultiplier becomes a high sensitivity detector permitting use of the apparatus as a simple secondary ion mass spectrometer.
4) Measurement of Ion Current form a Small Area : In this case, the aperture, located at the image point of the converter, limits the electron flux to the scintillator to a fine beam corresponding to a small area on the specimen. This mode of operation then permits a mass spectrometer analysis on the scale of a few microns (Figure 7).

The choice of these different modes of measurement is made by use of two devices, as follows :

1) A movable magnetic prism used to deflect the electron beam. This prism, formed by a permanent magnet placed in front of the immersion lens of the converter, is almost without action on the incident ion beam, but deflects the secondary electron beam and laterally displaces the electron image. An external control permits the prism to be rotated around the axis of the converter so that the electron image may be on the camera or in the position used for the other three modes of observation or analysis.
2) An aperture holder with three position. This device permits, when the prism is in the observation-analysis position, selection among the other three modes, that is :

   to receive the image on the fluorescent screen;
   to replace the screen by an aperture for analysis of large areas;
   or to use an aperture for point analysis (for example for analysis of an area of the specimen having a diameter of 5 microns).

It must be noted that the movable parts of the converter (the prism, the aperture holder, and the mechanism for advancing the film) are at the post-acceleration potential (25 kV positive or negative with respect to the envelop of the converter), and that they are therefore mounted on insulators.

Finally, one uses a special 35 mm film in the camera which degasses poorly. Each charge permits several tens of exposures and the interruption to change the camera is of the order of 10 minutes.

IV. - Performance and Characteristics

A. Primary ion beam

The "chemical effect", shown by Castaing (3) to enhance the secondary ion emission, must be taken into consideration in selecting the conditions for primary ion bombardment.

When bombarding a specimen having oxygen adsorbed on the surface, there is enhancement of the secondary ion emission for certain elements. It is assumed that oxygen forms compounds with these elements for which the ionization yield is greater

than for the pure element.

Enhancement by the "chemical effect" may also occur when atmospheric oxygen in the specimen chamber is adsorbed. This phenomenon is easily observed with aluminum for example, the emission from which can reach ten times the normal value at the start of the bombardment or under poor vacuum conditions.

Although bombardment with oxygen ions is deliberately used in some cases to obtain a selective effect, the enhancement due to the "chemical effect" is generally undesirable. To render the effect negligible, it is necessary to establis a good vacuum in the vicinity of the specimen, and to maintain a heavy flux of ion bombardment on the area being analysed.

In practice these conditions are met with a vacuum of 5×10^{-8} torr in the specimen chamber, and an ion beam flux of 200 $\mu A/mm^2$ obtained with a beam of 15 μA on an area with a diameter of 0.3 mm.

In connection with these conditions of primary ion bombardment, it should be pointed out that the Ion Microanalyser of the Castaing design has the following advantages over an Ion Microprobe of the scanning type :

1) The brightness (secondary ion emission per unit area of sample) for the Castaing Microanalyser is far superior because, in order to obtain the same average density of primary ion bombardment, a scanning Microprobe of 1 micron diameter must carry the same beam current as a 300 micron diameter beam in the Castaing Microanalyser

2) In the Castaing Microanalyser, all the points within the analysed area are bombarded simultaneously, keeping the surface clean and making the enhancement by "chemical effect" negligible. The scanning probe, of course, does not bombard all the points successively.

B. Mass Resolution

The double filtering system provides a mass resolving power sufficient to analyse all of the elements of the periodic table. Figure 8 gives, for example, a recording of the spectrum of tungsten obtained using an entrance aperture of 0.2 mm and a selection (exit) aperture of 0.4 mm, and an upper limit of initial energy of 2 volts. The observed resolution, calculated for a 10 % valley, is 1/350.

C. Sensitivity

Two factors contribute to the sensitivity, the transmission of the system, and the sensitivity of the detector. The system has a very high transmission factor because a large fraction of the ions extracted from the specimen are collected by the immersion lens and pass through the entrance aperture and the mass spectrometer, having circular apertures instead of slits and having these apertures in stigmatic focus, transmits a high fraction of the ions collected. For example, with the extraction field of 1 kV/mm normally used, and with the entrance aperture of 0.2 mm used to obtain maximum resolution, the limiting angle of collection for ions from the center of the field is 20° for 1 volt ions and 9° for 5 volt ions. With an aperture of 0.4 mm used when lower resolution is acceptable, the angles are 45° for 1 volt ions and 17° for volt ions.

The ion detector incorporated into the converter makes a conversion of ions into high energy electrons as described by Daly (5), but has the advantage over the Daly detector of being able to detect negative ions as well as positive. The optical system used for concentrating the lifht emitted by the scintillator, permits use of a photomultiplier with a small diameter photo cathode, thereby giving a low noise level. As with the Daly detector, when used in connection with a pulse height analyser and counter, one can detect currents corresponding to a few ions per second. For current measurements not requiring such sensitivity, one can use a DC amplifier and can obtain a detection limit of 10^{-16} A (equal to noise) with a response time of 1 second.

D. Spatial Resolution

The magnification of the image at the focal plane of the image converter is variable between 75 and 150, a factor of ten being due to the converter itself. The beam observed in a 25 mm diameter picture on the film then comes from an area with a diameter 165 to 330 microns in diameter.

The limit of resolution is in general of the order of a micron at the center of the image. Figure 9 shows a test of resolution using aluminum and calcium which have high secondary ion yields. The limit of resolution observed is better than 1 micron throughout the field of 190 micron diameter.

E. Sensitivity for Recording Images

Since the electron images are recorded directly on film placed within the vacuum system, the exposure time required is very short, between a few milliseconds and a few tens or seconds. Figure 10, for example, showing an image for aluminum ions for a specimen consisting of a grid of copper pressed onto a block of aluminum, was obtained with an exposure of 5 milliseconds.

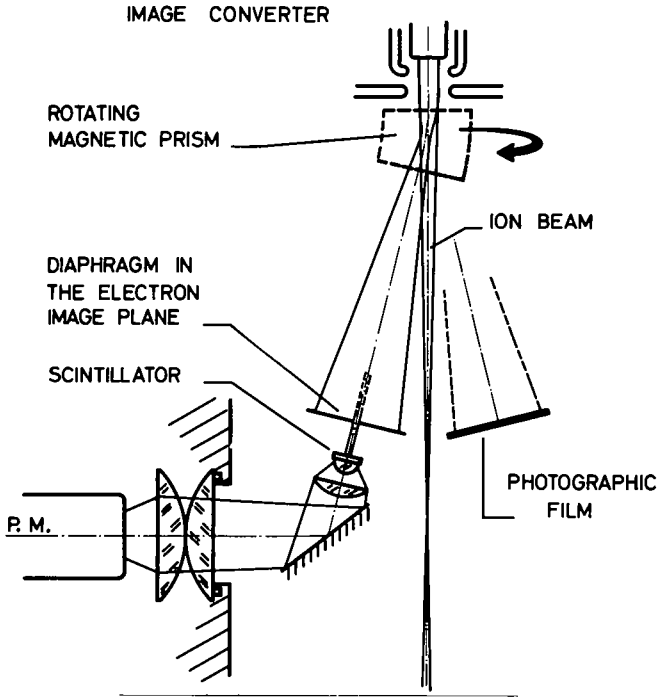

PRINCIPLE OF THE IMAGE RECORDING AND LOCAL ANALYSIS

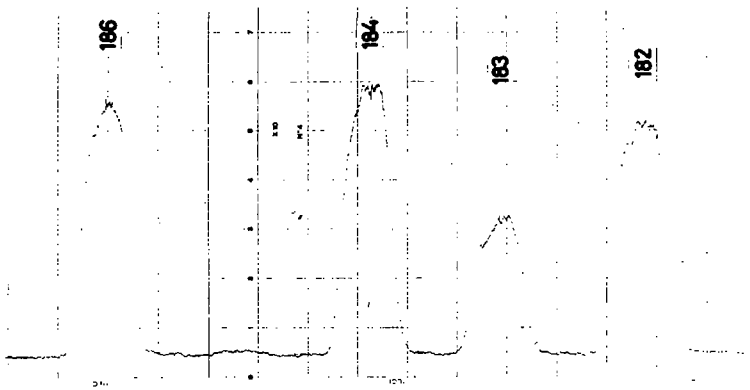

TEST OF RESOLUTION

TUNGSTEN SPECTRUM		ACCELERATING VOLTAGE	4.5 kV
ENTRANCE DIAPHRAGM	0.2 mm	ENERGY THRESHOLD	2 Volts
SELECTING DIAPHRAGM	0.4 mm	RESOLUTION (10% VALLEY)	$\frac{M}{\Delta M} = 350$

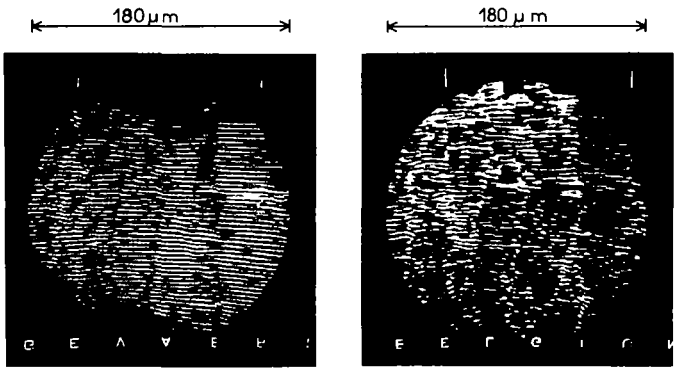

Al^+ IMAGE Ca^+ IMAGE

TEST OF SPATIAL RESOLUTION
Al-Ca ALLOY

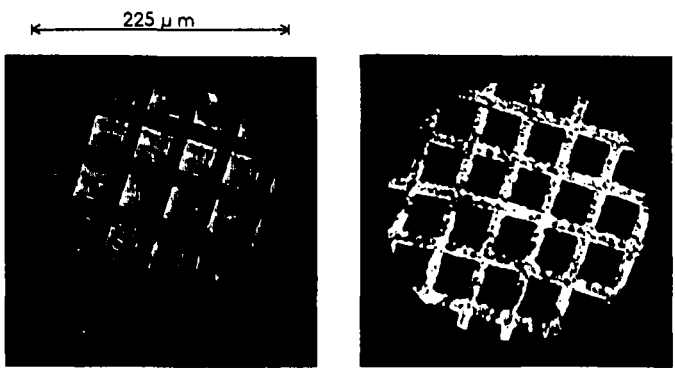

Al^+ IMAGE
TIME OF EXPOSURE : 0.005 SECOND

$^{63}Cu^+$ IMAGE
TIME OF EXPOSURE : 1 SECOND

COPPER GRID PRESSED ON AN ALUMINIUM BLOCK
(PRIMARY IONS : Ar^+)

The number of atomic layers which must be sputtered to make such an image can be estimated with the following assumptions :

1) the yield of aluminum ions is about 0.1 % of the total atoms of aluminum sputtered

2) a low resolving power is sufficient for resolution of aluminum, so that about 50 % of the ions emitted can be used to form the image;

3) an aluminum ion on the average produces two electrons in the converter;

4) finally, the film must receive about 1 electron per square micron to be darkened to an optical density of unity.

A simple calculation shows that the amount of material sputtered while forming an image is of the order of one atomic layer.

One cannot assume, however, that the resolution of depth is of the order of a single atomic layer, because account must be taken of the penetration of the primary ions into the target. The resolution in depth has not yet been determined by precise experiments, but it appears to be between 50 and 100 Angstroms (0.005 to 0.01 microns).

We note also that the image definition exceeds the resolution of the apparatus. The image is obtained from 5×10^8 electrons while, from the point of view of resolution, the image contains only about 5×10^4 elements.

V. Applications

There is not, unfortunately, any simple law relating intensity of secondary ion emission for an element to its concentration in the specimen. Because of this, ion microanalysis will not generally replace electron probe microanalysis for measurement of local elemental concentration. The new possibilities of the Ion Microanalyser are however, so attractive that one can predict a development in the area of research analagous to that of the electron microprobe.

First, isotopic analysis is possible and, in this case, the results can be quantitative. As examples, we can cite the study of isotopic segregation in mineralogy, and the study of self-diffusion using two isotopes of the same element. Figure 11 shows an application of self-diffusion. In order to study the diffusion of oxygen in UO_2, one diffuses ^{18}O into UO_2 containing mainly ^{16}O and records the images for ^{18}O and ^{16}O.

Second, we point out that there is no limitation with regard to atomic number; the lightest elements can be reached (see for example in Figure 12 the image for berylium).

But it is chiefly in its resolution in depth that ion microanalysis is superior to electron probe microanalysis. One can then consider study of surface phenomena, or the tracing of diffusion curves in very thin depths while eroding, layer after layer, the specimen surface. Figure 13 is a simple example of the results obtained by this method. It shows the diffusion of boron in a monocrystal of silicon.

Another important advantage of Ion Microanalysis is that there does not exists any phenomenon equivalent to the continuous background of X-rays which limits the sensitivity of the electron microprobe method. The analysis of very small quantities can be considered, and even give, if the elements are coalesced, images with good contrast.

Finally, the ion microanalyser gives images immediately. This is a practical and important advantage. The specimen can be explored as rapidly as with an ordinary metallographic microscope. In comparison with the electron microprobe, the scanning system limits the displacement speed of the sample under examination.

REFERENCES

(1) R. CASTAING et G. SLODZIAN - J. de Microscopie, 1, 395 (1962)

(2) OPTIQUE des RAYONS X et MICROANALYSE p. 48
Hermann Editeur, PARIS

(3) G. SLODZIAN et J-F. HENNEQUIN C.R.A.S., 263, 1246-1249.

(5) N.R. DALY - Rev. of Sc.Instr. 31, 3, 264-267.

83. Performance Characteristics of New Two-Stage Mass Spectrometer

W. E. Duffy

General Electric Company
Nucleonics Laboratory
Vallecitos Nuclear Center
Pleasanton, California

The instrument described here is a direction focusing, two magnetic stage, thermal emission mass spectrometer. It is used principally for isotopic analysis and combines some of the better features of recent developments, in this laboratory and elsewhere, related to ion yield, transmission, detection and abundance sensitivity. An unusually versatile and stable magnet system has been added which permits sweeping or fixed point operation. Commercially available electronic and mechanical components are used wherever possible.

The sample changer,[1] the ion source,[1] the Daly scintillation ion detector[2,3] and the pulse counting equipment[2] have been described in previous meetings so will not be discussed here.

The two magnets and associated controls were built to our general specifications by Magnion, Inc. They have a radius of curvature of 15", a sector angle of 90° and a fixed gap of 0.80". The energizing coils are low impedance, air cooled, copper foil, wound with Mylar insulation. The magnet yoke is "C" frame construction and cast from low carbon steel. The pole pieces contain 0.02% carbon (+ .03% - .01%). The magnetic field is uniform within ± 1 gauss along the ion path and within 1.5" from the pole cap at a maximum field strength of 9000 gauss. Rogowski-shaped pole edges minimize fringing effects, which are less than 100 gauss at a point 7" from the pole cap edge, along the ion path. A highly stable, precisely adjustable magnet base provides for linear movement at 45° along the radius of curvature, vertical leveling of four legs and angular movement about the center point of the pole caps.

The single magnet power supply and control instrumentation use rotating coil and rate coil type field control. Short term (100 sec) field stability is 1 part in 10^6. Long term (100 min) field stability is 5 parts in 10^6. The fields of both magnets are held to within 1 part in 10^5 at all times. This tracking specification holds when sweeping in either direction over the range of the magnet above 1000 gauss. The sweep rate is adjustable in 10 steps from 2000 gauss/min to 4 gauss/min. Field set accuracy is 2 parts in 10^4.

The magnets are located so that the ion beam passes clockwise through the two 90° sectors in a general "C" configuration.

The high voltage power supply for the ion source was built specially by Beva Electronics. It is adjustable from 1 to 15 kV, has a maximum output current of 10 mA and line-load regulation of 0.001%. An unusual feature is its rapid slewing time. Less than 80 milliseconds are required for a change of 200 volts at 15 kV. The various ion lens voltage controls are incorporated in the supply.

The sliding piston sample changer employs a 140 L/m mechanical pump on the first stage and a cold trap, air-cooled oil diffusion pump, mechanical pump on the second stage. Complete sample change requires five minutes. Overall system pressure remains in the 10^{-8}-10^{-9} torr region. The source and detector assemblies each have 6" Granville-Phillips cold traps, followed by a 140 L/s and 80 L/s Varian ion pump respectively. The middle slit also uses an 80 L/s ion pump. The three pumps share a common power supply. The source and detector may be isolated from the analyzer regions by 1" gate valves.

Changes in the ion optics from those of a conventional instrument have resulted in significant improvements in ion transmission and abundance sensitivity. The single V-shaped filament ion gun, employing adjustable Z-focus, is identical, dimensionally, with that described by Dietz. However, to overcome the known defocusing action of a narrow slit, a second pair of identical Z-focus plates was placed after the final collimating slit of the source. Ion transmission increased approximately 10% when using these plates. Defocusing in the Z-direction also occurs when entering and leaving a magnetic field. To compensate for the effects of the first magnet and the middle slit a larger pair of Z-focus plates were located immediately following the middle slit. These were separated by a distance equal to the length of the slit. Use of these center Z-focus plates increased the number of ions reaching the detector by 50-150%, depending

upon the sample. These measurements were made using both samples loaded from solution and rhenium ions emitting from the full face of the rhenium filament. There was no significant difference between the two sets of measurements. In order to corroborate this effect identical plates were installed in a second operating two-stage mass spectrometer. Identical behavior was noted.

The abundance sensitivity of the conventional two magnetic stage, direction focusing mass spectrometer is approximately 1 part in 10^6. Workers in two laboratories[4] recently reported the use of a simple retardation lens to increase this value to 1 part in 10^9. A similar lens was installed in this instrument and a similar improvement was noted. A common characteristic of about 50% loss in ion transmission to the detector was also noted. Therefore the lens is used only for special analyses.

The Daly scintillation ion detector has an overall gain of about 2×10^9. In addition to its very high gain a unique property of this detector is its relative independence of changes in source voltage. To test this behavior a constant Re^+ ion beam from a rhenium filament was maintained in the source while the ion accelerating voltage was changed in 50-volt increments. All controls were optimized at each point. There was negligible change in beam intensity throughout a 2000 volt change in ion accelerating voltage. Voltage changes beyond this affected the ion-electron optics of this particularly small scintillator and caused a loss of signal. A larger scintillator probably would eliminate this problem. Since a 2000 volt spread is greater than normally used for most isotopic analysis the Daly scintillation detector is particularly desirable when employing conventional voltage scanning techniques. Effects which have been attributed previously to source and detector efficiency largely are eliminated. The very high efficiency of the Dietz ion source probably contributes also to the overall flat response curve.

The first and second beam collimating slits in the ion source are fixed at 40 mils and 20 mils respectively. The middle slit and detector slit are adjustable. The ion beam at these points averages 20 mils and 30 mils respectively.

Acknowledgement

The diligent help of E. W. Skoog in the construction, assembly and testing of this instrument is gratefully acknowledged. The advice of C. P. Ruiz is also appreciated.

References

1. ASTM E-14 Proceedings 1962, p. 280.

2. ASTM E-14 Proceedings 1966, paper 68.

3. ASTM E-14 Proceedings 1967, p. 358.

4. ASTM E-14 Proceedings 1967, pp. 406, 562.

84. An Improved High-Resolution Mass Spectrometer for Organic Structure Studies

J. Okamoto, H. Tsuyama, Y. Nakajima, T. Noda

Hitachi Perkin-Elmer Ltd., Tokyo, Japan

F. W. McLafferty and J. W. Amy

Department of Chemistry, Purdue University, Lafayette, Indiana 47907

To study the usefulness of increased resolution and mass-measuring accuracy for structural analysis of organic compounds, an improved high-resolution double-focusing mass spectrometer (Hitachi RMH-2) has been constructed. Due to the requirements of high-speed high-resolution data acquisition over a wide mass range, a modified Nier-Johnson geometry was chosen with symmetrical positioning of source and detector. For mechanical stability and simplified alignment and operation the system employs horizontal ion trajectory. 50 centimeter electrostatic and 40 centimeter electromagnetic sectors with equal deflection angles of 70 degrees yield a resulting ion optical trajectory of just under 3 meters, giving improved sensitivity for metastable ion detection. The ion source, electrostatic sector, analyzer tube, and electron multiplier detection system are mounted onto a rigid pedestal base while the electromagnet is placed on a precision optical alignment stage. A unique high efficiency ion source is used with maximum accelerating voltage of 9,600 volts.

86. APPLICATIONS OF MASS SPECTROMETRY TO STRUCTURAL PROBLEMS IN NUCLEIC ACID CHEMISTRY

D. M. Desiderio, N. R. Earle, P. M. Krueger, A. M. Lawson, L. C. Smith

R. N. Stillwell, K. Tsuboyama, J. Wijtvliet and J. A. McCloskey

Baylor University College of Medicine, Houston, Texas

We have undertaken a broad investigation of the applications of mass spectrometry to structural problems in nucleic acid chemistry. Previous work on the mass spectra of free nucleosides (1) has clearly demonstrated (2) the usefulness of this technique. The present investigation has included studies of the mass spectra of (free) adenosine analogs, O-isopropylidine derivatives of nucleosides, nucleoside acetates, and trimethylsilyl (TMS) derivatives of bases, nucleosides and nucleotides (3).

Although the spectra of free nucleosides are very useful in many respects (e. g., location of methyl substituents), nucleotides and the more polar nucleosides (guanosine, cytidine) are precluded because of their low volatility. The use of either isopropylidine (Fig. 1) or acetate (4) (Fig. 2) derivatives permits the recording of spectra of all nucleosides, reflecting essentially the same structural relationships as in the case of the free compounds. The use of TMS derivatives (5) increases volatility enough to include not only bases (Fig. 3) and nucleosides, but also mononucleotides. Mass spectra of purine and pyrimidine base TMS derivatives are dominated by M and M-CH_3, indicating potential analytical usefulness for dealing with these compounds in mixtures. Spectra of nucleoside and nucleotide derivatives generally follow the interpretation shown for adenosine monophosphate-$(TMS)_5$ shown in Fig. 4. Several TMS migrations have been observed in these spectra, including those indicated in Fig. 4.

TMS derivatives have been employed in studies of the direct analysis of RNA and DNA hydrolysates, using high resolution mass spectrometry and related computer techniques. This work has necessitated the partial solution to the following two intermediate, related, problems.

(1) Coupling of the high resolution instrument (CEC 21-110B) to a gas-liquid chromatograph so as to permit use with compounds of very high molecular weight and polarity (e. g., nucleotide TMS derivatives). This has been accomplished with a porous stainless steel carrier gas separator (6), built into a probe handle. The effluent is introduced through a probe into the ion source using the standard CEC

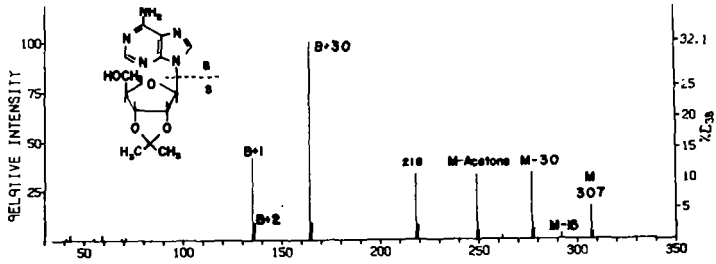

Fig. 1

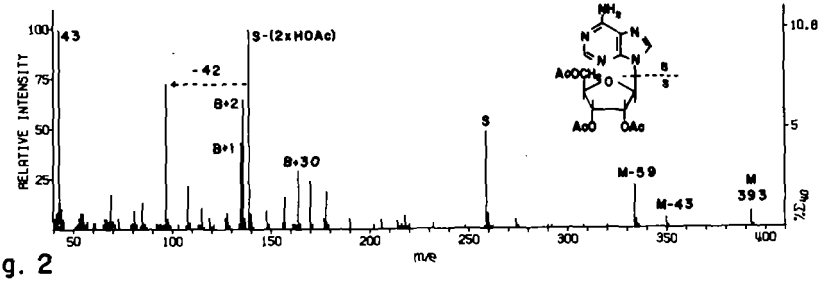

Fig. 2

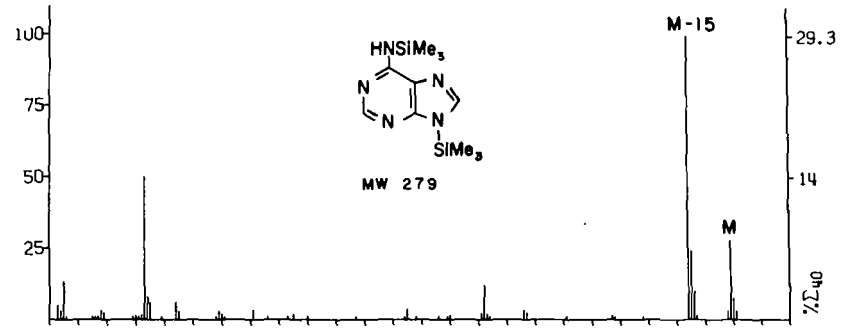

Fig. 3

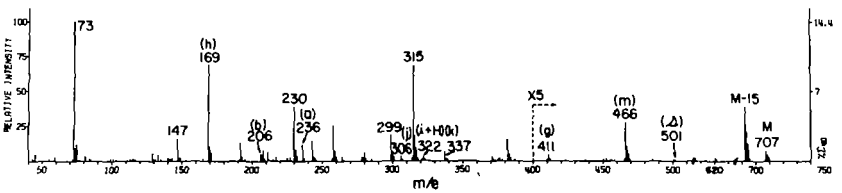

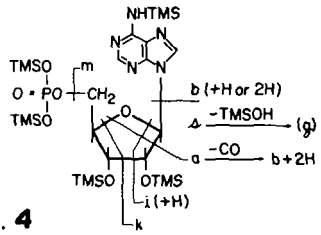

Fig. 4

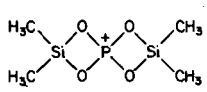

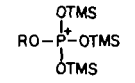

R = H m/e 315
R = OTMS m/e 387

CCl_5^+ ION ABUNDANCE CALIBRATION DATA
(8 KV, RESOL. 20,000, KODAK SWR PHOTOPLATE,
KODAK HRP DEVELOPER)

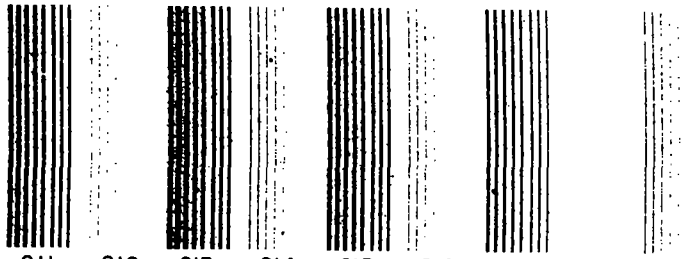

m/e	211	212	213	214	215	216	217	218	219
REL. ABUNDANCE	625	21.	1000	33	640	21	205	7	33

Fig. 5

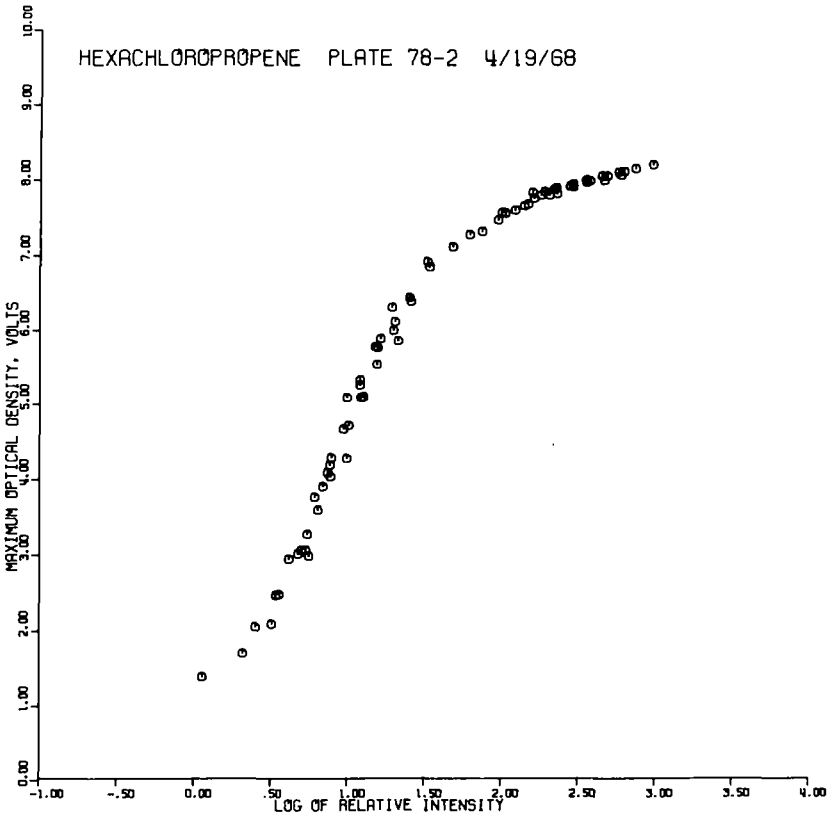

Fig. 6

direct inlet vacuum lock. This separator system (7) is normally operated at 35 cc/min He input, giving a source pressure (as measured) of 2×10^{-5} mm Hg or less, with a 40% efficiency (at M. W. 370) and a separation factor of 110. The porous stainless steel separator possessed the following advantages: inexpensive, nonbreakable, excellent heat transfer characteristics, easily cleaned and disassembled, and permits considerable versatility (dimensions, design) in construction.

(2) Calibration of the photographic plate for semi-quantitative ion abundance measurements over several orders of magnitude. A system has been developed utilizing the nine usable isotopic ions of $M\text{-}Cl^+$ from hexachloropropene. A completely automatic device has been built which permits the recording of eight separate exposures of the calibration compound at different levels (see Fig. 5), by offsetting the electric sector voltage slightly between exposures. Each exposure integral is read by the beam monitor into an integrator and is printed. From these data an approximately 72 point ion abundance - optical density calibration curve can be constructed and plotted (Fig. 6, using peak heights for the ordinate). The data (Fig. 5) requires only one line of the photoplate, is subjected to the same developing conditions as the data on the remainder of the plate, and is read by the microdensitometer in less than a minute.

A representative approach to the analysis and identification of components of crude nucleic acid hydrolysates is as follows: (1) degradation of unfractionated transfer RNA by snake venom and bacterial alkaline phosphatase, (2) dry over P_2O_5, (3) derivitization (TMS) of the nucleosides thus produced, (4) introduction of the entire mixture by direct inlet probe (or alternatively by GLC) into the mass spectrometer, with photographic recording of the spectrum. The resulting high resolution data (absolute and relative abundances and exact masses of all ions) are then obtained (via microdensitometer, recording on intermediate magnetic tape) by the computer, and then stored on a disk at the site of a central computer (IBM 360-50). The data are then at any time interrogated by remote terminals (teleprocessing: IBM 2260, typewriter: IBM 2740) located in the laboratory. Interrogation programs are in use which search the high resolution data by any of three categories: (1) exact masses, (2) compound name (using preselected and stored characteristic exact masses), (3) class name (e. g., "RIBONUCLEOSIDE TMS", using preselected and stored compound

names and corresponding masses.

Initial results with this system indicate that it may offer a powerful approach to certain of the structural and analytical problems confronting the nucleic acid chemist and biochemist.

References and Footnotes

(1) K. Biemann and J. A. McCloskey, J. Am. Chem. Soc., 84, 2005 (1962).

(2) See literature citations listed under ref (2) in ref (3) below.

(3) J. A. McCloskey, A. M. Lawson, K. Tsuboyama, P. M. Krueger and R. N. Stillwell, J. Am. Chem. Soc., July 17 (1968).

(4) S. J. Shaw and J. A. McCloskey, unpublished results.

(5) See, for instance: (a) Y. Sasaki and T. Hashizume, Anal. Biochem., 16, 1 (1966), (b) R. L. Hancock, J. Gas Chrom., 363 (1966), (c) C. W. Gehrke, D. L. Stalling and D. C. Ruyle, Biochem. Biophys. Res. Commun., 28, 869 (1967).

(6) See also: A. M. Lawson, F. A. J. M. Leemans, and J. A. McCloskey, Fifteenth Annual Conference on Mass Spectrometry and Allied Topics, Denver, 1967.

(7) Filter length 4", o.d. 1/2", wall thickness 1/8", mean pore diameter 0.1 micron. Obtained on special order from Mott Metallurgical Corp., Hartford, Conn. The separator was silanized according to instructions given in ref (5).

87. Determination of the Structures of Sphingolipid Bases by Combined Gas Chromatography-Mass Spectrometry

Charles C. Sweeley* and Alan J. Polito
Department of Biochemistry and Nutrition
Graduate School of Public Health
University of Pittsburgh

A relatively large number of long-chain aliphatic amines, of the general type $R\text{-}CH(OH)CH(NH_2)CH_2OH$, have been found in sphingolipids isolated from animals and plants. Many of these sphingolipid bases can be identified by gas chromatography of the volatile O-trimethylsilyl derivatives (1,2), or of the aldehydes liberated by periodate oxidation (3). Recent evidence for branching in the aliphatic chains of some bases (4,5), and for more than one olefinic group in others (6,7), makes structural assignments from retention times less certain.

We have used combined gas chromatography-mass spectrometry to determine the structures of N-acetyl-O-trimethylsilyl derivatives of the sphingolipid bases. Several characteristic types of fragmentation can be used in mass spectral identifications, as illustrated in the structure of the sphingosine derivative below. A molecular ion is rarely apparent but

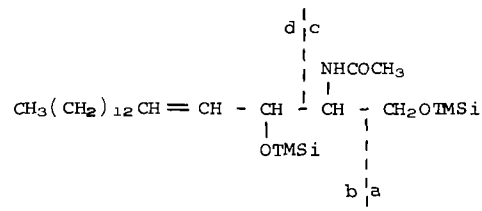

the molecular weight can be derived from peaks at M - 15, M - 90 (loss of trimethylsilanol), M - 103 (M - a), and M - 15 - 90. Cleavage between carbons 2 and 3 is always observed with charge retention on both fragments (c and d), and the peak at m/e 174 (c) is especially intense with an olefinic group in an allylic position as shown. The m/e of the d ion indicates chain length and degree of unsaturation in the parent sphingolipid base. In mass spectra of the C_{18} bases, for example, ions of the d type are at m/e 313 for the saturated base, sphinganine, m/e 311 for

*Present address: Department of Biochemistry, Michigan State University, East Lansing, Michigan

sphingosine, and m/e 309 for the doubly unsaturated sphinga-4,14-dienine.

We have developed a method for the definitive location of olefinic groups, based on previous studies of the osmium tetroxide oxidation of unsaturated fatty acids (8,9). The N-acetyl derivative of a base is oxidized with osmium tetroxide, and the double bond positions are then determined from characteristic fragmentations of the poly-O-trimethylsilyl derivative. Both double bonds of sphinga-4,14-dienine are oxidized by this procedure, and the structure of the N-acetyl-O-trimethylsilyl derivative is shown below. The position of the olefinic group at Δ^{14} is

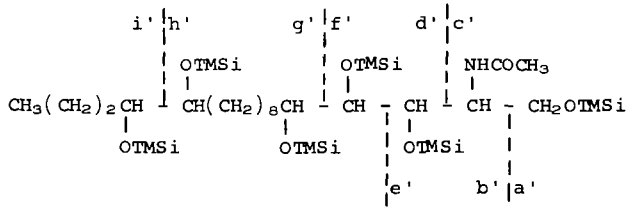

confirmed by the peaks at m/e 145 (i') and m/e 694 (h'), while the Δ^4 double bond gives a structure with characteristic ions at m/e 276 (e'), 378 (f') and 461 (g'). The molecular weight (839) is calculated from ions at M - 15, M - 103 (b'), M - 105 and M - 174 (d').

The mass spectral information obtained with N-acetyl-O-trimethylsilyl derivatives after osmium tetroxide oxidation can be utilized in a program for the computer interpretation of various sphingolipid bases. Such a program is now being developed in this laboratory. Full details of this study will be published at a later date (10).

1. Gaver, R. C., and Sweeley, C. C. (1965), J. Am. Oil. Chem. Soc. 42, 295.
2. Carter, H. E., and Gaver, R. C. (1967), J. Lipid Res. 8, 391.
3. Sweeley, C. C., and Moscatelli, E. A. (1959), J. Lipid Res. 1, 40.
4. Carter, H. E., and Gaver, R. C. (1967), Biochem. Biophys. Res. Communs. 29, 886.
5. Carter, H. E., and Hirschberg, C. B. (1968), Biochemistry 7, 2296.
6. Karlsson, K. A. (1967), Acta Chem. Scand. 21, 2577.

7. Polito, A. J., Akita, T., and Sweeley, C. C. (1968), Biochemistry, in press.

8. McCloskey, J. A., and McClelland, M. J. (1965), J. Am. Chem. Soc. 87, 5090.

9. Niehaus, Jr., W. G., and Ryhage, R. (1967), Tetrahedron Letters, 5021.

10. Sweeley, C. C., Naworal, J., Wood, W. C., and Polito, A. J., J. Lipid Research, in press.

89. Some Examples of the Use of High and Low Resolution Mass Spectroscopy in Biology and Medicine

H. M. Fales, National Heart Institute, Bethesda, Maryland

1. Ureasterone, a metabolite of testosterone was shown to have structure I, instead of the isourea structure II on the basis of the formulae of its high molecular weight (C_{17})

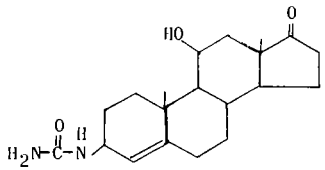

I

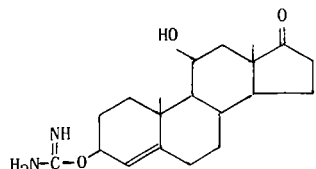

II

fragments which were shown to contain nitrogen and two oxygen atoms.[1]

2. The first naturally occurring thiouridine was identified as 4-thiouridylic acid after obtaining its pyrolytic mass spectrum which disclosed a weak ion possessing the formula $C_4H_4N_2SO$.[2]

3. Material from an Escherichia coli broth was identified as 2,3-dihydroxybenzoylserine[3] after consideration of the mass spectrum of its methylation product (III) which disclosed the formula of the parent ion and fragments. Its thermal dehydration product (IV) was also identified.

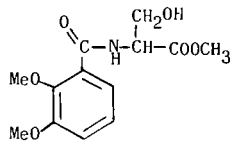

III

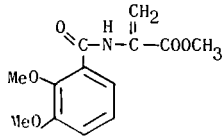

IV

4. Refsum's disease[4] is characterized by a high concentration of phytanic acid (V) in the tissues and sera. It was shown to be exogenous in origin since patients receiving D_2O did not incorporate deuterium into this substance while cholesterol was labeled as expected with approximately half as much deuterium as present in the body fluids.

These analyses, comparing P+/P ratios for the two substances, were carried out at high resolution ($\sim$6000) with the aid of a mass ratiometer[5] which sums areas of two peaks scanned successively, electronically obtains their ratios and displays the value on a digital voltmeter.

Normal oxidation of phytanic acid follows the β-oxidation pathway after an initial α-oxidation (via α-hydroxyphytanate) to pristanic acid (VII).

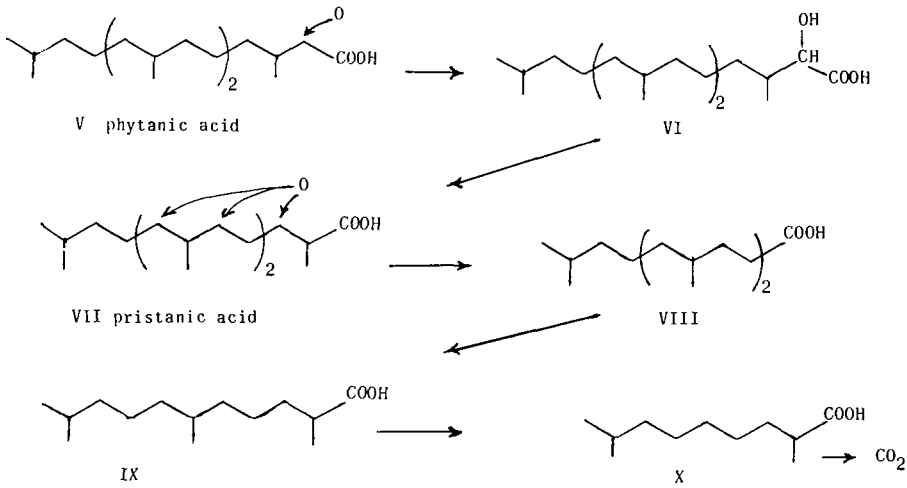

The metabolites (VI-X) were all identified by combined GLC-low-resolution mass spectra using high resolution measurements to confirm formulae. Fragmentations via the McLafferty rearrangement and methyl branching readily disclosed their structures.

Refsum's disease patients and their tissue cell cultures were able to oxidize ^{14}C-labeled α-hydroxyphytanate and pristanate at the same rate as normal individuals. In contrast they were unable to oxidize phytanate indicating that the metabolic block is associated with α-hydroxylation in the first step.

---

1. D. Fukushima and T. W. Gallagher, J. Biol. Chem., 241, 5336 (1966); S. Noguchi and D. K. Fukushima, J. Biol. Chem., 241, 761 (1966).

2. M. N. Lipsett, Biochem. & Biophys. Res. Comm., 20, 224 (1965); M. N. Lipsett, J. Biol. Chem., 240, 3975 (1965).

3. N. Brot, J. Goodwin, and H. M. Fales, Biochem. & Biophys. Res. Comm., 25, 454 (1966).

4. See S. C. Tsai, J. H. Herndon, Jr., B. W. Uhlendorf, H. M. Fales, C. E. Mize, and D. Steinberg, Biochem. & Biophys. Res. Comm., 28, 571 (1967) for leading references and D. Steinberg for future articles.

5. H. M. Fales, M. Greifner, D. Steinberg, and G. W. A. Milne, Paper #115, Fifteenth Annual Conf. on Mass Spectroscopy, May 14, 1967, Denver, Colorado.

90. USE OF HIGH RESOLUTION MASS SPECTROMETRY IN DETERMINING

THE STRUCTURE OF A COMPLEX AND BIOLOGICALLY SIGNIFICANT ORGANIC COMPOUND

G. P. Arsenault

Department of Chemistry, Massachusetts Institute of Technology,
Cambridge, Massachusetts 02139

Compounds of biological interest are often isolated only in small amounts, in a somewhat impure state. Determining the structure of these compounds is further complicated if no precedent is available concerning the structure of compounds having similar biological activity. High resolution mass spectrometry is particularly useful at the early stage of investigations in which structure determination is hampered by any one of the above factors, that is, trace quantities, impurities or unknown class of compound. Our investigation of the structure of antheridiol illustrates the application of high resolution mass spectrometry to such problems.

Antheridiol initiates the sexual reproduction cycle in fungi of the genus Achlya. Although the existence of this compound was postulated by Raper in 1939[1], its isolation was not achieved until much later.[2] Other compounds with similar biological activity have been isolated[3] but their structures were still unknown at the start of our work on antheridiol. Because of the scarcity of material (about 1 mg. was isolated initially) a high resolution mass spectrum was taken, using a few micrograms of the crude substance.

The element map [4] of antheridiol showed the elemental composition to be $C_{29}H_{42}O_5$. In addition, the distribution of the elemental composition of the fragment ions was strongly suggestive of a steroid containing two oxygen functions and two double bonds in the steroid nucleus, the remaining 10 carbons and three oxygens representing a side chain at C-17. The position of the third oxygen atom was revealed by the fact that the most intense peak in the spectrum corresponded to $C_{22}H_{32}O_3$, suggesting C-22 as the point of attachment. Thus, a single element map was sufficient to suggest a working hypothesis which was the starting point for an efficient and systematic design of further experiments. Later work done on crude derivatives of antheridiol led to structure I being proposed for this compound.[5]

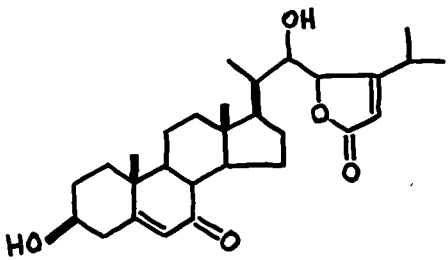

I

REFERENCES

1. J.R. Raper, Amer. J. Bot., 26, 639 (1939).

2. T.C. McMorris and A.W. Barksdale, Nature, 215, 321 (1967).

3. L. Machlis in "The Fungi", Vol. II, 415, G.C. Ainsworth and A.S. Sussman, Editors, Academic Press, New York, N.Y., 1966.

4. K. Biemann, P. Bommer, and D.M. Desiderio, Tetrahedron Letters, 1725 (1964).

5. G.P. Arsenault, K. Biemann, A.W. Barksdale, and T.C. McMorris, J. Am. Chem. Soc., in press.

91. The Effect of Halogens on the Ion Emission from a Hot Tungsten Filament

Kumasaburo Kodera, Isao Kusunoki and Hiroshi Kishi

(Department of Chemistry, Kyoto University, Kyoto, Japan)

INTRODUCTION

For the detection of alkaline atomic beam, a hot tungsten filament is usually used as a surface ionization detector. It was found that residual or background positive ion emission increased extraordinarily by exposing the filament to halide molecules. The purpose of this paper is to clarify the reason of this increase.

EXPERIMENTAL AND RESULTS

Tungsten filaments examined were a commercial doped filament and specially prepared undoped filament. Purity of the filaments were examined by a Mattauch-Herzog type double focussing mass spectrograph with a spark ion source. K, Na, Li, Al, Si, Fe, Ca, Ni, and Cr were found in both filaments. The difference between the two filaments was only the amount of impurities.

Total positive ion emission was measured by a diode tube with a doped filament at the center. After the filament was flashed under the vacuum of 10^{-6} torr, positive ion emission was measured at several temperatures above 1000°C. Then, chlorine gas was introduced to the pressure of $10^{-3} - 10^{-4}$ torr. At the instant of the introduction of the chlorine gas, positive ion emission was increased at once and then decreased rather rapidly but it did not go down to the original value. When the chlorine gas was pumped out the emission decreased again.

Species of the positive ions emitted from the filaments were examined by the same mass spectrograph using the filaments as surface ionization source. Main ions observed were K^+ and Na^+. In the atmosphere of chlorine K^+ and Na^+ were increased with Cr^+, Fe^+, and Ca^+ which were very small in vacua. Besides, Cl^+ and Cl_2^+ were also observed. With bromine similar phenomena were seen. Besides K^+ and Na^+, ions found were Al^+, Si^+, Cr^+, Mn^+, Fe^+, Co^+, and Ni^+. Br^+ and Br^{2+} were observed also but Br_2^+ was outside the range of observation.

Neutral molecules evaporated from the filament were examined by electron bombard method. A special ion source was not used for this

purpose. About 70 V was applied between the hot filament and the first slit of the mass spectrograph and electrons emitted from the filament itself were utilized to bombard the evaporated molecules. In the chlorine gas W^+, WO^+, WOH^+, WO_2^+, WCl^+, $WOCl^+$, WO_2Cl^+, WCl_2^+, $WOCl_2^+$, $WO_2Cl_2^+$, WCl_3^+, $(WO_2Cl_3^+?)$, WCl_4^+, WCl_5^+ were found. Similar results were obtained with the undoped filament.

CONCLUSION

From the above experiments it was concluded that, when chlorine was introduced around the filament, chlorine molecules reacted with the tungsten surface producing tungsten chlorides and oxychlorides. Evaporation of the products brought about the emission of alkaline ions which existed in the bulk of the tungsten metal. Instantaneous increase of positive ions after the introduction of chlorine is explained by the existance of a concentrated layer of alkaline ions under the surface. After the removal of this layer, the rate of positive ion emission is determined by the rate of corrosion of the tungsten surface. In vacua the rate determining process of positive ion emission is the rate of diffusion of positive ions in the tungsten metal.

The increase of work function of tungsten in the halogens cannot be considered as the reason of this increase, because ionization of potassium on clean tungsten surface is nearly complete and cannot increase hundreds times.

Cl^+, Cl_2^+, Br^+, and Br^{2+} found in the case of surface ionization may be produced by bombardment of surrounding halogen molecules by K^+ and Na^+.

This work will be published in Bull. Chem. Soc., Japan.

92. MASS MARKER FOR MAGNETIC SECTOR MASS SPECTROMETERS

by A.E. Banner
GEC-AEI (Electronics) Limited
Scientific Apparatus Division
Barton Dock Road, Urmston,
Manchester, England.

A description is given of a mass marker system designed for use with magnetic scanning mass spectrometers. The basic principle involved is the fundamental law of electromagnetic induction, and a novel integrating technique is employed. An output signal is provided for marking the recorder chart or magnetic tape record every 5 mass numbers, with a larger signal every 20. A digital display using four neon indicating tabes is also provided, the resolution being 0.1 atomic mass units. Calibration of the unit against a reference sample takes only a few minutes.

A mass range of 50 to greater than 900 can be covered with an accuracy of mass indication of ± 0.4 a.m.u., and scan times down to 5 seconds for a factor of 10 in mass can be followed. Results obtained from the mass marker with an AEI MS9 and an MS12 are presented. The drift of the system over five hours was within ± 0.2 a.m.u.

1. Introduction

For some time, mass spectrometry has been generally acknowledged as one of the most powerful analytical techniques. It is, of course, basic to the system to assign to each spectrum peak its mass number, or m/e ratio. The original method of counting the peaks from a known starting point is very time consuming, and in many cases, where large gaps occur between groups of peaks, liable to serious error. With recent developments such as continuous, direct sampling from a gas chromatograph, and fast scanning and recording of the resulting mass spectra, the high rate of information output now attainable demands some automatic means of marking the spectra every few mass numbers.

2. Requirements of a Mass Marker

(a) Accuracy

The consideration of prime importance in the design of a mass marker is that it shall be capable of providing unambiguous knowledge of the mass number of any peak within the range of the mass spectrometer. It is, therefore, necessary for the system to be accurate to ± 0.4 atomic mass units, over the whole mass range.

(b) Stability

The system should be able to maintain this accuracy for as long as possible after calibration against a reference compound. It is considered desirable to calibrate only once or twice a day. The mass marker must also correct for variations in the ion accelerating voltage or electrostatic analyser voltage, for single - and double-focusing instruments respectively.

(c) Fast Scanning

The accuracy of marking must be maintained under the fast scanning conditions imposed by the combination of a mass spectrometer with a gas chromatograph. In general the maximum mass number in such cases will be approximately m/e 600.

(d) Visual Display

Some means of visual display of the mass number must be provided, both to facilitate calibration and, in general, to assist in peak finding.

3. Traditional Methods

Various methods of magnetic field sensing have been tried by other workers. Tromp and Wijhbergen (1967) measured the magnetic induction indirectly by means of the current in the magnet coils, but found that this current had to be automatically programmed before each measurement in order to overcome hysteresis effects.

Two of the most important methods depend upon the Hall plate and rotating coil, the present limit of accuracy in both cases being about 0.01%, which is necessary for mass marking purposes, but they both suffer from the disadvantage of sensing the magnetic field over a very small area. Thus, although the sensors may well be linear with the field traversing them, they are unable to take account of changing inhomogeneities in magnetic field which may easily occur along the path followed by the ions, particularly under fast scanning conditions when eddy currents induced in the magnet pole pieces become significant. The combined system is, therefore, liable to non-linearity.

The Hall plate also has the disadvantage of being temperature dependent, and it is necessary to provide either a means of maintaining a constant temperature at the probe itself, within the magnet, or a probe temperature sensing element and temperature compensation.

The rotating coil is not temperature dependent, but is by no means ideal for fast scanning work, which would require an exceptionally high speed of rotation. Thus, assuming the coil to be a single-plane multi-turn winding, the required speed to give ± 0.4 a.m.u. accuracy at m/e 1000 on a 5 second scan for a decade in mass would be 30,000 revs/minute.

4. Instrumental

(a) The System

In order to avoid these disadvantages, a different method has been employed in the AEI "Massmaster", depending for its operation on the fundamental law of electromagnetic induction. A large area coil, specially shaped to follow the ion path, is fitted to the analyser tube. It does not rotate or vibrate, but simply gives an output e.m.f. when the magnetic flux linked with it is changed.

The associated induced current is integrated by means of a high quality operational amplifier and capacitor, and the output voltage from the integrator is proportional to the change of magnetic flux. It is independent of the time taken to change the flux. This output voltage is added to a fixed potential, which is adjusted to the required value by calibrating the system against a reference compound. As seen in figure 1, the resulting voltage, which is then proportional to the magnetic field, H, is applied to the input of a Squaring Circuit. Another input, a potential $V_{Acc.}$, proportional to the accelerating voltage, is also applied to the Squaring Circuit, the output of which is then proportional to $H^2/V_{Acc.}$, and, therefore, to m/e. This signal is examined by a special form of built-in potentiometric digital voltmeter, giving a four digit visual display (maximum mass 999.9) and driving a galvanometer in the recorder to give marks every five mass numbers (e.g. m/e 10, 15, 20, 25 .....) Double size marks occur at every even twenty mass numbers (e.g. m/e 20, 40, 60, 80 .....), and a unique treble size mark

is provided at m/e 200 to serve as a "landmark" in the spectrum. Setting-up of the equipment is made very easy by means of the built-in test circuit.

(b) Flux Integrator

The flux integrator is shown schematically in simplified form in figure 2. The fixed search coil is connected through the integrating resistor R to the input of a high gain operational amplifier, which has extremely low drift characteristics. The balance control enables the drift of the integrator to be reduced to a very low value (equivalent to about 0.07 a.m.u. per hour or better). The dielectric of the integrating capacitor, C, is P.T.F.E., and has a suitably low absorption coefficient (0.01%), and a very high insulation resistance (the time constant being greater than 250,000 seconds). Nevertheless, the electrical leakage of the capacitor is typically 100 times worse than can be tolerated, and a method of correcting for the resulting errors is necessary. This is achieved by means of a special circuit connected to a compensation control on the front panel of the unit.

In operation, the magnetic field of the mass spectrometer is set so that a suitable reference peak at about m/e 500 is tuned in at the collector. The integrating capacitor, C, is shorted out by means of a high insulation resistance relay, (so making $\Delta H = 0$), and a calibration potentiometer on the front panel of the unit is adjusted to give the correct mass number on the neon indicating tube four digit visual display. The mass spectrometer is then tuned to another suitable reference peak at a low mass number (m/e approximately 70), and a gain control on the front panel is set to give the correct display. Accurate operation is attained at high molecular weight (up to 800 and 950 with the MS12 and MS9, respectively) with the aid of two preset potentiometers, which are adjusted by means of a suitable reference compound.

(c) Squaring Circuit

A special circuit has been devized, which, in its general form, acts as an analogue multiplier/divider, performing the operation xy/z. In the Massmaster, the potential proportional to H, from the Flux Integrator circuit, is applied to both x and y, and the attenuated accelerating voltage $V_{Acc.}$ is applied to z. The circuit, therefore, determines $H^2/V_{Acc.}$, which is proportional to m/e.

The maximum error of the Squaring Circuit can be made as small as ± 0.1 a.m.u. from m/e 1000 to m/e 10, for variations of magnetic field, or ± 0.2 a.m.u. from m/e 500 to m/e 1000 for variations of accelerating voltage.

(d) The Marker and Indicator Unit

As shown in figure 3, the output signal proportional to mass number obtained from the Squaring Circuit is applied to the input of a comparator circuit. The other input is connected to a tapping point on a precision resistor chain fed by a reference voltage, the individual resistors being switched by associated high speed reed relays. The required switching sequence is obtained by means of two reversible decade counters which drive the relays, and suitable decoding circuits operate the first two neon indicating tubes.

The resistor values are arranged so that the resistor chain output voltage changes in steps of 5 atomic mass units, and in operation the comparator output is, therefore, equivalent to between 0 and 5 a.m.u. This analogue signal is applied to an analogue-to-digital converter, the output of which drives the third and fourth neon tubes.

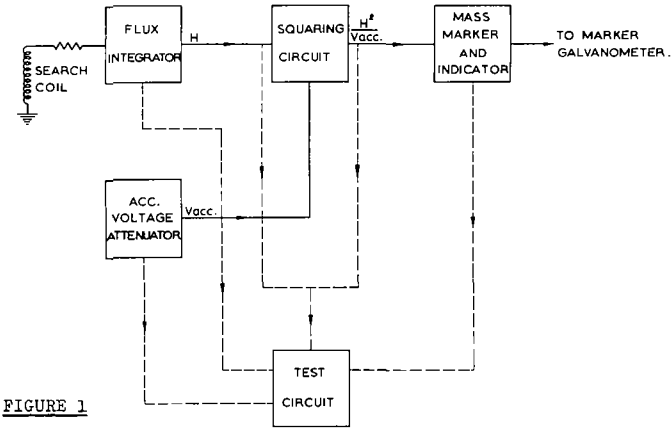

FIGURE 1

BLOCK SCHEMATIC OF MASSMASTER

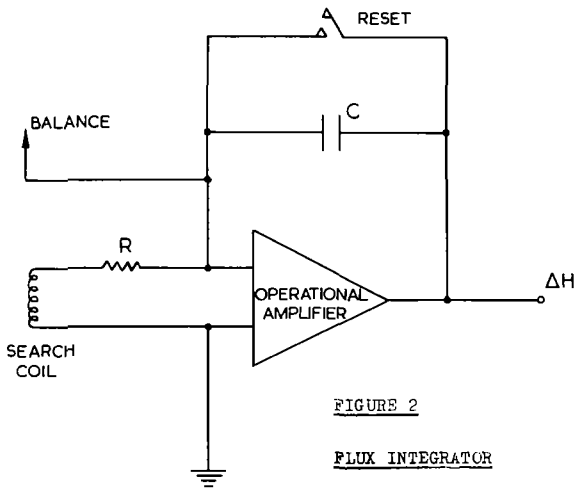

FIGURE 2

FLUX INTEGRATOR

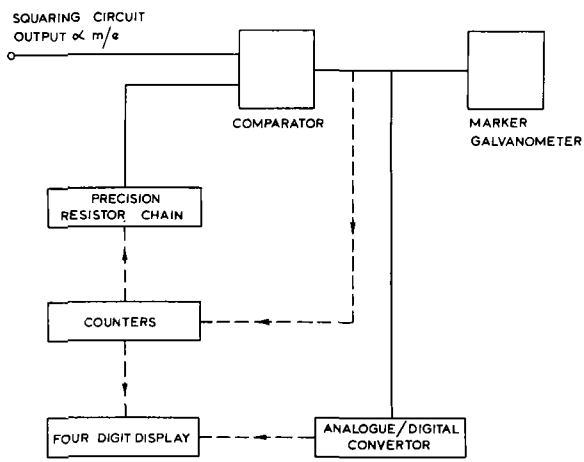

FIGURE 3

MARKER AND INDICATOR UNIT

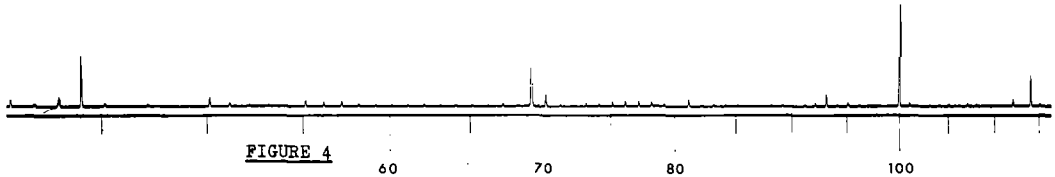

FIGURE 4

LOW MASS PORTION OF SPECTRUM, AT 8 SECONDS/DECADE

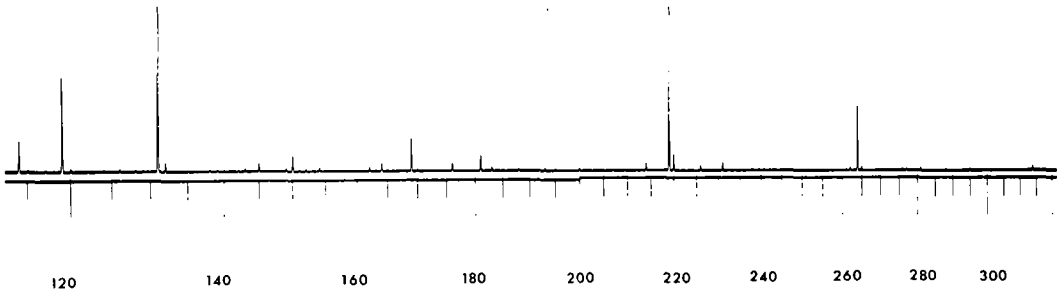

FIGURE 5

CENTRE PORTION OF SPECTRUM, AT 8 SECONDS/DECADE

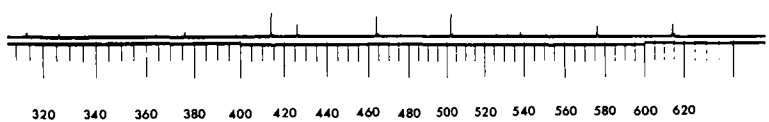

FIGURE 6

HIGH MASS PORTION OF SPECTRUM, AT 8 SECONDS/DECADE

Under scanning conditions, when the two inputs to the comparator pass through parity, an output pulse from the comparator is applied to the marking galvanometer in the recorder of the mass spectrometer, and another pulse is simultaneously fed into the decade counters, so causing the resistor chain to be switched to the next 5 a.m.u. step. The relays operate in less than 2ms, and the system is, therefore, readily able to follow a scan of 5 seconds per mass decade from m/e 1000 to 100.

5. Results

(a) Accuracy

The accuracy of the AEI Massmaster with the MS12, under static conditions, is ± 0.4 a.m.u. from m/e 70 to 800. With the MS9, this accuracy is extended up to m/e 950.

Typical sets of results with the MS12 are shown in Table 1, the reference samples being heptacosafluorotributylamine and a fluorinated phosphorus-nitrogen heterocyclic compound of molecular weight 972. It is clear that the Massmaster errors (true-indicated reading) are all less than ± 0.4 a.m.u.

Moreover, it is observed that the general trend of the errors with a particular set of equipment is characteristic of the system. Thus, for example, the error in the m/e 264 to 376 region is repeatedly found to be approximately -0.2 a.m.u. Clearly, it is possible to allow for this characteristic trend, so permitting even higher inherent accuracy than ± 0.4 a.m.u. to be obtained.

(b) Stability

With the balance and compensation controls correctly adjusted, which is a very simple matter by virtue of the built-in test circuit, the drift of the Massmaster is sufficiently small to allow unambiguous peak identification for about 5 hours after calibration with the mass spectrometer and reference compound. (The calibration process takes only about five minutes). Table 2 shows the drift at the calibration peak, which in this case was m/e 502.

Normal variations of the accelerating voltage are fully corrected by the Squaring Circuit

(c) Fast Scanning Performance

On scans of 5 seconds per mass decade from m/e 600, the accuracy of marking of the recorded spectrum is better than ± 0.4 a.m.u. Figures 4, 5 and 6 show various parts of the same spectrum of heptacosafluorotributylamine, taken at 8 seconds per mass decade with an AEI MS9. Figures 7, 8 and 9 show the regions at m/e 119, 219 and 464 in greater detail, from the same scan. The marking accuracy may be readily judged, since the mass deficiency of this reference compound is only about 0.04 a.m.u. at m/e 614, 0.02 a.m.u. at m/e 414 and 0.01 a.m.u. at m/e 100.

(d) High Mass Performance on Scan

The spectrum shown in figure 10 is the high mass end of an 8 second per mass decade scan, taken with an MS9 and the fluorinated phosphorus-nitrogen heterocyclic reference sample of molecular weight 972. The mass deficiency of this compound is approximately 0.05 a.m.u. at m/e 972 and 0.06 a.m.u. at m/e 791.

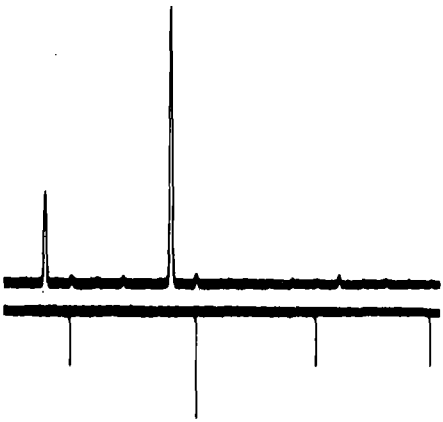

FIGURE 7

ENLARGED VIEW OF M/E 119 REGION

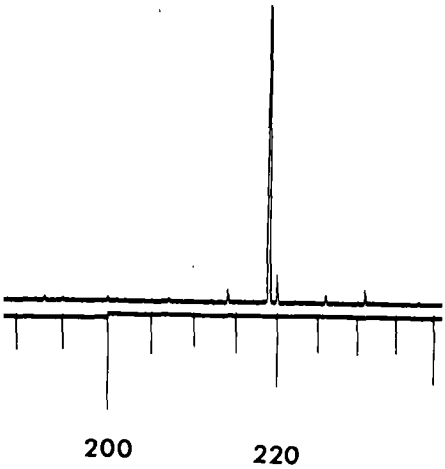

FIGURE 8

ENLARGED VIEW OF M/E 219 REGION

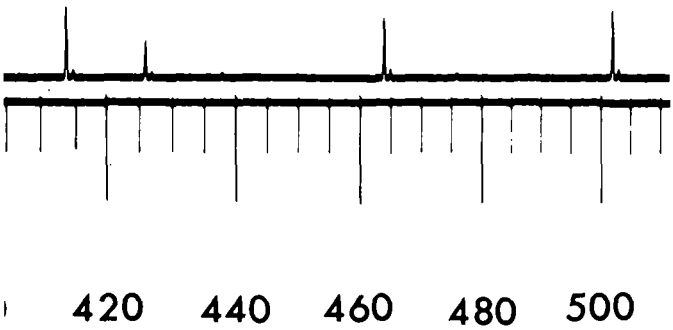

FIGURE 9

ENLARGED VIEW OF M/E 464 REGION

TABLE 1

STATIC LINEARITY OF MASSMASTER WITH MS12

HIGH MASS PERFORMANCE		LOW MASS PERFORMANCE	
m/e (a.m.u)	MASSMASTER ERROR (a.m.u)	m/e (a.m.u)	MASSMASTER ERROR (a.m.u)
873	+0.2	502	0.0
791	-0.2	414	-0.1
691	-0.3	376	-0.2
630	0.0	264	-0.2
530	+0.2	219	-0.1
		131	-0.1
		50	+0.1

TABLE 2 STABILITY OF MASSMASTER

TIME (HOURS)	MASSMASTER DRIFT (A. M. U.)
0.0	0.0
0.7	-0.1
1.3	0.0
1.8	+0.1
3.8	0.0
4.2	+0.1
4.7	+0.2
5.2	+0.2

Acknowledgements

This paper is published with the permission of Dr. J.D. Waldron, Director and General Manager of Scientific Apparatus Division, G.E.C.-A.E.I. (Electronics) Limited.

The author wishes to thank is colleagues for their help and encouragement, and in particular, he is extremely grateful to Mr. C. Cannon-Brookes, whose very active assistance and many helpful suggestions were greatly appreciated.

Reference

TROMP, F.M. and WIJNBERGEN, J.J. 1967, J. Sci. Instrum., 44, 209-11.

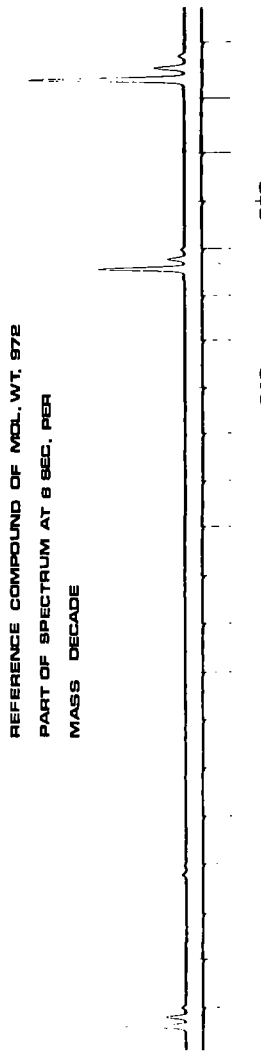

FIGURE 10

HIGH MASS PORTION OF REFERENCE SAMPLE OF M.W. 972, AT 8 SECONDS/DECADE

33. A PROBLEM IN STUDIES RELATED TO MASS SPECTROMETRY: SURFACE CHARGES

Y. Petit-Clerc et J.D. Carette
Centre de Recherche sur les Atomes et Molécules
Université Laval, CARDE, Québec

The purpose of this paper is to summarize what has been done on the subject of surface charges, in the laboratories of CRAM at Laval.

It has been found that local changes in surface potential induced by incident electrons or ions on a metallic surface in high vacuum are large enough to cause difficulties in many measurements. For instance, measurements of the ionization efficiency by electron impact of various gases, specially near threshold, have certainly been strongly influenced in the past by surface charges.

The apparatus used has been described earlier[1,2] and it consists essentially in a continously recording Kelvin probe used to observe the surface potential along a circumference of a disc after one spot has been exposed to an electron or an ion bombardment.

On figure 1, the first trace represents the surface potential along a circumference on an aluminum disc before any bombardment. The zero on the scale is, of course, arbitrary. The second trace has been registrated after one spot has been bombarded for few minutes. The surface potential was recorded immediatly after. We can see the negative valley obtained only at the bombarded spot.

The results on the drawing of figure 2 show typical negative valleys produced by electrons for various energies of the incident beam. As may be seen, the energy of incident electrons influence the magnitude of the charge.

Other parameters affecting the magnitude of the charge are the time during which the surface is exposed, the current density, the temperature of the surface and the vacuum system itself. In fact the charge is built up on a dielectric which is formed under the bombardment itself. In any usual vacuum system, there are organic contaminant vapors coming from pump oils or organic gaskets.

The monolayer or few monolayers adsorbed on the surface is probably not very important however. What makes the contaminants undesirable is the fact that organic molecules are cross linked by the incident electron or ion beam and they stay on the surface to form a dielectric film which is continously growing at each bombardment.

The drawing of figure 3 shows the effect of an ionic bombardment on the potential of a point of the circumference on stainless steel disc. The behaviour of the charge for ions is very similar to the one observed with electrons. The energy dependence is different however, the magnitude of the peak is independant of the ion energy in the range of 25 to 400 eV. Below 25 eV it decreases. In the case of electrons, it increases at lower energies and has a maximum around 5 eV.

Once formed a peak decays quite rapidly at the beginning and much slowlier after few minutes. The decay is slowlier than exponential. The decay in case of ions has been studied. If one plots ΔV, the change in surface potential of the peak, as a function of time on a logarithmic scale, breaks in the curve are seen and are very neat. At room temperature with argon we have observed up to six breaks, the first one being at 50 sec. the second one at 200 sec., after that at 660, 1900, 5900, 13000 sec. Some of those breaks are shown at figure 4.

If one assumes that charges are produced in the film at discrete and equal distances from the metal lattice and that each layer is neutralized by tunnelling of electrons from the metal lattice to the various layers one can find that each layer is neutralized at a different speed and breaks are to be found in the decay curve. Since the time constants are very different from one another, those breaks are given, from the tunnel effect, by the equation $K_1 n e^{K_2 n}$ where n is the number of the layer. Now if two points are used to find the two constants K_1 and K_2 in the equation, we may predict the position of the following breaks. Some of them are indicated by the arrows on figure 4. One may see that this interpretation is in good agreement with measured values.

Surface charges are expected to be present in a very large number of apparatus. Every focusing or deflecting system is thus subject to misfunction to a certain extent. It seems useless to apply precise calculations to electron optical systems at low energy if surface charges change the surface potential by a large amount. As an example we have observed the splitting of an ion beam into two parts after a focusing grid was contaminated and charged.

Another example is the study of the ionization efficiency curves near

threshold. We have constructed an usual apparatus to measure the ionization efficiency of argon near threshold. It consists in a 127^{o} selector as electron source and an ion box. The back of the usual ion box which is the surface collecting electrons has been replaced by a cylinder which can be rotated to bring the surface to a Kelvin probe and also to bring a fresh surface at the back of the ionization chamber. Even with the very low current density found is this apparatus, we have observed a quick contamination and the ionization curve is very different when the surface is fresh or contaminated. It seems that many fine structures attributed to the gaz itself may be a surface effect. One solution to the problem would be to use a dry ultra high vacuum system.

Moreover we have observed that an oxyde layer may contribute to the charging of a surface. So even in a baked out UH vacuum system, oxyded surfaces are to be avoided. However such a system is not always usable for a particular experiment. Then the only solution is to focalise charged particules is such a way they don't strike critical surfaces. A frequent cleaning is a must since it takes few hours to contaminate a surface and charge it a 1/2 volt for a current density of about 10^{-11} amp/mm^{2}. Another way to get rid of the problems caused by charged surfaces is to heat these surfaces as we have already demonstrated it[3], and keep them hot during measurements.

1.- Y. Petit-Clerc and J.D. Carette, Vacuum, 18, 7 (1968)

2.- Y. Petit-Clerc and J.D. Carette, Rev. Sci. Instr. 39, 933 (1968)

3.- Y. Petit-Clerc and J.D. Carette, App. Phys. Lett. 12, 227 (1968)

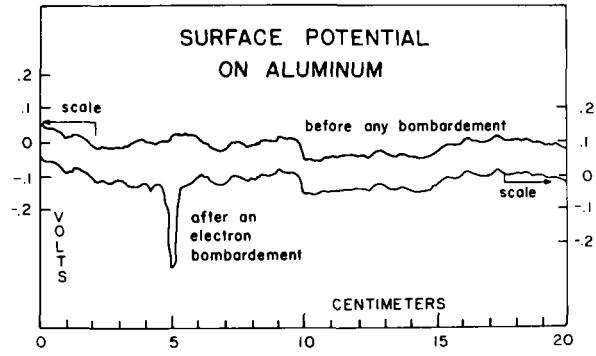

FIGURE 1

Potential along a circumference on an aluminum disc. a) before any bombardment, b) after one point of the circumference has been bombarded with a electron beam.

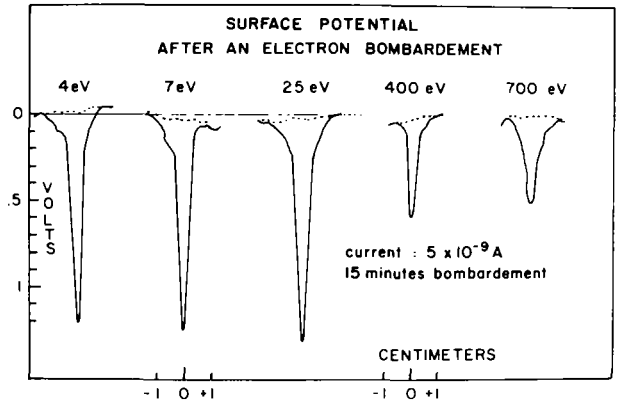

FIGURE 2

The intensity of the induced negative charges by an electron beam as a function of electron incident energy.

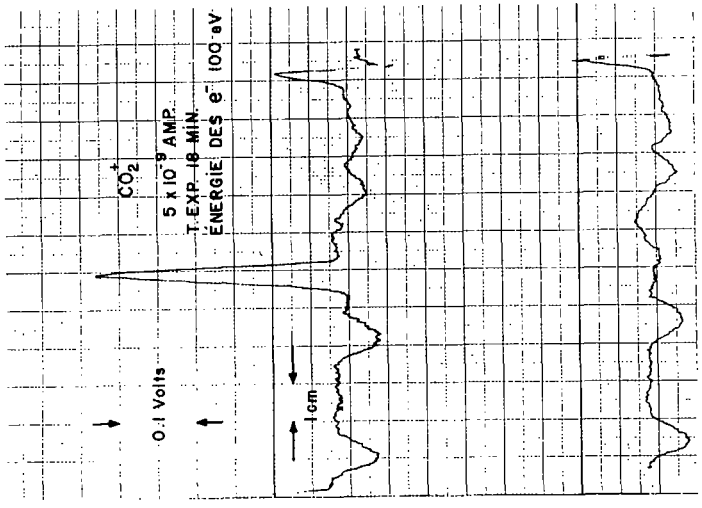

FIGURE 3

The direct recorder trace of the surface potential along a circumference on an stainless steel disc. a) before any bombardment; b) after one point of the circumference has been exposed to an ion beam.

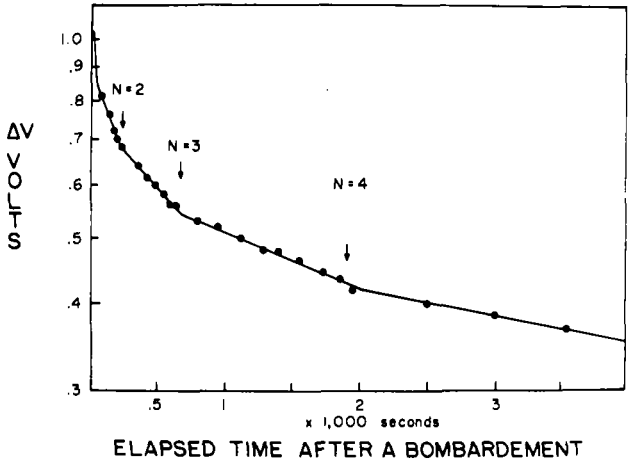

FIGURE 4

Amplitude of a positive peak, once formed, as a function of time.

94. COMPARISON OF QUADRUPOLES WITH ROUND AND HYPERBOLIC SURFACES*

W. M. Brubaker and W. S. Chamberlin

Bell & Howell Research Center
Pasadena, California **

INTRODUCTION

The formal theory of the operation of the quadrupole mass filter assumes that the equipotential surfaces are hyperbolic. However, almost all of the many quadrupole instruments in use have field-forming surfaces which are circular in cross section. This substitution of round for hyperbolic rods obviously is a compromise.

The object of this study is the evaluation of the price which is paid in the performance of the quadrupole by the use of round instead of hyperbolic rods. A computer is used to determine the perturbations in the electric fields which result from the use of the round rods. Selected trajectories are computed for normal and perturbed fields, and the differences noted. Experiments are made with two quadrupole units which differ only in the shape of the rods (round and hyperbolic). The experiments confirm the calculations. The performance of the quadrupole with hyperbolic rods is very significantly superior to that of the quadrupole with the round rods.

COMPUTER STUDIES

The computer was used to determine the equipotential surfaces when the radius of the round rods is 16 percent greater than the instrument radius, r_o. From a knowledge of the potentials, the fields were evaluated.

A few selected trajectories were computed for ions injected radially into fields which result from hyperbolic rods and from round rods. The perturbations in the fields caused by the use of round rods have a very pronounced influence on the ionic trajectories, particularly at the higher resolving powers. In general, the magnitude of the perturbations is very small in the vicinity of the instrument axis, but it becomes large at greater distances from the axis. These larger perturbations cause the trajectory to become unstable. Thus, the ions reach a point-of-no-return and proceed to the rods. This phenomenon reduces the effective size of the quadrupole. As the resolving power is increased, the effective dimensions continue to contract.

APPARATUS

Two quadrupole units were assembled. They differ only in the contours of the rods. These units are mounted symmetrically on a common vacuum system. They are energized in parallel from a common oscillator and dc power supply. The instrument radius, r_o, is 0.66 cm and the rod length is 25 cm. An insulated segment at the ion entrance end of each rod permits

---

*This research was supported in whole or in part by the National Aeronautics and Space Administration under Contract No. NASW-1298, monitored by Dr. Donald P. Easter.

**Present Address: Earth Sciences, A Teledyne Company, Pasadena, California.

operation of the units in the delayed dc mode[1] in which the segments are energized with ac voltages only. Excitation frequencies of 0.7, 1.0 and 1.4 MHz were used.

EXPERIMENTAL DATA

When the quadrupole is operated in the delayed dc ramp mode, the transmission efficiency is high for ions which are incident at low as well as high velocities. This circumstance leads to high resolving power capabilities because the low velocity ions spend more time within the quadrupole.

Krypton gas was used to display the resolving power capabilities of the two quadrupole mass filters. Sensitivity of the units was explored as functions of resolving power, ion injection energy, power and excitation frequency. A general conclusion which may be drawn from these data is that the resolving power of the hyperbolic unit is about twice that of the round when the operating conditions are identical for both and the transmission efficiency is less than 100 percent.

Of particular interest is the set of data which relates the sensitivity to the resolving power for low (one volt) ion injection energy when the frequency is varied. The most striking feature of these data is the observation that the hyperbolic unit excited at 0.7 MHz outperforms the round when the excitation frequency is 1.4 MHz! The rate at which power is dissipated in the tank coil which resonates the capacitance of the quadrupole varies as the excitation frequency to the fifth power. And 2^5 is 32!

The resolving power capabilities of the hyperbolic unit when the excitation frequency is 1.4 MHz and the ion injection energy is one volt is of particular interest. Flat topped peaks of krypton isotopes are obtained at a resolving power of 400, as calculated at 10 percent of the peak height. At 50 percent transmission, it is 850 and at 25 percent, it is 975.

CONCLUSIONS

The deterioration in the performance of the quadrupole mass spectrometer which results from the use of round instead of hyperbolic rods is quite appreciable. Computer studies of ionic trajectories in the perturbed fields (produced by round rods) demonstrate that ions reach a point-of-no-return before they come close to the rods. As the resolving power is raised, this point becomes closer to the axis. Thus, it is apparent that the effective radius of the quadrupole is considerably smaller than the actual radius when the field-forming surfaces are round rods.

The use of hyperbolic rods is of particular importance on instruments to be used in the space program because equivalent performance is obtainable in an instrument of smaller size operated at greatly reduced power.

---

[1] "Improved Quadrupole," presented at the International Mass Spectrometry Conference in Berlin, September, 1967, and published in "Advances in Mass Spectrometry," Vol. 4.

95. ION SAMPLING FROM SUPERSONIC GAS STREAMS*

by Rudolf R. Burke

AeroChem Research Laboratories, Inc.

Princeton, New Jersey

a subsidiary of Ritter Pfaudler Corporation

INTRODUCTION

Rocket-borne mass spectrometers[1] are the major tool for determining the ion composition of the lower ionosphere (50 to 80 km altitude). A rocket flying at supersonic speed through these relatively dense regions (1 to 10^{-3} Torr) sets up a shock wave, thus aggravating the difficulties associated with any technique for species sampling. Laboratory experiments are required to determine the nature and magnitude of these problems. In the present work positive and negative ion sampling from supersonic streams is explored, using both conical and blunt-faced inlet sampling systems. The sampled ions are identified with the aid of a quadrupole mass filter.

The conical inlet configuration is so designed as to penetrate or attach the shock wave, thus allowing direct undisturbed sampling of ions from the supersonic stream. The other sampling system consists of an orifice in a flat plate; with this configuration, the sample is obtained from the subsonic gas stream behind the bow shock wave. The results obtained from the two sampling configurations are compared in order to establish the relationships between charged species concentrations in the ambient stream and those apparent from mass spectra taken behind the shock. The results appear to be consistent with a recombination-dominated ion loss mechanism in the post-shock region, accompanied by electron attachment to produce increased concentrations of negative ions.

APPARATUS

A schematic of the experimental apparatus used in the present study is shown in Fig. 1. Supersonic streams of partially ionized gases are produced in a plasma generator, which has been described previously.[2,3] In the reservoir section of this facility, the working fluid (nitrogen or oxygen) is passed through a high pressure (10 to 30 Torr) glow discharge maintained between a copper electrode (cathode) and an outlet nozzle (anode). The plasma is then expanded through the nozzle, which is contoured to produce a shock-free Mach ~3 free jet. The discharge voltage is typically 1200 V; currents range from 0.18 to 0.6 A. Static pressures in the free jet range from 0.4 to 1.1 Torr.

Gas is sampled from the plasma jet with either the conical sampling probe or the sampling probe consisting of an orifice in a flat plate. Ion collection is achieved by biasing the probes at -30 V and + 2.5 V (for positive and negative ions, respectively). The separation of the ions from neutrals and their transfer to the analyzer is achieved by an ion lens system positioned in the extraction chamber. The ions are analyzed according to their mass-to-charge ratio in a quadrupole mass filter. The mass filter may also be operated without mass discrimination; it then transmits the total ion current. The ions which pass through the mass filter are detected with a Bendix magnetic electron multiplier. Electrons are not detected since the fringing magnetic field of the multiplier is strong enough to deflect them from the cathode.

* This research was sponsored by but does not necessarily constitute the opinion of the Air Force Systems Command and the Air Force Cambridge Research Laboratories, Office of Aerospace Research, under Contract No. F19628-67-C-0325. Funding for this research was supplied by DASA under Subtask No. 11BHAX 504 (07.504).

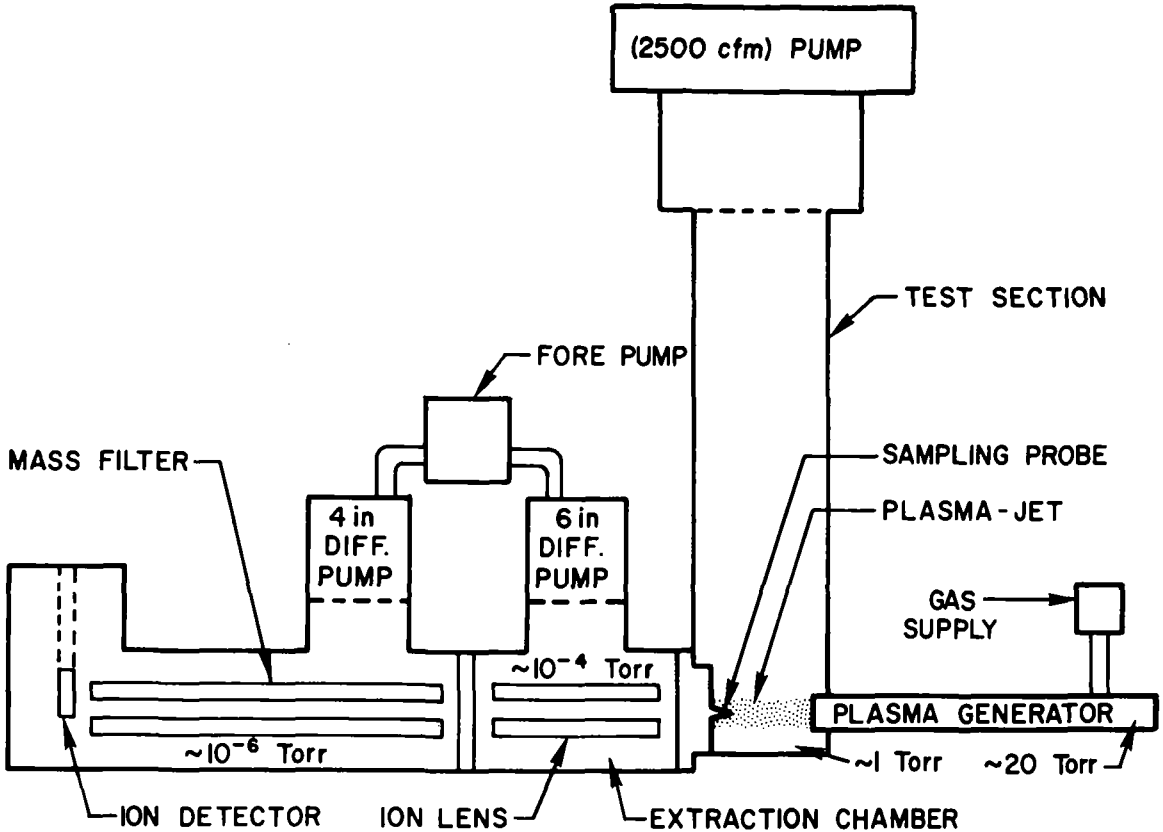

FIG. 1 BLOCK DIAGRAM OF APPARATUS FOR THE STUDY OF MASS SPECTROMETRIC ION SAMPLING PROCESSES

RESULTS AND DISCUSSION

The total and the mass-analyzed normalized ion currents observed (in coulombs per molecule sampled) in two typical experiments are reported in Tables I and II. An obvious feature of these results is the large decrease of total positive ion current and the increase of total negative ion current which occurs when the cone is replaced by the blunt-faced sampling probe.

If it is assumed that the positive ion current decrease is due entirely to recombination, it is possible to calculate an initial free jet ion concentration, n_+, which can then be compared with previous measurements in similar jets. Integration and rearrangement of the second order rate expression for recombination behind the shock yields the following equation

$$n_{+0} = \frac{1}{kt}\left(\frac{n_{+0}}{n_{+t}} - 1\right)$$

in which n_{+0} is the post-shock ion concentration and n_{+t} is the ion concentration after the decay time t. By making use of the relations $n_{+0}/\rho_0 = n_+/\rho$ and $n_{+0}/n_{+t} = x_{+0}/x_{+t} = i_0/i_t$ (in which x_+ and i are ion mole fraction and normalized current, respectively), the above equation becomes

$$n_+ = \frac{1}{kt}\,\frac{\rho_0}{\rho}\left(\frac{i_0}{i_t} - 1\right)$$

Since t (flow time from shock to probe) and k (recombination coefficient) are known, it is thus possible to calculate n_+ from the observed positive ion responses of the two probes. For example, for the experiment for which the results are shown in Table I (with O_2^+ the dominant ion), this calculation (with $k = 2.2 \times 10^{-7}\,(T/300)^{-0.7}\,cm^3$ $molecule^{-1}\,sec^{-1}$ (ref. 4), T = 650K, t = 28μ sec and $\rho/\rho_0 = 3.5$*) gives $n_+ = 2\times10^{13} cm^{-3}$. The value of n_+ in plasma jets similar to ours has been previously reported[2] to range from 10^{12} to 10^{13} cm^{-3}. The effects of ion molecule reactions in the post-shock region are currently being examined.

The increase in negative ion concentration is very likely due to three-body electron attachment to O_2. This is indicated by the fact that in the experiment reported in Table II the total negative ion increase is almost entirely due to the increase in O_2^-. An analysis of the type applied above is much more complicated in this case since attachment is accompanied by recombination and it is therefore necessary to consider the several processes which are occurring simultaneously.

CONCLUSIONS

The results appear to indicate that in the post-shock region positive ions are destroyed by recombination processes, whereas negative ions are produced by electron attachment. Since the ion and electron densities in the D region are much lower than in the laboratory plasma jet, recombination and electron attachment processes can be expected to be much less significant for sampling into rocket-borne mass spectrometers in the D region.

REFERENCES

1. Narcisi, R.S. and Bailey, A.D., "Mass Spectrometric Measurements of Positive Ions at Altitudes from 64 to 112 Kilometers," J. Geophys. Res. 20, 3607 (1965).

2. Wilkinson, J.B., "Magnetohydrodynamic Effects on Stagnation-Point Heat Transfer from Partially-Ionized Nonequilibrium Gases in Supersonic Flow," Engineering Aspects of Magnetohydrodynamics, ed. Norman W. Mather and George W. Sutton (Gordon and Breach Science Publishers, New York, 1964), pp. 413-438.

* T, t and ρ/ρ_0 are calculated from shock flow equations.

3. Fontijn, A., Rosner, D.E. and Kurzius, S.C., "Chemical Scavenger Probe Studies of Atom and Excited Molecule Reactivity in Active Nitrogen from a Supersonic Stream," Can. J. Chem. 42, 2440 (1964).

4. Kasner, W.H. and Biondi, M.A., "Electron-Ion Recombination Studies in Oxygen," Bull. Am. Phys. Soc. 12, 218 (1967).

TABLE I

TOTAL AND MASS-ANALYZED NORMALIZED POSITIVE ION CURRENTS (coulomb molecule^{-1} × 10^{28}) IN A MACH 2.7 OXYGEN JET AT 0.46 TORR AND 285K*

Mass	Formula	Cone	Plate
Total		7.3 (+2)	3.6
19	H_3O^+	5.5 (-2)	
30	NO^+	4.0	3.0 (-1)
32	O_2^+	1.3 (+2)	5.2 (-1)
34	$(^{16}O\text{-}^{18}O)^+$	5.1 (-1)	
46	NO_2^+	9.2 (-2)	
63	$^{63}Cu^+$	1.0	1.4 (-1)
65	$^{65}Cu^+$	4.8 (-1)	6.8 (-2)
67		3 (-2)	

TABLE II

TOTAL AND MASS-ANALYZED NORMALIZED NEGATIVE ION CURRENTS (coulomb molecule^{-1} × 10^{28}) IN A MACH 2.9 OXYGEN JET AT 1 TORR AND 185K*

Mass	Formula	Cone	Plate
Total		9.8 (-1)	7.2
16	O^-	1.1 (-2)	2.7 (-1)
32	O_2^-	2.0 (-1)	9.8 (-1)
35	$^{35}Cl^-$	4 (-3)	5.6 (-2)
37	$^{37}Cl^-$		2.5 (-2)
46	NO_2^-		3.9 (-2)
48	O_3^-		2.8 (-2)

* Numbers in parentheses are powers of ten.

96. THREE DIMENSIONAL MASS SPECTROMETER DISPLAY

R. O. Engh and R. L. Sperling
Honeywell Corporate Research Center
Hopkins, Minnesota 55343

During the study of the behavior of a gas discharge device[1] it was desirable to observe the ionic composition, including impurities, under various operating conditions. Point-by-point plotting would have been excessively slow, so a technique of "3-D" oscillographic representation was adopted. In order to project the solid formed by a function of three variables, X, Y and Z on to the screen of an oscilloscope, the variables must be mixed and distributed between the X and Y deflections in the proper proportions. By changing the distribution, the image can be rotated and viewed from any aspect. This mixing of signals and the rotation of coordinates is ordinarily accomplished by circuits involving ganged sine-cosine potentiometers and phase inverters, that are fairly complex and quite expensive. However, using a circuit approximation reported by MacKay,[2] a very simple and inexpensive three-dimensional display circuit can be built. MacKay's sine-cosine approximation is shown in Fig. 1.

The potentiometer, with its sliding contact grounded, resolves the angle, θ, into components proportional to the sine and the cosine of the angle and multiplies the X and Y inputs by the appropriate trigonometric function. (θ is the fraction of the full rotation of the potentiometer times $\pi/2$, in other words, at full rotation $\cos \theta = 1$ occurs.) MacKay has shown that if R_s (including the source impedance) is 70% of R, the maximum deviation from the trigonometric function is less than 7%.

A 3-D display circuit adopted from MacKay's designs was built for the purposes of this study, the schematic for which is shown in Fig. 2. Its application is illustrated in the block diagram, Fig. 3. X, Y and Z are the three inputs; X and Y being generally the independent variables, in this case the raster signals; and Z being the dependent variable--the peak height. The viewing aspect is determined by potentiometers P_1 and P_2, which control horizontal and vertical rotation respectively.

The outputs, X_1 and X_2, supply signals to the horizontal differential preamplifier of the oscilloscope. Y goes to the vertical preamplifier. A Tektronix Type 536 XY oscilloscope is probably the best to use for this display, with the Type 502 nearly as good. These have the advantages of (1) large active screen area, (2) differential inputs available and (3) capability of intensity modulation--for retrace blanking and trace intensification where needed.

The raster, of course, is composed of the two sawtooth signals, one used to sweep the mass range of mass spectrometer, and the other, whatever parameter, generally in the source, that is under study. The two sweep rates should differ by a factor of 100 or more depending on the resolution desired. Which one is the fast one depends on the

[1] Ions Observed in Field-free Regions of Self-sustaining Discharges in Penning Mixtures-R. L. Sperling and R. O. Engh-This conference.

[2] MacKay, D.M. A Simple Multi-dimensional CRT Display Unit. Electronic Engineering 32 June 1960, pp. 344-347.

nature of the experiment. Interesting displays may be had by allowing the sweep generators to run free, but for greater precision and stability, a time mark generator was used to synchronize the sweeps. The time mark generator was also used to trigger pulse generators, whose output was used to brighten the trace at appropriate intervals, providing a precision reference grid. Gating signals from the sweep generators were also mixed in with the trace brightness input to provide retrace blanking for the X and Y signals. The display was improved by including some of the mass peak signal to brighten the tips of the peaks.

With suitably decreased sweep rates, an XY recorder may be used in place of the oscilloscope.

Examples are shown of photographs of several of the displays obtained during the gas discharge investigation using a 10 centimeter quadruple mass spectrometer, with a multiplier for detector. The system was unbaked. The details of the experiment and the interpretation are discussed in the reference paper.

The first slide shows the mass range from 10 to 30 being swept at the rate of 10 sweeps per second on the X axis. The extraction potential--the voltage used to draw ions out of the discharge through the gas to the aperture is swept along the Y axis. It can be seen that the various species appear at different voltages and grow at different rates.

In the second picture, the entire source, including the aperture is swept along the Y axis. Since all peaks begin at the same Y value (which is close to zero) it is apparent that all ions emerge from the aperture with very little energy.

The last picture shows the results of an attempt to determine whether ions of any species might persist for a detectable length of time after a pulsed discharge. The mass sweep on the X axis was the slow one; the fast Y sweep was triggered with each discharge pulse. No persistant ionization was apparent within the limitations of the equipment.

Other interesting displays might be obtained with conventional sources with a swept retardation potential analyzed performance or by sweeping the ionizing energy of the electrons to give a display of appearance potentials.

The main advantages of the system described are, the ability to survey a large area in the field of interest with a minimum of data taking, and as a graphic demonstration of the effects of such variables as appearance potentials.

APPROXIMATION FOR SINE - COSINE POTENTIOMETER

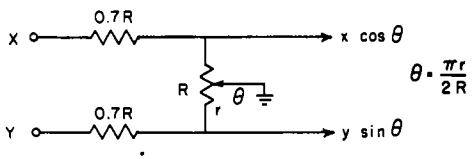

A SIMPLE MULTI-DIMENSIONAL CRT DISPLAY UNIT

D. M. McKAY
ELECTRONIC ENGINEERING 32
JUNE 1960 pp 344-347

FIG. 1

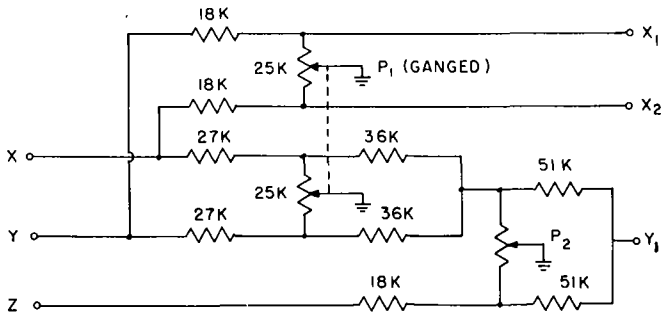

PROJECTIVE 3-D DISPLAY CIRCUIT

FIG. 2

BLOCK DIAGRAM FOR 3-D DISPLAY

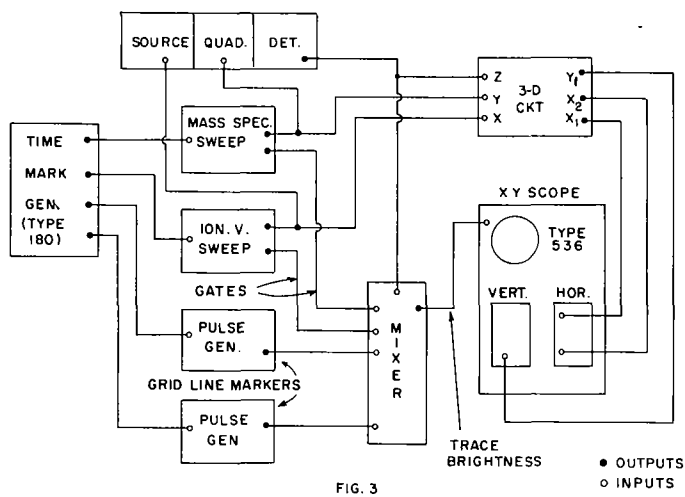

FIG. 3

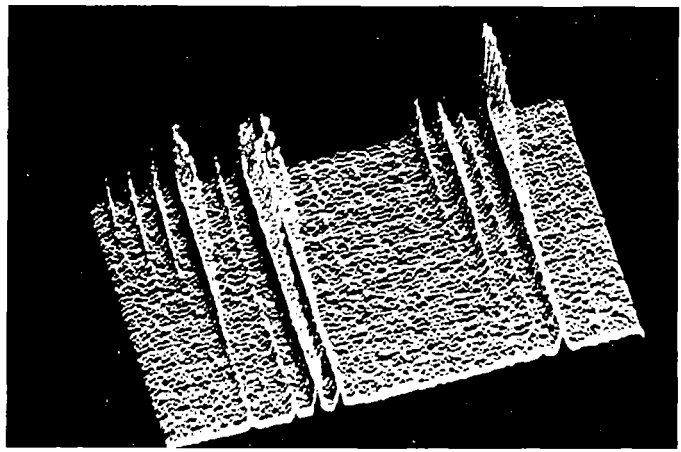

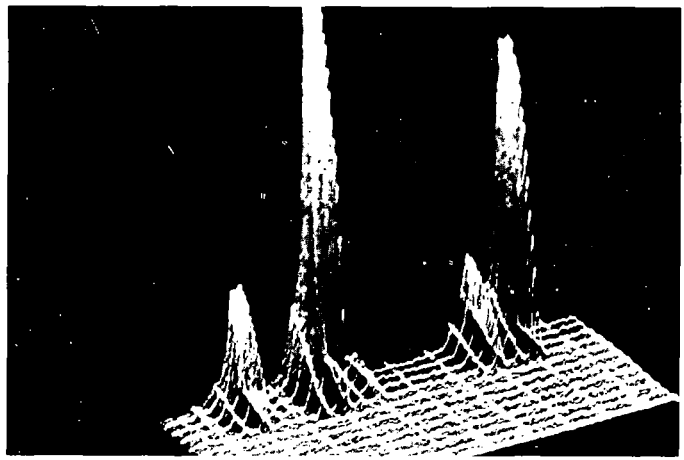

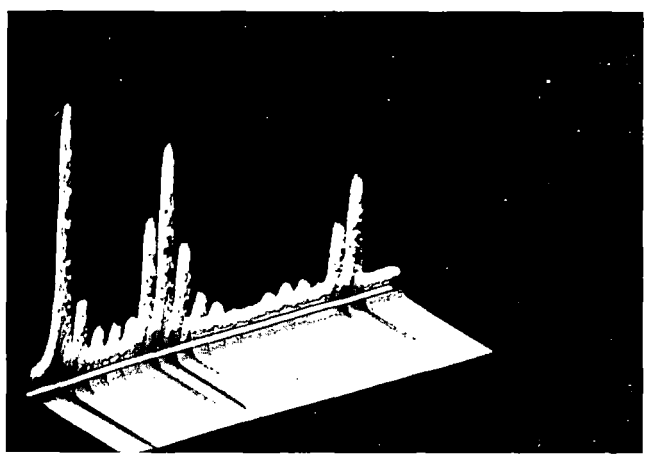

97. IONS OBSERVED IN RARE GAS-HYDROGEN DISCHARGES

R. L. Sperling and R. O. Engh

Honeywell Corporate Research Center
Hopkins, Minnesota 55343

SUMMARY

This work was undertaken to better understand the residual ionization decay processes occurring in discharges in mixtures predominantly composed of rare gases and hydrogen. A quadrupole mass spectrometer, simultaneous three parameter output display techniques, and suitable cathode-anode configuration were used for the analysis. The results have yielded descriptive classifications of the ionic content of these discharges as affected by gas composition and extraction field. Findings of particular interest are the presence of hydride peaks, their dependence on extraction fields, and the role of H_1^+ ions in the discharge.

PERFORATED CATHODE STUDY

The objectives of this study were to determine the species and energies of ions impacting on the cathode. The cathode was perforated to permit analysis of the ions in a differentially pumped quadrupole mass spectrometer chamber (see Fig. 1). Pressures were typically 20 to 40 Torr (inlet) and 10^{-4} to 10^{-5} Torr (quadrupole chamber). The composite spectra of observed ion species for mixtures of neon, helium, and argon with hydrogen was compiled (see Table I).

Retarding potential measurements were then employed to ascertain the energies of the impacting ions. The procedure was to raise or lower the source potential relative to the collector potential until the ion current was zero at which point the ions returned to the source. (Refer to Potential Profile Fig. 2) The retardation voltage curves for H_1^+ and Ne_{20}^+ are shown in Fig. 3.

The perforated cathode study has shown that:

a) the predominant ion in those rare gas-hydrogen mixtures we studied is H_1^+. The second most abundant ion is H_3^+ which could be regarded as the hydride ion of H_2,
b) H_1^+ does not charge exchange readily with H_2 molecules,
c) the hydrogen ion is the predominant current carrier,
d) Ne^+ suffers frequent charge exchange collisions,
e) residual impurities such as H_2O and N_2 lend themselves readily to hydride formation and
f) under certain conditions these hydride peaks (particularly H_3O^+ mass 19 and N_2H^+ mass 29) may be the most prominent feature of the mass spectrum.

EXTRACTION FIELD STUDY

The objective of this study was to determine if hydride ions were present in the low field region at an appreciable distance (.1875") behind the anode. The instrument shown in Fig. 4 was used with the aperture at a distance of .1875" from the anode. It is now required that a new parameter be included in the study - an extraction field or the potential difference between anode mesh electrode and aperture. With the introduction of a new parameter, very profitable use can be made of the 3-D display technique described in a companion paper.(1) By using the 3-D technique 8 seconds of successful running can allow information to be gathered over the whole range of the extraction field parameter.

To determine whether any ions having appreciable energy exit from the aperture, the potential profile condition of Fig. 5 was used. Both the source and aperture voltages were swept keeping the extraction field constant. Should ions of any appreciable energy exit from the aperture they would emerge prior to the aperture voltage reaching zero. Fig. 6 illustrates the results. Note that all ion peaks commence at the zero potential brightened trace. The effect of a slight potential "push" to ions by the aperture being biased even slightly positive is quite striking. The conclusions derived from this experiment are:

a) that all the ions exit by diffusion through the aperture, and
b) all ions suffer many charge transfer collisions enroute to the aperture. (Unlike the case of hydrogen in the earlier study.)

It must also be demonstrated that the detected ions are not formed on the analyzer side of the aperture such as the neon ions of the earlier study. For this experiment, the profile shown in Fig. 7 was used. The peak heights should diminish because the extraction field is decreasing as the scan progresses; however, throughout the scan the field is sufficient to ensure ions reaching the aperture. The results are shown in Fig. 8. If ions were formed on the analyzer side of the aperture, they could only be observed at a positive aperture bias. Peaks of this nature were not observed.

(1) "Three Dimensional Mass Spectrometer Display", R. O. Engh and R. L. Sperling

CATHODE STUDY - EQUIPMENT SCHEMATIC

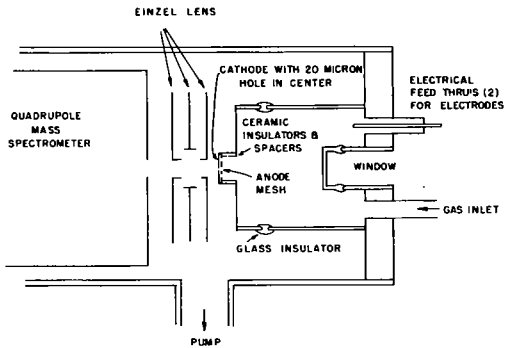

FIGURE 1

GENERAL POTENTIAL PROFILE - PERFORATED CATHODE STUDY

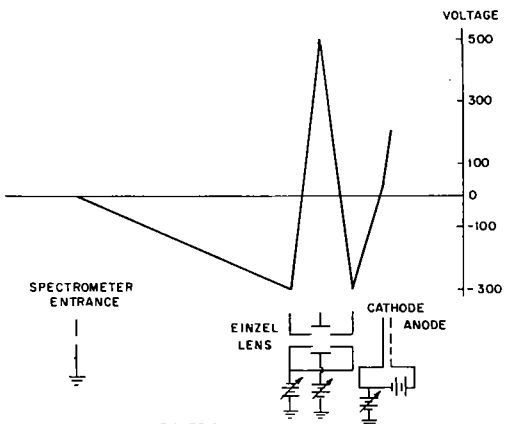

FIGURE 2

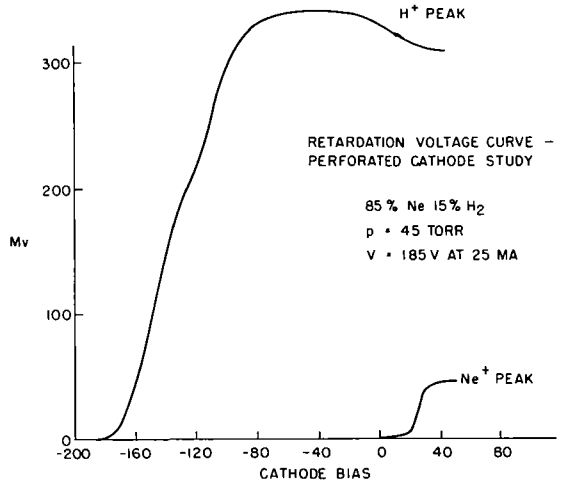

FIGURE 3

APPARATUS LAYOUT - EXTRACTION FIELD STUDY

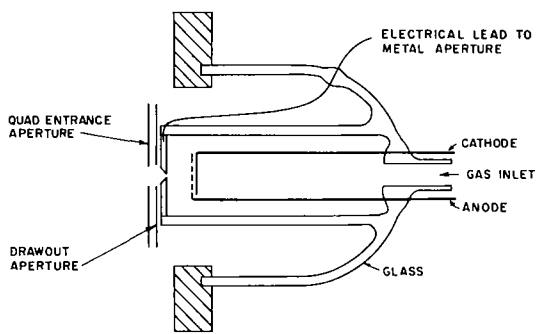

FIGURE 4

FIG. 5

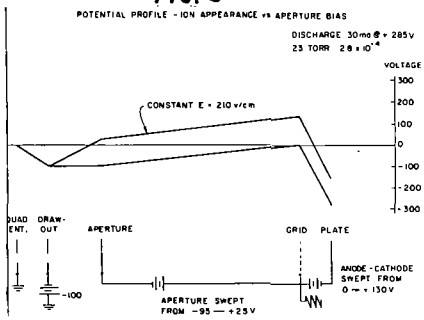

FIG. 6
ION EXIT ENERGY

FIG. 7

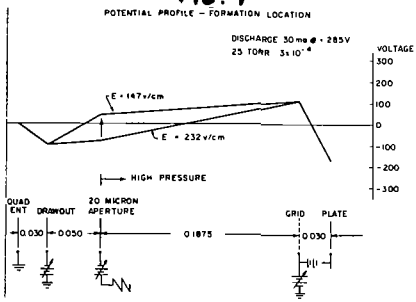

FIG, 8
FORMATION LOCATION

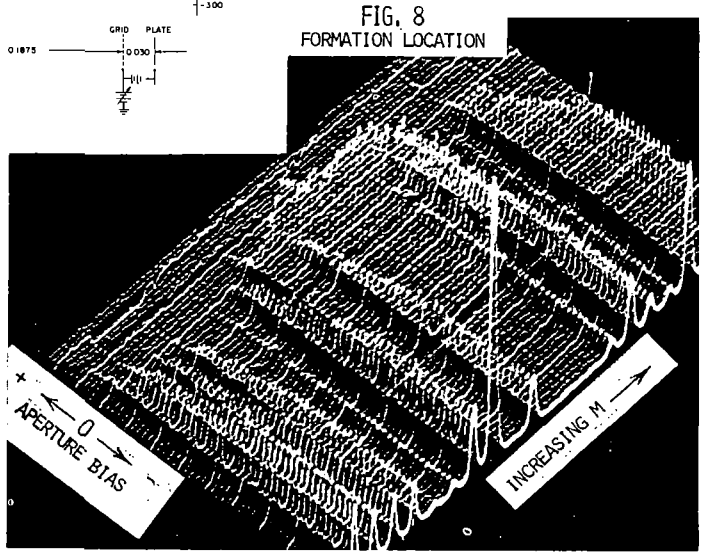

FIG. 9

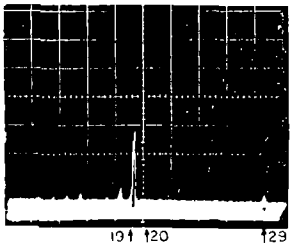

E = 157 VOLTS/CM

EFFECT OF EXTRACTION FIELD — MASS 10 → 29

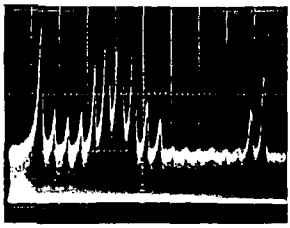

E = 250 VOLTS/CM

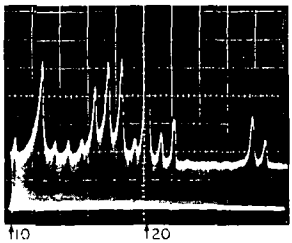

E = 380 VOLTS/CM

FIG. 10

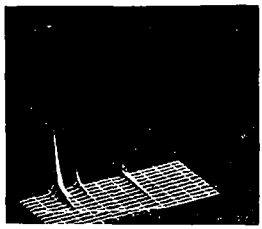

EFFECT OF EXTRACTION FIELD - MASS 1 → 5

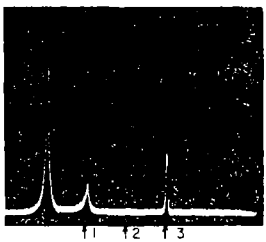

INCREASE E

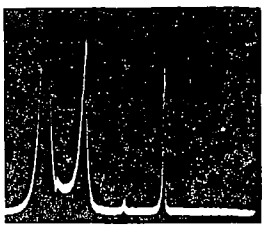

The Fig. 9 mass displays demonstrate the changes which occur in ion species with increased extraction field. The gas used was 15% H_2 85% N_e at 23 Torr. The discharge current was essentially the same for all three displays. Their respective extraction fields are shown to the right. The hydride peaks of mass 19 (H_3O^+) and mass 29 (N_2H^+) are dominant under low extraction fields. Other higher mass hydrides may be present but are beyond the mass range capability of the present quadrupole. As the extraction field increases, the 19 and 29 peaks diminish and other recessive peaks (in particular Ne_{20}^+) become dominant.

Fig. 10 illustrates the effect of increased extraction field on the low mass range 1 to 5. Notice the increase of H_1^+ over H_3^+ with increased field and the appearance of H_2^+. From these last two figures it is apparent that with higher extraction fields hydride ion formation is inhibited.

The extraction field studies have demonstrated that:
a) the hydride ions are present in the low field region behind the anode,
b) the hydride ions are present at an appreciable distance from the anode,
c) the hydride ions are dominant under conditions of low extraction field,
d) as the extraction field increases the hydride peaks diminish and other recessive peaks (notably Ne_{20}^+) become dominant.

The following hypotheses appear to be a reasonable explanation of the observed dependence of mass peaks on extraction field: At a pressure of 20 Torr, extraction fields of a few hundred volts/cm acting on ions having a mean free path of approximately 10^{-4}cm(at 20 Torr)probably will not impart sufficient kinetic energy to the ions to cause hydride dissociation by ion impact.

A substantially higher field exists in the cathode fall region of the discharge. This field is likely to be insufficient for field dissociation. Consideration of E/p suggests, however, that sufficient energy may be imparted to these ions to cause dissociation by impact. However, the latter case would then be independent of extraction field (which is not the case). We, therefore, conclude that the hydride formation reactions occur outside the discharge region.

For a given pressure, the presence of a high extraction field decreases the overall reactant path length. This permits more unaffected reactants to emerge from the aperture. The presence of high fields (i.e. more energetic ions) may also inhibit some reactions and promote others.

TABLE I
MASS COMPOSITE SPECTRUM

Mass No.	Species	Mass No.	Species
1	H^+	24	$HeNe^+$ C_2^+
2	H_2^+ D^+	25	C_2H^+
3	H_3^+ HD^+	26	$C_2H_2^+$
4	He^+	27	$C_2H_3^+$
5	HeH^+	28	N_2^+ $C_2H_4^+$ CO^+
6		29	N_2H^+ $C_2H_5^+$
7		30	NO^+ $C_2H_6^+$
8	He_2^+	31	
9		32	O_2^+
10	$^{20}Ne^{++}$	33	O_2H^+
11	$^{22}Ne^{++}$	34	
12	C^+	35	
13	CH^+	36	$^{36}A^+$
14	CH_2^+ N^+	37	$H_5O_2^+$
15	CH_3^+ NH^+	38	
16	CH_4^+ NH_2^+ O^+	39	
17	CH_5^+ NH_3^+ HO^+	40	$^{40}A^+$
18	NH_4^+ H_2O^+	41	$^{40}ArH^+$
19	H_3O^+	42	N_3^+
20	$^{20}Ne^+$ A^{++}	43	
21	$^{20}NeH^+$	44	CO_2^+ H_2O^+
22	$^{22}Ne^+$	45	
23	$^{22}Ne H^+$ NA^+	46	NO_2^+

98. A GAS DISCHARGE ION SOURCE FOR MASS SPECTROMETERS

Lowell P. Theard

Douglas Advanced Research Laboratories, Huntington Beach, California

A hot-cathode gas discharge ion source which can generate intense beams of positive ions with a relatively small spread in energy is described. By substituting the gas discharge source for the low-pressure type source commonly used with a magnetic deflection mass spectrometer, it may be possible to convert the instrument into a mass selector which could generate intense beams of those ions present in gas discharges. With most mass spectrometers, the loss of mass resolution due to ion beam energy dispersion would not be extreme.

The source is relatively simple to build and operate, and can be used to generate intense beams of both primary and secondary ions. Total beam currents in the range of 10^{-5}A can be extracted with a beam energy of 3 keV. The ion energy distribution in the extracted beam was measured for a variety of source conditions using an electrostatic parallel-plate energy analyzer. Under optimum source conditions, the ion energy distribution curve is a narrow peak with a tail that diminishes towards lower energies. Full-width of the peak at half-maximum is 1.1 eV and the shape of the curve is such that more than 81% of the beam ions have energies within a 10-eV interval.

Details will be published.

99. Homogeneity of Ion Sensitive Emulsions and Precision of Ion Beam Measurements in Spark Source Mass Spectrometry (A Summary)

A. J. Ahearn
Spectrochemical Analysis Section
National Bureau of Standards
Washington, D. C. 20234

1. Introduction

The precision and accuracy with which the chemical analysis of materials can be made by mass spectrometry are determined by (1) the precision with which mass analyzed ion beams can be measured, (2) the accuracy with which ion beam ratios can be measured and (3) the precision and accuracy of the numerical information on the degree by which the ion sample, presented to the mass spectrometer detector, represents the composition of the solid sample.

In spark source mass spectrometric analysis of solids, particularly for trace quantities, these precision and accuracy problems take the following form. In the ion beam measurement, it is the precision with which this can be done photographically. The ion beam ratio measurement is a combination electrical and photographic problem. The degree of representation is determined by measurements with standard samples.

2. Method

To determine the precision achievable in the photographic measure of an ion beam, a series of replicate exposures was made in which the successive mass spectra covered nearly the full 5 cm width and extended over a 15 cm length of the Q-2 emulsion. The major component rather than a minor component of a solid sample was recorded in the replicate exposures. This circumvents fluctuations that might be caused by sample inhomogeneities and/or variations in degree of representation of the specimen composition by the ion sample.

Platinum is a very suitable material for these replicate tests. By utilizing the low abundance isotopes of mass 190 and 192, the exposure -- an electrical measurement of charge at the monitor electrode -- can be replicated with greater precision than with an element that has no low abundance isotopes. Other desirable properties of platinum will be indicated in the section on results.

3. Results

Ion beam measurements on replicate spectra all recorded at the same magnetic field and made by racking the plate indicated the following. The number N^{+1} of singly charged ions plus the number N^{+2} of doubly charged ions is an adequate measure of the total number of platinum ions. The fluctuations in N^{+2} do not compensate those in N^{+1}. The average value of $N^{+1}/(N^{+1}+N^{+2})$ is 0.90 with a relative standard deviation as low as 1 to 2% in typical cases. Consequently N^{+1} is an equally adequate measure of the total number of platinum ions.

Data like the above show that for many but not all Q-2 plates, the relative standard deviation is $\leq$ 5%. This indicates that widthwise the inhomogeneity of the emulsion is within this limit but it tells nothing about how it may vary lengthwise. This was investigated with replicate exposures made at different values of the magnetic field. Three typical plates are represented in the 3 dimensional drawing of Fig. 1 in which a 5 by 16 cm emulsion is portrayed. At each of the 12 magnetic field settings, 12 replicate spectra were recorded widthwise by racking the plate.

These curves delineate averages made as follows. In the widthwise ones all the data at each racking position were averaged. In the lengthwise curves, all the data at each magnetic field were averaged. The individual curves do not seriously disagree with the average curves for a particular plate.

For plate 153D, the emulsion measure of the ion beam is quite constant both lengthwise and widthwise. Plate 14E shows a 20% trend lengthwise and a 30% trend widthwise. Plate 15E shows a trend of about 10% widthwise but a large overall change of 60% lengthwise.

The ZY curves clearly show the widthwise variation in the emulsion sensitivity. The XY curves are not so easily interpreted. When the magnetic field is increased, the length of the trajectory of the platinum (+1) ions is decreased. Consequently, the Z axis spread -- the ions spreading by radial projection in the unfocused direction -- decreases, and the number of ions/cm^2 producing the mass line increases. Thus, the emulsion measure of the ion beam is determined by two factors, the Z axis spread factor which increases with magnetic field, and the emulsion sensitivity factor, for which the lengthwise variation is not predictable.

The Z axis spread factor F can be experimentally measured by recording replicate spectra at several values of magnetic field, and then after reversing the plate in its holder, recording a second set of replicates. Thus, in one set of replicates, the factor F increases to the right of the reference end of the plate, whereas, in the other set, F decreases.

Tests of this sort indicate that, for the 21-110 spark source mass spectrograph being used, this Z axis spread factor F amounts to about 20% over a 20 cm length of ion sensitive plate, the standard plate being 38 cm long in this instrument.

4. Circumvention of Inhomogeneities in Ion Sensitive Emulsions

When samples are being compared, their spectra can be interspersed to neutralize widthwise variations in emulsion sensitivity. When a conventional graded series of exposures is being made, the exposures can be interspersed with replicate spectra of platinum to determine the magnitude of the correction factor introduced by a widthwise inhomogeneity.

Lengthwise inhomogeneities can be offset by measuring the Z axis spread factor for the spark source mass spectrometer being used, and then recording appropriate replicate spectra on the plate containing the spectra of the sample under analysis.

5. Summary and Interpretation of Results

1. The total number of platinum ions to the plate and the precision

of this quantity can be derived from measurements on the isotopic mass line of the singly charged ion of mass 192.

2. Tests with Q-2 plates from different lots indicate that the sensitivity fluctuations about an average may be $\leq$ 5% relative standard deviation in a 5 cm length or there may be as much as a 30% change in sensitivity over this distance.

3. A more detailed account of this work will be submitted for publication.

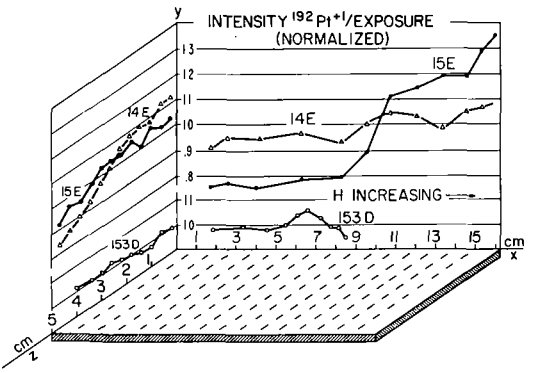

Fig. 1. Ion beam measurements by integration of ion intensity profile of platinum mass lines in replicate spectra on Q-2 ion sensitive emulsions.

100. THE MASS RESPONSE OF ION-SENSITIVE PLATES USED IN MASS SPECTROGRAPHY

by

J. R. Woolston, W. L. Harrington, R. E. Honig,
E. M. Botnick, and D. A. Kramer

RCA Laboratories
Princeton, N. J.

In the past decade or so, the analysis of solids by spark-source mass spectrography has been widely accepted as a valuable analytical technique. To enjoy even wider acceptance, the quantitative aspects of the technique must be improved. One of the more important factors which contribute to quantitative accuracy is a precise knowledge of the response of the ion-sensitive plates to ions of different mass. In effect, the situation is like a chain which is no stronger than its weakest link. This can be appreciated by examining the equation below, which serves to calculate impurity concentrations in solids mass spectrography:

$$C_i = \frac{a_r}{a_i} \cdot \frac{E_r}{E_i} \cdot \frac{\int I_i dx}{\int I_r dx} \cdot \frac{S_r}{S_i} \cdot \frac{g(M_i)}{g(M_r)} \cdot 10^6 \text{ ppma}$$

where

subscript "i" refers to a given sample component (impurity)

subscript "r" refers to a reference component (usually the matrix)

a = isotopic abundance

E = exposure used

I = ion intensity which is a function of optical blackening B, saturation blackening B_S, and background blackening B_B

x = distance along the photoplate (normal to the line)

S = relative sensitivity coefficient

M = isotopic mass

g = mass-response function of the emulsion.

Each quotient is a link in this chain. This paper deals with the last link: the mass-response function of the emulsion.

There have been several prior studies of this function,[1-5] yet the results obtained to date show little agreement. In most cases, very few data were obtained, and the experimental approaches taken often involved other factors that could not be separated from the mass response. In the present work, the experimental approach adopted permitted spark-source ions to be used, yet isolated the mass response from all other parameters. This work was carried out in an AEI type MS7 double-focusing mass spectrograph with the help of the special combination cassette shown in Fig. 1. This cassette contained a "sandwich" consisting of a metal mask with a one-inch square window, an electrical pickup plate which extended about half-way over the window, and the ion-sensitive plate to be studied together with one of several spacers whose lengths could be chosen in 3/4" increments. The electrical pickup consisted of a 1 1/8" wide conductive strip on a glass plate. Its low-mass end was connected via contacts and a feedthrough to an external amplifier and integrator. By precise adjustment of magnetic field strength, the low-mass isotope(s) of any poly-isotopic

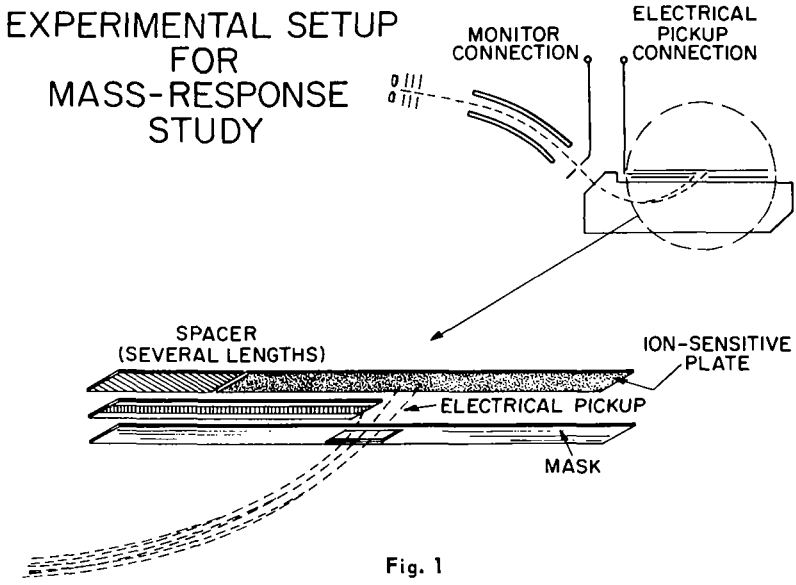
EXPERIMENTAL SETUP
FOR
MASS-RESPONSE
STUDY
MONITOR
CONNECTION
ELECTRICAL
PICKUP
CONNECTION
SPACER
(SEVERAL LENGTHS)
ION-SENSITIVE
PLATE
ELECTRICAL PICKUP
MASK

Fig. 1

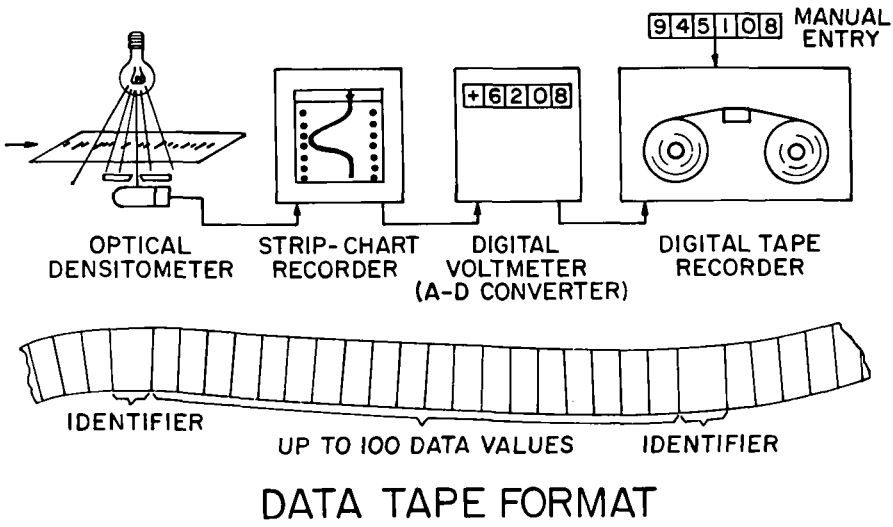
DATA COLLECTION EQUIPMENT
9 4 5 1 0 8
MANUAL
ENTRY
+ 6 2 0 8
OPTICAL
DENSITOMETER
STRIP-CHART
RECORDER
DIGITAL
VOLTMETER
(A-D CONVERTER)
DIGITAL TAPE
RECORDER
IDENTIFIER
UP TO 100 DATA VALUES
IDENTIFIER
DATA TAPE FORMAT

Fig. 2

DATA REDUCTION PROCEDURE

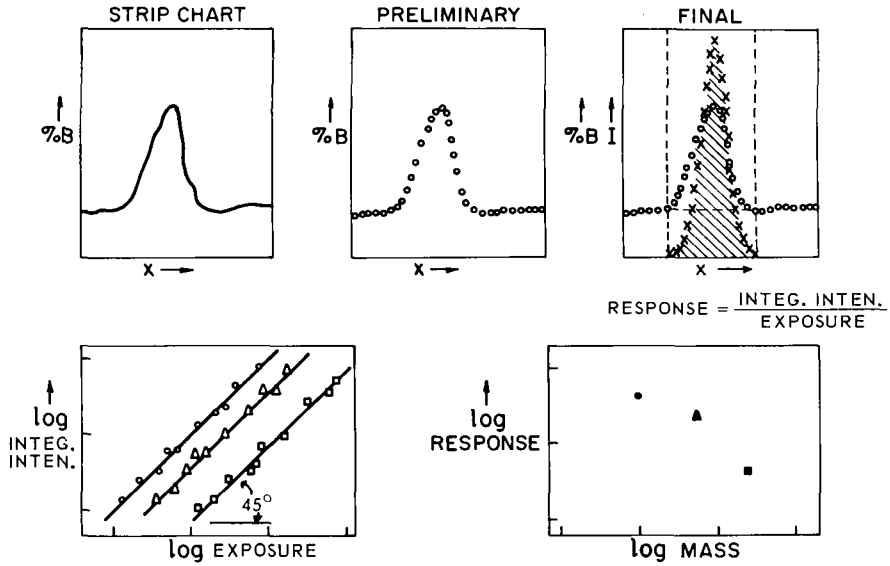

Fig. 3

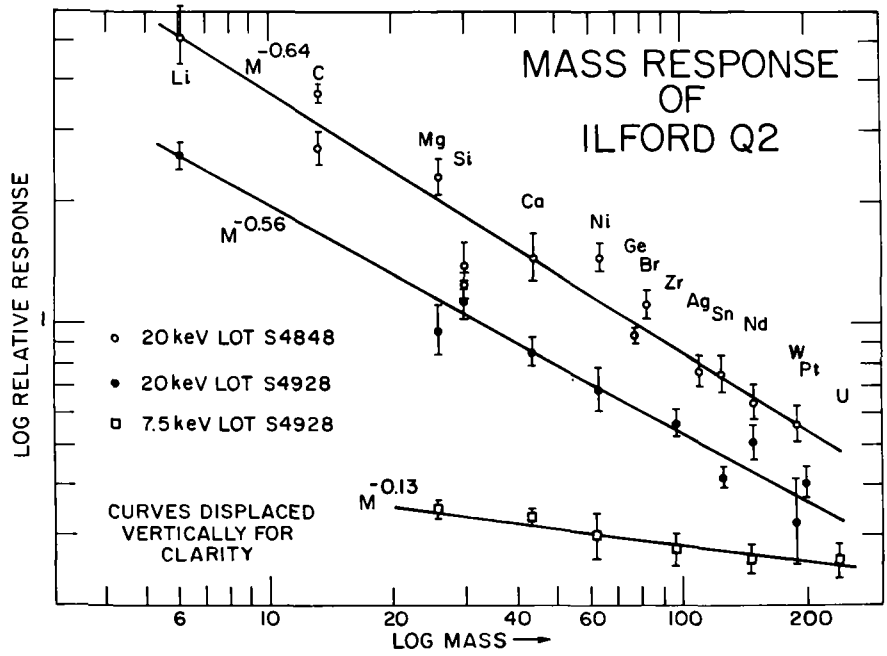

Fig. 4

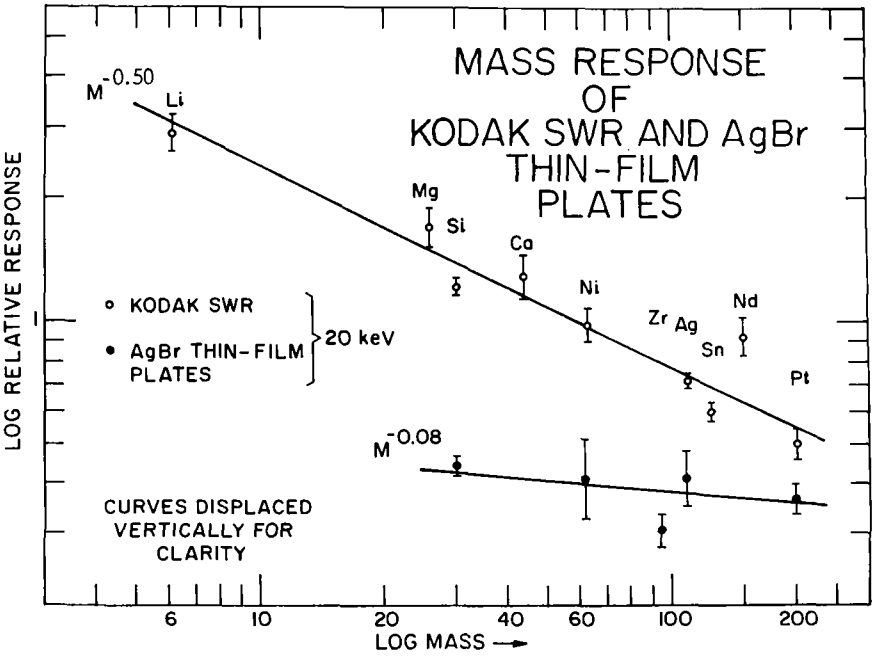
MASS RESPONSE
OF
KODAK SWR AND AgBr
THIN-FILM
PLATES
M^-0.50
Li
Mg
Si
Ca
Ni
Zr
Ag
Nd
Sn
Pt
KODAK SWR
AgBr THIN-FILM PLATES
20 keV
M^-0.08
CURVES DISPLACED VERTICALLY FOR CLARITY
LOG RELATIVE RESPONSE
6
10
20
40
60
100
200
LOG MASS

Fig. 5

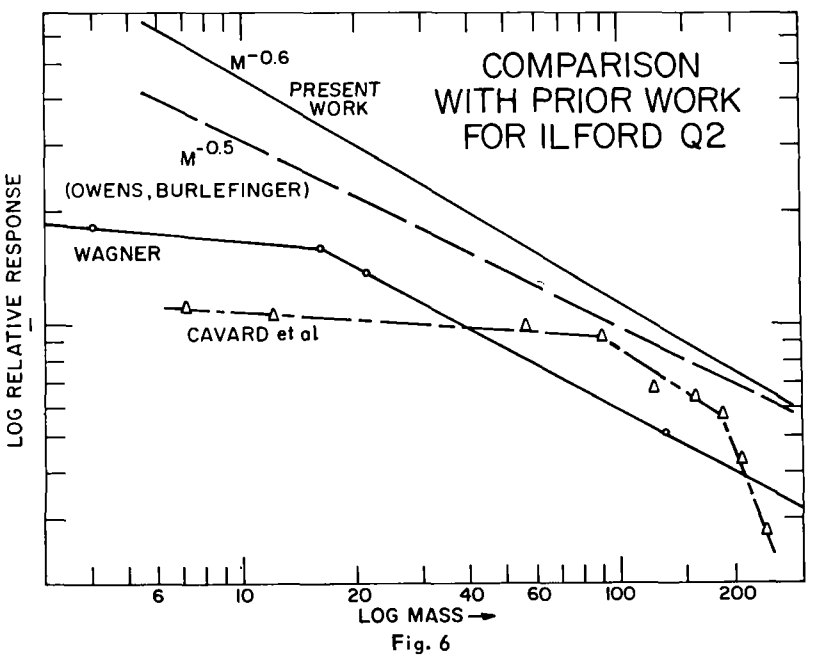
COMPARISON
WITH PRIOR WORK
FOR ILFORD Q2
M^-0.6
PRESENT WORK
M^-0.5
(OWENS, BURLEFINGER)
WAGNER
CAVARD et al
LOG RELATIVE RESPONSE
6
10
20
40
60
100
200
LOG MASS

Fig. 6

element could be made to fall on the electrical pickup, while the high-mass isotope(s) passed on to the ion-sensitive plate. Therefore, the amount of charge--hence, the number of ions-- corresponding to each line on the ion-sensitive plate could be determined from the known relative abundances of the isotopes of a given element. To optimize the accuracy of the results, the major isotope(s) should always be collected on the electrical pickup, and the less abundant ones on the ion-sensitive plate. To this end, a "reverse" electrical pickup was also constructed and used where indicated, e.g. for lithium and uranium. In changing from one element to another, the only instrumental parameter varied was the magnetic field strength since the ion trajectory remained constant. In actuality, to encompass the wide mass range from lithium to uranium, two such cassettes had to be constructed: one with the window near the low-mass end, the other, with the window near the high-mass end. Data were normalized by making runs with a reference element, nickel, through both windows. By successively employing the various spacers, and by turning the ion-sensitive plate end-for-end, data for up to ten different elements could be collected on a given plate, which eliminated plate-to-plate and development variations. Each plate used included data for nickel, in order to normalize its sensitivity. By closely spacing successive exposures across the one-inch window width, up to 14 exposures per element could be accommodated. These exposures provided a closely-spaced, graded blackening series ranging from 5 to 95% and produced complete response curves for each element. Data were obtained mostly for 20 keV ions, but the same set-up was also used for doubly-charged ions (equivalent to 40 keV particles) and, in one case, for 7.5 keV ions. The only precaution necessary in obtaining data was to ensure that no ions other than those being studied passed through the window onto the electrical pickup. This was accomplished by examining a full-spectrum plate produced in the usual manner immediately before or after running the mass-response plate. All questionable or "contaminated" data were rejected.

Altogether, more than 2000 spectral lines were recorded which had to be evaluated as precisely as possible. Because of line width and profile variations, simple peak-height measurements (maximum blackening) were inadequate. Therefore, a modification of the data-reduction procedure described previously[6] was used. This procedure involves integration of the true intensity profile which produces a total intensity directly proportional to exposure. The equipment set up for this purpose is shown diagrammatically in Fig. 2, while the data reduction procedure is illustrated schematically in Fig. 3. As seen in Fig. 2, the percent blackening signal from the Jarrell-Ash 23-100 optical densitometer was fed to a strip chart recorder fitted with a re-transmitting slidewire. This output was monitored by a Hewlett-Packard digital voltmeter whose BCD output was then used as input to a Hamner Electronics Data-Scanner and Control Unit, and Tally paper-tape perforator. The Hamner unit provided for a six-digit manual entry onto the tape which was used as a coded indentifier for each spectral line. A timer (not shown) caused a blackening value to be punched every 0.6 seconds as the spectral line was scanned at a rate of 0.5 mm/min. Including some background on each side of the spectral line, between 50 and 80 blackening values were punched for each line. The data reduction (see Fig. 3) proceeded as follows. The strip chart recorded the peak profile in analog fashion. A first, or "preliminary", computer program produced the same blackening profile in digital fashion in the form of a page plot together with a

tabulation of the actual blackening value for each plotted point. From this computer output, appropriate integration limits and background level values were manually selected and fed, via punched cards, to a second, or "final", computer program. Using the Hull equation,[7] this program converted each point between the integration limits to an intensity, corrected for background, and integrated the resulting intensity profile. As shown, the final page plot graphically displayed the integration limits, the interpolated background values, the intensity profile, and the original blackening profile. Since the response is proportional to sensitivity, it may be expressed as the integrated intensity divided by the exposure producing the line. Thus, for a given element, all isotopic lines for all exposures should result in the same response value. In order to check on the validity of individual data, log-log plots of integrated intensity versus exposure were made, as shown in Fig. 3. For a given element, valid data should fall closely on a 45° straight line. For each element, the response values for all acceptable spectral lines were then geometrically averaged and plotted versus mass in log-log fashion. In addition, the error factors for all mass-points were calculated and are shown as vertical bars on Fig. 4 and 5.

Fig. 4 shows the results obtained with Ilford Q2 emulsion. Plates from two emulsion lot numbers were studied and are shown as separate curves, displaced vertically for clarity. It is apparent that the mass response can be closely approximated by a straight line on a log-log plot, and that the two emulsion lot numbers exhibit straight lines with different slopes, the average slope being about -0.6. This value is significantly different from -0.5, the value which is commonly assumed to represent the mass response of Ilford Q2. Also shown on Fig. 4 are data obtained with 7.5 keV ions on Q2. These data indicate a surprisingly small mass-dependence compared to those for 20 keV. All the 7.5 keV data were obtained from one photoplate, and we can find no reason to suspect or reject them, but further work is clearly necessary to verify this unexpected result.

Fig. 5 presents the results obtained for 20 keV ions with Kodak SWR plates and with evaporated AgBr thin-film plates.[8] Again, the mass response closely approximates straight lines when plotted logarithmically. The SWR plates exhibit a slope slightly less than those for Q2, while the evaporated AgBr plates, as anticipated, are seen to display almost no mass-dependence.

Finally, Fig. 6 compares the present results with those of prior studies and with the $M^{-0.5}$ response widely used for Ilford Q2. Except for the helium point at mass 4, the data of Wagner[4] closely match the present work. The results published by Cavard et al.[5] present a wholly different picture which cannot be readily explained.

The pertinence of this work to the mass spectrographic analysis of solids can be summarized as follows: whenever analyses are not, or cannot, be accomplished with valid standards (which is the usual case), a precise knowledge of the mass response of the emulsion used is necessary to avoid introducing error into the analytical results. The mass response of Ilford Q2 closely approximates $M^{-0.6}$, but can vary slightly between emulsion lot numbers. Clearly, a simple means of determining the mass response would be desirable.

Further work along these lines is planned by the present authors, including in

particular studies with ions of energy lower than 20 keV, with multiply-charged ions, molecular ions, and with other emulsions. An attempt was made to study Kodak Special 101-01 in this work, but difficulties were encountered because the film base was unstable.

The authors wish to acknowledge the cooperation of the personnel of the RCA Laboratories Computer Center who processed over a mile of punched paper tape and turned out over 10,000 pages of output in a relatively short time.

References

(1) E. Burlefinger and H. Ewald, Z. Naturforsch. 16a, 430 (1961).

(2) W. Rudloff, Z. Naturforsch. 16a, 1263 (1961); 17a, 414 (1962).

(3) E. B. Owens and N. A. Giardino, Anal. Chem. 35, 1172 (1963).

(4) H. Wagner, Ann. Physik 13, 189 (1964).

(5) A. Cavard, R. Stefani, and R. Bourguillot, Compt. Rend. Acad. Sci. B263, 928 (1966).

(6) J. R. Woolston, R. E. Honig, and E. M. Botnick, Rev. Sci. Instr. 38, 1708 (1967).

(7) C. W. Hull, ASTM E-14 Mass Spectrometry Conference, New Orleans (1962), paper 72.

(8) R. E. Honig, J. R. Woolston, and D. A. Kramer, Rev. Sci. Instr. 38, 1703 (1967).

101. DIGITAL MASS SPECTROGRAPHIC PLATE READER

RW Bonham and JO Humphries
General Electric Company
Neutron Devices Department
St. Petersburg, Florida

INTRODUCTION

A need for fast semi-quantitative spark source analysis is becoming extremely important in industry today. This need is predicated upon the increased demand for such analyses and the fact that impurity level requirements are getting lower and lower. The time required to read photographic plate data and to perform corrections to the data is one of the basic hindrances in speeding up spark source analyses.

The use of a scanning densitometer is usually one of the first steps that is taken to reduce the time required for plate reading. Unfortunately, the densitometer creates as many problems as it solves for the output data is in the form of transmission percentages. A conversion to ion density, using plate calibration, and the application of "width at half height" corrections are time consuming. Furthermore, unless the line under consideration is Gaussian, the width correction is a poor approximation of the area correction it is intended to approach.

This paper describes an integrating mass spectrographic plate reader, which has been developed at the General Electric Neutron Devices Department (NDD) to reduce the time required for spark source analyses. This unit, used in conjunction with a standard scanning densitometer, features digital readout and a background compensation circuit.

DESCRIPTION

There are several existing methods to calibrate a photoplate and to read out ion density (1) (2). The method described in this paper automatically makes the conversion from percentage transmission (T) to ion density. It also integrates over the peak area to give a digital readout of the ion intensity expressed as atomic parts per million of gold. Mass corrections are made manually using the following ratio:

$$\frac{M_x^{2/3}}{M_{Au}^{2/3}}$$

Before starting each line scan, the operator can zero out background.

Figure 1 is a block diagram of the digital mass spectrographic plate reader system. The slave slidewire on the densitometer is installed with taps corresponding to 10 percent transmission increments. Voltage is fed to each tap from a resistor divider. The tap voltage is adjusted by the pots. This voltage is picked off by the sliding contact and it is fed to a potentiometric recorder for the original calibration. A Churchill calibration (3) provides the conversion of percentage T to relative exposure. The percentage T values are manually set on Recorder 1 and the pots are adjusted to give the correct reading on Recorder 2.

After completion of the original calibration, Recorder 2 is switched out of the circuit and the signal is fed to a voltage-to-frequency converter and then to a scaler. The zero balancing circuit applies a small bucking voltage to the voltage-to-frequency

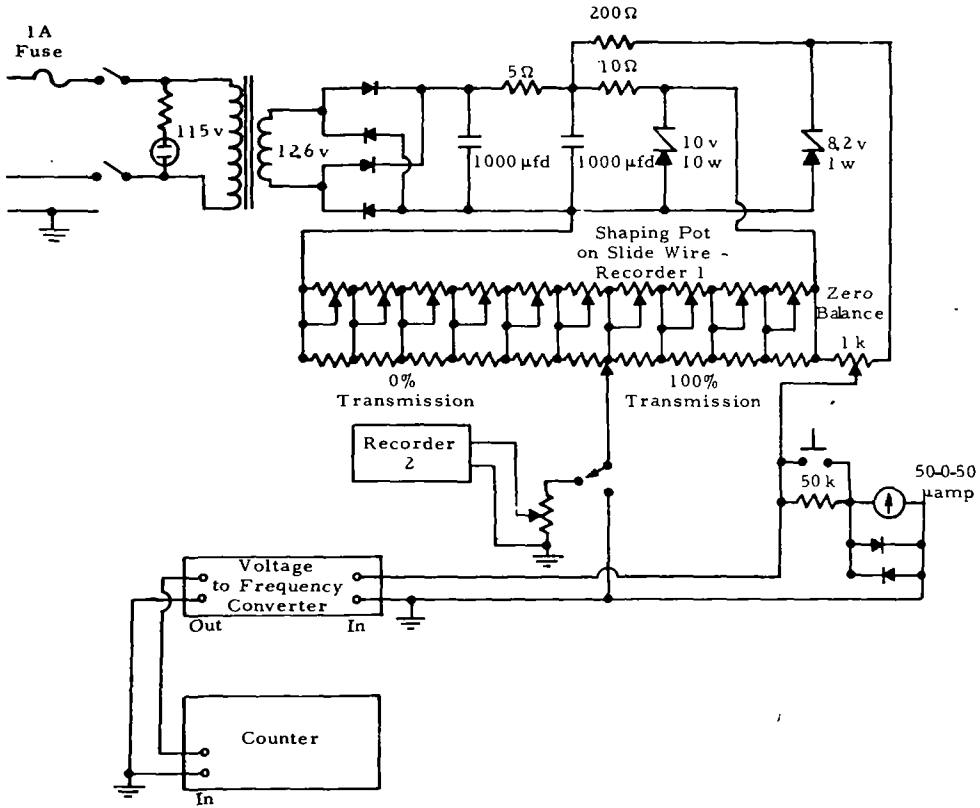

Figure 1. Block Diagram of Digital Mass Spectrographic Plate Reader

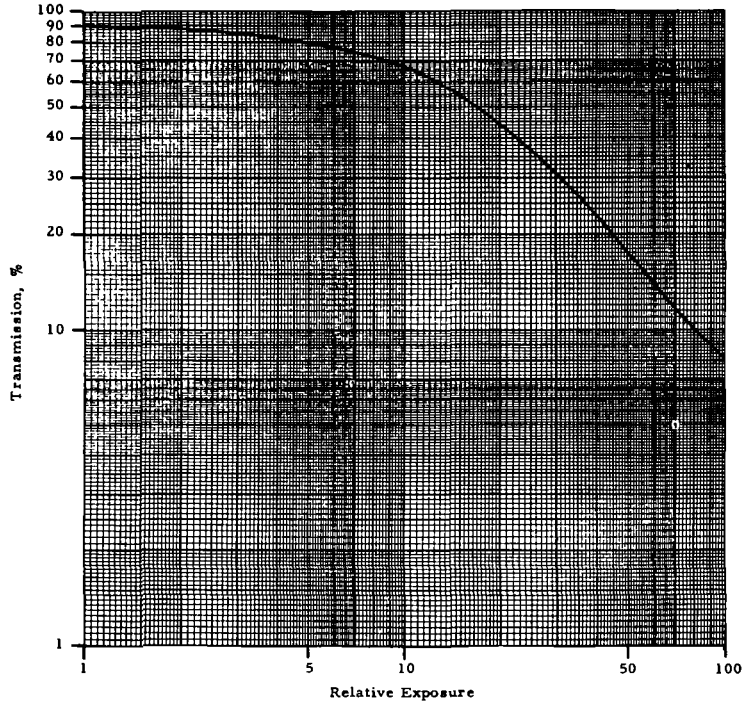

Figure 2. Photoplate Response Curve

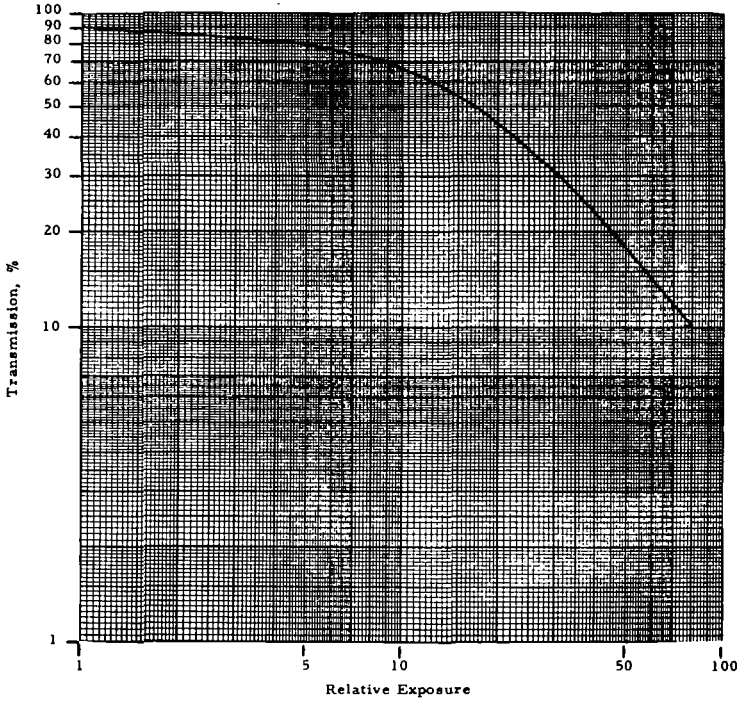

Figure 3. Approximation of Photoplate Response Curve

input to balance a signal resulting from a high background. The scaler reads the integrated signal less background.

The method of applying bucking voltage permits background corrections as low as 40 percent transmission and retains correct sensitivity for faint signals. This method is advantageous on traces near heavy matrix peaks.

Figure 2 is a plot of the photoplate response curve obtained from the Churchill calibration. Three separate photoplates, representing over 300 individual pieces of information, were used to generate the curve shown in Figure 2. Figure 3 is a plot of an approximation of the photoplate response curve using data from the slave slidewire. The integrated signal from the calibration plates is plotted in Figure 4. Signals of the same exposure from Er 166 and 167 were used to generate the experimental line plot shown in Figure 4. If the calibration is valid, a straight line with slope 1.456 will result. Although the scatter shown in Figure 4 is more than desired, the average of the individual ratios is 1.430, an error of less than two percent.

The gain of the combined system is set so that pure gold sparked to an exposure of 10^{-12} coulombs gives an integrated readout of 100 counts. Thus, gold sparked to 10^{-14} coulombs reads a count of 1. If the gold line reads 1 at an exposure of 10^{-8} coulombs in some other matrix, a one-ppma impurity level can be assumed. The final results are corrected for mass effect, and the weight is corrected to yield results in parts per million by weight.

In summary, the digital mass spectrographic plate reader automatically integrates over the peak area to give a digital readout of ion density, and it converts from percentage transmission to relative exposure. This capability eliminates the laborious calculation of "widths at half height," thus reducing plate evaluation time by approximately 80 percent. Furthermore, operator errors are minimized since the amount of data handling is also reduced.

EXPERIMENTAL RESULTS

As a check on the integrating mass spectrographic plate reader system, pure platinum was sparked and the isotopic abundances were calculated. The results of ten different exposure readings for the platinum sample were averaged. These results are given in Table I, and the stated errors are calculated standard deviations.

Table I
PLATINUM ISOTOPE ABUNDANCES

Isotope	Accepted Value (%)	Spectrographic Value (%)
190	0.0127	0.011 ±0.0014
192	0.7800	0.880 ±0.1100
194	32.9000	29.400 ±3.8000
195	33.8000	36.800 ±4.8000
196	25.3000	25.900 ±3.4000
198	7.2100	7.100 ±0.9200

Table II gives a comparison of true values and spectrographic plate reader values for various elements in a sample of NBS Standard 1165, which is an iron base alloy. With the exceptions of arsenic, copper, manganese, and carbon, these single-plate

values are fairly close to NBS values. The copper, manganese, and carbon are background from a previous sample, whereas the high arsenic value is confusing and no explanation can be offered at this time.

Table II
NBS STANDARD 1165

Element	True Value	Spectrographic Value
W	10	6
Ta	10	14
Sn	10	27
Ag	3	12
Mo	50	22
Nb	10	10
As	100	240
Cu	190	290
Mn	320	590
Cr	40	21
V	20	19
Ti	2000	2000
S	100	150
Co	80	60
C	370	700
P	80	110

Table III gives a comparison of certified values and mass spectrographic plate reader values for various elements in a sample of NBS Standard 1156, which is a maraging steel material. These values are from two plates; however, the sample was the same two electrodes in both cases. These double-plate values are fairly close to NBS values.

Table III
NBS STANDARD 1156

Element	Certified Value (%)	Spectrographic Value (%)
Mo	3.100	2.600, 2.400
Cu	0.025	0.029, 0.025
Ni	19.000	18.700, 16.400
Co	7.300	7.400, 6.300
Fe	69.700 (by difference)	70.800, 74.500
Mn	0.210	0.290, 0.250
Cr	0.200	0.200, 0.170
C	0.023	0.011, 0.012

CONCLUSIONS

In conclusion, the digital mass spectrographic plate reader can reduce the time required for evaluating a spark source photoplate from four to five hours to about one hour. Operator errors are also minimized since the amount of data handling is reduced.

Although spark source mass spectrography is still a semi-quantitative technique, the addition of a digital plate reader does provide a definite improvement in precision and reliability. The platinum isotope calculation (Table I) shows the precision to be expected on replicates, since the standard deviation is approximately ±10 percent of the amount present. Furthermore, the precision and reliability for the NBS Standards (Tables II and III) is reasonably good, since no relative sensitivity corrections were made.

REFERENCES

1. Paulsen, P. J. and Branch, P. E., "Electronic Analog Computer for Measuring Intensity Areas on Mass Spectrographic Plates," Mass Spectrometry Conference, Dallas, Texas, May 1966.

2. Kennicott, P. R., "A System for the Quantitative Evaluation of Mass Spectrographic Plates," Mass Spectrometry Conference, Dallas, Texas, May 1966.

3. Owens, E. B. and Giardino, N. A., "Quantitative Mass Spectrometry of Solids," Analytical Chemistry, Vol. 35, pp. 9 and 1172, August 1963.

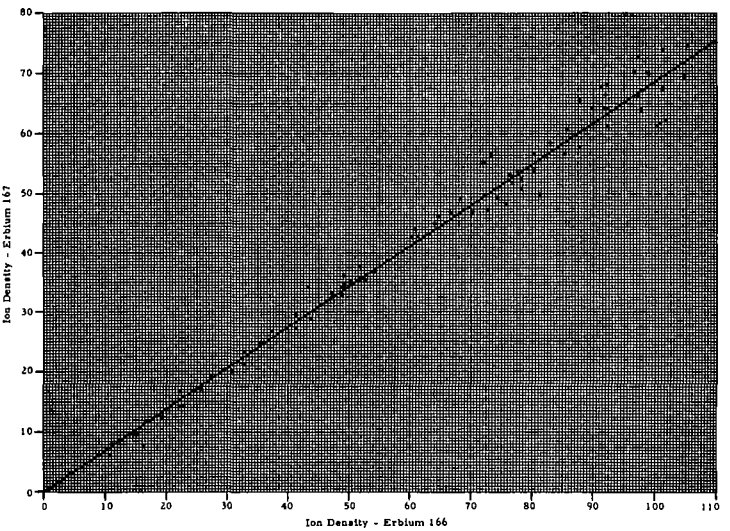

Figure 4. Integrated Ion Densities of Erbium 166 Versus Erbium 167

102. MASS SPECTRA OF SOME PHOTO-CYCLOADDITION PRODUCTS OF NUCLEOTIDE BASES

Catherine Fenselau, A. J. Varghese and S. Y. Wang

The Johns Hopkins University School of Medicine and
School of Hygiene and Public Health
Baltimore, Maryland 21205

The discovery in 1877 that ultraviolet irradiation can kill bacteria initiated research which is still continuing on the effects of radiation on living organisms. In 1928 it was suggested[1] that the biological effects were due to chemical changes in nucleic acids, especially in deoxyribonucleic acid (DNA). These chemical changes are now considered to involve intrastrand polymerization of certain of the bases in DNA. Dimers I and II, isolated from native DNA irradiated with UV doses comparable to biological studies, have recently been characterized.[2] Dimers I and III have been structurally identified as irradiation products of thymine in ice[3] and compound IV was obtained from III by chemical dehydration.

We have analyzed the fragmentation patterns on electron impact of these photodimers to facilitate the application of mass spectrometry to structural characterization of additional polymeric photoproducts of unknown structure.

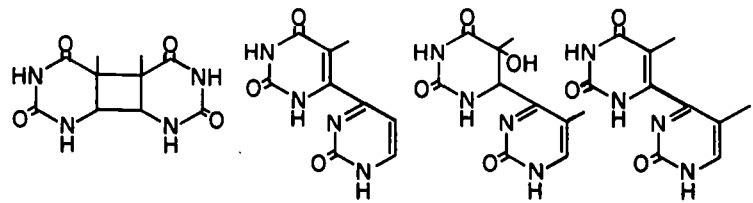

I II III IV

The spectrum of compound I contains no molecular ion; the peaks at highest mass correspond to monomeric thymine (m/e 126) and protonated thymine (m/e 127). In large part the rest of the spectrum resembles that of monomeric thymine.[4] Pyrolytic decomposition may be occurring in addition to electron impact processes.

The fragmentation of the homologous pair of compounds II and IV may be viewed as a combination of thymine fragmentation and pyrimid-2-one fragmentation. Some of the ions identified in the high resolution mass spectrum are generated by elimination of small neutral molecules from both rings, and the elimination of ammonia appears to require the interaction of both heterocycles.

Elimination of water in the fragmentation of dimer III generates a daughter ion and subsequent fragmentation similar to ionized compound IV. The fragmentation pattern characteristic of pyrimidone is also present in the high resolution spectrum of III. The elimination of carbon dioxide from the molecular ion suggests that some rearrangement of oxygen is occurring. In addition, several prominent peaks reflect the hydroxy

dihydrothymine structure specifically, and delineation of the processes generating these ions has established criteria for the identification of this linkage in photopolymers of unknown structure.

The research was supported by grant AT (30-1)-2798 from the Atomic Energy Commission, grant 5-K-3-GM-4134 from the National Institutes of Health and United States Public Health Service Training Grant GM 1183.

We wish to acknowledge and thank for mass spectra the Purdue Mass Spectrometry Center and Mr. W. R. Landis of the National Institutes of Health. A complete account of this work will be submitted for publication.

1. F. L. Gates, Science, 68, 479 (1928).

2. S. Y. Wang and A. J. Varghese, Biochem. Biophys. Res. Commun., 29, 543 (1967).

3. A. J. Varghese and S. Y. Wang, Science, 160, 186 (1968).

4. J. M. Rice, G. O. Dudek and M. Barber, J. Am. Chem. Soc., 87, 4569 (1965).

103. MASS SPECTROMETRIC INVESTIGATION OF COMPOUNDS RELATED TO THE "A" RING OF TETRACYCLINE

Ward M. Scott and Morton E. Wacks
University of Arizona
C. D. Eskelson, J. Towne, and C. Cazee
Radioisotope Service, Veterans Administration Hospital
Tucson, Arizona

There is a great deal of interest in the chemistry of tetracyclines because of the known tumor locating properties of these compounds.[1] Since tetracyclines readily rearrange on exposure to air and light, it is difficult to control the course of reactions involving these compounds. Acridines and acridones are also known tumor locators;[2] therefore the synthesis of these compounds substituted similarly to that of the "A" ring of tetracycline was undertaken with a view to internally locating and destroying tumor tissue with radioactively labeled compounds of high specific activity.

The initial steps in the synthesis (Fig. 1) necessitated the preparation of many substituted salicylic acids (Table I); the early work of Emery[3] in 1960 has been of great help in the interpretation of fragmentation mechanisms of these compounds. Only low resolution data from an Hitachi RMU-6E mass spectrometer are discussed.

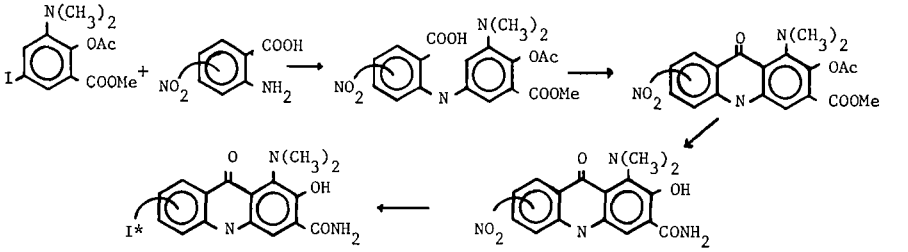

Fig. 1. Synthesis route for production of I-131 labeled acridones.

TABLE I

Substituted Salicylic Acids and Derivatives Investigated

Substitution / Acid	None	5-I	3-NO_2	5-NO_2	3-NO_2,5-I	3-NH_2,5-I
Salicylic Acid	X	X	X	X	X	X
Methyl Salicylate	X	X			X	X
Salicyl Acetate	X	X			X	
Methyl Salicyl Acetate	X	X			X	

The fragmentation pathways of salicylic acid, methyl salicylate, aspirin, and methylated aspirin are outlined in Fig. 2. Salicylic acid itself first loses a neutral water molecule, then breaks down further by eliminating two molecules of carbon monoxide, to give C_5 and C_3 ions as indicated. Methyl salicylate first eliminates methanol in a manner analogous to that of loss of water from salicylic acid and then fragments in the same manner as the acid. The o-acetyl acid first eliminates a neutral ketene molecule and then decomposes as the acid. The methyl ester of the o-acetyl acid also first eliminates ketene with subsequent fragmentation as indicated.

The acetylated compounds have small parent ions relative to the base peak at m/e 120, while salicylic acid and its methyl ester both have large parent ions; the base peak in these spectra was at m/e 120. Metastable ions were located for several transitions indicated in Fig. 2.

The high mass regions of the spectra of the corresponding derivatives of 5-iodo salicylic acid are shown in Fig. 3. The iodine behaves as a hydrogen atom; C_5 and C_3 ions are formed with and without the iodine atom. Again the acetylated derivatives are characterized by small parent ions and large ions formed by elimination of neutral ketene, while the acid and its methyl ester have large parent ions.

Fig. 4 indicates the fragmentation pathways of 3- and 5-nitro salicylic acids. After elimination of a neutral water molecule, the presence of the electron withdrawing nitro group in the aromatic nucleus causes a change in the fragmentation pathway. No CO is eliminated until the nitrogen atom is lost either as NO or NO_2. Small peaks (< 10% of the parent ion intensity) are found at 16, 30, and 46 mass units below m/e=165, corresponding to loss of O, NO, or NO_2. Two further modes of decomposition are possible

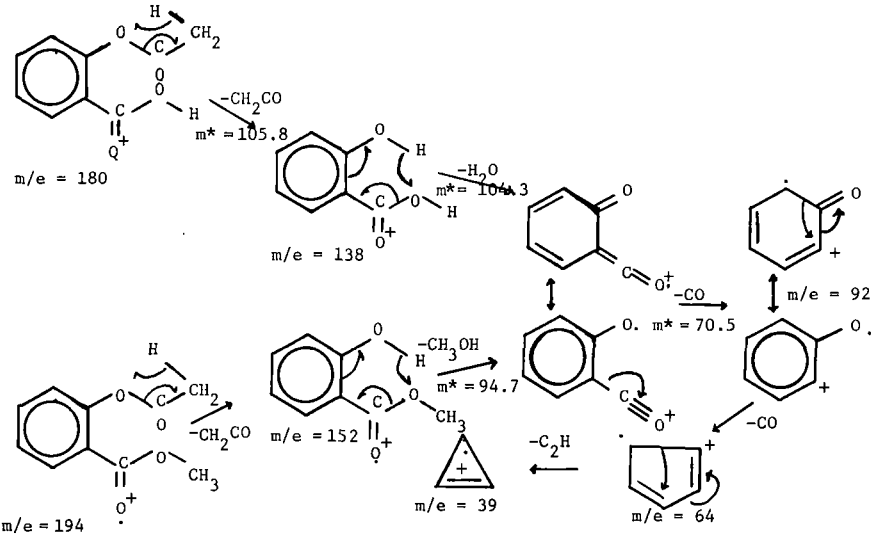

Fig. 2. FRAGMENTATION PATHWAYS FOR SALICYLIC ACID AND ITS ESTERS.

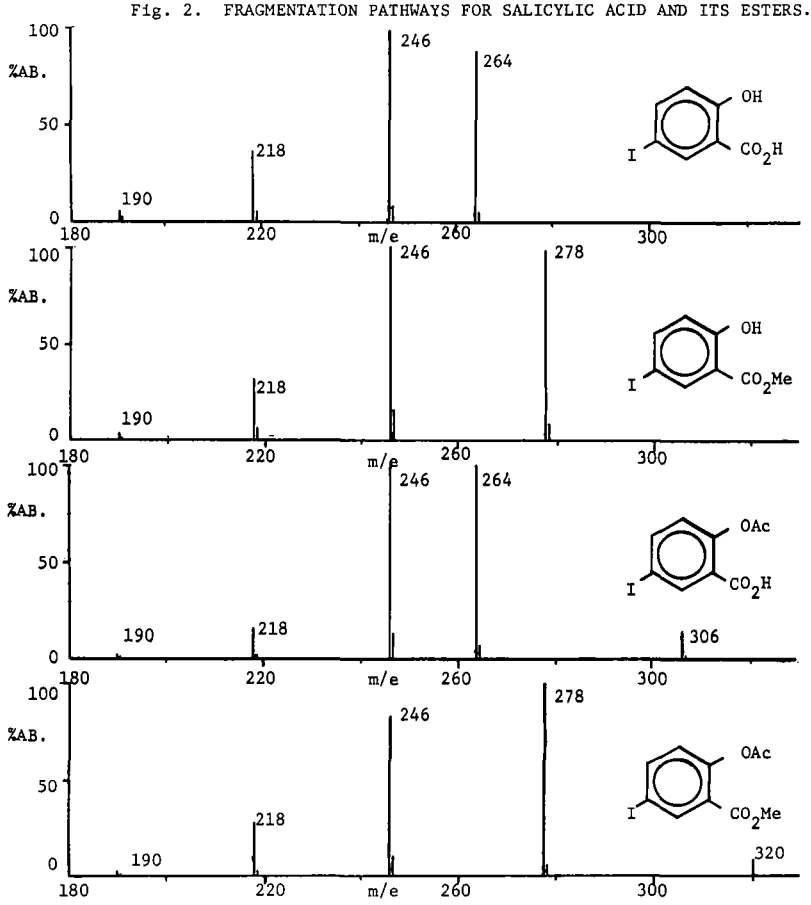

Fig. 3. MASS SPECTRA OF 5-IODO SALICYLIC ACID DERIVATIVES (HIGH MASS END).

by expulsion of neutral CO molecules. One occurs after loss of NO_2, which may occur by either (or both) a one or two step process, the other follows expulsion of NO to give a substituted orthoquinone ion.

This information coupled with that obtained from the spectra of the 5-iodo compounds, permits prediction of the spectra of 3-nitro, 5-iodo salicylic acid and its derivatives. The recorded spectra are shown in Fig. 5.

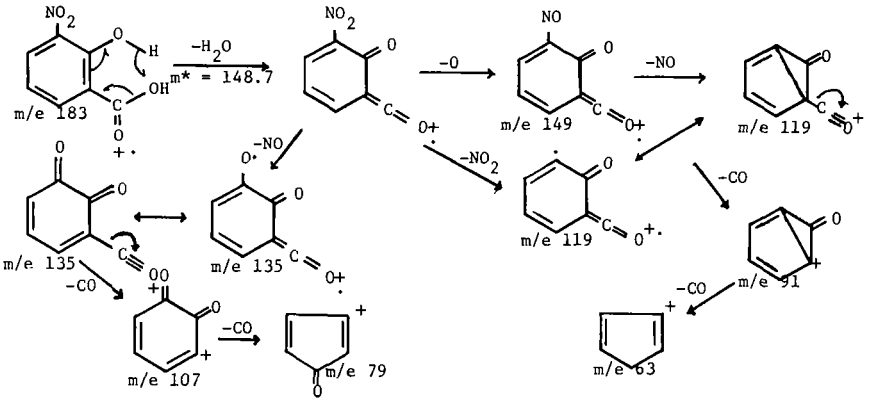

Fig. 4. FRAGMENTATION PATHWAYS FOR NITRO-SALICYLIC ACIDS.

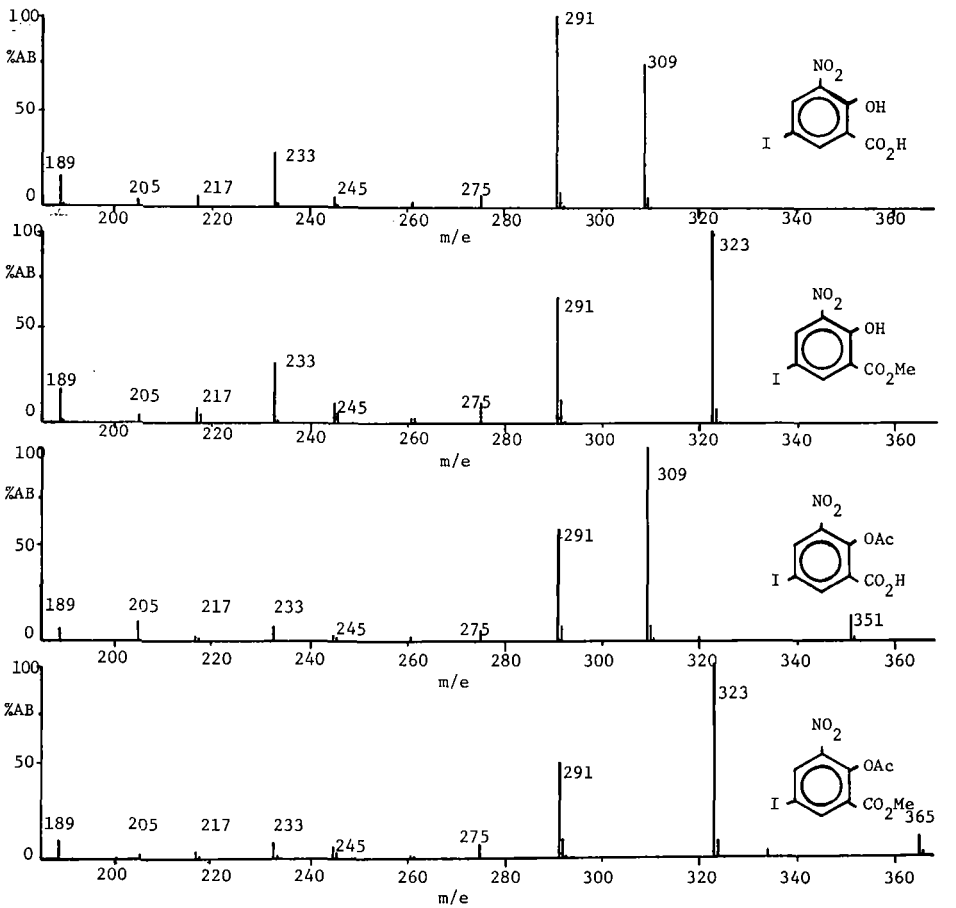

Fig. 5. MASS SPECTRA OF 3-NO_2,5-I SALICYLIC ACID DERIVATIVES (HIGH MASS END).

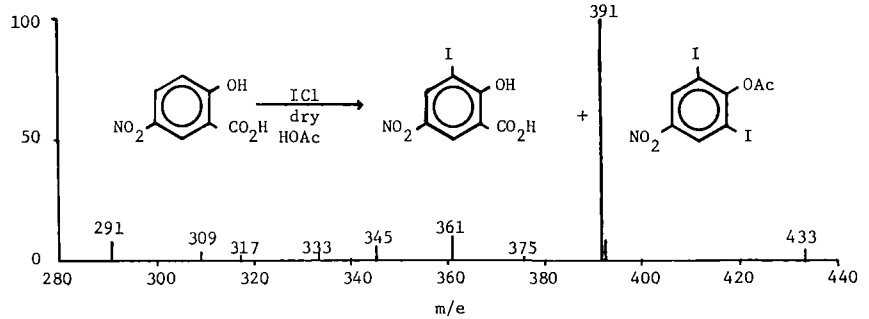

Fig. 6. Mass Spectrum of Additional Reaction Product (High Mass End).

This rationale has permitted the identification of several completely unexpected reaction products, e.g., as shown in Fig. 6. This compound corresponds to a second crop of crystals gathered in addition to the expected reaction product of the iodination of 5-NO_2 salicylic acid. The expected product had a large parent ion (at m/e 309) and a large $(P-18)^+$ ion corresponding to loss of water. In addition to showing these two peaks (present in small abundance) the mass spectrum indicated the presence of another compound of higher molecular weight. This compound had a small parent ion at m/e 433 and a large $(P-42)^+$ ion at m/e 399, formed by elimination of ketene, a process which has been shown to be indicative of an acetylated phenol. Peaks at 16, 30, and 46 mass units below 391 imply the presence of a nitro group, but only one further loss of CO is observed. No loss of 18 or 32 mass units (typical of a carboxyl or methyl carboxyl group adjacent to the phenol group) suggests that decarboxylation had occurred, while the presence of further ions in the low mass end of the spectrum corresponding to two losses of 127 mass units lead to the di-iodo acetylated phenol structure for this compound.

The fragmentation pathways of 3-amino, 5-iodo salicylic acid and its methyl ester are indicated in Fig. 7. The amino group does not have the electron withdrawing power of the nitro group and thus the NH_2 stays on the ring until after expulsion of two molecules of CO as indicated. The stability of the m/e 78 ion is attributed to resonance between ions of the type shown here, and this further fragments (as does pyridine)[4] by loss of 27 mass units (probably HCN). High resolution measurements will clarify this point completely in the very near future.

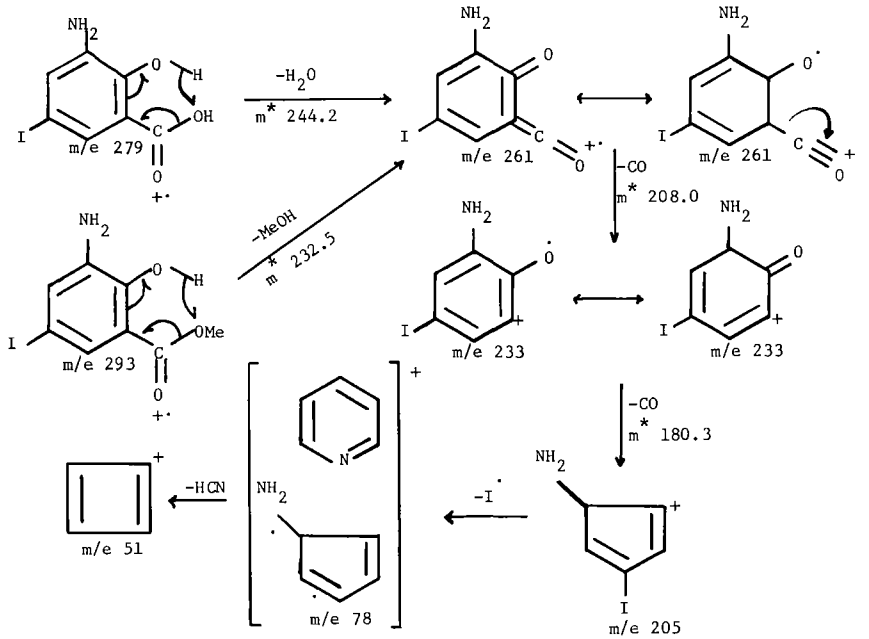

Fig. 7. Fragmentation Pathways for 3-Amino, 5-Iodo Salicylic Acid Derivatives

Due to the predictability of the masss spectra of these compounds, the framentation pattern of the reduction product from the methyl ester of the acetylated 3-nitro, 5-iodo salicylic acid (Fig. 8a) was not anticipated.

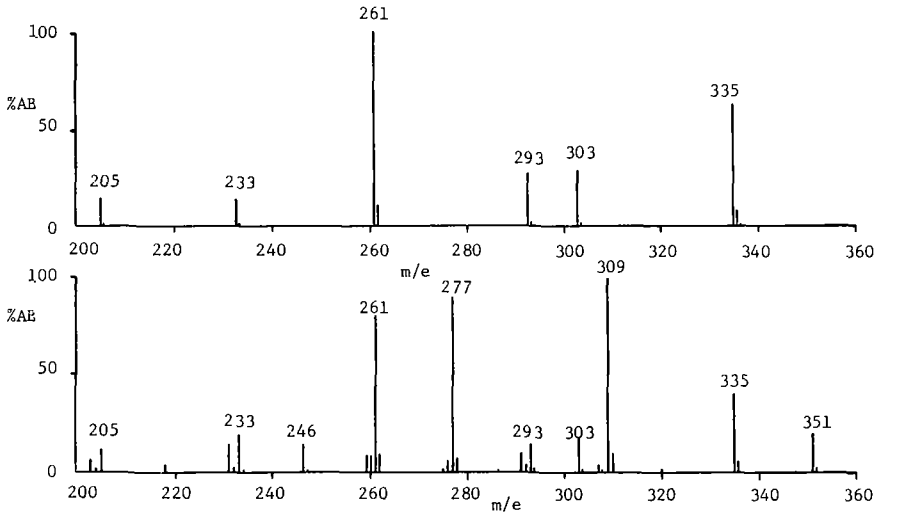

Fig. 8. Mass Spectra of Reduction Products (High Mass End).
(a) $SnCl_2$; H_2S (b) H_2/Pt/C.

If this were the corresponding amino compound, its mass spectrum should show a small parent ion followed by a large ion produced by elimination of ketene, to perhaps give the base peak in the spectrum. There is a $(P-42)^+$ ion but also a $(P-32)^+$ ion. Metastable ions indicated that both these ions were formed by one step decomposition from the parent ion. The presence of a free phenol group is indicated by the $(P-32)^+$ ion while the $(P-42)^+$ ion indicates the presence of an acetyl group. However, the compound has the correct molecular weight and, after loss of 74 mass units, fragmentation is as expected for the methyl ester of 3-amino, 5-iodo salicylic acid (Fig. 7). This implies that the acetyl group has migrated to the nitrogen atom of the amino group, leaving a methyl salicylic acid derivative, which should have a large parent ion, as has this compound. The spectrum in Figure 8b shows this compound as well as the hydroxylamine from reduction of the 3-nitro, 5-iodo derivative and indicates that migration of the acetyl group only occurs after complete reduction to the free amine.

This mass spectral investigation has been very helpful in following the preparation of the intermediates prepared in the synthesis of the desired acridines and acridones. In addition, it has provided information on the fragmentation pathways of a large number of compounds for which mass spectral data have not been readily available.

ACKNOWLEDGEMENTS

The authors acknowledge the help of Mr. J. Teets in obtaining the mass spectra and the Veterans Administration for financial support in the synthesis of these compounds.

REFERENCES

1. C. D. Eskelson, A. L. Dunn, R. E. Osborn, J. F. McLeay, J. Nucl. Medicine 4, 382 (1963).
2. A. F. Lalli, Cancer 18, 1493 (1965).
3. E. M. Emery, Anal. Chem., 32, 386 (1960).
4. Catalog of Mass Spectral Data, American Petroleum Institute Research Project 44, Carnegie Institute of Technology, Pittsburgh, P., Spectrum No. 633.

104.

MASS SPECTROMETRIC ANALYSIS OF N-SUBSTITUTED CYCLOHEXENE-1,2-DICARBOXIMIDES[1,2]

by

E. D. Mitchell and G. R. Waller

Department of Biochemistry
Agricultural Experiment Station
Oklahoma State University
Stillwater, Oklahoma 74074

The fragmentations induced by electron impact of the sugar beet germination inhibitor cis-4-cyclohexene-1,2-dicarboximide (1), its N-alkyl derivatives and cyclohexane-1,2-dicarboximide have been studied at 70 ev using both low and high resolution mass spectrometry. Previous studies (2-4) on N-substituted phthalimides indicated that a major fragmentation pathway was the loss of CO_2 from the molecular ions. It was observed that this rearrangement, which involved the migration of an oxygen atom, occurred only when the substituent on the nitrogen atom was a methyl or phenyl group (4) and when the ionization voltage was above 12.6 ev. Consequently, it was concluded that this was not an energetically favored pathway of fragmentation of these molecules. It was suggested (5) that the $(M\text{-}CO_2)^+$ ion might arise from artifacts produced by thermal isomerization or that it might be an impurity; however, these phthalimides need to be examined further so that the results can be clarified. No evidence of the loss of CO_2 from the cyclohexene dicarboximides reported herein was observed. A study of the fragmentation of N-propyl and N-butyl succinimides (6) reveal that the most abundant peak in their spectra arose from the loss of the N-alkyl sidechain but involved a double hydrogen transfer from the N-alkyl fragment.

RESULTS AND DISCUSSION

The mass spectra of cis-4-cyclohexene-1,2-dicarboximide and its N-methyl, N-ethyl, N-propyl and N-butyl derivatives and 4-cyclohexane-1,2-dicarboximide was obtained; however, only the parent compound, the N-methyl and N-ethyl derivatives will be discussed. Certain similarities were observed in these group of spectra: a) each compound gave an intense molecular ion, b) a cluster of peaks at 77, 78, 79, 80 and 81 were formed in which the peak at m/e 80^+ was the most intense except in the case of cis-4-cyclohexane-1,2-dicarboximide where the ion had shifted to m/e 82, and c) each of the spectra exhibited characteristic interpretive ions at nominal masses m/e 151^+, m/e 136^+ and m/e 123^+; however, in some cases doublets and triplets were observed.

Cis-4-cyclohexene-1,2-dicarboximide. A partial interpretation of the fragmentation of cis-4-cyclohexene-1,2-dicarboximide (Figure 1) is shown in Figure 3. The loss of CO from the imide ring was a major decomposition pathway; however, high resolution analysis showed that the peak at m/e 123^+ was a doublet of elemental compositions C_7H_9NO $(M\text{-}CO)^+$ and $C_7H_7O_2$ $(M\text{-}H_2CN)^+$. The formation of the $C_7H_7O_2$ ion probably arises from the transition $150^+ \longrightarrow 123^+ + HCN$ ($m^* = 100.8$). A plausible mechanism would involve opening the cyclic imide ring with cleavage of one of the carbon-nitrogen bonds, then a ring involving a new carbon-oxygen bond could be formed. Loss of HCN which involves a 1,2-hydrogen migration would give rise to the unstable lactone which stabilizes when the oxygen becomes attached to the alternate bridge-head carbon atom. The formation of the m/e 136^+ ion involves either the loss of CH_3 or NH. This ion resulting from the decomposition of cis-4-cyclohexene-1,2-dicarboximide appears as a singlet ($C_7H_6NO_2$) clearly indicating the loss of CH_3. Cyclohexene and transΔ^2-decalin are reported (7) to produce an $M\text{-}15^+$ ion and this unusual fragmentation was later shown to involve a hydrogen migration (8). An analogous situation occurs in the mass spectrum of cyclohexane-1,2-dicarboximide (spectrum not shown) which shows a peak at 138 corresponding to the loss of a methyl group. Another analogous transition occurs in the cyclohexane compound in the peak at m/e 125^+ which can arise by the direct expulsion of carbon monoxide from the ($m^* = 102.1$). One of the most intense ions in the spectrum of cis-4-cyclohexene-1,2-dicarboximide appears at m/e 80^+ whereas in the cyclohexene compound it appears at m/e 82. This ion may arise from direct cleavage of the cyclic imide ring or it may arise from at least two stepwise fragmentation pathways in which the cyclic imide fragments as indicated in Figure 2. Ions at mass 106 C_7H_8N and C_7H_6O, can be formed from either of the mass 123 ions as shown in Figure 3. The expulsion of NHCO from m/e 123^+ (C_7H_9NO) also provides a direct route for the production of m/e 80^+. The ion at m/e 65^+ is probably formed by the successive loss of NHCO and CO from m/e 136^+.

N-Methyl cis-4-cyclohexene-1,2-dicarboximide. The mass spectrum of the N-methyl derivative (M^+ = 165) shows a higher $(M-1)^+$peak than other members of this series. The m/e 136^+ ion is formed in a two-step process; either first by loss of a proton and second by loss of CO or the reverse. The loss of CO directly gives rise to m/e 137^+. The contrast between the routes of formation of m/e 136^+ ($C_8H_{10}NO$) from the N-methyl derivative and the parent compound, m/e 136^+ ($C_7H_6NO_2$) is striking, since there is no evidence for the loss of a methyl radical from the cyclohexene ring in the N-methyl derivative.

The N-methyl cis-4-cyclohexene-1,2-dicarboximide exhibits a single ion at m/e 123^+ ($C_7H_7O_2$). This ion probably arises from a pathway analogous to that described for the parent compound, but it may also arise from the loss of CH_3CN from the ion at m/e 164^+; however, no metastable transition was observed to confirm this hypotheses.

The ion at mass 106 may be formed either from m/e 123^+ ($C_7H_7O_2$) or it may arise by a sequential process involving the successive loss of CH_3, NCO, H, and H yielding the intermediate ions at m/e 150^+, 108^+ and 107^+.

The origin of the multiple group of six carbon ions at m/e 77^+, 79^+, and 80^+ and 81^+ are similar to that indicated for the parent compound in Figure 2. Additional peaks in the spectrum of the N-methyl derivative are m/e 110^+ (C_6H_6NO) which can be formed by the loss of C_2H_2 from m/e 136^+ and m/e 91^+ (C_7H_7; tropylium ion) which can be formed by expulsion of an oxygen atom from m/e 107^+ (C_7H_7O).

N-Ethyl-cis-4-cyclohexene-1,2-dicarboximide. The fragmentation of the N-ethyl derivative has some similar features to those of the previous compounds; however, certain notable differences do exist. Two ions of m/e 151^+ are formed; one of these ($C_9H_{13}NO$) arises from the expulsion of CO and the other ($C_8H_9NO_2$) arises from the loss of C_2H_4 from the N-alkyl sidechain. The formation of $C_8H_9NO_2$ involves a single hydrogen shift.

Two ions with mass 136 ($C_7H_6NO_2$ and $C_8H_{10}NO$) are present in the spectra of the N-ethyl derivative. It is notable that the $C_7H_6NO_2$ ion, which was probably formed from m/e 151^+ by the expulsion of a methyl group from the cyclohexene ring, was not observed in the N-methyl derivative (no m/e 151^+ ($C_8H_9NO_2$) was observed in the N-methyl derivative either). However, in the N-methyl derivative the ion at m/e 136^+ ($C_8H_{10}NO$) is formed in a two-step process involving the loss of CO and H sequentially whereas in the N-ethyl derivative the two-step process involves the sequential loss of CH_3 and CO. The ion at m/e 136^+ ($C_7H_6NO_2$) fragments to give m/e 93^+ (C_6H_5O) which is followed by the loss of CO to give m/e 65^+ (C_5H_5). The latter two ions were not present in the N-methyl derivative.

A single peak was observed for the ion at m/e 123^+ ($C_7H_7NO_2$) and it was assumed that it originated from m/e 151^+ ($C_8H_9NO_2$) in the same manner as shown for the parent compound (Figure 3).

A minor pathway involves a 1,2-hydrogen shift in a retro Diels-Alder reaction to give the ion m/e 126^+ ($C_6H_8NO_2$) which can further decompose to give m/e 98^+ ($C_4H_4NO_2$).

N-n-propyl- and N-n-butyl cis-4-cyclohexene-1,2-dicarboximide. The mass spectra of the N-n-propyl and the N-n-butyl derivatives were quite similar. Both of these compounds exhibit relatively intense molecular ions and, in general, their fragmentation pattern could be predicted in part based on the studies done on the N-n-propyl succinimides (6).

A detailed study of their spectra shows some ions not observed in lower homologues of this series. A 1,3-hydrogen shift that involved the N-alkyl side-chain was observed.

EXPERIMENTAL

Mass Spectra. Mass spectra were obtained, using the direct and gas-chromatograph inlets on the prototype of the LKB Model-9000 combination mass spectrometer-gas chromatogarph (9,10). All spectra were corrected for background. The mass spectrometer was operated at an electron energy of 70 ev at an accelerator voltage of 3.5 kv and a trap current of 65 μA. The ion source was kept at 290°. The electron multiplier voltage was maintained at 1.7 kv except to obtain metastable peaks when it was raised to 2.1 kv.

High resolution spectra were obtained on a CEC 21-103 instrument at the Mass Spectrometry Center, Lafayette, Indiana.

The spectra were computer plotted from tabular intensity data (11). The tabular values were computed from raw data (mm intensity values) introduced to an IBM 7040 computer through punched cards (11).

Synthesis. The synthesis of the unlabeled compounds has been described previously (1).

ACKNOWLEDGEMENTS

We wish to thank Dr. Fred W. McLafferty and Dr. George Van Lear of the Purdue University Mass Spectrometry Center (supported under U.S. Public Health Service Grant No. FR-00354) for the high resolution mass spectral data, Dr. N. E. Tolbert of Michigan State University for samples of the unlabeled compounds and Dr. Stuart E. Scheppele of Oklahoma State University for helpful discussions.

FOOTNOTES

[1]This work was supported in part by Research Grants GB-3482 and GB-7731 from the National Science Foundation, Washington, D. C., U.S.A.

[2]To be submitted for publication in Organic Mass Spectrometry.

REFERENCES

1. E. D. Mitchell and N. E. Tolbert, Biochemistry, 7, 1019 (1968).

2. R. A. W. Johnstone, B. J. Millard and D. S. Millington, Chem. Comm. 600 (1966).

3. R. L. Cotler, R. A. Dine-Hart, Chem. Comm. 809 (1966).

4. J. Scharvit and A. Mandelbaum, Israel Journ. Chem., 5, 33 (1967).

5. R. T. Alzpin and J. H. Jones, Chem. Comm. 261 (1967).

6. A. M. Duffield, H. Budzikiewicz and C. Djerassi, J. Am. Chem. Soc., 87, 2913 (1965).

7. H. Budzikiewicz, J. I. Brauman and C. Djerassi, Tetrahedron, 21, 1855 (1965).

8. R. T. Aplin, H. E. Browning and P. Chamberlain, Chem. Comm., 1071 (1967).

9. R. Ryhage, Arkiv. Kemi., 26, 305 (1967).

10. G. R. Waller, Proc. Okla. Acad. Sci., 47 (1967), in press.

11. H-Y Li, D. Etter, J. Walden and G. R. Waller, Proc. Okla. Acad. Sci., 48 (1968), in press.

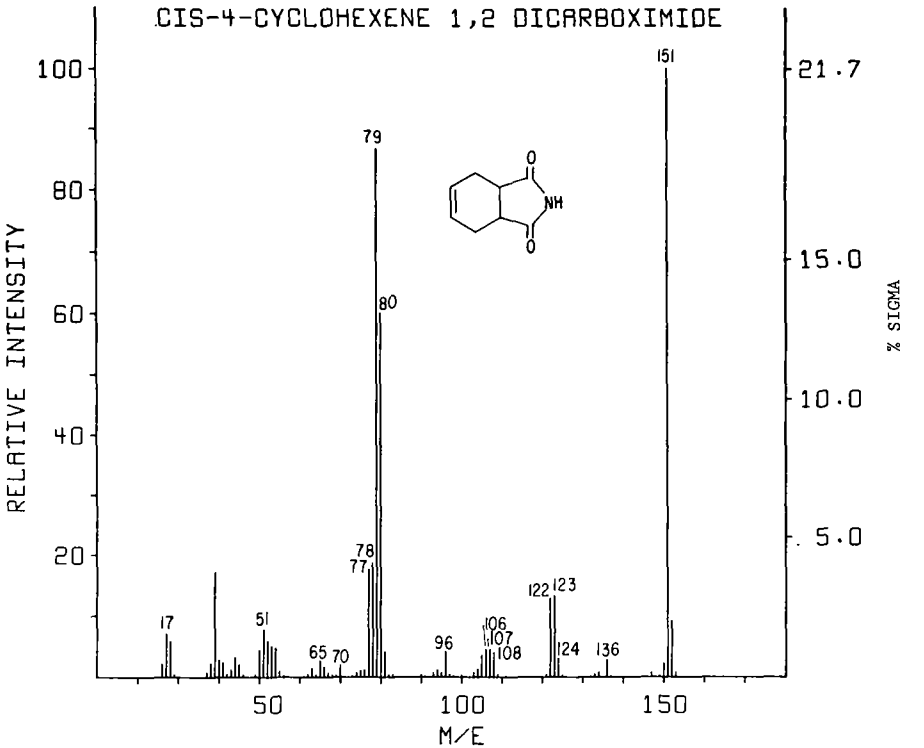

Figure 1

Mass Spectrum of cis-4-cyclohexene-1,2-dicarboximide

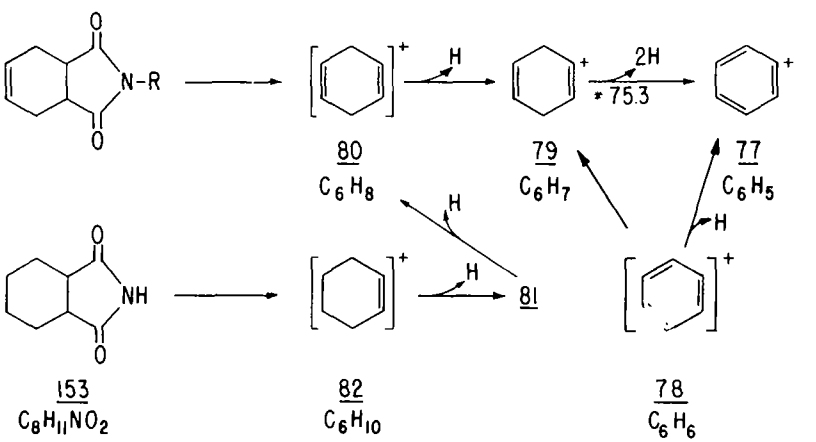

Figure 2

Proposed Mechanism for the Formation of the Ions Containing Six Carbon Atoms

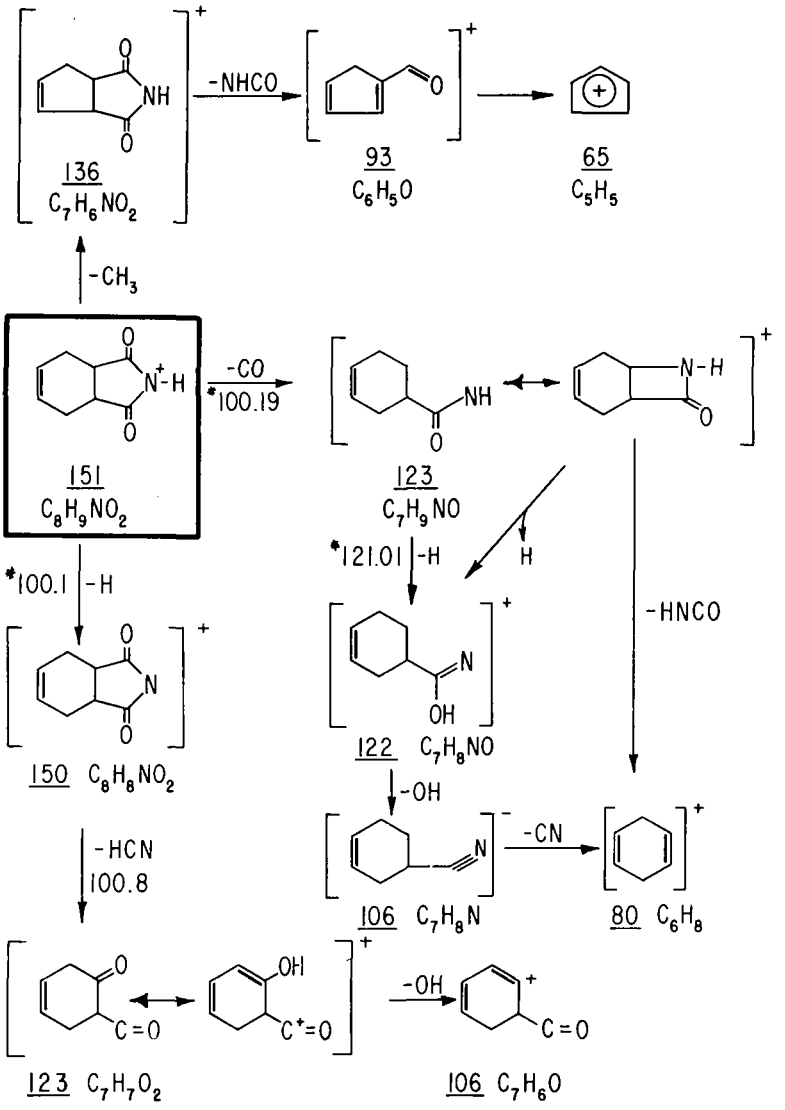

Figure 3

PARTIAL FRAGMENTATION OF CIS-4-CYCLOHEXENE 1,2 DICARBOXIMIDE

105. Analysis of Biological Related Organic Salts by Laser Ionization

F. J. Vastola, A. J. Pirone and R. O. Mumma
Pennsylvania State University
University Park, Pa.

Introduction

While studying the species produced by laser pyrolysis of polymeric materials it was found that organic ions could be produced by laser irradiation (1). Because of the simplicity of the spectra produced by this method of ionization its use as a technique of analysis of organic solids would appear promising. To test the scope of this technique the analysis of some organic salts was attempted. Organic salts (phosphates, sulfates, sulfonates and thiosulfates) are of biological interest because they play an important role in the metabolism of all living organisms. These organic salts are also of considerable importance because man has contaminated his environment with these molecules in the form of synthetic detergents and pesticides. These organic salts present some difficulty in analysis because they are not volatile and cannot be gas chromatographed. Normal mass spectra of these molecules can't be obtained since the spectra represent only the pyrolysis products. The positive ion mass spectra, produced by laser irradiation, of nine organic salts (sulfates, thiosulfates and sulfonates) are presented in this paper.

Experimental

The equipment has been described in detail (2). It consists of a small pulsed ruby laser (wavelength 6943 Å, output 0.1 joule) whose output is focused through a 2X microscope objective on a sample placed in the ionization chamber of a Bendix model 12-107 TOF mass spectrometer. Since the laser pluse length is approximately 300 μ sec. the 10 KHz repetition rate of the mass spectrometer allows 2-3 analysis to be made during the irradiation period. Ions are produced only during the laser pulse. By the synchronization of an oscilloscope with a raster type display and the master oscillator of the TOF spectrometer with the laser pulse, the laser ion spectrum can be recorded. When using the laser as the mass spectrometer ionizing source the standard electron bombardment source is deactivated.

The samples were prepaired for analysis by compacting about 1 mg of material into a disk 3 mm in diameter. Several of these disks could be placed on a pedestal which could be inserted into the mass spectrometer ionization chamber through a vacuum lock assembly. To insure uniform coupling of the laser output to the samples a sparce covering of pyrographite flakes (1-10 microns in diameter) was placed on their surface.

Materials

A number of simple organic sulfate, thiosulfate and sulfonate salts were chosen for this investigation (Table I). The sulfate (3) and the thiosulfates esters (4) were prepared in our laboratory. Sodium hexylsulfonate was purchased from Mann Research Laboratories and the potassium and cesium salts were prepared by means of ion exchange columns.

TABLE I

SALTS USED

Ident. Number	Salt	MW
Ib	$C_6H_{13}SO_3Na$	188
Ic	$C_6H_{13}SO_3K$	204
Id	$C_6H_{13}SO_3C_s$	298
IIa	$C_6H_{13}SO_4Na$	204
IIe	$C_{16}H_{33}SO_4K$	388
IIb	$C_6H_{13}SO_4C_s$	314
IIIf	$C_{16}H_{33}S_2O_2Na$	360
IIIh	$C_{14}H_{29}S_2O_2Na$	332
IIIc	$C_8H_{17}S_2O_2K$	264

Spectra

Mass spectral intensities of thesalts given in Table I are depicted in Table II.

TABLE II

MASS SPECTRA

Ib			Ic			Id		
m/e	Rel. Int.*	Species	m/e	Rel. Int.	Species	m/e	Rel. Int.	Species
126	*	Na_2SO_3	105	2		133	13	Cs
149	*	Na_3SO_3	113	4		142	4	
165	*	Na_3SO_4	158	2	K_2SO_3	298	14	Cs_2O_2
211	20	P + Na	197	2	K_3SO_3	321	2	P + Na
239	*		213	3	K_3SO_4	337	6	P + K
			226	2		341	20	P + Cs
			243	20	P + K	490	1	Cs_3SO_4
	IIa			IIc			IIb	
142	20	Na_2SO_4	110	4	K_2O_2	133	20	Cs
149	2	Na_3SO_3	158	6	K_2SO_3	193	1	
165	8	Na_3SO_4	174	10	K_2SO_4	208	3	
227	10	P + Na	197	6	K_3SO_3	291	2	$CsKNaSO_4$
			213	20	K_3SO_4	298	13	Cs_2O_2
			427	20	P + K	307	1	CsK_2SO_4
						337	1	P + Na
						353	4	P + K
						385	5	Cs_2NaSO_4
						401	5	Cs_2KSO_4
						429	2	
						447	14	P + Cs
						495	9	Cs_3SO_4
	IIIf			IIIh			IIIc	
135	20	NaS_2O_3	135	8	NaS_2O_3	110	20	K_2O_2
149	8	Na_3SO_3	149	12	Na_3SO_4	158	12	K_2SO_3
165	10	Na_3SO_4	165	14	Na_3SO_4	174	8	K_3SO_3
298	4		355	20	P + Na	197	20	K_2SO_4
355	2		371	14	P + K	213	13	K_3SO_4
383	16	P + Na	387	6	$P^{\dagger}$ + K	224	6	
399	13	P + K				303	17	P + K
415	4	$P^{\dagger}$ + K						

* = < 1%, † Potassium impurity parent.

The spectra cover a mass range from m/e 100 to slightly more than the molecular weight of the salt. The mass spectra were taken from Polaroid photographs of the oscilloscope raster. Due to the relatively low dynamic range of this technique spectra could only be recorded over a twenty to one range. The accuracy of mass assignment is presently limited by factors such as the linearity of the oscilloscope sweep. For these spectra the authors have used the salts and their fragments as internal mass standards. The mass adjustments necessary were usually less than 1%. The following generalizations can be drawn from those spectra. The only major organic salt ion produced is that of the parent (i.e., RSO_3Na = P) plus a cation. There are no major peaks produced by carbon-carbon bond breakage. The majority of the ions produced are inorganic. The cesium salt produces a much more intense ion burst for a given laser power than the sodium salt.

The major ion for the sulfonates is the parent plus a cation. The inorganic ion intensity is relatively small, this is best illustrated by the sodium salt (Ib) which

produces essentially a one peak spectrum. It is interesting to note how impurities in the cesium salt (Id) produce peaks at the parent plus sodium and also potassium together with the parent plus cesium. These peaks could be the sodium or potassium salt plus cesium as well.

With the sulfate salts the parent plus a cation is not always the major peak. The inorganic ions are greater in intensity than in the spectra of the sulfonates indicating that the carbon-sulfur bond is stronger than the carbon-oxygen bond.

The thiosulfate spectra are similar to those of the sulfates. Masses 135 and 142 can be used to differentiate between the thisulfate and sulfate sodium salts. The sodium salts (IIIf and IIIh) are contaminated with potassium, relatively large amounts of the potassium parent plus potassium are detected.

Conclusion

Laser ionization has been used to analyze a series of alkali metal sulfonate, sulfate and thiosulfate salts. These materials tend to decompose on heating however this technique produces simple mass spectra where the only major organic ion is that of the parent plus a cation.

References

1. Vastola, F. J., Pirone, A. J., "Advances in Mass Spectrometry", Institute of Petroleum (in press).

2. Vastola, F. J., Pirone, A. J., Knox, B. E., Proceedings Fourteenth Annaul Conference on Mass Spectrometry and Allied Topics, 78 (1966).

3. Mumma, R. O., Lipids 1, 221 (1966).

4. Mumma, R. O., Unpublished work.

105. Applications of GC-MS Systems to Organic and Biomedical Problems

R.A. Hites, S. Markey, R.C. Murphy, and K. Biemann

Department of Chemistry
Massachusetts Institute of Technology
Cambridge, Massachusetts 02139

In work on organic and biomedical problems one is often faced with complex mixtures of organic compounds. We would like to describe here one approach to those problems which are amenable to gas chromatography as a separation technique. Direct coupling with mass spectrometry as a highly sophisticated structure sensitive detector using a computer to handle the large volume of data produced, makes the system a rather powerful one.

An IBM 1800 computer handles raw data generated by a single focusing, magnetic scanning mass spectrometer (Hitachi RMU-6D) with its ion source connected to the effluent of a gas chromatograph via a helium separator. The computer converts this raw data into mass-intensity tables (mass spectra) (1). The key to this system is the reproducible, repetitive scanning of the magnet which allows reliable conversion of time units to masses. This reproducibility is best achieved by having the computer precisely time the start and end of the magnet scan. A mass spectrum is recorded and stored on magnetic disks every four seconds during the entire course of the gas chromatogram. Rather than using the ion beam monitor to produce the gas chromatogram that the mass spectrometer sees (a flame ionization curve is run parallel mainly for control purposes), the digitized signals are summed for each scan (thus producing a value analagous to the ion beam monitor output) and plotted vs. scan index number (Figure 1).

The availability of complete spectral data for each four second interval of the gas chromatogram regardless of the apparent emergence of a fraction not only eliminates the need for any decision making during the course of the experiment but also makes it possible to manipulate and use the data in a variety of ways, many of them not otherwise feasible, at the option of the investigator. For example, each one of the 378 mass spectra from the 25 minute chromatogram in Figure 1 can be randomly accessed and plotted as a conventional bar graph for manual interpretation. Furthermore, an automated comparison of any spectrum with those contained in a library of known mass spectra is an alternative mode of interpretation (2). Table 1 shows the results of such a library search for scan number 179.

Table 1: Library Search of Scan Number 179 in Figure 1

MVD 24-2-3, Methylated	Scan No. 179
Results	Similarity Index
*Methyl octane-1,8-dioate	0.721
Methyl 4-methylheptane-1,7-dioate	0.390
Methyl 10-methyl-octadecanoate	0.196
Methyl 14-methyl-heptadecanoate	0.184
Methyl hexadecanoate	0.180
Methyl nonanoate	0.173
Methyl heptadecanoate	0.168
Methyl pentadecanoate	0.168
Methyl tridecanoate	0.165
Methyl 16-methyl-heptadecanoate	0.161

The searching program involves the following: 1) the unknown spectrum is reduced to an abbreviated spectrum containing the two most intense ions for every 14 mass units, and 2) this is then compared with the abreviated spectra of the known compounds in the library. The similarity index indicates the weighted averaged relative ratios of intensities of each mass in the known versus the same mass in the unknown.

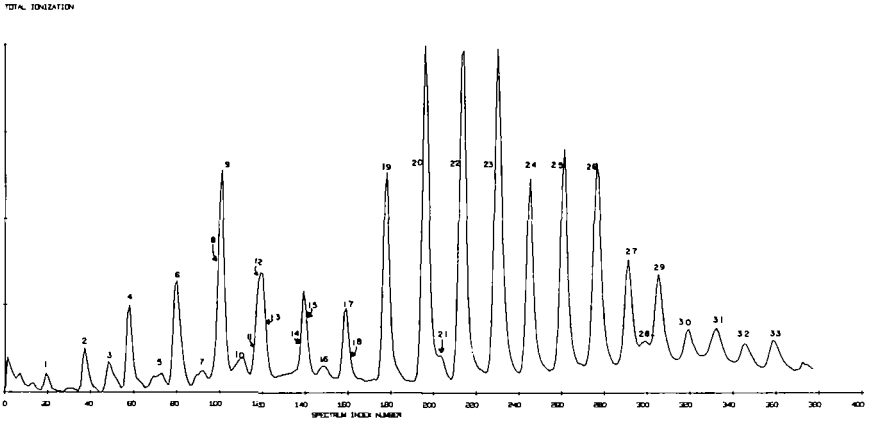

FIGURE 1

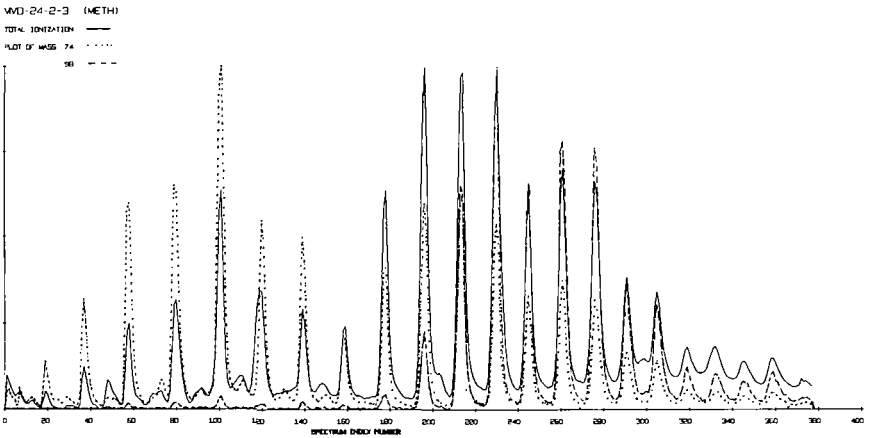

FIGURE 2

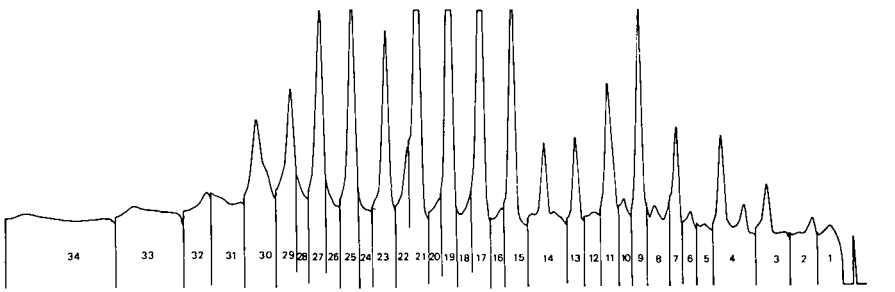

FIGURE 3

An index of 1.0 is perfect , but anything above 0.5 is good considering the fact that the library spectra have been mainly assembled from published data and were thus obtained in other laboratories on other mass spectrometers and on stationary samples rather than GC effluents. In the above example it is rather clear that the scan number 179 is methyl octane-1,8-dioate and that the technique distinguishes it well from the branched isomer listed in the second line. As a final check one could ask the computer to plot the spectra of the known and unknown side by side for individual inspection of the details of the similarity.

One approach we have found to be extremely useful involves plotting the abundance of a specific ion in the consecutive spectra as a function of spectrum number. This is illustrated in Figure 2. The solid trace is the same as Figure 1. Since the mixture represented an acid fraction which was converted to methyl esters, it was expected that there may be present aliphatic mono- and di- methyl esters. The former give rise to a peak at m/e 74 and the latter to m/e 98 (if the $(CH_2)_n$ chain is long enough). Plots of these two masses (dotted and broken line respectively) show exact coincidence (in terms of the x-axis parameter) with some of the GC-peaks, indicating that in the earlier part of the chromatogram mono-methyl esters are eluted while the later part consists mainly of α,ω dimethyl esters. However, some peaks are broad on the total ion plot but sharp when individual masses are plotted (see for example, the area around spectrum index 120), indicating that other components are present in the peak, or at places where the trace seems flat (as between indexes 120-140), individual ion intensities clearly indicate the emergence of different compounds.

In some instances it is necessary to have high resolution data to facilitate the interpretation of low resolution scans. For this purpose the mixture is also run on a gas chromatograph connected to a high resolution mass spectrometer of Mattauch-Herzog geometry (CEC 21-110B) using a photographic plate to continuously record the spectra (3). Because of the simultaneous focusing of all ions and the integrating properties of the photographic emulsion, each spectrum (as many as 60 per plate) contains all the elemental composition data of that part of the gas chromatogram emerging during the particular exposure. Figure 3 shows the beam monitor recording of the same mixture as in Figure 1 run on this GC-HRMS system. The photographic plate is read on an automatic comparator operated on-line with the computer (4). To mention an example of the performance, exposure 27 of Figure 2, which was 22 seconds long, indicated a resolution of 22,000. The masses of 89% of the ions were found within ±1.0 millimass unit of the theoretical value. The computer time required from the beginning of the reading of the photoplate to the final printing of the elemental compositions was under 10 minutes.

The results of such interpretative techniques applied to the methylated acidic fraction of Green River shale (shown in Figures 1 to 3) have led to the identifications shown in Table 2.

Table 2: Identification of Labeled GC Peaks in Figure 1

1. Methyl hexanoate
2. Methyl heptanoate
3. Methyl 2,6-dimethyl-heptanoate
4. Methyl octanoate
5. Methyl 2,6-dimethyl-octanoate
6. Methyl nonanoate
7. Methyl 2,6-dimethyl-nonanoate
8. Methyl butane-1,4-dioate
9. Methyl decanoate
10. $C_{10}H_{19}COOCH_3$
11. $C_8H_{11}NO_2$
12. Methyl pentane-1,5-dioate
13. Methyl undecanoate
14. Methyl hexane-1,6-dioate
15. Methyl dodecanoate
16. Methyl 2,6,10-trimethyl-undecanoate
17. Methyl heptane-1,7-dioate
18. Methyl tridecanoate
19. Methyl octane-1,8-dioate
20. Methyl nonane-1,9-dioate
21. Intense M/e 155 ($C_8H_{11}O_3$)
22. Methyl decane-1,10-dioate
23. Methyl undecane-1,11-dioate
24. Methyl dodecane-1,12-dioate
25. Methyl tridecane-1,13-dioate
26. Methyl tetradecane-1,14-dioate
27. Methyl pentadecane-1,15-dioate
28. $M^+ = 296$ $C_{20}H_{24}O_2$
29. Methyl hexadecane-1,16-dioate
30. Methyl heptadecane-1,17-dioate
31. Methyl octadecane-1,18-dioate
32. Methyl nonadecane-1,19-dioate
33. Methyl eicosane-1,20-dioate

Another example of the use of this system in medical research will be mentioned briefly. In the course of an investigation (conducted by Prof. J. Hedley-Whyte at Harvard Medical School) of the materials extractable from human blood serum, a sample was encountered that exhibited a series of gas chromatographic peaks in an area devoid of components in normal blood. In an effort to identify these substances, a sample of the extract was run on the system described above. Surprisingly enough, the bar graph plot of a scan recorded during the emergence of one of the major GC fractions revealed the features of a straight chain hydrocarbon of 17 carbon atoms. As a test for the presence of other homologous hydrocarbons, M/e = 57, 71, 85, and 99, abundant ions in the mass spectra of normal alkanes, were plotted as described above. The coincidence of the abundance of all these alkyl ions with most (but not all) gas chromatographic peaks indeed indicated the presence of a series of normal alkanes. The main differences in the ion abundance plots and the total ionization plot reside in the components of very long retention times. These seem to be the beginning of the elution of the steroid components.

References.

1. R. A. Hites and K. Biemann, Anal. Chem., 40, 1217 (1968).

2. R. A. Hites and K. Biemann, International Conference on Mass Spectrometry, Berlin, September 1967.

3. J. T. Watson and K. Biemann, Anal. Chem., 37, 844 (1965).

4. C. Cone, P. Fennessey, R. Hites, N. Mancuso, and K. Biemann, 15th Annual Conference on Mass Spectrometry and Allied Topics, Denver, May 1967.

Acknowledgement

This work was supported by research grants from the National Institutes of Health (FR-00317) and the National Aeronautics and Space Administration (NsG 211-62 and NGR-22-009-102).

107. DIGITALIZATION AND RECORDING OF MASS SPECTRA FROM A COMBINATION GAS CHROMATOGRAPH - MASS SPECTROMETER.

P.-Å Jansson, S. Melkersson, R. Ryhage and S. Wikström

Laboratory for Mass Spectrometry
Karolinska Institutet, Stockholm, Sweden

ABSTRACT

A mass spectrum digitizer has been developed and used in a combination gas - chromatograph - mass spectrometer (LKB 9000). The digital data is recorded by an incremental tape recorder Ampex TM7. An electronic mass marker working with a Hall-element, senses a change in the magnetic field at constant accelerating voltage and generates a trigger pulse for each mass number. The recording speed of the system is limited by the incremental tape recorder (max. 300 peaks per second). The trigger pulse starts the analog to digital signal conversion as well as the recording onto the magnetic tape. The digitally recorded mass spectra are given to a computer where back-ground spectra are substracted from the actual mass spectra and the results are conveniently readable in table form or can be plotted as "bar graphs".

The mass marker is also used for fast analog recording of mass spectra where one channel is used for recording the mass marker, one for the analog data in logarithmic form and on a third channel the start/stop function of the mass spectrometer scan is recorded. A computer (IBM 1800) reads the analog tape and the computer program uses the mass marker signals to calculate a m/e value for each analog recorded peak intensity. Consequently, there is no need for a reference compound for comparison and spectra can be taken at random rates. Mixtures of different organic compounds run by the GC-MS instrument were studied and some results are given.

INTRODUCTION

After the construction of a combined gas chromatograph and a mass spectrometer with a molecule separator as an integrated part of the system was completed, the number of mass spectra obtained has increased continuously, and this increased production of mass spectra has often become difficult to handle. The developmental advantages made in electronic and computer fields during the past few years have completely changed the registration and information possibilities. These factors have made it desirable to begin using computers to evaluate mass spectral data. Most laboratories do not have the advantage of using a computer of their own, connected "on line" with the mass spectrometer, as would be the best solution. It is therefore conceivable that a less expensive data acquisition system could fulfill the need of a mass spectrometer in many cases. The data could then be processed on a central computer in the vicinity.

Such data acquisition systems have been developed at our laboratory. These systems will reduce the time required for obtaining a mass spectrum and presenting it in tabular form or as a plotted "bar graph".

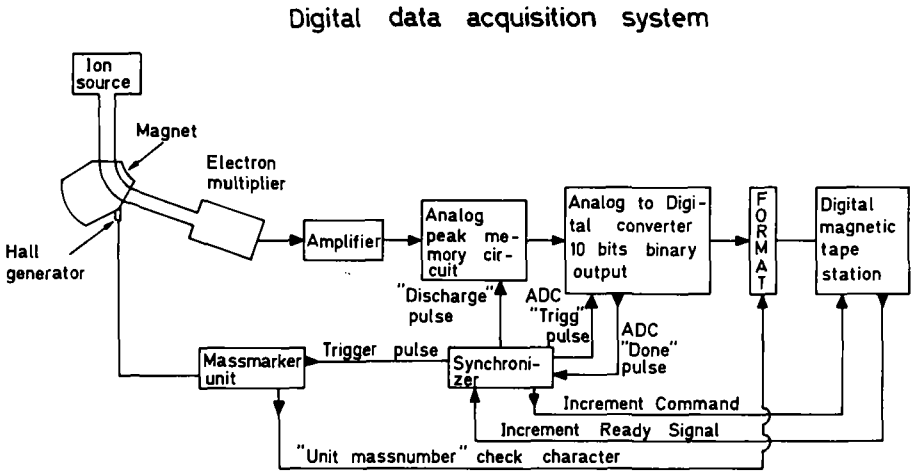

Fig. 1. Function diagram of the incremental data acquisition system.

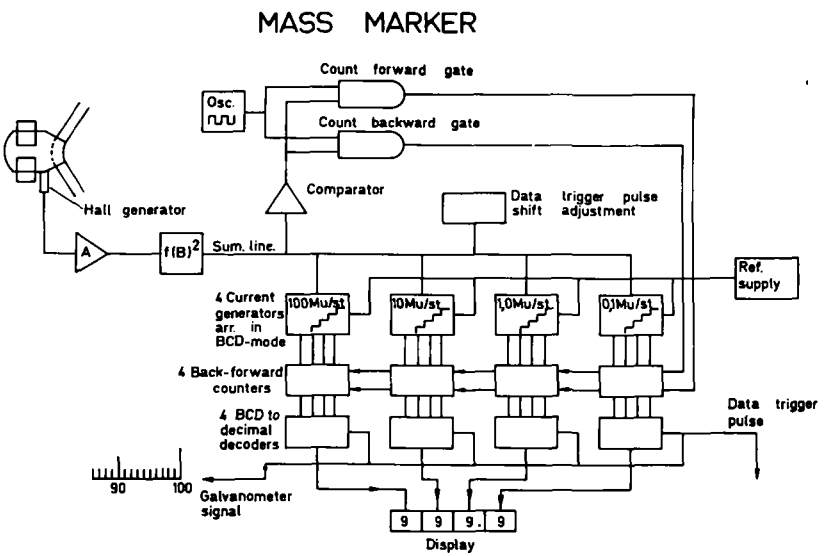

Fig. 2. Block diagram of the mass marker.

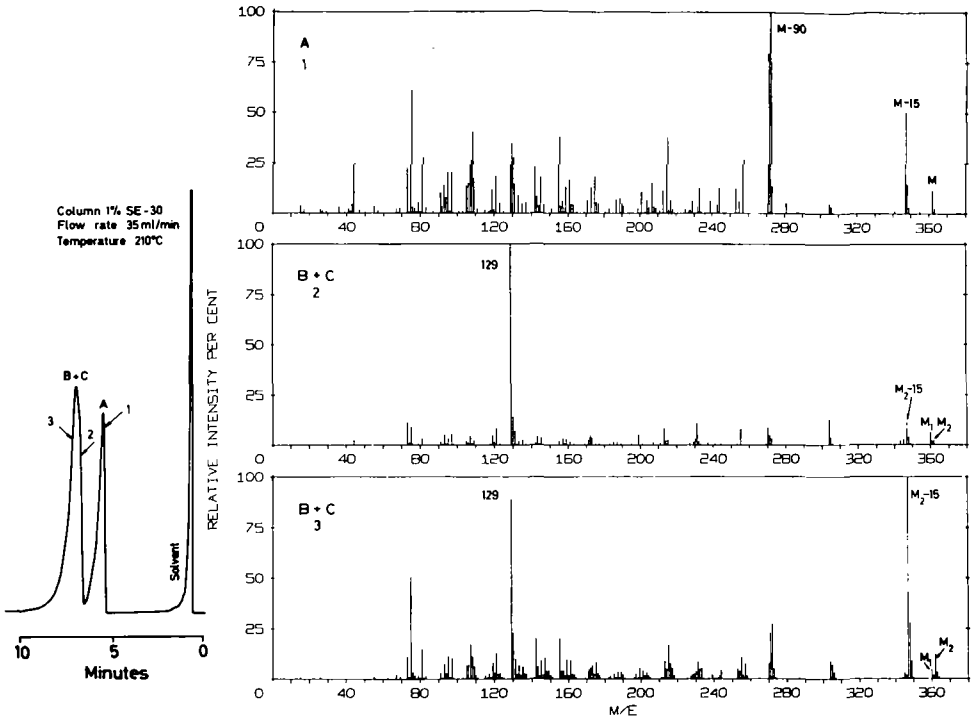

Fig. 3. Gas chromatogram of Androsterone, epiAndrosterone and Dehydroandrosterone TMSi derivative and mass spectra taken at the marks of the two peaks.

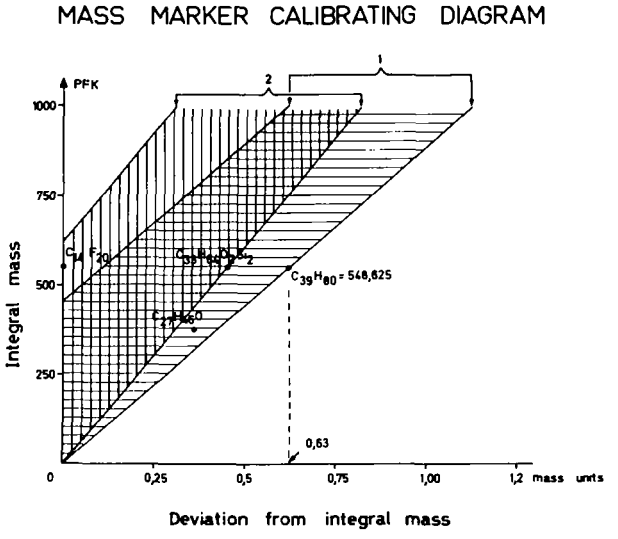

Fig. 4. Integral mass as a function of the positive deviation from integral mass.

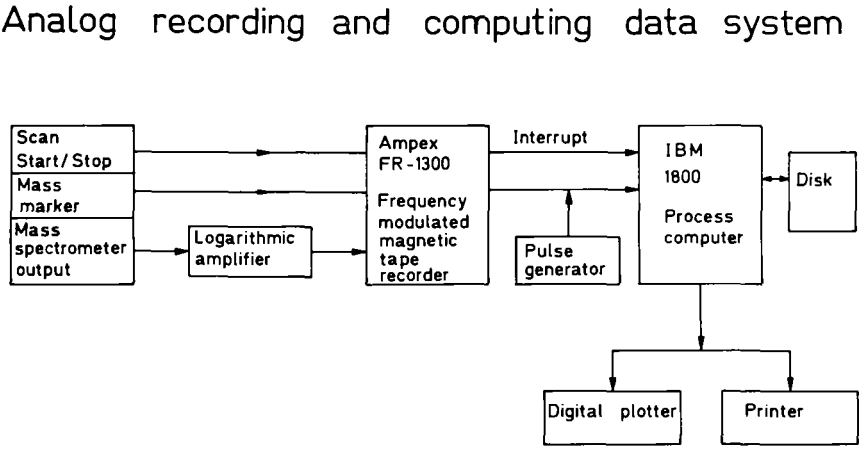

Fig. 5. Block diagram of the analog recording and computing data system.

Previously a data acquisition system which continuously samples the output of a mass - spectrometer, manufactured by Radiation Incorporated in the United States, has been used by Hites and Biemann, MIT. A cyclic magnetic scan of the mass spectrometer and reference compounds for calibration of the mass number were used in this case.

In the data systems we have developed a mass marker used for calibration of the mass number, which means that mass spectra can be taken at random rates without reference compounds.

INSTRUMENTATION

Fig. 1 shows the incremental digital data acquisition system, when it is connected to a mass spectrometer with an operating electronic mass marker. The mass marker pulse is placed about 0.3 mass units behind every mass number and is used to give a read command to a fast A/D converter (10 μs, 10-bits binary word), which reads the analog signal from the mass spectrometer, stored in the analog peak memory circuit. When the A/D converter has read the amplitude value of the analog peak, it gives out a discharge command to the peak memory circuit, which from that moment is ready to take care of the next analog signal. The synchronizer then forwards the digital value of the analog peak to the digital magnetic tape recorder where it is recorded together with a mass number check character supplied by the mass marker unit. The maximum speed of the tape station is 650 characters per second and each intensity requires two characters. The maximum scanning speed will therefore be 325 mass numbers per second. The actual mass spectrometer scanning time over a mass range m/e 10-800 will be about 3 seconds, which will be satisfactory for most of the gas chromatography work. The scanning speed is limited by the time difference between two adjacent mass numbers at the highest studied mass and consequently, the linear scan is favoured over the exponential scan when the digital recording system is used in the incremental mode of operation.

Fig. 2 shows the principal of the mass marker which has been developed to enable a fast and accurate evaluation of the mass numbers. A Hall-generator is used as a sensor of the magnetic field of the mass spectrometer and its output voltage is applied to an electronic function converter. The output current from the converter is proportional to the square of the input, that is, to the square of the magnetic field and therefore also to the corresponding mass number. Four decades of current generators are connected to the output of the function converter to balance this output. The generators are switched on and off from the outputs of a 4 decade back-and-forth counter and by decoding the positions of the switches it is possible to read the mass number directly on a 3-4 unit display. A pulse is also generated for each mass number passed during a scan, which is used either to give a mark on the UV-paper or to trigger a data acquisition system. The marks are also shown in the lower left side of the figure 2 and as can be seen, their amplitude differs for units, tenths and hundredths of a mass. The maximum scan speed which can be tolerated by the mass marker is 1-1000 mass units in 0.8 seconds. The maximum error of the mass marker is about 0.3 mass units.

RESULTS AND DISCUSSION

The incremental digital data acquisition system has been used to record mass spectra of eluents from a gas chromatograph. A mixture of Androsterone (A), epiAndrosterone (C) and Dehydroepiandrosterone (B) was converted to trimethylsilylethers and then injected on a 1% XE-60 column. On this column, all three compounds were nearly separated and good mass spectra were obtained. Fig. 3 shows the same mixture injected on a 1% SE-30 column, where a separation between Dehydroepiandrosterone and epiAndrosterone can hardly be noticed on the GLC diagram. However, the obtained mass spectra which are marked B + C, 2 and 3, shows that these compounds can be identified without too much difficulty. The plot of these mass spectra by the digital plotter took about 3 minutes for each in computing time.

The program for processing the digital magnetic tape is written in programming language one (PL-1) and works as follows: First; it reads all spectra into the computer where each spectrum is checked for a correct sequence of mass numbers. When this is done the computer takes the "background" spectra and subtracts it from the actual sample mass spectra. The resulting data is then converted into relative intensities. One can then decide whether a table or a plot as "bar graph" should be made. Using a line printer the table is made in less than 10 sec. The computer can also make up a new so called library magnetic tape with spectra which are considered to be valuable.

The mass marker for low resolution mass spectrometers should indicate each mass number with good accuracy independent of the combination of different atoms. This is, however, not always possible since the masses of all different atoms are given relative to the mass standard ^{12}C and all other atomic combinations give always a m/e value of more or less deflection from the integral mass numbers. Fig. 4 shows a diagram of the integral mass number, which is nearly equivalent to Perfluorokerosine, given as a function of the positive mass difference from integral mass. Experimentation has shown that a difference in mass up to 0.5 mass units can be accepted without changing the scale factor. When the scale factor is set for hydrocarbons, area 1 shows the working range of the incremental digital registration system. Within this area most organic compounds are found, only highly aromatic compounds with a molecular weight above 500, or compounds which have halogens incorporated, need another setting of the scale factor, and the diagram will change as shown in area 2. Saturated hydrocarbons and Perfluorokerosine with a molecular weight up to about 450 can be recorded without changing the scale factor.

The mass marker pulses are at the center of the peaks for registration on UV-paper, but, with the digital data acquisition system in operation the pulses are placed about 0.3 mass units after the peaks, to be certain the peaks will be correctly recorded. A change of the mass marking position is easily created. A digital data acquisition system used to continuously record the output from a mass spectrometer has been reported earlier by Hites and Biemann, MIT. It should therefore only be noted here, that the mass marker data is added to the intensity data on the magnetic tape. This will make the recording procedure somewhat easier, since no cyclic magnetic scan is necessary.

The computer program to evaluate the data will be simpler, since no calibration run has to be done to receive a reference mass marker table within the computer. The main difference between the incremental and continuous digital registrations it that in

the incremental mode only one intensity is recorded for each mass number, but, with the continuous system the A/D converter samples the output of the mass spectrometer 3 to 12 000 times every second, as the mass spectrometer scan runs. The approximate total amount of data will be about 50 times greater as compared to the incrementally operated system.

Mass spectra have also been recorded on an analog magnetic tape using a 7-channel Ampex FR-1300 recorder.

Fig. 5 shows a block diagram of the analog registration system. To enable a dynamic range of 1:1000 on one channel, the analog signal from the mass spectrometer output is fed to the recorder via a logarithmic amplifier. On another channel the mass marker signals are recorded and are used to monitor the mass scale during the computer processing.

On a third channel the start/stop function of the mass spectrometer scan is recorded. It is used by the process computer as an interrupt channel to start and stop sampling of the analog input. The sampling speed of the analog input of the computer can be externally controlled up to 20 kc and the data is stored on disk.

In the program to process this magnetic tape the mass marker is used as a monitor where a peak is expected to be found. When a maximum value of this peak is found and if this intensity is above a cut-off level, a curve-fitting method is performed between a model curve and the peak. If the peak is high enough it is used as a calibration peak; that is, to record the new mass mark position in relation to the peak center deviation. This eliminates all mistakes in mass number counting due to differences in the empirical composition of compounds.

The peak intensity maximum is stored together with the corresponding mass number and the relative intensities in percentages are calculated. A decision can be made as to whether the output format of the data should be in table-form, plot-form or both. The recording speed of this system is very fast. This means that most scanning speeds of the mass spectrometer can be used, since the tape recorder can be played back into the computer if necessary, with a reduction factor of 1:30 in speed.

Of the systems described, the incremental system gives an easily read tape which can be handled by a small computer. The continuously sampling and digitally recording system and the analog recording systems give a lot more data to handle for the computer, however, these give a more detailed picture of the mass spectra where metastable and doubly charged ions can be studied.

The electronic mass marker has been very useful in all three methods since the mass scale can be established without the use of reference compounds.

REFERENCES

1. Hites, R.A. and Biemann, K.. Analyt. Chem., 1967, 39, 965.

108. ON-LINE DATA ACQUISITION AND PROCESSING OF GLC-MS DATA

J.R. Chapman, S. Evans and J.M. Holmes,
Consultant Laboratory,
Scientific Apparatus Division,
GEC-AEI (Electronics) Limited,
Manchester, England.

INTRODUCTION

The recording of complete high resolution mass spectra using a fast scanning double focusing instrument of Nier-Johnson geometry is now a well established technique.[1,2,3] The use of single focusing instruments for similar work has until recently not been considered feasible, largely because of the limited resolving power i.e. about 1000 of such machines and the expected inaccuracy of mass measurement due to kinetic energy of formation of fragment ions.

The performance of the GEC-AEI MS12 single focusing mass spectrometer has been improved so that a static resolving power of 7500 can be routinely achieved. A spectrum can also be scanned at the rate of 8 seconds per decade in mass at a resolving power up to 6000. This increased performance is sufficient for the separation of reference peaks from unknown sample peaks occuring at the same nominal mass up to about mass 500 if one considers 0.055 as typical of the smaller mass defects for organic compounds containing nitrogen and oxygen. Higher resolving power would be required if more mass deficient elements, e.g. sulphur or silicon were present. A resolving power of 6000 is also sufficient to fully separate CH_4-O doublets up to about m/e 200. These considerations indicate that it should be possible using a data acquisition and analysis system to accurately mass measure each peak in the spectrum and finally obtain a listing of the atomic compositions.

EXPERIMENTAL

In order to establish the achievable mass measurement accuracy, the initial experiments were carried out using hexachlorobutadiene as the "unknown" sample. This compound was admitted to the mass spectrometer via a conventional heated reservoir inlet system. For assessment of the basic mass measurement accuracy of the system it has the advantage that its mass spectrum contains no CH-^{13}C doublets. The reference compound for the measurements was perfluorokerosene which was also admitted via the same inlet system.

The gas chromatographic work was carried out using a Pye 104 type packed column system. This was connected to the mass spectrometer source via a Biemann Molecular Separator[4]. The components eluted from the GLC column were detected by the total ion monitor of the mass spectrometer. After amplification the signal from the monitor plate was displayed on a pen recorder to provide a record of the GLC effluent. Whilst monitoring the effluent in this manner the mass spectrometer is operating with an ionizing electron voltage of 20eV. At this potential the residual helium carrier gas entering the source is not ionized and the stability of the ion current monitor reading is improved. When the total ion current monitor indicates the presence of a component of the mixture in the source, the mass spectrometer scan switch is operated. The ionizing electron energy is then automatically increased to 70eV for the duration of the scan, returning to 20eV when the scan is terminated.

The output of the mass spectrometer collector amplifier was connected directly to the data acquisition and analysis system based on a small computer (Digital Equipment Corporation PDP8). The digitization rate of this system is such that when operating on-line to the mass spectrometer a spectrum may be scanned at the rate of 8 seconds per decade in mass at a resolving power of 5000. These conditions will give about ten digital samples per peak in the mass spectrum.

During the course of the mass spectrometer scan the digital peak data is partly processed. The peak centroids and areas are determined and the time interval between peaks is also stored. When the scan is terminated this data may be further processed immediately or, alternatively, it may be punched out on paper tape to await subsequent processing. This paper tape provides a convenient permanent record of the part-processed digital data. The time required to produce a tape is about 1½ minutes

for a spectrum containing about 300 peaks. Thus, for operation on-line when recording GLC eluates, this time interval is required between peaks if mass spectra of two successive peaks are to be recorded on-line. This restriction does not, of course, apply when the high resolution spectra are initially recorded on analogue magnetic tape. However, in some cases more than one spectrum may be recorded on-line before the maximum number of peaks, i.e. 560, is reached and punch-out of the data is necessary. For example, for low molecular weight compounds the digitization can be started at about mass 250, and the spectrum of the reference compound plus the unknown will probably contain less than 250 peaks. In these circumstances the computer is put onto "pause" while the magnet scan is reset and onto "continue" for the next scan. The time lag between the scans in such a case is about 5 seconds.

During the mass spectrometer scans, the spectrum was also recorded in analogue form on the conventional U.V. chart recorder.

RESULTS

Figure 1 shows histograms summarizing the results of mass measurements taken on the peaks in the spectrum of hexachlorobutadiene. The mass measurements were performed using the normal perfluorokerosene peaks which occur 12 mass units apart. The scan conditions were 8 seconds per decade in mass at a resolving power of 4000. Sixteen scans were taken and the results include measurements on 46 different peaks. It can be seen that the standard deviation of the errors for single scans is 14 ppm. The shaded area shows the results after averaging the values for 4 repeat scans. The standard deviation is then reduced to about 7 ppm.

These results thus showed that the accuracy which can be obtained, though not as high as that obtainable from double focusing instruments[3], should be quite adequate for many analytical purposes. The following examples of the on-line analysis of some GLC eluates further illustrate this point.

Figure 2 shows the total ion current monitor trace for the GLC separation of two natural organic sulphur-containing compounds. Figure 3 shows the computer print-out of the listing of elemental compositions for this spectrum. The molecular ion of the compound occurs at m/e 101 and was identified as C_4H_7NS. (SA and SB as heteroatoms in this print-out refer to ^{32}S and ^{34}S respectively). The peak at m/e 102 is the ^{13}C containing ion, $^{12}C_3{}^{13}CH_7NS$ and m/e 103 is identified as $C_4H_7N^{34}S$. The doublet peak at m/e 100 due to the reference ion C_2F_4 and C_4H_6NS requires a theoretical resolving power of 3500. However, at a resolving power of 4000, these two peaks were not resolved by the on-line system. This was because the intensities of the two peaks resulted in the valley between them, although less than 10% the mean peak height, not being below the computer threshold for peak detection. The two peaks were thus treated by the digitizer as a singlet. To overcome this effect the mass spectrum was re-recorded and digitized at a resolving power of 6000. This compound was tentatively identified as n-propyl isothiocyanate.

Figure 4 shows the total ion monitor trace of an unresolved GLC peak obtained from a mixture of amyl acetate and methyl amyl ketone. The composite peak lasted for approximately 30 seconds. This allowed time for a scan at the rate of 8 seconds per decade in mass to be made, for the magnet to be reset, and for a further scan at the same speed without intermediate punch-out of peak data. Both scans were run at a resolving power of 4000. Figure 5 shows the computer print-out for the first scan and Figure 6 that for the second. In Figure 5, as expected, the results show only the presence of amyl acetate. The molecular ion peak, m/e 130, does not appear in the print-out since its intensity was at this point too low. The $M-CH_3$ peak is, however, identified at m/e 115 ($C_6H_{11}O_2$). Figure 6 shows clearly the presence of two components during the scan taken on the "hump" of the GLC peak. In this case the molecular ions of both constituents are identified at m/e 130 ($C_7H_{14}O_2$) and m/e 114 ($C_7H_{14}O$). The corresponding $M-CH_3$ ions are also present and comparison of the two computer print-outs would quickly reveal the presence of two different compounds.

Figure 7 shows the trace from the total ion monitor for a mixture of steroids. Again the spectra were scanned at 8 seconds per decade in mass at a resolving power of 4000. Figure 8 shows the computer print-out for the first peak, 5α-pregnan-20-one, with the molecular ion at m/e 302 ($C_{21}H_{34}O$) and other peaks including $M-CH_3$, $M-H_2O$, $M-C_2H_3O$ and $M-C_5H_9O$. Figure 9 shows the result for androst-4-ene,3,17 dione.

It has been shown that the MS12 single focusing mass spectrometer can be used to obtain complete high resolution mass spectra when attached on-line to a data acquisition and analysis system. However, the mass measurement accuracy is lower than that obtained from double focusing instruments. The data acquisition and analysis system based on the small PDP8 computer can be used to record on-line scans covering a factor of 10 in

HEXACHLORO—BUTA—DIENE C_4Cl_6

HISTOGRAMS OF INDIVIDUAL ERRORS (ppm) MASS RANGE 70—266

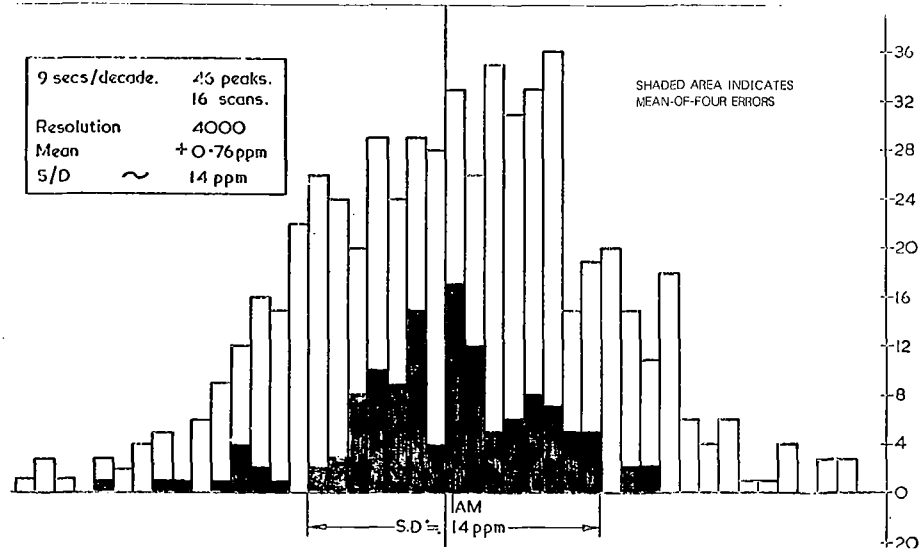

PART OF MONITOR TRACE FROM 0.1μl MIXTURE OF ISOTHIOCYANATES
10% SILICONE OIL COLUMN AT 125°

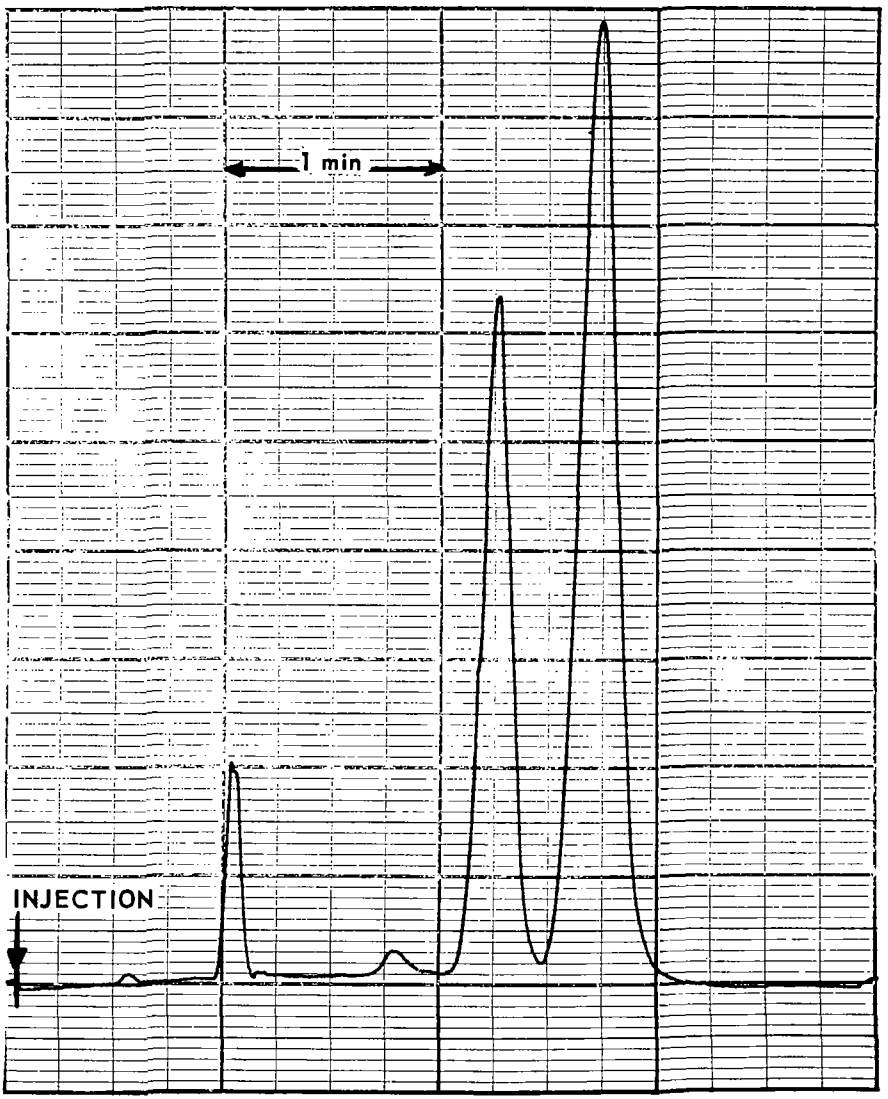

LOW MOLECULAR WEIGHT SULPHUR COMPOUND

1 1

(Propyl isothiocyanate C_3H_7NCS?)

CALCULATED MASS	ERR	C12/13	H	N	O	SA	SB	MEASURED MASS	NO. PTS	INTENSITY
REFERENCE								118.9919	27	++++++++++++
REFERENCE								111.9935	7	++++++
103.0257	-1.28	4/0	7	1	0	0	1	103.0244	8	+++++++
103.0211	3.20	3/1	6	1	0	0	1			
102.0343	-4.33	7/0	4	1	0	0	0	102.0300	10	++++++++
102.0299	.13	6/1	3	1	0	0	0			
102.0332	-3.21	3/1	7	1	0	1	0			
102.0304	- .41	5/0	8	0	0	0	1			
102.0259	4.05	4/1	7	0	0	0	1			
101.0265	2.15	7/0	3	1	0	0	0	101.0286	34	++++++++++++
101.0299	-1.22	4/0	7	1	0	1	0			
101.0254	3.26	3/1	6	1	0	1	0			
100.0187	2.41	7/0	2	1	0	0	0	100.0211	8	+++++++
100.0220	- .96	4/0	6	1	0	1	0			
100.0175	3.50	3/1	5	1	0	1	0			
REFERENCE								99.9935	12	+++++++++
96.9941	-2.91	3/1	2	1	0	1	0	96.9912	4	++++
96.9913	- .10	5/0	3	0	0	0	1			
96.9868	4.36	4/1	2	0	0	0	1			
96.9902	1.00	1/1	6	0	0	1	1			
REFERENCE								92.9951	10	++++++++
88.0022	- .27	3/0	4	1	0	0	1	88.0019	6	+++++
87.9977	4.21	2/1	3	1	0	0	1			
87.0108	-1.48	6/0	1	1	0	0	0	87.0093	5	+++++
87.0064	2.97	5/1	0	1	0	0	0			
87.0097	- .38	2/1	4	1	0	1	0			
87.0069	2.42	4/0	5	0	0	0	1			
87.0058	3.54	0/1	8	0	0	1	1			
86.0030	3.52	6/0	0	1	0	0	0	86.0065	13	++++++++++
86.0064	.15	3/0	4	1	0	1	0			
83.9907	.91	3/0	2	1	0	1	0	83.9917	5	++++++
REFERENCE								80.9951	6	++++++
71.9907	.67	2/0	2	1	0	1	0	71.9914	8	+++++++

MONITOR TRACE FROM 0.1μl MIXTURE OF AMYL ACETATE AND METHYL AMYL KETONE
10% SILICONE OIL COLUMN AT 125°

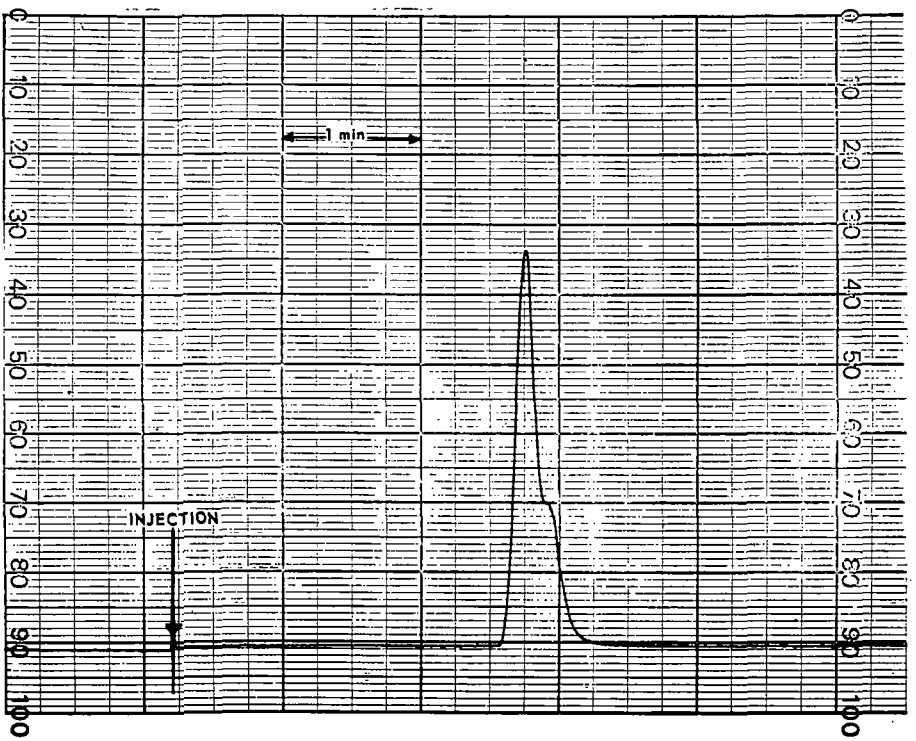

AMYL ACETATE ($C_5H_{11}OCOCH_3$) ONLY

REFERENCE						142.9919	14	+++++++++
137.0027	- .27	10/0	1	3	1	137.0024	6	++++++
136.9982	4.18	9/1	0	3	1			
REFERENCE						130.9919	48	+++++++++++++
REFERENCE						118.9919	50	+++++++++++++
115.0758	- .93	6/0	11	0	2	115.0749	6	++++++ $M^+ - CH_3$ (Amyl acetate)
115.0714	3.52	5/1	10	0	2			
REFERENCE						111.9935	11	++++++++
REFERENCE						99.9935	18	++++++++++++
REFERENCE						92.9951	15	+++++++++
88.0524	.07	4/0	8	0	2	88.0524	13	++++++++
87.0809	2.04	5/0	11	0	1	87.0830	8	++++++
87.0445	1.80	4/0	7	0	2	87.0463	17	++++++++++
86.0731	1.19	5/0	10	0	1	86.0743	7	++++++
85.0653	.22	5/0	9	0	1	85.0655	10	+++++++
REFERENCE						80.9951	11	++++++++
74.0367	-1.35	3/0	6	0	2	74.0354	14	++++++++
74.0323	3.09	2/1	5	0	2			
73.0653	- .99	4/0	9	0	1	73.0643	6	++++++
73.0608	3.47	3/1	8	0	1			
73.0289	.10	3/0	5	0	2	73.0290	19	++++++++++
72.0575	- .50	4/0	8	0	1	72.0570	12	++++++++

CALCULATED MASS	ERR	C12/13	H	N	O	MEASURED MASS	NO. PTS	INTENSITY
71.0815	- .77	4/1	10	0	0	71.0808	15	+++++++++
71.0496	-2.07	4/0	7	0	1	71.0476	11	+++++++
71.0451	2.41	3/1	6	0	1			
NO COMP CALC						70.1219	8	++++++
70.0782	- .48	5/0	10	0	0	70.0777	54	+++++++++++++ $M^+ - CH_3CO_2H$
REFERENCE						69.9985	23	+++++++++ (Amyl acetate)

AMYL ACETATE ($C_5H_{11}OCOCH_3$) – METHYL AMYL KETONE ($CH_3COC_5H_{11}$)

REFERENCE						142.9919	14	+++++++++
131.1071	-3.54	7/0	15	0	2	131.1036	8	++++++
131.1027	.91	6/1	14	3	2			
REFERENCE						130.9919	40	+++++++++++
130.0993	.85	7/0	14	0	2	130.1002	7	++++++ M^+ (Amyl acetate)
130.0948	5.34	6/1	13	0	2			
NO COMP CALC						119.0599	8	++++++
REFERENCE						118.9919	48	+++++++++++++
115.1122	-4.11	7/0	15	0	1	115.1081	8	++++++
115.1078	.35	6/1	14	0	1			
115.0758	- .32	6/0	11	0	2	115.0755	10	+++++++ $M^+ - CH_3$ (Amyl acetate)
115.0714	4.13	5/1	10	0	2			
114.1044	- .56	7/0	14	0	1	114.1038	14	+++++++++ M^+ (Methyl amyl ketone)
114.0999	3.90	6/1	13	0	1			
REFERENCE						111.9935	11	++++++++
101.0602	-2.50	5/0	9	0	2	101.0577	9	+++++++
101.0557	1.96	4/1	8	0	2			
100.0887	-2.60	6/0	12	0	1	100.0861	8	++++++
100.0843	1.86	5/1	11	0	1			
REFERENCE						99.9935	21	++++++++++
99.0809	-1.00	6/0	11	0	1	99.0799	14	++++++++ $M^+ - CH_3$ (Methyl amyl ketone)
99.0764	3.44	5/1	10	0	1			
97.0653	.22	6/0	9	0	1	97.0655	7	++++++
97.0608	4.69	5/1	8	0	1			
REFERENCE						92.9951	15	+++++++++

CALCULATED MASS	ERR	C12/13	H	N	O	MEASURED MASS	NO. PTS	INTENSITY
88.0524	- .16	4/0	8	0	2	88.0522	12	++++++++
88.0479	4.30	3/1	7	0	2			
87.0809	.94	5/0	11	0	1	87.0819	11	+++++++
87.0445	1.92	4/0	7	0	2	87.0465	18	++++++++++
86.0731	.94	5/0	10	0	1	86.0741	10	+++++++
85.0653	.96	5/0	9	0	1	85.0662	15	+++++++++

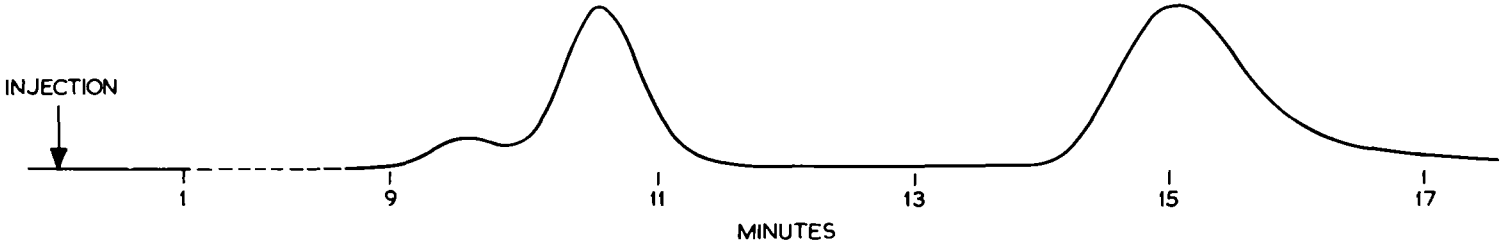

MONITOR TRACE FROM 2μg MIXTURE OF 5α-PREGNAN-20-ONE & ANDROST-4-ENE-3, 17-DIONE

3% SE 30 COLUMN AT 245°

5α – PREGNAN – 20 – ONE

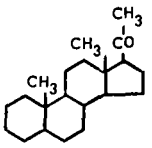

---

1 1

CALCULATED MASS	ERR	C12/13	H	N	O	MEASURED MASS	NO. PTS	INTENSITY	
REFERENCE						318.9793	9	++++++	
REFERENCE						304.9825	8	++++++	
303.2687	-3.72	21/0	35	0	1	303.2650	6	++++	
303.2642	.79	20/1	34	0	1				
302.2608	6.46	21/0	34	0	1	302.2673	9	++++++	M^+
REFERENCE						292.9825	10	+++++++	
287.2374	.61	20/0	31	0	1	287.2380	8	++++++	
287.2329	5.06	19/1	30	0	1				
284.2503	-4.02	21/0	32	0	0	284.2463	6	+++++	
284.2458	.48	20/1	31	0	0				
REFERENCE						280.9825	16	++++++++	
269.2269	1.64	20/0	29	0	0	269.2285	5	++++	
269.2223	6.10	19/1	28	0	0				
REFERENCE						268.9824	12	+++++++	
259.2425	7.08	19/0	31	0	0	259.2496	5	++++	
257.2268	5.43	19/0	29	0	0	257.2323	5	+++	
257.2224	9.88	18/1	28	0	0				
REFERENCE						254.9855	10	+++++++	
244.2191	-3.14	18/0	28	0	0	244.2159	5	++++	
244.2145	1.37	17/1	27	0	0				
REFERENCE						242.9856	11	++++++++	
REFERENCE						230.9856	12	++++++++	
REFERENCE						218.9856	13	++++++++	
218.2034	-2.25	16/0	26	0	0	218.2011	6	+++++	
218.1989	2.22	15/1	25	0	0				
217.1956	1.64	16/0	25	0	0	217.1972	9	+++++++	
217.1910	6.16	15/1	24	0	0				

mass in 8 seconds at a resolving power up to 6000.

REFERENCES

1. W.J. McMurray, B.N. Green and S.R. Lipsky, Anal. Chem., 38, 1195, 1966.

2. W.J. McMurray, S.R. Lipsky and B.N. Green, "Advances in Mass Spectrometry", Vol. 4, Ed. E. Kendrick, Inst. Petroleum, 1968, p.77.

3. A.L. Burlingame, D.H. Smith, R.W. Olsen and T.O. Merren, 16th Annual A.S.T.M. E-14 Meeting, Pittsburgh, 1968, paper 38.

4. J.T. Watson and K. Biemann, Anal. Chem., 36, 1135, 1964.

ACKNOWLEDGMENT

The authors wish to thank Dr. J.D. Waldron, Director and General Manager of GEC-AEI (Electronics) Limited for permission to publish this paper.

ANDROST - 4 - ENE - 3,17 - DIONE

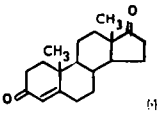

CALCULATED MASS	ERR	C12/13	H	N	O	MEASURED MASS	NO. PTS	INTENSITY	
REFERENCE						292.9825	14	+++++++	
287.2010	1.74	19/0	27	0	2	287.2027	5	++++	
287.1966	6.16	18/1	26	0	2				
286.1932	-3.17	19/0	26	0	2	286.1900	8	+++++++	M+
286.1887	1.28	18/1	25	0	2				
REFERENCE						283.9825	16	++++++++	
271.1697	-5.79	18/0	23	0	2	271.1639	5	+++	
271.1652	-1.34	17/1	22	0	2				
REFERENCE						268.9824	11	+++++++	
REFERENCE						254.9855	10	+++++++	
245.1935	-1.80	17/0	25	0	1	245.1887	5	++++	
245.1860	2.68	16/1	24	0	1				
244.1826	- .79	17/0	24	0	1	244.1819	8	++++++	
244.1782	3.66	16/1	23	0	1				
REFERENCE						242.9856	10	++++++++	
242.1669	-1.86	17/0	22	0	1	242.1651	5	++++	
242.1625	2.59	16/1	21	0	1				
REFERENCE						230.9856	14	+++++++++	
REFERENCE						218.9856	12	++++++++	

109. AN IMPROVED MEASUREMENT OF R-F SPARK SOURCE OPERATING CONDITIONS

T. J. Eskew

Nuclide Corporation
State College, Pennsylvania

The electronics group at Nuclide Corporation has been aware for several years of a certain looseness of terminology with respect to the r-f spark source voltage. But the particular magnitude of this voltage has not seemed to influence the instrument performance, and we have been satisfied to specify only the maximum output of the r-f generator, and to ignore the question of what is the actual voltage across the spark gap.

We have lately found, however, that a quantitative display of this voltage can serve as a useful index of the spark source adjustment. I would like to show how this is done.

To measure very high a-c voltages, electrical engineers use a more or less standard arrangement: the calibrated capacitive divider. When an a-c voltage is impressed across a pair of capacitors connected in series, each capacitor receives a fraction of the total which is inversely proportional to its capacitance. For very high voltages, it is convenient to let the smaller capacitor - which withstands nearly the entire voltage — be simply the stray capacitance between the circuit under test and some small sensing electrode. If the arrangement is rigidly mounted, the stray capacitance will be quite stable and can be accurately calibrated. The small stray capacitance, of course, does not disturb the tuning of the r-f circuit.

Figure 1 shows the arrangement used in the experiments described here. This drawing shows the output transformer of a Nuclide Model FA-3 r-f amplifier, which is mounted in a shielded cabinet under the source housing of the GRAF-3 spectrograph. C_1, the upper branch of the capacitive divider, is the stray capacitance between the anti-corona ring at the rf end of the output coil and a small copper disc about 10 cm away. The disc is supported by a brass screw mounted through a ventilating screen in the wall of the r-f cabinet, and insulated with fiber washers. The lower branch of the divider is formed by an oscilloscope probe, plus the stray capacitance of the mounting. Since the probe and its ground lead are outside the metal enclosure, the set-up cannot respond to the transformer's magnetic or electromagnetic field.

To calibrate this arrangement, a second divider, formed of a pair of low-voltage mica capacitors, was connected across the secondary, and the output from a signal generator was coupled to the circuit by means of a few turns of wire wrapped loosely around the lower end of the secondary. This second divider reduced the resonant frequency to about 60 kHz; when the signal generator was tuned to this frequency about 70 volts peak-to-peak appeared across the coil. The mica capacitors were separately calibrated on a capacitance bridge. The ratio of the high voltage divider was thus found to be 540-to-1, within about 5%.

C_2 - the combined capacitance of the 'scope probe and the mounting hardware — was measured by adjusting a trimmer capacitor parallel with C_2 to reduce the signal to half-amplitude. The trimmer capacitance was then equal to C_2, and could conveniently be measured on a capacitance bridge. The value of C_2 was found to be 11 pF, giving a value of 2×10^{-14} farad for C_1. But note that the ratio of C_1 to C_2 is known more accurately than either capacitance separately.

Figure 2a shows a typical r-f pulse waveform, with the sample electrodes separated too far to allow a spark. The time axis is 10 microseconds per centimeter, and the vertical axis is 20V/cm times the divider ratio, giving 10.8 kV/cm. We see that the r-f frequency is very nearly one MHz, and the peak voltage about 21 kV.

The pulse at the grid of the driver tube was precisely rectangular, and of 32 μs duration. During the first few cycles, energy is stored in the tuned circuits at the driver

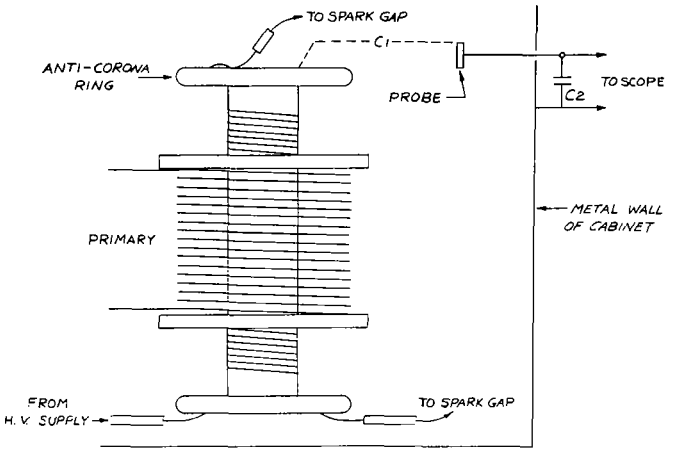

FIGURE 1

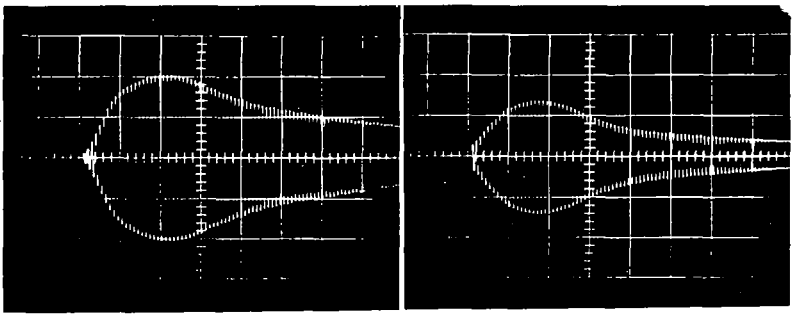

A
Low-power pulse
10.8 kV/cm
Open gap

B
High-power pulse
27.4 kV/cm
Open gap

FIGURE 2

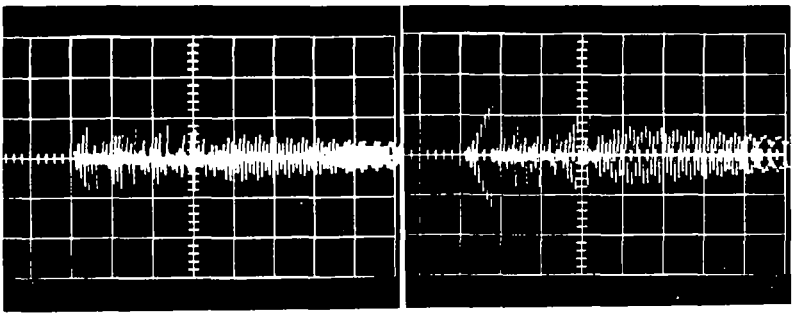

A
Low-power pulse
10.8 kV/cm
50 micron gap

B
Low-power pulse
10.8 kV/cm
75 micron gap

FIGURE 3

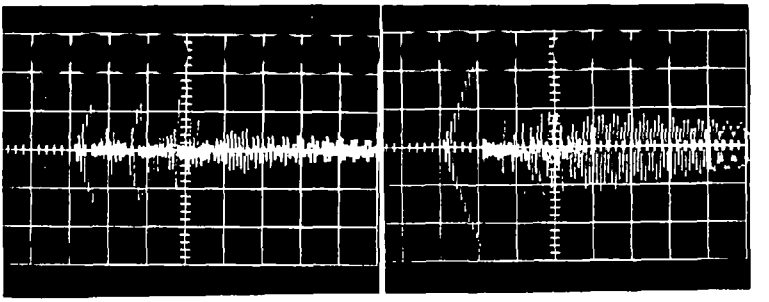

A
High-power pulse
10.8 kV/cm
75 micron gap

B
High-power pulse
10.8 kV/cm
300 micron gap

FIGURE 4

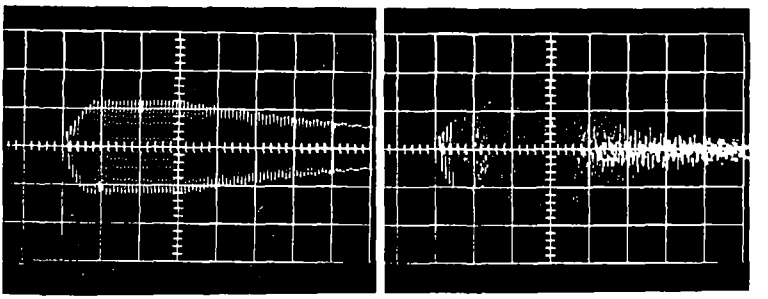

A
Output of pick-up coil
Uncertain calibration
Open gap

B
Output of pick-up coil
Uncertain calibration
100 micron gap

FIGURE 5

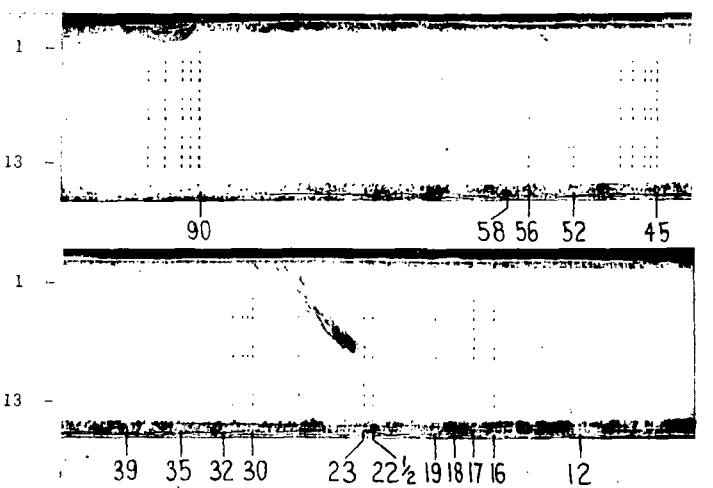

FIGURE 6

plate and final grids; the output tubes begin to conduct on about the fourth or fifth cycle. With no spark, the "Q" of the output transformer primary and secondary is rather high, and the pulse approaches equilibrium amplitude only near the end of the 32 μ sec duration. The exact rate of build-up depends on the output plate-supply voltage and especially on the grid-drive power; the final equilibrium amplitude is controlled mainly by the plate-supply voltage, and to a smaller extent by the drivepower. The tuning adjustments also influence the build-up in a complex manner. (It should be mentioned that both the driver and output transformers are over-coupled; in fact, as closely coupled as they can be with aircore design and consistent with the insulation voltage requirement between windings.) The build-up is more rapid when the driver plate and output plate circuits are de-tuned slightly to the high-frequency side of resonance, with the output grid de-tuned to the low-frequency side. Also, the system can be tuned to quench the ringing after the end of the pulse: the slightly different ringing frequencies drift out of phase with each other, and can produce a cancellation effect. This mode of tuning can produce a series of beats in the trailing portion of the pulse, and has been avoided in these photographs, since it would make some of the waveforms more difficult to interpret.

For Figure 2a, the final plate supply was set at 3000 volts and 80% maximum grid drive; in the discussion that follows I shall refer to this as the "low-power" condition.

Figure 2b shows the output waveform with the plate supply setting increased to 6000 volts, and a y-axis calibration of 27.4 KV/cm — that is, 2/5's the previous setting. Here the peak-to-peak amplitude is 76,000 volts. Note that the total build-up time is about the same as in the previous figure — about 18 μs, allowing for an extra two cycles before the sweep triggered. Thus the build-up rate is about 1.8 times faster than before. As suggested by the rounded shape, the amplitude is in this case limited by the 32 μs duration of the drive pulse, rather than by the output plate-supply voltage. In the following discussion I shall refer to this as the high-power condition.

Figure 3a shows a spark voltage waveform, produced with a very narrow setting of the spark gap - perhaps about 50 microns - and under the low-power condition. The sensitivity is again 10,800 V/cm. The build-up proceeds as before until the potential reaches about 8600 volts; then the spark breakdown abruptly removes energy from the output tank, and prevents further increase in the voltage. The detailed behavior of the waveform during the spark discharge is erratic, but note that the peak amplitude does not at any time exceed 0.8 cm, and that the breakdown begins after about 4 1/2 cycles.

In Figure 3b the gap has been opened slightly - to perhaps 75 microns. There are now 7 r-f cycles before the breakdown begins; the peak potential at this point is about 14,000 volts.

In Figure 4a, the output plate voltage has been increased to 6000 volts — the high-power condition mentioned previously - but the gap width is unchanged. As in the previous figure, the breakdown begins at 14,000 volts, but the voltage now reaches this value after only 5 r-f cycles.

The factor-of-two increase in plate voltage nearly doubled the plate current to the output stage; thus the power input to the final amplifier and spark is nearly four times greater than in the previous slide. The spark appears brighter to the eye, and the erratic waveform in the trailing edge of the pulse suggests that a discharge continues in the spark gap far beyond the nominal 32 μs pulse duration. This four-fold power increase made the ion current somewhat more steady, and produced about a 20% increase in the average ion current.

In Figure 4b, the power setting is unchanged, but the gap has been opened to the widest setting that will sustain a satisfactory spark - about 300 microns. The peak potential now reaches 28,000 volts before the spark begins.

In every case, the details of the voltage waveform during the spark are erratic: when the 'scope is allowed to scan repetitively, the spark-portion of the trace is a confused blur. But the intial build-up is precisely repeated, and the breakdown generally begins on the same cycle in each pulse. As the sparking continues, the breakdown voltage gradually tends to increase. After a time, the increase allows an additional r-f

cycle to appear in the initial build-up. With the high-power, wide-gap spark, and a fairly high duty ratio, the increase becomes apparent in less than a minute: it represents the increase in gap width as the sample is consumed.

Some experimenters have used a one-or two-turn pick-up coil to monitor the spark source operation. Figure 5a shows the output of a two-turn coil wound loosely around the lower or d-c end of the transformer secondary, with a wide gap and no spark. The coil was connected by a twisted pair of leads to the 'scope probe; perhaps the high frequency ringing could have been reduced by a suitable damping resistor. There is not a simple one-to-one correspondence between the output of this pick-up coil and the output of the capacitive divider. Rather, the relationship depends on the tuning of both the oscillator and the plate tank circuit. Worse, the maximum output from this coil does not occur at the same tuning that produces maximum sparkgap voltage. Further, the effects mentioned previously - small de-tunings to enhance the build-up rate — cannot be observed with this arrangement.

The pick-up coil, of course, does not sense voltage directly, but rather the combined magnetic field of the transformer primary and secondary windings. Since the transformer windings are both tuned and are over-coupled, there is no simple relationship between voltage and current.

When the gap is closed to allow sparking, the pick-up coil produces the waveform shown in Figure 5b. The sudden discharge of the energy stored in the secondary tank produces high peak currents and magnetic fields. The waveform here is a sort of current-complement to the voltage waveform observed with the capacitive divider.

If the spark gap is to be used for quantitative analyses, the factors which influence its sensitivity to the various constituents of the sample must be kept under control. Figure 6 and Table 1 illustrate some effects produced by changing the gap width. The plate shows thirteen exposures of the mass spectrum of a Zircaloy -2F sample (NBS standard No. 1215) containing a few tenths of a percent of tin, iron, chromium and nickel, and smaller amounts of several other elements. The mass spectrograph, a Nuclide model Graf-3, was operated at an ion accelerating potential of 20,000 volts, and the magnet current was adjusted to bring the singly-charged zirconium lines (90 thru 96) near the high-mass end of the plate.

Exposures were made for three conditions: narrow gap at low power, narrow gap at high power, and wide gap at high power. The photographs shown as examples of these conditions were, in fact, made just before each group of exposures on this plate. For each condition, four exposures were made, as shown in the table; the pulse repetition frequencies were 1, 3.2, 10 and 32 per second, keeping the exposure time more or less constant. For exposure 13, the repetition frequency was decreased to 3.2 per second, giving a .01% duty ratio. The numbers in the table are the raw photometer readings, with the plate background taken as 100% transmission.

The abundance of zirconium -96 is about 2.8%; for this line in the 3×10^{-12} coulomb exposures (No. 4, 8, 12 and 13) the transmissions are about equal - perhaps slightly more 96 in the wide-gap exposure No. 12, but hardly outside the spread one might expect in a hand-developed plate.

For iron at mass 56 and chromium at mass 52, the situation is quite different: the wide-gap, high-voltage exposures are markedly biased in favor of these elements.

The bias is in the opposite direction for multiply-charged zirconium: compare the transmissions at mass 47, and the lines at mass 30.

The most drastic anomalies can be seen at masses 19, 18 and 17: 19 is almost completely absent from the wide-gap exposure, and 18 from the narrow-gap exposures. With the narrow gap, 17 is more intense than any except the zirconium peaks, but with the wide gap is fainter by perhaps a factor of 100.

There is a curious situation in exposure No. 11: peaks at masses 23, 27, 39 and several other points are too dark with respect to their counterparts in exposure No. 12.

Perhaps the sparking reached a severe inhomogeneity at this point; the NBS analysis does not mention either sodium or aluminum.

To conclude: there is a simple one-to-one correspondence between spark breakdown voltage and gap width; this relationship is not influenced by adjustments of the electronics, although it may be changed somewhat by different types of sample. The capacitive divider can be given an absolute calibration by a simple experiment, and can be used to repeat previously noted gap settings, with better reproducibility than a micrometer calibration of the gap adjustment knobs, since it takes into account the consumption of the electrode material.

This type of calibration could easily be used to compare operating conditions between mass spectrometers of different manufacture.

TABLE 1

	EXPOSURE		% TRANSMISSION FOR MASS:							
			96	56	52	48	32	19	18	17
1.	10^{-13} COULOMB									
2.	3×10^{-13}	NARROW GAP								22
3.	10^{-12}	¼ POWER								9
4.	3×10^{-12}		25	56	53	19	66	48	92	5
5.	10^{-13}									
6.	3×10^{-13}	NARROW GAP								16
7.	10^{-12}	FULL POWER								7
8.	3×10^{-12}		24	51	50	20	69	48		5
9.	10^{-13}	WIDE GAP								
10.	3×10^{-13}	FULL POWER								86
11.	10^{-12}									93
12.	3×10^{-12}	.1% duty ratio	20	34	26	27	85	97	59	85
13.	3×10^{-12}	.01% duty ratio	22	38	35	28	83			

110. THE USE OF A ROTATING DISC ELECTRODE METHOD FOR THE SPARK SOURCE MASS SPECTROMETRIC ANALYSIS OF THIN FILMS AND LIQUIDS

R. Brown, W.J. Richardson and P. Swift
Scientific Apparatus Division
GEC-AEI (Electronics) Limited
Barton Dock Road
Urmston, Manchester.

INTRODUCTION

The analysis of thin films, using a GEC-AEI MS702, has been made possible by the development of a simple spinning electrode apparatus. This apparatus allows the sample to be rotated whilst the surface upon which the film is deposited is scanned against a stationary counter-electrode.

This technique has been used to investigate the composition of films including the detection of impurities down to the sub-ppm level. Surface layers of as little as 5000°A have been examined using the method.

Liquids may be analysed by evaporating the sample onto a thin disc and then scanning the deposited residue whilst rotating the disc. Elements whose concentrations have been as little as 10^{-12} gram in the liquid sample have been detected by the method.

APPARATUS

Figure 1 illustrates the experimental set-up schematically.

The right-hand insulator (A) is shorter than normal to facilitate the fitting of the small electric motor (B) which is mounted on the adjustable bracket (C). The motor is driven at a speed of approximately 300 revolutions per minute by a rechargeable 1.5 volt mercury dry cell (D). The sample disc (E) is mounted on the motor by fixing it to the backplate (F) with a very thin layer of impact adhesive, (e.g. evostick). A spectroscopically pure counter-electrode (G) is mounted in a standard sample clamp (H) on the left hand insulator.

The drive shaft of the motor is off-set by its reduction gear assembly (see Figure 2) which makes it particularly suitable for this application since the disc can be brought as close as required to the first slit in the ion source of the MS702.

Figure 2 is a photograph of the ion source of the MS702 with the rotating disc apparatus mounted.

EXPERIMENTAL

Usually, samples containing a thin film for examination are, themselves, in the form of discs, platelets or wafers and pieces of up to approximately 1 cm square can be mounted on the back-plate for analysis. Hence, all or part of the sample may be fixed to the backplate with a very thin layer of evostick so that the surface for examination can be scanned across the stationary counter-electrode whilst recording analytical exposures.

Figure 3 shows the surface of a silicon wafer after sparking.

The evaporation of a liquid sample is carried out under an infra red lamp and the residue is usually deposited on a spectroscopically pure gold disc approximately 1 cm diameter x 0.5 mm thick. The gold disc is then fixed to the backplate with evostick such that the surface upon which the residue has been deposited can be scanned whilst recording analytical exposures.

The counter-electrode material usually used for either films or liquid residues is spectroscopically pure gold wire 0.02 inches diameter.

FIGURE 1 Schematic diagram of rotating disc apparatus

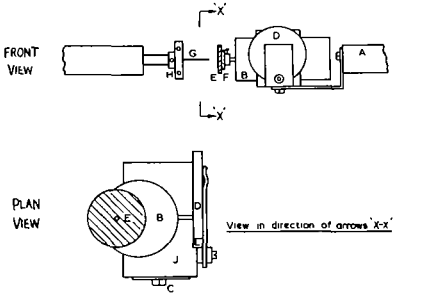

A — SHORTENED GLASS INSULATOR
B — MOTOR.
C — ADJUSTABLE BRACKET.
D — ½ VOLT MERCURY DRY CELL
E — DISC
F — BACKPLATE
G — COUNTER ELECTRODE
H — STANDARD SAMPLE CLAMP
J — MOTOR CLAMP
L — GLASS SPACER.

DIAGRAM OF SPINNING DISC ELECTRODE SYSTEM

FIGURE 2 Rotating disc apparatus mounted in MS702 ion source chamber

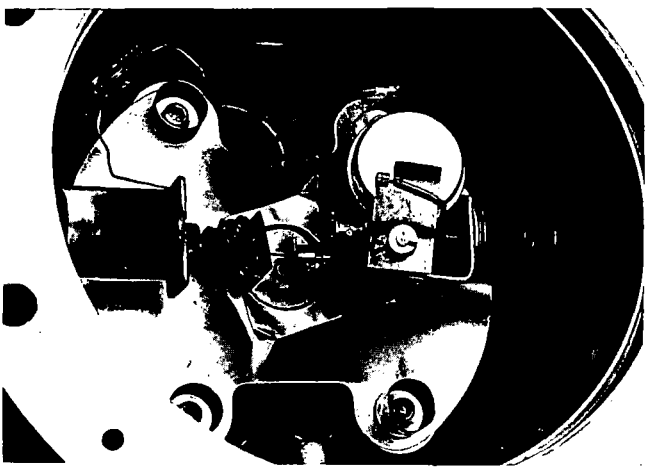

FIGURE 3 The surface of a silicon wafer after sparking

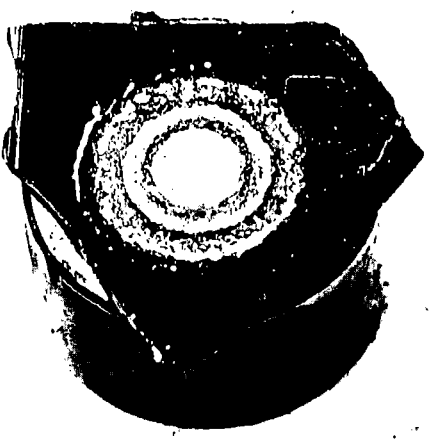

EXAMPLES OF ANALYTICAL APPLICATIONS

THIN FILMS:

(a) The Analysis of Glass Films

The samples were in the form of films deposited on a copper substrate. These had been prepared by electron beam volatilization of the glass under vacuum and subsequent condensation of the vapours onto a copper sheet. The specimens submitted for analysis were approximately 1 cm square by 1 mm thick, each piece having a glass film of between 4 and 10 microns thick.

The purpose of the analysis was to determine the difference between the glass composition of bulk material used and the condensed films. The results are summarised in Table 1.

TABLE 1

ANALYSIS OF VACUUM DEPOSITED GLASS

Values in % Weight

		Bulk	Film
Sample 1	SiO_2	35	97.8
4.5 microns	Al_2O_2	35	0.28
thick	CaO	30	1.9
Sample 2	SiO_2	50	78.2
8 microns	B_2O_3	15	15.4
thick	Al_2O_3	10	0.17
	BaO	25	5.9
	As_2O_3	0.3	0.27

Bulk analyses by chemical methods.

Film analyses by mass spectrometry.

Comparison of the concentrations of the oxides in the two columns of results above shows how the composition of the film has changed from that of the glass because of the different volatilities of the components.

(b) The Analysis of Boron in Silica Films

The samples were in the form of silicon slices 1 cm square by 1 mm thick. One surface of each slice had been oxidised to yield a layer of silica approximately 5000°A thick into which boron oxide vapour had diffused.

The purpose of the analysis was to determine the atomic concentration of boron per cubic centimeter of the silica layer. The results are summarized in Table 2.

TABLE 2

ANALYSIS OF BORON IN SILICA LAYERS

Sample A Boron at 1×10^{18} atoms per cc

Sample B Boron at 3×10^{17} atoms per cc

Sample C Boron at 4×10^{19} atoms per cc

LIQUIDS:

(a) The Analysis of a Geological Water Sample

Approximately 1 millilitre of the sample was pipetted onto the surface of a high purity gold disc and then gently evaporated to dryness under an infra red lamp. The gold disc was mounted on the motor and scanned against a stationary gold counter-electrode.

The concentrations of a few elements in the sample had been estimated previously by atomic absorption spectroscopic methods. From these copper was chosen as internal standard for the mass spectrometric analysis. The results are summarised in Table 3.

TABLE 3

ANALYSIS OF GEOLOGICAL WATER SAMPLE

Values in ppb (weight)

a	Lead	300	Calcium	20,000
	Strontium	95	Potassium	20,000
	Arsenic	80	Chlorine	25,000
a	Zinc	550	Sulphur	8,500
a	Copper	100	Phosphorus	10,000
a	Iron	7,200	Silicon	9,000
	Manganese	60	Aluminium	3,000
	Chromium	20	Magnesium	2,500
	Vanadium	9	Fluorine	100
	Titanium	160	Boron	35
	Sodium	major component		

a Atomic absorption values for these elements in ppb (weight)

Lead	500	Copper	100
Zinc	500	Iron	6,400

(b) The Analysis of a Microgram Quantity of a Black Deposit

A few specks of the black deposit, estimated to be of the order of a few micrograms, were brushed from a faulty brazed joint onto a watch glass. One drop of approximately 10% nitric acid was added and the deposit became suspended in the acid solution. This drop was pipetted onto a gold disc and evaporated to dryness under an infra red lamp.

The purpose of the analysis was to determine whether the black deposit was associated with either the copper-silver braze or a ceramic material which was in close proximity to the joint and could have broken down under the temperature of the tungsten arc whilst the brazing was being carried out.

Figure 4 shows the spectra obtained from the analysis of the deposit. It can be seen that copper and silver are present in the spectrum whilst the aluminium level is the same in both the blank and sample spectra. Therefore, it was deduced that the deposit was associated with the braze material.

The presence of tungsten in the sample spectrum has arisen from the filament used in the high temperature arc which is used for the brazing process. The iron, cobalt and nickel has arisen from the base metal which was nilo-k.

SUMMARY

The application of the spinning disc technique has made possible the analysis of thin films and evaporated residues on the GEC-AEI spark source mass spectrometer. The sensitivity of the technique has allowed impurities of sub ppm concentration to be determined in films whilst an element concentration of as little as 10^{-12} grams per millilitre have been detected in liquid samples.

ACKNOWLEDGMENT

This paper is published with the permission of Dr. J.D. Waldron, Director and General Manager of Scientific Apparatus Division, GEC-AEI (Electronics) Limited.

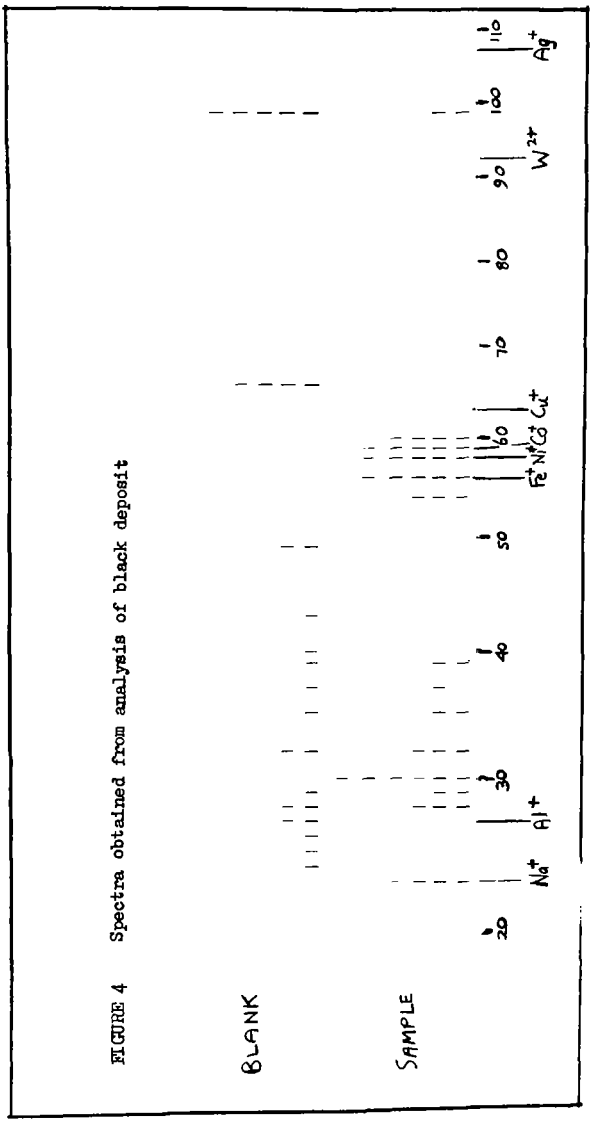

FIGURE 4 Spectra obtained from analysis of black deposit

111. ELECTRICAL DETECTION METHODS FOR IMPROVING QUANTITATIVE ANALYSIS BY SPARK SOURCE MASS SPECTROMETRY

R.A. Bingham and P. Powers
Scientific Apparatus Division
G.E.C.-A.E.I. (Electronics) Limited
Manchester England

INTRODUCTION

Quantitative spark source mass spectrometry is a very well established technique for the analysis of impurities in a wide variety of materials.(1) Up to the present time it has been usual to use photographic detection since this allows integration of the fluctuating ion beam. More recently Conzemius, Svec at Iowa State University and ourselves at this laboratory have both carried out investigations into the suitability of electrical detection techniques. (2, 3)

Figure 1 shows a schematic layout of the apparatus used here. The electron multiplier is positioned at the principal radius of the spectrometer and is used to collect each individual ionic species.

The monitor collector, between the analysers, collects a fixed fraction of the total ion beam before mass separation.

In this work the apparatus has been used in two ways. These are electromagnetic peak scanning and voltage peak-switching. Peak scanning is achieved by initiating an exponential scan of the magnet current so that ions of different mass are swept successively over the collector. An exponential scan ensures that equal times are spent on each peak so that quantitative results can be obtained even on fast scans. With peak switching on the other hand the operator changes his attention from one peak to the next by changing the accelerating and ESA voltages by a suitable amount. Quantitative analyses are made by integrating the collector current, from each peak of interest, whilst a particular charge is collected at the monitor.

Both techniques are complimentary. Peak scanning is generally used for rapid surveys of impurity content with a precision only slightly better than that of the photoplate. Peak switching, which is less fast, is used for measurements of the highest precision.

Peak Scanning

The inherent fluctuation of the r.f. spark discharge can cause severe changes in ion beam intensity even over the time that one peak takes to pass the collector. Furthermore these fluctuations mean that quantitative analysis is made very difficult. Figure 2 shows a straight output from a fairly slow scan of a steel sample. Although it is possible to make a qualitative assessment from this scan, quantitative results are not feasible.

In order to correct this a double logarithmic amplifier arrangement has been used to present a ratio signal to a recorder. This ratio is logarithm of $\frac{\text{collector current}}{\text{monitor current}}$.

Figure 3 shows a recorder trace from such a system. It can be seen that the peak noise has been substantially reduced. The spectrum is of the antimony and tin region of a Johnson-Matthey copper CA2 sample. The horizontal line marked A10 represents a concentration level of 2 p.p.m. atomic. The A100 line represents 20 p.p.m. etc. The detection limit at this setting of multiplier and amplifier gains is therefore about 0.1 p.p.m.

Two features of this sort of output are worth mention. The region over which the dynamic range of 1000:1 can be displayed can be adjusted by changing the amplifier or multiplier gain.

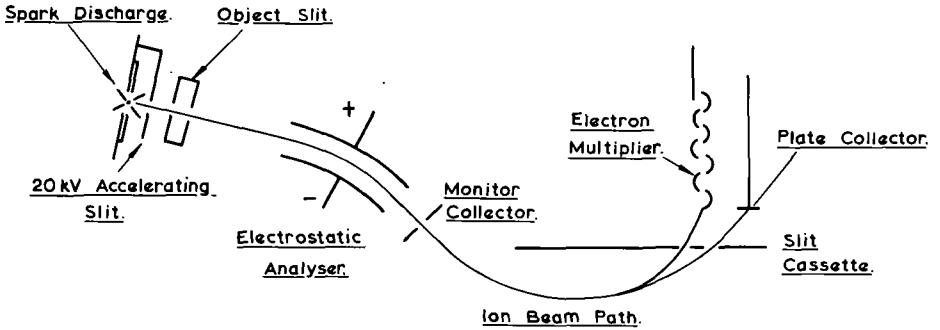

FIG. 1. DIRECT READING ARRANGEMENT OF THE M.S.7.

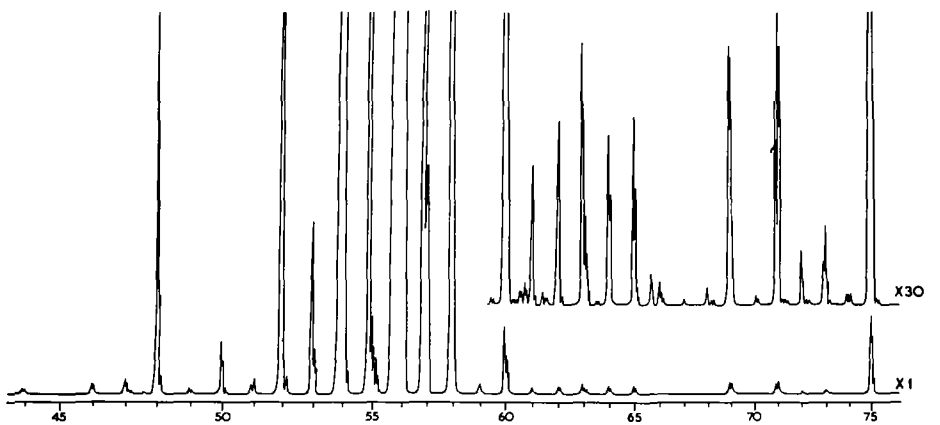

ELECTRICALLY RECORDED SCAN OF SPECTRUM OF STEEL STANDARD SS54 WITH R.F. SPARK DISCHARGE. MS702.

TIN AND ANTIMONY REGION OF RATIO SCAN

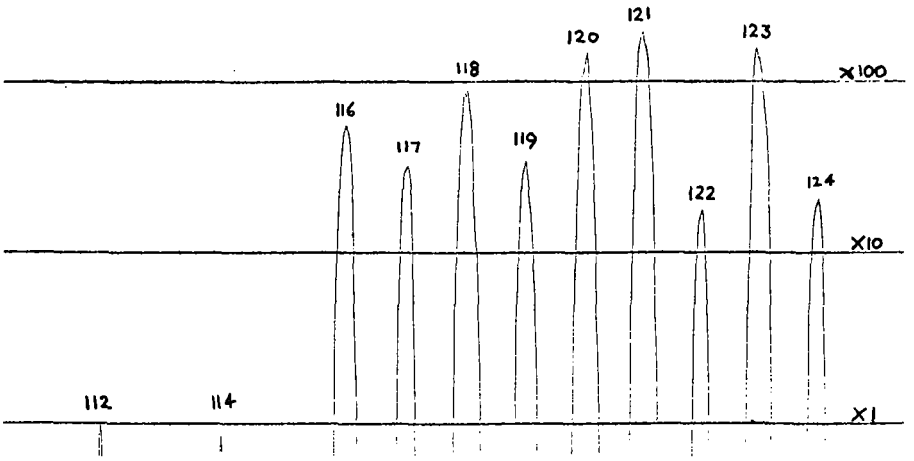

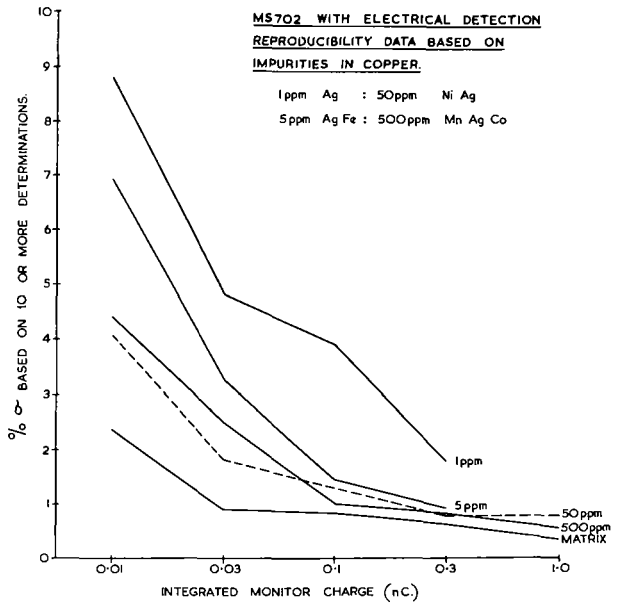

This means that one can display the range 0.2-200 p.p.m. or 200 p.p.m.-20% etc. Secondly it can be seen that peaks from components with a concentration exceeding the dynamic range will still be visible (although not measurable) on the chart.

Table I and II show results taken from scans at two different speeds, 18 minutes and 110 seconds per decade.

TABLE I

REPRODUCIBILITY OF TEN REPEAT ANALYSES ON COPPER STANDARD CA2 WITH RATIO SCANNING

Scan speed 18 minutes/decade; Results in p.p.m. atomic

	Measured	Quoted
Bi	59.4 ± 15.8	40
Pb	33.8 ± 7.2	30
Sb	59.9 ± 10.4	60
Sn	64.2 ± 14.6	65
Ga	54.1 ± 7.3	75
Cr	49.0 ± 10.8	70

Spark conditions 24kV, 1000pps, 200μs

TABLE II

REPRODUCIBILITY OF NINE REPEAT ANALYSES ON COPPER STANDARD CA2 WITH RATIO SCANNING

Scan speed 110 seconds/decade; Results in p.p.m. atomic

	Measured	Quoted
Bi	44 ± 14	40
Pb	36 ± 15	30
Sb	68 ± 24	60
Sn	57 ± 21	65
Ga	79 ± 30	75
Cr	83 ± 31	70

Spark conditions 24kV, 1000pps, 200μs

The results in Table I have a mean standard deviation of 21% with the worst (Bi) 27% and the best (Ga) 13%.

Those in Table II have a mean standard deviation of 35% with the worst (Pb) 42% and the best (Ag and Bi) 33%.

Peak Switching

For the highest analytical precision it is necessary to spend longer on each peak and the most convenient way of doing this is to use a peak switching method. Any number of peaks can be arranged to be preset and switched onto the collector in turn, although in this work a maximum of 10 peaks was used with a factor 2 mass range. Results were obtained by integrating the collector current whilst a fixed charge (the integrated monitor charge) is collected at the monitor.

Figure 4 shows how analytical precision changes with integrated monitor charge and with concentration level. In this graph all elements present at a particular level have been grouped together to provide the data.

To illustrate the performance of this system Table III shows results of an analysis of four samples of Johnson-Mattheys CA series using the high impurity level CA0 as standard. This series was chosen because it contains lead and bismuth, both notoriously poor elements in copper from an analytical point of view.

TABLE III

ANALYSIS OF COPPER STANDARDS (CA SERIES) BY ELECTRICAL DETECTION

Average of 10 determinations

	Lead (p.p.m. atomic)		Bismuth (p.p.m. atomic)	
	Measured	Quoted	Measured	Quoted
CA2	36.4 ± 0.9	30	45.4 ± 2.7	40
CA3	14.2 ± 1.6	15	19.6 ± 2.7	25
CA4	7.0 ± 0.2	9	9.2 ± 0.6	15
CA8	1.2 ± 0.7	1	1.4 ± 0.06	0.6

TABLE IV

ANALYSIS OF COPPER STANDARDS (CB SERIES) BY ELECTRICAL DETECTION

Average of 5 determinations

	Cobalt (p.p.m. atomic)		Nickel (p.p.m. atomic)	
	Measured	Quoted	Measured	Quoted
CB1	244 ± 1.9	220	156 ± 1.5	150
CB2	109 ± 2.1	110	68 ± 1.9	50-100
CB3	58 ± 1.8	60	17 ± 0.8	50
CB8	1.6 ± 0.08	1	2 ± 0.1	2

Table IV shows the analysis of two impurities in copper which have a good analytical reputation. These are cobalt and nickel. For this the Johnson-Matthey CB series was used and the high level CB0 was used as standard. In this case only five determinations were made.

DISCUSSION

The results from peak scanning show that easily interpreted quantitative data can be obtained from a scan taking only 110 seconds per decade in mass. This corresponds to three minutes for the mass range m/e 250-8. The standard deviation of the results from repeat analyses is of the same order as that ordinarily achieved with the photoplate, and if time permits a significant improvement in precision can be achieved if the scan time is increased to 18 minutes/decade.

The additional features of peak switching allow higher precision to be achieved on selected peaks of interest. An analysis time of 7½ minutes for 10 elements is typical although single determinations on 10 peaks can be made in times down to 90 seconds.

This is a technique which now makes feasible the spark source analysis of a range of impurity levels from one of the same order as the matrix down to a level less than 10ppb. Table V in fact shows that with only a 0.1nC integrated monitor charge sensible results can be obtained even from isotopes present to only 7ppb.

TABLE V

EXAMINATION OF % ABUNDANCE OF LEAD ISOTOPES IN A COMPACTED ROCK SAMPLE

Average of 20 determinations

	Isotope Concentration (p.p.m. atomic)	% Abundance Found	Normal
Pb208	0.25	50.3	52.3
Pb207	0.11	21.3	22.6
Pb206	0.11	26.4	23.6
Pb204	0.007	2.0	1.5

Integrated Monitor Charge 0.1nC, multiplier gain 3 x 10^7
Total lead concentration of mix 0.48 p.p.m. atomic
S.D. Pb204 = 32% (20 determinations).

SUMMARY

A.E.I. MS702 RF SPARK SOURCE ELECTRICAL DETECTION

Peak Scanning (at a resolving power of 500, 10% valley)

Speed	Precision	Detection Limit
18 minutes/decade	S.D. = 21%	<0.1 p.p.m.
10 minutes/decade	-	0.1 p.p.m.
2 minutes/decade	S.D. = 35%	0.5 p.p.m.

Peak Switching (using 1nC integrated monitor charge and at 500 resolving power)

Speed — 7½ minutes to prepare complete analysis on 10 peaks, and down to 90 seconds for single determinations on 10 peaks using 0.1nC.

Precision — S.D. = 0.5% at matrix level; 5% at 1 p.p.m. level

Detection Limit — much lessthan 10ppb

REFERENCES

(1) J.S. Halliday, P. Swift and W.A. Wolstenholme "Quantitative Analysis by Spark Source Mass Spectrometry". Advances in Mass Spectrometry Vol. 3 ed. W.E. Mead p. 143-161.

(2) H.J. Svec, R.J. Conzemius, International Mass Spectrometry Conference, Berlin 25-29th September, 1967.

(3) R.A. Bingham, R. Brown and P. Powers "Electrical Detection Spark Source Mass Spectrometry". paper 201, 1968 Pittsburgh Conference on Analytical Chemistry and Applied Spectroscopy, March 3-8 1968.

ACKNOWLEDGEMENT

The authors wish to thank Mr. R. Brown for very helpful discussions and Dr. J.D. Waldron, Director, Scientific Apparatus Division, G.E.C.-A.E.I. (Electronics) Limited for permission to publish this paper.

112. High Energy Irradiation of Solid Dielectrics as an Aid to Analysis by Spark Source Mass Spectrometry

J. G. Allard
U. S. Naval Research Laboratory, Washington, D. C. 20390

A program for the preparation and characterization of highly purified single crystals of alkali halides has been under active investigation at the Naval Research Laboratory for several years. The analysis of these materials by mass spectrometry has proved to be difficult and laborious. Frequently the spectra obtained from these materials contained broad lines, large ratios of the singly to the multiply charged ions of the matrix elements, and in some instances fewer singly than doubly charged species, making the interpretation difficult and quantitative analyses uncertain.

To produce a spark between electrodes of KBr, it is normally necessary to apply an r-f voltage of approximately 50 kv for a period of one hour or more. Ohkura and Maurer[1] reported that the waiting time to obtain the first spark was dependent on the geometrical configuration of the electrodes and that electrical breakdown was preceded by the injection of F-centers--that is, electrons trapped at negative ion vacancies into the crystal. Electrical breakdown frequently occurs on the surface of the crystal and when a surface arc is established and maintained, the ion beam is very erratic, constant manipulation of the sample electrode is necessary to maintain ion production, and the magnitude of the ion beam is insufficient to be practical for high exposures. In addition the electrical arc is accompanied by a large luminescent plasma which frequently supports electrical breakdown within the ion source region, and it is thought that the abnormalities observed in the large ratios of the matrix ions as well as the very high ratios of the successive degrees of ionization of the matrix elements is related to the luminexcent plasma.

In view of the above, since it is well documented that exposure of these materials to high energy radiation produces negative ion vacancies, single crystals of KBr were irradiated at room temperature with gamma rays from cobalt-60 at a dose rate of 1×10^6 r/hr. for a total dose of 10^8 roentgen. It is estimated that the exposure to the gamma-rays increased the negative ion vacancy population by 3 or 4 decades to a population of approximately 10^{18} negative ion vacancies per cubic centimeter. The irradiated samples, after removal from the radiation, were heated at 400°C for 20 minutes to thermally remove trapped electrons from the radiation inducted negative ion vacancies.

In practice, the crystals were cleaved into cubes approximately 2 mm on edge and mounted on 1 mm platinum wires by heat-fusing the salt to the platinum. The crystals were then irradiated, thermally bleached, etched in a mixture of deionized water and absolute ethyl alcohol, and placed in the r-f ground sample-holder of the mass spectrograph. A pointed counterelectrode of platinum was used in the remaining sample holder.

With the gap between the electrodes very short, it has been found that application of the sparking voltage usually produces an ion beam immediately, or after a few seconds. Ion beams of 2×10^{-10} amperes are not unusual at pulse rates of 100 or 300. The ion beam is relatively stable and normally the electrode geometry does not require adjustment to maintain the ion output. In addition, the irradiation treatment eliminates the luminescent plasma and the abnormalities observed in the large ratios of the successive degrees of ionization of the matrix elements. Another unusual feature of the irradiated salts is the characteristic change in the appearance of the spark itself. Visually one observes a very small, unimpressive spark between the sample and the counterelectrode similar to sparks often observed when sparking conductors. However, care must be exercised in maintaining the sparking voltages and repetition rates below values that would support surface arc-over, in which case the spectra revert to those obtained from unirradiated salts.

Table I shows the ratio of the singly charged matrix ions of non-irradiated KBr and KCl as well as gamma-irradiated KBr. The ratio given for KCl was from a report by Ohkura and Maurer[1].

TABLE I

Ratio of $Alkali^+ / Halogen^+$

		K^+/Br^+	K^+/Cl^+
NRL	Non-Irr.	3-48	
	γ-Irr.	5-6	
Univ. of Ill. -Non-Irr.			10

Table II gives the ratio of the single to the successively increasing degrees of ionization of the matrix elements of gamma-irradiated and non-irradiated KBr and of non-irradiated KCl. The irradiated salt indicates a decrease in the ratios of 2 to 3 decades.

The line widths of the singly and multiply charged ions of the matrix elements were found proportional to $M^{1/2}$ except the singly charged alkali which showed some broadening thought due to space charge or thermal ionization.

TABLE II

Ratio of N^+/N^{x+}

	Element	N^+/N^{2+}	N^+/N^{3+}	N^+/N^{4+}
NRL γ-Irr.	K	3.8×10^{1}	1.6×10^{2}	1.0×10^{3}
	Br	7.5×10^{0}	6.3×10^{1}	5.3×10^{2}
NRL Non-Irr.	K	4.0×10^{3}	2.5×10^{5}	NA
	Br	1.0×10^{1}	2.5×10^{3}	NA
U. of Ill. Non-Irr.	K	1.4×10^{4}	5.0×10^{5}	2.1×10^{6}
	Cl	1.2×10^{3}	6.1×10^{4}	1.7×10^{5}

Table III shows the analysis of a doped sample of KBr. The analysis by flame photometry, activation analysis, wet chemistry and atomic absorption was performed by C. T. Butler at Oak Ridge National Laboratory. Concentrations from mass spectrometry determined by the visual method using 81_{Br^+} as an internal standard; the alkali metals were corrected using 6 as the ratio of the K^+/Br^+. All concentrations have been rounded off to one significant figure.

TABLE III

Impurities in KBr

	Concentration PPM (wgt.)				
Element	Mass. Spec.	Activation Analysis	Flame Photo.	Wet Chemistry	Atomic Absorption
Mg	4				3
Cu	2	<1			
Sr	10		12.3		
Rb	150		134		
Mn	1		< 1		
Li	0.1		< 0.1		
S	0.6			< 1	
P	Not Found			0.3	

In an effort to see if the irradiation treatment would improve the ionization of non-crystalline solids, samples of high purity iron-doped sodium silicate glass were irradiated with 2 Mev electrons and run using a gold counterelectrode.

Little is known about the radiation-induced defects in non-crystalline materials such as glass. Recent experimental results indicate that the electrical conductivity of alkali glasses is due to alkali-metal ions. Although satisfactory spectra on samples of alkali glass have been obtained some of the time, the enhancement of the ionization characteristic was inadequate to completely eliminate thermal ionization, especially of the alkali matrix element. Despite considerable effort to analyze for iron in doped alkali glasses, reproducibility was poor. In general, the glass was difficult to spark and ion output was erratic and low. In addition, constant manipulation of the electrodes was necessary and a large luminescent plasma was observed about the tips of the electrodes and frequently between the sample and the sample holder. At the present time the spark source analysis of electron irradiated alkali glass is considered to be qualitative.

When crystalline material, such as the alkali halides, is irradiated with high energy ionizing radiation, different kinds of color centers and other defects are produced simultaneously and the experimentally observed facts are difficult to interpret in a simple manner. The precise mechanism responsible for the enhancement of the ionization characteristics in alkali halides is not known; it appears to be related to the induced negative ion vacancies. Although the irradiation and thermal bleaching treatment favorably alters the ionization characteristic of alkali halides in the conditions of the r-f spark, any surface arc-over is a source of thermal ions that impose limitations on the quality of the analysis.

It would seem probable that other crystalline material in which electron and hole centers could be radiation-induced may respond in a similar fashion so that improved ionization and analysis could be achieved.

REFERENCES:

(1) R. J. Maurer and H. Ohkura, Technical Report No. 8, Contract Nonr 1834(19) NR017-412 (Sept. 1964).

113. RELATIVE SENSITIVITIES OF TWENTY ELEMENTS IN THE IRON MATRIX FOR SPARK-SOURCE MASS SPECTROMETRY

J. M. McCrea
Applied Research Laboratory
United States Steel Corporation
Monroeville, Pa. 15146

An experimental investigation of the relative sensitivities for various trace elements in the iron matrix then undertaken in an effort to resolve these inconsistencies noticed in interlaboratory comparisons, particularly for elements lying below titanium in the periodic table.

Well-characterized samples of good micron-range homogeneity with respect to the distribution of trace impurities are not readily available. After due consideration, No. 461, 465, and 466 of the National Bureau of Standards 460 series of ingot-iron and low-alloy steel reference materials were selected for the calibration work. In addition to other considerations, a distinct advantage in using members of the NBS 460 series for calibration accrues from the availability of sensitivity data from other laboratories that have worked with these materials.

Electrode pairs were retipped and repolished after analysis for subsequent analyses. The sample sequence for the instrument was scrambled to offset time and memory effects.

After a standard calculation of sample composition, assuming equal sensitivity per atom in the mass spectrometer, the results obtained were compared with the data for composition on a parts per million by atoms (ppma) basis obtained from the weight percent data given by NBS. Sensitivities for 20 elements in the iron and low-alloy-steel matrixes were calculated and summarized as geometric means. All data for lines without blemishes and with a minimum relative transmittance greater than 0.18 were weighted equally in the averaging. In all over 1500 lines were measured photometrically; Table I shows data for NBS 466 and geometric means for all data.

Experience with analytical use of the average sensitivities in Table I is largely satisfactory. The practice removes much of the interlaboratory discrepancy associated with data on manganese, copper, phosphorus, and sulfur. With nickel, cobalt, and molybdenum the agreement is not as good when experimental sensitivities are used to obtain results as when the equal sensitivity assumption is made. Overall, the agreement among the data from mass spectrographic and activation analysis laboratories is better when experimental sensitivities are used than when they are not.

Added justification for analytical use of experimental sensitivities is obtained from a critical comparison of data published during the period that spark-source mass spectrometers have been available commercially. Difficulties inherent in making such a comparison derive from choice of reference elements and use or nonuse of corrections for effects such as linewidth, background, and the relation between emulsion response and ion mass. This situation is not utterly bleak; the original articles reveal many of the idiosyncrasies, and data can usually be recomputed to a common basis for valid comparisons. The author has chosen to delete any correction made for the effect of ion mass on instrument transmission or emulsion sensitivity from the published data, and to use iron as a reference element with the assigned value of unity. The effects of background corrections and differences in the techniques of emulsion calibration

Table I

Relative Mass Spectral Sensitivities of Elements in an Iron Matrix

Element	Individual Runs on NBS 466				Geometric Means NBS 461	NBS 465	NBS 466	All Data
B	9.68	2.44	6.85	3.83	6.04	4.72	4.90	5.11
P	4.66	2.60	4.14	4.00	5.36	4.27	3.76	4.34
S	8.58	4.12	7.12	7.52	10.2	7.09	6.59	7.57
Ti	2.32	1.94	1.78	2.04	1.74	2.19	2.01	2.01
V	2.11	2.44	1.19	1.43	1.24	1.51	1.72	1.50
Cr	1.24	1.15	1.03	1.18	1.29	0.84	1.15	1.04
Mn	2.06	1.89	2.06	2.35	2.57	2.24	2.08	2.27
Co	0.72	0.80	0.62	0.68	0.82	0.63	0.70	0.70
Ni	0.65	0.67	0.42	0.78	0.78	0.68	0.61	0.68
Cu	2.18	1.61	1.44	2.56	1.98	1.75	1.90	1.85
Ge	1.97	1.25	1.03	2.28	2.28	1.29	1.57	1.58
As	5.11	2.40	1.44	5.22	3.87	3.07	3.10	3.26
Zr	0.63	0.57	0.33	0.73	0.34		0.54	0.44
Nb	0.93	0.88	0.72	1.20	1.08	0.66	0.92	0.85
Mo	0.63	0.76	0.31	0.48	0.79	0.35	0.52	0.54
Ag	5.57	2.63	2.69	10.25	5.92	4.64	4.48	4.93
Sn	1.77	1.01	0.91	2.79	3.99	1.86	1.46	2.16
Ta					0.42			0.42
W					0.28			0.28
Pb	1.65	1.55		2.02	3.01		1.73	2.28
Fe	- - - - -Unity- - - -				- - - Unity - - -			Unity

Note: These data apply to the radio-frequency-spark source and the Ilford Q2 plate ion detector, based on maximum line intensity of a 1+ line and without correction for line width.

are judged to be unimportant. The greatest obstacle to comparison is the treatment of line shape or width.
A qualitative classification of results according to use or non-use of a correction for line shape or width is easily made, and the gap between the two cases is partially bridged by the author's and another laboratory's data calculated both ways. From a comparison of data from 10 laboratories in 5 countries and using 5 different makes of instruments, it is concluded that factors related to spark-source operation can apparently influence sensitivity results as much as any linewidth treatment. Several correlations of sensitivity and elemental properties have been suggested empirically or from theoretical consideration by various workers. The author has tested these and some additional relations graphically using experimental data for the iron matrix. The most attractive data pattern is given by a semilogarithmic plot of the temperature required for a given vapor pressure of the pure element and the sensitivity based on triangulated estimates of integrated line exposure. A vapor pressure of 10^{-6} torr, corresponding to spark-source operating pressures, was selected for the temperature axis. Most of the data concentrate in a band, but the silver and boron data are anomalous. The reference values for silver are not certified, and erroneously low values for the three samples could raise the apparent silver sensitivity. The discrepancy for boron, the only sensitivity for the second row of the periodic table determined, is considered related to its periodic table position and possibly to segregation.

Some prognosticated values for the relative sensitivities of other elements are presented in Table II. These values were obtained from the correlation with linear interpolation from linewidths for Ti, S, P, and Na used to estimate the linewidth for elements below Ti in the periodic table. The alkali metals are listed as a separate group because the phenomenon of surface ionization may also enhance their sensitivities. The author is now using prognosticated sensitivities rather than the popular assumption of equal sensitivity. Only extended experience can justify this action, but to date this experience has been consistently favorable with metallic samples.

In this summary of the work, it is not practical to provide citations to all the literature considered, and for this reason no citations are given. It is hoped to provide these elsewhere in a fuller account of the work.

Table II

Sensitivity Estimates for the Iron Matrix

Element	Sensitivity Estimate	Element	Sensitivity Estimate	Element	Sensitivity Estimate	Element	Sens. Est. (Area) /1/
Be	3.3	Ba	2.8	Au	1.4	Be	1.7
C	1.0	La	1.1	Hg	4.4	C	0.5
Mg	4.7	Ce	1.2	Tl	2.8	Mg	4.7
Al	2.5	Pr	1.4	Bi	2.6	Al	2.5
Si	1.7	Nd	1.6	Po	3.5	Si	1.7
Ca	3.3	Sm	2.5	At	4.6	Ca	3.3
Sc	1.6	Eu	2.8	Ra	2.9	Sc	1.6
Zn	3.4	Gd	1.5	Th	0.7	---	---
Ga	1.8	Tb	1.4	U	1.0	Li	2.9
Se	3.7	Dy	1.5	Pu	1.4	Na	3.6
						K	3.8
Sr	2.9	Ho	1.8	Am	1.9		
Y	1.2	Er	1.8	---	---		
Tc	0.6	Tm	2.2	Li	6		
Ru	0.6	Yb	2.9	Na	5.6		
Rh	0.8	Lu	1.3	K	4.6		
Pd	1.3	Hf	0.6	Rb	3.9		
Cd	3.6	Re	0.35	Cs	4.1		
In	2.1	Os	0.4	Fr	4.6		
Sb	2.8	Ir	0.6				
Te	3.3	Pt	0.8				

Note: Estimates for use where no corrections are applied for variation of emulsion sensitivity with ion or for ion transmission from source to detector. Those in column designated /1/ for use with peak area triangulation; other data are for maximum line exposure and also with peak area triangulation if separate values are not shown. Elements are arranged in order of increasing atomic number, with alkali metals as a separate group.

114. The Sensitivity, Accuracy and Speed of Spark Source Electrical Detection

Charles W. Hull

Analytical Instruments Division
Consolidated Electrodynamics Corporation
Monrovia, California

An experimental electrical detection spark source mass spectrometer has been built in our laboratory which is much more sensitive, and is faster than a conventional photoplate instrument. This spectrometer has been tested by determining the relative sensitivity factors and detection limits of 17 elements in eight NBS 460 series iron samples. It has also been used to study the accuracy characteristics of a spark source.

This work will shortly be submitted for formal publication. Therefore, only a brief description of the instrument and tests follows.

An electrical detector was built which effectively discriminates against the baseline background in the spark source spectra. This is diagrammed in Figure 1. The multiplier detector is shielded against both charge exchange ions, and reflected ions. These are the primary backgrounds in a spark source spectrum, and with this detector the baseline background was generally less than one part in 10^9.

Figure 2 is a sketch of the electrical detection apparatus. The electromagnet was driven by a precision magnet field regulator. This regulator was referenced to a "peak selector", whose dials were calibrated directly in units of $\sqrt{\text{a.m.u}}$ Thus, in operation an m/e was chosen, its square root set into the peak selector, and the field regulator automatically adjusted the field so that if the chosen m/e existed in the ion beam, it was brought into register at the collector. The peak intensity was then defined as the charge from the multiplier divided by a standard total beam charge integrated at the beam monitor.

The electrical detector has a more favorable signal to background law than the photoplate does. A typical comparison is shown in Figure 3. The time advantage of doing an electrical analysis compared to doing a photoplate analysis for typical manual operation is shown in Figure 4. If both systems are automated, the advantage shifts more in favor of the electrical method, as is shown in Figure 5.

The response of 17 elements in iron was quite similar to that found with the photoplate. Figure 6 is a tabulation of the response data. Tin had the highest response, but also the largest standard deviation. Tungsten had the lowest response, and Niobium had the smallest standard deviation.

FIGURE 1

ELECTRICAL DETECTION COLLECTOR

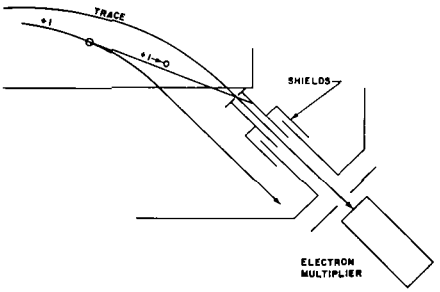

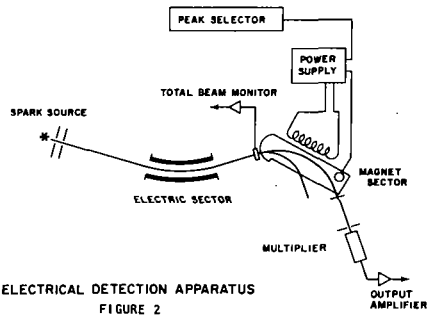

ELECTRICAL DETECTION APPARATUS

FIGURE 2

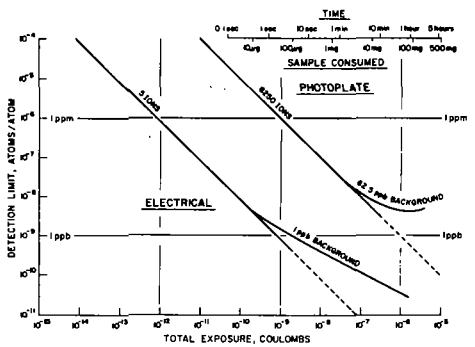

Figure 3 - Typical Detection Limit Functions for Electrical and Photoplate Detectors

FIGURE 4

MANUAL PHOTOPLATE DETECTION COMPARED TO MANUAL ELECTRICAL DETECTION

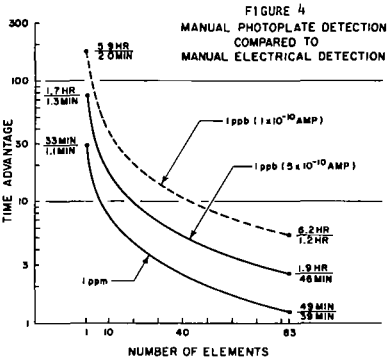

FIGURE 5

AUTOMATED PHOTOPLATE DETECTION COMPARED TO AUTOMATED ELECTRICAL DETECTION

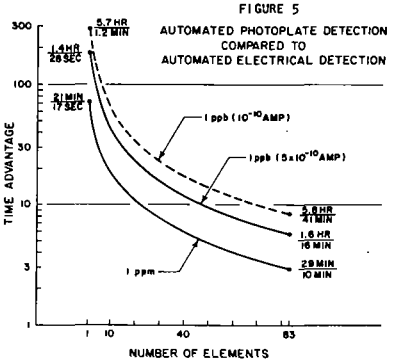

Based on the measured elemental response and the measured baseline background, two types of detection limits were calculated: the standard detection limit, as the actual detectability with exposure sufficient to give 1 ppb elemental detectability with the isotope used, then corrected for measured background and measured element response. This is the type of detection limit one might find in a many-element survey. Next, the individual detection limit was defined as the detection limit with a total exposure of 1×10^{-6} coulombs, with half used to accurately measure the background. This is the detection limit available if one wants to take advantage of the favorable signal to background law of electrical detection and search for only one or a few elements in the sample. Figure 7 is a tabulation of these two limits for the 17 elements measured. Tungsten had the highest limits, since it had the poorest response, a small isotope, and a rather high background. Arsenic had the lowest limits, since it had high response, a 100% isotope, and low background. The standard limits are comparable to the ultimate available with photoplate detection, and those elements near the matrix, V, Cr, Mn, Co, and Ni, are far more detectable than with a photoplate. The individual detection limits vary from one to two orders of magnitude lower than possible with photoplate detection.

FIGURE 6

SUMMARY OF 123 ELEMENT CONCENTRATION DETERMINATIONS IN EIGHT NBS 460 SERIES IRON SAMPLES

ELEMENT	(#) OF SAMPLES	AVERAGE NORMALIZED RESPONSE	
B	(6)	0.75 ±31%	
C	(7)	0.70 ±28%	
P	(8)	2.2 ±24%	
Ti	(7)	1.5 ±25%	
V	(8)	1.0 ±16%	
Cr	(8)	0.93 ±9.1%	
Mn	(8)	1.6 ±19%	
Co	(8)	0.65 ±26%	
Ni	(7)	0.60 ±19%	
Cu	(8)	1.3 ±17%	
As	(8)	3.9 ±22%	
Zr	(4)	1.6 ±8.3%	
Nb	(7)	1.1 ±7.2%	(BEST DATA)
Mo	(8)	0.78 ±7.8%	
Sn	(8)	4.2 ±35%	(WORST DATA)
Ta	(7)	0.50 ±21%	
W	(6)	0.35 ±17%	

FIGURE 7

DETECTION LIMITS FOR 17 ELEMENTS IN IRON

ELEMENT	ISOTOPE	STANDARD DETECTION LIMIT	INDIVIDUAL DETECTION LIMIT	
		ppB		
B	11	3.2	0.12	
C	12	2.6	0.09	
P	31	0.69	0.09	
Ti	47	1.9	0.24	
*	48		0.02	
V	51	1.2	0.03	
Cr	52	2.1	0.07	
Mn	55	3.9	0.13	
Co	59	2.2	0.07	
Ni	60	6.9	0.46	
Cu	63	1.2	0.04	
As	75	0.40	0.01	(LOWEST)
Zr	90	1.5	0.06	
Nb	93	1.8	0.05	
Mo	95	4.7	0.39	
Sn	118	1.2	0.08	
Ta	181	4.2	0.12	
W	182	25	1.7	(HIGHEST)

115. Time Resolution in Spark Source Mass Spectrography

C. A. Evans, Jr.* and G. H. Morrison
Department of Chemistry
Cornell University
Ithaca, New York 14850

Several workers[1,2] have predicted time variations during the individual spark breakdowns which last for less than 0.1 μsec and are repeated throughout the rf pulse packet. In the present study time resolution of the rf pulse has shown variations on the order of 1-100 μsec.

A pulse generator external to the mass spectrometer synchronizes the rf spark and the square pulse used for time resolution. At a predetermined time after the rf pulse is initiated, a square pulse is generated and imposed on the ion deflector plates. In contrast to Jackson, Whitehead, and Vossen[3] and Franzen and Schuy[4], the defelctor plates are located after the ESA, not before. Therefore, when no voltage is on the deflector plate, a normal spectrum is produced on the photoplate. When the voltage pulse is imposed on the deflector plate, another spectrum is formed on the plate slightly up or down mass from that of the undisturbed beam. The ion intensity for a given time segment is then ratioed to the total ion intensity.

A dual beam oscilloscope proved to be invaluable to this study. Not only did it allow the determination of the time relations under study, but correlations were found between the ion yield vs. time curves and the oscillographic traces. In order to observe the characteristic signal from the rf spark, a coil of wire was placed on the Tesla coil axis and connected to the oscilloscope. Figure 1 presents the traces for two matrices studied, iron rod and 50:50 biological-ash: graphite[5]. The upper traces present the driving pulse and the lower trace, the spark signal. In the iron trace the rf signal is constant throughout the rf pulse packet. When the ash: graphite electrodes are sparked, the rf signal varies during the pulse packet. During the early discharges there is the characteristic rf discharge whereas there is a low-voltage signal during the latter portion of the signal. This low-voltage signal is very similar to the trace obtained when the electrodes are shorted together. In addition, the discharge from the biological ash-graphite lasts well past the "cut-off" time noted with the iron electrodes.

Ion yield vs. time studies of the iron electrodes showed the ion production to be reasonably constant throughout the rf pulse for all ionic species as shown in Figure 2. The intensity of the initial maximum was found to vary with the accelerating potential. This could be caused by a loading down of the accelerating voltage power supply and a shift in the energy distribution at the entrance to the magnetic sector. Alternatively, the intensity of this maximum could be varying with the initial energy of the ions.

The ion yield for the biological ash-graphite exhibited a drastically different behavior. In the ash-graphite electrodes, the +2 ions were preferentially produced in the early portion of the discharge. Little or no +2 ion production was found after 60-70 μsec even though singly-charged species were found as late as 110 μsec.

---

*Present address: Ledgemont Laboratory
Kennecott Copper Corporation
128 Spring Street, Lexington, Massachusetts 02173

From the oscilloscopic traces of the ash-graphite electrodes it seems the rf discharges induce a very large number of charge carriers into the electrode gap, the gap resistance drops and a low-voltage type of discharge is established. Correlating the oscillographic and the ion yield data, it would seem the doubly-charged ion production is suppressed during the low-voltage portion. Franzen[6] has obtained similar results using the pulsed-dc discharge[4], where he found decreased production of the doubly-charged species during the dc portion of the discharge when using potassium halide-graphite electrodes.

A more extensive discussion of this study has been submitted for publication in Analytical Chemistry.

References

1. R. E. Honig in Mass Spectrometric Analysis of Solids, A. J. Ahearn, Editor, p. 16, Elsivier, New York, 1966.
2. J. Franzen, K. D. Schuy, and H. Hintenberger, Twelfth Annual Conference on Mass Spectrometry and Allied Topics, Montreal, Canada, 1964, p. 251.
3. P. F. S. Jackson, J. Whitehead, and P. G. T. Vossen, Anal. Chem., 39, 1737, (1967).
4. J. Franzen and K. D. Schuy, Z. Naturforsch., 209, 176(1965).
5. C. A. Evans, Jr. and G. H. Morrison, Anal. Chem., 40, 869 (1968).
6. J. Franzen, personal communication.

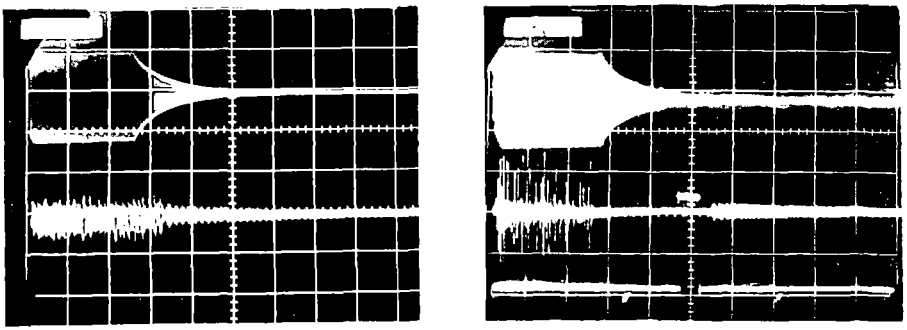

a. Iron Electrodes b. Biological Ash-Graphite Electrodes

(20 μsec. / div.)

Figure 1. Oscillographic Traces of the rf Spark Pulses

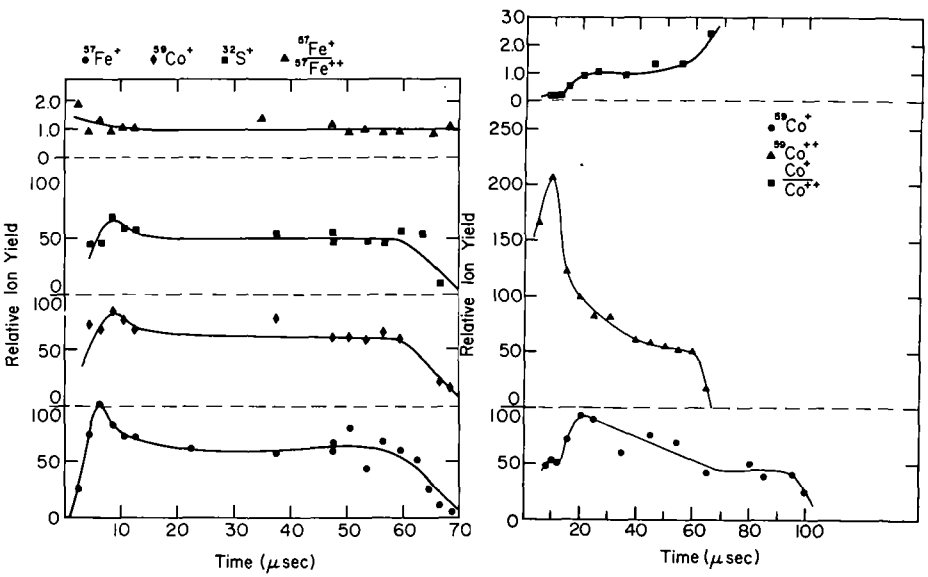

a. Iron Electrodes b. Biological Ash-Graphite Electrodes

Figure 2. Ion Yield vs. Time for Various Ions

116. USE OF A SPARK SOURCE MASS SPECTROGRAPH FOR THE GENERAL ANALYSIS OF GEOLOGICAL SAMPLES

Riley D. Carver and Paul G. Johnson

Lawrence Radiation Laboratory, University of California
Livermore, California

For many years the spark source mass spectrograph has been used to analyze geological samples for trace impurities,[1,4] but when the gross composition is desired the older, classical techniques usually are relied upon. The spark source mass spectrograph, however, has many virtues which would make it a desirable instrument for survey analysis at all composition levels.

Atomic masses 7 - 250 can be determined from a single analysis. These include all elements except helium and hydrogen. The analysis is extremely sensitive, and impurity abundances of a few parts per billion are frequently reported. This sensitivity is fairly uniform, with variations up to a factor of two or three. A variation of this magnitude is usually satisfactory in determining trace impurities, but would not be acceptable for major constituent analysis.

If, however, the deviation of any particular element were relatively constant in all samples of a given type, then an empirical correction could be made for that element in samples of that type. Several geological materials of known composition[5,6] have been analyzed by spark source mass spectrography to determine the reliability of this procedure.

The instrument used in this work is a Consolidated Electrodynamics Corporation 21-110 spark source mass spectrograph of Mattauch and Herzog design.[9] This geometry is necessary because the wide spread of ion energy and fluctuations of the spark require double focusing and an integrating collector such as a photographic plate. Ions are made in the source by passing a 100 KV radio-frequency electric spark between two pieces of the sample. These ions are accelerated through a 20 KV potential and focused in the electrostatic sector to a narrow energy spread. Approximately one-half of the ion beam is intercepted by the beam monitor electrodes and is displayed on a current meter. Circuitry is provided to integrate this current and show cumulative ionic charge. All ions which enter the magnet sector are focused along the plane of the photographic plate. Their position on the photoplate defines their atomic mass number, and the extent of photographic blackening is a measure of their relative abundance in the original sample.

The standard geological samples are obtained in a finely ground homogeneous form. Since all samples for this instrument must be in some sort of electrically conductive state, 400 mg of sample are mixed with 400 mg of National Carbon Company SP-1 grade graphite and pelletized in a small laboratory press at 10,000 psi. The outside surface of the rod-like pellet is machined away to remove any possible contamination from the die. The rod is then broken into two pieces and mounted in the electrode holders of the instrument so that the freshly broken surfaces are exposed to the spark. The source is then sealed, and a high vacuum is obtained (10^{-7} torr), usually within a few hours. Similar vacuum (10^{-8} torr) is constantly maintained in the analyzer portion of the instrument by a source isolation valve. Neither of these pressures changes significantly during the sparking. The sample electrodes are pre-sparked for several minutes to insure surface cleanliness; then the isolation valve is opened, and the photographic collection is made.

Because of the limited dynamic range of photographic emulsions, a series of graded exposures is made, from 4×10^{-13} to 1×10^{-7} Coulombs in increasing factors of two, a total of nineteen exposures. An additional exposure is made on each photoplate for an emulsion calibration. For this, rhenium metal is sparked for several values of ionic exposure, changing the magnet strength slightly after each sparking. The known isotope ratio of rhenium is used to fit the Hull[10] equation for emulsion calibration.

The photoplates used in this study are Ilford Q-2. These Schumann type plates are very abrasion sensitive, and extreme care must be taken to prevent accidental damage to the surface. After all exposures are made, the photoplates are developed in a darkroom for three minutes with commercial Kodak D-19 developer. A ten second quick-stop in 2% acetic acid solution is followed by a three minute fix in commercial Kodak rapid fix with hardener. The plates are then washed for five minutes with tap water and for one minute with distilled water. After air drying at room temperature, every line of interest is interpreted automatically using a Grant comparator-microphotometer and a Digital Equipment PDP-8 computer. This system will be described elsewhere. Each line is corrected for mass effect by multiplying times $(\text{mass})^{1/2}$, but no correction is attempted for line widths. The elemental abundances are referenced to silicon as an internal standard using the atomic mass number 29 and 30 lines.

TABLE I

ACCEPTED VALUES, EXPRESSED AS WEIGHT PERCENT, FOR GROSS ELEMENTAL COMPOSITION IN SEVERAL GEOLOGICAL STANDARD MATERIALS COMPARED WITH EXPERIMENTAL MEASUREMENT

Element	Granite (b) G - 1	Correction factor exp/std	Diabase (b) W - 1	Correction factor exp/std	Syenite (c) 1	Correction factor exp/std	Tonalite (d) T - 1	Correction factor exp/std	Andesite (e) AGV - 1	Correction factor exp/std	Sulfide (c) 1	Correction factor exp/std
Na	2.44	3.97	1.59	2.26	2.40	3.82	3.20	3.43	3.14	2.52	0.76	2.61
Mg	0.21	1.78	3.93	1.66	2.45	1.98	1.10	1.36	0.90	1.16	2.37	1.53
Al(a)	7.87	1.03	7.91	0.83	5.07	1.14	8.63	1.14	9.07	0.86	5.01	0.55
Si	33.90	1.00	24.58	1.00	27.79	1.00	29.49	1.00	27.63	1.00	16.14	1.00
P	0.04	2.41	0.06	1.41	0.09	1.60	0.07	1.92	0.21	1.12	0.04	2.14
K	4.58	2.52	0.52	1.92	2.28	3.23	1.02	2.35	2.37	2.06	0.52	2.61
Ca	0.97	0.72	7.80	0.78	7.38	1.03	3.66	0.54	3.50	0.94	3.96	0.45
Ti	0.16	0.99	0.65	0.91	0.29	1.38	0.34	1.18	0.63	1.52	0.48	1.04
Fe	1.36	0.95	7.79	1.28	6.08	1.09	4.10	1.12	4.65	1.16	22.87	1.33

(a) reference element

(b) preferred value, see Ref. 5

(c) preferred value, see Ref. 6

(d) preferred value, see Ref. 7

(e) preferred value, see Ref. 8

TABLE II

ACCEPTED VALUES, EXPRESSED AS WEIGHT PARTS PER MILLION,
FOR SOME TRACE IMPURITIES IN TWO GEOLOGICAL STANDARD MATERIALS
COMPARED WITH EXPERIMENTAL MEASUREMENT

	Granite		Diabase	
	(a)		(a)	
Element	G - 1	experimental	W - 1	experimental
Pr	17	15	3.31	2.40
Nd	55	80	18.8	33.0
Sm	8.9	6.8	4.08	5.00
Eu	1.5	1.4	1.24	3.10
Gd	5.6	11.8	4.18	8.20
Tb	1.1	0.4	0.7	0.7
Dy	4.6	2.6	3.45	7.70
Ho	0.96	0.28	0.86	3.50
Er	1.95	0.73	2.4	2.8
Tm	0.24	0.20	0.31	0.46
Yb	0.84	0.37	1.95	2.30
Lu	0.13	0.20	0.24	0.21

(a) preferred values, see Ref. 1-5

Table I shows the ratio of our measured elemental abundances to the listed "standard" values for major constituents. These ratios are fairly constant for each element in samples of the same general composition and could be used as empirical correction factors to improve survey-type analyses.

Because of the lack of geological materials whose compositions are well established at the trace impurity level, no attempt has been made to determine any correction factors for these elements. As mentioned earlier, however, the expected sensitivities are fairly uniform and usually are acceptable in trace analysis. Table II shows the measured along with the "standard" values for some trace impurities in two geological materials.

These results show that spark source may be used for the general survey analysis of geological samples at all levels of elemental composition, especially if extreme accuracy and precision are not required.

This work was performed under the auspices of the United States Atomic Energy Commission.

REFERENCES

1. Brown, R., and W. A. Wolstenholme, Nature, London 201, 598 (1964).
2. Taylor, S. R., Nature, London 205, 34 (1965).
3. Taylor, S. R., Geochim. Cosmochim. Acta 29, 1243 (1965).
4. Nicholls, G. D. A. L. Graham, E. Williams, and M. Wood, Anal. Chem. 39, 584 (1967).
5. Fleischer, M. and R. E. Stevens, Geochim. Cosmochim. Acta 26, 525 (1962).
6. Webber, G. R., Geochim. Cosmochim. Acta 29, 229 (1965).
7. Ingamells, C. O., and N. H. Suhr, Geochim. Cosmochim. Acta 27, 897 (1963).
8. Flanagan, F. J. Geochim. Cosmochim. Acta 31, 289 (1967).
9. Mattauch, J., and R. Herzog, Z. Physik 89, 786 (1934).
10. Hull, C. W., Proc. Tenth Conf. A. S. T. M. Comm. E-14, 404 (1962).

117. COMPOSITION OF PYRIDINE EXTRACTS FROM REDUCED AND UNTREATED COALS AS DETERMINED BY HIGH-RESOLUTION MASS SPECTROMETRY

T. Kessler, R. Raymond, and A. G. Sharkey, Jr.

U.S. Department of the Interior, Bureau of Mines
Pittsburgh Coal Research Center, Pittsburgh, Pa. 15213

INTRODUCTION

The purpose of this investigation at the Bureau of Mines was to determine the factors required for the solvation of coal.

Reggel and coworkers reported greater pyridine solubility for vitrains after reduction with lithium-ethylenediamine.[1,2] These workers suggested that the increased solubility of reduced coals might be attributed to (1) splitting of ether linkages in the coal and partial elimination of sulfur from the coal structure to produce smaller, more soluble units, and (2) the addition of hydrogen to aromatic rings in the coal structure to form hydroaromatic compounds which are generally more soluble than the corresponding aromatic molecules.

Because of the complexity of coal, in situ investigations of the chemical structure of coal often cannot be conducted. Coal extracts have been used by many investigators to study the constitution of coal.[3]

Chemical changes produced by the reduction of coal should be detected in the pyridine extracts. For example, a pyridine extract of a reduced vitrain should contain less sulfur than the corresponding untreated vitrain extract, as indicated by ultimate analyses of the coals.

Several papers have been published describing the general technique of high-resolution mass spectrometry for the identification of organic compounds.[4-7]

EXPERIMENTAL

The reduced sample used in this investigation was prepared by reacting vitrain from Pittsburgh seam hvab coal with lithium-ethylenediamine using a previously described procedure.[1] The reduced vitrain contained 16 added hydrogen atoms per 100 carbon atoms.[2]

Samples consisting of 0.25 g of vitrain (-325 mesh) and 20 ml of pyridine (99.5 percent pure) were mechanically agitated for 24 hours at ambient temperature. The resulting extract was separated from the coal residue by centrifugation. Pyridine was removed from the extract for subsequent mass spectrometric investigations by passing nitrogen over the sample at room temperature. The residue was then air dried to constant weight at 100° C and was used as the basis for determining the amount of pyridine solvation according to the method of Curran and others.[8] The following results were obtained:

Sample	Weight percent solvated	
	This investigation	Previous investigation[1]
Reduced vitrain	41	31
Untreated vitrain	17	21

Mass spectra of the extracts were obtained using a Consolidated Electrodynamics Corporation model 21-110B high-resolution mass spectrometer. The mass spectrometer inlet and source temperatures were 300° C. A resolution of 1 part in 5,000 was sufficient to resolve the multiplets of interest for peak matching. Precise masses were determined manually using a Nier peak matcher.[9] The low ionizing voltage technique was used to obtain mass spectra for semi-quantitative analyses.[10] Data were based on percent of total ionization of all multiplets in the mass spectra, assuming equal sensitivity for all compounds. This method gives only approximate values but is useful in studying changes in concentration.

RESULTS AND DISCUSSION OF RESULTS

Approximately 30 percent of both the reduced and untreated vitrain were volatilized at 300° C in the mass spectrometer. Precise masses were determined for all multiplets that occurred at even numbered nominal masses from 94 to 270. Above mass 270 ion intensities were too low for accurate mass measurement. Only empirical formulas which deviated less than ± 0.005 amu from measured values were considered. In the mass range investigated, empirical formulas were assigned to 155 precise masses measured for the reduced vitrain and 158 masses for the untreated vitrain. The two samples were found to contain structural types having the following elemental compositions:

Elemental composition[a/]	Number of possible structures[b/] Reduced	Untreated
C,H	19	18
C,H,O	7	7
C,H,O_2	-	2
C,H,S	4	10
C,H,S_2	-	1
C,H,N_2	3	1

The above are minimum values because isomeric forms are not included.

a/ Only the number of heteroatoms is specified.

b/ In the discussion to follow reference to "structure" merely denotes an example of a possible compound that can correspond to an empirical formula determined by precise mass measurement.

Oxygenated compounds. The total oxygenate concentration (based on percent of total ionization) for the reduced and untreated vitrains were 21.2 and 11.8 percent respectively. The reduced vitrain contained 8.0 percent phenols compared to 2.9 percent in the untreated vitrain. The increase in phenols in the reduced vitrain is evidence for the rupture of the ether linkage in coal to form lower molecular weight compounds. Five other series of oxygenated structures were higher in the reduced vitrain extract compared to the untreated vitrain extract. Empirical formulas of the first member and examples of these series are: C_8H_6O (benzofurans), C_8H_8O (indanols), $C_{10}H_8O$ (naphthols), $C_{12}H_{10}O$ (phenylphenols), and $C_{16}H_{10}O$ (naphthylphenols).

Sulfur compounds. An example of the elimination of a sulfur compound(s) from coal by reduction is shown in table 1. The nominal mass 208 for the untreated vitrain consists of a triplet composed of a sulfur-, an oxygen-, and a hydrocarbon compound. The spectrum of the extract of the reduced vitrain contains only the oxygen- and hydrocarbon compounds.

Table 1.- Evidence for elimination of sulfur from coal at nominal mass 208

Sample	Empirical formula	Relative intensity
Reduced vitrain	$C_{15}H_{12}O$	1.0
	$C_{16}H_{16}$	17.0
Untreated vitrain	$C_{14}H_8S$	4.0
	$C_{15}H_{12}O$	1.0
	$C_{16}H_{16}$	17.0

The total ionization for sulfur compounds in the reduced vitrain was only 0.3 percent compared to 2.6 percent for the untreated vitrain. Sulfur values from ultimate analyses of the reduced and untreated vitrains were 0.14 and 0.94 percent, respectively. The decrease in sulfur compounds determined by mass spectrometry is the same order of magnitude as the decrease in total sulfur determined by ultimate analyses.

Hydrocarbon compounds. If reduction produces rupture of the coal-ether linkages and the elimination of sulfur to form smaller and more soluble coal units, there should be a change in the concentrations of hydrocarbons volatile at 300° C. Using the molecular weight series of cyclohexadiene and its alkyl derivatives as an example of a smaller structural unit, the reduced vitrain contains approximately 13 times more of this compound type than the starting vitrain. For homologous series of higher molecular weight structures, such as 3-ring aromatics, the total concentrations of the compound types in the mass range investigated are lower following reduction. From these data it appears that reduction causes smaller and more soluble coal units to be formed.

Hydroaromatic compounds. Comparison of the total naphthalene and hydronaphthalene series was used to determine differences in hydroaromatic content for the extracts. The concentration of naphthalenes was lower by a factor of 2 in the reduced vitrain compared to the untreated vitrain. The total dihydro-, tetrahydro-, and hexahydronaphthalenes are greater by factors of 4, 5, and 3, respectively, following reduction. These changes indicate that reduction occurred. The changes in concentration of the hydroaromatics are based on maximum values as corrections have not been made for the alkyl derivatives of indene, indan, and benzene, which have the same precise masses as these hydroaromatic compounds. The above hydroaromatics represented 29 percent (of total ionization) of the reduced vitrain compared to 7 percent for the untreated vitrain. The large difference between the naphthalene values (9.9 percent for the reduced versus 28.8 percent for the starting vitrain) is reflected, as expected, in the formation of hydroaromatic compounds. The differences in concentration of the series with the first member having an empirical formula $C_{10}H_{16}$ (octahydronaphthalenes), which is free of interference from alkyl derivatives of indene, indan, and benzene, is further evidence that hydroaromatic compounds were formed during the reduction of the vitrain. The reduced vitrain contains 2.8 percent octahydronaphthalenes compared to 0.9 percent for the untreated vitrain. From these data it appears that the conclusions of Reggel and coworkers that reduction of vitrain causes the formation of hydroaromatic compounds which are more soluble is substantiated.

SUMMARY

High-resolution mass spectrometric analyses of pyridine extracts obtained from reduced and untreated vitrain have shown:

1. A greater concentration of oxygen-containing compounds in the reduced vitrain compared to the untreated vitrain.

2. An approximate 8-fold decrease in organic sulfur compounds in the vitrain following reduction, which is consistent with the decrease in S as shown by ultimate analyses.

3. A lower concentration of higher molecular weight hydrocarbons such as 3-ring aromatics in the reduced vitrain.

4. A significant increase in the amount of hydroaromatic compounds in the reduced vitrain.

REFERENCES

1. Reggel, L., Raymond, R., Steiner, W. A., Friedel, R. A., and Wender, I. Fuel, Lond., 1961, 40, 339.

2. Reggel, L., Wender, I., and Raymond, R., Fuel, Lond, 1964, 43, 75.

3. Dryden, I. G. C. in Chemistry of Coal Utilization, Suppl. vol., p. 237, H. H. Lowry, Ed., Wiley: New York, 1963.

4. Biemann, K., Bommer, P., and Desiderio, D. G., Tetrahedron Letters, 1964, 1725.

5. Biemann, K., and Fennessey, P. U., Chimia, 1967, 21, 226.

6. Sharkey, A. G., Jr., Shultz, J. L., and Kessler, T. Proc. 15th Ann. Conf. on Mass Spectrometry and Allied Topics, May 1967, pp. 443-446. ASTM E-14, Denver, Col.

7. Sharkey, A. G., Jr., Shultz, J. L., Kessler, T., and Friedel, R. A. Preprints of papers, Div. of Fuel Chem., 154th Nat'l Meeting, Sept. 1967, pp. 232-239, Amer. Chem. Soc., Chicago, Ill.

8. Curran, G. P., Struck, R. T., and Gorin, E. Preprints of papers, Div. of Fuel Chem., 151st Nat'l Meeting, March 1966, pp. C-130-C-148. Amer. Chem. Soc., Pittsburgh, Pa.

9. Quiesenberry, K. S., Scolman, T. T., and Nier, A. O., Phys. Rev., 1956, 102, 1071.

10. Lumpkin, H. F., Anal. Chem., 1958, 30, 321.

118. HIGH-RESOLUTION MASS SPECTROMETRIC INVESTIGATION OF HETEROATOM SPECIES IN COAL-CARBONIZATION PRODUCTS

J. L. Shultz, T. Kessler, R. A. Friedel, and A. G. Sharkey, Jr.

U.S. Department of the Interior, Bureau of Mines
Pittsburgh Coal Research Center, Pittsburgh, Pa. 15213

INTRODUCTION

High-resolution mass spectrometry is being used to study (1) the effect of different coal-carbonization processes on the chemical composition of the coal-tar product, and (2) the changes in the composition of tar fractions, distillates, and residues in various atmospheres. The present objective of this investigation at the Pittsburgh Coal Research Center of the Federal Bureau of Mines is to determine which specific organic structures impart the most desirable properties to commercially important fractions of coal tars, such as road tar and electrode binder pitch.

A literature review of coal-tar pitch chemistry was published by Greenhow and Sugowdz in 1961.[1] Subsequently, Wood reported high-temperature gas-liquid chromatographic analyses of solvent extracts and vacuum distillates[2] and Shultz, Friedel, and Sharkey obtained semi-quantitative data for structural types in an 80°-85° C coal-tar pitch using low-resolution, low-ionizing voltage mass spectrometric techniques.[3]

The current status of high-resolution mass spectrometry in the structural analysis of organic compounds has been reviewed by Biemann and Fennessey.[4] Some applications of the technique to the analysis of complex mixtures of petroleum origin include a study of waxes by Reid,[5] a low-ionizing voltage characterization of aromatic materials by Johnson and Aczel,[6] and a group-type analysis described by Gallegos, et al.[7]

High-resolution mass spectrometry offers a new approach to the study of species present in coal-carbonization products.[8] It is particularly useful in providing information concerning heteroatom species, as these are present in lower concentrations than polynuclear aromatic hydrocarbons. While mass spectral determination of elemental composition does not distinguish specific structural types (many isomeric variants or positional isomers are possible), differences in composition and/or concentration of organic species present in coal-carbonization products can be detected. Correlation of these differences with physical parameters should lead to improved processes and increase the potential market for coal-tar products.

EXPERIMENTAL PROCEDURE

All data were obtained with a Consolidated Electrodynamics Corporation model 21-110B high-resolution mass spectrometer. Mass spectra were obtained at a resolution of 1 part in 15,000. Precise mass measurements were made using the Nier peak matching system. Only empirical formulas whose molecular weights deviated less than $\pm$ .003 amu from the measured values were considered.

The 80°-85° C softening point coal-tar pitch represented approximately 70 percent of the crude pitch after the low-boiling oils were removed. The xylene-insoluble fraction of the coal-tar pitch, a concentrate of the heteroatom species, was obtained using a solvent separation technique which separates components by chemical type rather than molecular weight.[9] All other samples investigated were obtained through the cooperation of the British Coal Tar Research Association. Data for the original and weathered road-tar fractions and coke-oven pitches are based on percent of total ionization calculated from the high-resolution mass spectra.

RESULTS

A. Coal-Tar Pitch. A total of 239 molecular formulas corresponding to 108 structural types and their alkyl derivatives were detected in this study. Previous workers have identified less than 100 components in coal-tar pitch--many of these are isomers.[1]

Sixteen different elemental combinations of C, H, O, N, and S were detected in the coal-tar pitch and its xylene-insoluble fraction. Eight of these combinations, CH, CHO, CHO_2, CHN, CHN_2, CHS, CHON, and CHO_2N_2, representing 76 structural types, have either been identified by previous workers or are closely related to previously identified components of coal tar. Only the number of heteroatoms is specified for the elemental combinations as the carbon-hydrogen content varies with the degree of condensation of the aromatic rings. Including alkyl derivatives, 198 molecular formulas were derived from these data. The number of structural types is a minimum since isomeric variants cannot be determined.

Eight additional elemental combinations containing O_3, O_4, N_3, OS, O_2N, N_2S, O_2S, and O_6 in the heteroatom groups, were detected. These empirical formulas, indicating at least 32 structural types (41 molecular formulas), are chemically possible but may also result from rearrangement ions produced by fragmentation of more complex heterocyclic hydrocarbons. In either case, these structures indicate the presence of material previously unidentified in pitch.

Analogous structures detected in the coal-tar pitch can be illustrated using fluorene (5,6,6) as a base structure.[10] Formulas determined from precise mass measurements indicate similar structures in which carbon-hydrogen(s) are replaced by N, O, N_2, S, O_2, NO, and OS. Known compounds corresponding to these elemental combinations suggest the presence of carbazole, dibenzofuran, dibenzothiophene, and other 5,6,6 aromatic or heterocyclic nuclei. In most cases these structures also form homologous series. Thus, empirical formulas corresponding to benzcarbazoles, dibenzcarbazoles, etc., are indicated by the precise masses measured at 217, 267, etc., through mass 320. At masses greater than 320 the peaks in the mass spectrum are too small to obtain precise mass measurements. These data represent approximately 70 percent of the pitch; the remaining 30 percent of the sample was not vaporized at 300° C.

B. Weathered Road Tars. Use of the high-resolution mass spectrometric technique to study the compositional changes occurring in samples exposed to various atmospheres is illustrated by an investigation of a vertical-retort road tar. The mass spectra of the unprecipitated fractions from the original tar and the tar after 12 and 24 months of weathering under road conditions were obtained. Percent of total ionization represented by the various combinations of atoms was used as the basis for comparison. At molecular weights less than 200, decreases in ionization attributable to the polynuclear aromatics, the oxygenated components, and the total sample are similar. The increase in percent of total ionization of the oxygen-containing material between masses 200 and 320, relative to the original road tar, is more than double that of the polynuclear aromatic ring systems after 12 months exposure and 50 percent higher after 24 months exposure. Increases in both the average molecular weight and average number of rings per structural unit occur during weathering for all structural types observed. Approximately 95 percent by weight of these road-tar fractions was vaporized in the mass spectrometer.

C. Coke-Oven Pitches. High-resolution mass spectra were obtained to study the compositional differences between 2 coke-oven pitches, one described as having "average stability" and a second described as having "low reactivity" on exposure to air.

Preliminary data for polynuclear aromatic hydrocarbons indicate that the low-reactivity pitch contains a higher percentage of 5- and 6-ring structural types (and less 2- and 3-ring structures) than the average stability pitch. With high-resolution, accurate peak intensities can be obtained for the polynuclear aromatic hydrocarbons and their alkyl derivatives. From these data, the ratio of the peri-condensed ring systems (e.g., pyrene) to the cata-condensed ring systems (e.g., chrysene) was determined for the coke-oven pitches. This ratio is 1.8 for the low-reactivity pitch and 1.2 for the average-stability pitch, indicating that the degree of condensation of the polynuclear aromatic ring systems in a tar may be a significant parameter in determining its stability.

CONCLUSIONS

This investigation of the high-resolution mass spectra of coal-tar pitch and a concentrate containing the heteroatom species has resulted in the detection of approximately twice the number of structural types previously reported in the literature. Application of the high-resolution mass spectrometric technique in detecting changes in the concentration or composition of organic structures in complex mixtures has also been demonstrated by the studies of weathered road tars and coke-oven pitches. The concentration of organic structures containing oxygen increases more rapidly than other classes or organic compounds in tars weathered on road surfaces. Data obtained for polynuclear aromatic ring systems in two coke-oven pitches indicate that the degree of condensation as well as the average molecular weight and average number of rings per structural unit could be a factor in determining reactivity of pitches. The ratio of peri-condensed to cata-condensed aromatic hydrocarbons was 50 percent higher for the low-reactivity pitch than for the average-stability pitch investigated.

These studies of the high-resolution mass spectra of complex mixtures indicate the power of this technique to detect species containing heteroatoms in highly aromatic matrices and to provide data relating compositional changes to chemical or physical properties.

REFERENCES

1. Greenhow, E. J., and G. Sugowdz. Coal Research in C.S.I.R.O., No. 15, 10 (1961).

2. Wood, L. J. J. Appl. Chem., Lond. 11, 130 (1961).

3. Shultz, J. L., R. A. Friedel, and A. G. Sharkey, Jr. Fuel 44, 55 (1965).

4. Biemann, K., and P. V. Fennessey. Chimia 21, 226 (1967).

5. Reid, W. K. Anal. Chem. 38, 445 (1966).

6. Johnson, B. H., and T. Aczel. Anal. Chem. 39, 682 (1967).

7. Gallegos, E. J., J. W. Green, L. P. Lindeman, R. L. LeTourneau, and R. M. Teeter. Anal. Chem. 39, 1833 (1967).

8. Sharkey, A. G., Jr., J. L. Shultz, T. Kessler, and R. A. Friedel. Proc. 15th Ann. Conf. on Mass Spectrometry and Allied Topics, May 14-19, 1967, Denver, Col., ASTM Committee E-14, pp. 443-446.

9. Smith, J. W. Fuel 45, 233 (1966).

10. Patterson, A. M., L. T. Capell, and D. F. Walker. The Ring Index. Am. Chem. Soc., Washington, D. C., 2nd ed. (1960).

120. ELECTRON IMPACT FRAGMENTATION OF PORPHINE

by

Earl W. Baker

Mellon Institute
Carnegie-Mellon University
4400 Fifth Avenue
Pittsburgh, Pennsylvania, 15213

Since the widespread availability of the direct insertion probe, there have been a number of studies of the mass spectra of substituted porphyrins.[1] As is expected, the 70 ev spectrum is dominated by the parent molecular ion. There is also, as expected of such a hyperaromatic system, doubly charged spectrum with 15 to 30% of the intensity of the singly charged spectrum and a noticeable triply charged spectrum. The region of the spectrum on which most of the discussion to date has dwelled is the singly charged portion corresponding to side chain fragmentation. Such fragmentation is concentrated in the bond β to porphyrin ring and depending on the particular side chain(s) has an intensity 10 to 50% that of the parent ion.

Subordinate to these larger peaks are seen a series of envelopes of peaks extending on down to the doubly charged spectrum. Some of these peaks result from the simultaneous loss of two or more side chains, but some were not accountable this way, and suggested that there was some disintegration of the porphyrin nucleus. It was this suggestion that led to the study on the parent compound, porphine.[2]

In the spectrum of porphine between the singly charged molecular ion at m/e = 310 (P^+) and the doubly charged molecular ion at m/e = 155 (P^{++}), there are 11 envelopes and a 12th buried under the group of peaks around the P^{++}. Additional groups, though less distinct, occur at lower m/e values. This sort of spectrum is reminiscent of the straight chain alkanes. In this case, since the molecule is a $C_{20}N_4$, the observation of 12 or more envelopes of roughly equal intensity implies that all possible losses of C-N structural units occur.

Table I indicates the elemental losses required to account for the largest peak in each of the envelopes. To determine which of these possibilities was actually involved, the exact mass of a number of these

TABLE I

COMPOSITION OF FRAGMENTS

Envelope m/e Maximum	Δ	Cumulative Loss	Loss		
310					
293	17	17	CH_5	NH_3	
282	11	28	C_2H_4	CNH_2	N_2(?)
267	15	43	C_3H_7	C_2NH_5	$C_1N_2H_3$
255	12	55	C_4H_7	C_3NH_5	C_3NH_5
242	13	68	C_5H_8	C_4NH_6	$C_2N_2H_3$
231	11	79	C_6H_7	C_5NH_5	$C_4N_2H_3$
217	14	93	C_7H_9	C_6NH_7	$C_5N_2H_5$
205	12	105	C_8H_9	C_7NH_7	etc.
192	13	118	C_9H_{10}	etc.	
179	13	131	$C_{10}H_{11}$		
167	12	143	$C_{11}H_{12}$		
	Average = 13				

was measured. The results are shown in Table II. The low intensities and the complexity of the spectrum make such measurements difficult and could, of course, lead to errors large enough to prevent interpretation. However, on such known peaks such as the P^+ and $P + 1^+$, agreement between calculated and observed peak masses on the MS-9 were within a few tenths

TABLE II

HIGH RESOLUTION MEASUREMENTS ON SELECTED PEAKS AND HYDROGEN ENRICHMENT OF THE LOWER M.W. FRAGMENTS

Peak Nominal Mass	Obs.[a] m/e	Calc.[a] m/e	Loss	H/C+N of Fragment	Possible Formulation
		$C_{20}N_4H_{14}$			
310	.1221	.1218		0.58	
		$C_{20}N_3H_{11}$			
293	.0951	.0953	NH_3	3.0	NH_3
		$C_{19}N_3H_{12}$			
282	.1024	.1031	CH_2N	1.0	CH=NH
267	.0789	.0796	C_2H_5N	1.6	CH_3CH=NH
	.0926	.0922	CH_3N_2	1.0	?
255	.0797	.0795	C_3H_5N	1.25	CH_2=CH-CH=NH
	.0924	.0921	$C_2H_3N_2$	1.0	?
242	.0713	.0718	C_4H_6N	1.2	?
	.0842	.0844	$C_3H_4N_2$	0.8	
231	.0789	.0796	C_5H_5N	0.83	?
	.0920	.0922	$C_4H_3N_2$	0.60	
217	.0765	.0766	C_6H_7N		
	.0655	.0653	$C_5H_5N_2$		

[a]Plus nominal mass.

of a millimass unit. This precision and accuracy led us to proceed to the fragment peaks with some confidence that meaningful results could be obtained. The 293 peak must result from the loss of a nitrogen and three hydrogens (of course, not necessarily as ammonia) as the 282 peak must be the result of the loss of H_2CN. In fact, every fragment peak in the spectrum seems to be the result of the loss of at least one nitrogen. In addition to the main peak in each envelope, at least one subsidiary peak on either side was also measured, and it was confirmed that these also resulted from the loss of one or more nitrogens. For example, the 267 peak was found to be a doublet with one branch being a one nitrogen loss and the second branch a two nitrogen loss.

As shown in Table II, there appears to be a large amount of hydrogen transfer to the small departing fragments. Note for example, the 267 peak (Table II) where the loss corresponds to C_2H_5N. Since no carbon atom in the parent compound ($C_{20}H_{14}N_4$) is attached to more than one proton and 8 carbons have no protons, this fragment appears to have "collected" protons from other sites in the molecule. As the size of the fragment increases its H to C+N (Col. 5, Table II) ratio tends to approach that of the parent substance. This suggests that in the excited state, the protons are very "fluid".

It has been previously pointed out that all possible losses of C-N structural units are lost with approximately equal probability. Since porphine is a very symmetric molecule, this result is not completely unexpected. The next step in the investigation was to introduce some asymmetry and observe the effects. For this purpose, we chose dihydroporphin (trivially named chlorin). Actually, the spectrum of chlorin showed a remarkable resemblance to porphine with the envelopes near the P^+ two mass units higher. These results are summarized in Table III. We had expected that these extra protons would be supplied to the fragments or at least

TABLE III

COMPARISON OF LOSSES FROM PORPHINE AND CHLORIN

Porphine		Chlorin	
Envelope Maximum	Cumulative Loss	Envelope Maximum	Cumulative Loss
293	17	295	17
282	28	283	29
267	43	270	42
255	55	256	56
242	68	244	68
231	79	231	81
217	93	219	93

lost very easily upon electron impact. This expectation was not confirmed and only far down in the spectrum near the P^{++} is there evidence of the extra protons being incorporated into the fragments or lost concurrently with them.

Our next attempt to produce some asymmetry and thus a selectivity of fragment loss was to prepare metalloderivatives. Comparing the Mn and Ni derivatives with porphine shows quite clearly that the loss of NH_3 has been retarded. In fact, it appears that the intensities of all of the early odd numbered envelopes have been reduced. The largest fragment peak in the Mn porphine spectrum and the only peak for which a metastable has been observed corresponds to the loss of H_2CN.

In an attempt to learn more about the origin of the hydrogens in the small hydrogen rich fragments, N,N dideuteroporphine was prepared by exchange. The ammonia loss peak centers at 294 which formulates as NH_2D. Tentatively, we interpret this to mean that the favored mechanism of ammonia loss includes only one of the imino protons.

It is concluded that the fragmentation is initiated at a C-N bond followed by the breaking of bonds to the β carbons of the pyrrole rings. At this point, in free base porphine essentially an open chain molecule has resulted and subsequent nearly non-selective bond breakage results in losses corresponding to C_1 through C_{12} units. Substitution patterns may produce limited selectivity but the method does not look especially promising as an isomer identification method.

ACKNOWLEDGEMENTS

The author thanks Mr. J. R. Boal for recording the mass spectra. This investigation was supported by Public Health Service research grant FR 55801-5 from the General Research Support Branch.

[1] See A. H. Jackson, G. W. Kenner, K. M. Smith, R. T. Aplin, H. Budzikiewicz and C. Djerrassi, Tetrahedron, 21, 2913 (1965) and references therein.

[2] For structure and synthesis, see J. E. Falk, "Porphyrins and Metalloporphyrins", Elsevier Publishing Company, New York, 1964, p. 4.

121. Computer Techniques for the Quantitative High Resolution Mass Spectral Analysis of Complex Hydrocarbon Mixtures

by

Thomas Aczel, D. E. Allan*, J. H. Harding & E. A. Knipp
Esso Research and Engineering Company
Baytown, Texas

This paper deals with the computer techniques developed in these laboratories for the quantitative analysis of complex aromatic and polar mixtures related to or derived from petroleum. The analytical method to be handled by the computer system was the high resolution-low voltage technique, also developed in these laboratories and described in the literature.(1)(2) This method has several advantages. The use of a resolving power of about 1 part in 10,000 permits one to separate the most important multiplets occurring in the spectra of materials related to petroleum. The use of low ionizing voltages, resulting in essentially parent peak spectra, eliminates interferences among the various components and thus makes the method applicable to any sample regardless of origin, treatment, and boiling range (up to 1100°F).

Automatic data acquisition and reduction from high resolution-low voltage spectra must satisfy several requirements peculiar to this mode of operation. All the 500 to 1000 parent peaks in the average sample must be identified, including peaks as large as 250,000 ppm and as small as 50 ppm or two times the three millivolts noise level. New reference compounds must be used for mass measurement, as conventional standards do not yield peaks at low voltages. The data output must be in a format which can easily be converted to quantitative analysis.

The physical system used for the data acquisition is an IBM 1802 computer interfaced to the mass spectrometer, an Associated Electrical Industries Model MS9 instrument. The 1802 system converts the analog voltage signals to digital data, yields precise time values, and writes the data on a digital tape. All subsequent calculations, including the identification of peaks, measurement of peak areas and of occurrence times, recognition of reference standards, mass measurement, formula assignment, and quantitative computations are carried out by an IBM 360/50 computer system.

The programs used for the determination of peak areas and occurrence times are similar to those described in the literature(3) for magnetic scanning instruments.

The reference standards used consist of a blend of halogenated aromatic compounds, mostly benzenes, naphthalenes, and diphenyls, covering a mass range from m/e 96 to m/e 458. These reference peaks can easily be recognized by the computer, with a logic based on historical occurrence times and the known ratios among the isotopic peaks given by the halogenated compounds. To facilitate the recognition process, the scan is started at a fixed position in the spectrum, determined by focusing the peak at m/e 614 in perfluorotertiarybutylamine on the scope of the instrument. If so desired, the standard peaks can also be recognized by human intervention.

Precise mass measurement is achieved by relating the occurrence times of known standard peaks to those of the sample peaks. This can be done using equation (1)

$$(1)\quad \ln M_x = \ln M_{ref} + \frac{t_x - t_{ref}}{\tau}$$

where M_x, M_{ref}, t_x, t_{ref} are the masses and the occurrence times of the sample and reference peak, and τ is the time constant calculated in the mass interval between the two bracketing reference peaks. As τ is not constant, but changes with mass, (1) does not give the most accurate mass measurement. Therefore, two new approaches have been explored in this work. One is the use of Lagrangian interpolation; the other is the linear extrapolation of τ in (1) to the mass interval between the sample peak being measured and the closest reference peak. The new approaches resulted in decreasing the average error of 2.09 mmu, observed using equation (1), to 1.54 and 1.26 mmu, respectively. The error calculations were made on 670 individual mass measurements. The Lagrange interpolation selected to be used results in about 80 percent of the peaks being correctly identified in low voltage spectra. This degree of accuracy is considered quite good, as this statistic includes both very small and very large peaks, with a dynamic ratio of about 1 to 5000 and the height of the average peak in the very complex mixtures analyzed is only about 100 mv (30 times the noise level). Analysis of complex mixtures at low voltages requires, however, that all peaks be correctly identified, as each and every peak corresponds to a different component.

---

* Present address: Louisiana State University, Baton Rouge, Louisiana.

A technique was therefore developed which resulted in the increase of correctly identified peaks to 92-98 percent. This technique can be summarized as follows. Mass measurements are carried out with the Lagrange interpolation for all peaks, but formulas are calculated with conventional algorithms only for peaks in the immediate neighborhood of the halogenated standards, where the mass measurement error is minimum. The remaining formulas are calculated using each identified sample peak as reference standard for the adjacent sample peaks within two integer mass units, equating the measured mass intervals with differential formulas. In this way, the distance between sample peak and reference standard peak is effectively reduced to a maximum of two integer mass units with a consequent drastic reduction of systematic errors. This interpolation method is applicable, however, only to petroleum type samples.

In addition to the elemental formula, the program also assigns each peak to the appropriate homologous series and yields a final list in which the components are tabulated according to homologous series and in order of increasing molecular weight. This information is also punched on cards and is used as input for the quantitative analysis.

At the present, quantitative data are obtained routinely for up to 58 aromatic compound types and 2900 components per sample, including S and O compounds. The average sample consists of 40 to 50 compound types and 500 components. The parameters determined include weight percent of each component and the weight percent, average molecular weight, average number of carbon atoms, average number of carbon atoms in side chains of each compound type. Weight percent of atomic S and O are also calculated.

The use of the computerized data acquisition and reduction system allows us to obtain this detailed information in about three hours per sample, including instrument time.

Another advantage of the computer system is that it permits one to interpret the spectra of very complex mixtures. This capability is best illustrated by the identification of the components in the low intensity heptuplet shown below.

Intensity, % ΣI	Mass	Error, mmu	Formula
0.0306	150.142	1.3	$C_{11}H_{18}$
0.0830	150.127	-3.2	$C_9{}^{13}CH_{15}N$
0.8373	150.103	-1.1	$C_{10}H_{14}O$
0.0736	150.068	0.1	$C_9H_{10}O_2$
0.1916	150.049	-1.8	$C_9H_{10}S$
0.1667	150.013	-0.5	C_8H_6SO
0.0563	149.963	-	Reference

In the spectrum containing this particular heptuplet 300 components, belonging to 75 C, H, O, S, N compound types were identified in a matter of hours.

A paper on the subject matter discussed here will be submitted to Analytical Chemistry in the near future.

---

1. B. H. Johnson and Thomas Aczel, Anal. Chem. 39, 682 (1967).
2. Thomas Aczel and B. H. Johnson, paper presented at the 153rd National Meeting of the American Chemical Society, Miami Beach, Florida, April 9-13, 1967.
3. W. J. McMurray, B. N. Greene, and S. R. Lipsky, Anal. Chem. 38, 1194 (1966).

122. HIGH RESOLUTION MASS SPECTROMETRIC STUDIES OF THE ACIDS OF THE COLORADO GREEN RIVER SHALE

Pat Haug, H. K. Schnoes and A. L. Burlingame
Department of Chemistry
University of California
Berkeley, California

Among the organic constituents of shales, hydrocarbons have received the most prominent attention and a considerable number of biologically interesting compounds such as isoprenoid hydrocarbons (i.e. pristane and phytane), iso and anteiso alkanes, steranes and triterpanes have been isolated and either completely or partially identified. A number of sediments ranging in age from the very recent to the ancient, among which the Soudan and Fig Tree are the oldest, have been investigated; the work of Calvin, Eglinton, Oro, and others is representative of these efforts. The heteroatomic compounds such as the acidic and basic constituents have received less study by comparison, but there is now a reasonable amount of information on the simple acid constituents in shales available. We wish to present a summary report on our data covering the acids of the Green River Formation, an eocene sediment which is extremely rich in organic material.

At the time that our comprehensive study of the acids of the Colorado Green River Shale was begun, Abelson and Parker had reported n C_{12} and n C_{13} acids (1), Lawlor and Robinson n C_{10}-C_{34} acids (2), Leo and Parker n C_{12}-C_{18} as well as iso and anteiso acids (not previously reported) (3), and Eglinton the C_{13}-C_{20} (with the exception of C_{18}) isoprenoid acids (which corresponds nicely with the hydrocarbons pristane and phytane)(4). The extract obtained by extracting the shale with benzene/methanol (4:1) was extracted with base, neutralized and subsequently esterified. A preliminary high resolution mass spectrum of the methyl esterified (hexane soluable) acid extract revealed the distribution of compound types in addition to the expected McLafferty rearrangement ion m/e 74 and m/e 88 for α methyl branched esters and the expected cleavage fragments at m/e 87, 101 and 115; For example, one finds a series of cyclic esters dominated by the $C_{11}H_{20}O_2$ (m/e 184) ion and the cyclic fragment at m/e 169. Also evident are a series of aromatic esters: 150,164, 178, 192, 206, 220 and two napthyl carboxylic esters of composition $C_{13}H_{12}O_2$ and $C_{14}H_{14}O_2$. Consequently individual esters were separated on a 5% SE-30 gas chromatography column followed by a more polar cyclohexanediol succinate (3% HIEPF 8 BP) column. High and low resolution spectra were obtained on the numerous fractions so isolated. The C_7-C_{11} normal methyl esters were isolated and characterized by the rearrangement ion at m/e 74, the loss of 31 methoxy mass units, 29 mass units composing the α and β carbons, and 43 mass units from the α, β and γ carbons, along with the absence of further branching.

The methyl ester of the C_{10} isoprenoidal acid, 3,7 dimethyloctanoate, was readily identified by comparison with a standard. The presence of the methyl ester of the C_9 isoprenoidal acid, methyl 2,6 dimethylheptanoate, is based on the rearrangement peak at m/e 88, the expulsion of the α and β carbons at M-43 and the α, β, and γ carbons at M-57, as well as the strong loss of 43 and 15 mass units from the end isopropyl group. The suggestion of methyl 2-methyl octanoate for Ester 10 Fraction 1 is on the basis of its rearrangement peak at m/e 88, apparent lack of further branching, and glc retention time.

The esters of two C_8 cyclic acids, four C_9, three C_{10}, four C_{11} and two C_{12} were found. It should be noted that the most abundant of the cyclic esters was indeed of mass 184 indicated by their empirical formulas as was also seen in the high resolution spectrum of the total mixture. Although one can speculate on structures, none can be conclusively identified. It should be noted that stereochemical and substituent variation exert dramatic effects on the mass spectra and therefore synthetic standards are necessary for structural detail. Assignment is based on empirical composition. There is some tentative evidence for the unsaturated esters but distinction is not definative. It might be pointed out that Cason has recently identified several cyclopentyl acids from petroleum such as trans 2,2,6-trimethylcyclohexylacetic (5) and 3-ethyl 4-methylcyclopentylacetic acids (6).

A very interesting series found were the aromatics ranging from simple methyl benzoates to the higher phenylalkyl acids up to molecular weight 234. The mass spectra of m and p toluate were identified by the loss of 31 and 31 plus 28 and the absence of the loss of 15 and 32 mass units. Four ortho dimethylbenzoate fractions were characterized by their strong loss of 32 mass units. The trimethyl benzoates of molecular weight 178 were also found although substituent position assignment cannot be made in the absence of standards.

One phenylalkyl ester of molecular weight 192 was isolated, five of molecular weight 206, seven of molecular weight 220, and three of molecular weight 234. The presence of methyl monomethyl substituted and dimethyl substituted 4-phenylvalerate are possible by comparison with the mass spectrum of authentic methyl 4-phenylvalerate.

Ester 30 Fraction 1 is indicative of methyl 2-methyl 4-dimethylphenylbutyrate (I) on the basis of the intense peak at m/e 88 requiring α branching and by the intense peak at m/e 119 representing the dimethyl tropyllium ion. It should be noted that the composition of the latter peak has been verified by high resolution mass spectrometry to be indeed C_9H_{11}. A plausible diorthosubstituted precursor would be a hydrocarbon of the β carotene-type (II) where one methyl group could be lost in aromazation during diagenesis.

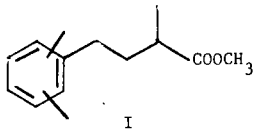

I

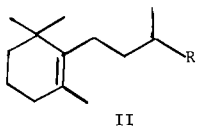

II

Two substituted napthyl carboxylic esters of molecular weight 200 were found. High resolution verifies the compositions (which have the same nominal mass as saturated fragments) as m/e 200 as $C_{13}H_{12}O_2$, 169 as $C_{12}H_9O$, and 141 as $C_{11}H_9$. The fragmentation patterns and high resolution establish the presence of other members of the series of molecular weight 214, 228 and 242 in small quantities. Aside from this, a series of cyclo aromatic acid methyl esters were determined from the high resolution mass spectra of molecular weight 204, 218 and 232 representing tetrahydro napthyl or indane. The finding of these aromatic components in a shale are of interest since aromatic acids have not previously been reported in sediments.

A series of C_{13}-C_{18} α, ω dicarboxylic acid esters was characterized by the ion of m/e 98 and loss of 31 and 73 mass units. High resolution mass spectrometric data verify that the composition of m/e 98 is $C_6H_{10}O$, 112 is $C_7H_{12}O$, 126 is $C_8H_{14}O$, 185 is $C_{11}H_{21}O_2$. The methyl esters of α methyl branched dicarboxylic acid esters (III) are indicated by the prominent loss of m/e 87 as well as 73 and intense peaks at both 74 and 88 as well as 98 and 112. It is conceivable that they might result from oxidation of iso acids. Also it should be noted that in one other report Eglinton has reported the presence of normal dicarboxylic acids in Scottish Torbanite (7).

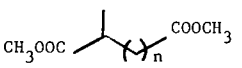

III n = 9, 11, 12

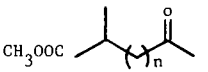

IV n = 8, 11

Two keto esters, methyl 10-oxyundecanoate and methyl 13-oxytetradecanoate, (IV) were identified by the sequence M-31, M-57 and M-57-32 together with the McLafferty rearrangement resulting in the intense peak at m/e 58. Again high resolution spectra verify the compositions.

In summary, we have found several interesting types of acids not previously reported by other investigators. We have not found iso or anteiso acids and Eglinton in his experiments also found no evidence for these. We did not detect any appreciable amounts of the higher normal and isoprenoidal acids and it is felt that this may be due to the extraction method utilized since subsequent experiments in our lab with demineralized shales have shown that these acids are indeed present. Currently experiments are being carried out to determine the composition of acids in the mineral matrix of kerogen (8).

REFERENCES

1. Abelson, P. H., and P. L. Parker, "Fatty Acids in Sedimentary Rocks," Carnegie Institute Wash. Year Book, 61, 181 (1962).

2. Lawlor, D. L., and W. E. Robinson, "Fatty Acids in Green River Formation Oil Shale," Div. Pet. Chem., Amer. Chem. Soc., Detroit, May 9, 1965.

3. Leo, R. F., and P. L. Parker, "Branched Chain Fatty Acids in Sediments," Science, 152, 649 (1966).

4. Eglinton, G., A. G. Douglas, J. R. Maxwell, J. N. Ramsay and S. Stallberg-Stenhagen, "Occurrence of Isoprenoid Fatty Acids in the Green River Shale," Science, 153, 1133 (1966).

5. Cason, J., and K. Liauw, "Characterization and Synthesis of a Monocyclic Eleven Carbon Acid Isolated from a California Petroleum," J. Org. Chem., 30, 1763 (1965).

6. Cason, J. and A. I. A. Khodair, "Separation from a California Petroleum and Characterization of Geometric Isomers of 3-Ethyl- 4-Methylcylopentylacetic Acid," J. Org. Chem., 31, (1966).

7. Douglas, A. G., K. Douraghi-Zadeh, G. Eglinton, J. R. Maxwell and J. N. Ramsay, "Fatty Acids in Sediments Including the Green River Shale (Eocene) and Scottish Torbanite (Carboniferous)", Advances in Organic Geochemistry, Pergamon Press, New York (1967).

8. Full paper will be published in Geochim. Cosmochim. Acta.

123. ELECTRON IMPACT STUDIES OF MANGANESE AND RHENIUM PENTACARBONYL HALIDES[1]

G. A. Junk, H. J. Svec and R. J. Angelici

Institute for Atomic Research and Department of Chemistry
Iowa State University, Ames, Iowa 50010

Abstract: The energetics of the ionization and dissociation of manganese and rhenium pentacarbonyl halides are reported. The ionization potentials are: $Re(CO)_5Cl$ = 9.18 eV; $Re(CO)_5Br$ = 9.07 eV; $Re(CO)_5I$ = 8.64 eV; $Mn(CO)_5Cl$ = 9.12 eV; $Mn(CO)_5Br$ = 8.97 eV; and $Mn(CO)_5I$ = 8.55 eV. These values are shown to be related to the ionization potentials of Re and Mn and to the relative electron donating abilities of the halogen ligands. Appearance potentials for fragment ions were measured and used to calculate average ionic bond dissociation energies. The Re-CO bond is shown to be much stronger than the Mn-CO bond. Within the halogen series for each metal atom, the energy requirements for rupture of a single metal-CO bond follows the trend; IM-CO > BrM-CO > ClM-CO. These results correlate well with the relative kinetic reactivities of $M(CO)_5X$ compounds in reactions where M-CO bond rupture is rate determining. Similarities and significant differences in the mass spectra are briefly discussed.

A recent report by Foffani et al.[2] relates the ligand donor ability to the measured ionization potentials of transition metal carbonyl nitrosyl complexes. The ionization potentials of $Co(CO)_3NO$ and $Fe(CO)_2(NO)_2$ are significantly lowered when PCl_3 or $P(OEt)_3$ is substituted for one of the CO groups in each complex.[3] The reduction in the ionization potential is attributed to the greater donor capacities of PCl_3 or $P(OEt)_3$ relative to CO. This donor ability through the sigma bond between the metal atom and the ligand is related to the ionization potential of the ligand itself.

In this report the conclusions of Foffani et al.[2] are shown to be valid for the two series, $Mn(CO)_5X$ and $Re(CO)_5X$, where X = Cl, Br or I. The effect of the central transition metal atom on the ionization potential is also considered. In the unsubstituted carbonyls, $M(CO)_x$ [M = Ni, Fe, Cr, Mo or W and x = 4, 5 or 6] investigations[3-8] have shown that the ionization potentials of these compounds are more closely related to the ionization potentials of the metal atoms than the carbon monoxide ligands. For example, the ionization potential of CO is 14.1 eV while the ionization potentials of all $M(CO)_x$ compounds are 8 to 9 eV compared to M atom ionization potentials of 7 to 8 eV. However, discrepancies exist when the trend of the ionization potentials of the metal carbonyls are compared with the trend of the ionization potentials of the metal atoms. In three early reports[4,5,8] the expected variation is observed for the series; $Cr(CO)_6$, $Mo(CO)_6$ and $W(CO)_6$.[8a] However, two recent reports[6,7] suggest that any trend in this series is within the experimental limits of reproducibility. Thus the exact influence of the metal atoms on the molecular ionization potentials is debatable. Additional results for other metal atom systems are desirable for clarification. These results are provided by the comparison of the known ionization potentials of Re and Mn atoms with the values reported here for the metal pentacarbonyl halide pairs, [$Re(CO)_5Cl$ and $Mn(CO)_5Cl$], [$Re(CO)_5Br$ and $Mn(CO)_5Br$] and [$Re(CO)_5I$ and $Mn(CO)_5I$].

This report then considers the influence of both the ligands and the metal atom on the ionization potentials. Additional considerations are the mass spectral features, the bond energy measurements from appearance potential data, and the correlation between electron impact measurements and kinetic reactivities.

Mass Spectrometer Sampling. Four different sampling procedures were employed.

1. Heated Inlet - An all glass MicroTek universal heated inlet system was used. However, some thermal decomposition was detectable with all samples. The thermal stabilities were in the order Re > Mn and I > Br > Cl.

2. Direct Insertion - The high vapor pressure of $M(CO)_5X$ compounds limited the successful application of this sampling technique. Sample consumption and ion source contamination were extensive. Fluctuations of the ion intensities appreciably affected the quality of the mass spectra and the appearance potential measurements.

3. Cold Probe - The probe used here was similar to that described by Haddon et al.[11] This technique is not yet convenient to employ and poor spectral reproducibility made it undesirable for accurate mass spectral and appearance potential measurements. However, the technique was employed to guarantee that thermal decomposition was not affecting the mass spectra[12] obtained by use of a modified direct insertion technique.

4. Modified Direct Insertion - A probe similar in design to that described by Shadoff and Westover[13] was used extensively for these studies. It was found advantageous to substitute Teflon for the metal ferrules normally used to provide the vacuum seal around the sample tube. Much less torque is required to seal the Teflon-metal surface and sample changeover is accomplished easily and rapidly. All the $M(CO)_5X$ samples had sufficient vapor pressure, at room temperature for obtaining the mass spectra. Under these temperature conditions, thermal decomposition is negligible provided the ion source is cool and the inside surfaces of the metal probe have not been contaminated by deposits from previously decomposed metal carbonyls.

Ionization and Appearance Potential Measurements. All the ionization and appearance potential measurements were obtained using Warren's[14] extrapolated difference technique for evaluation of the ionization efficiency curves. These curves were plotted using an automatic device[15] to reduce the time necessary for each measurement. With this device, a single complete curve (55 to 5 eV) is plotted in less than two minutes. Multiple partial curves within a few volts of onset may be accumulated in a matter of minutes. Reproducibility of measurements is of the order of ±0.03 eV for parent ions to±0.2 eV for some of the bare metal fragment ions.

Results and Discussion

Ionization Potentials. The measured ionization potentials are tabulated in Table I. It is evident that the trend in the ionization potentials of the halogen ligands is reflected in the ionization potentials of the $M(CO)_5X$ compounds. Thus, the influence of the electron donor ability of the ligand[2] has been established for two series of three compounds. In each case the difference in the ionization potentials of the halogens is considerably attenuated. For instance, the difference in the ionization potential of Cl and Br, ΔI.P. [Cl-Br], is 1.2 eV while the ΔI.P. $[Re(CO)_5Cl\text{-}Re(CO)_5Br]$ is only 0.11 eV. Similar comparisons can be made for the remainder of the data in the table and those of Foffani et al.[2] for $Fe(NO)_2(CO)P(OEt)_3$ and $Co(NO)(CO)_2(PCl_3)$. From these results one can predict that the exchange of a ligand in a metal carbonyl will cause a shift in the ionization potential by about 20% of the difference in the ionization potentials of the ligands exchanged.

Table I. Ionization Potentials in eV of $M(CO)_5X$ Compounds and the M and X Atoms

Sample	I.P.	I.P. of X[a]	I.P. of M[a]
$Re(CO)_5I$	8.64±0.03	10.4	7.87
$Re(CO)_5Br$	9.07±0.02	11.8	7.87
$Re(CO)_5Cl$	9.18±0.03	13.0	7.87
$Mn(CO)_5I$	8.55±0.02	10.4	7.43
$Mn(CO)_5Br$	8.97±0.03	11.8	7.43
$Mn(CO)_5Cl$	9.12±0.08	13.0	7.43

[a]Taken from ref. 19.

When the metal atoms are interchanged, a trend parallel to the ligand effect is observed. The difference in the ionization potentials of Re and Mn are reflected in the ionization potential of the $M(CO)_5X$ compounds. Three series of two compounds, $M(CO)_5Cl$, $M(CO)_5Br$ and $M(CO)_5I$, can be compared on the basis of the data reported in Table I.

The shift is again about 20% of the difference in the ionization potentials of exchanged metals. Thus, the ionization potential of a $M(CO)_5X$ compound is related to both the ionization potential of the metal atom and the halogen ligand. The ligand effect (donor ability across a sigma bond) supports the conclusions of Foffani et al.[2] about the ionization and probably bonding in metal carbonyls. The parallel metal atom effect adds further support to these conclusions and is supplementary evidence for ionization associated primarily with a transition metal electronic orbital.[2-7,20] It seems probable that these observations are generally applicable to metal carbonyl derivatives.

Appearance Potentials and Bond Energies. The appearance potentials (A.P.) of most of the $[M(CO)_yX]^+$ fragment ions were measured. These values are listed in Table II. Previous results for mono-metal carbonyls[6,7] have shown that the average ionic bond energies calculated from appearance potential data are equal to the average neutral energies within 0.3 eV. If this is also true for these halogen derivatives, conclusions based on the results for ionic bond energies may be extended to the neutral bond energies. The average bond energies are calculated from the ionization potentials given in Table I, the appearance potentials given in Table II and the equation,

$$\text{Ave. Ionic B.E.} = \frac{\text{A.P. of } [M(CO)_yX]^+ - \text{I.P. of } M(CO)_5X}{(5-y)} \approx \text{Ave. Neutral B.E.} \quad (1)$$

Table II. Appearance Potentials of $[M(CO)_yX]^+$ and Selected $[M(CO)_y]^+$ Fragment Ions in eV[a]

	$[M(CO)_4X]^+$	$[M(CO)_3X]^+$	$[M(CO)_2X]^+$	$[M(CO)_X]^+$	$[MX]^+$
$Re(CO)_5I$	10.29	12.04	14.65	19.69	19.20
$Mn(CO)_5I$	--	9.49	10.46	12.37[b]	14.0
$Re(CO)_5Br$	10.50	11.97	15.02	16.94	19.51
$Mn(CO)_5Br$	--	9.55	10.47	11.72	12.4
$Re(CO)_5Cl$	10.45	11.92	14.85	16.84	19.27
$Mn(CO)_5Cl$	--	--	10.6[b]	11.3[b]	13.8[b]

[a]All values except those noted were obtained using Warren's[14] procedure.

[b]Vanishing current procedure used (see Ref. 21).

Table III. Average Ionic Bond Energies for $[M(CO)_5X]^+$ Molecule Ions in eV.

	Substituents Lost							
Sample	1CO	2CO	3CO	4CO	5CO	2CO+X	4CO+X	5CO+X
$Re(CO)_5Cl$	1.3	1.4	1.9	1.9	2.0	--	--	2.3
$Mn(CO)_5Cl$	--[a]	--	0.5	0.6	1.0[b]	--	--	1.0
$Re(CO)_5Br$	1.4	1.5	2.0	2.0	2.1	2.2	--	>2.4
$Mn(CO)_5Br$	--[a]	0.3	0.5	0.7	0.7	1.3	1.2	1.3
$Re(CO)_5I$	1.6	1.7	1.9	2.1	2.1	2.1	--	>2.4
$Mn(CO)_5I$	--[a]	0.5	0.6	1.0	1.1	1.2	1.2	1.3

[a]The $[Mn(CO)_4X]^+$ fragment ion is absent in the mass spectrum.

[b]Questionable value due to experimental complications.

These values are tabulated in Table III. Inspection of these results leads to interesting conclusions about relative bond strengths in $M(CO)_5X$ compounds. First, the Re-CO bonds are much stronger than the Mn-CO bonds. Second, the first two M-CO bonds are weaker than the last three. Third, the energetics for loss of the first and second CO groups follow the trend, $M(CO)_5I > M(CO)_5Br > M(CO)_5Cl$. Fourth, no consistent halogen effect is observed for the average M-CO bond energy for rupture of three, four or five CO groups. Last, the the difference in the M-X vs. M-CO bond strength (compare columns four to seven) is greatest for the manganese derivatives. Unequivocal experimental evidence that the Re-X

bond is stronger than the Re-CO bond does not exist. When all the data are analyzed, the only reasonable conclusion is that Re-X ≈ Re-CO.

The first and third conclusions given above may be used to qualitatively predict the kinetic reactivities of $M(CO)_5X$ compounds when S_N1 mechanisms are involved. All other factors being equal, the trend in the rates of S_N1 mechanistic reactions should be inversely proportional to the M-CO bond energy. The rate predictions based on mass spectrometric bond energy measurements for $M(CO)_5X$ compounds are Cl > Br > I and Mn > Re. Kinetic results for formation of cis-$M(CO)_4(L)X$ compounds[22,23] by reaction of $M(CO)_5X$ with phosphines, phosphites and other ligands confirm these predictions. This correlation of mass spectrometric data with kinetic results is satisfying and may indicate that other more extensive relationships exist.

Mass Spectra. The mass spectra of all these $M(CO)_5X$ compounds, except $Re(CO)_5Br$, have been previously reported.[24,25] These earlier studies were done with an A.E.I. MS-9 mass spectrometer using the direct insertion sampling technique. We have converted the tabulations in these reports to bar graphs and include results in Figs. 1 and 2. Very satisfactory agreement exists for $Re(CO)_5Cl$, $Mn(CO)_5Br$ and $Mn(CO)_5Cl$. A probable decimal point error in the tabulation[25] for $[Mn(CO)_5Br]^+$ and $[Mn(CO)_3Br]^+$ explains the poor correspondence for these ion currents. Less gratifying agreement occurs for $Re(CO)_5I$ and $Mn(CO)_5I$, but this may be due to difficulties which are experienced in maintaining constant sample pressure of these volatile substances when direct insertion is employed.[25]

The 22 eV mass spectra of $M(CO)_5X$ compounds have also been measured in our laboratory and these results are shown in Fig. 3. The mass spectra of the three $Re(CO)_5X$ samples are very similar. The same is true, although to a somewhat lesser degree, for the $Mn(CO)_5X$ samples. Increased fragmentation of the manganese compounds is evident, and this may be caused by a combination of relative ionic stabilities and energy requirements for unimolecular decompositions. Another notable and unexpected difference between the Re and Mn compound spectra is the absence of $[Mn(CO)_4X]$ fragments, while the $[Re(CO)_4X]^+$ fragments are intense peaks.

References

1. Work was performed in the Ames Laboratory of the U. S. Atomic Energy Commission. Contribution No. 2265.
2. A. Foffani, S. Pignataro, G. Distifano and G. Innorta, J. Organomet. Chem., 7, 473 (1967).
3. R. E. Winters and R. W. Kiser, Inorg. Chem., 3, 699 (1965).
4. Ibid, 4, 157 (1965).
5. A Foffani and S. Pignatro, Z.Physik. Chem. Neue Folge, 45, 79 (1965).
6. G. A. Junk and H. J. Svec, Z. Naturforsch., 23b, 1, (1968).
7. D. R. Bidinosti and N. S. McIntyre, Can. J. Chem., 45, 641 (1967).
8. F. I. Vilesov and B. L, Kurbatov, Dokl. Akad. Nauk SSSR, 140, 1364 (1961)

8a. $Ni(CO)_4$ and $Fe(CO)_5$ do not follow the predicted trend. It seems necessary to restrict the exact influence of the effect to carbonyls within one group in the periodic table.

11. W. F. Haddon, Em. M. Chait and F. W. McLafferty, Anal. Chem., 88, 1968 (1966).
12. H. J. Svec and G. A. Junk, Unpublished results.
13. L. A. Shadoff and L. B. Westover, Anal. Chem., 39, 1948 (1967).
14. J. W. Warren, Nature, 165, 810 (1950).
15. G. A. Junk and H. J. Svec, Unpublished work.

19. R. W. Kiser, "Tables of Ionization Potentials", TID-6142, USAEC, Office of Technical Information, June (1960).
20. H. J. Svec and G. A. Junk, J. Am. Chem. Soc., 89, 2836, (1967).
21. F. H. Field and J. L. Franklin "Electron Impact Phenomena," Academic Press Inc., New York, N.Y., 1957, p. 30.
22. R. J. Zngelici and F. Basolo, J. Am. Chem. Soc., 84, 2495 (1962).
23. F. Zingales, M. Grasizni, F. Faraone and U. Belluco, Inorg. Chim. Acta, 1, 172 (1967).
24. J. Lewis, A. R. Manning, J. R. Miller and J. Wilson, JACS, A, 1663 (1966).
25. K. Edgar, B. F. G. Johnson, J. Lewis, I. G. Williams and J. M. Wilson, J. Chem. Soc., A, 379 (1967).

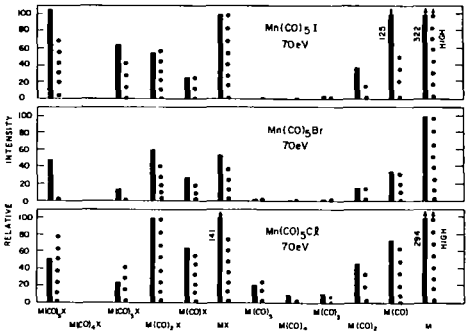

Figure 1. Comparative 70eV mass spectra of $Mn(CO)_5X$ samples. Solid bar—this report; Broken bar—from refs. 24 and 25.

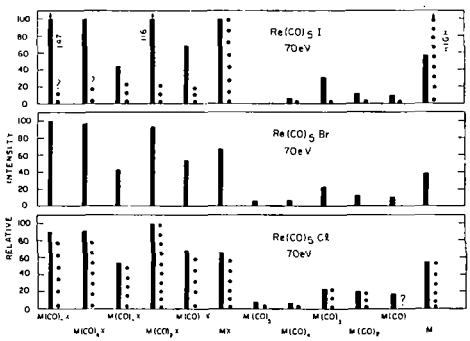

Figure 2. Comparative 70eV mass spectra of $Re(CO)_5X$ samples. Solid bar - this report; Broken bar - from ref. 25.

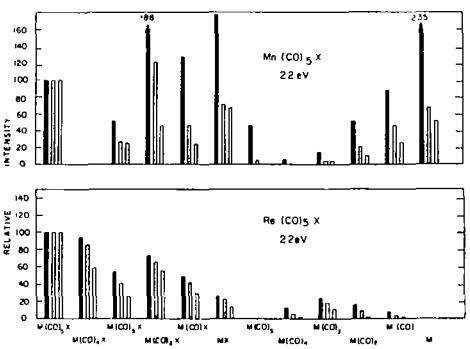

Figure 3. Parent ion normalized mass spectra (22eV) of $Mn(CO)_5X$ and $Re(CO)_5X$ samples. Solid bar - X=Cl; shaded bar - X=Br; open bar - X=I.

124. The Mass Spectrum of Trifluorosilyltetracarbonyl Cobalt

F. E. Saalfeld and M. V. McDowell
Naval Research Laboratory
Washington, D. C. 20390

and

A. P. Hagen and A. G. MacDiarmid
John Harrison Laboratory of Chemistry
and the
Laboratory for Research on the Structure of Matter
University of Pennsylvania
Philadelphia, Pa. 19104

The fragmentation patterns and appearance potential results for trifluorosilyltetracarbonyl cobalt have been discussed elsewhere.[1] The pertinent values derived from this study were: $\Delta H_f^\circ(SiF_3Co(CO)_4) = -490 \pm 10$ Kcal/mole and $DE(F_3Si\text{-}Co(CO)_4) = 105 \pm 12$ Kcal/mole. In addition, the fragmentation patterns of a series of cobalt carbonyl derivates, $RCoL_4$, where R = H, CH_3SeF_2 or SiF_3 and L = CO or PF_3 ligands, have been correlated in terms of the molecular structure of these compounds.

Edgell, et al.[2,3] have indicated that the structure of $HCo(CO)_4$ is a distorted trigonal bipyramid, with the equatorial ligands bent toward the axial hydrogen. They also presented evidence for an interaction between the axial hydrogen atom and the equatorial ligands. We believe that the fragmentation patterns shown in Table I, which we have observed for a series of compounds of structure $RCoL_4$, indicate that there is an interaction between the axial R substituent and the equatorial ligands. From a comparison of the ion intensities of the $RCoL_{x-1}^+$ and CoL_x^+ ions it is apparent that following the ionization of the molecule, the initial bond broken is a ligand-Co bond, not the R-Co bond. If the ligand lost in this step is in the axial position on the molecule, the equatorial ligands can assume a more planar configuration, thus weakening the R-L interaction. Accordingly in the next step, while loss of the ligand is still the favored mechanism, some breakage of the very weak H-Co bond[4] is observed. The next successive bond breakage, however, appears to strongly favor the loss of R instead of L, suggesting that the R-L interaction has been greatly weakened or terminated except for $CH_3SiF_2Co(CO)_4$ and perhaps $HCo(PF_3)_4$.

It has been shown[4] that the H-Co bond energy is the same in all of the hydrogen cobalt carbonyl phosphorus trifluoride compounds reported in Table 1. Thus, by comparing the ratio of the intensity of CoL_x^+ ion to that of the $HCoL_{x-1}^+$, a measure of the change in H-L interaction with ligand substitution can be visualized. This is shown in Table 2, where a smaller ratio is indicative of a greater interaction. The ratios become smaller with increasing PF_3 substitution, suggesting that the PF_3 ligand has a greater interaction with the axial hydrogen atom than does the carbon monoxide. Such an interaction should increase the stability of the compound, thus one would predict that these compounds would become more stable with increasing phosphorus trifluoride substitution. This prediction agrees with the chemistry of this series of compounds where replacement of the carbon monoxide by PF_3 ligands greatly increases the thermal stability of the compounds.

References

1. Accepted for publication in Inorganic Chemistry.
2. W. F. Edgell, C. Magee and G. Gallup, J. Am. Chem. Soc. 78, 4185 (1956).
3. W. F. Edgell and G. Gallup, J. Am. Chem. Soc. 78, 4188 (1956).
4. F. E. Saalfeld, M. V. McDowell, S. K. Gondal and A. G. MacDiarmid, J. Am. Chem. Soc., in press.

Table 1

Comparison of % Total Current of the CoL_x^+ to the $RCoL_{x-1}^+$ Ions[a]

	$SiF_3[Co(CO)_4]$	$CH_3SiF_2[Co(CO)_4]$	$H[Co(CO)_4]$	$H[Co(CO)_3(PF_3)]$	$H[Co(CO)_2(PF_3)_2]$	$H[Co(CO)(PF_3)_3]$	$H[Co(PF_3)_4]$
$RCoL_4^+$	2.8	1.4	4.5	2.0	3.1	1.7	2.8
CoL_4^+	0	0	0	0	0	0	0
$RCoL_3^+$	4.3	2.7	7.6	4.8	6.9	4.0	6.7
CoL_3^+	0	0	2.2	1.7	1.3	1.0	1.6
$RCoL_2^+$	3.5	1.2	3.7	4.7	5.9	5.6	9.4
CoL_2^+	12.1	4.0	15.6	14.2	14.8	9.4	7.8
$RCoL^+$	3.0	4.8	1.6	5.2	5.8	7.6	7.7
CoL^+	18.9	8.0	20.0	22.7	25.7	27.1	28.1
RCo^+	12.5	12.3	1.0	1.6	1.8	2.2	2.7
Co^+	23.3	11.4	19.5	21.7	21.9	22.6	24.3

[a]Spectra observed with a Bendix TOF mass spectrometer operated in the pulsed mode with ion lens on; electron energy 70 V, ionizing current 0.125 μa.

Table 2

Ratio of the $\frac{CoL_x^+}{HCoL_{x-1}^+}$ Ion Currents

	$HCo(CO)_4$	$HCo(CO)_3(PF_3)$	$HCo(CO)_2(PF_3)_2$	$HCo(CO)(PF_3)_3$	$HCo(PF_3)_4$
$\frac{CoL_4^+}{HCoL_3^+}$	0	0	0	0	0
$\frac{CoL_3^+}{HCoL_2^+}$	.59	.36	.22	.18	.17
$\frac{CoL_2^+}{HCoL^+}$	9.75	2.73	2.55	1.24	1.01
$\frac{CoL^+}{HCo^+}$	20.00	14.19	14.28	12.32	10.41

125. The Mass Spectra of Arsenic Trifluoride and Arsenic Pentafluoride

M. V. McDowell and F. E. Saalfeld
Naval Research Laboratory
Washington, D. C. 20390

Introduction

We have studied the mass spectra of the series $HCoL_4$ where L = CO or PF_3, and wish to extend this series to include the arsenic fluorides. Since the compounds, $HCoL_4$, are prone to decompose thermally in the ion source of a mass spectrometer with the formation of the ligand L, it is imperative that fragmentation patterns and appearance potentials of the ions produced from L alone be known if the spectrum of $HCoL_4$ is to be successfully interpreted. Therefore, we have undertaken the mass spectral study of the arsenic fluorides, AsF_3 and AsF_5.

Experimental

The AsF_3 and AsF_5 (Ozark-Mahoning Co.) were free of any detectable impurities and were used as supplied. Both fluorides were introduced into the mass spectrometer through a gaseous inlet system with regulation of the gas flow by a molecular leak. Passivation of the mass spectrometer was accomplished by introducing a relatively high pressure (approximately 0.2 torr) of the sample into the inlet system and allowing it to expand into the mass spectrometer for a few minutes. This procedure was repeated until stable mass spectra were obtained.

Mass Spectral Data

The data reported were obtained on a Bendix T-O-F mass spectrometer which has been modified[1] for appearance potential measurements. Seventy-volt fragmentation patterns of the compounds, obtained using a regulated ionizing current of 0.125 μa, are given in Table 1. The mass spectrometer was always operated in the pulsed mode with the ion lens on.

Ion intensities reported in Table 1 are the mean of ten independent measurements, averaged by a computer program which rejects any datum deviating from the average value by more than 3σ. As observed with most inorganic fluorides, the parent minus a fluorine atom ion is the most abundant ion in both spectra. Further, no parent positive ion current was detectable for AsF_5.

Several negative ions of low intensity were observed in the spectra of these compounds. In AsF_3 the F^- ion appears to be formed both by ion pair and dissociative capture processes. It was observed over a considerable electron energy range, disappeared, then reappeared, and finally vanished again in a very narrow range of electron energy as the electron energy was continuously decreased from 70 V. AsF_2^- ions were also observed, and appeared to be produced by an electron capture process. This conclusion must be considered tentative because the intensity of the AsF_2^- ion was only slightly greater than the noise level.

The negative ion spectra of AsF_5 consisted of F^-, produced both by ion pair and dissociative capture processes, and AsF_4^- and AsF_5^-, both produced by electron capture. Although the ion currents observed for these last ions are extremely small, it is interesting to note that the parent positive ion of AsF_5 is not detected at all.

Table 2 cites the appearance potentials for the principal positive ions formed from AsF_3 and AsF_5. The values of the appearance potentials were determined by the extrapolated difference method of Warren using both Ar and Xe as internal standards. The errors quoted in Table 2 are the standard deviation of the mean; the absolute accuracy has been estimated to be ± 0.2 V. Since the heats of formation of both AsF_3 and AsF_5 are known (-218.3[2] and -295.6,[3] respectively), the heats of formation for the positive ions of AsF_3 and AsF_5 could be calculated if the ionic processes were known or could be safely assumed. While it is tempting to assume such processes, the authors have chosen not to report in detail the ion source reactions here. It should be pointed out, however, that reasonable processes for the various ion source reactions can be postulated and the ionic heats of formation calculated. If this calculation is made, the heat of formation of the ions produced from AsF_3 are approximately 20 Kcal/mole more positive than the ions of the same elemental composition formed from AsF_5. This difference can be ascribed to structural differences in the AsF_3^+ ions where energy is required to produce a planar ion from the pyramidal molecule of AsF_3. The equatorial fluorines in AsF_5 are already planar; therefore, the conversion energy is not required. We have also noted the same trend for PF_3, POF_3 and PF_5, where the heats of formation of the ions from PF_3 and POF_3 which have

fluorine atoms arranged in a pyramidal structure, are greater than the same ions from PF_5 which has three planar fluorine atoms. It is also interesting to note that the ionization potential of AsF_3 is greater than the ionization of PF_3 (11.5 e.v.). Although a decrease in the ionization potential with increasing atomic weight in a chemical group is normally expected, the fourth row elements (in this case arsenic) are well known for their anomalous behavior.

References

1. R. S. Olfky and F. E. Saalfeld, Report of NRL Progress, June 1965, p. 56.
2. F. D. Rossini, D. D. Wagman, W. H. Evans, S. Levine, and I. Jaffe; "Selected Values of Chemical Thermodynamics," NBS Cir. 500, Washington, D. C., 1952.
3. P. A. G. O'Hare and W. N. Hubbard, J. Phys. Chem. 69, 4358 (1965).

Table 1
Fragmentation Patterns of AsF_3 and AsF_5

Ion	m/e	Percent of Total Ion Current AsF_3	AsF_5
AsF_5^+	170	--	0
AsF_4^+	151	--	63.5
AsF_3^+	132	25.0	9.8
AsF_2^+	113	55.4	6.7
AsF^+	94	4.6	5.6
As^+	75	3.9	4.8
AsF_3^{++}	66	0.3	3.2
AsF_2^{++}	56.5	0.9	0.6
AsF^{++}	47	4.0	2.1
As^{++}	37.5	1.0	--
F^+	19	4.8	3.7

Table 2
Appearance Potential Results

Ion	AsF_3 A.P. (e.v.)	AsF_5 A.P. (e.v.)
AsF_5^+	-	-
AsF_4^+	-	15.7 ± .01[a]
AsF_3^+	12.5 ± .02[a]	13.2 ± .02
AsF_2^+	14.9 ± .01	15.1 ± .01
AsF^+	20.8 ± .04	21.5 ± .04
As^+	26.0 ± .05	28.4 ± .03
F^+	31.1 ± .04	35.2 ± .02
AsF_3^{++}	34.8 ± .04	39.9 ± .04
AsF_2^{++}	36.9 ± .04	40.6 ± .06
AsF^{++}	37.0 ± .05	46.5 ± .07
As^{++}	45.7 ± .03	-

[a]Standard deviation of the mean for seven independent measurements.

126. Ionization Efficiency Curves and Dissociation Energies of Antimony and Arsenic Vapor Species*

James E. Hudson and Gerd M. Rosenblatt
Department of Chemistry
The Pennsylvania State University
University Park, Pennsylvania

ABSTRACT

Ionization-efficiency curves of the ions formed upon electron impact of arsenic vapor at 550°K (As_4^+, As_3^+, As_2^+, As^+) and antimony vapor at 650°K (Sb_4^+, Sb_3^+, Sb_2^+, Sb^+) have been obtained using a Nuclide 12-90G, single-focusing, 90° sector, magnetic-scanning mass spectrometer equipped with an 100kHz pulsed RPD source[1]. The samples were composed of tightly pressed, ground, metallic poly-crystals of 99.9999% quoted purity. They were vaporized one cm. from the ionizing electron beam in aluminum-foil Knudsen-effusion cells, conductively heated by the source block. Xenon and krypton were used to calibrate the electron-energy scale.

The ionization efficiencies, the differences in ion intensity at one retarding potential and a retarding potential 0.1 ev. lower, were plotted as a function of electron energy. The curves show changes in slope due to the onset of new ionization or fragmentation processes. A number of these changes in slope or "breaks" can be assigned to explicit fragmentation processes. For example, the first break above appearance in the As_2^+ curve is assigned to the process $As_4 \rightarrow As_2^+ + As_2 + e$ and the third break in the As_2^+ curve to $As_4 \rightarrow As_2^+ + 2\,As + e$. Comparing the energies at which these two processes occur yields the dissociation energy of As_2. An independent value of $D_o(As_2)$ may be obtained by taking the appearance potential of As^+, which corresponds to $As_2 \rightarrow As^+ + As + e$, and subtracting the spectroscopic ionization potential of As. The values obtained for $D_o(As_2)$ by these methods are, respectively, 3.93 ev. and 3.79 ev. In addition to internal agreement, the data agree well with the literature spectroscopic convergence limit, 3.93 ev.

In a similar manner the dissociation energies of most of the neutral and singly-ionized vapor species in the arsenic and antimony system can be obtained by comparing the energies of assigned breaks in the ionization efficiency curves. The dissociation energies, ionization potentials and appearance potentials obtained are summarized in Table I, along with available literature values. The data have been calculated under the assumption that the fragmentation processes occur with no excess kinetic energy. The data for antimony are preliminary and are quite uncertain.

The present method of obtaining dissociation energies in these and similar polyatomic systems is independent of the high-temperature mass-spectrometric vapor-pressure method normally employed. The data are not subject to errors which may arise in second and third-law evaluations of mass-spectrometric vapor-pressure data, such as fragmentation processes preventing accurate measurement of partial pressures, uncertainty in cross sections or cross-section ratios, uncertainty in temperature measurement, low vaporization coefficients leading to difficulty in establishing equilibrium conditions, or uncertainties in free-energy and enthalpy functions.

Table I. Summary of Results (ev.)

	This work	Literature	Reference
IP(As)	----	9.81	(8)
$IP(As_2)$	9.91±0.05	11.0±0.5	(4)
$AP(As_3^+)$	11.55±0.06	----	
$IP(As_4)$	9.04±0.06	9.9±0.2	(4)
$D_o(As_2)$	3.88±0.06	3.93	(6)
$D_o(As_2\text{-}As_2)$	3.11±0.05	3.03, 3.13	(3) (4)
$D_o(As_4^+ \rightarrow As_3^+ + As)$	2.53±0.1		
$D_o(As_3^+ \rightarrow As_2^+ + As)$	5.54±0.1		
$D_o(As_2^+ \rightarrow As^+ + As)$	3.80±0.1		
IP(Sb)	8.77±0.2	8.64	(7)
$IP(Sb_2)$	8.54±0.2	8.4±0.3	(2)
$AP(Sb_3^+)$	10.85±0.2	10.8±0.3	(2)
$IP(Sb_4)$	8.10±0.2	7.7±0.3	(2)
$D_o(Sb_2)$	2.98±0.2	3.07	(2)
$D_o(Sb_2 - Sb_2)$	2.83±0.2	2.69,2.76,2.94	(3) (4) (5)
$D_o(Sb_4^+ \rightarrow Sb_3^+ + Sb)$	2.75±0.2		
$D_o(Sb_3^+ \rightarrow Sb_2^+ + Sb)$	3.50±0.2		
$D_o(Sb_2^+ \rightarrow Sb^+ + Sb)$	3.21±0.2		

*Supported in part by the U. S. Army Research Office-Durham

REFERENCES

1. R. E. Fox, W. M. Hickam, D. J. Grove, and T. Kjeldaas, Jr., Rev. Sci. Instr. 26, 1101 (1955).

2. G. DeMaria, J. Drowart, and M. G. Inghram, J. Chem. Phys. 31, 1076 (1959).

3. P. Goldfinger and M. Jeunehomme, Advances in Mass Spectrometry, Vol. 1, Pergamon press, London, 1959, p. 534.

4. H. Gutbier, Z. Naturforschung 17, 268 (1961).

5. A. J. H. Boerboom, H. W. Reyn, H. F. Vugts and J. Kistemaker, Advances in Mass Spectrometry, Vol. 3, Pergamon Press, London, 1966, p. 945.

6. G. D. Kinzer and G. M. Almy, Phys. Rev. 52, 814 (1937).

7. G. Herzberg, Molecular Spectra and Molecular Structure, Van Nostrand, New York, 1950.

8. C. E. Moore, Atomic Energy Levels, Vol. II, Natl. Bur. Stds. Circular 467 (1952).

127. MASS SPECTROMETRIC STUDIES OF THE LASER-INDUCED VAPORIZATION OF ARSENIC AND VARIOUS ARSENIC SELENIDES*

Bruce E. Knox and Vladimir S. Ban

Materials Research Laboratory
The Pennsylvania State University

Procedure

The laser - mass spectrometer has been used to study the vaporization of arsenic metal and several glassy compositions from the arsenic-selenium system. Basically, the instrument consists of a TRG Model 104A laser system coupled with a Bendix 12-107 time-of-flight mass spectrometer. Both ruby and neodymium-doped glass laser rods were used in the same system, giving the experimenter a choice of either 6,943 Å or 10,600 Å radiation. The laser output consisted of a pulse 800 to 1000 microseconds in width with a maximum (but controllable) energy of about 5 joules. Details of the system have been reported elsewhere (1,2).

Crystals of pure arsenic were obtained from the Department of Chemistry of this university. As_2Se_3 single crystals and glassy samples of arsenic-selenium containing 4, 10, 20, 30, 40, 45, 48, 50 and 55 atomic percent arsenic were obtained from the research laboratories of the Xerox Corporation. Because of the tendency of arsenic to oxidize rather quickly in air, even when combined with selenium, freshly cleaved surfaces were always presented to the laser beam in these studies. Both ionic and neutral spectra were recorded; to minimize fragmentation without sacrificing too much sensitivity, 15ev ionizing electrons were used in obtaining the neutral spectra.

Results

The major ionic and neutral species in the vapor above arsenic was As_4. Other ionic species observed were (in decreasing order of importance) As_5, As_3 and some As_7; other neutral species were As_2 and As_3 with minor amounts of As_5, As and As_7. In no case was either As_6 or As_8 observed.

As_3Se was the dominant species in the vapor in both the ionic and neutral spectra at glass compositions containing more than 30 atomic percent arsenic. As these glasses became more selenium-rich As_3Se_4 increased in importance until it became the dominant species in the vapor above glasses with less than 20 percent arsenic. In the neutral spectra Se_2 was important at all compositions below 30 to 40 percent arsenic. A single crystal of As_2Se_3 was compared with a glass of the same composition; both the ionic and neutral spectra were almost identical from the glass and the single crystal.

Discussion

The results of the laser-induced vaporization of arsenic were somewhat different

*The full manuscript will be published in the Materials Research Bulletin, Vol. 3 (1968).

from those obtained from conventional vaporization experiments where As_4 is the only species observed until As_2 appears at temperatures above 800°C (3). In the ionic spectra As_3 and As_5 conceivably result from the asymmetric fragmentation of two arsenic tetrahedrons during their removal from the solid. The small amounts of As and As_7 observed in the neutral spectra as well as the more important As_3 and As_5 probably originate in the same manner. The fragmentation of a single arsenic tetrahedron can explain the neutral As_2 in the vapor. Thus it is quite apparent that the stable SRO structure is As_4 in its well-known tetrahedral configuration.

In the arsenic-selenium system As_3Se was the most important species in the vapor, just as Bi_3Se dominated its analogous system (4). Thus it would appear that this is a stable SRO structural unit; unlike the Bi-Se system, however, it is not as easy to visualize the build-up of a long-range-order lattice from these units. As_3Se_4 dominated the vapor as the glass became more selenium rich. This is a stable species formed by the clustering of three more selenium atoms about the As_3Se structural unit. No As_2Se_3 was observed in the vapor, even above the single crystal.

In order to determine whether As_3Se actually was removed from the solid structure as such or was formed in a solid- or vapor-phase reaction, two additional experiments were conducted. The first consisted of vaporizing a 2:3 mixture of powdered arsenic and selenium; the spectra contained some small contributions from As_3Se and As_3Se_4 species, thus indicating that some solid-solid reaction probably had occurred. The second experiment consisted of simultaneously vaporizing powdered arsenic and selenium in such a way that the solids could not react but the vapors were well mixed. The spectra showed no As_3Se or As_3Se_4 but appeared to be the additive spectra of pure selenium and pure arsenic. One final experiment was conducted to compare the results of laser vaporization with those obtained from flash vaporization of As_2Se_3. In the flash spectra Se_2 was by far the most dominant species in the vapor; other Se_n and mixed arsenic-selenium species contributed relatively small amounts to these spectra. The mixed species had such wide energy distributions that the TOF resolution was drastically reduced.

Acknowledgements

The authors wish to acknowledge the financial assistance provided by NSF Grant GP-3232 and NASA Institutional Grant NGR-39-009-015.

References

(1) Vastola, F. J., A. J. Pirone and B. E. Knox, Proceedings of the 14th Annual Conference on Mass Spectrometry and Allied Topics, ASTM Committee E-14, Dallas, 1966, pp 78-82.
(2) Vastola, F. J. and A. J. Pirone, Advances in Mass Spectrometry, Vol. 4, Institute of Petroleum, London, 1968, pp 107-111.
(3) Nesmeyanov, A. N., Vapor Pressure of the Elements, Academic Press, New York, 1963, pp 297-302.
(4) Knox, B. E., V. S. Ban and J. Schottmiller, Materials Research Bulletin 3, 337 (1968).

129. Dissociation Energies of Gaseous AlCu, AlAg, and AlAu

Gary D. Blue
Department of Chemistry
The Ohio State University
Columbus, Ohio 43210

Karl A. Gingerich
Battelle Memorial Institute
Columbus Laboratories
Columbus, Ohio 43201

Previous investigations have established the existence of numerous gaseous diatomic molecules involving metal-metal bonding. Both homonuclear diatomic[1,2] and heteronuclear diatomic[2] metal-metal molecules have been studied and found to have a wide range of stabilities. Of particular interest is the general high stability of gaseous intermetallic molecules such as UAu,[3] AlAu,[4] SnAu,[5] CrAu[6] and others[2] in which gold is a constituent atom. Prior investigations in our laboratories on the bond energies of gaseous GaAg and InAg[7] appeared to establish a correlation between the bond energies of the homonuclear diatomic molecules of the constituent atoms and their electronegativity difference. Predictions of the bond energies of heteronuclear diatomic molecules formed between Group IIIA and IB metals were made using a Pauling model[8] and tested experimentally for the series AlCu, AlAg, and AlAu reported here.

The gaseous equilibria AlM = Al + M, Al + M_2 = AlM + M, and M_2 = 2 M where M is either Cu, Ag, or Au have been studied by means of Knudsen effusion high-temperature mass spectrometry, using both second and third law methods. In all cases the high purity metals were placed in a tantalum Knudsen cell which was resistance heated using a tungsten helix. Shutter effects, ionization efficiency curves, and isotopic abundance data were used to identify the neutral molecular precursor of the observed ions. Pressure calibrations were made by total vaporization of a known mass of metal such as Ag. Temperatures were measured with a calibrated optical pyrometer sighted on a black-body hole in the bottom of the cell and were checked at the conclusion of a run by sighting through the orifice of the cell.

For the Al-Au system, the equilibrium AlAu(g) = Al(g) + Au(g) was studied over the temperature range 1550°K-2050°K, while the equilibrium AlAu(g) + Au(g) = Au_2(g) + Al(g) was studied over the range 1850°K-2050°K. In addition some data were obtained on the homonuclear diatomics. The thermochemical data are summarized in the first table. The dissociation energy, D_0°(AlAu) = 75.8 kcal/mole, is the highest known at the present time for diatomic molecules between metal atoms.

SUMMARY OF REACTION HEATS IN THE Al-Au SYSTEM

Reaction	Method	ΔH_o^o kcal/mole	D_o^o(AB) kcal/mole	AB
$AlAu(g) = Al(g) + Au(g)$	2nd law	76.9	76.9	AlAu
	3rd law	75.8	75.8	
$AlAu(g) + Au(g) = Au_2(g) + Al(g)$	3rd law	23.8	75.8[a]	AlAu
$Au_2(g) = 2\ Au(g)$	3rd law	53	53	Au_2
$Al_2(g) = 2\ Al(g)$	3rd law	≤ 41.5	≤ 41.5	Al_2

(a) Using $D_o^o(Au_2)$ = 52 kcal/mole: Siegel, Quart. Rev., 19, 77 (1965).

HEATS OF REACTION IN THE Al-Cu SYSTEM

Reaction	Method	ΔH_o^o kcal/mole	D_o^o(AB) kcal/mole	AB
$AlCu(g) = Al(g) + Cu(g)$	2nd law	50.3	50.3	AlCu
	3rd law	50.6	50.6	
$AlCu(g) + Cu(g) = Cu_2(g) + Al(g)$	2nd law	4.9	50.9[a]	AlCu
	3rd law	5.4	51.4[a]	
$AlAu(g) + Cu(g) = AlCu(g) + Au(g)$	3rd law	24.0	51.8[b]	AlCu
$Cu_2(g) = 2\ Cu(g)$	2nd law	47.1	47.1	Cu_2
	3rd law	44.8	44.8	

(a) Assuming $D_o^o(Cu_2)$ = 46 kcal/mole: Siegel, Quart. Rev., 19, 77 (1965).

(b) Assuming $D_o^o(AlAu)$ = 75.8 kcal/mole: This work.

SUMMARY OF REACTION HEATS IN THE Al-Ag SYSTEM

Reaction	Method	ΔH_0° kcal/mole	$D_0^\circ(AB)$ kcal/mole	AB
$AlAg(g) = Al(g) + Ag(g)$	3rd law	~43.0	~43.0	AlAg
$AlAg(g) + Ag(g) = Ag_2(g) + Al(g)$	3rd law	6.7	44.3[a]	AlAg
$Ag_2(g) = 2\ Ag(g)$	3rd law	37.8	37.8	Ag_2
$Al_2(g) = 2\ Al(g)$	3rd law	~41.5	~41.5	Al_2
$AlAu(g) + Al(g) = Al_2(g) + Au(g)$	3rd law	37.5	38.5[b]	Al_2

(a) Assuming $D_0^\circ(Ag_2)$= 37.6 kcal/mole: Siegel, Quart. Rev., 19, 77 (1965).

(b) Assuming $D_0^\circ(AlAu)$ = 76 kcal/mole: this work.

ELECTRONEGATIVITY AND PREDICTED BOND ENERGIES (IN EV)

A	B	D(AA)	D(BB)	$[D(AA)\cdot D(BB)]^{\frac{1}{2}}$	Expl. D(AB)	Calc. D(AB)	Expl. X(A)-X(B)	Calc. X(A)-X(B)
B	Cu	2.86	1.97	2.38	--	2.39	--	0.1
Al	Cu	1.80	1.97	1.88	2.30	2.20		0.5
Ga	Cu	1.47	1.97	1.70		2.02		0.5
In	Cu	0.96	1.97	1.37		1.69		0.5
Tl	Cu	0.61	1.97	1.10	--	1.31	--	0.4
B	Ag	2.86	1.63	2.16		2.17	--	0.1
Al	Ag	1.80	1.63	1.71	1.90	2.03	0.38	0.5
Ga	Ag	1.47	1.63	1.55	1.83	1.87	0.47	0.5
In	Ag	0.96	1.63	1.25	1.62	1.57	0.53	0.5
Tl	Ag	0.61	1.63	1.00	--	1.21	--	0.4
B	Au	2.86	2.23	2.53	--	3.00	--	0.6
Al	Au	1.80	2.23	2.00	3.28	3.30	1.01	1.0
Ga	Au	1.47	2.23	1.81		3.11		1.0
In	Au	0.96	2.23	1.46		2.76		1.0
Tl	Au	0.61	2.23	1.17	--	2.22	--	0.9

For the Al-Cu system, the equilibrium $AlCu(g) = Al(g) + Cu(g)$ was studied over the temperature range 1520°K-1840°K, while the exchange reaction was studied over the range 1610°K-1840°K. The results are summarized in the second table.

Due to the much higher vapor pressure of Ag, temperature dependences were difficult to obtain for the Al-Ag system, but 3rd law data are presented in the third table for various reactions studied within the 1320°K-1490°K range.

In the third-law thermochemical calculations relative ionization cross sections were taken from Mann,[9] relative multiplier gains computed according to the findings of Pottie,[10,3] and free energy functions calculated from standard formulas using known values of we and re when available[4,2] and estimates such as addition of metallic radii[8] in other cases. It appears that in each case the use of such estimates would tend to make the $D_0^\circ(AlM)$ values slightly lower than if experimental molecular parameters were used.

The high experimentally measured values for the metal-metal bond energies may be interpreted in terms of a Pauling model[8] of an extra ionic resonance energy, which for AlM may be formulated as $\Delta(Al\text{-}M) = 30\,[X(M)-X(Al)]^2$, which is related to the bond energy in kilocalories per mole by the equation.

$D(Al\text{-}M) = [D(Al)D(M\text{-}M)]^{\frac{1}{2}} + \Delta(Al\text{-}M)$ where $X(M)-X(Al)$ is the electronegativity difference of the univalent atoms. The predictions for the Group IIIA-Group IB molecules are shown in the fourth table, together with our experimental results for comparison. The agreement is very gratifying and one is therefore lead to make predictions of other intermetallic molecules which would appear to have high stabilities. Among the more interesting predictions for bond energies in electron volts are $D_0^\circ(LaAu) = 4.5$, $D_0^\circ(LaCu) = 3.0$, $D_0^\circ(NiAu) = 2.8$ and $D_0^\circ(NiCu) = 2.2$. According to the model high stability molecules are also to be expected for other metals of low electronegativity and moderate dimer bond energies, such as some other lanthanides, bonded to metals of relatively high electronegativity and dimer bond energy. Finally, one may use an observed value for D(MAu), for example, to roughly approximate the dimer bond energy of M_2 if it is unknown.[3]

Work is presently in progress to test the predicted high stability of LaAu(g) and the gaseous metallic boride BAu.

References

1) B. Siegel, Quart Rev. (London), 19, 77 (1965).

2) J. Drowart: In "Phase Stability in Metals and Alloys" (P. S. Rudman, J. Stringer, and R. I. Jaffee, editors), McGraw-Hill Book Co., New York, 1966.

3) K. A. Gingerich and G. D. Blue, J. Chem. Phys., 47, 5447 (1967).

4) R. F. Barrow and D. N. Travis, Proc. Roy. Soc. A273, 133 (1963).

5) M. Ackerman, F. E. Stafford, and G. Verhagen, J. Chem. Phys., 36, 1557 (1962).

6) M. Ackerman, F. E. Stafford, and G. Verhagen, J. Chem. Phys., 36, 1560 (1962).

7) G. D. Blue and K. A. Gingerich (unpublished).

8) L. Pauling, "The Nature of the Chemical Bond," (Cornell University Press, Ithaca, N. Y., 1960), 3rd ed., Chap. 3.

9) J. B. Mann, J. Chem. Phys., 46, 1646 (1967).

10) R. F. Pottie, J. Chem. Phys., 44, 916 (1966).

130. A MASS SPECTROMETRIC STUDY OF THE VAPOR SPECIES IN THE B-S AND B-O-S SYSTEMS

P. J. Ficalora*, M. Uy, D. Muenow and J. L. Margrave

Department of Chemistry

Rice University

Houston, Texas 77001

*Present Address: Syracuse University, Department of Chemical Engineering and Metallurgy, Syracuse, New York 13210

A Bendix time of flight mass spectrometer was used to investigate the reactions of sulfur vapor, generated through the decomposition of Cr_2S_3[1], with solid boron and gaseous boric oxide. Initial studies with amorphous boron gave $B_2S_3^+$, $B_2S_2^+$, B_2S^+, BS_2^+, BS^+ and $B_2S_2O^+$ species whose intensity varied with time at a constant temperature. An x-ray diffraction pattern of the gray residue recovered from the Knudsen cell showed it to be B and B_2O_3. It was concluded that the $B_2S_2O^+$ ion, which was first thought to be a reaction product of a boron-sulfur specie with background oxygen, was formed from $B_2O_3(g)$ and $S_2(g)$.

Subsequent investigations with boron crystal rod (99.99%) remedied the above trouble and allowed the reactions leading to parent species to be studied. A second series of experiments were carried out with gaseous B_2O_3 and a series of oxysulfides which are completely analogous to the gaseous oxides were discovered and studied.

Species effusing from the Knudsen cell are listed in Table I together with their relative intensities and appearance potentials

TABLE I

Appearance Potentials of Observed Ions

GASEOUS B-S SYSTEM

Species	Relative Intensity (1125°K)	A.P. (ev)	Data Collected (ev)
BS^+	0.007	10.2 ± 1.0	-----
B_2S^+	0.08	9.8 ± 0.3	14
BS_2^+	0.33	11.4 ± 0.3	14
$B_2S_2^+$	0.55	11.8 ± 0.3	40
$B_2S_3^+$	1.0	10.2 ± 0.3(10.4±0.2)[2]	40
S_2	0.32	-----	40
$B_2S_2O^+$	0.38	-----	-----

GASEOUS B-O-S SYSTEM

Species	Relative Intensity (1300°K)	A.P. (ev)	Data Collected (ev)
$B_2O_3^+$	1.0	11.8 ± 0.3	40
BOS^+	0.18	9.8 ± 0.3	15
B_2OS^+	0.32	12.6 ± 0.3	15
$B_2O_2S^+$	0.29	9.4 ± 0.3	40
$B_2S_2O^+$	0.03	9.0 ± 0.3	40
S_2	0.59	-----	40
BO_2S^+	0.68	14.0 ± 0.3	-----

It was concluded from the shapes of the ionization efficiency curves and the appearance potentials that all of the above species except BS^+ and BO_2S^+ are parents. The relative intensity of $B_2S_2O^+$ from early experiments is included for comparison with the intensities of the B-S species. Ion intensity data were recorded at several ev. above the appearance potentials to prevent interference from fragment ions.

Ion intensities were converted into pressures [3] by using a Ag calibration, in the B-S studies, or B_2O_3 as an internal standard in the B-O-S studies. The heat of vaporization of B_2O_3 measured in this study (ΔH°_{298} = 90.4±2.0 kcal/mole) is in good agreement with the accepted value [4] suggesting that $B_2O_3(l)$ was probably at unit activity. An X-ray diffraction pattern of the solid residues showed that solid B or B_2O_3 were recoverable; no evidence of a second phase was found. Cross sections were estimated using the Otvos and Stevenson [5] rule and the data of Mann [6]. Efficiency terms relative to Ag or B_2O_3 were calculated from the relation [7]:

$$\frac{e_1}{e_2} = \left[\frac{M_2}{M_1}\right]^{\frac{1}{2}}$$

With these partial pressures the enthalpies for the various reactions were obtained as given in Table II.

TABLE II

SECOND LAW ENTHALPIES[a]

Reaction	$\Delta H^{\circ}_{1370^{\circ}K}$ (Kcal/mole)
$2B(s) + \frac{1}{2} S_2(g) = B_2S(g)$	-14.0
$B(s) + S_2(g) = BS_2(g)$	-8.7
$2B(s) + S_2(g) = B_2S_2(g)$	-12.8
$2B(s) + 3/2\ S_2(g) = B_2S_3(g)$	-30.1
	$\Delta H^{\circ}_{1365^{\circ}K}$ (Kcal/mole)
$B_2S_2O(g) + O_2(g) = S_2(g) + B_2O_3(g)$	-144.8
$B_2O_2S(g) + \frac{1}{2} O_2(g) = \frac{1}{2} S_2(g) + B_2O_3(g)$	-75.1
$2BOS(g) + \frac{1}{2} O_2(g) = S_2(g) + B_2O_3(g)$	-30.7
$B_2OS(g) + O_2(g) = \frac{1}{2} S_2(g) + B_2O_3(g)$	-104.2

a - uncertainties are $\sim$ 4-6%

References

1. P. J. Ficalora, J. W. Hastie and J. L. Margrave, J. Phys. Chem. 72, 1660 (1968).
2. F. T. Greene and P.W. Gilles, J. Am. Chem. Soc. 86, 3964 (1964).
3. R. Colen and J. Drowart, J. Chem. Phys. 37, 1120 (1962).
4. JANAF Thermochemical Tables (The Dow Chemical Company, Midland, Michigan; 1963).
5. J. W. Otvos and D. P. Stevenson, J. Am. Chem. Soc. 78, 546 (1956).
6. J. B. Mann, J. Chem. Phys. 46, 1646 (1967).
7. R.C.Schoonmaker and R. F. Porter, J. Chem. Phys. 30, 283 (1959).

132. Mass Spectrometric Studies of the Reactions of Atomic Nitrogen with Organic Compounds

Robert E. Huie and John T. Herron

National Bureau of Standards
Washington, D. C. 20234

Mass spectrometry has been used successfully in the field of reaction kinetics as an aid in the elucidation of reaction mechanisms, and in the determination of rate constants. We have applied this technique to the study of the reactions of atomic nitrogen.

The apparatus which was basically a discharge-flow system connected to a mass spectrometer, has been described previously (1). Highly purified nitrogen was subjected to a microwave discharge which dissociated about 0.1% of the molecules. This gas then passed thru a 40 cm long, 20 mm i.d. Pyrex reactor tube, which was surrounded by a heater. The total pressure in the reactor was kept at about 3 torr. The compound to be studied was introduced into the reactor thru a movable multi-holed, central inlet tube.

A glass "leak" of about 30 μm diameter was located at the base of the reactor. This was located directly above the electron beam in an open-type ion source which was part of a conventional mass spectrometer.

For a simple bimolecular reaction, N + A → Products, the bimolecular rate expression is:

$$-\frac{dA}{dt} = k[A]\,[N]$$

which may be integrated to

$$k = \ln(A_o/A_t)/\int_o^t [N]dt$$

where A_o and A_t are the concentrations of the reactant at times zero and t, respectively, and [N] is the nitrogen atom concentration. Under our conditions, the integral can be replaced by the average value of the nitrogen atom concentration times the reaction time.

(A_o/A_t) was determined as the ratio of the ion currents with the discharge off and on. The relative nitrogen atom concentration was determined at mass 14 at reduced electron energy. This relative concentration was then put on an absolute basis by titration with nitric oxide (2).

The rate constants were determined over a temperature range of 370 to 550 K. From plots of log k vs 1/T, the Arrhenius parameters, A and E, were determined. These are given in Table I. The uncertainties are standard deviations based on a least squares treatment of the data.

Table 1. Arrhenius Parameters for the Reactions of Atomic Nitrogen with Some Olefins and Acetylenes.[a]

Reactant	Log(A, cm^3 mol^{-1} s^{-1})	E, cal mol^{-1}	E, J mol^{-1}
	Olefins		
Ethylene, C_2HD_3	10.425 ± 0.208	760 ± 380	3200 ± 1590
Ethylene[b]	10.204	700	-
Ethylene[c]	11.394	1900	-
Isobutene	10.893 ± 0.154	550 ± 270	2300 ± 1130
Propene, C_3D_6	10.948 ± 0.145	1020 ± 270	4270 ± 1130
Propene[b]	11.176	1650	-
2-methyl-2-Butene	10.966 ± 0.140	860 ± 250	3600 ± 1050
1-Butene	11.190 ± 0.129	1310 ± 230	5480 ± 960
2,3-dimethyl-2-Butene	11.226 ± 0.099	1370 ± 170	5730 ± 710
cis-2-Butene	11.369 ± 0.082	1980 ± 150	8280 ± 630
trans-2-Butene	11.525 ± 0.071	2100 ± 125	8790 ± 520
	Acetylenes		
Acetylene[d]	-	-	-
Propyne	10.839 ± 0.153	1480 ± 280	6190 ± 1170
2-Butyne	11.265 ± 0.133	1840 ± 250	7700 ± 1050
1-Pentyne	11.468 ± 0.163	2080 ± 300	8700 ± 1260
3-Hexyne	11.526 ± 0.122	2190 ± 220	9160 ± 920
1-Butyne	11.539 ± 0.114	2240 ± 210	9370 ± 880
1-Hexyne	11.664 ± 0.130	2450 ± 240	10250 ± 1000

[a] This work except as noted.

[b] Reference 5.

[c] Reference 6. A and E were recomputed from the original data.

[d] From 330 to 550 K, $k \leq 2 \times 10^9$ cm^3 mol^{-1} s^{-1}. L. I. Avramenko and V. M. Kransnen'kov, Izvest. Akad. Nauk. S.S.S.R., Ser. Khim. 822 (1964), give $k = 5.4 \times 10^8$ $T^{\frac{1}{2}}$ exp(-2300 ± 299/RT) cm^3 mol^{-1} s^{-1}. At 550 K this leads to a rate constant approximately equal to our limiting value.

The A factors for these reactions, when compared to analogous oxygen or hydrogen atom reactions, are quite low. Typically, one would expect log A on the order of 13-14. The main reason for this difference is that the N-atom reactions are spin-forbidden -- they involve a spin-forbidden transition between the potential energy surfaces of reactants and products. These reactions, therefore, are much slower than the analogous oxygen or hydrogen atom reactions. As a result, a small amount of a oxygen or hydrogen atom producing impurity in the discharge, or the production of substantial amounts of H atoms in the reaction, could lead to erroneously high results. We, therefore, have taken care to purify the nitrogen used, and added only a small amount of reactant -- to suppress H atom production in the reaction. It has also been suggested that excited nitrogen molecules, produced by recombination, can act as an initator in a spin-allowed reaction. This was checked by a variation of the N atom concentration. A dependence of the rate on the square of the N atom concentration would have indicated that the reaction was initiated by excited nitrogen molecules. This was not observed.

A particularly striking example of the effect of an impurity on a reaction is given by the N + C_2H_2 reaction. The reaction normally is too slow for us to observe, but upon the addition of a small amount of hydrogen before the discharge, the reaction proceeds rapidly. Recently, Michael and Niki (3) have shown that hydrogen atoms react rapidly with C_2H_2 to produce vinyl radicals -- which may then react further to produce hydrogen and C_2H_2. They found no net consumption of C_2H_2. We feel that

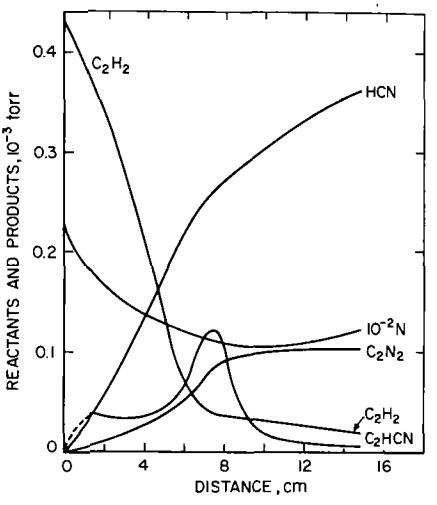

FIGURE 1

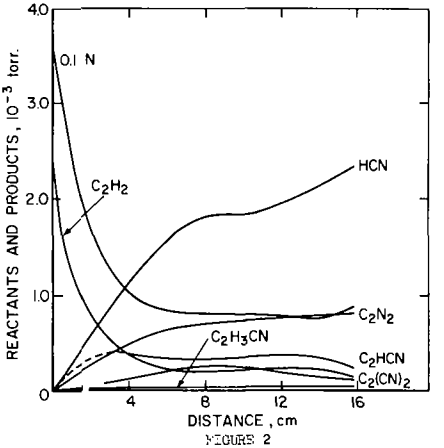

FIGURE 2

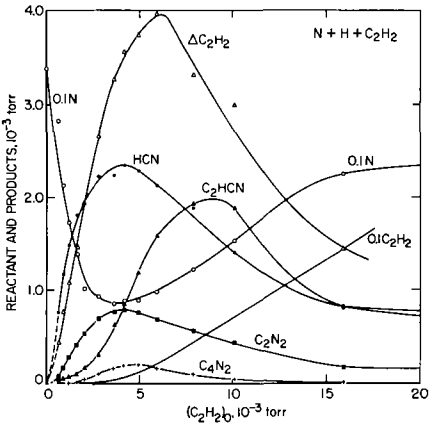

FIGURE 3

the production of vinyl radicals by the hydrogen atom reaction may be the reason for the increase in apparent rate.

The products of the N + H + C_2H_2 reaction seem to indicate that cyanogen radicals played an important role in their formation. Figures 1 and 2 show the variation of product yield as a function of reactor length, or time. The products corresponding to cyanogen attack seem to level off, or decrease, after reaching a maximum. Also, the nitrogen atoms seem to start to increase after reaching a minimum.

Figure 3 shows the variation of product yield as a function of the initial acetylene concentration. The product curves go through a maximum, and then fall off while the reactant partial pressures go through a minimum before arising again. Clearly the reaction is self-inhibiting.

Some of the observed reaction products may be accounted for by the following reaction scheme, involving the cyanogen radical:

$$CN + C_2H_2 \rightleftharpoons C_2H_2CN^* \rightarrow C_2HCN + H$$
$$\xrightarrow{M} C_2H_2CN$$

$$C_2H_2CN + H \rightarrow C_2HCN + H_2$$
$$\rightarrow C_2H_2 + HCN$$

$$CN + C_2HCN \rightleftharpoons C_2H(CN)_2^* \rightarrow C_2(CN)_2 + H$$
$$\xrightarrow{M} C_2H(CN)_2$$

$$C_2H(CN)_2 + H \rightarrow C_2(CN)_2 + H_2$$
$$\rightarrow C_2H(CN) + HCN$$

$$CN + CN \overset{M?}{\underset{W?}{\rightleftharpoons}} C_2N_2$$

However, the nature of the initiating steps has not been established.

References

(1). J. T. Herron, J. Phys. Chem. 70, 2803 (1966).

(2). G. B. Kistiakowsky and G. G. Volpi, J. Chem. Phys. 28, 665 (1958).

(3). J. V. Michael and H. Niki, J. Chem. Phys. 46, 4969 (1967).

133. APPLICATIONS OF THE MASS SPECTROMETRIC STANDARD MIXTURE CALIBRATION TECHNIQUE

John M. Ruth

Entomology Research Division, Agricultural Research Service
USDA, Beltsville, Md.

and

Joseph N. Damico

Food and Drug Administration, Department of Health, Education,
and Welfare, Washington, D. C.

The familiar method for the quantitative mass spectrometric analysis of multicomponent mixtures requires sensitivity coefficients, which are expressible as spectral intensity per unit pressure. An alternative method, for which no pressure measurements are needed, makes use of the spectrum and known composition of a calibration mixture. The mathematical development of the latter method has been described elsewhere (1). The purpose here is to provide some experimental data illustrating its applicability.

I. Use with molecular leaks and reservoirs lacking micromanometers. Many laboratories not routinely engaged in quantitative analysis do have occasional need for it. A large number of mass spectrometers exist which have vapor reservoirs equipped with molecular leaks but are without any provision for reservoir pressure measurements. Although the professional quantitative analyst, in such circumstances, may respond by suggesting the purchase of an instrument specialized for analytical use, the research organization having only a limited need for that particular service does not always find that solution applicable to its problem.

An example of the situation just described was encountered in the operation of a Consolidated Electrodynamics Model 21-110B high resolution spectrometer. With a source slit opened to 8 mils and the collector slit to 10 mils, singlet peaks as exhibited by the electron multiplier and 5-124 oscillograph have flat tops, and the range of amplitude of the noise, which need not be the same as that in the baseline, is immediately seen. The first analysis of a mixture of heptane, 2,4-dimethylpentane, 2,4,4-trimethyl-2-pentene, and 1-octene, made up by weight to 34.5, 17.0, 32.5, and 16.0 mole percent, respectively, yielded the values 33.6, 16.3, 33.0, and 17.1 mole percent. For the applications contemplated, the results are quite satisfactory.

In a somewhat different example, in which a needle valve substituted for the leak, the analysis was applied to a mixture of three hydrocarbons occurring in a single gas chromatographic fraction which was transferred to a Bendix time-of-flight mass spectrometer by means of a small glass trap fitted with stopcocks and ground joints (2). The trap served as the reservoir.

II. Application to the direct inlet probe. It is sometimes desired to estimate the concentrations of the components of mixtures introduced directly into the ion source by means of a probe. Requests for this sort of analysis usually are received when the sample, because of small size, low volatility, or thermal instability, cannot be handled in a heated reservoir. Also, its usefulness is naturally limited to mixtures having rather narrow boiling ranges, such as gas chromatographic fractions produced in the study of biochemical materials. As an example, the chromatographic separation of a plant or animal wax may yield trapped fractions which are still mixtures of isomers (3,4). Since the scarcity of reference materials of that sort is always a problem, it was decided to investigate the analytical method by applying it to some more easily available model systems.

The compounds chosen are isomeric diesters of dibasic acids. No fractional evaporation was detected. A Bendix Model 14 time-of-flight mass spectrometer was used. With this instrument, it is a simple matter to make eight or ten moderately fast scans, each of which in the present case covered the range between m/e 50 and 120 in about 40 seconds. In such sets, the effect of small intensity variations, perhaps caused by fluctuations in the rate of evaporation, tends to be averaged out, and any effect of a slow drift in sample pressure is similarly reduced, which makes the result preferable to that of a single slow scan. The probe data reported here are averages of such sets.

In a representative experiment, a mixture of dimethyl sebacate, diethyl suberate, dipropyl adipate, and dibutyl succinate was examined. The composition prepared by weight was 32.8, 16.9, 33.5, and 16.8 mole percent, respectively, and the corresponding values found were 30.0, 18.2, 32.8, and 19.0.

III. Use in place of sensitivity coefficient method with analytical instruments. Although a comparison of the two methods would be of interest, it remains to be done.

References

(1) John M. Ruth, "Mathematical Solution of the Mass Spectrometric Standard Mixture Problem," Fifteenth Annual Conference on Mass Spectrometry and Allied Topics, Denver, Colorado, May 14-19, 1967; Analytical Chemistry 40, 747-750 (1968).

(2) Roger J. Philippe, Robert G. Hunnicutt, and John M. Ruth, Journal of Chromatography 20, 250-259 (1965).

(3) James D. Mold, Robert K. Stevens, Richard E. Means, and John M. Ruth, Biochemistry 2, 605-610 (1963).

(4) James D. Mold, Richard E. Means, Robert K. Stevens, and John M. Ruth, Biochemistry 3, 1293-1298 (1964).

134. LASER-QUADRUPOLE MASS SPECTROMETER SYSTEM AS APPLIED TO ANALYSIS OF INORGANIC SALTS

M. O. Hobbs and A. J. Getzkin, North American Rockwell Corporation, Autonetics Division, Life Sciences Operations, Anaheim, California, and R. A. Meyer, North American Rockwell Corporation, Science Center, Thousand Oaks, California

Laser energy was used to vaporize inorganic solids and the vapor produced was subsequently analyzed with an EAI Quadrupole Mass Spectrometer, Model 250. These tests were conducted to evaluate the feasibility of using a laser-quadrupole system as the basis for a rapid, automatic method to determine the elemental content of blood serum samples.

A continuous wave carbon dioxide laser, Perkin Elmer Model 6200, was employed with a shutter system to permit exposure of the sample to the laser for 2 milliseconds (ms). The sample was positioned immediately adjacent to the quadrupole ionization chamber. In addition, a neodymium, pulsed laser (0.5 ms pulse) was similarly evaluated to compare vaporization selectivities. The quadrupole was modified to provide a scan rate of one ms per spectrum in order to obtain valid analytical data during the short duration of the laser-produced sample plume.

Mass spectral data were obtained from the plumes produced by action of each laser on seven inorganic salts and one complex salt mixture. Four of the selected salts exhibited an absorption band at the CO_2 laser wavelength (10.6 microns) and all were transparent at the neodymium wavelength (1.06 microns). The data obtained did not include m/e values greater than 60 because of severe base-line broadening and great loss in sensitivity observed at higher mass numbers. This condition does not normally exist with the quadrupole mass spectrometer and was probably caused by breadboard modifications made to increase the scanning rate. Although the neodymium laser had a power output significantly greater than that of the CO_2 laser, 3 of the 4 inorganic salts tested which absorb at the CO_2 laser wavelength produced as much or more mass spectral data when the lower powered CO_2 laser was employed. All compounds transparent at both wavelengths produced more mass spectral data when the higher powered neodymium laser was used.

These studies demonstrated that inorganic salts may be selectively vaporized when subjected to laser exposures and that selectivity is probably dependent on the laser wavelength and the transmission spectrum of the sample at that wavelength. This proved to be a major disadvantage in our specific application, but this finding could

be used to advantage for analytical applications if the components to be analyzed may be selectively vaporized out of the sample matrix by employing appropriate laser energy. In addition, these studies demonstrated that the quadrupole-type mass spectrometer may be used to perform analyses of solid samples using a laser as the vaporization source.

This work was supported in part by U.S. Air Force Contract AF41(609)-3072.

It is anticipated that the detailed text of this paper will be submitted for publication to Journal of Applied Spectroscopy.

136. IMPROVED MASS SPECTROMETRIC ISOTOPIC ANALYSIS USING AN AMPLITUDE SELECTOR FOR PULSE COUNTING WITH A SCINTILLATION ION DETECTOR

A. C. Tyrrell, R. G. Ridley and N. R. Daly

Atomic Weapons Research Establishment, Aldermaston, Berkshire, England

Isotopic analyses of nanogram sized solid samples can be made difficult if background peaks are present on the spectrum. This technique utilizes the difference in secondary electron coefficients obtained from a scintillation ion detector for metal and polyatomic ions. An amplitude selector is used in place of the normal discriminator in the pulse counting system, to reduce the background by over a factor of 10.

Published in the International Journal of Mass Spectrometry and Ion Physics, Vol. 1, No. 1, 69 - 73, 1968.

137. Absolute Isotope Ratio Determination of a Natural Boron Standard

P.J. De Bièvre and G.H. Debus

Central Bureau for Nuclear Measurements

EURATOM GEEL BELGIUM

1. Introduction

The natural isotopic composition of boron cited in literature shows large variations exceeding the uncertainties quoted.
This could be due to variations in the natural isotopic composition of boron. This laboratory found significant variations between natural boron stocks used as references in different nuclear research establishments.

2. Experimental

The CBNM decided to establish a 100 Kg boric acid stock and to define it isotopically so that it could be used as a standard for the calibration of mass spectrometers and for the preparation of boron samples for nuclear measurements. The isotopic analyses were performed on the $Na_2BO_2^+$ ions, from borax ($Na_2B_4O_7$), at masses 88 and 89. The contribution of the $Na_2\ ^{10}B\ ^{16}O\ ^{17}O^+$ ion to mass 89 (experimentally evaluated from masses 89 and 90 of enriched ^{11}B samples) was 0.000790 ± 0.000012 times peak 88.
The mass spectrometer used was a 90° - 15" instrument with a triple Re filament and thermal ionization source. Samples (about 100 µg) were taken from 3 mg B/ml solutions and measured, on a plate collector VRE with a 10^{11} ohm input resistor, at 7 kV and varying magnetic field. A carefully controlled zero suppression circuit was used to reduce the recorder error.

3. Determination of mass spectrometer bias factor

The bias factor K, defined as the ratio of true (R true) and observed (R_{obs}) isotope ratios, was determined by measuring samples of accurately known isotopic compositions, prepared by mixing precisely known amounts of chemically defined ^{10}B and ^{11}B enriched isotope solutions (with respectively $^{10}B/^{11}B$ ratios of R_A and R_B). The isotope ratio R_c of these blends can be computed from

$$K_c R_c = \frac{q\,K_A R_A(1+K_B R_B)+K_B R_B(1+K_A R_A)}{q(1+K_B R_B)+(1+K_A R_A)}$$

q is obtained from the masses M_A and M_B of the components and from their chemical concentrations C_A and C_B

$$q = \frac{M_A C_A}{M_B C_B}$$

Subscripts A and B refer to respectively the enriched ^{10}B and enriched ^{11}B.

The starting solutions were defined as indicated in Table 1 :

TABLE 1

Isotopic and chemical definition of the enriched isotopes solutions

	Solution A	Solution B
$^{10}B/^{11}B$ atom ratio	R_A = 28.571 ± 0.024 (n=4)	R_B = 0.017283 ±0.000020 (n=4)
^{10}B atom conc. ^{11}B atom conc.	(96.6183 ± 0.0027)% (3.3817 ± 0.0027)%	(1.6989 ± 0.0020)% (98.3011 ± 0.0020)%
C (coulombs/g)	C_A = 35.702 ± 0.011 (n=19)	C_B = 29.869 ± 0.009 (n=11)
$\frac{C_A}{C_B}$	1.19529 ± 0.00052	

Note : uncertainties given are standard deviations for a single measurement.

The chemical determination was performed by the CBNM Analytical Chemistry Department and has been described elsewhere [1)2)3)4)5)]. The mass determinations were carried out at the CBNM Metrology Department. Eleven blends were prepared at about 10-19.8-35-50-65-80 and 90 atom % ^{10}B nominal concentrations. These synthetic mixtures were measured on the mass spectrometer together with samples from the standard stock. The 11 K-values were the same with a standard deviation on a single determination of 0.06 % as can be seen in Table 2. A least square fit showed that K is independant of the isotopic composition.

Hence $K_c = K_A = K_B = K$ in the equation above and

$$K = \frac{q(R_c - R_A) - (R_B - R_c)}{(R_B - R_c)R_A - q(R_c - R_A)R_B}$$

An extrapolation to R_A = 28.571 and R_B = 0.017283 was made in order to correct these for the observed bias. A new set of K-values calculated from these corrected starting materials yielded a mean value 0.99874, slightly different from the first one (0.99892). After 2 more iterations the process leads to a constant K = 0.99870 ± 0.0006 (n=11)(standard deviation on the single determination).

TABLE 2

^{10}B nominal atom %	$K = \frac{R_c}{R_{obs}}$
10	0.99821
19.8	0.99960
	0.99807
	0.99939
35	0.99864
50	0.99917
65	0.99952
80	0.99954
	0.99900
	0.99865
90	0.99840

4. Results

The measurements on the standard stock yielded a $^{10}B/^{11}B$ atom ratio of 0.24757 ± 0.00024 (n=22) (standard deviation of a single determination). Hence the absolute value is 0.99870 x 0.24757 = 0.24726. The different error contributions, expressed as 95 % confidence limits on the mean, are :

- K determination (n=11) 0.040 %
- Standard (n=22) 0.044 %
- Error due to chemical preparation of blends (n=11) 0.038 %

$$\frac{\delta K}{\delta(C_A/C_B)} \; s\left(\frac{C_A}{C_B}\right)$$

- Error due to uncertainty on enriched B_{10} (n=4)

$$\frac{\delta K}{\delta R_A} \; s(R_A)$$ 0.006 %

- Error due to uncertainty on enriched B_{11} (n=4)

$$\frac{\delta K}{\delta R_B} \; s\,(R_B)$$ 0.018 %

The Central Bureau of Nuclear Measurements considered the possible contributions of these partial errors to the total accuracy of the natural Boron standard, and decided to emit a certificate stating an accuracy of 0.1 % on the ^{10}B isotopic concentration of the natural Boron standard (Table 3).

TABLE 3

Results	
$^{10}B/^{11}B$ atom ratio	0.24726 ± 0.00032
^{10}B atom concentration	19.824 ± 0.020
^{11}B atom concentration	80.176 ± 0.020
^{10}B weight percent	18.359 ± 0.020
^{11}B weight percent	81.641 ± 0.020
Atomic weight (^{12}C=12)	10.81178 ± 0.00020
(Nuclidic masses :	
^{10}B : 10.012939	
^{11}B : 11.009305	

The authors express their gratitude to J. Spaepen, Director of the CBNM (Euratom), who initiated the project, for stimulating advice and support. They are indebted to K.F. Lauer and Y.Le Duigou for the chemical analyses, to H. Moret and J. Brulmans for the mass determinations, to H. Moret for statistical evaluation of the results and to M. Gallet for collecting the mass spectrometric data.

(1) Lauer K.F., Le Duigou Y.
Z. Anal. Chem.
184 4 (1961)

(2) Lauer K.F., Le Duigou Y.
Analytical Chim. Acta
29 87 (1963)

(3) Le Duigou Y., Lauer K.F.
Anal.Chim.Acta
33 222 (1965)

(4) Le Duigou Y.
EUR. 2240 (1965)

(5) Le Duigou Y., Lauer K.F.
EUR. 3490 (1967)

Note: A full account of this measurement will be published elsewhere.

138. AUTOMATED MASS SPECTROMETRIC THERMAL ANALYSIS OF SOME ORGANO-NICKEL COMPLEXES

H. G. Langer and T. P. Brady
The Dow Chemical Company
Eastern Research Laboratory
Wayland, Massachusetts 01778

and

M. D. Rausch and H. B. Gordon
Department of Chemistry
University of Massachusetts
Amherst, Massachusetts

The MASTA (Mass Spectrometric Automatically Scanning Thermal Analyser) system used for this study has been previously described.[1] It consists of a combination of thermal analysis and mass spectrometry by which a sample can be heated either outside or within the mass spectrometer and a constant record of thermal changes as well as complete mass spectra at a rate of 10 per second can be obtained. The information is stored on magnetic tape from which the data are normally recorded as a plot of mass peak intensity versus temperature. The preparation and chemical properties of the compounds described in Table I will be reported elsewhere. For this study, it was of interest to correlate mass spectrometric thermal data with bond strengths of the various compounds and differences in chemical degradation reactions.

Table I

$CpNiCl$	·	$\emptyset_3P$
$CpNi\emptyset$	·	$\emptyset_3P$
$CpNi\emptyset_{Cl}$	·	$\emptyset_3P$
$CpNi\emptyset_{F}$	·	$\emptyset_3P$

Cp = cyclopentadienyl-, = C_5H_5

$\emptyset$ = phenyl-, = C_6H_5

$\emptyset_{Cl}$ = perchlorophenyl-, = C_6Cl_5

$\emptyset_F$ = perfluorophenyl-, = C_6F_5

All four compounds were decomposed within the mass spectrometer up to a temperature of approximately 400°. The decomposition of the triphenylphosphine complex of cyclopentadienyl nickel chloride (Figure 2) is readily explained as a disproportionation reaction with the formation of highly volatile nickelocene (Cp_2Ni) and the triphenylphosphine complex of nickel dichloride. The latter compound is

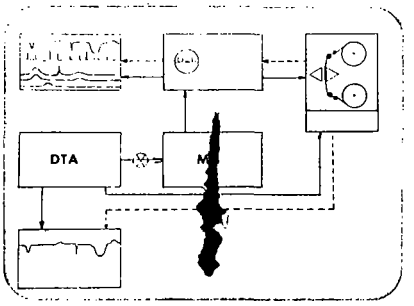

FIG. 1 MASTA SCHEMATIC

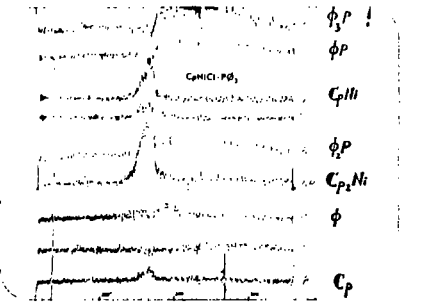

FIG. 2

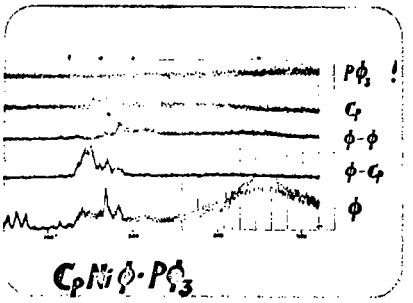

FIG. 3

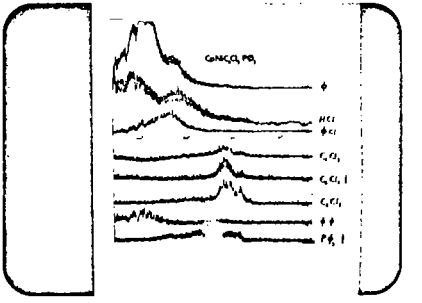

FIG. 4

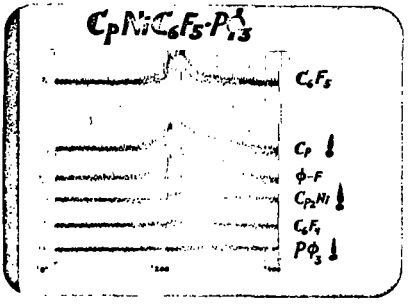

FIG. 5

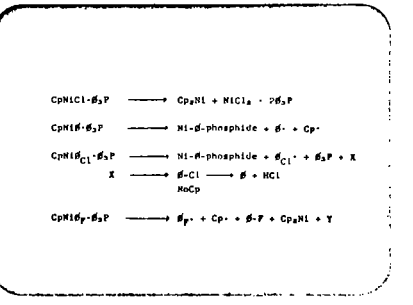

FIG. 6 OBSERVED DECOMPOSITIONS

thermally unstable and produces triphenylphosphine which is not only fragmented in the ion source but also decomposed with formation of phenyl radicals and biphenyl as shown in separate experiments. If the chloride is replaced by phenyl (Figure 3), a disproportionation is no longer observed. Here the reaction is apparently initiated by homolytic cleavage of the nickel to phenyl bond which causes a complete molecular breakdown. This is demonstrated by the appearance of both phenyl and cyclopentadienyl radicals and their recombination products, the absence of a strong peak for triphenylphosphine at the decomposition range and also the complete absence of any volatile nickel compounds. The resulting nickel compound therefore must be of a phosphide type: polymeric phenylphosphide initially and nickel phosphide after prolonged heating. For the pentachlorophenyl compound (Figure 4) the pyrolysis is further complicated by secondary reaction of the initially formed pentachlorophenyl radical. This radical acts as a chlorinating agent with formation of a thermally stable compound which upon further heating produces chlorobenzene and finally phenyl and hydrochloric acid. A small amount of triphenylphosphine is released from the metal apparently through replacement by chlorine. As a final example (Figure 5) the perfluorophenyl-nickel complex is more reminiscent of the nickel chloride complex shown in Figure 2. The presence of nickelocene indicates partial disproportionation, yet the low intensity of the triphenylphosphine peak, and the presence of fluorobenzene show the effect of the pentafluorophenyl radical as a fluorinating agent and the formation of polymeric nickel phenylphosphide observed earlier.

In summary (Figure 6), using the MASTA system we could readily demonstrate a fundamental difference in the decomposition of the cyclopentadienyl nickel chloride complex and the three organometallic nickel compounds. It was further shown that the latter three compounds decompose in a fashion which is similar to a template reaction, since organic reactions are observed to take place essentially on the surface of a nickel atom. Despite the formal similarity of the three compounds, each one has its own characteristic decomposition pattern and path. Finally, it was shown that the thermal stability increased from the phenyl compound over the perchlorophenyl to the perfluorophenyl complex.

REFERENCES

1. H. G. Langer and F. J. Karle, "Automated Mass Spectrometric Thermal Analysis", presented at the 15th Annual Conference on Mass Spectrometry and Allied Topics, Colorado, May 1967.

139. IMPROVEMENTS OF THE METHOD FOR THE DETERMINATION OF PLUTONIUM CONTENT IN NUCLEAR FUELS

R. BIR - G. FREJAVILLE*

This paper will describe some improvements brought to the classical procedure (1, 2, 4) for uranium to plutonium ratio determinations by isotopic dilution in order to increase their rate and precision.

INTRODUCTION -

The procedure used before is as follow :

1) SPIKE -SOLUTION MIXTURE
- Spike : $^{233}U + ^{242}Pu$
- Solution : U + Pu + fission products

2) PLUTONIUM VALENCE CYCLE
- Pu + hydroxylamine chlorhydrate $\longrightarrow Pu^{III}$
- Pu^{III} + 8N nitric acid $\longrightarrow Pu^{IV}$

3) URANIUM PLUTONIUM SEPARATION

Anion exchange column (Dowex AG 1 X 4 - 100 - 200 mesh)
Adsorbtion of 2 cc of 8N nitric acid uranium plutonium solution
Uranium and fission products elution with 8N nitric acid
Plutonium elution with hydroxylamine chlorhydrate

4) Decomposition of the hydroxylamine chlorhydrate.

Using this procedure two days are necessary to obtain four samples for mass spectrometry measurements and the result of a determination is available four days after the beginning of the analytical procedure.

In order to increase the rate of the measurements the chemical procedure duration has to be reduced.

In order to know the possible ways for increasing the precision fo the uranium-plutonium ratio determinations a statistical study of the results obtained previously was performed and leads to the following results :

- the overall variance appears to be the sum of two nearly equal terms : the variance of the chemical procedure and that of the mass spectrometry measurements.
- the reproducibility of the ratio determinations is (Fig 1) directly correlated to the internal dispersion of the isotopic measurements. The internal dispersion has been estimated by the quadratic sum of the dispersions spectra necessary to obtain a pair of uranium plutonium ratios.

---

* - Commissariat à l'Energie Atomique - Services des Isotopes Stables - Service de Spectrométrie de Masse - BP N° 2 - GIF-sur-YVETTE (91) France .

Then it may be thought that the overall precision can be improved by reducing the random errors coming from the chemical treatment and by modifying the method of isotopic ratio measurements.

SIMPLIFICATION OF THE CHEMICAL PROCEDURE -

1) Plutonium valence cycle suppression : it is well known (3, 4, 5, 6, 7) that, for a nitric concentration lower than 8N a dismutation of plutonium according to :

$3\ Pu^{IV} \longrightarrow 2\ Pu^{III} + Pu^{VI}$ occurs. So it may be thought that when both spike and solution were in 8N nitric acid the plutonium valence cycle was not required. So all spikes and samples were made and kept in 8N nitric acid media.

To make sure that, in such conditions, the valence cycle can actually be suppressed the following experiments were carried out : for each run of four spike-solution mixtures, two were analysed according to the previous procedure and two without the plutonium valence cycle. These experiments were carried out on a number of samples large enough to make statistical tests significant.

The tests showed that there is no systematic difference between the results obtained using the two procedures, and that the reproducibility of the results obtained without the plutonium valence cycle is not affected by the suppression.

The routine operating procedure no longer includes the valence cycle, which saves more than two hours.

2) The classical procedure for the uranium plutonium separation was also improved. The method used is given below :

1) Adsorbtion of plutonium :

Stir up for 30 mn
- 100 mg of resin DOWEX AG 1 X 4 (100 - 200 mesh)
- 2,5 cc of 8N nitric acid
- 2,5 cc of uranium plutonium solution

2) Elimination of uranium and fission products :

Eliminate 4 cc of solution

Repeat 3 times the following operation:

Add 7 cc of 8N nitric acid

Stir up for 2 mn

Eliminate 7 cc of solution

3) Plutonium elution :

Stir up for 5 mn
- 7 cc of 1 % hydroxylamine chlorhydrate solution
- Few drops of 20 % hydroxylamine chlorhydrate solution

Filter to eliminate the resin

Decompose the hydroxylamine chlorhydrate by nitric acid.

This method of separation is four times as quick as the previous one. A separation lasts one hour only. The performances are equivalent to those obtained on an ion exchange column. As an example, for a uranium to plutonium ratio of 2500, the efficiency of plutonium recovery is greater than 90 % and the uranium to plutonium ratio in the plutonium fraction is lower than two.

IMPROVEMENTS OF THE ISOTOPIC RATIO MEASUREMENTS -

1) We already saw it is possible to increase the reproducibility of uranium to plutonium ratio measurements by selecting the mass spectra according to a statistical test of internal coherence.

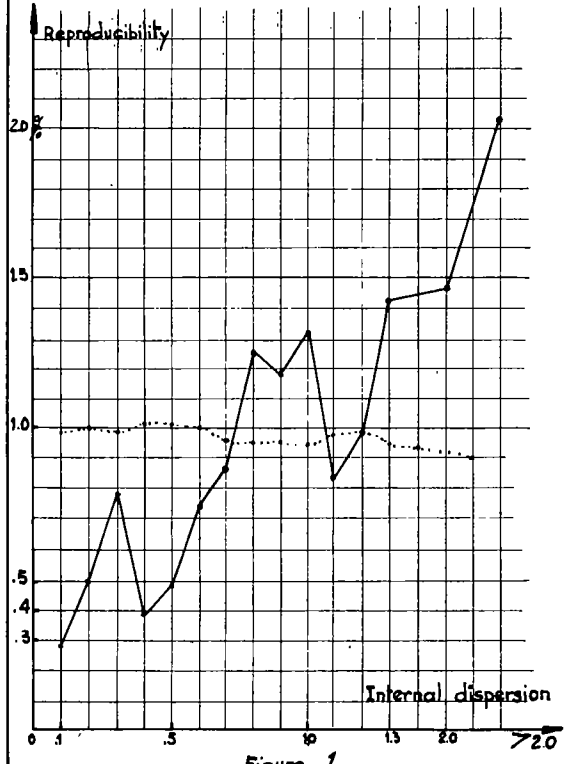

Figure. 1

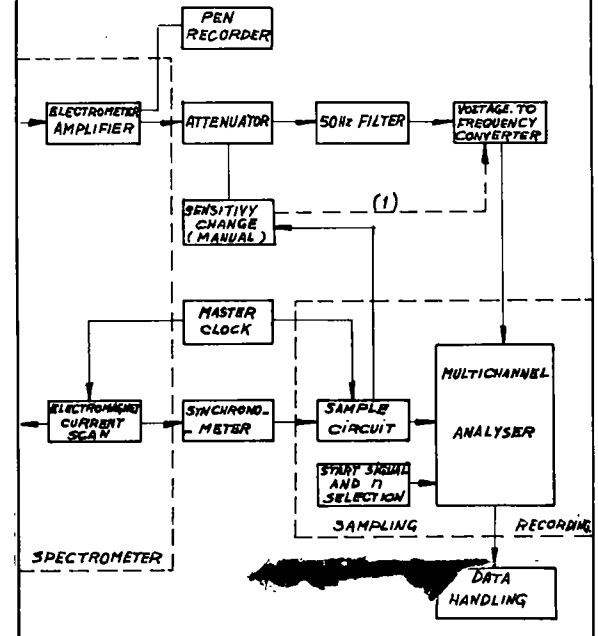

Figure. 2

General schematic of the digitizer system

(1) OPTIONAL

If both ^{238}U - ^{233}U and ^{239}Pu - ^{242}Pu isotopic ratios are as close as possible to one, the exploitation of experimental data is of course easier. It is possible to calculate the spike to solution ratio which leads to isotopic ratios included within two limits.
Then the volumes of solution and spike to be mixed have to be carefully measured. Such a measurement is, in principle, not necessary in the case of mixed spike technique. However, this drawback actually leads to a gain of time, as the proportion of good isotopic measurements is better than that obtained without volumes measurements.

2) In order to increase the rate and the precision of the mass spectrometry determinations themselves a peak height digitizer of isotopic mass spectra was designed (8).
The method normally used to digitalize the information given by a mass spectrometer is to count directly the number of ions collected during a given time interval (9, 10, 11, 12). Its main disadvantage lies in the limitation of the maximum current measurable, the resolution time of the usual counting units being effectively not less than 0,02 μ s . The counting loss on the equivalent of a 10^{-14} ampere current is greater than 0.1 % . Very elaborate devices to compensate for these counting losses are necessary as soon as the ion current exceeds 10^{-13} ampere .
The system which was developed works on a different principle. The current to be measured feeds into the input circuit of an ordinary amplifier which delivers a voltage proportional to the average current. This voltage is applied to the input of a voltage frequency converter. The essential property of such a converter is to deliver, during a time interval, a number of pulses proportional to the charge collected during this time interval. Such a system therefore fulfills essentially the same function as a direct ion counter but the proportionality factor between the number of pulses and the number of ions can have any value eitheir below or above one. We thus abolish the upper ion current limit previously mentionned without introducing a lower limit.
Figure 2 shows the general flow sheet of the system . The mass spectrometer amplifier output is fed into a conventional pen recorder and an attenuator mounted in parallel. The pen recorder is used to test the overall quality of the analysis and to verify the absence of electrical discharges. The attenuator can be adjusted manually to approach as closely as possible the full scale of the converter.
Next comes a 50 Hz low pass filter which brings the hum down to a negligible level. This is followed by a voltage frequency converter which sends the pulses into the sampling and recording circuit.
The sampling and recording circuit are made of a multichannel analyser with ferrite memories and its electronics which permits the selection and the triggering of the recording periods. A time base consisting of a master clock and its logic circuits synchronises the sampling and recording with the scanning of the magnetic field obtained by the rotation of a functional potentiometer fixed to a stepped motion motor. In this way there is a correlation between the possition of the channel and the value of the magnetic field. Each element of successive mass spectra is always recorded in the same channel.
Lastly the data is delivered in the desired form by the reading unit. Punched tapes are used and processed on a small computer.
Using such a digitizer system increases greatly the rate of the isotopic analyses. The analysis time is about twenty minutes, that is, about half that required if a pen recorder is used. The digitalization of the information dispenses with the laborious peak height measurements and also with the subjective factor influencing them. The final result is available forty minutes only after starting the analysis.
On the other hand, the $^{240}Pu/\,^{239}Pu$, $^{241}Pu/\,^{239}Pu$, $^{236}U\,/\,^{238}U$, $^{235}U/\,^{238}U$ isotopic ratios

can be evaluated from routine procedure. This is not the case when a pen recorder is used. To test the precision of the measurements obtained by this method, number of analyses were performed with double recordings. The statistical study of these results made it clear that the numerical reading leads to an appreciable decrease of random errors.

CONCLUSION -

The application of all the improvements described leads to a weekly rate of ten uranium-plutonium ratio determinations for one mass spectrometer with a 0.6 % relative precision.

This corresponds to an increase by a factor four on the rate and by a factor two on the precision, compared with the previous conditions.

BIBLIOGRAPHY -

1) CHENOUARD. J. , LUCAS. M. Rapport CEA . R 2563. (1963)

2) LUCAS.M. Rapport CEA R 2564. (1964)

3) CROCKER.H.I. CRDC - 697 . AECL NO 488 (1957)

4) WEBSTER. R. K, SMALES.A.A, DANCE .D.F, SLEE.L.J. AERE. R 3327 - R 3378 (1960)

5) SEABORG.G.T, KATZ.J, MANNING.W.M. The Transuranium Elements (Res Pap) Part I - II (1949)

6) SEABORG.G.T, KATZ.J. The Actinide Elements (1954)

7) SEABORG.G.T, KATZ.J. The Chemistry of the Actinide Elements (1957)

8) CARRE.J.C, BIR.R, FREJAVILLE.G. Advances in Mass Spectrometry . V IV (1968)

9) DALLY.N.R. Rev Sci Inst V 31 - 264 (1960)

10) CALDECOURT.V.J. Appl Spectrosc - 12 - N° 2 - 40 (1958)

11) DIETZ.A.L. Rev Sci Inst V 36 - 1763 (1965)

12) BARTON.G.W, GIBSON.L.E, TOLMAN.L.F. Anal Chem 32 - 1599 (1960)

ADDENDUM

1. Proton Affinities of Organic Molecules in the Gas Phase

J. L. Beauchamp and R. C. Dunbar

Arthur Amos Noyes Laboratory of Chemical Physics,
California Institute of Technology
Pasadena, California 91109

ABSTRACT

Proton and hydrogen affinities are defined, respectively, as the negative of the enthalpy change for the processes

$$M + H^+ \rightarrow MH^+ \qquad PA(M) = -\Delta H \qquad 1$$

and

$$M^+ + H \rightarrow MH^+ \qquad HA(M^+) = -\Delta H . \qquad 2$$

Proton and hydrogen affinities are related simply by the expression

$$PA(M) - HA(M^+) = IP(H) - IP(M) \qquad 3$$

where IP(X) is the adiabatic ionization potential of the species X. By definition, the hydrogen affinity of a species M^+ corresponds to the $\overset{+}{M}$—H bond dissociation energy.

In that ion-molecule reactions do not involve activation energies, it is possible to determine the relative proton affinities of the species M_1 and M_2 by an examination of reactions of the type

$$M_1H^+ + M_2 \rightleftharpoons M_1 + M_2H^+ \qquad 4$$

for which the enthalpy change is the difference in proton affinities of the species M_1 and M_2. The proton affinities of simple alkenes and ketones can be calculated from available electron and photon impact data and permit absolute values in the scale of relative proton affinities to be established.

Using ion cyclotron resonance techniques to identify processes such as reaction (4)[1] the above considerations have been applied to determine the proton affinities of a variety of alkenes, aldehydes, and ketones in addition to alcohols, ethers and their sulfur containing analogs.

The assumption that the hydrogen affinities of structurally related species containing the same functional group are approximately equal provides a uniform interpretation of the proton affinity data derived from ion-molecule reactions. The proton affinity scale has a fundamental significance for a wide range of ion chemistry studies.

---

[1] J. L. Beauchamp and S. E. Buttrill, Jr., J. Chem. Phys. 48, 1783 (1968).

Author Index

Author Index

Author Index

A.S.T[illegible] Publications on Mass Spectrometry*

A. Recommended [illegible]actices and Methods of Test**

Title an[illegible]itations in 1968 Book of ASTM Standards

Designation	
D1137-53	An[illegible]is of Natural Gases and Related Types of Gaseous Mi[illegible]es by the Mass Spectrometer, Part 19, pp. 213-223.
D1302-61T	An[illegible]is of Carburetted Water Gas by the Mass Spectrometer, P[illegible]9, pp. 288-294.
D1658-63	Ca[illegible]n Number Distribution of Aromatic Compounds in Na[illegible]as by Mass Spectrometry, Part 17, pp. 599-602.
D2424-67	Hy[illegible]carbon Types in Propylene Polymer by Mass Spectrometry [illegible]18, pp. 574-582.
D2425-67	[illegible] carbon Types in Middle Distillates by Mass Sp[illegible]trometry, Part 17, pp. 875-884.
D2498-66T	Isomer Distribution of Straight-Chain Detergent Alkylate by Mass Spectrometry, Part 18, pp. 622-627.
D2567-66T	Molecular Distribution Analysis of Monoalkylbenzenes by Mass Spectrometry, Part 18, pp. 751-753.
D2601-67T	Low-Voltage Mass Spectrometric Analysis of Propylene Tetramer, Part 18, pp. 779-782.
D2650-67T	Chemical Composition of Gases by Mass Spectrometry, Part 18, pp. 796-804.
E137-65	Evaluation of Mass Spectrometers for Use in Chemical Analysis, Part 30, pp. 339-342.
E244-64T	Atom Percent Fission in Uranium Fuel, Mass Spectrometric Method, Part 30, pp. 767-772.
E304-66T	Use and Evaluation of Mass Spectrometers for Mass Spectrochemical Analysis of Solids, Part 30, pp. 1003-1009.

Title and Citation in Other ASTM Publications

Proposed	Hydrocarbon Types in Olefinic Gasoline by Mass Spectrometry ASTM Standards on Petroleum Product and Lubricants, App. VIII, Vol. I, p. 1128 (October, 1961). (Published as information only.)
Proposed	Hydrocarbon Types in Low Olefinic Gasoline by Mass Spectrometry: App. VII, Report of Committee D-2, 1961; republished for information.
Proposed	Carbon Number Distribution of Saturate and Aromatic Classes in Distillate Waxes by Mass Spectrometry: App. III, Report of Committee D-2, 1967; published for information.

B. Other ASTM Mass Spectrometric Information

DS27	Index of Mass Spectral Data, published Sept., 1964, 248 pages (Initially published as STP No. 356).
DS27-1a	Mass Spectral Data - Punched Card Index—3200 cards
DS27-1b	Mass Spectral Name Formula - Punched Card Index—3500 cards
STP No. 149	Chemical Analysis of Inorganic Solids by Means of Mass Spectrometer, published 1951.

* Prepared by Subcommittee VI, ASTM Committee E-14, June, 1968.

** Committee jurisdiction for the mass spectrometric practices and methods is as follows:

Committee D3 - D1137 and D1302
Committee E10 - E244
Committee E14 - E137 and E304
Committee D2 - all others listed.